INFORMATION TO USERS

This manuscript has been reproduced from the microfilm master. UMI films the text directly from the original or copy submitted. Thus, some thesis and dissertation copies are in typewriter face, while others may be from any type of computer printer.

The quality of this reproduction is dependent upon the quality of the copy submitted. Broken or indistinct print, colored or poor quality illustrations and photographs, print bleedthrough, substandard margins, and improper alignment can adversely affect reproduction.

In the unlikely event that the author did not send UMI a complete manuscript and there are missing pages, these will be noted. Also, if unauthorized copyright material had to be removed, a note will indicate the deletion.

Oversize materials (e.g., maps, drawings, charts) are reproduced by sectioning the original, beginning at the upper left-hand corner and continuing from left to right in equal sections with small overlaps.

Photographs included in the original manuscript have been reproduced xerographically in this copy. Higher quality 6" x 9" black and white photographic prints are available for any photographs or illustrations appearing in this copy for an additional charge. Contact UMI directly to order.

ProQuest Information and Learning
300 North Zeeb Road, Ann Arbor, MI 48106-1346 USA
800-521-0600

UMI®

Reproduced with permission of the copyright owner. Further reproduction prohibited without permission.

DISSERTATION

DROP SIZE-DEPENDENT CHEMICAL COMPOSITION IN CLOUDS AND FOGS

VOLUME I: CHAPTERS 1 – 11

Submitted by

Katharine F. Moore

Department of Atmospheric Science

In partial fulfullment of the requirements

for the Degree of Doctor of Philosophy

Colorado State University

Fort Collins, Colorado

Spring 2002

Reproduced with permission of the copyright owner. Further reproduction prohibited without permission.

UMI Number: 3053433

UMI®

UMI Microform 3053433
Copyright 2002 by ProQuest Information and Learning Company.
All rights reserved. This microform edition is protected against
unauthorized copying under Title 17, United States Code.

ProQuest Information and Learning Company
300 North Zeeb Road
P.O. Box 1346
Ann Arbor, MI 48106-1346

Reproduced with permission of the copyright owner. Further reproduction prohibited without permission.

COLORADO STATE UNIVERSITY

November 12, 2001

We hereby recommend that the dissertation prepared under our supervision by Katharine F. Moore entitled DROP SIZE-DEPENDENT CHEMICAL COMPOSITION IN CLOUDS AND FOGS be accepted as fulfilling in part requirements for the degree of Doctor of Philosophy.

Committee on Graduate Work

Advisor

Department Head

Reproduced with permission of the copyright owner. Further reproduction prohibited without permission.

ABSTRACT OF DISSERTATION

DROP SIZE-DEPENDENT CHEMICAL COMPOSITION IN CLOUDS AND FOGS

Cloud drop composition varies as function of drop size. More sophisticated atmospheric chemistry models predict this and observations at many locations around the world by multiple techniques confirm this. This variation can influence the cloud processing of atmospheric species. Aqueous-phase reaction and atmospheric removal rates for scavenged species, among other processes, can be affected by drop size-dependent composition. Inferences to these processes drawn upon single bulk cloud composition measurements can be misleading according to observations obtained using cloud water collectors that separate drops into two or more size-resolved fractions. Improved measurements of size-dependent drop composition are needed to further examine these and related issues.

Two active multi-stage cloud water collectors were developed for sampling super-cooled drops in mixed-phase clouds and warm cloud drops, respectively. Both use the principles of cascade inertial impaction to separate drops into three fractions (super-cooled drop collector) and five fractions (warm cloud drop collector). While calibration suggests there is more drop overlap between stages than desired, consistently different drop fractions are still collected.

FROSTY – the super-cooled drop collector – has been used successfully to obtain size-resolved drop composition information during two field campaigns in Colorado. While the data are limited, FROSTY's field performance appears to be reasonably consistent during individual cloud events, although not predictable based solely upon its collection efficiency curves. Additional factors must be considering in evaluating its performance in future campaigns. Nevertheless, the ability

Reproduced with permission of the copyright owner. Further reproduction prohibited without permission.

to obtain consistent size-resolved drop composition information from super-cooled clouds was not previously possible.

Field data indicate that the warm cloud collector – the CSU 5-Stage – is able to resolve variations in the drop size-dependent composition not discernible with the two-stage size-fractionating Caltech Active Strand Cloud water Collector (sf-CASCC). Field performance evaluations suggest that the 5-Stage and the sf-CASCC compare well to each other for the range of sampling conditions experienced. Both collectors' performances differ from measurements made by the Caltech Active Strand Cloud water Collector #2 (CASCC2) in some specific sampling conditions, but otherwise agreement between the three collectors is good. Where the sf-CASCC indicates little drop variation in an orographic cloud study at Whiteface Mtn., NY, the 5-Stage indicates up to a factor of two difference may exist between the maximum and minimum drop concentrations for the major inorganic ions (ammonium, nitrate and sulfate). The sf-CASCC data suggest that typically a factor of 3 – 5 difference exists between large and small drop species' concentrations in radiation fogs measured in Davis, CA. Concurrent 5-Stage samples suggest the actual variation may be up to at least a factor of 4 – 5 greater, and that the smallest drops (approximately < 11 μm in diameter) are principally responsible for the strong observed concentration gradients between sizes. While the data are limited, the 5-Stage's results are consistent for all of the sample sets obtained during both field campaigns. Data from the 5-Stage emphasize that cloud drop chemical composition cannot be considered separately from the sampled cloud's microphysics and dynamics. Interpreting the 5-Stage's results necessarily draws upon both.

During the Davis campaign, additional measurements were performed to investigate species removal from the atmosphere via drop deposition and gas/liquid partitioning in-fog. Although subject to confounding effects, these investigations benefited from the additional insight 5-Stage data provided into the processes occurring. In particular, 5-Stage data and between-fog aerosol measurements suggest that deposition of the largest fog drops resulted in the relative removal of

Reproduced with permission of the copyright owner. Further reproduction prohibited without permission.

coarse mode aerosol particles from the atmosphere. 5-Stage data and gas-phase measurements suggest the ammonia/ammonium system may not be at equilibrium and provide some information about the nitrous acid/nitrite system not otherwise available. The 5-Stage has the potential to be a valuable tool in investigating the effects of fog and fog processing on the fate of ambient species.

Katharine F. Moore
Department of Atmospheric Science
Colorado State University
Fort Collins, CO 80523
Spring 2002

Reproduced with permission of the copyright owner. Further reproduction prohibited without permission.

Acknowledgements

I need to recognize and thank the faculty who served upon my committee: Professor Jeff Collett, Professor Sonia Kreidenweis, Professor Roger Pielke and Professor Roy Buchan. In particular I specifically thank my advisor, Jeff, who I'm quite sure had no idea what he was getting into when he accepted my application. I have occasionally wondered since then if he would have still extended the offer if he had really known me then as well as he does now (to which my response is "Hah – too late!"). Further, I thank Sonia for giving generously of her time and equipment whenever I asked for it.

I have been very fortunate to have been the recipient of a US Environmental Protection Agency "Science to Achieve Results" (STAR) continuing doctoral fellowship for the last 3 years (#U-915364). I am grateful to my project officer, Ms. Georgette Boddie, and the other staff at both the US EPA and CSU who helped administer it.

Funding for the development of the CSU 5-Stage collector and subsequent field campaigns was provided by the National Science Foundation under grants ATM-9509596, ATM-9712603, and ATM-9980540. Funding for the development of the FROSTY collector and associated field work was supported by the US Environmental Protection Agency National Center for Environmental Research and Quality Assurance under grant R82-3979-010. Additional field work during the December 1998 – January 1999 Davis, CA field campaign was supported by the San Joaquin Valleywide Air Pollution Study Agency.

Table i lists the seven field campaigns that I have participated in during my time at CSU and the additional Group members who took part. The success of these field campaigns depended upon

Reproduced with permission of the copyright owner. Further reproduction prohibited without permission.

the work and cooperation of them all, and I am grateful for their collective efforts. Eli Sherman was the once constant for every campaign. I would not have a dissertation without him.

I appreciate the help, encouragement and advice of the various members of the Atmospheric Chemistry Group over the last five years. This particularly includes Sandy Progen. I have used the results of Derek Straub's M.S. thesis extensively, and have very much benefited from his help. I am indebted to Betsy Andrews and Mike Hannigan for their continuing friendship.

Fredi Boston almost always knew where to find the latest obscure reference I absolutely positively had to have immediately. I am very grateful for her help.

Our participation at the ACE2 project "HILLCLOUD" was significantly assisted by Dr. Keith Bower of UMIST. The Davis, CA and Whiteface Mountain, NY field campaigns were conducted in conjunction with Professor L. Husain's group of the New York State Department of Health (Wadsworth Laboratory)/SUNY Albany. At Whiteface, the help of the staff of the Atmospheric Science Research Center is gratefully acknowledged, as well as the assistance of Professor C. Anastasio and Mr. Mike Mata at UC Davis.

The ACE2 wind speed, temperature, pressure, liquid water content, and drop size distributions were obtained from the ACE2 main database after data quality controls by the investigators – UMIST and the Risø National Laboratory (Denmark). I am grateful to both of those organizations for providing the data, and particularly for a helpful discussions with Keith Bower. I believe K. Bower (UMIST), M. Gallagher (UMIST), and M. Nielsen (RNL) are responsible for the data.

At various times, many people have assisted this work. They include: Capt. S. Emert, Dr. C.-H. Kim, Dr. P. Herckes, Prof. J. C. Wilson, W. Dawson (Drop Measurement Technologies), D. Bloudoff (Cal-EPA), Prof. M. Wendisch, Dr. H. Gerber, Dr. C. Ortiz, Prof. A. Gertler, Prof. (emeritus) S. Self, Prof. A. Berner, Dr. R. Borys, Prof. C. Anastasio, Prof. R. Vong, R. Burkhard,

Reproduced with permission of the copyright owner. Further reproduction prohibited without permission.

Prof. W. Eugster, T. Wrzesinsky, Dr. M. Millet, and the librarians at the Desert Research Institute and Stanford University, among others.

Table i: Field Campaigns

Campaign	Dates	Collett Group Field Participants
Storm Peak Laboratory Steamboat Springs, CO	January 1997	D. E. Sherman, E. Andrews, X. Rao, X. Gang, D. J. Straub, K. Hoag
ACE-2 HILLCLOUD Tenerife, the Canary Islands	July 1997	D. E. Sherman
Davis, CA	January 1998	D. E. Sherman, D. J. Straub
Horsetooth Mountain, Fort Collins, CO	April 1998	D. E. Sherman, X. Gang, (E. Andrews)
Whiteface Mountain, NY	July 1998	D. E. Sherman, J. E. Reilly
Davis, CA	December 1998 – January 1999	D. E. Sherman, J. E. Reilly, M. P. Hannigan, T. Lee
Corcoran, CA	December 1999 – January 2000	D. E. Sherman, P. Herckes

Finally, I do need to thank my friends and family for their support, encouragement, and putting up with me. While I don't usually admit it, I am very much aware of how blessed I am to live the life I lead and to have them all on my side. I do not have the space to thank everyone individually, however I do not know what I would do without my M M (and Rupert).

Reproduced with permission of the copyright owner. Further reproduction prohibited without permission.

Table of Contents

Volume I

1. Introduction 2
   1.1 Why cloud composition is important 2
   1.2 Chemical composition of clouds 4
   1.3 Size-dependent cloud drop chemistry 6
      1.3.1 Models 9
      1.3.2 Observations 10
   1.4 Goals of this research 13
   1.5 Dissertation format 14
      1.5.1 Comment on the appendices 15

2. Cloud water collectors: design and development 16
   2.1 Existing cloud water collectors 16
      2.1.1 The Caltech series of active strand cloud water collectors 17
   2.2 The new cloud water collectors 19
      2.2.1 FROSTY 20
      2.2.2 The 5-Stage collector 22
   2.3 Collector design/use considerations 24
      2.3.1 Physical Performance Criteria 24
         2.3.1.1 Principles of Cascade Impactor Design 25
         2.3.1.2 Sampling Time Requirements 27
         2.3.1.3 Drop Integrity 27
         2.3.1.4 Aspiration Efficiency 29
         2.3.1.5 Windshield Design 35
         2.3.1.6 Preliminary Performance Evaluation and Resulting Modifications 36
      2.3.2 Chemical integrity 36
         2.3.2.1 Material Inertness 36
         2.3.2.2 Evaporation and condensation within the collectors 37
      2.3.3 Ease-of-use 38
      2.3.4 Comparability 39

Reproduced with permission of the copyright owner. Further reproduction prohibited without permission.

3. Field Performance of the Caltech Heated Rod Cloud water collector (CHRCC) and the FROSTY collector 40
3.1 Rationale behind field performance validation 40
3.2 The Storm Peak Laboratory Field Campaign 43
3.3 CHRCC Evaluation 48
3.4 FROSTY evaluation 51
3.5 CHRCC vs. FROSTY 56
3.6 Concluding Discussion 59
3.7 Further issues related to FROSTY's performance 63

4. Field performance of the warm cloud collectors – the Caltech Active Strand Cloud water Collector #2 (CASCC2), the size-fractionating Caltech Active Strand Cloud water Collector (sf-CASCC), and the 5-Stage 66
4.1 sf-CASCC side-by-side comparison 67
4.1.1 Side-by-side results 68
4.1.2 Side-by-side discussion 68
4.2 CASCC2 and sf-CASCC mass comparisons 72
4.2.1 CASCC2 vs. sf-CASCC collected mass 72
4.2.2 CASCC2 and sf-CASCC collected mass vs. measured LWC 72
4.2.2.1 Revised Davis LWC data 74
4.2.2.2 Evaluation of a previously proposed CASCC2-LWC equation 78
4.2.3 Collector orientation 78
4.3 Evaluation of CASCC2 and sf-CASCC collection efficiency curves 79
4.3.1 Drop distribution data 80
4.3.1.1 Cloud microphysical parameters at ACE2 80
4.3.1.2 Cloud microphysical parameters at Whiteface 82
4.3.2 Collector efficiency curves 82
4.3.3 CASCC2 and sf-CASCC predicted/collected mass results 83
4.3.4 Discussion 86
4.4 5-Stage predicted and collected mass 88
4.4.1 Experimental collection efficiency curves 89
4.4.2 5-Stage predicted and collected mass performance 90
4.4.2.1 Results 90
4.4.2.2 Discussion 91
4.5 Derived "bulk" vs. bulk cloud water composition 96
4.5.1 Results 97

Reproduced with permission of the copyright owner. Further reproduction prohibited without permission.

4.5.2 Discussion 98
4.6 Summarizing discussion 104

5. Sampling and analytical protocol 107
5.1 Field sampling 108
5.1.1 Preparation 108
5.1.1.1 Collectors 108
5.1.1.2 Aliquot Chemicals 108
5.1.2 Field Installation 109
5.1.2.1 Equipment 109
5.1.3 Field Measurements 109
5.1.3.1 Cloud water 109
5.1.3.2 Cloud physics and meteorological measurements 110
5.1.3.3 Gas-phase species 110
5.1.3.3.1 SO_2 and H_2O_2 110
5.1.3.3.2 NH_3 and HNO_3 111
5.1.3.3.3 Additional gas phase measurements 112
5.1.3.4 Aerosol measurements 112
5.1.4 Field aliquot preparation 113
5.2 Chemical analysis 114
5.2.1 pH 114
5.2.2 IC (Inorganic ions) 114
5.2.3 GFAAS (Metals) 116
5.2.4 $H_2O_{2(aq)}$ 117
5.2.5 $S(IV)_{(aq)}$ 117
5.2.6 $HCHO_{(aq)}$ 117
5.3 Analytical uncertainty 118
5.3.1 pH 118
5.3.2 IC 118
5.3.3 GFAAS 120
5.3.4 $H_2O_{2(aq)}$ 120
5.3.5 $S(IV)_{(aq)}$ 122
5.3.6 $HCHO_{(aq)}$ 123
5.3.7 Gas data 123
5.4 Other measurement uncertainty 124
5.4.1 Meteorological measurements 125
5.4.2 Flow rates 125

Reproduced with permission of the copyright owner. Further reproduction prohibited without permission.

5.5 Analytical data validation 126
5.5.1 Charge balance 126
5.5.2 Comments specific to particular analyses/campaigns 127
5.5.2.1 Low concentrations of divalent cations 127
5.5.2.2 GFAAS methods 128
5.5.2.3 5-Stage HCHO and S(IV) aliquots 129
5.5.2.4 Whiteface DI contamination 130
5.5.2.5 Sample stability 130

6. Horsetooth 134
6.1 The Horsetooth Mountain site 134
6.2 Why study mixed-phase clouds? 135
6.3 The Storm Peak Laboratory Winter 1996/7 Results 136
6.4 Results 137
6.4.1 Data Validation 138
6.4.2 Drop size-dependent composition 139
6.4.3 Sampling protocol 146
6.5 Discussion 148

7. ACE2 150
7.1 Project overview and site description 150
7.2 Summary of first reported results 154
7.3 CSU's contribution to HILLCLOUD 155
7.3.1 sf-CASCC data 155
7.3.2 5-Stage data 156
7.4 Ambient conditions during cloud events 158
7.5 Results and discussion 158

8. Whiteface 172
8.1 Site description 172
8.1.1 Equipment and protocols 173
8.2 Review of the sf-CASCC results 174
8.3 5-Stage results and discussion 180

9. Davis 200
9.1 Site description 200
9.2 Fog events and ambient conditions 201

Reproduced with permission of the copyright owner. Further reproduction prohibited without permission.

9.2.1 Fog events 201
9.2.2 Ambient conditions 202
9.3 Review of the sf-CASCC data 207
9.3.1 Davis timelines 207
9.3.2 Large and Small Davis fog drop composition 208
9.4 5-Stage in Davis 216
9.4.1 Results and discussion 216
9.5 Gas and aerosol measurements 230
9.5.1 Results and discussion 231
9.6 In-fog deposition 239
9.6.1 Results and discussion 240
9.7 Gas/Liquid equilibria in-fog 243
9.7.1 NH_4^+/NH_3 and NO_3^-/HNO_3 results and discussion 246
9.7.2 $HONO/NO_2^-$ results and discussion 250
9.8 Equivalent air concentrations 254
9.9 Scale data 257
9.10 Summarizing remarks 258

10. Conclusions and recommendations 261
10.1 Conclusions 261
10.2 Recommendations 265

11. References 270

Volume II

A. Appendix: Review of Cloud Chemistry Measurements 309

B. Appendix: Cloud water collectors – review, characterization and reported field comparisons 345

C. Appendix: The FROSTY Collector: Cleaning, Assembly and Sampling Protocol 411

D. Appendix: The CSU 5-Stage Collector: Cleaning & Sampling Protocol 419

E. Appendix: Drop stopping distance and characteristic times for varying ambient conditions 429

Reproduced with permission of the copyright owner. Further reproduction prohibited without permission.

F. Appendix: the wind shield (baffle) 437

G. Appendix: Drop size distributions – instruments, problems and processing 444

H. Appendix: Data tables 474

I. Appendix: Performance of the Gerber PVM-100 510

J. Appendix: Microorifice Uniform Deposit Impactor (MOUDI) protocol 515

K. Appendix: Compiled IC statistics 518

Reproduced with permission of the copyright owner. Further reproduction prohibited without permission.

List of Tables

Table 2-1: FROSTY operating/design parameters 21
Table 2-2: 5-Stage operating/design parameters 24
Table 2-3: Anisokinetic sampling conditions by warm-cloud collector 30
Table 3-1: SPL EVENT 2 data available 45
Table 3-2: SPL EVENT 8 data available 46
Table 3-3: SPL EVENT 9 data available 46
Table 3-4: SPL EVENT 10 data available 47
Table 3-5: SPL EVENT 14 data available 47
Table 4-1: W188 sf-CASCC side-by-side comparison – tabulated results 70
Table 4-2: Summary of revised LWC data for Davis 77
Table 4-3: Compiled CASCC2 and sf-CASCC predicted/measured mass results 86
Table 4-4: CASCC2 and sf-CASCC measured mass results 86
Table 4-5: sf-CASCC to CASCC2 derived "bulk" to bulk concentration comparison for all data 97
Table 4-6: 5-Stage and sf-CASCC to CASCC2 derived "bulk" to bulk concentration comparison for 5-Stage sampling periods only 98
Table 5-1: Davis campaign aliquot protocol (abridged) 115
Table 5-2: Fe compiled statistics 121
Table 5-3: Mn compiled statistics 121
Table 5-4: Cu compiled statistics 122
Table 5-5: Compiled $H_2O_{2(aq)}$ statistics 122
Table 5-6: Compiled S(IV) statistics 123
Table 5-7: Compiled HCHO statistics 124
Table 7-1: ACE2 event and sampling period summary 156
Table 7-2: ACE2 wind speed and temperature means/standard deviations by event 158
Table 7-3: Non-sea salt/total amount ratios by species for all data and clean event only .. 170
Table 8-1: sf-CASCC results from the Whiteface Campaign (July 1998) 179
Table 8-2: W198 sample range by collector for selected species 183
Table 8-3: sf-CASCC and 5-Stage maximum/minimum concentration ratio for selected species on W198 and 5-Stage-to-sf-CASCC ratio comparison 195
Table 9-1: Fog events and samples 203

Reproduced with permission of the copyright owner. Further reproduction prohibited without permission.

Table 9-2: MOUDI and denuder sampling periods between the D009, D010 and D010B events (denuders also sampled during events) 203
Table 9-3: Davis Campaign overall sf-CASCC composition results 215
Table 9-4: sf-CASCC, 5-Stage, and 5-Stage to sf-CASCC maximum/minimum concentration ratios for the major species 228
Table 9-5: Deposition drop diameters 241

Reproduced with permission of the copyright owner. Further reproduction prohibited without permission.

List of Figures

Figure 1-1: Size-dependent cloud drop chemistry schematic. 7
Figure 2-1: Schematic of sf-CASCC (top) and CASCC2 (bottom) 17
Figure 2-2: sf-CASCC installed in Davis, CA (December, 1998) 18
Figure 2-3: FROSTY installed at the Storm Peak Laboratory, Steamboat Springs, CO (January, 1997) 20
Figure 2-4: FROSTY top view schematic 21
Figure 2-5: 5-Stage collector schematic (side view) 23
Figure 2-6: The 5-Stage collector installed at the summit of Whiteface Mountain, NY (July, 1998) 23
Figure 3-1: The theoretical CHRCC and experimental FROSTY collection efficiency curves for SPL conditions. 48
Figure 3-2: CHRCC predicted vs. collected mass (EVENT 8, 8 samples). 51
Figure 3-3: CHRCC collected mass vs. PVM LWC at SPL (2 events, 11 samples). 52
Figure 3-4: FROSTY LARGE predicted vs. collected at SPL (3 events, 15 samples) 52
Figure 3-5: FROSTY MEDIUM predicted vs. collected at SPL (3 events, 15 samples). 53
Figure 3-6: FROSTY SMALL predicted vs. collected at SPL (3 events, 15 samples). 53
Figure 3-7: FROSTY relative predicted vs. collected performance, EVENT 9 #2 at SPL 54
Figure 3-8: FROSTY relative predicted vs. collected water mass performance at Horsetooth Mtn (4/14/98, 1 – 2 a.m.) 56
Figure 3-9: FROSTY vs. PVM at SPL (3 events, 21 samples). 57
Figure 3-10: FROSTY vs. CHRCC collected mass at SPL (7 points, 3 events). 57
Figure 3-11: Temporal evolution of sulfate for FROSTY at SPL (EVENT 8). 60
Figure 4-1: W188 sf-CASCC side-by-side comparison – collected mass 68
Figure 4-2: W188 sf-CASCC side-by-side comparison – nitrate 69
Figure 4-3: W188 sf-CASCC side-by-side comparison – potassium ion 69
Figure 4-4: W188 sf-CASCC side-by-side comparison – iron 70
Figure 4-5: Total sf-CASCC vs. CASCC2 collected mass for the Whiteface and Davis campaigns. 73
Figure 4-6: Total sf-CASCC collected mass vs. PVM LWC 75
Figure 4-7: CASCC2 collected mass vs. PVM LWC 75

Reproduced with permission of the copyright owner. Further reproduction prohibited without permission.

Figure 4-8: Filtered sf-CASCC collected mass vs. PVM LWC with reduced major axis fit equation shown 76
Figure 4-9: Filtered CASCC2 collected mass vs. PVM LWC with reduced major axis fit equation shown 76
Figure 4-10: CASCC2 collected mass vs. PVM LWC by event at Whiteface 79
Figure 4-11: ACE2 T189 event dLWC distribution 81
Figure 4-12: ACE2 T203 event dLWC distribution 81
Figure 4-13: CASCC2 and sf-CASCC collection efficiency curves 83
Figure 4-14: sf-CASCC net theoretical and modeled collection efficiency curves 84
Figure 4-15: CASCC2 predicted vs. measured mass (12 samples) 85
Figure 4-16: sf-CASCC predicted vs. measured mass via Fluent curves (33 samples) 85
Figure 4-17: sf-CASCC predicted vs. measured mass via theoretical curves (33 samples) 86
Figure 4-18: 5-Stage experimental collection efficiency curves (Straub and Collett, 1999) . 89
Figure 4-19: Overall collection efficiency curves for the CASCC2, sf-CASCC and the 5-Stage 90
Figure 4-20: 5-Stage predicted and collected mass for the W198 event (a) 6 – 7 a. m., (b) 8 – 9 a. m., and (c) 10 – 11 a. m. Predicted interstage losses are shown only in (c) for clarity 92
Figure 4-21: 5-Stage simulation of the sf-CASCC's collected mass performance (W198, 10 – 11 a. m.) 93
Figure 4-22: 5-Stage and sf-CASCC total mass compared to the CASCC2 for validated time periods 93
Figure 4-23: sf-CASCC (open) and 5-Stage (solid) derived bulk concentrations for major species compared to the CASCC2 – filtered for >LOQ and >120 mg m^{-3} LWC 99
Figure 4-24: sf-CASCC (open) and 5-Stage (solid) derived bulk concentrations vs. CASCC2 concentration for selected species – filtered data > LOQ and < 120 mg m^{-3} LWC 99
Figure 4-25: Sulfate distribution – observed and modeled (D010 event, 4 – 6 a. m.) 100
Figure 4-26: Manganese concentration – observed and modeled (W198 event, 6 – 7 a. m.) 100
Figure 5-1: Davis: ammonium stability in IC vials after approximately 1 month of storage 132
Figure 6-1: pH in all validated Horsetooth samples (4/14/98) 140
Figure 6-2: Nitrate concentrations in all validated Horsetooth samples (4/14/98) 141
Figure 6-3: Calcium ion concentrations in all validated data at Horsetooth (4/14/98) 141
Figure 6-4: Horsetooth temporal evolution in calcium ion (April 15, 1998) 143

Reproduced with permission of the copyright owner. Further reproduction prohibited without permission.

Figure 6-5: Horsetooth temporal evolution in nitrate (April 15, 1998). 143
Figure 6-6: Horsetooth temporal evolution in sulfate (April 15, 1998). 144
Figure 6-7: Horsetooth temporal evolution in ammonium (April 15, 1998) 145
Figure 6-8: Horsetooth temporal evolution in pH (April 15, 1998) 145
Figure 6-9: Horsetooth comparison of pH measurements for samples melted in the field and kept frozen until measurement in the lab 146
Figure 6-10: Frozen vs. "regular" concentrations for selected species in the three LARGE sample pairs 147
Figure 7-1: Map of Tenerife 151
Figure 7-2: Taganana as seen from El Bailadero (July 1997) 151
Figure 7-3: Looking up to El Bailadero from Taganana (July 1997) 152
Figure 7-4: The view of Paiba from El Bailadero (July 1997) 152
Figure 7-5: Cloud sampling equipment installation at El Bailadero 153
Figure 7-6: The sf-CASCC installed at El Bailadero (July 1997) 153
Figure 7-7: T189 3 – 4 a. m. Large fraction sf-CASCC sample (polluted) 160
Figure 7-8: T189 3 – 4 a. m. Small fraction sf-CASCC sample (polluted) 160
Figure 7-9: T203 9 – 10 p. m. Large sf-CASCC fraction sample (clean) 161
Figure 7-10: T203 9 – 10 p. m. Small fraction sf-CASCC sample (clean) 161
Figure 7-11: Large vs. Small sf-CASCC – pH for all events 162
Figure 7-12: Large vs. Small sf-CASCC collected sample mass for all events 163
Figure 7-13: Large vs. Small sf-CASCC cation concentrations for polluted and intermediate events 164
Figure 7-14: Large vs. Small sf-CASCC cation concentrations for the clean event 165
Figure 7-15: Large vs. Small sf-CASCC anion composition (including non-sea salt (nss) sulfate) for polluted and intermediate events 166
Figure 7-16: Large vs. Small sf-CASCC anion composition (including non-sea salt (nss) sulfate) for the clean event 167
Figure 7-17: Large vs. Small sf-CASCC total peroxides for all events 167
Figure 7-18: Large vs. Small sf-CASCC Fe and Mn for polluted and intermediate events 168
Figure 7-19: Large vs. Small sf-CASCC Fe and Mn for the clean event 168
Figure 7-20: Sodium vs. chloride concentrations for all ACE2 data 169
Figure 7-21: Non-sea salt vs. total sulfate concentrations for all ACE2 data 170
Figure 8-1: The Whiteface field site (July 1998) 173
Figure 8-2: Large vs. Small sf-CASCC -- pH 176
Figure 8-3: Large vs. Small sf-CASCC -- ammonium 176
Figure 8-4: Large vs. Small sf-CASCC – nitrate 177
Figure 8-5: Large vs. Small sf-CASCC – sulfate 177

Reproduced with permission of the copyright owner. Further reproduction prohibited without permission.

Figure 8-6: Large vs. Small sf-CASCC – calcium ion 178
Figure 8-7: Large vs. Small sf-CASCC – manganese 178
Figure 8-8: Large vs. Small sf-CASCC – copper 179
Figure 8-9: W198 2 – 3 a. m. pH (all collectors) 184
Figure 8-10: W198 8 – 9 a. m. pH (all collectors) 184
Figure 8-11: W198 CASCC2 temporal evolution -- ammonium 185
Figure 8-12: W198 sf-CASCC temporal evolution - ammonium 185
Figure 8-13: W198 5-Stage temporal evolution – ammonium 186
Figure 8-14: W198 6 – 7 a. m. nitrate (all collectors) 187
Figure 8-15: W198 6 – 7 a. m. sulfate (all collectors) 187
Figure 8-16: W198 8 – 9 a. m. sulfate (all collectors) 188
Figure 8-17: W198 10 – 11 a. m. sulfate (all collectors) 188
Figure 8-18: W198 CASCC2 temporal evolution -- manganese 190
Figure 8-19: W198 sf-CASCC temporal evolution -- manganese 190
Figure 8-20: W198 5-Stage temporal evolution -- manganese 191
Figure 8-21: W198 6 – 7 a. m. calcium ion (all collectors) 191
Figure 8-22: W198 8 – 9 a. m. calcium ion (all collectors) 192
Figure 8-23: W198 10 – 11 a. m. calcium ion (all collectors) 192
Figure 8-24: W198 6 – 7 a. m. potassium ion (all collectors) 193
Figure 8-25: W198 8 – 9 a. m. potassium ion (all collectors) 193
Figure 8-26: W198 10 – 11 a. m. chloride (all collectors) 194
Figure 8-27: W198 10 – 11 a. m. total peroxides (all collectors) 194
Figure 8-28: W198 5-Stage temporal evolution – total measured inorganic concentration 197
Figure 9-1: The Davis field site (December 1998) 201
Figure 9-2: Eli Sherman collecting sample from the large Teflon deposition plates in Davis (December 1998). 202
Figure 9-3: Large vs. Small sf-CASCC – pH 209
Figure 9-4: Large vs. Small sf-CASCC – ammonium 209
Figure 9-5: Large vs. Small sf-CASCC – nitrate 210
Figure 9-6: Large vs. Small sf-CASCC – potassium ion 210
Figure 9-7: Large vs. Small sf-CASCC – nitrite 211
Figure 9-8: Large vs. Small sf-CASCC – iron 214
Figure 9-9: Large vs. Small sf-CASCC – copper 214
Figure 9-10: Sulfate – all three collectors (D004, 20:08 – 22:00) 217
Figure 9-11: Sulfate – all three collectors (D004, 23:00 – 01:00) 217
Figure 9-12: Sulfate – all three collectors (D004, 02:00 – 04:00) 218

Reproduced with permission of the copyright owner. Further reproduction prohibited without permission.

Figure 9-13: Chloride – all three collectors (D004, 02:00 – 04:00) 218
Figure 9-14: pH – all three collectors (D004, 23:00 – 01:00) 219
Figure 9-15: pH – all three collectors (D004, 02:00 – 04:00) 220
Figure 9-16: Nitrite – all three collectors (D004, 23:00 – 01:00) 220
Figure 9-17: Nitrite – all three collectors (D004, 02:00 – 04:00) 221
Figure 9-18: distributed water mass – all three collectors (D009) 222
Figure 9-19: Ammonium – all three collectors (D009) 222
Figure 9-20: pH – all three collectors (D009) 223
Figure 9-21: Nitrite – all three collectors (D009) 223
Figure 9-22: Copper – all three collectors (D009, 04:00 – 06:00) 224
Figure 9-23: Distributed water mass – all three collectors (D010) 225
Figure 9-24: Ammonium – all three collectors (D010) 226
Figure 9-25: Calcium ion – all three collectors (D010) 226
Figure 9-26: pH – all three collectors (D010) 227
Figure 9-27: Nitrite – all three collectors (D010) 227
Figure 9-28: Total measured inorganic ion concentration for the two 5-Stage sampling periods on D010 229
Figure 9-29: 5-Stage ammonium and nitrate ratios by stage to the respective sum of measured cations or anions (mean of all sample sets) 230
Figure 9-30: Ammonia concentrations in Davis (January). In-fog events are noted 232
Figure 9-31: Nitric acid gas concentrations in Davis (January). In-fog events are noted .. 232
Figure 9-32: Size-resolved aerosol mass measurements before and after the D009 event for (a) nitrate, (b) sulfate, and (c) ammonium 233
Figure 9-33: Same as figure 9-32, except mass is now normalized to show the relative change 234
Figure 9-34: Same as figure 9-32 except before and after the D010 event 235
Figure 9-35: Same as figure 9-33, except normalized mass concentrations are shown 236
Figure 9-36: Davis deposition velocities for selected species 241
Figure 9-37: Equilibrium fraction of NH_4^+ predicted for varying pH and LWC 245
Figure 9-38: Equilibrium partitioning of NO_2^- in the aqueous-phase as a function of LWC and pH. 246
Figure 9-39: Actual/equilibrium aqueous-phase mole fraction ratio for ammonium by event mean. 247
Figure 9-40: Measured/equilibrium aqueous-phase ammonium mole fraction ratio for a 5-Stage sampling period (D009, 4 – 6 a. m.) 248
Figure 9-41: Measured/equilibrium aqueous-phase ammonium mole fraction ratio for a 5-Stage sampling period (D010, 6:52 – 9 a. m.). 249

Reproduced with permission of the copyright owner. Further reproduction prohibited without permission.

Figure 9-42: $HONO_{(g)}$ derived from aqueous-phase measurements plotted by event/sample. 251
Figure 9-43: Same as figure 9-42 with LWC added on the secondary axis..... 252
Figure 9-44: $HONO_{(g)}$ derived from the 5-Stage for all seven samples. 252
Figure 9-45: Equivalent nitrate air concentrations plotted by event and collector 255
Figure 9-46: Equivalent nitrate and nitrite air concentrations derived from 5-Stage data plotted by event sample set (Stage 1 through Stage 5) 257
Figure 9-47: D004: 1/4/99 10:10 p.m. to 1/5/99 8:00 a.m. scale vs. deposition plate flux 258

Reproduced with permission of the copyright owner. Further reproduction prohibited without permission.

List of Symbols

(includes regularly used acronyms and notation)

Symbol	meaning
A	measured activity correction
Area	for the gaussian fits – the area under the curve
C	Cunningham slip correction factor
C_{aq}	the aqueous-phase species concentration (expressed in terms of air concentration)
CASCC	Caltech Active Strand Cloud water Collector
CASCCs	all collectors in the Caltech "family" of active strand collectors
CASCC2	Caltech Active Strand Cloud water Collector #2
$C_{bc,i}$	bulk cloud concentration of species i [usually μN]
CCN	Cloud condensation nuclei
C_D	coefficient of drag (dimensionless)
$C_{dp,i}$	deposition plate concentration of species i [usually μN]
C_g	the gas-phase species concentration
CHRCC	Caltech Heated Rod Cloud water Collector
C_i	concentration of species i [usually μN for chemical species, and g m^{-3} for water]
CL	Confidence Limit (95% is used)
CSASP	Classical Scattering Active Spectrophotometer Probe (PMS, Inc., Boulder, CO)
C2	index notation for the CASCC2
D_{cnt}	critical drop size (collected with 0% efficiency)
D_{eff}	effective diameter
D_i	the midpoint diameter in bin i
dLWC	the liquid water content in the bin
dN	the number concentration in the bin
D_{nozzle}	diameter of the aspirating nozzle
D_p	particle diameter

Reproduced with permission of the copyright owner. Further reproduction prohibited without permission.

D_{p50}	drop cut-point diameter with collected with 50% efficiency
dV	the volume concentration in the bin
$D_{\#}$	drop diameter corresponding to #% collection efficiency
emp	empirical factor for the 2 UMIST FSSPs studied
f_{act}	distribution factor based upon measurements (as defined)
f_{calm}	parameter in Grinshpun *et al.* (1993)
f_{equil}	distribution factor based upon assuming gas-/aqueous-phase equilibrium (as defined)
F_i	flux of species i [quantity/area-time][usually g m^{-2} s^{-1}]
f_i	frequency factor generated from particle transit times
FSSP	Forward Scattering Spectrophotometer Probe (PMS, Inc., Boulder, CO)
H_{eff}	the effective Henry's constant
i	index/species of interest
j	index used for calculating the aqueous-phase mole fraction
L	jet length (cascade impactor)
Large	when capitalized refers to Stage 1 of the sf-CASCC
LARGE	in all capitals refers to FROSTY Stage 1
Le	length of the tube
L_i	distance to the mid-point of the first bank of collection surfaces in collector I
LOQ	Level of Quantitation
lwc	LWC (in mg m^{-3}) calculated in Chapter 4 based upon collected CASCC2/sf-CASCC masses
LWC	Liquid Water Content (in appropriate units)
m	emprical factor applied to activity correction
M	Molar (moles $liter^{-1}$)
mass	mass (in grams) of water collected by either the CASCC2 or the sf-CASCC (Chapter 4)
mb	milli-bars (unit of pressure → 1013 mb = 101300 Pa)
MDL	Minimum Detection Limit
MEDIUM	in all capitals refers to FROSTY Stage 2

Reproduced with permission of the copyright owner. Further reproduction prohibited without permission.

Metals	when capitalized refers to Fe, Mn and Cu concentrations (derived from the acidified aliquot)
mN	milli-Normal (milli-equivalents liter^{-1}, or 10^{-3} moles of charge liter^{-1})
N_a	actual number concentration (in a bin)
N_{drops}	drop concentration
n_i	the number concentration in bin i
N_m	measured number concentrion (in a bin)
P	pressure
PVM	The Gerber Particle Volume Monitor (model 100)
Q	volumetric flow rate
R	the universal gas constant
Re	Reynolds number (as defined)
Re_f	Reynolds number calculated based upon the fluid flow
R_{eff}	Effective radius
Re_i	impactor jet Reynolds number
Re_p	particle Reynolds number
Re_0	initial Reynolds number (as defined)
RSD	relative standard deviation
S	distance between the bottom of the impactor jet and the impaction surface
SA	the total surface area measured by the PVM [cm^2 m^{-3}]
sfC	index notation for the sf-CASCC
sf-CASCC	size-fractionating Caltech Active Strand Cloud water Collector
Small	when capitalized refers to Stage 2 of the sf-CASCC
SMALL	in all capitals refers to FROSTY Stage 3
St	stopping distance
St_{crit}	critical Stokes number
Stk	Stokes number (particle stopping distance/characteristic length)(a measure of particle inertia)
Stk_{asp}	Stokes number as defined by Vincent (1989) for blunt sampling devices
T	temperature (expressed in Kelvin)
t	time

Reproduced with permission of the copyright owner. Further reproduction prohibited without permission.

Th	jet throat length (cascade impactor)
T_i	residence time in collector i
u_a	ambient velocity down the throat of the FSSP
u_b	fan-induced velocity in the sampling volume of an FSSP
U_s	sampling velocity (=V_0 in the jets)
U_0	free-stream/ambient velocity
V	the total volume measured by the PVM [mg m^{-3}]
$v_{d,i}$	deposition velocity of species i [length/time][usually expressed as cm s^{-1}]
Vel	generic particle velocity
Vel_i	sampling velocity of collector i
V_i	manufacturer's quoted sample volume
V_i'	actual sample volume
V_{imp}	relative impaction velocity
VMD	Volume median diameter
V_p	particle velocity (typically assumed to be the flow velocity)
V_0	initial jet velocity
V1	Stage 1 (5-Stage)
V2	Stage 2 (5-Stage)
V3	Stage 3 (5-Stage)
V4	Stage 4 (5-Stage)
V5	Stage 5 (5-Stage)
V_+	dimensionless deposition velocity
V_t	turbulent inertial deposition velocity
W	nozzle width (cascade impactor/Chapter 2) or (equivalent) diameter for the wind shield (Appendix F)
w	for the gaussian fits – the width of the distribution
We	Weber number (inertia/surface tension)
We_{imp}	impaction Weber number (for drop shatter)
x	for the gaussian fits – midpoint bin diameter [μm]
x_c	for the gaussian fits – the central value of the distribution
y	for the gaussian fits – dN [# cm^{-3}]
y_0	for the gaussian fits – the offset from the y-axis

Reproduced with permission of the copyright owner. Further reproduction prohibited without permission.

χ^2	chi-squared – a measure of the goodness of fit
η_{asp}	aspiration efficiency
$\eta_{tube,turb_inert}$	efficiency of inertial turbulent deposition in a tube
μ	dynamic viscosity of air
μN	micro-Normal (micro-equivalents liter^{-1}, or 10^{-6} moles of charge liter^{-1})
#	number (percentage in this case)
ν	kinematic viscosity of air
ρ_a	density of air
ρ_p	particle density
ρ_{H2O}	density of water
σ	surface tension of the water/air interface
τ'	Stokes law characteristic time
τ	characteristic time to 95% of the stopping distance
τ_+	dimensionless particle relaxation time

Reproduced with permission of the copyright owner. Further reproduction prohibited without permission.

1. Introduction

The goal of this section is to briefly review why the chemical composition of clouds has been studied, why it is important, and what has been observed. This segues into a discussion of the theoretical basis for and observations of size-dependent drop composition, and its relevance to atmospheric chemistry. The goals of this research are developed within this context and the ensuing chapters outlined.

1.1 Why cloud composition is important

Although estimates vary, at any one time approximately 50% of the Earth's surface area is covered by clouds, and 7 – 15% of the troposphere by volume contains clouds (Ravishankara, 1997; Lelieveld and Crutzen, 1991; 1990). While much of the research in tropospheric chemistry has primarily focused on the gas-phase, cloud prevalence suggests that multi-phase reactions in clouds have the potential to play an important role in the atmospheric chemistry of many species. For example, eighty to ninety percent of global atmospheric production of sulfate – a key component in acid precipitation and suspended aerosol particles – from $SO_{2(g)}$ is thought to occur in-cloud (Lelieveld and Heintzenberg, 1992). Several studies have reported evidence of in-cloud sulfate production (Liu *et al.*, 1993; Gervat *et al.*, 1988; Hegg and Hobbs, 1988; 1986; Hegg *et al.*, 1984; Hegg and Hobbs, 1982; 1981). Models have also suggested that clouds can perturb HO_x chemistry (Lelieveld and Crutzen, 1991, among others), and thus affect the atmosphere's oxidative capacity. While the implications for global budgets of species such as O_3 remain controversial (Jacob, 2000), recent measurements confirm this prediction locally (Mauldin *et al.*,

Reproduced with permission of the copyright owner. Further reproduction prohibited without permission.

1997). Further, only 10% of clouds precipitate (Lelieveld and Crutzen, 1990), and an aerosol particle on which cloud drops form – a cloud condensation nuclei (CCN) – may go through 3 – 7 cloud cycles prior to removal (Lelieveld and Heintzenberg, 1992). Thus clouds can affect atmospheric gas-, solid-, and aqueous-phase chemistry.

Different chemical and physical processes affect clouds. In the atmospheric multi-phase system there are emissions, gas-to-particle conversion processes, dry deposition, condensation, nucleation scavenging, dissolution (e.g. gas partitioning into liquid drops), precipitation formation, wet deposition, impaction scavenging of aerosol particles, evaporation, freezing/melting (if mixed-phase), and chemical reactions within and between phases. All of these factors can affect the atmosphere's chemistry and the radiative balance (Leriche *et al.*, 2000; Fuzzi, 1997b). Chemical reactions include oxidation, reduction, complexation and hydrolysis, among others (Sedlak *et al.*, 1997). Their importance depends particularly on the time available for reaction which varies between clouds. Drops within clouds can also have different life-spans than the clouds themselves. For example, stratiform clouds may last for hours giving aqueous-phase reactions significant time to proceed while convective clouds with their short life-spans may serve only to re-distribute species between different levels in the atmosphere (Lelieveld and Crutzen, 1991). Of the processes listed above, nucleation scavenging and gas dissolution are thought to be the principal mechanisms to introduce species into non-precipitating cloud drops where subsequent in-cloud transformation of species may occur. Additionally, clouds are not closed systems (Heintzenberg, 1992), and, as implied above, entrainment/detrainment can be important (Fuzzi, 1997a).

Several issues drive research in cloud drop composition within the context of atmospheric chemistry – species' production and deposition, their subsequent impact on local ecosystems (including health effects), and global climate change. First, the 1980s boom in cloud composition research was fueled by the recognition that cloud drops were a major source and route of acid species into some environments and were likely playing a critical role in observed environmental

Reproduced with permission of the copyright owner. Further reproduction prohibited without permission.

degradation. For example, cloud capture can contribute 30 – 60% of total deposition of nitrogen and sulfur species to high elevation environments at Mt. Mitchell, NC and Whiteface Mtn., NY (Miller *et al.*, 1993; Lin and Saxena, 1991). In-cloud species production and subsequent deposition can negatively impact buildings, too (Del Monte and Rossi, 1997). Deposition studies have historical precedent: as early as 1853 investigators were also studying cloud drop chemistry to discern the role of fog in providing nutrients to agriculture (Eriksson, 1952a and references therein). Second, clouds impact climate both directly and indirectly, although the magnitudes of these effects are highly uncertain. Clouds modify aerosols (which have their own direct climate effect) and their presence also modifies the Earth's radiative balance. Further, the 1st cloud indirect effect ("Twomey") where changes in CCN result in cloud albedo changes, and the 2nd indirect effect – which concerns how anthropogenic pollution may lead to changes in drizzle formation and cloud lifetime – both have important climate ramifications (Charlson *et al.*, 2001; IPCC, 2001; Osborne *et al.*, 2001, and references therein). While cloud effects on climate are more widely recognized now, early 20th century drop composition measurements were in part prompted by the study of CCN (Eriksson, 1952b and references therein). Third, dense winter fogs are associated with high levels of both PM_{10} and $PM_{2.5}$[†] in the San Joaquin Valley, CA (Chow *et al.*, 1996; Chow *et al.*, 1993), although the fogs themselves may be instrumental in the removal of particles from the atmosphere (Lillis *et al.*, 1999; Forkel *et al.*, 1990; Pandis and Seinfeld, 1989; Waldman and Hoffmann, 1987). Recent work has associated fine particulate matter with excess morbidity and mortality (Dockery *et al.*, 1992, among others). This is a continuation, in many ways, of studies begun in the 1950s that sought to determine the causes behind the high mortality associated with some London fogs (Wilkins, 1956). Thus, knowledge of cloud drop composition can help to interpret the various roles clouds play in the environment.

1.2 Chemical composition of clouds

[†] PM_{10} and $PM_{2.5}$ refer to particulate matter less than or equal to 10 and 2.5 μm in aerodynamic

Reproduced with permission of the copyright owner. Further reproduction prohibited without permission.

In a 1986 compilation, 11 inorganic species, 1 ketone, 5 aldehydes, and 7 carboxylic acids were reported to have been found in clouds and fog for a total of up to 23 compounds (Graedel *et al.*, 1986, p. 506). Since then, many more inorganic species (particularly metals) and organic compounds have been identified, primarily in bulk cloud samples (see Appendix A for a review). As the focus of this dissertation concerns mainly measurements of selected inorganic species – principally ions and metals – in cloud water, my discussion of the composition will be limited. It is important to recognize, however, that many more species co-exist in the cloud with the ones measured and that these species may have an unrecognized effect on the cloud chemistry. Further, it is also important to recognize that any cloud chemistry measurements (including those presented here) are very much a function of the collector used (discussed in later chapters), the working definition of a "cloud" (e.g. minimum liquid water content (LWC)), the sampling and analytical protocols used, and, of course, the cloud itself (e.g. precipitating or not). While the discussion that follows is primarily based upon bulk cloud water measurements, the ranges reported are relevant to size-resolved cloud drop chemistry. Both bulk and size-dependent cloud drop composition can vary within and between clouds.

Cloud drop inorganic ion concentrations are typically dominated by NH_4^+, NO_3^-, and $SO_4^=$. The hydrogen (or hydronium) ion, H^+, is also important if the pH is low (< 4) (see (Wrzesinsky and Klemm, 2000; Fuzzi *et al.*, 1998a; Choularton *et al.*, 1997; Fuzzi *et al.*, 1984; Munger *et al.*, 1983), among others). Observed concentrations have been reported up to mN levels, although μN is more typical depending upon local conditions[††]. Air mass back trajectories have been successfully used to interpret cloud drop composition observations. Air masses from "clean" regions typically contain clouds with lower solute concentrations than drops formed in air masses from "polluted" regions ((Vong *et al.*, 1990; Saxena and Yeh, 1988; Castillo and Jiusto, 1984), among others). In marine environments, Na^+, Cl^- and other sea salt-associated ions may also be

---

diameter, respectively.

[††] Ionic species are generally reported in units of equivalents liter^{-1} (or "Normal" (N)) in this dissertation. Normal is related to Molar (moles liter^{-1} (M)) by multiplying the latter by the number of charges per mole of the species. For monovalent cations and anions, Normal and Molar are equivalent.

Reproduced with permission of the copyright owner. Further reproduction prohibited without permission.

present in high concentrations (see Chapter 7). High Cl^- concentrations have also been reported in several urban European locations (Millet *et al.*, 1996; Sigg *et al.*, 1987).

A pH value of approximately 5.6 is considered "neutral" for the atmosphere as it reflects equilibrium with the carbonate system. Actual observations of pH vary from < 3 to > 7, with values in the 2s often reported in continental locations. Low pH values are typically associated with highly polluted conditions. High pH values often result from either elevated concentrations of dust (e.g. Ca^{2+}), as observed over China and India ((Lai *et al.*, 1997; Khemani *et al.*, 1987), among others), or NH_3. NH_3 is the most important basic gas in the atmosphere and plays an important role in enhancing the solubility of some species and buffering acid-producing reactions in-cloud (Behra *et al.*, 1989). pH values as low as 1.69 (Corona del Mar, CA), 1.94 (Japan), 1.94 (Switzerland) and 1.7 (Germany), and as high as 10.1 (Japan) have been reported (Igawa *et al.*, 1998; Kroll and Winkler, 1988; Sigg *et al.*, 1987; Hileman, 1983; Okita, 1965). Of the trace metals, Fe concentrations tend to be the largest (up to 1000s of $\mu g\ l^{-1}$) and have been the most widely reported due to its recognized potential as a catalyst in some aqueous-phase reactions. Other inorganic ions and metals are often present in important, but lower, concentrations.

1.3 Size-dependent cloud drop chemistry

If the input aerosol particles are "externally mixed", then the resulting cloud drops will be as well. An external mixture indicates that a collection of aerosol particles do not individually have the same composition as the overall sample mean. For example, if 45% of the overall sample mean composition is sulfate, 45% of each particle in an "internal" mixture would be sulfate, but in an external mixture the sulfate amount in the individual particles could vary. Observational evidence for this based upon individual drop analyses has existed for some time (Kuriowa, 1956; 1953; 1951). The external mixture, whether hygroscopic or not, influences the resulting cloud (Svenningsson *et al.*, 1994), and individual species may show different drop size-dependencies.

Reproduced with permission of the copyright owner. Further reproduction prohibited without permission.

Some of the first theoretical development of size-dependent cloud drop chemistry was suggested by Ogren and Charlson (1992). Incorporating this work with additional modeling development by others ((Flossmann *et al.*, 1987; Flossmann *et al.*, 1985), among others), Prupaccher and Klett (1997, pp. 700 - 785) use different microphysical regions to describe the resulting size-dependent drop composition (figure 1.1).

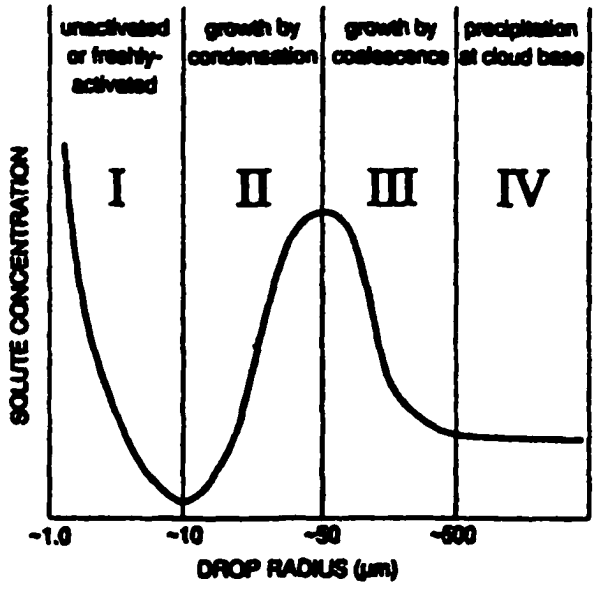

Figure 1-1: Size-dependent cloud drop chemistry schematic (from (Pruppacher and Klett, 1997)).

In Region I are unactivated or newly activated drops. Solute concentrations decrease as water uptake increases. As the smallest drops dilute faster (r^{-1} dependence for condensation), the concentration decreases as drop diameters* increase between approximately 2 and 20 μm (all drop sizes given are approximate). In-cloud there are always some new drops activating, so this should be a persistent feature. Region I is sometimes referred to as the "growth to equilibrium" region (Ogren and Charlson, 1992). In Region II (20 – 100 μm), drops are in the "growth by

*Unless otherwise specifically indicated, references to cloud drop or aerosol particle "size" throughout this work will be to their diameter, not radius.

Reproduced with permission of the copyright owner. Further reproduction prohibited without permission.

condensation" stage and total solute (or total non-volatile solute) concentrations increase because larger drops grow slower. Ogren and Charlson (1992) suggest that up to a 10^4 difference in solute concentration could be observed between the minimum and maximum concentrations in these two regions. In Region III (100 – 1000 μm), in-cloud collision/coalescence processes become important and drop concentrations start to dilute again due to mixing between sizes. In Region IV (> 1 mm), drops are now precipitation-sized and their composition is thought to be uniform due to in-cloud mixing. "Region V" (not shown) is an extension of figure 1.1 and is where below-cloud processes may affect individual precipitation drops, potentially inducing a size-dependent composition in them. While this discussion has been sequential, various cloud physical parameters will affect whether drops actually follow this progression. In particular, all CCN, which are the aerosol particles that drops form on, are not uniform in either size or composition and thus will activate under different conditions. Further, gas dissolution into and volatilization from the aqueous-phase will also affect observed drop concentrations of many species. Both of these factors have the ability to affect observations of drop size-dependent cloud water chemistry.

Recent attempts to interpret field observations within this theoretical framework emphasize the distinction between "fresh" and "aged" clouds. Fresh clouds include orographically-induced ones and aged clouds include longer-lived clouds, such as stratus, particularly associated with frontal systems. Fresh cloud drops activate once, in-cloud supersaturations and coarse particle concentrations are high, and the species are highly soluble. As a result, solute concentrations increase with drop diameter due to "growth by condensation" (Region II). Older aged cloud drops have been through several activation/deactivation cycles. Solute concentrations decrease with drop size (Region I) as there are low in-cloud supersaturations, few coarse particles and overall low species solubility (possibly due in part to hydrophobic coatings on the CCN). Modeling suggests that with the absence of the coarse mode, no evidence of Region II behaviour will be found in these clouds. Diffusive drop growth and gas uptake compete. If the former dominates, then Region II behaviour will be observed: if the latter, Region I. Clearly size-dependent cloud

Reproduced with permission of the copyright owner. Further reproduction prohibited without permission.

drop composition depends both upon the physics and chemistry of the local environment (Jaeschke *et al.*, 1997; Schell *et al.*, 1997b; Ogren and Charlson, 1992). Further, it is specifically worth mentioning that entrainment (e.g. changing cloud microphysics) will affect observed concentrations, and the mixing inherent in the drop collection processes will mitigate some of the actual concentration variations observed between drops (Ogren and Charlson, 1992). Observations will also be a function of altitude which is not specifically addressed in figure 1.1 (Ogren and Charlson, 1992). Although many processes are not specifically addressed by the simple theoretical development, a useful interpretive basis is provided for size-dependent cloud drop composition.

There are important caveats to this description of size-dependent cloud drop chemistry, particularly as it will be addressed herein. Recent modeling and field work suggests that classical Köhler theory may not adequately describe all the nuances of the competing/interacting processes when cloud drops form. The complex interaction of soluble trace gases, slightly soluble substances and mass transfer issues suggests that in actuality, large (e.g. > 10 μm in diameter) stable, technically unactivated cloud drops may form, particularly in polluted conditions (Charlson *et al.*, 2001; Nenes *et al.*, 2001; Laaksonen *et al.*, 1998; Chuang *et al.*, 1997; Kulmala *et al.*, 1997; Kulmala *et al.*, 1993). For the purposes of this work, a "cloud drop" is any particle aerodynamically large enough to be sampled by our cloud water collectors. Drops with a range of lifetimes are collected during one sampling period in-cloud (Fuzzi, 1997a), and the sampled clouds and fogs presented here were non-precipitating. Thus the behaviour characteristic of Regions I and II only should apply.

1.3.1 Models

There are a wide variety of atmospheric chemistry models of varying degrees of sophistication that consider size-dependent drop chemistry in fogs and clouds ((Majeed and Wexler, 2001; O'Dowd *et al.*, 2000; Wurzler *et al.*, 2000; Bott, 1999; Zhang *et al.*, 1999; Wurzler, 1998; Bower *et al.*, 1997; Gurciullo and Pandis, 1997; Wurzler *et al.*, 1995; Colvile *et al.*, 1994; Müller and

Reproduced with permission of the copyright owner. Further reproduction prohibited without permission.

Mauersberger, 1994; Bott and Carmichael, 1993; Roelofs, 1993; Hegg *et al.*, 1992; Roelofs, 1992a; b; Bower *et al.*, 1991; Ayers and Larson, 1990; Hegg and Larson, 1990; Pandis *et al.*, 1990a; b; Seidl, 1989; Twohy *et al.*, 1989a; Flossmann *et al.*, 1987; Flossmann *et al.*, 1985), among others). It is often difficult to compare model predictions due to the differences in assumptions between them. Despite this limitation, the model simulations reported suggest the importance of considering size-resolved drop chemistry compared to bulk treatments for some atmospheric conditions. In particular, sulfur oxidation tends to be enhanced compared to predictions based upon the mean bulk cloud composition when size-dependence is considered. This is largely due to the highly non-linear O_3 and metal-catalyzed auto-oxidation S(IV)-to-S(VI) transformation pathways (O'Dowd *et al.*, 2000; Gurciullo and Pandis, 1997). The models also indicate that species (including water) can re-partition between the gas-phase and different drop sizes while in-cloud or as the cloud evaporates, which impacts the resulting gas- and solid-phase atmospheric composition (see (Majeed and Wexler, 2001; Flynn *et al.*, 2000; Bower *et al.*, 1999a; Bradbury *et al.*, 1999; Bower *et al.*, 1997), among others). Several studies suggest that clouds can play a role in the processing/production of fine aerosol particles (of the size of concern for health effects) (Majeed and Wexler, 2001), and that the history of the aerosol particles either in-cloud or pre-/post-cloud can impact their evolution, distribution, and ability to act as CCN (Zhang *et al.*, 1999; Zhang *et al.*, 1998). Further, in order to validate these models (and it is difficult to interpret observations without the use of models), field observations of size-resolved drop composition are important (Iribarne and Cho, 1989).

1.3.2 Observations

Approximately 50 papers exist in the literature that report specifically on observations of size-dependent cloud drop chemistry, although some data may be "double-reported" particularly for the large-scale campaigns. Papers where the methods and assumptions make the interpretation of results difficult have been omitted from this discussion. For the purposes of this overview it is

Reproduced with permission of the copyright owner. Further reproduction prohibited without permission.

important to note that these observations are subject to the same limitations described in section 1.2. Further, many of the authors indicate that while their results are generally "typical", exceptions often occur. Individual drop or residue studies are included, but reported cloud composition results – whether size-resolved or not – are typically aggregated in time. The majority of size-resolved cloud composition measurements have been reported based upon the collection and subsequent analysis of the cloud water itself (not the residues). This permits direct observation and quantification of drop composition.

Three studies specifically considered size-dependent rime chemistry – at Storm Peak Laboratory, Steamboat Springs, CO (SPL) (Xu *et al.*, 1999; Carter and Borys, 1993) and at Mt. Washington Observatory, NH (Rancourt and Howe, 1987). While the data are limited, they suggest that smaller drops have lower pHs and that at SPL sulfate, for example, tended to be found in higher concentrations in smaller drops and chloride in the larger ones.

Several investigators at a variety of locations have studied individual drops (or their residues) in some detail (Kasahara *et al.*, 2001; Tenberken and Bächmann, 1998; Ganor *et al.*, 1993; Levin *et al.*, 1990; Noruse and Maruyama, 1971). In general, higher solute concentrations were associated with larger drops, including H^+ (thus pH tended to be lower). One study did report a shift in large/small drop concentrations which they interpreted in terms of aged vs. fresh drops as described in section 1.3 (Tenberken and Bächmann, 1998). The Counterflow Virtual Impactor (CVI) (Noone *et al.*, 1988a) and the related Droplet Aerosol Analyzer (DAA) (Martinsson *et al.*, 1997b) have been widely used recently to measure the "non-volatile" (operationally-defined) drop solute mass and compare it to the initial drop size. CVI and DAA measurements at a variety of locations – Mt. Åreskutan (Sweden), Cheeka Peak, WA, and the Great Dun Fell (England) – studying primarily orographic clouds have suggested that non-volatile solute concentrations in larger drops are greater than in smaller drops (Martinsson *et al.*, 1999; Martinsson *et al.*, 1997a; Heintzenberg *et al.*, 1989; Ogren *et al.*, 1989; Noone *et al.*, 1988b). For example, at Mt. Åreskutan, 22 μm drops had approximately three times the non-volatile solute concentration of 8

Reproduced with permission of the copyright owner. Further reproduction prohibited without permission.

μm drops (Heintzenberg *et al.*, 1989). The DAA results from two campaigns at Great Dun Fell, however, indicate that the least evidence of size-dependence is associated with multi-activated drops, solute concentrations can become inverted, and that each drop can behave very differently (Martinsson *et al.*, 1999; Martinsson *et al.*, 1997a). In contrast, studies of (primarily) radiation fogs in the Po Valley using a CVI indicated that drops < 15 μm in diameter were sharply more concentrated than larger drops (Ogren *et al.*, 1992). This observation was confirmed by simultaneous operation of a jet cloud water impactor collecting liquid drops.

Observations have been made with a variety of liquid water collectors which generally separate drops into two, somewhat overlapping, size fractions. For inorganic ions in radiation fogs, NH_4^+, $SO_4^=$, NO_3^- and H^+ tend to be concentrated in the smaller drops while "crustal" species (e.g. Ca^{2+}, Mg^{2+}) tend to be found in larger drops (Reilly *et al.*, 2001; Reilly, 2000; Collett *et al.*, 1999; Hoag *et al.*, 1999; Chérif *et al.*, 1998; Fuzzi *et al.*, 1998b; Fuzzi *et al.*, 1998a; Hoag, 1998; Bator and Collett, 1997; Rao, 1997; Fuzzi *et al.*, 1996; Millet *et al.*, 1996; Collett *et al.*, 1995; Collett *et al.*, 1994; Ogren *et al.*, 1992; Schell and Georgii, 1989). In these fogs trace metals (e.g. Fe, Mn) may exhibit varying size-dependencies (Reilly *et al.*, 2001; Reilly, 2000; Hoag *et al.*, 1999; Rao and Collett, 1998; Schwanz *et al.*, 1998; Rao, 1997). Low molecular weight organic acids and carbonyls may exhibit some size-dependency, and also may not (Hoag, 1998; Millet *et al.*, 1997; Rao and Collett, 1995). In a variety of orographic clouds at both clean and polluted locations, concentrations in larger drops for the inorganic ions can be higher than in small drops, but here again little size-dependence or higher concentrations in smaller drops for particular species are sometimes observed (Acker *et al.*, 2001; Herckes *et al.*, 2001b; Rattigan *et al.*, 2001; Menon *et al.*, 2000; Reilly, 2000; Bator and Collett, 1997; Rao, 1997; Schell *et al.*, 1997a; Schell *et al.*, 1997b; Vong *et al.*, 1997; Collett *et al.*, 1994; Wobrock *et al.*, 1994; Munger *et al.*, 1989b). Low molecular weight organic acids and carbonyls can also exhibit varying size-dependencies as in fogs (Rao and Collett, 1998; Rao, 1997; Keene *et al.*, 1995; Munger *et al.*, 1995; Munger *et al.*, 1989b). Recent airborne size-resolved measurements of cumulus and stratus drop concentrations over the North Sea indicate that species drop concentration can be highly variable

Reproduced with permission of the copyright owner. Further reproduction prohibited without permission.

as a function of elevation and cloud type (Jaeschke and Günther, 2001). Finally, collectors that are able to separate drops into more drop fractions in these locations suggest that drop composition is much more varied than the simple "either/or" approach via the two-stage collectors. "U"-shaped profiles where both smaller and larger drops are more concentrated than intermediate sized ones for some species are not uncommon, as are the reverse and "N"-shaped profiles (Bower *et al.*, 2000; Fuzzi *et al.*, 1998b; Fuzzi *et al.*, 1998a; Laj *et al.*, 1998; Fuzzi *et al.*, 1996; Collett *et al.*, 1995). An earlier study using a somewhat different technique by Ludwig and Robinson (1970), also suggested a "U"-shaped profile for sulfate in California stratus.

From the preceding discussion, it may appear as though any size-dependence may be observed for any particular species. However, these observations can generally be interpreted within the context of the preceding theoretical discussion of size-dependent cloud composition. For fresh, orographic clouds, activated drops growing by condensation are consistent with observations of large drops being relatively more concentrated than smaller ones (which dilute more rapidly). Higher concentrations of coarse mode CCN also would contribute to this observation. In orographic clouds influenced by pre-existing stratus or frontal systems and fogs, cloud drops are more likely to be aged and have previously been through multiple activation/evaporation cycles. In combination with low concentrations of coarse mode particles and lower supersaturations, relatively higher concentrations may be observed in smaller drops. A lack of size-dependence in non-volatile species has been attributed to the input aerosol having been through many previous cloud cycles which would tend to remove composition differences, although cloud microphysics suggests that Region I or II should still be discernible (depending upon the CCN mixture and drop spectral width). The time for drop growth under both scenarios has been identified as a key parameter in observations (Schell *et al.*, 1997b). While nucleation scavenging is important for the non-volatile (and some volatile) compounds, species that partition into the drops from the gas-phase may or may not exhibit size-dependency based upon their own solubility, kinetic limitations and their ability to achieve equilibrium within the time resolution of cloud water collection. The

Reproduced with permission of the copyright owner. Further reproduction prohibited without permission.

solubility of gas-phase species may depend upon the pH of the drop as well as relevant in-drop chemical reactions.

It is important to recognize that the ability to resolve size-dependent drop composition may be compromised by mixing between different drop sizes inducing chemical changes, and/or the arbitrary or weak size-cuts between stages (addressed in detail in later chapters). Further, the CVI uses an operational definition of "non-volatile" as some species cannot form salts and are lost during drying (Gieray *et al.*, 1993). Therefore, while it is possible to interpret the observations to the first order within a theoretical framework, the conclusions reached are not unequivocal for all species due to measurement uncertainty. Despite this, cloud water collectors that are able to resolve the size-dependent drop chemistry into more fractions would be useful to understanding the role of clouds in atmospheric chemistry (Ogren and Charlson, 1992).

Poor time resolution of sampled cloud waters is an identified problem (Fuzzi *et al.*, 1994; Heintzenberg, 1992). In addition, in order to interpret what is observed in clouds, detailed aerosol composition and size-distribution data, liquid water content, cloud drop distribution and distance from cloud base data are required (Jaeschke *et al.*, 1997). Of course, collector characteristics and the drop spectrum need to be taken into consideration while evaluating the chemistry (Fuzzi *et al.*, 1984).

1.4 Goals of this research

Real measurements are required of cloud composition, not just modeling studies (Hobbs, 1986). Better measurements to resolve size-dependent drop chemistry are needed as well as improved time resolution. Two new multi-stage cloud water collectors for super-cooled and warm clouds/fogs have been developed which complement existing experimental equipment within our research group. The two collectors extend our ability to separate drops into size-resolved

Reproduced with permission of the copyright owner. Further reproduction prohibited without permission.

fractions, thus increasing our ability to discern composition differences across the drop size spectrum. They were designed to improve temporal resolution. The FROSTY collector for super-cooled clouds separates drops into three fractions, and the 5-Stage collector for warm clouds separates drops into five fractions. In both instances, this represents two more fractions than previously possible in our group. The collectors were designed, constructed (by outside vendors), and subsequently operated in the field. The size-dependent cloud composition results from four of these campaigns will be presented and interpreted in terms of the preceding discussion. While modeling is required to fully interpret the implications of these observations, useful insights into the role of clouds in the fate of atmospheric species are still discernible. The data presented here should be useful for size-resolved cloud drop model validation.

1.5 Dissertation format

This dissertation can be roughly divided into two parts. The first considers the design and development of the new collectors, and uses observations to evaluate their field performance – both "absolutely" and in comparison to some of our pre-existing cloud water collectors. It became clear while trying to inter-compare collectors that the field performance of these older collectors also needed to be evaluated and included. Finally, the first part includes a review of the sampling and analytical protocols used in the field and the laboratory. This information provides the basis for interpreting the second part which presents the size-dependent cloud drop composition measured during the four campaigns. Where additional measurements are available, the effects of clouds and the implications of the drop size-dependent composition in terms of the local atmospheric chemistry are explored. The composition data will be presented campaign-by-campaign.

Specifically, Chapter 2 will present the final FROSTY and 5-Stage collector designs, and the factors considered in their development. The Caltech "family" of cloud water collectors will also

Reproduced with permission of the copyright owner. Further reproduction prohibited without permission.

be introduced as data from them will be presented and evaluated throughout. Chapters 3 and 4 discuss the field performance validation of the super-cooled and warm cloud water collectors, respectively. Chapter 5 describes our sampling and analytical protocols with some comments regarding their validation. Chapters 6, 7, 8, and 9 describe the results from field campaigns at Horsetooth Mountain, CO (April 1998); Tenerife, the Canary Islands (ACE2 HILLCLOUD project, July 1997); Whiteface Mountain, NY (July 1998); and Davis, CA (December 1998 – January 1999), respectively. Hereafter, each of these campaigns will be referred to as "Horsetooth", "ACE2", "Whiteface" and "Davis". Horsetooth is described first, although this is out of chronological order, as it is the only one considering super-cooled clouds. Conclusions and recommendations for future work to answer some of the questions raised by this research are in Chapter 10.

1.5.1 Comment on the appendices

I have made extensive use of appendices. They serve two purposes. The first is that while the focus of the dissertation is size-dependent cloud drop chemistry, many disparate factors have to be taken into consideration in the different chapters. Therefore, in the interests of keeping the main body of manageable length, the detailed discussion of some facets of the design and field performance validation in particular are in the appendices. The main conclusions from the appendices and the primary literature citations are, of course, included in the main body. The second purpose is to provide documentation on both how to use the new collectors and how the field performance analyses described here were performed. While there may be relevant factors that I have ignored or errors in my interpretation and calculations, I believe that in order to compare data between campaigns it is important to use the same consistent approach to both obtain and interpret the results.

Reproduced with permission of the copyright owner. Further reproduction prohibited without permission.

2. Cloud water collectors: design and development

This chapter's goal is to introduce the FROSTY and 5-Stage collectors and describe the factors relevant to their design. The Caltech series of active strand collectors and issues related to their use are included in this discussion as field observations made with them will be presented, evaluated and used to validate the newer collectors in later chapters. The collectors are presented before the discussion of the design factors so the latter can be considered in context. While this chapter is largely based upon part of an accepted 5-Stage collector manuscript*, the discussion has been expanded to include both FROSTY and aspects relevant to the Caltech collectors.

2.1 Existing cloud water collectors

Cloud water collectors depend primarily upon inertial impaction to sample drops. Passive collectors rely upon the local wind to give drops sufficient inertia to impact and be collected while active collectors, with the notable exception of the rotating arm collectors, use pumped flow to achieve the same end. There are a wide variety of passive and active collectors available for varying ambient conditions (see Appendix B for a review of techniques to sample cloud water). Typically, both passive and active samplers utilize flow past collecting strands or rods. The Caltech series of active strand collectors are examples. Some active collectors use jet-driven impaction onto solid surfaces. Size-resolved cloud composition is usually obtained via active collectors with multiple jet/impaction surface combinations, or stages, and varying cut-point diameters. However, in some instances two sets of differently-sized rods/strands (Vong *et al.*,

* Moore, K.F., Sherman, D.E., Reilly, J.E. and J.L. Collett, Jr. (2001) Development of a multi-stage cloud water collector: 1. Design and field performance evaluation (in press, *Atmospheric Environment*)

Reproduced with permission of the copyright owner. Further reproduction prohibited without permission.

1997; Demoz *et al.*, 1996; Munger *et al.*, 1995) constitute separate stages, or a combination of a strand stage and a jet-impaction stage (Schell and Georgii, 1989) are used to separate collected drops into two fractions.

2.1.1 The Caltech series of active strand cloud water collectors

We use three versions of the Caltech Active Strand Cloud water Collectors (CASCCs) – the CASCC2, the size-fractionating CASCC (sf-CASCC), and the Caltech Heated Rod Cloud water Collector (CHRCC) – as described by Demoz *et al.*, (1996). (The Caltech Rotating Arm Collector (Jacob *et al.*, 1984a) is considered in Appendix B). A schematic of the CASCC2 and sf-CASCC is shown in figure 2-1, and a field photo of the sf-CASCC is shown in figure 2-2.

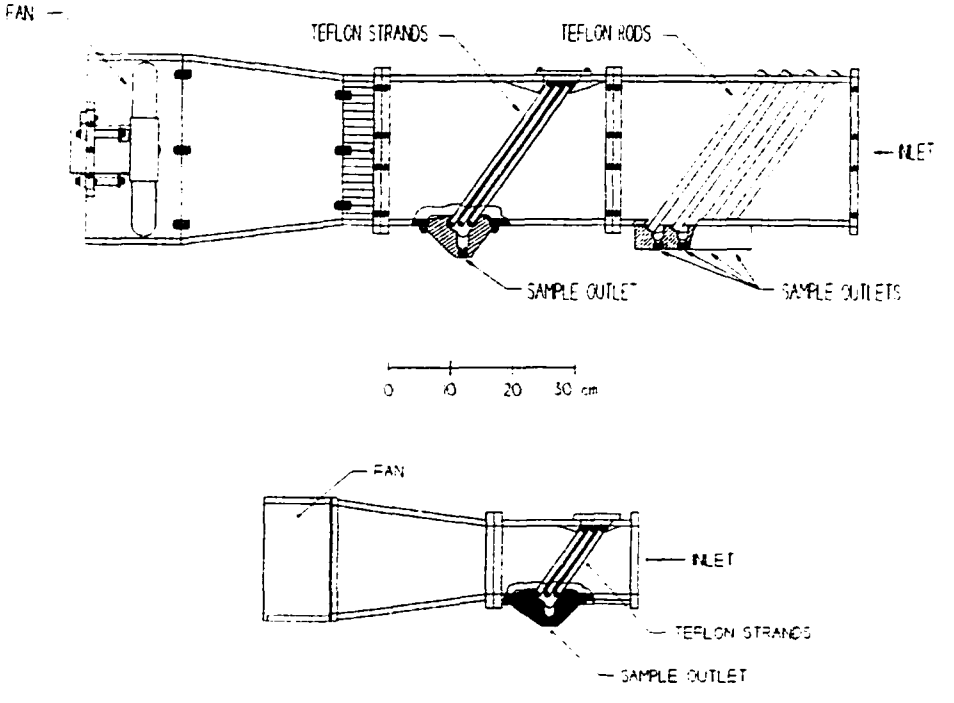

Figure 2-1: Schematic of sf-CASCC (top) and CASCC2 (bottom) (Demoz *et al.*, 1996, figure 1)

Reproduced with permission of the copyright owner. Further reproduction prohibited without permission.

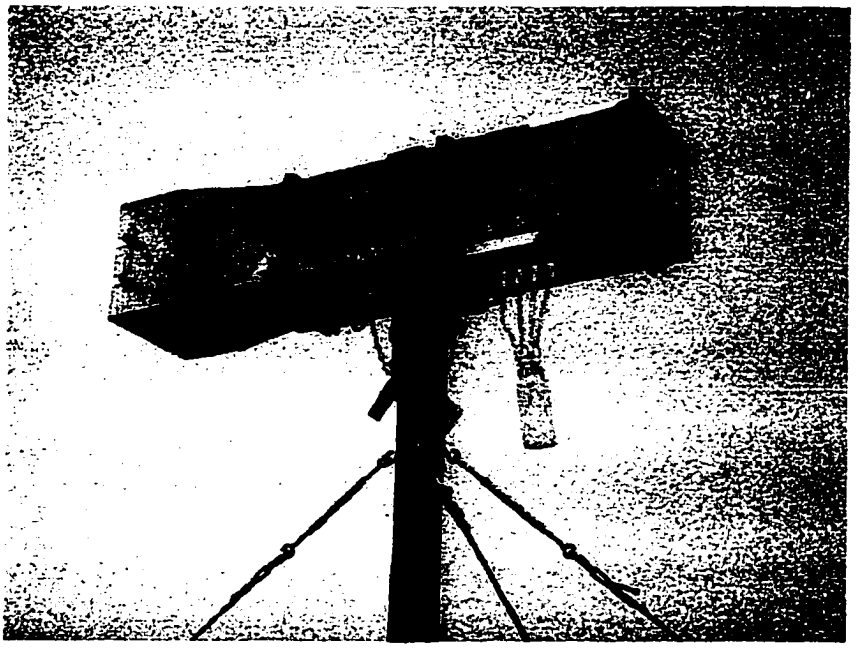

Figure 2-2: sf-CASCC installed in Davis, CA (December, 1998)

A photo of the CHRCC is not shown, but it is very similar in appearance and size to the CASCC2. The principle of operation for all of these collectors is the same. The rear fan pulls drop-laden air through the collector past banks of rods/strands. Drops with too much inertia to follow the fluid streamlines around the cylinders impact. In the warm cloud collectors, these drops coalesce and subsequently are collected after they flow down the rods/strands into the collecting troughs and then into the attached bottles. In the CASCC2 there are 6 rows of 0.508 mm diameter Teflon strands (on three cartridges), the volumetric flow rate is 5.8 m^3 min^{-1}, the velocity at the strands is 8.6 m s^{-1} and the theoretical D_{p50} is calculated to be 3.5 μm. The CASCC2 is a smaller version of the original CASCC (not shown). In the sf-CASCC the 6 rows of strands are downstream of 4 rows of eight 12.7 mm diameter Teflon rods. The sf-CASCC's volumetric flow rate is 19 m^3 min^{-1} and its velocity at the strands is 6.7 m s^{-1}. Recent modeling work (see Chapter 4) suggests that theoretical calculations of the front (Large** fraction) cut-size which neglect flow interactions between rods overestimate the Large D_{p50}. This is consistent with measurements of the amount

**In this dissertation "Large" uniformly refers to the front section (1st stage) of the sf-CASCC. The rear section (2nd stage) is uniformly referred to as the "Small". This notation will be consistently used throughout.

Reproduced with permission of the copyright owner. Further reproduction prohibited without permission.

of water collected by each bank of rods (Demoz *et al.*, 1996). The Large D_{p50} is approximately 17 – 18 μm (depending upon how it is calculated[#]), and the rear (Small) fraction's D_{p50} is still theoretically calculated to be 4 μm. The CHRCC can be used in either warm or super-cooled clouds where drops will freeze upon impact. In lieu of Teflon strands, it has 6 rows of 3.2 mm diameter hollow stainless steel rods. The rods have internal heating elements which can be used to periodically melt the collected rime when the fan is turned off between sampling periods. Once melted, water collection proceeds similarly to the other CASCCs. For the CHRCC data reported in this work, external heating to the collector body was also applied to help melt the sample. The CHRCC flow rate and velocity are the same as the CASCC2's, although the theoretical D_{p50} is approximately 9 μm.

Finally, the D_{p50}s vary between the three collectors, although the collection efficiency curve shapes are all similar (shown in Chapters 3 and 4). Full collection characterization requires knowledge of both the shape of the efficiency curve and the D_{p50} (to locate the curve), although when only theoretical efficiencies are calculated, the D_{p50}s alone are generally sufficient. For these three collectors only theoretical collection efficiency curves based upon idealized flow patterns through the collecting rods/strands are available. The sole exception is the Large sf-CASCC fraction whose collection efficiency curve is based upon a numerical simulation of the flow. Further information on this collector family can be found in Demoz *et al.* (1996) and Appendix B.

2.2 The new cloud water collectors

[#] For smaller (< 10 μm) rod/strand D_{p50}s, the D_{p50} is typically reported as calculated because within the drop size range considered (up to 50 – 100 μm) nearly 100% collection efficiency is ultimately achieved. For larger rod/strand D_{p50}s, 100% collection efficiency is usually not reached. In this case, the D_{p50} may be reported scaled to whatever the maximum collection efficiency is. For example, if 80% collection efficiency is the maximum achieved, the "collected" D_{p50} may, in fact, be the "total" D_{p40}. The sf-CASCC's Large fraction D_{p50} appears to be scaled in the literature. See Appendix B for more information.

Reproduced with permission of the copyright owner. Further reproduction prohibited without permission.

FROSTY and the 5-Stage are introduced so the design discussion in section 2.3 can consider them. Derek Straub calibrated both of these collectors and his experimental calibration data will be referred to as needed (Straub and Collett, 2001a; b; Straub and Collett, 1999).

2.2.1 FROSTY

FROSTY is a three-stage rectangular jet cascade impactor built to sample super-cooled cloud drops from precipitating or non-precipitating mixed-phase clouds in conditions consistent with the U.S. Standard Atmosphere at 3000 m elevation (Lide, 1998, pp. 14-16 – 14-22). Figure 2-3 is a photo of the collector, figure 2-4 is a schematic, and table 2-1 contains its major design parameters.

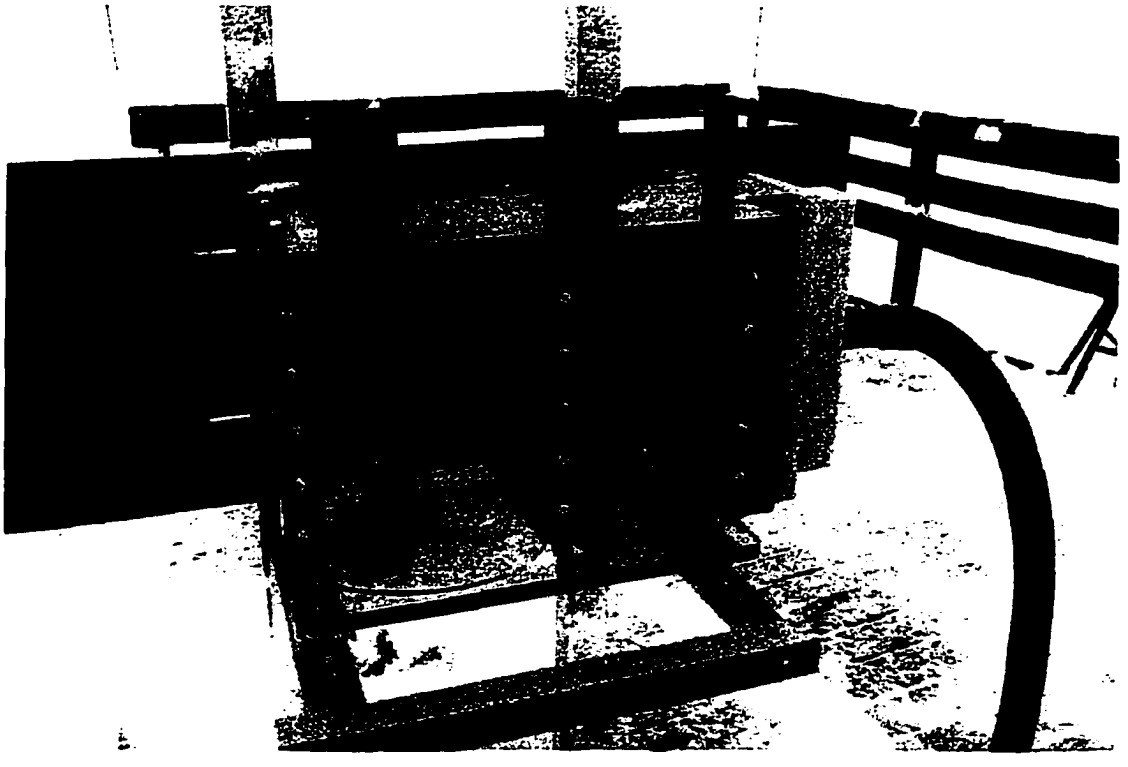

Figure 2-3: FROSTY installed at the Storm Peak Laboratory, Steamboat Springs, CO (January, 1997). Note the wind shield mounted to the stand. (photo by D. E. Sherman)

Reproduced with permission of the copyright owner. Further reproduction prohibited without permission.

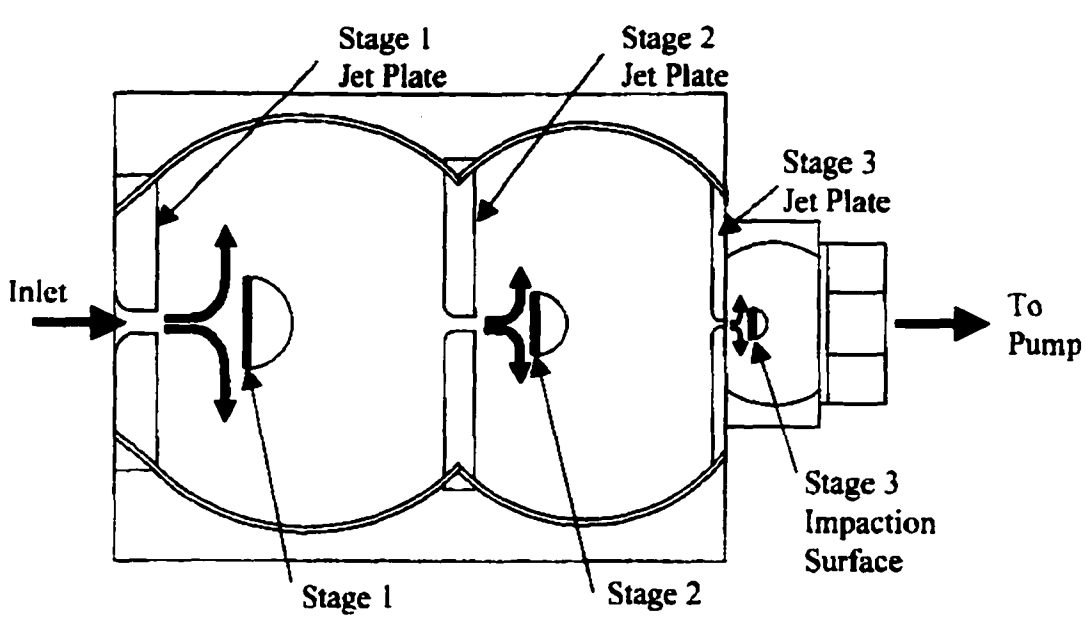

Figure 2-4: FROSTY top view schematic. The air flow pattern is shown with heavy arrows. The overall collector dimensions are approximately 60 cm long by 30 cm wide and 30 cm high. (Straub and Collett, 1999, figure 1.9)

Table 2-1: FROSTY operating/design parameters

FROSTY operating/design parameters									
Stage	Design D_{p50} [μm]	Experimental D_{p50} [μm]	Jet Re, [--]	Jet velocity (V_0) [m s^{-1}]	Jet length (L) [cm]	Jet width (W) [cm]	Jet aspect ratio (L/W) [--]	Pressure drop	
								Design [Pa]	Cumulative [Pa]
1/LARGE	15	17	10,000	5.83	26.8	1.65	16	15	15
2/MEDIUM	10	11	10,000	8.48	26.8	1.09	25	33	48
3/SMALL	4	4	10,000	18.66	26.8	0.46	58	158	206

note: flow rate = 1.5 m^3 min^{-1}
design conditions are U.S. Standard Atmosphere @ 3000 m elevation
experimental D_{p50}s from Straub and Collett (1999)

FROSTY's design 50% collection efficiency cut-point diameters, D_{p50}s, (15, 10 and 4 μm for Stage 1/LARGE through Stage 3/SMALL[##]) were chosen to span the range of expected super-cooled cloud drop sizes (table 2-1). Drop-laden air is pulled through the collector via a downstream pump. However, in this case the air is accelerated through a series of progressively

[##] In this dissertation, the front (1st) stage of FROSTY is uniformly referred to as the LARGE stage or fraction. The 2nd and 3rd stages are referred to as the MEDIUM and SMALL stages. This notation is used consistently throughout.

Reproduced with permission of the copyright owner. Further reproduction prohibited without permission.

smaller jets to increasingly higher velocities (table 2-1). Drops of progressively smaller diameters are collected on each stage as those with too much inertia cannot follow the fluid streamlines and impact. The collection surfaces are vertically-oriented because drops should freeze upon contact (see Chapter 3 for a discussion of this point). To avoid aspiration of any large frozen precipitation which could contaminate the LARGE drop stage, the collector is oriented perpendicular to the wind during operation. A downstream wind shield should aid aspiration of the cloud drops (figure 2-3). The main body is composed of polycarbonate, although the beige-colored exit stage is ABS. The removable collection rods are a combination of Delrin (black) and Teflon (white). The sampling surface itself is Teflon. At the end of each sampling period, each collection rod is removed, placed in a clean plastic bag and a duplicate rod is inserted. The collection rod with sample can then be taken into the lab for subsequent sample handling. Appendix C contains a protocol for the use of the FROSTY collector, and Chapters 3 and 6 contain further information on sampling with FROSTY.

FROSTY is not an acronym; when stood on one end the collector resembles a snowman.

2.2.2 The 5-Stage collector

A schematic of the final 5-Stage collector design is shown in figure 2-5; figure 2-6 shows it installed in the field. The 5-Stage is also a cascade impactor and consists of five stages, each with a single, one-sided rectangular jet arranged in a "staircase" configuration. Most drops in non-precipitating radiation fogs vary from approximately 5 – 35 μm in diameter (Jiusto, 1981). The design D_{p50}s of the 5-Stage (30, 25, 15, 10 and 4 μm for Stage 1 through Stage 5 (V1 – V5)[‡]) were chosen to span this range (table 2-2). During operation, the collector is mounted at 45° to the horizontal so sampled drops coalesce and run down to polypropylene vials threaded directly into each stage. Using one-sided jets (figure 2-5) minimized the collector size and was useful for

Reproduced with permission of the copyright owner. Further reproduction prohibited without permission.

liquid drops. The collector is oriented into the wind during operation, subject only to site restrictions and its own geometry. Except for the Plexiglas lids, the main body is constructed entirely of Delrin, and the seams sealed with a two-part epoxy (Resiweld #FE-7004, H.B. Fuller and Company).

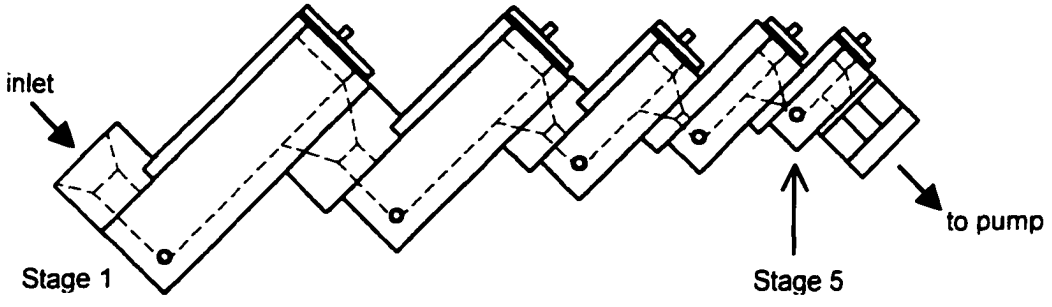

Figure 2-5: 5-Stage collector schematic (side view). The collector dimensions are approximately 1 m long by 60 cm wide by 50 cm tall.

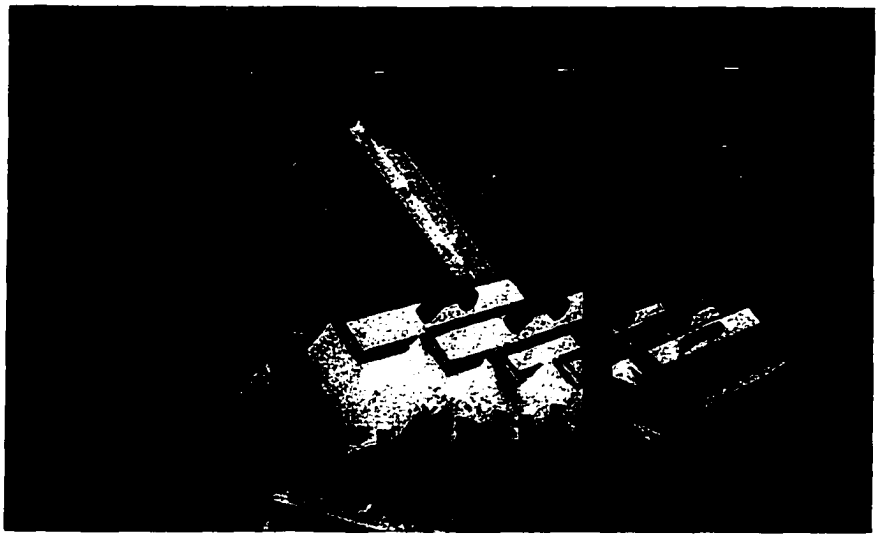

Figure 2-6: The 5-Stage collector installed at the summit of Whiteface Mountain, NY (July, 1998). The wind shield is shown extending forward over the inlet and attached to a precipitation cover. On Stages 1 and 2, vial-to-bottle adapters are attached.

‡ Notation may be used to refer to the five stages of the 5-Stage collector as follows: Stage 1 (V1), Stage 2 (V2), Stage 3 (V3), Stage 4 (V4), and Stage 5 (V5). Stage 1 is the first and largest stage, and Stage 5 is the smallest and last.

Reproduced with permission of the copyright owner. Further reproduction prohibited without permission.

Table 2-2: 5-Stage operating/design parameters

5-Stage operating/design parameters										
Stage	Design D_{p50} [μm]	Exp. D_{p50} [μm]	Jet Re_j [--]	Jet velocity (V_0) [m s^{-1}]	Jet length (L) [cm]	Jet width (W) [cm]	Jet aspect ratio (L/W) [--]	Pressure drop		
								Design [Pa]	Cumulative [Pa]	Measured [Pa]
1	30	25.5	10,000	2.67	43.4	2.87	15	4	4	< 5
2	25	29	10,000	3.22	43.4	2.39	18	6	10	< 5
3	15	17.5	10,000	5.31	43.4	1.45	30	16	25	20
4	10	11.5	10,000	7.97	43.4	0.97	45	35	60	52
5	4	4.5	10,000	20.18	43.4	0.38	114	224	284	337

note: flow rate = 2.0 m^3 min^{-1}
design conditions are for a radiation fog at 1 atmosphere and 20°C
experimental D_{p50}s from Straub and Collett (1999)
pressure measurements performed in the laboratory

While the collector is designed for low wind environments, a baffle or wind shield parallel to the inlet is added for higher winds such as those found in orographic clouds. A precipitation cover may also be used. At the end of a sampling period, each stage's lid is removed and any remaining water on the impaction surface is pushed down to the attached vial using a clean rubber spatula. Appendix D contains a protocol for the use of the 5-Stage collector, and Chapters 4 and 7 (in particular) contain further information on sampling with the 5-Stage.

2.3 Collector design/use considerations

Factors to consider in the design of a cloud water collector have been given in various forms by many authors (Mohnen and Kadlecek, 1989; Däumer *et al.*, 1988; Dröscher, 1986; Jacob *et al.*, 1984a; May, 1961; Houghton and Radford, 1938). A synthesis and discussion of these criteria and additional ones specific to the development of FROSTY and the 5-Stage are given here. Where relevant, the CASCCs are also included in this discussion.

2.3.1 Physical Performance Criteria

Reproduced with permission of the copyright owner. Further reproduction prohibited without permission.

To facilitate comparison, a collector should perform consistently – sample drops in the range of interest with the same overall efficiency – between different cloud events over a reasonable range of atmospheric conditions. Thus, both the 5-Stage and FROSTY are active cloud water collectors, since collection efficiency curves for passive collectors vary with wind speed. Only cloud drops should be collected and they should not be re-entrained into the flow. Sampling time periods, while a function of the liquid water content and drop size spectrum, should be minimized to provide adequate temporal resolution. For multi-stage collectors the collection efficiency curves should be as sharp as possible to minimize overlap between drop fractions. For many designs the sampling inlet velocity is constant, thus anisokinetic sampling conditions will be common. Therefore the collector's aspiration efficiency – the fraction of drops that enters the inlet for subsequent collection – should minimally distort the ambient drop size distribution during sampling. Overall sampling efficiency is the product of the aspiration, collection and transmission efficiencies (see Appendix B).

2.3.1.1 Principles of Cascade Impactor Design

We used the design principles of cascade inertial jet impaction developed by Marple and co-workers (Marple and Rubow, 1986; Marple and Willeke, 1975; Marple, 1970) to design FROSTY and the 5-Stage collector. Their jet impactor designs should provide FROSTY and the 5-Stage with steeper collection efficiency curves than theoretically achievable with strands and minimize collection overlap between stages (see Appendix B). Both round (Berner *et al.*, 1998; Collett *et al.*, 1995; Millet *et al.*, 1995; Collett *et al.*, 1993a) and rectangular (Laj *et al.*, 1998; Winkler, 1992; Schell and Georgii, 1989) jet cloud water collectors have been reported. Excessive size requirements for a "ring" arrangement of multiple round jets, and the problems of jet interference and water collection in a more dense arrangement (Fang *et al.*, 1991) resulted in the rectangular jet design for the new collectors. The relevant equations for rectangular jet impactors are:

$$Stk = \frac{\rho_p V_0 C D_p^2}{9\mu W} \qquad (2\text{-}1),$$

Reproduced with permission of the copyright owner. Further reproduction prohibited without permission.

$$\mathrm{Re}_i = \frac{2\rho_a W V_0}{\mu} \quad (2\text{-}2),$$

$$S/W \geq 1.5 \quad (2\text{-}3),$$

$$L/W \geq 10 \quad (2\text{-}4),$$

$$Th/W = 1 \quad (2\text{-}5), \text{ and}$$

$$\Delta P = \frac{1}{2}\rho_a V_0^2 \quad (2\text{-}6).$$

All of the symbols used are defined in the List of Symbols at the beginning of this dissertation. The Stokes number (Stk) (equation 2-1) is often used to parameterize the relative inertia of particles/drops and as defined here is the ratio of the drop stopping distance (in Stokes flow) to the characteristic dimension (jet width) of the collector. The impactor Reynolds number (Re_i) was set to 10,000 which is higher than optimal (500 – 3000) to accommodate the high flow rate (1.5 (FROSTY) $m^3\ min^{-1}$ and 2.0 (5-Stage) $m^3\ min^{-1}$) chosen for adequate temporal resolution. Given the volumetric flow rates ($=LWV_0$), sampling conditions, Re_i and D_p for each stage, equations 2-1 through 2-5 are solved for the primary collector dimensions – jet length (L) and jet width (W) (tables 2-1 and 2-2).

The aspect ratio of each jet, L/W, should be at least 10 (Marple and Rubow, 1986) to limit jet end effects (equation 2-4), although Mercer and Chow (1968) suggest a higher minimum value. The aspect ratio ranges in FROSTY and the 5-Stage are high enough to mitigate these non-idealities (tables 2-1 and 2-2). In the 5-Stage, the impaction surfaces were lengthened (5 – 8W) relative to design guidelines (4W) due to the asymmetric design (Marple, 1970). The entrance to each jet was tapered to minimize inlet losses (Marple and Willeke, 1975), and for FROSTY parabolic inlets were machined. The pressure drop through both collectors is very small (< 0.5% of an atmosphere by equation 2-6). In the 5-Stage, the difference between measured and calculated

Reproduced with permission of the copyright owner. Further reproduction prohibited without permission.

pressure of approximately ±20% on Stages 4 and 5 (table 2-2) is not surprising given the turbulence within the collector and the limitations of this calculation.

Several of the design decisions made for the 5-Stage – one-sided rectangular jet, extended impaction surfaces, high Re_i, sharp turns between stages, relatively large drops – can be expected to result in a decrease in the sharpness of the collection efficiency curves (Marple and Rubow, 1986; Marple and Willeke, 1975) and/or large internal losses (Schell and Georgii, 1989). Although not all of these factors apply to FROSTY, some lack of sharpness in the collection efficiency curves would likely also occur. However given the expected sampling conditions and criteria, the ultimate designs represented a compromise between competing objectives.

2.3.1.2 Sampling Time Requirements

The combination of flow rates and overall sampling efficiency of some of the pre-existing multi-stage collectors (Collett *et al.*, 1995; Collett *et al.*, 1993a) require long multi-hour sampling periods to collect sufficient sample for analysis. FROSTY and the 5-Stage's flow rates were chosen to minimize sample collection time subject to Re_i and collector size requirements. The 5-Stage's field results suggest time periods as short as 0.5 hour can be used, although one to two hour samples are more typical. One hour sampling periods were usually used for FROSTY, but 0.5 hour could be possible depending upon ambient conditions and sample volume requirements. The current FROSTY sampling protocol (see Chapter 6) which calls for melting each collected sample prior to removing it from the collection surface may limit sampling at sub-hourly intervals, if only two sets of impaction surfaces are available.

2.3.1.3 Drop Integrity

Drops sampled by the impactor should not deform or break up due to distortion in the collector's flow field and should not shatter upon impaction. Cascade impactor theory presumes drops are

Reproduced with permission of the copyright owner. Further reproduction prohibited without permission.

spherical which is true for drop Reynolds numbers (Re_p) < ≈ 300 (Pruppacher and Klett, 1997) where Re_p is defined as:

$$\mathrm{Re}_p = \frac{\rho_a D_p V_p}{\mu} \qquad (2\text{-}7).$$

The Weber number indicates the relative importance of drop kinetic energy to surface tension and is defined as:

$$We = \frac{\rho_a D_p V_0^2}{\sigma} \qquad (2\text{-}8)$$

(Pruppacher and Klett, 1997). To avoid self-induced drop break-up the maximum value for We should be approximately < 10 (Pruppacher and Klett, 1997). According to Reim (1993), another version of the Weber number related to drop shattering upon impact can be defined – the impact Weber number (We_{imp}) – where ρ_p and V_{imp} (the impaction velocity) are substituted into equation 2-8. A range of experimental values exists for the critical value of We_{imp}. Depending upon impaction surface properties, drop shattering may occur for We_{imp} as low as 28 to 70 (Hallett and Christensen, 1984) (Reim (1993) appears to make a calculation error in reporting the lower bound in Hallett and Christensen (1984)). Jacob *et al.* (1985a) suggest 150 as the critical value for We_{imp} based upon earlier work by Self and Keating (1980) in an unavailable internal report of the Stanford University Department of Mechanical Engineering. Several authors cite this value, although credit for the underlying source is often not clear. Professor Self recently indicated that the report cited by Jacob et al., (1985a) concerned ash drop measurements resulting from coal combustion (Self, 2001; Self, 1980). He estimated the critical We_{imp} value to be 500 for his application and suggested that Jacob et al. (1985a) chose a more conservative value based upon their application (Self, 2001). This remains unresolved, but the work by Hallett and Christensen (1984) suggests an even smaller critical value may be more appropriate. Additional drop shattering parameterizations are proposed in the literature that take into consideration surface characteristics by incorporating, for example, the *Ohnesorge* number and/or collection surface water film thickness (see (Cossali *et al.*, 1997; Mundo *et al.*, 1995; Reim, 1993)). These

Reproduced with permission of the copyright owner. Further reproduction prohibited without permission.

parameterizations yield essentially the same results: for the 5-Stage and FROSTY in relevant sampling conditions (0 – 20 m s^{-1} jet velocity, 1013 – 700 mb, -10 - 25°C, 4 < D_p < 50 μm) the conditions for drop integrity are uniformly satisfied.

While the largest drops are separated from the highest velocities within the collectors, this is not the case for drops which may impact the external surfaces of the collectors. Neglecting super-cooled drops, if drops shatter on or near the inlet, the resulting smaller drop fragments may be aspirated into the collectors and have the potential to contaminate the observed drop composition. At ambient wind speeds < 10 m s^{-1} (e.g. at Whiteface and Davis) drop shattering should not occur. For ACE2 conditions, where wind speeds as high as 17 m s^{-1} occurred, drops as small as ≈ 30 μm may shatter. Both the CASCC2 and the sf-CASCC have substantial flanges surrounding the inlets where drops have the opportunity to shatter and the fragments can be entrained. For these sub-isokinetic sampling conditions, however, it may be unlikely the drop fragments will be aspirated. The 5-Stage's geometry makes this a difficult point to evaluate. However, for high wind speeds, the possibility of drop shattering on the external surfaces of the collectors may produce some sampling artifact.

2.3.1.4 Aspiration Efficiency

If a sampling device is perfectly aligned (isoaxial) with the incident fluid streamlines and the sampler's velocity is the same as the ambient conditions (isokinetic) then the aspiration efficiency for suspended drops should be 100% (see Brockmann (1993) for a thorough discussion of this topic). The sampler theoretically does not disturb the ambient fluid streamlines. Unfortunately real samplers will disturb the ambient fluid streamlines and this is exacerbated if the sampler is blunt, mis-aligned with the ambient wind (anisoaxial), and/or the sampling velocity does not match the ambient one (anisokinetic). Drop size-dependent aspiration efficiency can be greater or less than 100%. Early investigators recognized that non-ideal aspiration efficiencies from anisokinetic and anisoaxial sampling for cloud water or drops was problematic (May, 1961; 1945; Houghton

Reproduced with permission of the copyright owner. Further reproduction prohibited without permission.

and Radford, 1938). This continues to be a problem as a range of ambient conditions may be experienced during collection (see Appendix B for mitigation techniques). Most of the laboratory or modeling work to evaluate and quantify the effects of anisoaxial and anisokinetic sampling on blunt or thin-walled sampling probes examine either highly idealized geometries or conditions not relevant to cloud water sampling which potentially limits their usefulness. In particular, cloud collector Re and drop Stk tend to be larger than in the systems studied, although turbulent Re were usually included. Therefore, care must be exercised in using the available aspiration efficiency corrections.

Table 2-3 illustrates the different sampling regimes for the 5-Stage, the sf-CASCC and the CASCC2 based upon ambient conditions and assuming all are oriented correctly (FROSTY and the CHRCC are difficult to compare as FROSTY is not oriented into the wind).

Table 2-3: Anisokinetic sampling conditions by warm-cloud collector

Free stream velocity [m s^{-1}]	Super- or sub-isokinetic sampling @ collector inlet		
	sf-CASCC	CASCC2	CSU 5-Stage
$U_0 < 2.7$	Super-	Super-	Super-
$2.7 < U_0 < 6.7$	Super-	Super-	Sub-
$6.7 < U_0 < 8.6$	Sub-	Super-	Sub-
$U_0 > 8.6$	Sub-	Sub-	Sub-

Table 2-3 illustrates that each collector may be subject to varying degrees of anisokinetic sampling simultaneously which may result in the aspiration of different drop populations. Varying collector orientation relative to the ambient wind (anisoaxial sampling) will also impact aspiration (isokinetic sampling conditions imply that the isoaxial condition is satisfied, however, the converse is not true). Overall drop sampling efficiency is dependent on both the internal collection efficiency and the sampler's aspiration efficiency (transmission efficiency is assumed to be 100% within the collectors upstream of the applicable collection efficiency curves, but see Appendix B

Reproduced with permission of the copyright owner. Further reproduction prohibited without permission.

for some consideration of this point). The aspiration efficiency may vary substantially between cloud events due to changing atmospheric conditions. Drop shattering and loss on external surfaces is neglected here. Based upon the preceding discussion, this should not occur in low wind conditions and in the absence of precipitation-sized drops (D_p > 100 μm). The following discussion starts with some consideration of the "blunt" collectors – the 5-Stage and then FROSTY. The more tractable thin-walled collectors (CASCCs) are then considered. The calculations included are relevant both as they lend insight into the CASCCs' performance, but also as they may help to interpret the blunt collectors' results. Finally, a discussion of "calm air" conditions for thin-walled tubes and their relevance to our samplers/sampling conditions is presented.

To consider the 5-Stage first, the critical factor affecting the aspiration efficiency is its blunt profile, which may substantially distort the flow field around the inlet. A 2-D model of a simple blunt sampler with a slot may be useful in providing a qualitative assessment of the collector's aspiration efficiency (Vincent and Mark, 1982). The equations that describe the model (equations 7.15, 7.16, 7.22 – 7.28 in Vincent (1989)) are not shown here in detail, but the aspiration efficiency can be thought of as:

$$\eta_{asp}=f(U_0/U_s,\ Stk_{asp},\ \textit{collector dimensions},\ \textit{empirical factors}) \qquad (2\text{-}9).$$

The first two parameters consider the effects of anisokinetic sampling conditions and the inertia of the drop to be collected. The latter two parameters consider how the flow field is changed by the presence of the blunt collector. The shapes used to determine the empirical factors are only generally similar to the 5-Stage, and are very limited in number (see (Tsai and Vincent, 1993; Vincent, 1989; 1987; Vincent *et al.*, 1982; Vincent and Mark, 1982)). Their direct applicability is unclear, and this geometry limitation should be considered wherever these parameterizations are invoked. The models found in the literature study highly idealized cases which suggests that an empirical approach is needed for "real" samplers (Vincent, 1987; Vincent *et al.*, 1982). In fact, the

Reproduced with permission of the copyright owner. Further reproduction prohibited without permission.

shape and "bluntness" of the collector affect the flow field (see (Dunnett and Ingham, 1988; Vincent and Mark, 1982), among others). Nevertheless, the 2-D model results suggest that for D_p < 40 μm in winds < 10 m s^{-1} with the collector oriented into the wind, the aspiration efficiency should approximately vary between 90 – 110% for any cloud drop size in the 5-Stage. Larger drops (with more inertia) tend to show the largest deviations. For larger drops (large Stk) the expected behavior as the yaw angle approaches 90° is for the aspiration efficiency to approach zero. Conversely, as the yaw angle goes to 0°, the aspiration efficiency ought to go to the ratio of the ambient over the sampling velocities (U_0/U_s). While the 2-D results are promising, this simple model does not include any parameter for inlet orientation into the wind, the angle of the inlet to the wind, and the complicating presence of the wind shield (see section 2.3.1.5).

A 3-D version of this model which includes anisoaxial operation (equations 7.33 – 7.42 in Vincent (1989)) limited to an axisymmetric spheroid with a central sampling orifice was also investigated. Its applicability to the 5-Stage is not clear, but it does suggest that very large deviations from 100% aspiration are possible for blunt samplers.

It is difficult to evaluate FROSTY's aspiration efficiency because it is operated at right angles to the ambient flow. While the presence of the wind shield (section 2.3.1.5) should theoretically promote 100% aspiration by creating a stagnation region in front of the sampler's inlet, there are few equations reported in the literature for very limited (and largely trivial) sampling conditions (e.g. see the limitations on the anisoaxial sampling correlations in Brockmann (1993)).

The CASCCs may be approximated as thin-walled sampling tubes and their aspiration efficiencies can be described by:

$$\eta_{asp} = 1 + \frac{\left(\frac{U_0}{U_s} - 1\right)}{\left(1 + \frac{0.418}{Stk}\right)}, \left(U_0 / U_s\right) > 1 \qquad \text{(2-10), and}$$

Reproduced with permission of the copyright owner. Further reproduction prohibited without permission.

$$\eta_{asp} = 1 + \frac{\left(\frac{U_0}{U_s} - 1\right)}{\left[1 + \frac{0.506\left(U_0 / U_s\right)^{0.5}}{Stk}\right]}, \left(U_0 / U_s\right) < 1 \qquad (2\text{-}11)$$

which are valid for $0.01 \leq Stk \leq 100$ and $0.1 \leq (U_0/U_s) \leq 10$ (Brockmann, 1993). As U_0/U_s goes to 1 (isokinetic sampling), the limiting behavior for both equations is correct. Where drop size distribution information is available, these equations are used to correct the CASCCs' aspiration efficiency in the chapters that follow. Given the dependence upon Stk, larger effects can be observed as drop sizes increase. In general for the data reported here, these corrections to the CASCCs' aspiration efficiency are negligible except potentially in Davis (see Chapter 4). Sampling anisoaxially can result in poor aspiration efficiencies as drops get larger and the angle increases (Wen and Ingham, 2000; Brockmann, 1993; Tsai and Vincent, 1993). However, one reasonably relevant study (Grinshpun *et al.*, 1990) suggests that for representative drop sizes and ambient conditions that a yaw angle of ± 15° results in less than a 5% variation in aspiration. Anisoaxial corrections are subsequently ignored, but this result suggests that if the wind direction is reasonably constant and the collector is oriented properly undue error may not be introduced.

One aspect related to the aspiration efficiency of the collectors – particularly the CASCCs – is whether or not high ambient velocities affect the size-resolved or overall collection efficiencies, and/or the sampler flow rate. This issue is addressed in Appendix E by focusing on stopping distances and characteristic times.

Calm air sampling has been addressed by several investigators and a variety of restrictions are reported in the literature for varying orientations and conditions (Grinshpun *et al.*, 1993; Agarwal and Liu, 1980; Gibson and Ogden, 1977; Kaslow and Emrich, 1974; Davies, 1968). While most of these references appear in Brockmann (1993), the original sources must be consulted to verify their relevance to cloud water sampling. In particular Agarwal and Liu (1980), and Gibson and

Reproduced with permission of the copyright owner. Further reproduction prohibited without permission.

Ogden (1977) (and the several references cited therein) are applicable over only a very limited range of relevant ambient velocities and drop sizes. Kaslow and Emrich (1974) consider thick-walled cylinders, but the geometry approximations required to apply their equations to the 5-Stage limits their usefulness. Grinshpun and co-workers (1993) link calm air sampling with higher velocity sampling (e.g. similar to equations 2-9 and 2-10). For the CASCCs, the results are generally similar to those using equation 2-10 at the limit of its applicability: drops > approximately 30 μm may have poorer aspiration by as much as 10%, but smaller drops should not be significantly affected. (I believe there is an a typographical error in the definition of "f_{calm}" in Grinshpun et al., (1993)[†]). Davies (1968) takes an alternate approach – for given conditions (including calm air) he defines the size of "small" and "large" sampling tubes. "Small" tubes may be oriented in any direction and have ideal aspiration efficiency, but "large" tubes have non-ideal aspiration. Both the sf-CASCC and the CASCC2 are "large" collectors, and the CASCC2 is, in some sense, relatively "larger" due to its higher sampling velocity. Therefore by this evaluation technique, the collectors by definition are likely to have non-ideal aspiration efficiencies. Finally any additional criteria given in Brockmann (1993) consider vertically-oriented tubes only.

Drop sedimentation, particularly in low ambient wind conditions (e.g. fogs), has the potential to affect the aspiration efficiency of the 5-Stage collector as its inlet is pointed partially up. This effect should be partially mitigated by the presence of the wind shield (if installed). Froude number correlations (often used to parameterize the effects of sedimentation (gravity) (Vincent, 1989)) were not particularly useful for assessing the impacts of sedimentation on the 5-Stage's aspiration. As with the other treatments, the parameter's applicability was questionable due to the different geometry between the 5-Stage and the simple object used as the basis for the parameterization. The CASCCs should not be similarly affected. Gravitational losses within the collectors during sampling should be negligible.

[†] The paper links the equations for calm air and "non-calm" air sampling together by the use of adjustable non-dimensional scaling factors. In order for the scaling factors to sum to 1.0, a negative sign must be inserted into the equation defining f_{calm}.

Reproduced with permission of the copyright owner. Further reproduction prohibited without permission.

The discussion above suggests that aspiration efficiency has the potential to affect the samplers' overall sampling efficiency. However, it is difficult to draw any firm conclusions about blunt sampler aspiration efficiency due to the significant approximations required to use any of the models/empirical correlations reported in the literature. For the CASCCs and the conditions studied, aspiration efficiency does not appear to markedly change except for larger drops (D_p > 30 μm approximately) in calm conditions (e.g. Davis fogs, but not at Whiteface or ACE2). For the blunt samplers, the presence of the wind shield theoretically may improve their aspiration up to 100% efficiency (Vincent, 1989 and references therein). As aspiration efficiency alone is difficult to evalute based upon field measurements, the overall sampling efficiency for the collectors is examined in Chapters 3 and 4. The aspiration efficiency (assuming it is the predominant factor in overall sampling efficiency) is likely not ideal if the total mass sampled cannot be predicted for the collectors.

2.3.1.5 Windshield Design

Berner and co-workers have reported successful results for sampling in high winds from the stagnation region created by a downstream baffle (Berner *et al.*, 1998; Berner and Kruisz, 1997; Kruisz *et al.*, 1992). Although constrained by the 5-Stage's geometry, the goal of the windshield was to not interfere with the drop sizes of interest (D_p < 50 μm) for approximately 10 m s^{-1} ambient winds. For FROSTY, higher ambient winds were considered (up to 15 m s^{-1}). For these design conditions, the wind shields' sizes were determined using the model of no drop collection by a disc in cross-flow (May and Clifford, 1967). The non-Stokes flow stopping distances (equation E-3) of relevant drop sizes were calculated as a check (Mercer, 1973). While these wind shields are based upon a very simplified model and may modify the flow field around the inlets, they should not interfere with and may aid the collection of drops. A more detailed discussion may be found in Appendix F.

Reproduced with permission of the copyright owner. Further reproduction prohibited without permission.

2.3.1.6 Preliminary Performance Evaluation and Resulting Modifications

Prototype laboratory testing of Stage 5 of the 5-Stage collector indicated that the combination of high velocity in that stage and the small impaction surface length might lead to the loss of collected drops to the exit via surface migration. This problem was not observed at the lower velocities of the preceding stages. A "lip" was added at the end of the Stage 5 impaction surface to prevent losses. According to the design guidelines of May and Clifford (1967) the lip should not change the stage's D_{p50}. Flow across the length of the nozzle was uniform in laboratory testing, although drop losses to surfaces other than the designated impaction area were observed. The overall pressure drop through the collector ($\approx$ 2900 Pa) was primarily due to the exit stage. This suggests that pump and flow meter sizing must take much larger total pressure drops into consideration than predicted by equation 2-6 for the drop collection stages alone.

Few laboratory measurements of the flow field inside FROSTY were performed prior to its calibration.

2.3.2 Chemical integrity

The process of drop impaction and subsequent collection must not chemically modify the sample. The collector itself should be chemically inert for the species of interest, and the potential for evaporation/condensation within the collector minimized.

2.3.2.1 Material Inertness

The 5-Stage and FROSTY are constructed entirely of plastic since the principal species of interest in their collected samples are the major inorganic ions (Na^+, NH_4^+, Mg^{2+}, K^+, Ca^{2+}, (NO_2^-), NO_3^-, SO_4^{2-}, Cl^-, H^+) and metals such as Fe, Mn, and Cu. The epoxy used to seal the 5-Stage seams was inert when dry, but care was taken to ensure that it was not present in any potential

Reproduced with permission of the copyright owner. Further reproduction prohibited without permission.

sample path regardless. No adhesives are used upstream of the exit stage in FROSTY. Both FROSTY and the 5-Stage's blanks are consistently clean for these ionic species and metals (see Chapter 5 for limitations for other species).

A new sf-CASCC was built in 1998 completely out of plastic as well. Metal fasteners and cartridge frames for the 2nd stage (Small fraction) were replaced, but critical dimensions for sampling stayed the same. It entered use with the Whiteface campaign.

2.3.2.2 Evaporation and condensation within the collectors

This discussion largely concerns the 5-Stage. The possibility of vapor deposition within FROSTY is addressed in Chapter 3.

Of particular concern in the cloud and fog sampling literature is the effect of collection on the local thermodynamic state. Slight changes can result in condensation or evaporation of the collected drops, which historically has been a problem (Mallant, 1988). There are three important factors to consider. The first, from an operational point of view, is to limit sampling to continuous clouds. The latter two are design parameters: to minimize both the drop residence time in the collector and pressure changes induced by the flow. Changes in pressure and thus temperature result in saturation differences and potential drop growth/evaporation. The net effect, however, is limited by the time available. Those drops that spend the most time prior to impaction (roughly $D_p < 11.5$ μm) are at the highest risk in the 5-Stage.

A theoretical evaluation of drop diameter changes prior to impaction inside a cascade impactor-style collector has been developed (Berner *et al.*, 1998; Berner, 1988). Drops experience alternating regions conducive to condensation and evaporation from high velocity (e.g. in the jet) and low velocity flow fields (e.g. between stages). The theory assumes that suspended drops have the same residence time within the collector as the fluid. Modeling suggests this

Reproduced with permission of the copyright owner. Further reproduction prohibited without permission.

assumption is not valid for all drops within the CSU 5-Stage due to its turbulent flow fields and re-circulation zones (Straub and Collett, 2001a). Making adjustments to reflect the different configuration of the 5-Stage but otherwise generally similar assumptions to Berner *et al.*'s approach, the calculated saturation changes varied at most by < 0.5%. The driving forces for drop size change prior to collection were thus negligible. As a consequence, drop growth calculations (equation 4.6 (Berner *et al.*, 1998)) indicate no more than a 1% change in diameter would occur (not shown). This result is robust for the expected drop size range and is not sensitive to a reasonable parameter range (e.g. varying accommodation coefficients from 0.01 to 1) or changing drop residence times to simulate a variety of drop paths within the collector. Therefore, suspended drops should not change measurably prior to impaction. Impacted drops, however, may be subject to condensation/evaporation during temporary exposure to the flow field. As previously indicated, the 5-Stage is mounted at an angle to promote run-off into the attached quiescent vials to mitigate this. No field evidence of evaporation/condensation has been found in chemical analysis of the collected drops and other investigators have also reported no evidence of condensation/evaporation for similar pressure drops (Schell *et al.*, 1992; Winkler, 1992; Däumer *et al.*, 1988).

2.3.3 Ease-of-use

Given the constraints to their designs, the collectors should be as easy and safe to use as possible. The 5-Stage weighs approximately 27 kg when fully assembled and can be placed into its dedicated stand by one operator. FROSTY is both smaller and lighter. Time-consuming disassembly is not required for sample collection from either, unlike some earlier multi-stage collectors (Collett *et al.*, 1995; Collett *et al.*, 1993a). A skilled operator can quickly (< 10 minutes) collect the 5-Stage samples, and less time is required for FROSTY. Appendices C and D contain the detailed sampling protocols for both collectors.

Reproduced with permission of the copyright owner. Further reproduction prohibited without permission.

2.3.4 Comparability

Ideally, new cloud water collectors should be comparable to pre-existing collectors and other measurement devices. While experimental calibrations exist for some collectors, only theoretical collection efficiencies have been reported for many others. It is important to verify that the collectors operate consistently and comparably under field conditions where they will actually be used. These issues are addressed in Chapters 3 and 4 where the field performance of the super-cooled and warm cloud collectors are evaluated. This ensures that no operational problems (particularly aspiration efficiency variations) are hidden in the lab and that theoretically and experimentally developed collection efficiency curves are accurate. Non-idealities in collector operation may result in actual collection efficiencies that vary from theory. It is important to quantitatively determine if the collectors sample the same drop populations. Previous side-by-side comparisons of collectors indicate that agreement can be fairly good if the same drop population is being consistently sampled, but changes in aspiration efficiency and internal losses can lead to quite different results as atmospheric conditions vary (Schell *et al.*, 1992; Collett *et al.*, 1990; Hering *et al.*, 1987). Appendix B discusses collector comparisons in the literature.

Reproduced with permission of the copyright owner. Further reproduction prohibited without permission.

3. Field Performance of the Caltech Heated Rod Cloud water collector (CHRCC) and the FROSTY collector

In this section, the CHRCC and FROSTY collectors' performances are evaluated from both a physical (i.e. collected mass) and chemical perspective based upon the data obtained during two field projects – at Storm Peak Laboratory (SPL) (December 1996/January 1997) and at Horsetooth Mountain (April 1998). The comparisons are made between results from the collectors and other concurrently operated equipment and are interpreted in view of the ambient conditions.

Following a brief discussion of the rationale behind this type of analysis (as it motivates Chapter 4 as well), selected aspects of the SPL campaign will be briefly described. Comparisons of the CHRCC's collected mass are presented first followed by FROSTY's. The collected mass and composition results from FROSTY and the CHRCC are comparatively evaluated. The results and their implications are discussed. Finally, a few remaining issues prompted by additional field observations and work by others are addressed.

3.1 Rationale behind field performance validation

Investigators use a variety of techniques to collect and analyze cloud water (reviewed in Appendix B). "Standard" techniques are readily available to evaluate the analytical methods which facilitates the comparison between results reported by different research groups. Inter-comparison of cloud chemistry results across different sites depends upon the assumption that the cloud water collectors sampled the drops consistently and with known efficiency under all the conditions experienced. In some sense, field performance evaluation is an "accuracy check" for

Reproduced with permission of the copyright owner. Further reproduction prohibited without permission.

cloud water collectors; it provides a means to evaluate the "representativeness" of the collected cloud water sample. In order to properly interpret results, any bias introduced by the collection device needs to be determined. Instead of asserting that the cloud drop composition obtained is as actually existed and reported without artifact, a preferable alternative is to be able to prove – albeit within the limitations of the analysis – that this is likely to be so.

Most cloud water collectors have some kind of theoretical performance characteristics reported in the literature (see Appendix B). Criteria often provided include collection surface area available, flow rate, 50% cut point diameter, and more. Few collectors have been rigourously evaluated experimentally either in wind tunnels or in the laboratory. Actual field performance, however, can vary substantially due to changing ambient conditions and may highlight limitations in the theoretical or experimental calibration. Often theoretical analysis makes simplifying assumptions for tractability, which may or may not be strictly true for "real" operating conditions. For both active and passive cloud water collectors, aspiration efficiency (often unknown or difficult to evaluate (Chapter 2)) can modify the drop distribution incident upon the collection surfaces. The overall collection efficiency curve is a function of both aspiration, transmission and the collector's efficiency curve. Therefore reported collector efficiency curves, even those based upon rigourous calibration, may not always be representative of overall field collection. Therefore, collector performance must always be evaluated as part of any field measurement campaign.

Two general types of comparisions can be performed – physical and chemical. Physical comparisons involve tracking water mass. Many pieces of equipment (e.g. PVM-100, FSSP-100) can measure the sampled cloud's LWC. Collected water is often correlated against cloud LWC to provide an estimate of the collector's sampling efficiency (see Appendix B). However, total water collection efficiency is a function of drop size and distribution. Therefore, a preferred method of evaluating collector physical performance would use available drop size distributions and collector efficiency curves. Insight into whether consistent collection occurs across all drop sizes and distributions should result. A simple comparison of total collected mass vs. ambient LWC

Reproduced with permission of the copyright owner. Further reproduction prohibited without permission.

cannot show that. It is important to know for what conditions collection is not predictable and which drop sizes are affected. This is a critical issue for size-resolving collectors. A limitation of this "mass approach" is that it may be much less sensitive to whether or not small drops (e.g. < 10 μm in diameter) are being collected, although this is a function of the peak and breadth of the overall drop size distribution.

One evaluation method that can be sensitive to small drops is chemical composition comparison between collectors. If the composition is drop-size dependent, over- or under-sampling of a particular size drop is more likely to be evident. This method should also reveal contamination, evaporation or condensation problems. For bulk cloud water collectors, observed concentrations can be compared. These results can be interpreted in terms of accompanying physical measurements. In other words if the two collectors have different sampling efficiencies for different size drops (and thus collect different amounts of mass for a standardized flow rate), then variations in composition are not unexpected. When size-resolving collectors are used, volume-weighted averages can be calculated to yield a derived "bulk" concentration. This type of calculation presumes that species are conserved during mixing which may not always be true (Pandis and Seinfeld, 1991; Perdue and Beck, 1988). Inherent in this approach is the assumption that the overall collection efficiency curves are similar between the collectors which is not always valid. However, a common basis for evaluation must be found and extending the comparison to multiple species can reinforce the results. Drop size distributions can be used to qualitatively interpret any variations in bulk and "derived" bulk composition, but their quantitative use would require detailed information of the size-dependent composition on as high a resolution as the distribution itself. Current high-volume cloud sampling techniques do not provide that data (however this idea is explored with the 5-Stage in Chapter 4). A limitation of this approach is that for drops with weak size-dependent composition, this technique may provide limited information about the collectors' performance and multiple biases may off-set each other.

Reproduced with permission of the copyright owner. Further reproduction prohibited without permission.

To summarize, collected mass, drop size distributions, LWC measurements and collection efficiency curves (assumed to be representative of overall sampling efficiency curves) are quantitatively useful for physical comparisons. For chemical comparisons, collected mass and drop composition measurements are also quantitatively useful, but collection efficiency curves, LWC and drop size distributions are only of qualitative benefit. Therefore for evaluation purposes, a complete data set would contain all of these measurements made with as little uncertainty as possible. In practice, however, data from all these instruments are not always available and some of their measurement uncertainties are considerable (e.g. drop size distribution measurements (Appendix G)). Although the resulting propagated error in the analysis can be quite high, the results are still useful in evaluating the performance of the collectors. The physical and chemical approaches complement each other: Each has its limitations and neither will definitively determine if a collector is working as specified. However, they can suggest to what degree the data are internally consistent and predictable between the cloud water collectors and the other instruments. Very inconsistent collector field performance should be evident.

Finally, inherent in a field evaluation is the assumption that each sampling instrument is exposed to the same population of drops. It is not always possible to co-locate equipment as closely together as might be needed to completely satisfy this requirement. Artifacts introduced by the act of sample collection itself also add some additional uncertainty to the results (e.g. mixing drops together of varying composition). Despite these limitations, however, field performance evaluations are necessary adjuncts to collector measurements and are required to compare results between campaigns, investigators, techniques, and equipment.

3.2 The Storm Peak Laboratory Field Campaign

A brief summary of the results of this campaign is included with the presentation and interpretation of the Horsetooth composition measurements in Chapter 6. The goal here is to

Reproduced with permission of the copyright owner. Further reproduction prohibited without permission.

describe the site and the measurements available from that campaign that are useful for collector performance validation.

The Storm Peak Laboratory is operated by the Dessert Research Institute (DRI) and is located at the summit of Mt. Werner (3210 m asl) in Colorado on the western side of the Rocky Mountains. The lab is located in the Steamboat Springs ski resort area. Mt. Werner is a tall, isolated peak (based upon prevailing wind direction), and is often located in the free troposphere. Clouds composed of super-cooled drops frequently surround the summit in the winter. The sampling location is on the roof of the lab; there are no immediate upstream obstructions except for a few individual trees in the usual flow direction. A variety of cloud and precipitation studies including both physical and chemical measurements have been performed there over many years (Borys *et al.*, 2000; Hindman *et al.*, 1994; Carter and Borys, 1993; Borys *et al.*, 1988).

During the study presented here, six super-cooled cloud events were sampled over approximately two weeks in January 1997 (1/2/97, 1/3/97, 1/8/97, 1/9/97, 1/10/97, and 1/14/97). These events are referred to hereafter as EVENT # where the number is the day the event started (1/2/97 = EVENT 2). In addition to the two collectors, DRI supplied FSSP-100 drop-size distribution and meteorological measurements. Cloud LWC was measured using the CSU PVM-100. The FSSP-100 was mounted to orient itself into the wind, while the CHRCC was fixed to the railing and could not be re-oriented. FROSTY was mounted on its stand which (theoretically) could be re-oriented if a substantial wind shift occurred. In practice it was difficult to rotate the stand due to accumulated snow. Both collectors were (more or less) oriented in the correct direction (CHRCC into the wind (with a downward facing inlet to prevent the aspiration of precipitation) and FROSTY perpendicular to the wind) during sampling. EVENT 2 had somewhat warmer temperatures ($\approx$ - 3°C) and milder ambient wind ($\approx$ 5 m/s) than the other days (< -10°C and $\approx$ 10 m/s (4 – 7 m/s during EVENT 14)). The wind was generally steady from the N or NW during the measurement periods. Due to the extreme conditions myriad difficulties with sampling equipment occurred. Heavy riming invalidated some FSSP, LWC, meteorological and collector

Reproduced with permission of the copyright owner. Further reproduction prohibited without permission.

measurements. All validated data available are included in the following analysis and are tabulated in Appendix H.

Rimed drops in the CHRCC can be melted by the application of heat or current to the collecting rods (Chapter 2). In order to limit rime buildup, sample was collected from the CHRCC two and sometimes three times per hour. As a result, to compare CHRCC results with the hourly FROSTY ones, CHRCC measurements must be averaged together. Gaps between sampling intervals (up to five minutes) when the CHRCC sample was being collected are also ignored in the FROSTY inter-comparisons. "CHRCC-only" evaluations do not suffer from these limitations. Several CHRCC and FROSTY samples where concurrent notes clearly indicate collection problems (e.g. FROSTY mass loss, retention of rime in the CHRCC between sample periods) were excluded. Tables 3-1 through 3-5 are included here to both show the range of conditions experienced (e.g. D_{eff}, LWC), but also to emphasize the approximations required to compare the two collectors to each other.

Table 3-1: SPL EVENT 2 data available

Collector sample	Sampling time period [local]	LWC [mg m^{-3}] (via PVM-100)	D_{eff} [μm] (via FSSP)	Predicted/ collected mass comparison	Collector intercomparison		PVM LWC compar.
					mass	composition	
CHRCC #2	1/2/97 23:50 – 1/3/97 0:20	n. a.	n. a.	no	*see below*	*see below*	no
CHRCC #3	1/3/97 0:25 – 0:50	n. a.	n. a.	no	*see below*	*see below*	no
CHRCC #4	1/3/97 0:55 – 1:25	n. a.	n. a.	no	*see below*	*see below*	no
CHRCC #5	1/3/97 1:30 – 1:55	n. a.	n. a.	no	*see below*	*see below*	no
FROSTY #2	1/2/97 23:50 – 1/3/97 0:50	n. a.	n. a.	no	CHRCC #2 & #3	CHRCC #2 & #3	no
FROSTY #3	1/3/97 0:55 – 1:56	n. a.	n. a.	no	CHRCC #4 & #5	CHRCC #4 & #5	no

n.a. indicates not availabe
collector intercomparison indicated by FROSTY samples as multi-CHRCC samples required

No LWC data are available during EVENTs 2 or 9: while LWC can be calculated using the FSSP, this was not done for consistency with the rest of the data. Where data are available, the cloud

Reproduced with permission of the copyright owner. Further reproduction prohibited without permission.

Table 3-2: SPL EVENT 8 data available

Collector sample	Sampling time period [local]	LWC [mg m^{-3}] (via PVM-100)	D_{eff} [µm] (via FSSP)	Predicted/ collected mass comparison	Collector intercomparison		PVM LWC compar.
					mass	composition	
CHRCC #3	1/8/97 21:56 – 22:22	72.2	11.3	yes	*see below*	*see below*	yes
CHRCC #4	1/8/97 22:26 – 22:56	93.0	12.0	yes	*see below*	*see below*	yes
CHRCC #5	1/8/97 23:02 – 23:32	93.0	11.8	yes	*see below*	*see below*	yes
CHRCC #6	1/8/97 23:36 – 23:57	104.1	12.3	yes	*see below*	*see below*	yes
CHRCC #7	1/9/97 0:03 – 0:28	129.5	13.2	yes	*see below*	*see below*	yes
CHRCC #8	1/9/97 0:32 – 0:57	144.3	14.6	yes	*see below*	*see below*	yes
CHRCC #9	1/9/97 1:02 – 1:27	171.1	15.6	yes	*see below*	*see below*	yes
CHRCC #10	1/9/97 1:31 – 1:52	184.5	16.2	yes	*see below*	*see below*	yes
FROSTY #1	1/8/97 21:00 – 21:57	44.7	n. a.	no	*see below*	*see below*	yes
FROSTY #2	1/8/97 22:02 – 23:00	85.9	11.7	yes	CHRCC #3 & #4	CHRCC #3 & #4	yes
FROSTY #3	1/8/97 23:02 – 24:00	98.3	12.1	yes	CHRCC #5 & #6	CHRCC #5 & #6	yes
FROSTY #4	1/9/97 0:03 – 1:00	137.4	14.0	yes	CHRCC #7 & #8	CHRCC #7 & #8	yes
FROSTY #5	1/9/97 1:02 – 2:00	178.2	15.9	yes	CHRCC #9 & #10	CHRCC #9 & #10	yes
FROSTY #6	1/9/97 2:03 – 3:00	209.3	16.3	yes	no	no	yes
FROSTY #7	1/9/97 3:02 – 4:00	255.1	16.9	yes	no	no	yes
FROSTY #8	1/9/97 4:02 – 5:00	278.0	17.3	yes	no	no	yes

n.a. indicates not availabe
collector intercomparison indicated by FROSTY samples as multi-CHRCC samples required

Table 3-3: SPL EVENT 9 data available

Collector sample	Sampling time period [local]	LWC [mg m^{-3}] (via PVM-100)	D_{eff} [µm] (via FSSP)	Predicted/ collected mass comparison	Collector intercomparison		PVM LWC compar.
					mass	composition	
CHRCC #3	1/9/97 18:03 – 18:18	n. a.	18.0	no	*see below*	*see below*	no
CHRCC #4	1/9/97 18:23 – 18:38	n. a.	17.4	no	*see below*	*see below*	no
CHRCC #5	1/9/97 18:43 – 18:58	n. a.	17.7	no	*see below*	*see below*	no
CHRCC #6	1/9/97 19:03 – 19:18	n. a.	18.9	no	no	no	no
FROSTY #2	1/9/97 18:02 – 19:00	n. a.	17.8	relative only	CHRCC #3, #4 % #5	CHRCC #3, #4 % #5	no
FROSTY #3	1/9/97 19:02 – 20:00	n. a.	18.8	relative only	no	no	no

n.a. indicates not availabe
collector intercomparison indicated by FROSTY samples as multi-CHRCC samples required

Reproduced with permission of the copyright owner. Further reproduction prohibited without permission.

Table 3-4: SPL EVENT 10 data available

Collector sample	Sampling time period [local]	LWC [mg m^{-3}] (via PVM-100)	D_{eff} [µm] (via FSSP)	Predicted/ collected mass comparison	Collector intercomparison		PVM LWC compar.
					mass	composition	
CHRCC #3	1/10/97 16:23 - 16:38	134.2	n. a.	no	no	no	yes
CHRCC #4	1/10/97 16:42 - 16:57	157.8	n. a.	no	no	no	yes
CHRCC #5	1/10/97 17:02 - 17:17	145.6	n. a.	no	no	no	yes
FROSTY #1	1/10/97 16:00 - 17:00	151.8	n. a.	no	no	no	yes
FROSTY #2	1/10/97 17:02 - 18:00	150.7	n. a.	no	no	no	yes
FROSTY #4	1/10/97 19:02 - 20:00	164.1	19.1	yes	no	no	yes
FROSTY #5	1/10/97 20:02 - 21:00	141.1	16.9	yes	no	no	yes
FROSTY #6	1/10/97 21:02 - 22:00	171.3	17.4	yes	no	no	yes
FROSTY #7	1/10/97 22:02 - 23:00	419.2	17.8	no	no	no	yes
FROSTY #9	1/11/97 0:02 - 1:00	276.9	19.2	yes	no	no	yes
FROSTY #10	1/11/97 1:02 - 2:00	283.2	18.3	yes	no	no	yes

n.a. indicates not availabe
collector intercomparison indicated by FROSTY samples as multi-CHRCC samples required

Table 3-5: SPL EVENT 14 data available

Collector sample	Sampling time period [local]	LWC [mg m^{-3}] (via PVM-100)	D_{eff} [µm] (via FSSP)	Predicted/ collected mass comparison	Collector intercomparison		PVM LWC compar.
					mass	composition	
FROSTY #1	1/14/97 13:30 - 14:30	179.4	14.6	yes	no	no	yes
FROSTY #3	1/14/97 15:30 - 16:30	258.6	15.3	yes	no	no	yes
FROSTY #4	1/14/97 16:32 - 17:30	297.1	n. a.	no	no	no	yes
FROSTY #5	1/14/97 17:32 - 18:30	271.3	n. a.	no	no	no	yes
FROSTY #6	1/14/97 18:32 - 19:30	389.1	n. a.	no	no	no	yes

n.a. indicates not availabe
collector intercomparison indicated by FROSTY samples as multi-CHRCC samples required

LWC tended to be in the 100 – 300 mg m^{-3} range and the effective diameters < 20 µm (usually 15 – 16 µm), although a pronounced shift is evident during EVENT 8 from 11 to 17 µm. Useful data were available from five of the six events (tables 3-1 through 3-5).

Reproduced with permission of the copyright owner. Further reproduction prohibited without permission.

3.3 CHRCC Evaluation

The theoretical CHRCC efficiency curve is shown in figure 3-1 (Demoz *et al.*, 1996) (as are the experimentally determined FROSTY curves (Straub and Collett, 1999)).

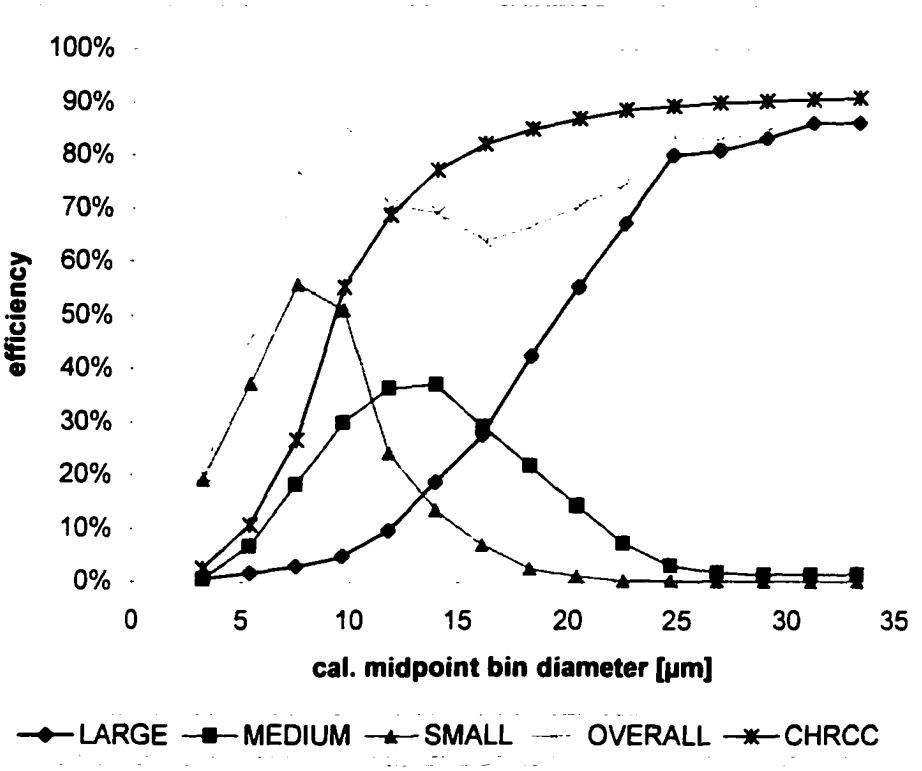

Figure 3-1: The theoretical CHRCC and experimental FROSTY collection efficiency curves for SPL conditions (Straub and Collett, 1999; Demoz *et al.*, 1996). "OVERALL" is the sum of the FROSTY curves.

The volume distributions calculated using the processed PVM-LWC and the FSSP data (Appendix G) were multiplied by the collector efficiency curve for each bin across the drop size distribution. The predicted mass for each bin was summed across all diameters to get the total predicted CHRCC mass for each time period. This prediction is compared to the actual mass collected. The propagated uncertainty in this calculation is a combination of the uncertainty in the FSSP (25% (Baumgardner, 1995)), the PVM-100 (10% (Gerber *et al.*, 1994)), flow rate (5%, estimated), weight measurement (0.1 g, estimated), and uncollected residual mass (3.0 g,

Reproduced with permission of the copyright owner. Further reproduction prohibited without permission.

estimated). The error bars shown are plus/minus the propagated uncertainty. The CHRCC comparison is shown in figure 3-2.

In these calculations and all of those that follow, estimated uncertainties are treated in the same manner as standard deviations, although, in fact, they are not. All error bars, except as otherwise specifically indicated, represent ± 1 uncertainty/standard deviation.

While there is considerable uncertainty expressed in the error bars, the variation between predicted and collected mass is much larger. For these samples the predicted/collected ratio varies from 150 – 552% (mean 391%). Unfortunately these data are all from one event (EVENT 8). However, it is worrisome that the trend between the predicted and collected masses differ as the event progresses. It appears that the CHRCC performance becomes worse with time. This is consistent with a build-up of uncollected rime which may affect the collection efficiency curves. However, D_{eff} is getting larger during this event and any rime build-up should affect smaller drops more. Using short sampling periods should help to mitigate rime build-up. The PVM and FSSP may not have been operating correctly, but they were routinely calibrated during the campaign. Further, a comparison of measured LWC between the two for the SPL campaign by Betsy Andrews exhibited high correlation. Therefore it is unlikely that the differences between predicted and collected mass observed result solely from them. A further possibility would be a poor and variable aspiration efficiency for the CHRCC. Wind speeds were high, but they did not appear to change appreciably during the event. Additionally, the wind direction was reasonably consistent during the sampling periods (see Appendix H) which suggests that the observed discrepancies between predicted and collected mass do not result from misalignment, although the downward facing inlet probably affected aspiration. They do not explain the apparent change in efficiency between samples #3 and #4 either. The CHRCC collection efficiency curve is theoretical and important factors (e.g. interaction between rods which are relatively closely spaced (see Chapter 4)) may result in "non-ideal" collection. The amount of heating used for each sample was similar

Reproduced with permission of the copyright owner. Further reproduction prohibited without permission.

during this event and the ambient temperature changed little. A combination of these factors may be responsible for this observed discrepancy between predicted and collected mass.

During the SPL campaign, we were aware of the possible inadequacy of the CHRCC's heating system and those data where ice was known to be retained in the CHRCC were removed from this analysis. The 3.0 g residual mass value assumed for the uncertainty calculations may be inadequate. Evaporation is not supported as a source of the discrepancy between predicted and collected masses (see discussion below). The PVM-100 was installed possibly up to 1 m higher vertically, but the FSSP-100 and FROSTY were essentially horizontally co-located. Therefore variations in LWC with height, while possible (Vong and Kowalski, 1995), likely cannot account for the observed discrepancies. The CHRCC was designed for warmer temperatures and lower wind speeds.

A comparison of the CHRCC collected mass to the PVM is shown in figure 3-3. The uncertainty is calculated and shown in a similar fashion to figure 3-2's. This comparison does not depend upon the drop size distribution and could suggest if the CHRCC is at least working consistently (if not necessarily as predicted).

In figure 3-3 the two largest CHRCC collected masses are the two data points (#3 and #4) that in figure 3-2 are the closest to the predicted value. This comparison was not adjusted for differences in sampling period but they were recorded to all be within one minute of each other. The r^2 value is < 0.2. The poor correlation is not surprising given the results in figure 3-2.

A comparison of CHRCC-derived LWC and PVM measured LWC from Mt. Rigi in the Swiss Alps has been reported and an equation proposed to derive LWC from the CHRCC collection rate (Demoz *et al.*, 1996). It is not clear, without knowledge of the "true" LWC as measured by the PVM, which correlation to choose – "high" or "low" LWC. Based upon the results shown in figure

Reproduced with permission of the copyright owner. Further reproduction prohibited without permission.

3-2 it is not surprising that even allowing for collection flow rate differences that the equation proposed yields very poor results for SPL – the derived LWC averages only 40% of the measured

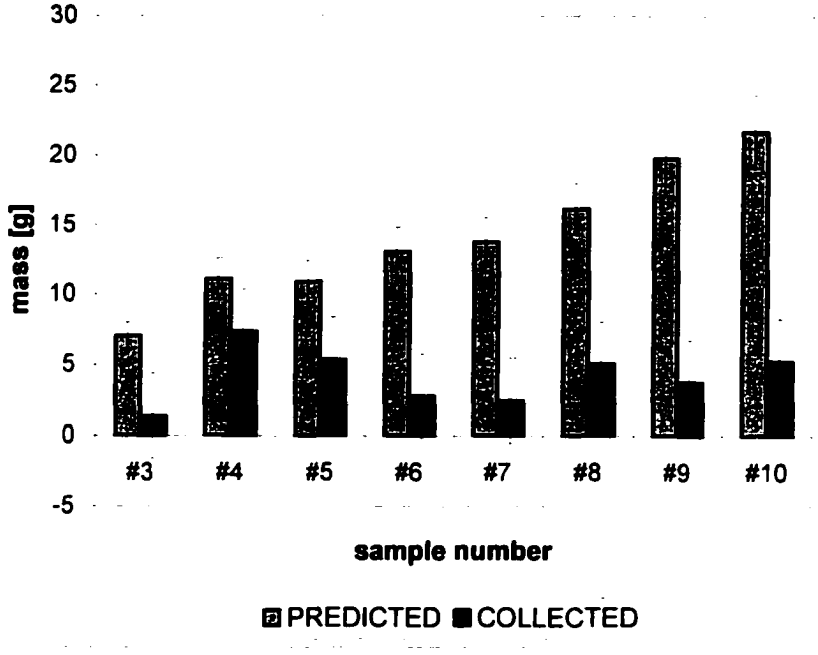

Figure 3-2: CHRCC predicted vs. collected mass (EVENT 8, 8 samples).

LWC (21% - 66% for 11 comparisons). This suggests that caution must be used when comparing correlations between different conditions (particularly when varying flow rates are used).

3.4 FROSTY evaluation

The FROSTY predicted vs. collected mass comparisons are shown by stage in figures 3-4, 3-5, and 3-6. These are calculated similarly to the CHRCC's predicted mass (section 3.3), but here the MEDIUM and SMALL stages cannot collect drops that impact upstream. An additional term has been added in the uncertainty calculations to reflect the fact that Straub (1999) reports confidence limits for the experimentally determined collection efficiency curves shown in figure 3-1 which vary up to 10% when converted to standard deviation. The uncertainty in collected mass is assumed to be 0.5 g as liquid water is pipetted directly from the collection surfaces, and flow

Reproduced with permission of the copyright owner. Further reproduction prohibited without permission.

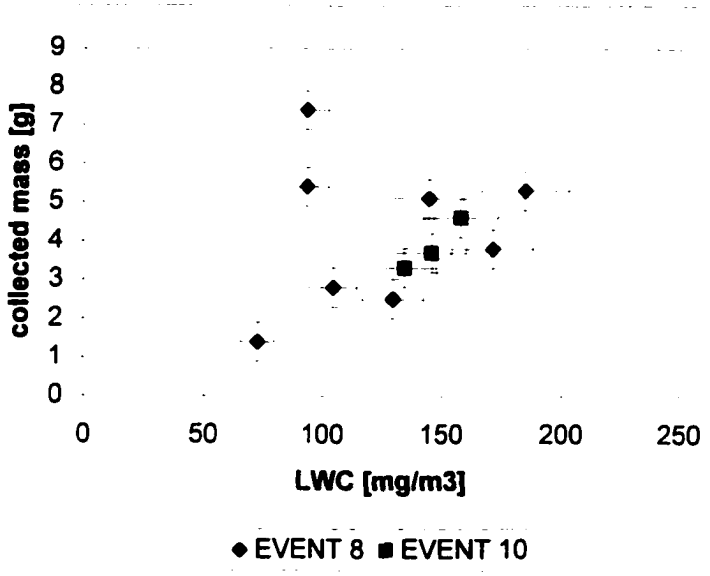

Figure 3-3: CHRCC collected mass vs. PVM LWC at SPL (2 events, 11 samples).

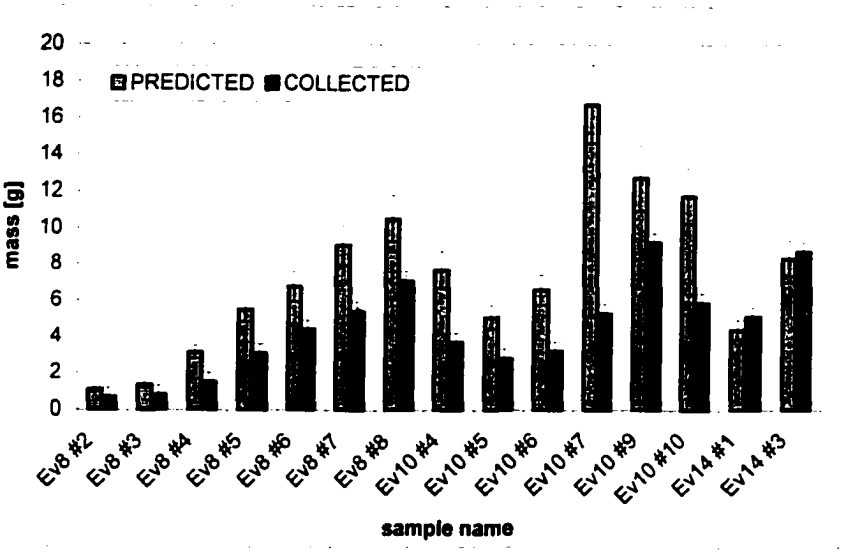

Figure 3-4: FROSTY LARGE predicted vs. collected at SPL (3 events, 15 samples).

rate uncertainty remains at an estimated 5%. The error bars shown represent plus/minus one propagated "standard deviation".

Reproduced with permission of the copyright owner. Further reproduction prohibited without permission.

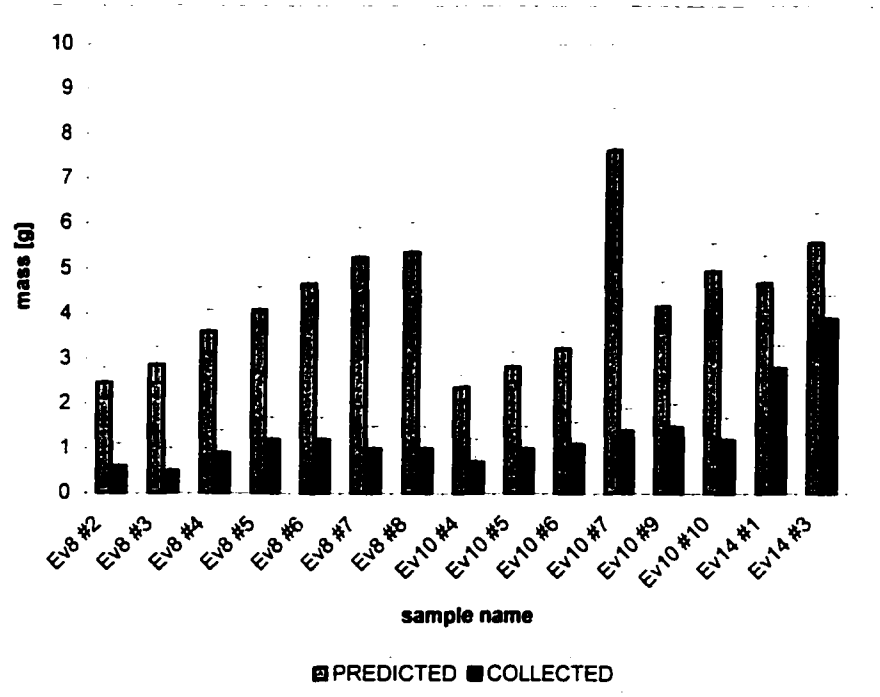

Figure 3-5: FROSTY MEDIUM predicted vs. collected at SPL (3 events, 15 samples).

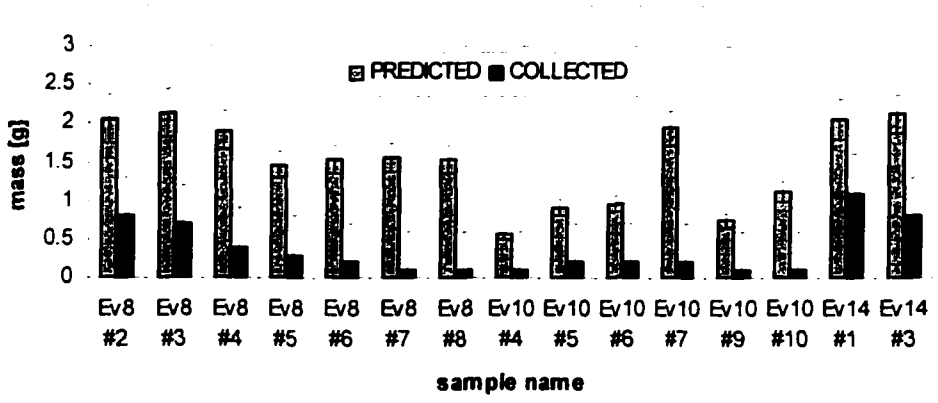

Figure 3-6: FROSTY SMALL predicted vs. collected at SPL (3 events, 15 samples).

While it is encouraging that the amounts of collected mass across the stages of FROSTY at least follow the trends in predicted mass reasonably for the data shown here, it also does not collect all the water predicted. Predicted/collected water mass is 86 – 316% (mean 174%), 143 – 575% (mean 376%) and 186 – 1573% (mean 679%) for the LARGE, MEDIUM and SMALL drop stages respectively. It is not known why the agreement for EVENT 14's two points is generally better

Reproduced with permission of the copyright owner. Further reproduction prohibited without permission.

than the others. The only difference in ambient conditions between these sampling periods and the end of EVENT 8 is a somewhat lower ambient wind velocity. This may suggest a change in aspiration efficiency or it just may be that the collector works more predictably at the start of an event as opposed to the end. The internal jets of FROSTY were observed to rime over during one time period (data excluded), but slight jet riming may be why the predicted/collected agreement gets relatively worse as the drops propagate through the collector. While there is considerable uncertainty in the measurements on the last stage, more water should still be collected. The limited amounts shown here jeopardize the ability to collect enough for analysis. Sample accretion on the impaction surfaces may also affect the collection efficiency curves for FROSTY to some degree, but ought to, in fact, lead to increased collection.

The FSSP data can be used for FROSTY where no PVM LWC data are available to investigate if proportionately the same relative amounts are being collected on each stage (figure 3–7). The total mass collected is used to normalize the drop distribution data so the sum of the LARGE, MEDIUM, and SMALL fractions is 100%.

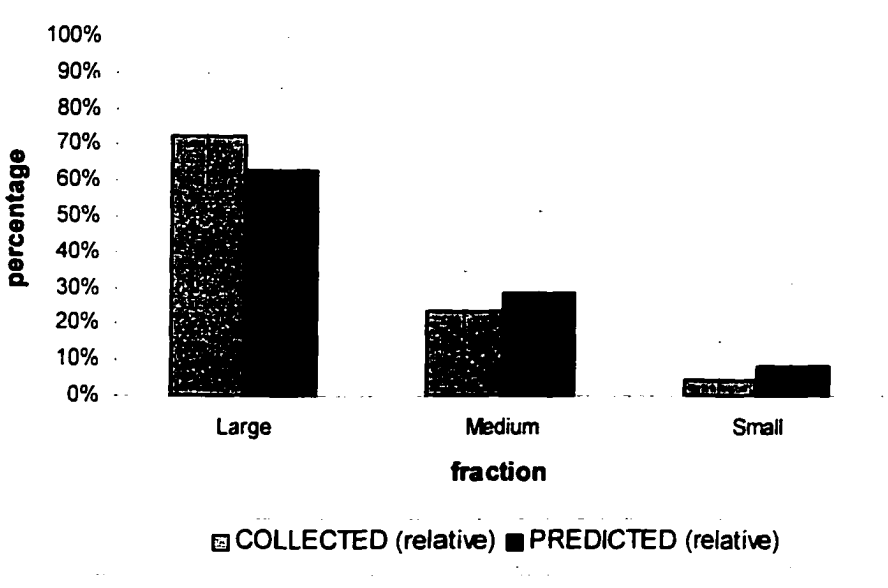

Figure 3-7: FROSTY relative predicted vs. collected performance, EVENT 9 #2 at SPL

Reproduced with permission of the copyright owner. Further reproduction prohibited without permission.

The predicted vs. collected performance shown in figure 3-7 is not surprising given the results shown in Figures 3-4 through 3-6 – while FROSTY appears to "underperform" it does so somewhat consistently. A random sampling of the other sample time periods where this calculation can be performed suggests this result is reasonably robust for Storm Peak.

The later campaign at Horsetooth Mtn. in Fort Collins (Chapter 6) permits this same kind of analysis for two sampling periods (figure 3-8). For both time periods the results are similar to each other but vary from those observed at SPL. While within the uncertainty, the LARGE fraction collects substantially more mass than predicted while the SMALL fraction collects consistently less. During these sampling periods at Horsetooth the calculated D_{eff}s were 10.2 and 7.7 μm, the wind speed was on the order of 1 m s^{-1}, and field notes indicate the cloud was relatively "light". As for SPL, this may be evidence of either non-ideal aspiration efficiency or a change in the surface collection efficiency resulting in smaller drops becoming collected earlier than predicted. There may be some size-dependent unquantified sampling problems that disproportionately affect smaller drops. It must be noted that at Horsetooth some mass on the large fraction was removed frozen prior to weighing the sample. As total mass is needed to perform this analysis, an amount "lost" was added to the calculations based upon the chemical analyses subsequently performed on the "lost" fraction in the laboratory. Even with generous estimates, it does not change the general result – too much water was collected on the LARGE fraction and too little in the SMALL compared to predictions, although the propagated uncertainty associated with this calculation is large.

FROSTY's collected mass at SPL correlates reasonably well with the PVM (r^2=0.58) for the samples shown. There is considerable noise, but notice that the EVENT 8 data points don't show similar outliers as the CHRCC's do.

Reproduced with permission of the copyright owner. Further reproduction prohibited without permission.

3.5 CHRCC vs. FROSTY

Two intercomparisons are possible – collected mass by each collector during comparable time

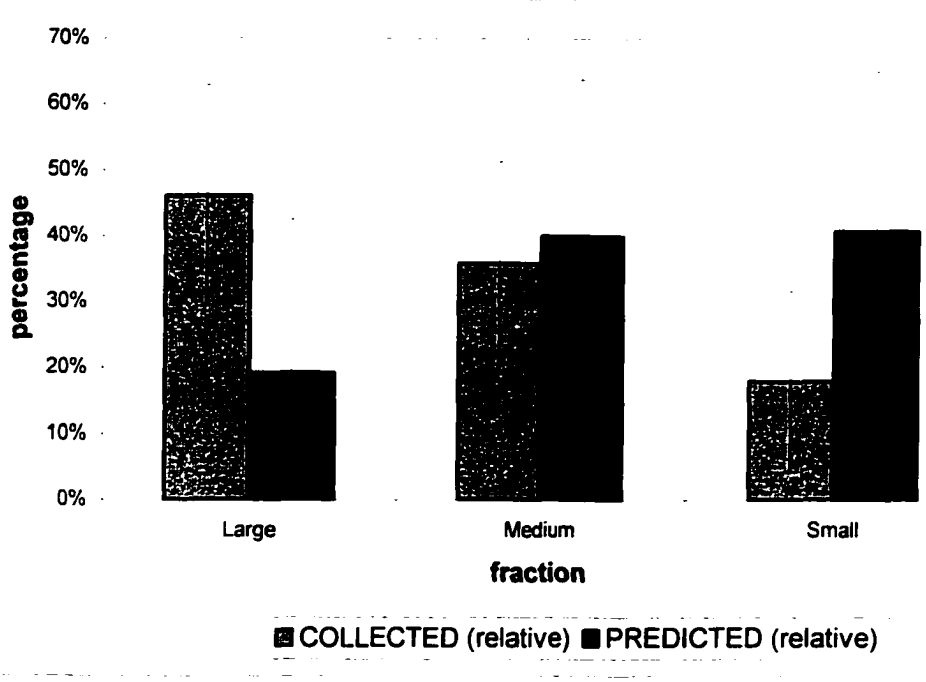

Figure 3-8: FROSTY relative predicted vs. collected water mass performance at Horsetooth Mtn (4/14/98, 1 – 2 a.m.).

periods (figure 3-10) and a "bulk" composition comparison. Given the preceding results, these comparisons must be interpreted appropriately. However, they do provide results useful for this type of analysis. The correlation between the masses of the two collectors was very high (r^2=0.94) and a reduced major axis fit yielded the following equation: y = 0.55x – 1.92 where x is the CHRCC collected mass in grams and y is FROSTY's in grams. FROSTY collected about double the mass of the CHRCC for a given time period despite the fact that the CHRCC flow rate is about 3.8 times larger. However, from this perspective the collectors do operate consistently relative to each other. Given the results presented above, however, this may just be fortuitous.

Reproduced with permission of the copyright owner. Further reproduction prohibited without permission.

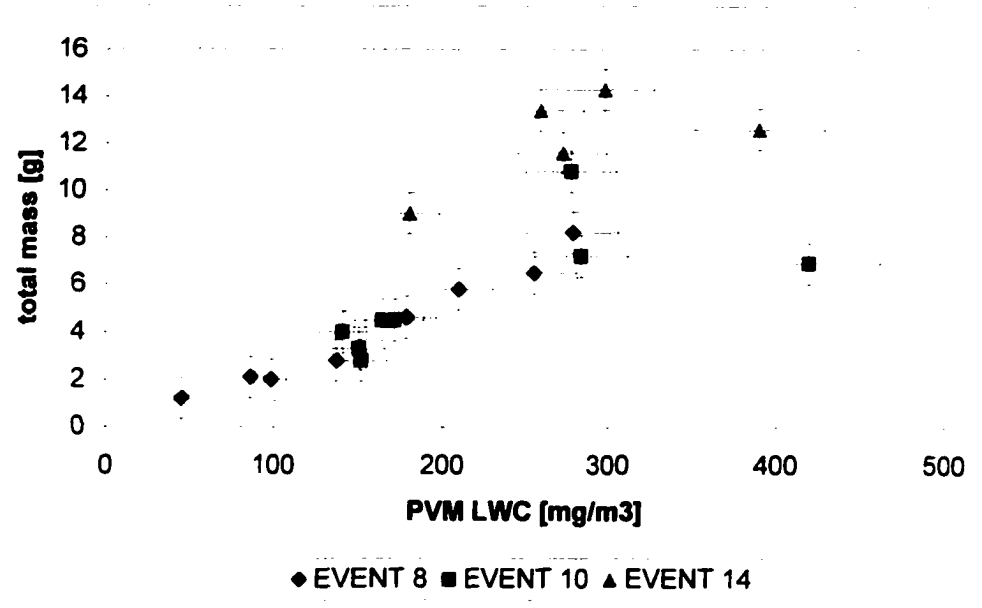

Figure 3-9: FROSTY vs. PVM at SPL (3 events, 21 samples).

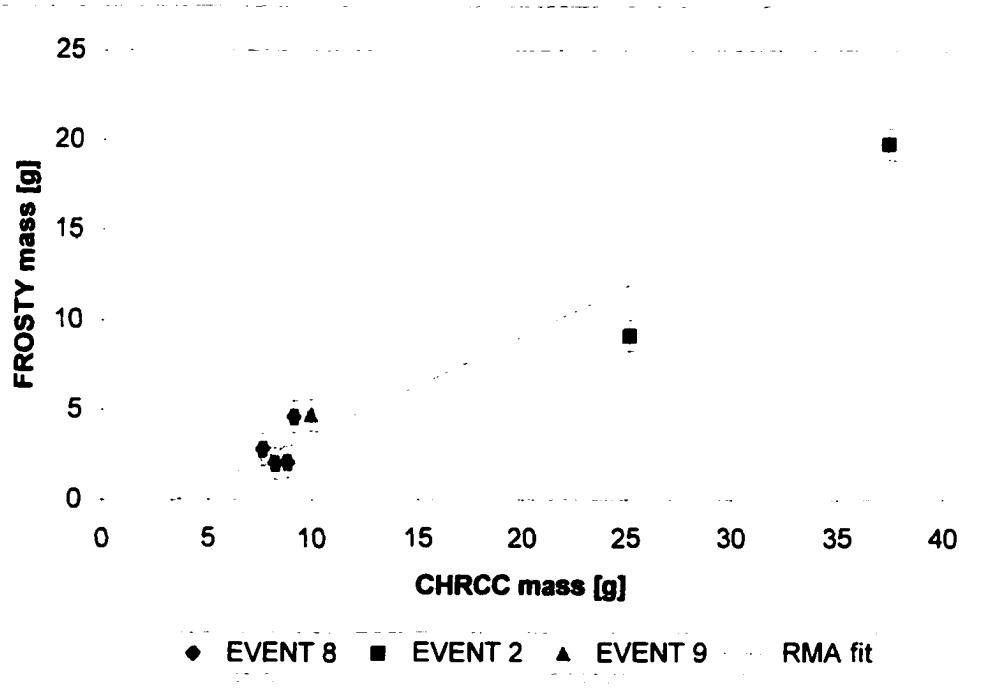

Figure 3-10: FROSTY vs. CHRCC collected mass at SPL (7 points, 3 events).

To perform a "bulk" composition comparison, the collectors must proportionately collect the same drops. It is evident in figure 3-1 that the overall collection curve for FROSTY is very much

Reproduced with permission of the copyright owner. Further reproduction prohibited without permission.

different from the CHRCC's (assuming both apply). A partial solution is to compare the composition of the LARGE and MEDIUM FROSTY stages only to the CHRCC. However, the CHRCC theoretically will collect substantially more small drops than either of those stages which will bias the calculation (as the smaller drops at SPL were more concentrated than the larger ones generally (see Chapter 6 or (Xu *et al.*, 1999)). As a compromise, 1/3 of the mass (and concentration) measured in the SMALL fraction can be added to these calculations as the resulting collection efficiency curve for FROSTY is a reasonable approximation to the CHRCC's curve. Calculations were performed with and without the SMALL fraction addition. The FROSTY derived "bulk" concentration is the volume-weighted average and the error bars shown include the analytical uncertainty. As before, the error bars shown are plus/minus one propagated "uncertainty". For the same seven samples shown in figure 3-10, a comparison of sulfate and nitrate (the species present in the largest concentrations which should not be affected by mixing) was performed.

For the MEDIUM and LARGE only comparison, the CHRCC/FROSTY sulfate and nitrate ratios were on average 139%, and their ranges were both from about 70% up to 200+% (standard deviation of 50%). Adding the 1/3 of the SMALL stage volume to the calculations did not change the results for nitrate, but variation in the sulfate range was reduced to 30% – 140%, with a 95% mean (standard deviation 40%). The sulfate and nitrate concentrations measured were in the range of approximately 20 – 200+ μN which should be quantified well. The explanation for the varying behaviour of sulfate and nitrate is that sulfate has a much shaper gradient in concentration between the MEDIUM and SMALL stages than nitrate (ratio of 1.8 on average compared to 1.3). Therefore adding some of the SMALL stage water disproportionately impacted the mean "bulk" sulfate concentration. Given the poor performance in the predicted/collected mass comparison for the collectors and the resulting likelihood that the collector efficiency curves may not adequately represent true collection characteristics at SPL, the agreement in this bulk chemical comparison is good. As a final note, it cannot be excluded that the relatively higher concentrations observed in the CHRCC may partly result from the fact that it is not quite sampling

Reproduced with permission of the copyright owner. Further reproduction prohibited without permission.

for the same time period as FROSTY. Further, the applied heating in the CHRCC needed for sample retrieval may result in some sample evaporation.

Figure 3-11 shows the FROSTY sulfate concentrations plotted as a function of the (theoretically collected) volume median drop diameter. Each point represents the actual composition measured on one of FROSTY's stages for a sampling period. The volume median diameter is calculated by multiplying the drop distribution data (dV form) by the collection efficiency curve across the entire drop spectrum. The predicted volume is summed for a particular stage and the median diameter determined. For the Caltech collectors, non-ideal aspiration efficiency as a function of wind speed is considered in this calculation. The evolution in concentration as the event progresses is clear and the gradient in concentrations decreases as the cloud drops become larger. Even if the collector efficiency curves themselves changed during the event and thus the composition represented for each stage is misleading, the figure nevertheless illustrates (if only qualitatively) the advantage of the FROSTY collector in representing size-dependent drop composition which cannot be done with the CHRCC. In particular, note that the calculated SMALL drop stage volume median diameter evolves from about 10 μm for the first time period shown to about 12 μm at the end (slightly greater than its experimental cut size). Plotting composition data as columns or lines that change in time miss this evolution in size (and also that the volume median drop diameter collected may be larger than the cut-size for the stage). Unlike the warm cloud collectors where the lower cut-sizes are approximately the same and theoretically similar "representative" cloud samples are obtained, the difference in lower cut-sizes (if accurate) for FROSTY and the CHRCC means that the concentrations obtained from each should not be plotted together unless some correction factor is taken into consideration.

3.6 Concluding Discussion

Reproduced with permission of the copyright owner. Further reproduction prohibited without permission.

The comparison between these two collectors and the additional measurement devices suggest that they did not predictably sample cloud drops at SPL. The limited nature of the Horsetooth comparison does not permit drawing firm conclusions, although the different results under

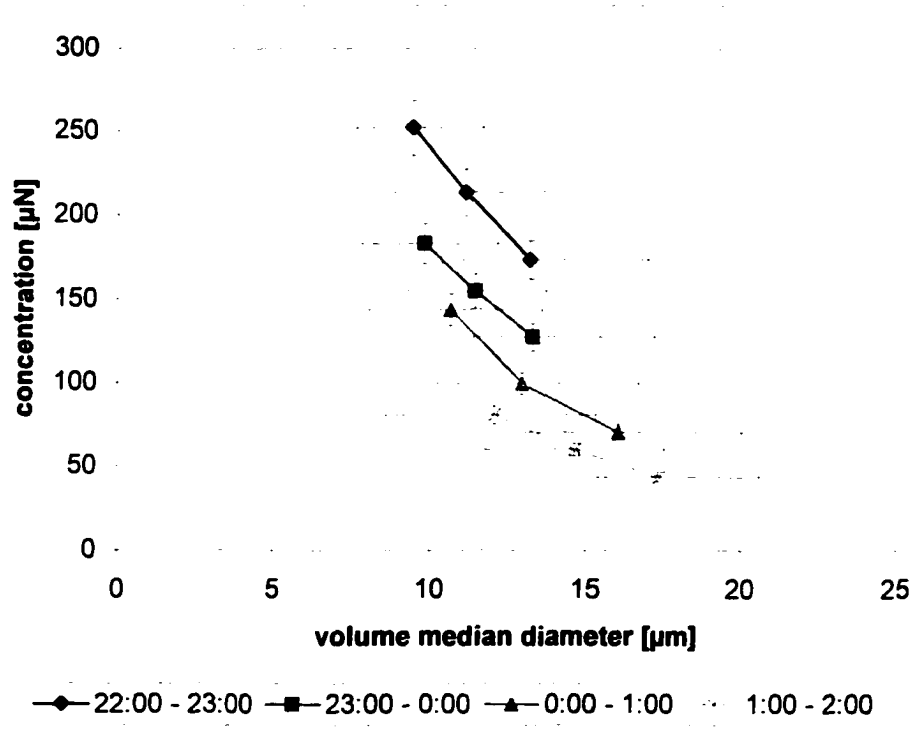

Figure 3-11: Temporal evolution of sulfate for FROSTY at SPL (EVENT 8). Horizontal error bars represent the diameters corresponding to 16% and 84% of the volume. Vertical error bars represent analytical uncertainty (RSD) only (6.6%).

dissimilar ambient conditions do suggest further questions to resolve regarding at least FROSTY's performance. While these are first results and have limitations, the observations suggest the collectors' field performance is not as well characterized as previously thought, at least for the ambient conditions experienced.

Comparing Horsetooth and SPL results, the FROSTY data suggest that drop size-dependent modification to either aspiration efficiency during sampling or due to possible changes in the internal configuration due to riming (either the jet or the collection area) may alter the overall collection efficiency. For the time periods studied, additional factors undoubtedly affect collection.

Reproduced with permission of the copyright owner. Further reproduction prohibited without permission.

It is worth noting that the experimental calibration technique (see Appendix B) could not, by its nature, address issues like these. Further, the apparent degradation in FROSTY's performance during EVENT 8 is consistent with internal riming (e.g. on the jets), although changes in aspiration due to the increasing D_{eff} cannot be excluded. That may in part explain why the data for EVENT 14 have a better fit – they were the first samples.

Poor aspiration efficiency and internal riming may also be affecting the performance of the CHRCC at SPL. In fact, the CHRCC's performance was much worse than FROSTY's. These results suggest that the CHRCC should not be used in conditions such as those at SPL in the future without (substantial) modification (assuming the sampling problems are identifiable and correctable). An important caveat, however, is that the CHRCC's theoretical collection efficiency has not been verified and may be an unquantified source of some of the mis-match between predicted/collected mass. While Demoz *et al.* (1996) found "reasonable" agreement in an earlier study the method used does not exclude this possibility. While available methods likely will not mimic the effect on collection that riming causes, an experimental or numerical investigation may indicate that the theoretical curve is not representative of actual performance. The magnitude of the discrepancy between predicted and collected mass, however, may be indicative of a larger problem (e.g. internal riming) than can be explained by an improved understanding of the collection efficiency curve. It should be emphasized that aside from the changes in ambient conditions previously mentioned there were no obvious wind shifts, for example, that should so sharply affect the overall collection efficiency and the collector was reasonably oriented into the wind.

As briefly mentioned earlier, bias in the PVM and FSSP at SPL could explain some of the results (e.g. the fairly constant over-prediction of sampled mass based upon the PVM's measurement of LWC). However, the volume intercomparison between the two was good, and, again, both pieces of equipment were routinely calibrated. The sizing corrections performed for the FSSP are extensive (see Appendix G), and the multi-event nature of most of the comparisons should

Reproduced with permission of the copyright owner. Further reproduction prohibited without permission.

indicate if a mis-calibration influences the result on a particular day. Within the data available, a problem like this is not clearly evident.

Unlike for the 5-Stage, the FROSTY wind shield did not appear to prevent a degradation in aspiration efficiency. It may be that the simple analysis used to size the wind shield was inadequate. Certainly the types of conditions experienced at the summit of Mt. Sonnblick where the CWS collector (Kruisz *et al.*, 1992) is routinely used should be more extreme than those at SPL, yet it is reported to work well. The drops at SPL were relatively small and should have been collected. This is true to a great degree at Horsetooth, although the lack of PVM data there hinders the analysis. A larger wind shield to more completely disrupt the ambient flow may improve results as may locating the inlet somewhat closer to the windshield. These are differences between the CWS collector's geometry and FROSTY's.

There does appear to be a clear benefit from using an impactor like FROSTY under these type of extreme atmospheric conditions. While removing sample from the CHRCC was very difficult, the FROSTY surfaces were easily replaced and sampling quickly re-started.

Several of the figures which "suggest" good agreement between the collectors were included to make the point that while one comparison (e.g. FROSTY vs. CHRCC collected mass) may be excellent, that others (e.g. predicted vs. collected mass for either collector) may indicate that performance is poor. This emphasizes the need to make as many measurements that can be compared as possible and to evaluate the equipment's performance using all possible methods. Internal consistency between all measurements is the goal. Field work using these two collectors in the future should certainly include measurements aimed at trying to resolve some of the performance issues raised here which are severe despite the limited size of the data set. More detailed knowledge regarding how different factors affect the collectors' field performance is needed in order to understand the results obtained.

Reproduced with permission of the copyright owner. Further reproduction prohibited without permission.

The variations observed in the predicted/collected mass comparison for FROSTY raise the issue of interpretation of size-dependent composition data when the ability to predict what drops are collected is poor. Given that anything other than individual drop-by-drop analysis represents some kind of average, if some drop sizes are preferentially excluded from the mixture, the resulting concentration may not be representative. While it may be the "best possible", it does not necessarily represent what actually occurred. In other words, if the mass in FROSTY cannot be predicted, the significance/interpretation of its observations with regard to the actual cloud is unclear. This issue applies to bulk collectors as well, but there, in fact, it is acknowledged that drop size-dependent variations are being averaged over. FROSTY, on the other hand, is intended to improve upon that and present a more accurate representation of cloud drop composition. While it does, in fact, show variation unobservable before, it is not clear what is being observed. Implicit in figure 3-11 is the assumption that the "right" drops are being proportionately sampled on each stage which the predicted/collected mass comparison does not necessarily support.

Finally, I do not believe that these results invalidate the interpretation of Xu et al., (1999), and, in fact, may help to explain some of the uncertainty observed in their analysis. They do represent, however, an additional caveat to the conclusions drawn regarding FROSTY's sample composition.

3.7 Further issues related to FROSTY's performance

During the SPL campaign at various times, I noted that the impaction pattern on the LARGE surface was somewhat different than expected. Typically, deposited material is located directly under the jets in impactors and this is what we observed on the MEDIUM and SMALL stages uniformly. On the LARGE stage this sometimes was observed. However, in other instances, two accreted ridges were observed to form parallel to the jet, but offset from the centerline equivalent

Reproduced with permission of the copyright owner. Further reproduction prohibited without permission.

distances in both directions. The design of FROSTY is predicated upon the condition that the collected supercooled drops freeze immediately upon impact. If they were not freezing immediately there was a possibility that collected sample was being lost and perhaps subsequently re-entrained in the flow with the potential to impact the results for the downstream stages.

For the conditions experienced at SPL, the residence time of the drops on the impaction surfaces assuming they were not frozen and moving at jet velocity is on the order of milli-seconds (neglecting friction, although Teflon itself has a very low friction coefficient). However, the approximate time required for the impacted drop to freeze for the SPL conditions (allowing for the collector's geometry in the drop freezing equation) is on the order of micro-seconds (equation 16.26, (Pruppacher and Klett, 1997) (p. 676)). While the use of this equation required making some assumptions which may not be entirely defensible, it is not likely that making more rigourous ones would change the results by the three orders of magnitude needed. Further, it cannot be ruled out that these observations were due to some kind of upstream turbulence or inlet effect which has been occasionally documented to cause non-ideal flow across ribbons (e.g. the impaction stage) (May and Clifford, 1967). This could explain why this pattern was observed on the LARGE stage and not the others. However, the more likely explanations involve two factors. The first is that impaction is a function of Stokes number and that drops with only "just" enough inertia to be collected will be located at a distance offset from the centerline (Sethi and John, 1993). This has been observed in impactors before. Secondly, the accreting drops as discussed above do alter the texture of the Teflon surface. This may produce different regions of "preferred" impaction on the surface (e.g. alter the collection efficiency curve). I am not sure if "wet growth" conditions similar to those observed for hail can occur within FROSTY, but it is clearly evident during operation if drops are not freezing (see Chapter 6).

One issue raised by many authors (Hindman *et al.*, 1992, among others) who work in the field of rime collection is whether or not vapor deposition will occur to the accreted drops during

Reproduced with permission of the copyright owner. Further reproduction prohibited without permission.

sampling. Vapor deposition, in this case, would represent contamination. Following the treatment of Baker and co-workers (1987) as suggested by Hindman *et al.* (1992) for likely FROSTY sampling conditions, calculations suggest that while some deposition may occur it is likely to be insignificant compared to the accreted mass. The same conclusion is reached based upon figure 13-29 in Pruppacher and Klett (1997) (p. 550) with similar approximations made to reflect collector geometry as in the drop freezing calculation. Here again, the calculations are only approximate, but neither seem worthy of a more thorough investigation barring additional field work raising new questions regarding FROSTY's performance. Most authors reach similar conclusions (Voisin *et al.*, 2000), except in both low LWC (< 0.08 g m^{-3}) and cold (< -11 to 12°C) conditions (Snider and Huang, 1998; Snider *et al.*, 1992) or where measured accreted masses are on the order of theoretical deposition masses (Hindman *et al.*, 1992).

Reproduced with permission of the copyright owner. Further reproduction prohibited without permission.

4. Field performance of the warm cloud collectors – the Caltech Active Strand Cloud water Collector #2 (CASCC2), the size-fractionating Caltech Active Strand Cloud water Collector (sf-CASCC), and the 5-Stage

In this chapter theoretical considerations and field measurements will be combined to assess how well the three warm cloud collectors – the CASCC2, sf-CASCC and 5-Stage* – work. While the original goal was solely to evaluate the 5-Stage's performance, it became clear as that work progressed that the other two collectors had to be included in order to resolve questions that arose. Different data sets are available for the three warm cloud campaigns – ACE2, Whiteface and Davis – which limit the calculations that can be performed. However, an overall sense of the collectors' field performance can be determined both compared to each other and to other equipment.

A series of comparisons are presented which use both collected mass and composition measurements. First, as two different sf-CASCCs were used during these campaigns, the data from a side-by-side comparison at Whiteface are included to show the validity of intermingling their results. Both sf-CASCC and CASCC2 collected masses are compared and their performance evaluated against simultaneous Gerber PVM-100 LWC measurements. For Whiteface and ACE2, drop size distribution data are available which permit evaluation of the sf-CASCC and CASCC2 collector efficiency curves. The 5-Stage's collection efficiency curves are similarly evaluated by comparing collected masses in the individual stages to the predicted masses. Finally, the three collectors' sampled mass and bulk or derived "bulk" composition are

*parts of the 5-Stage evaluation have been previously reported in Moore, K. F., Sherman, D. E., Reilly, J. E. and J. L. Collett, Jr. (2001) Development of a multi-stage cloud water collector: 1. Design and field performance evaluation (in press, *Atmospheric Environment*)

Reproduced with permission of the copyright owner. Further reproduction prohibited without permission.

compared. Discussion will follow each set of results, and there are some final summarizing comments.

This chapter uses data selectively from each of these campaigns. In order to prevent duplication, only the data most important to these comparisons will be included here. Each campaign chapter should be consulted for site descriptions and supporting information – ACE2 (Chapter 7), Whiteface (Chapter 8), and Davis (Chapter 9). Chapter 5 (Sampling protocols) may also be useful. Tabulated data for this chapter can be found in Appendix H.

4.1 sf-CASCC side-by-side comparison

The ACE2 sf-CASCC uses stainless steel fasteners and the cartridges for the Teflon strands are Teflon-coated metal. While these potential sources of metal contamination should rarely come in contact with any sampled cloud water, an improved approach is to construct the collector completely out of plastic similar to the modifications made by Klemm *et al.* (1991) (Appendix B). Prior to Whiteface, the "new" sf-CASCC was built and no metal parts were used. Its design and dimensions were virtually identical to the "old" (ACE2) sf-CASCC. All "official" Whiteface and Davis sf-CASCC data are from the new collector.

In order to establish experimentally that the collectors worked similarly, they were operated side-by-side during the W188 event at Whiteface. Although it was raining prior to the event, sampling did not commence until after the rain stopped. There was a light wind (4.4±0.9 m s^{-1}) from the S – SW, the temperature was 12.0±0.2°C and the LWC event average was 430 mg m^{-3}. Starting with sample period #2, side-by-side operation continued until 15 sample pairs were obtained from each collector. In most instances a full aliquot set was performed for both collectors. The first three samples were one hour in length and the next 12 were every thirty minutes.

Reproduced with permission of the copyright owner. Further reproduction prohibited without permission.

4.1.1 Side-by-side results

Timelines of the collected mass and nitrate concentrations for both collectors broken down by Large and Small drop fractions are shown in figures 4-1 and 4-2. The timelines are plotted to the mid-point of the sampling period. Figure 4-3 compares the potassium ion concentrations between the two collectors and table 4-1 summarizes the calculated residual standard deviations (RSDs) for each comparison. Figure 4-4 shows the measured iron timeline. Error bars represent analytical uncertainty only.

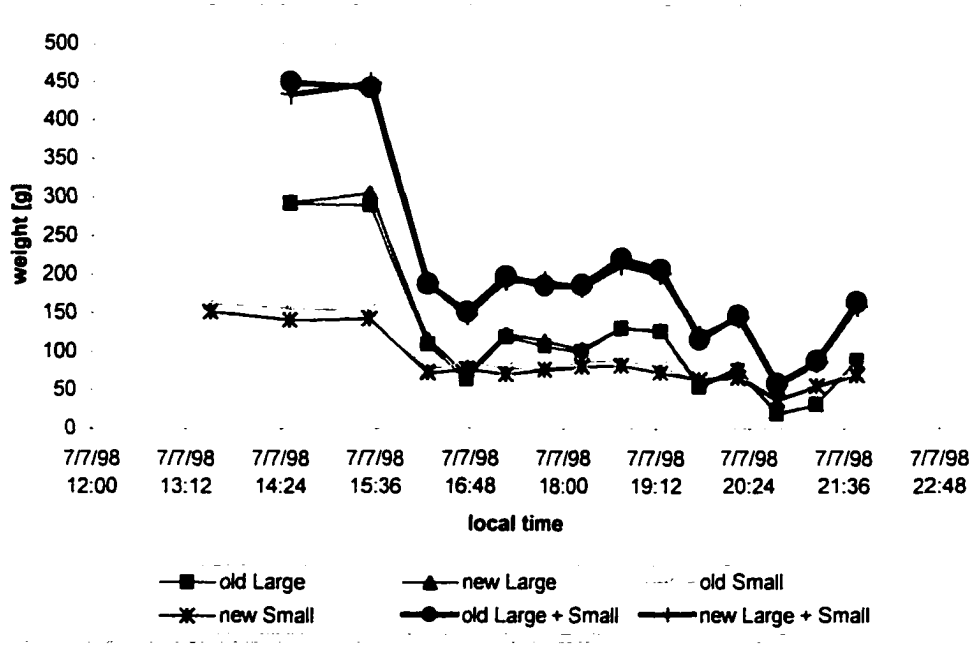

Figure 4-1: W188 sf-CASCC side-by-side comparison – collected mass

4.1.2 Side-by-side discussion

The collected mass comparison between the two collectors is very good, as is the nitrate comparison. The timelines track each other well (figures 4-1 and 4-2). Concentrations tended to be relatively low during W188 – possibly because of the earlier rain – but even ions measured at very low concentration (e.g. potassium) compare reasonably well in absolute terms between the

Reproduced with permission of the copyright owner. Further reproduction prohibited without permission.

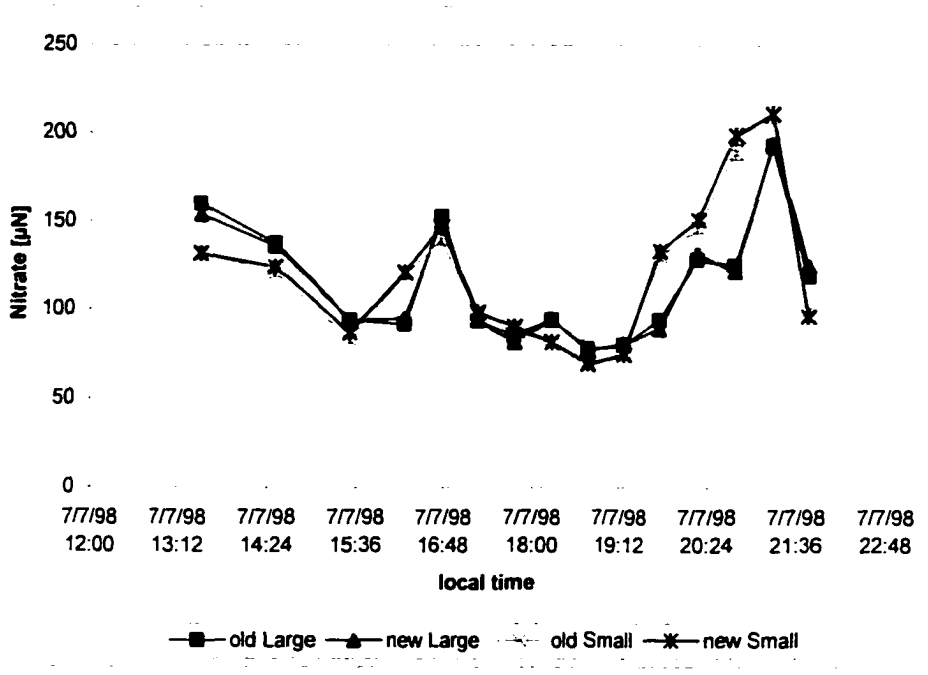

Figure 4-2: W188 sf-CASCC side-by-side comparison – nitrate

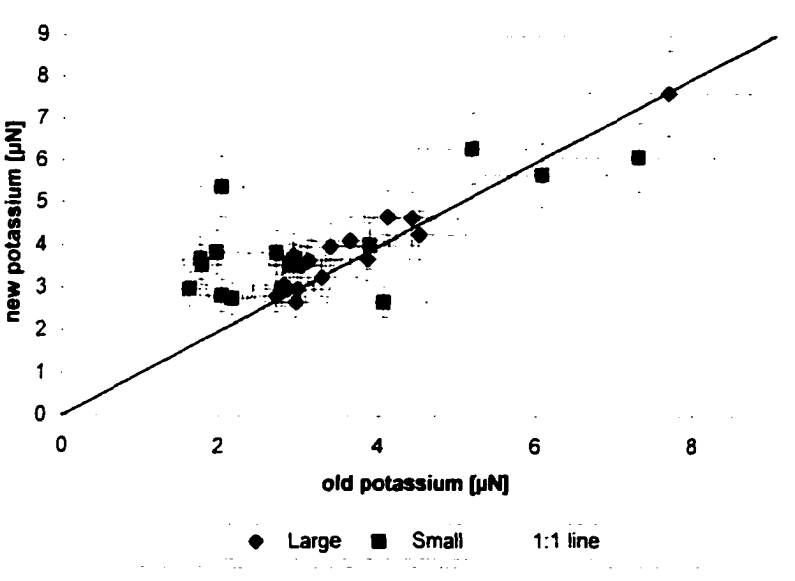

Figure 4-3: W188 sf-CASCC side-by-side comparison – potassium ion

Reproduced with permission of the copyright owner. Further reproduction prohibited without permission.

Table 4-1: W188 sf-CASCC side-by-side comparison – tabulated results

Results by fraction	mass	pH	Chloride	Nitrate	Sulfate	Sodium ion	Ammonium	Potassium ion	Magnesium ion	Calcium ion	Iron	Manganese	H_2O_2	HCHO
	[g]		[μN]	[μN]	[μN]	[μN]	[μN]	[μN]	[μN]	[μN]	[μg l^{-1}]	[μg l^{-1}]	[μM]	[μM]
Large														
n	14	15	15	15	15	15	15	15	15	15	15	15		
minimum	19.4	2.91	6.5	77.9	233	1.4	107.3	2.7	3.6	11.9	36.6	2.2		
maximum	305.7	3.54	19.4	193.7	1307	3.8	294	7.7	10.5	42.3	113	8.4		
mean	116.7	3.34	9.1	114.8	439.9	1.9	142.5	3.8	5	21.6	54.7	4		
RSD	3%	0.7%	13.6%	2%	5.4%	36.9%	1.7%	7.6%	25.9%	29.1%	27%	12.2%		
Small														
n	15	15	15	15	15	15	15	15	15	15	15	15		
minimum	36.8	2.9	6.9	68.4	212.7	0.8	106.3	1.8	2.5	6.9	15.2	0.7		
maximum	162.8	3.58	13.1	211.1	1422	5.1	319.3	7.3	13.9	36.7	73.5	5		
mean	87.1	3.33	9.5	120	496.9	2.4	159.4	3.6	4.3	12.1	35.5	2.2		
RSD	6%	0.3%	14.1%	2.3%	4.8%	56.4%	3.8%	28.2%	42.8%	47.4%	30.7%	19.3%		
Large + Small														
n	14												8 total*	8 total*
minimum	56.8												5.6	5.4
maximum	449.4												13	9.5
mean	198.8												9.3	7.3
RSD	2%												8.4%	6.6%

n = number of samples

** HCHO and H_2O_2 analysis grouped Large and Small pairs together due to low number*

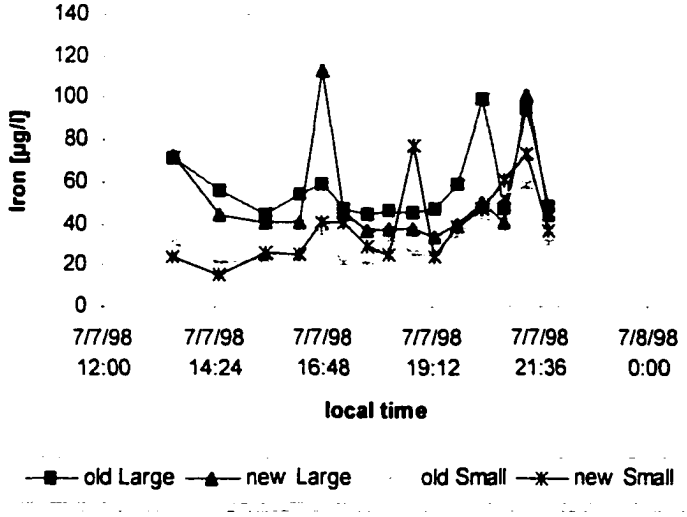

Figure 4-4: W188 sf-CASCC side-by-side comparison – iron

Reproduced with permission of the copyright owner. Further reproduction prohibited without permission.

two collectors (figure 4-3). Table 4-1 summarizes the results. For species measured at high concentrations (e.g. not sodium, potassium or chloride) the RSDs calculated between the two collectors are less than or on the order of the analytical RSDs (Chapter 5). Iron and manganese are two exceptions, however. Figure 4-4 illustrates that on different fractions at varying times an iron concentration spike may be observed, although concentrations resume tracking each other in the next sampling period. We do not generally filter the Metals aliquots prior to acidification/preservation ("Metals" refers specifically to the species Fe, Mn and (occasionally) Cu). These spikes may be evidence of colloidal material that is not homogeneously distributed in the cloud water. The analytical RSD for iron is 2.8% for this campaign and is much lower than the table 4-1 RSD. Similar results are found for manganese (not shown). The effects of filtering on reported cloud water concentrations for iron and other species can vary between events and locations (Siefert *et al.*, 1997, among others). The analytical uncertainty for Fe and Mn may not adequately capture the true variability between samples. An interesting feature of these iron results is that neither set has been blank-corrected. The old sf-CASCC had been cleaned at CSU and its blank concentrations were negligible. The new one had been field cleaned at Whiteface. The DI, Large fraction and Small fraction blanks for the new collector in this event are 39.0, 44.7, and 39.8 $\mu g\ l^{-1}$, respectively. The measured concentrations between the two collectors were highly similar without blank correction (figure 4-4). Blank correction would have markedly worsened the comparison – no blank correction appears to be "necessary" at all. This represents field evidence that blank-correcting metal concentrations is not necessarily straight-forward (at least for high-volume collectors).

These results suggest that data collected by the two versions of the sf-CASCC can be used interchangeably. As the collectors were very closely co-located horizontally and vertically, little can be gleaned about cloud inhomogeneity (with the possible exception of Fe and Mn).

Reproduced with permission of the copyright owner. Further reproduction prohibited without permission.

4.2 CASCC2 and sf-CASCC mass comparisons

The collected sample masses in the CASCC2 and sf-CASCC are compared to each other and to the LWC measured by the Gerber PVM-100 using data from all campaigns. Linear equations are derived to calculate the LWC given a CASCC2 or sf-CASCC total mass measurement. These results are used to evaluate the PVM-100's performance in the Davis fogs and an earlier equation proposed to calculate the LWC based upon the CASCC2 collection rate. Finally, some Whiteface data are used to illustrate how collection rates are affected when the collectors are not aligned with the ambient wind.

All of the data presented have been standardized to one hour sampling periods with the collectors oriented into the wind. For the sf-CASCC there are 30 ACE2, 49 Whiteface and 53 Davis sample pairs (132 total); there are 47 Whiteface and 53 Davis samples (100 total) for the CASCC2. These samples were obtained in orographic clouds of variable wind speed (up to 17 m s^{-1}) and radiation fogs where the ambient wind speed was < 2 m s^{-1} with validated LWC sampling period averages ranging from approximately 50 to 800 mg m^{-3}.

4.2.1 CASCC2 vs. sf-CASCC collected mass

CASCC2 and sf-CASCC collected mass correlate very well with each other (r^2 = 0.94) (figure 4-5). The data points cluster around a line representing the ratio of their nominal flow rates (19 m^3 min^{-1}/5.8 m^3 min^{-1}). This suggests that the collectors work consistently with respect to each other under varied conditions.

4.2.2 CASCC2 and sf-CASCC collected mass vs. measured LWC

At Whiteface and Davis, our PVM-100 was used to measure the LWC and was co-located with the collectors. At ACE2, the UMIST PVM-100 was used. Figures 4-6 and 4-7 show the CASCC2

Reproduced with permission of the copyright owner. Further reproduction prohibited without permission.

and the total sf-CASCC collected masses plotted against the PVM-100's measured LWC. The

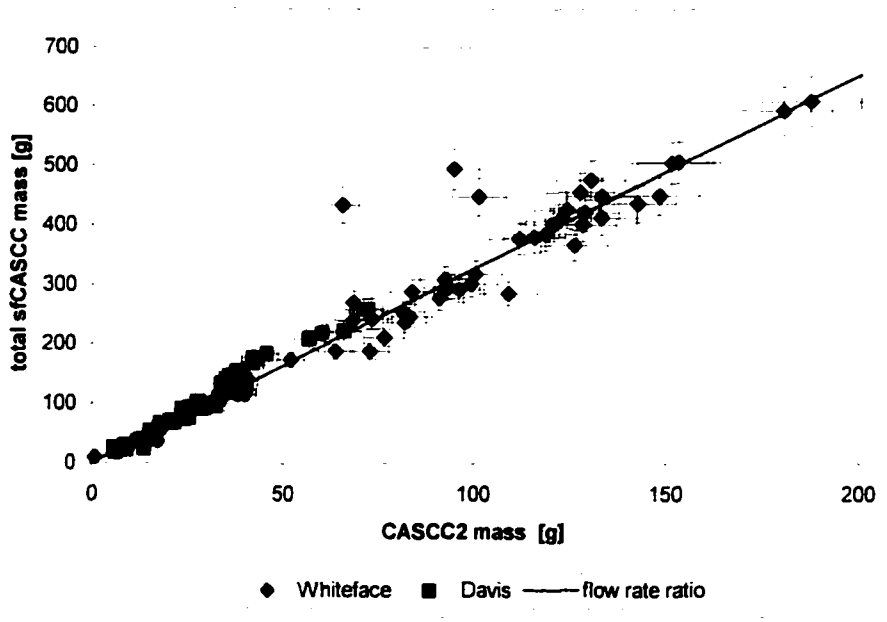

Figure 4-5: total sf-CASCC vs. CASCC2 collected mass for the Whiteface and Davis campaigns. Error bars represent combined estimated flow rate and residual mass uncertainty (7%).

PVM LWC measurement uncertainty is estimated to be 10% (Gerber *et al.*, 1994). ACE-2 data obtained in high wind conditions are consistent with Whiteface data at lower wind speeds suggesting that wind-ramming through the sf-CASCC may not have occurred to sufficient degree to impact the results. Correlation is very good for both comparisons ($r^2 > 0.90$); however, careful examination suggests that there may be a bias in some of the Davis data for LWC < 100 mg m^{-3}. There is a noticeable "hump" in both figures where collected mass is almost independent of measured LWC. A review of the literature on PVM-100 performance in clouds with high (approximately > 20 μm) volume median diameters (VMDs) is given in Appendix I. While somewhat controversial, studies in both controlled and ambient environments with high VMDs suggest that the PVM-100's performance may severely decline (see (Wendisch *et al.*, 2000; Wendisch, 1998), Appendix I, and references therein).

Reproduced with permission of the copyright owner. Further reproduction prohibited without permission.

4.2.2.1 Revised Davis LWC data

As figures 4-6 and 4-7 and the literature review indicated that the measured LWC in the Davis fogs might be incorrect, Davis LWC can be revised based upon collector performance at the other locations incorporating any "good" data from Davis where possible. Many investigators use collected mass measurements to derive ambient LWC (Appendix B and references therein). No independent measurements of the drop size distribution are available for Davis. Using the PVM-derived D_{eff} as a surrogate for VMD, all data points were removed where $D_{eff} > 20$ μm. As a result, many (43 out of the 53) Davis sampling periods were eliminated (figure 4-8 shows the remaining points). For both collectors, the parameters for a reduced major axis linear fit (Miller and Kahn, 1962, pp. 201 - 210) were calculated to relate collected mass to the PVM data. The reduced major axis approach was used in lieu of a standard least squares regression as both data sets were subject to error. If total sf-CASCC mass is available then the equation is:

$$mass = 0.827(lwc) - 24.7 \qquad (4\text{-}1)$$

where mass is in [g] and "lwc" is in [mg m^{-3}]. The CASCC2 equation is:

$$mass = 0.238(lwc) - 2.9 \qquad (4\text{-}2).$$

The standard error of the intercept and slope for the sf-CASCC are 5.80 and 0.016, respectively, for 88 points. The CASCC2 equation is based upon 58 points and the standard error of the intercept and slope are 3.74 and 0.009. In both figures, correlation is very good (r^2=0.96 (sf-CASCC) and r^2=0.92 (CASCC2)). The sf-CASCC equation with the filtered data set is shown in figure 4-8; figure 4-9 presents the CASCC2's results. Most of the apparent bias in the Davis PVM data is removed. Both equations 4-1 and 4-2 have negative intercepts suggesting that some threshold value of LWC must be achieved before sample volume can be obtained. This is not physically unrealistic. For the Davis campaign new LWC values need to be calculated for the

Reproduced with permission of the copyright owner. Further reproduction prohibited without permission.

sampling periods where PVM data has been discarded. Table 4-2 summarizes the changes made and the values represent the average of the LWC calculated using equations 4-1 and 4-2.

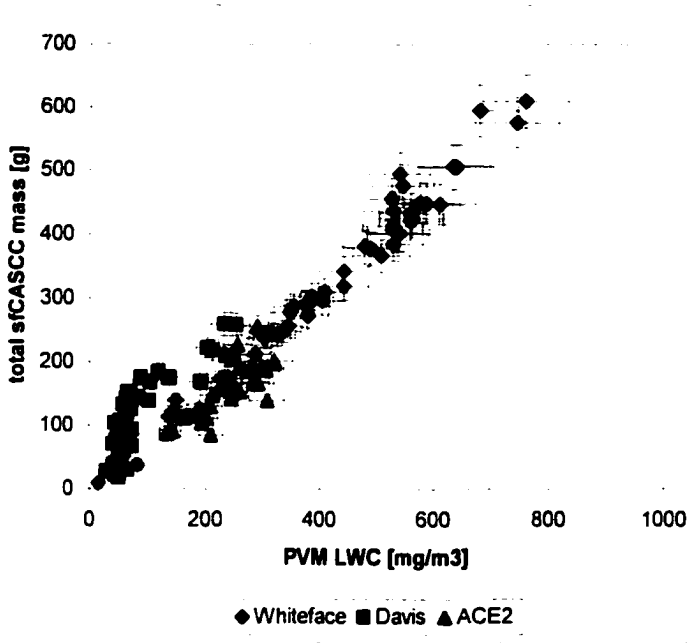

Figure 4-6: Total sf-CASCC collected mass vs. PVM LWC. Error bars represent mass and LWC measurement uncertainty

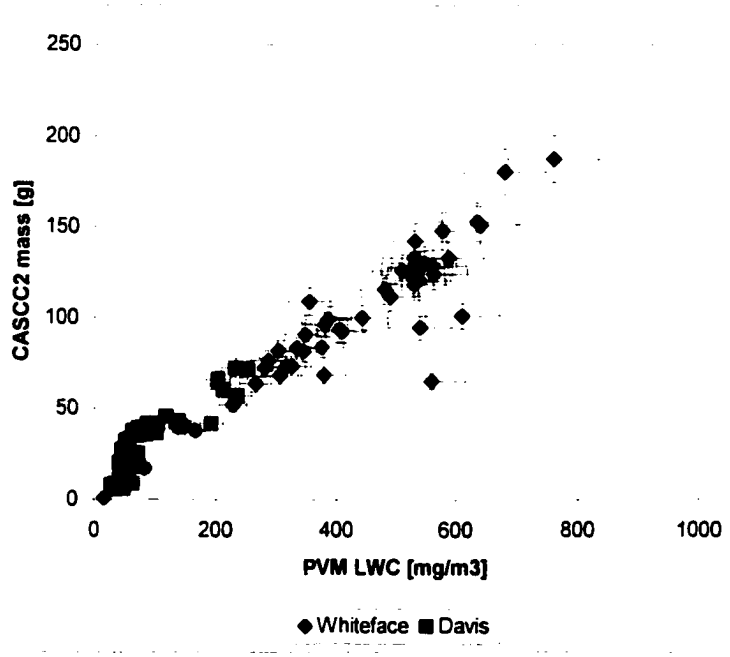

Figure 4-7: CASCC2 collected mass vs. PVM LWC. Error bars represent mass and LWC measurement uncertainty.

Reproduced with permission of the copyright owner. Further reproduction prohibited without permission.

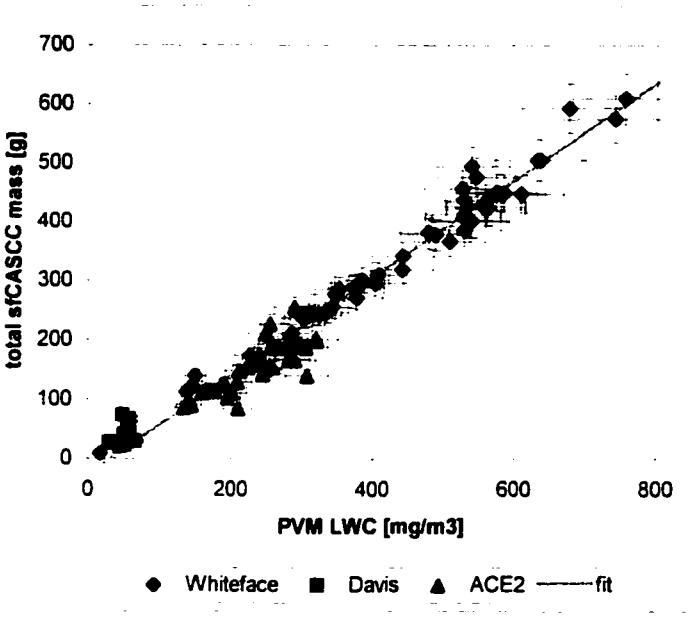

Figure 4-8: Filtered sf-CASCC collected mass vs. PVM LWC with reduced major axis fit equation shown

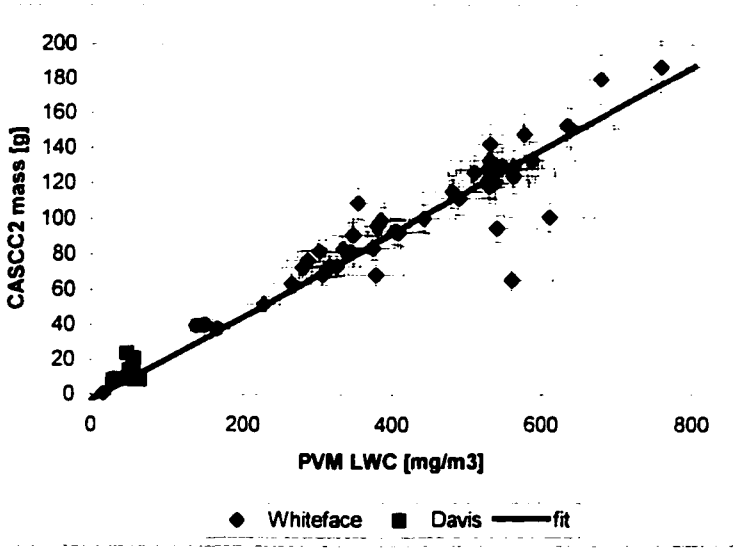

Figure 4-9: Filtered CASCC2 collected mass vs. PVM LWC with reduced major axis fit equation shown

While events D009 and D010 do not change significantly as fewer data points were revised, the other five events change substantially. Mean event LWC essentially doubles (the mean ratio of original to revised LWC for the 43 sampling periods is 56% (range 32% - 115%)). Several

Reproduced with permission of the copyright owner. Further reproduction prohibited without permission.

Table 4-2: Summary of revised LWC data for Davis

event	revised/ total samples	measured LWC range [mg m^{-3}]	mean measured LWC [mg m^{-3}]	revised LWC range [mg m^{-3}]	mean revised LWC [mg m^{-3}]
D352	8/9	50 - 252	171	44 - 330	222
D004	13/13	51 - 137	81	125 - 228	186
D009	3/8	29 - 65	51	29 - 177	81
D010	2/6	34 - 57	49	34 - 67	53
D010B	8/8	33 - 74	56	49 - 141	101
D011	8/8	42 - 72	59	70 - 179	133
D013	1/1		47		120

arguments support this revision. First, as indicated previously, the PVM appears to measure "low" in high VMD environments. The factor of 2 difference found here is larger than laboratory experiments indicate, but the combination of low LWC and high VMD found in these fogs is difficult to duplicate in controlled environments and each PVM may behave differently (Wendisch *et al.*, 2000). The high D_{eff} measured by the PVM – although subject to error – is supported by the collected water distribution in the 5-Stage and the sf-CASCC. While drop size distributions are not available for the Davis campaign, unpublished IMS95 data and the CHEMDROP94 campaign (Wendisch *et al.*, 1998) data obtained in radiation fogs are also consistent with the collected water distributions in the collectors and high D_{eff}s (possible drop distributions and a brief discussion of fog microphysics are included in Chapter 9). During the Davis campaign, Teflon deposition plates were placed around the cloud sampling site to measure water and species fluxes. If the measured LWC is correct, over an order of magnitude change occurred in the flux between sampling periods with no concurrent change in ambient LWC, although, of course, the flux depends upon the drop distribution as well. Revised LWC values tend to increase with the measured water flux (not shown). Calculations of the mean drop size (see Chapter 9) using the revised LWC and deposition data are more typical for radiation fogs (30 – 40 μm) observed in other locations than are calculated using the measured LWC data (up to and exceeding 70 μm). The sf-CASCC and CASCC are oriented parallel to the ground so sedimentation into the inlets should not occur and affect the collected mass results. Finally, as shown in figure 4-5, the two collectors appear to work consistently relative to each other in all locations.

Reproduced with permission of the copyright owner. Further reproduction prohibited without permission.

4.2.2.2 Evaluation of a previously proposed CASCC2-LWC equation

An equation has been proposed to calculate the cloud LWC (up to LWC = 500 mg m^{-3}) based upon the CASCC2 collection rate (Demoz *et al.*, 1996). The proposed equation uses an assumed drop distribution and the theoretical collection efficiency curve (figure 4-12) for the CASCC2 (Demoz *et al.*, 1996, and references therein). The proposed equation was evaluated against the measured LWC and collected CASCC2 data for these campaigns (36 validated data points for Whiteface and Davis). The RSD between the measured and calculated LWC is approximately 19% and the calculated LWC on average is 115% of the measured LWC (range 50% - 199%) which is a positive bias, although within the uncertainty. The estimated error in LWC via this proposed equation is ± 20% which is generally validated by this sample set. The positive bias is consistent with the CASCC2's performance evaluated using the drop size distributions (section 4.3). Advantages of equations 4-1 and 4-2 are that their validity is not limited to LWC < 500 mg m^{-3}, and the results are valid for the range of ambient conditions experienced in these campaigns.

4.2.3 Collector orientation

While some collectors – particularly passive ones – are omni-directional, most active collectors, including the CSU collectors, are designed to be oriented into the wind (see Appendix B). Figure 4-10 shows the Whiteface CASCC2 mass vs. PVM LWC data plotted by event (sf-CASCC results are similar).

The W185 data which have previously been excluded from figures 4-5 through 4-8 are included here. The W185 data have a markedly different slope than the other data. Following the evaluation steps outlined by Miller and Kahn (1962, pp. 201 - 210), the slopes of the two lines are statistically different and the two axes represent samples from statistically different populations

Reproduced with permission of the copyright owner. Further reproduction prohibited without permission.

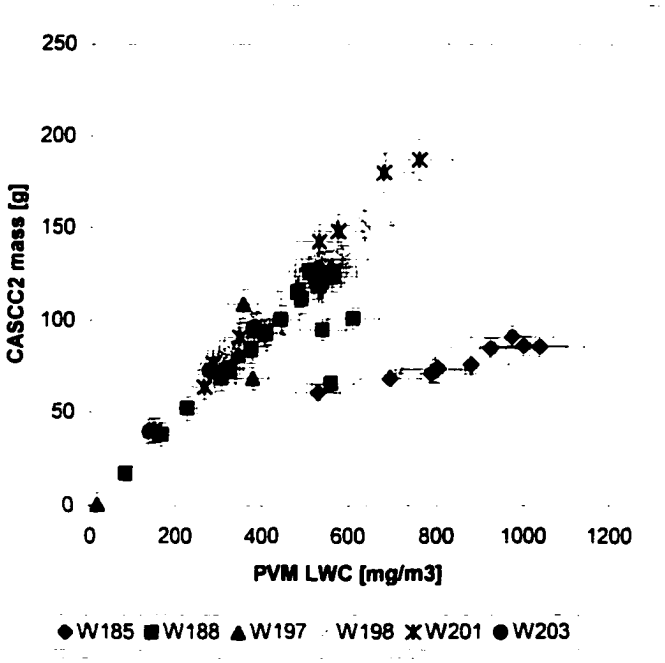

Figure 4-10: CASCC2 collected mass vs. PVM LWC by event at Whiteface. Error bars represent mass and LWC measurement uncertainty.

(the calculated "Z" statistic > 8 for both CASCC2 and sf-CASCC data sets). While very little meteorological data exist for the W185 event, field notes indicate that collectors were oriented at approximately 135° to the ambient wind. As a result total collection rates are lower and it is unknown how this misalignment affected the distribution of both aspirated and collected drops. Therefore, the W185 data are generally excluded from the analysis here and in other chapters.

4.3 Evaluation of CASCC2 and sf-CASCC collection efficiency curves

In this section, the collection efficiency curves for the CASCC2 and sf-CASCC are evaluated using drop distribution data from ACE2 and Whiteface. The goal is to determine if the collection efficiency curves adequately predict the physical mass of water sampled. Several theoretical treatments are given (Demoz *et al.*, 1996; Munger *et al.*, 1989a) in the literature, but no drop size distribution data were available. Relevant cloud microphysical parameters will be described first,

Reproduced with permission of the copyright owner. Further reproduction prohibited without permission.

followed by the collection efficiency curves and predicted vs. collected mass comparisons. Aspiration efficiency is specifically treated for the CASCC2 and sf-CASCC. The collection efficiency curves are assumed to include all other factors affecting drop collection.

4.3.1 Drop distribution data

Validated drop distribution data are available for 4 of the 5 ACE2 events and from 2 of the events at Whiteface (W188 and W198). Drop distribution data processing is described in Appendix G. Twenty sampling periods from ACE2 and 13 from Whiteface can be used to evaluate the sf-CASCC. Twelve periods from Whiteface are available for the CASCC2.

4.3.1.1 Cloud microphysical parameters at ACE2

The T188, T189 and T195 events had very similar LWC and drop distributions (figure 4-12, for example). The LWC varied from 134 – 282 mg m^{-3} (the overall peak was 320 mg m^{-3}, but that drop distribution is not available). The drop distributions did not vary much, with a sharp peak at ≈ 11 μm in the LWC distribution tailing off to larger drop sizes. Few drops were found > 20 μm in diameter. The calculated values of D_{eff} range from 10.7 – 11.8 μm consistent with this figure. The total drop number concentrations were on the order of 1000 cm^{-3} consistent with a polluted air mass (see Chapter 7 for a discussion of the meteorological conditions). LWC variability increased when the LWC decreased, and the LWC showed no discernible pattern during these events. In contrast, the T203 event (figure 4-13) was of maritime origin, and relatively clean. The LWC was higher (249 – 305 mg m^{-3}) and very stable throughout the event. The distribution was much broader and the peaks shifted to 18 – 20 μm with some drops > 40 μm being observed. The D_{eff}s ranged from 18.2 – 20.5 μm. Total drop number concentrations were ≈ 100 cm^{-3}.

Reproduced with permission of the copyright owner. Further reproduction prohibited without permission.

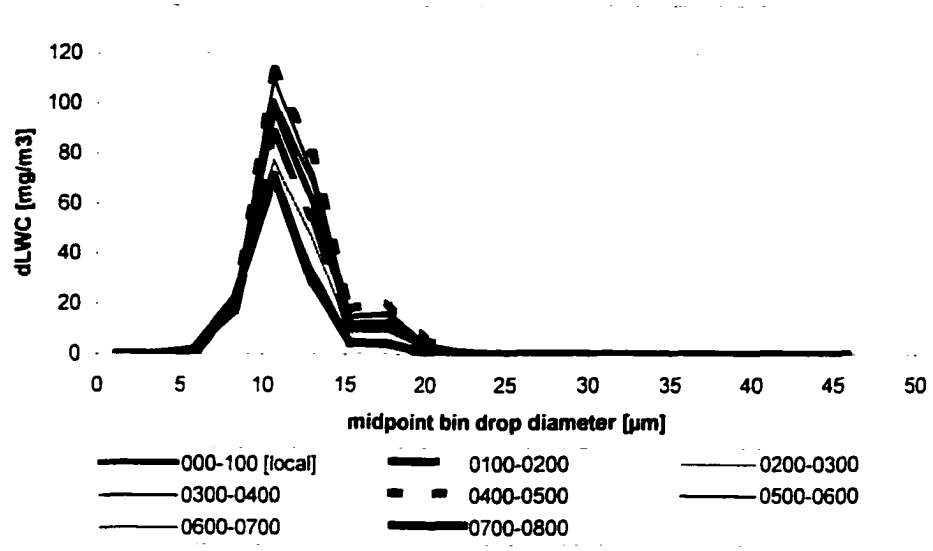

Figure 4-11: ACE2 T189 event dLWC distribution

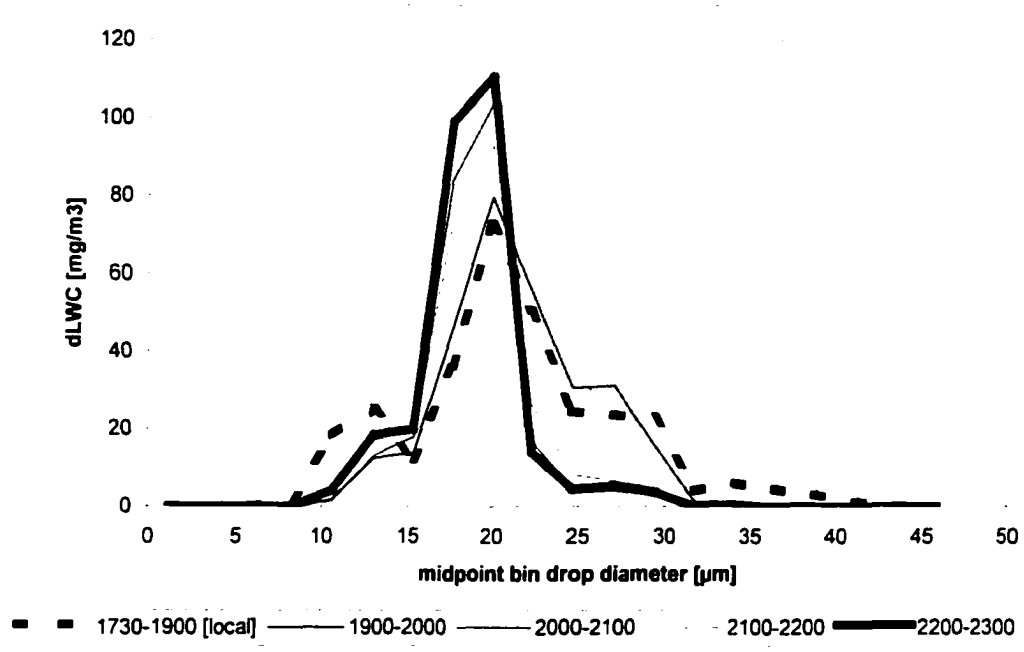

Figure 4-12: ACE2 T203 event dLWC distribution

Reproduced with permission of the copyright owner. Further reproduction prohibited without permission.

4.3.1.2 Cloud microphysical parameters at Whiteface

The W188 event has been described in section 4.1. The W188 D_{eff} was about 15 μm and similar results were obtained for the validated portions of W198 (see Appendix G). During W198 after cloud onset at 1:30 a.m. (local time – EDT), the summit stayed continuously in cloud past 11:00 a.m. The wind direction showed little variation (standard deviation ≈ 5°) and the collectors were oriented properly. The wind speed started at 6 m s^{-1} but then dropped to 4 m s^{-1} for the last sampling period (10 – 11 a. m.). The temperature was also stable at 15.6±0.3°C, and the mean event LWC was 521 g m^{-3}.

4.3.2 Collector efficiency curves

Demoz et al. (1996) gives equations to calculate the collection efficiency curves for the Caltech family of active strand collectors which start by considering the flow past a single cylinder and then revise that to account for several rows of cylinders (see Appendix B and references therein). Prior to building the new sf-CASCC described in section 4.1, Eli Sherman modeled the flow field in the sf-CASCC Large fraction in 2-D using Fluent v5.0 software for standard conditions following the methodology established in Straub and Collett (1999). With the calculated flow field, he was able to determine numerically drop collection efficiency. His results and the theoretical collection efficiency curves for the CASCC2, and sf-CASCC are shown in figure 4-13.

The modeling indicated that the fluid flow around the large rods was not independent of the upstream rods. Rods are arranged in each row in a "staggered" pattern. The resulting flow pattern became focused and an uneven drop collection pattern was found between the rows of rods. Unequal sample collection on the rod banks had been previously observed (Demoz *et al.*, 1996). As a result of the higher velocities approaching the downstream rods, smaller drops are collected in the Large stage and a D_{p50} of 16 – 17 μm is found, not 23 μm (Demoz *et al.*, 1996).

Reproduced with permission of the copyright owner. Further reproduction prohibited without permission.

The Fluent efficiency curve is steeper than the theoretical curve and the maximum efficiency is approximately 90%, slightly higher than theory predicts for both the Large fraction as well as the

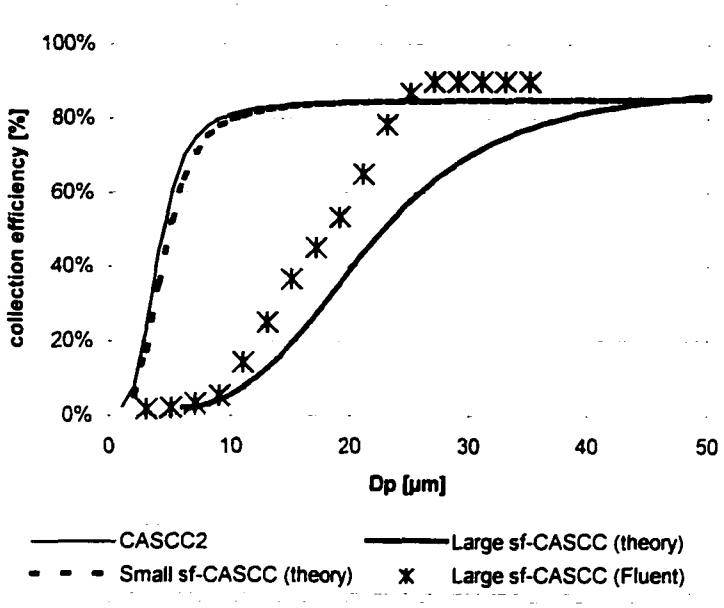

Figure 4-13: CASCC2 and sf-CASCC collection efficiency curves

Small and CASCC2 (85 – 86%). The Small fraction was not modeled (for consistency I will refer to its collection efficiency curve when used in conjunction with the Large modeled curve as the "Fluent" curve). Figure 4-14 shows the net collection efficiency curves determined for the Small fraction using both the theoretical and modeled Large fractions. The Small drop fraction will likely collect a larger volume of drops downstream of the Demoz *et al.* (1996) theoretical curve than downstream of the Fluent curve. Figures 4-13 and 4-14 suggest that the CASCC2 and sf-CASCC will collect most incident drops. The key for the sf-CASCC curves is where the cut-size between the two fractions actually is.

4.3.3 CASCC2 and sf-CASCC predicted/collected mass results

To obtain the predicted mass, the processed drop distribution (in terms of dLWC) was first adjusted for either super- or sub-isokinetic sampling conditions (equations 2-10 and 2-11) as

Reproduced with permission of the copyright owner. Further reproduction prohibited without permission.

needed for all drop sizes in (typically) 2 μm increments. Similar to the calculations for the super-cooled drop collectors in Chapter 3, the resulting distribution was multiplied by the collection

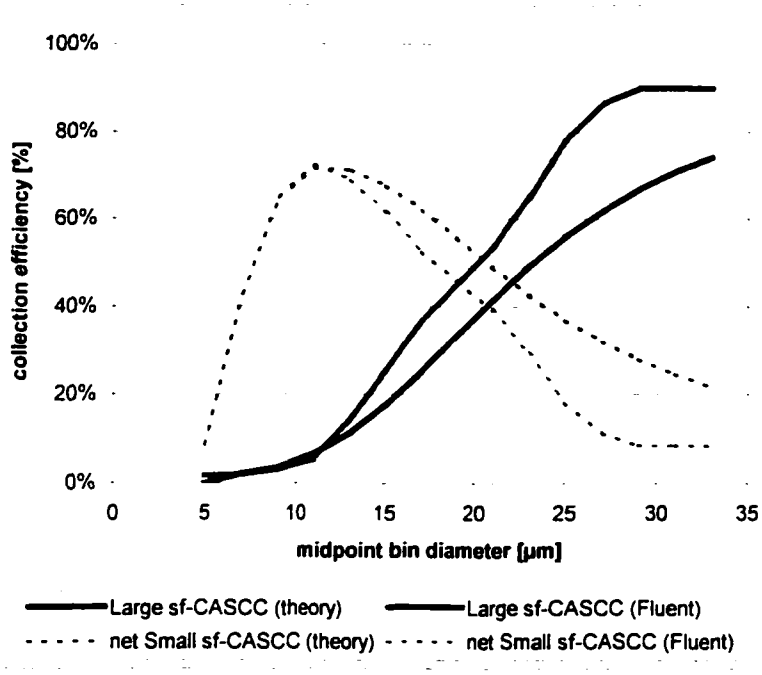

Figure 4-14: sf-CASCC net theoretical and modeled collection efficiency curves

efficiency curve, the nominal collector flow rate and sampling time. Predicted mass for a collector or fraction is the sum across all drop sizes. For the sf-CASCC Small fraction, the incoming drop size distribution reflected upstream collection. Measured mass is as collected. The error bars shown are appropriate combinations of the following sources of uncertainty: errors in the CSASP data (25%, Appendix G), PVM-100 (10%, (Gerber *et al.*, 1994)), collector flow rate (5%, estimated), mass measurement (0.1 g), and estimated uncollected residual mass in the collectors (3.0 g/CASCC2, 5.0 g/sf-CASCC). Due primarily to a low degree of confidence in the Whiteface drop size distribution data (Appendix G), the error bars shown have been multiplied by 2. The error bars do not include any uncertainty associated with the collection efficiency curves themselves.

Figures 4-15, 4 –16, and 4-17 show the results for the CASCC2, and sf-CASCC via both the Fluent and theoretical efficiency curves. For all of these figures the data presented are the

Reproduced with permission of the copyright owner. Further reproduction prohibited without permission.

means for the number of samples. The error bars shown are based upon the calculated standard deviation for the mean based upon the individual uncertainties in the measurements. Tables 4-3 and 4-4 contain tabulated results.

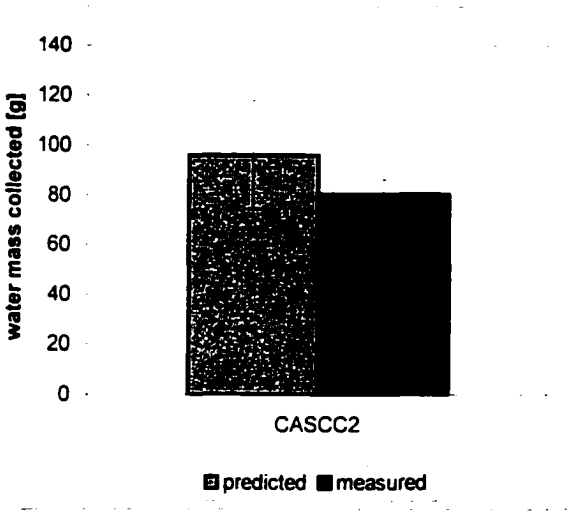

Figure 4-15: CASCC2 predicted vs. measured mass (12 samples)

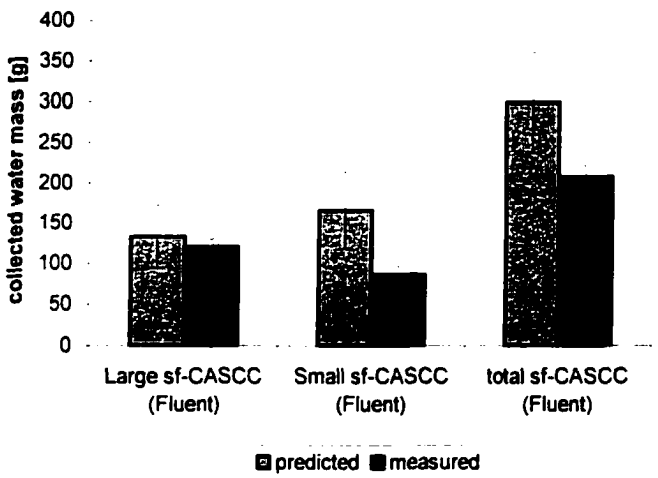

Figure 4-16: sf-CASCC predicted vs. measured mass via Fluent curves (33 samples)

Reproduced with permission of the copyright owner. Further reproduction prohibited without permission.

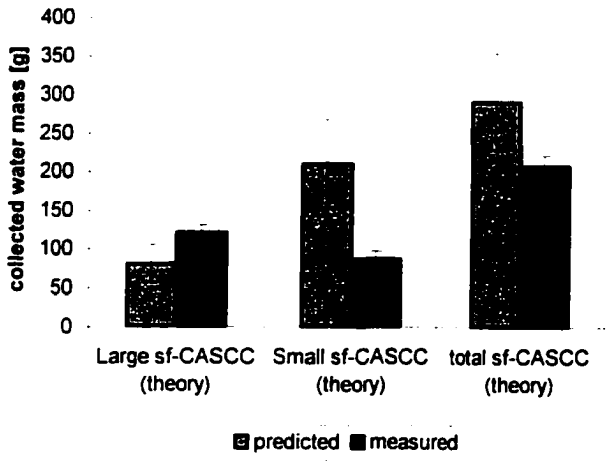

Figure 4-17: sf-CASCC predicted vs. measured mass via theoretical curves (33 samples)

Table 4-3: Compiled CASCC2 and sf-CASCC predicted/measured mass results

collector or fraction	predicted/measured mass	
	mean	Range
CASCC2	120%	116 – 123%
FLUENT MODEL		
Large sf-CASCC	111%	83 – 165%
Small sf-CASCC	190%	122 – 442%
total sf-CASCC	144%	116 – 241%
THEORY		
Large sf-CASCC	67%	48 – 107%
Small sf-CASCC	242%	153 – 643%

total theory sf-CASCC similar to Fluent results

Table 4-4: CASCC2 and sf-CASCC measured mass results

collector or fraction	measured mass [g]	
	mean	Range
CASCC2	80.3	18.9 – 152.9
Large sf-CASCC	120.6	14.1 – 392.1
Small sf-CASCC	87.1	31.4 – 183.3

4.3.4 Discussion

The CASCC2 collection efficiency curves consistently over-predict by about 20% the actual mass

Reproduced with permission of the copyright owner. Further reproduction prohibited without permission.

collected (figure 4-14, table 4-3) within a fairly narrow range of values. Table 4-4 is included and figure 4-14 plotted in terms of mass to emphasize that mass measurement error is probably not responsible for the difference unless substantial losses (10 – 15 ml) occur. This result is consistent with the results from the evaluation of the CASCC2 collection rate equation proposed in Demoz *et al.* (1996) (section 4.2.2.2).

The results for the two sets of curves for the sf-CASCC are more mixed, although total collection is over-predicted by about 45% overall (table 4-3). That high value is principally due to the inability to accurately predict collection on the Small stage. The Fluent collection efficiency curves tend to over-predict collection on both stages, but give more consistent results than the theoretical set of curves. The theoretical curves tend to under-predict Large fraction collection and over-predict strongly Small fraction collection (consistent with figure 4-14). The Fluent curves appear to represent more closely actual sf-CASCC measurements and will be used in comparisons with the 5-Stage. The changing D_{eff} between events did not appear to affect the results other than shifting collection back and forth between stages on the sf-CASCC, but the results do support the Fluent results that the Large D_{p50} is smaller than simple theory predicts.

Actual collection on the Small fraction is much lower than predicted. The 242% over-prediction for the theoretical Small fraction suggests that 210 g should have been collected not the 87 g actually measured. That is a large amount of "missing water". Field observations during collection have not focused on, for example, whether there is a large quantity of internal losses between stages. Flow measurements inside the sf-CASCC indicate that it is highly turbulent downstream of the Large rods. Turbulence may disproportionately affect smaller drops which have small inertia (large drops, in contrast, have high inertia and are more likely to continue upon their trajectories). There may be transmission losses between stages. However, it seems that a loss of 120 ml would have been readily observable. While the CASCC2 has a higher sampling velocity, there are no upstream banks of rods to interfere with collection on the strands which may be one reason why its collection efficiency curve performs better. At the sf-CASCC inlet, the

Reproduced with permission of the copyright owner. Further reproduction prohibited without permission.

upstream "bow waves" produced by the large rods may also affect sampling efficiency. The theoretical collection efficiency curve may be inadequate. No data currently exist to resolve this over-prediction issue.

The uncertainty in this calculation is quite large, and does not include any error in the collection efficiency curves. For the CASCC2, a higher nominal flow rate could easily account for the over-prediction (which is within the propagated error). In the sf-CASCC, flow rate may also be a factor, but even relatively large fluctuations could not account for the missing water mass. While the drop distribution is highly uncertain, affecting the split between stages, the overall total predicted is still 45% too high on average. These results suggest that there are unquantified factors which appear to affect sf-CASCC collection and particularly the Small fraction.

These results indicate that the 86% overall collection efficiency suggested for the CASCC2 is reasonable given the uncertainty in this analysis, and the evaluation in terms of volume. For the sf-CASCC, however, the overall collection efficiency appears to be somewhat lower on average than the collection efficiency curves suggest, although consistent (figure 4-5). There is more variability in the sf-CASCC data, particularly compared to the CASCC2 data. The ACE-2 data points, however, did not add any appreciable variability that was not already present in the Whiteface data used for the CASCC2. Both collectors were subject to the same changing ambient conditions.

4.4 5-Stage predicted and collected mass

The first part of the 5-Stage evaluation focuses on mass. The same approach is used as described in sections 4.2 and 4.3 for the CASCC2 and sf-CASCC. The experimental efficiency curves will be presented first, followed by a predicted/collected mass analysis and then a collected mass comparison to the other two collectors.

Reproduced with permission of the copyright owner. Further reproduction prohibited without permission.

4.4.1 Experimental collection efficiency curves

Experimental laboratory and numerical modeling techniques were used to calibrate the CSU 5-Stage (Straub and Collett, 2001a, and Appendix B). The experimental collection efficiency curves will be used for the field evaluation. These curves, however, do not include any upstream effects (such as from the windshield), or the lip downstream of the Stage 5 (V5) impaction surface. The curves are shown for each stage (figure 4-18), and also summed across them to yield the overall curve (figure 4-19). The total CASCC2 and sf-CASCC curves are included for comparison. The experimentally-determined standard deviation for the Stage 1 (V1) efficiency curve is 24.5% and for the other stages is 12.5%, although these are not shown in the figures for clarity. Overall 5-Stage collection efficiency ranges from 50 – 70%. This is due to large wall losses predicted in the collector (not shown). These are consistent with those reported for an aerosol sampler operating in a similar size range (Marple and Willeke, 1975), and are not unexpected given the relatively large inertia of the drops (Schell and Georgii, 1989). Large internal losses have been reported for similar multi-stage cloud water impactors (Schell *et al.*, 1997a, and Appendix B). One goal of the field evaluation is to investigate whether the predicted wall losses migrate and subsequently are collected.

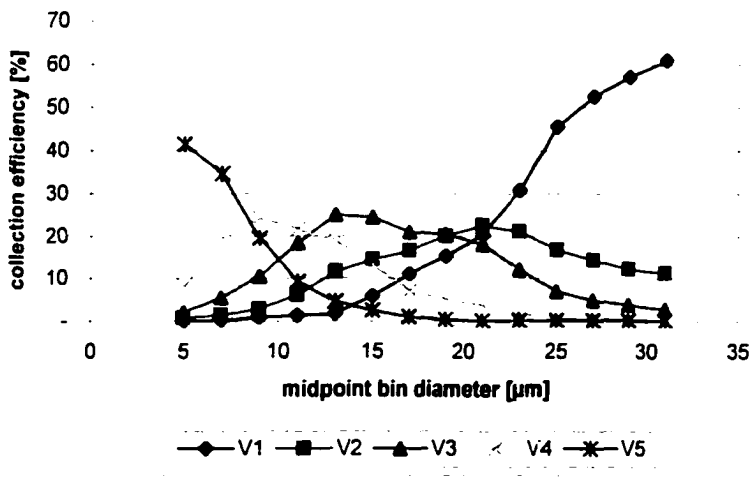

Figure 4-18: 5-Stage experimental collection efficiency curves (Straub and Collett, 1999)

Reproduced with permission of the copyright owner. Further reproduction prohibited without permission.

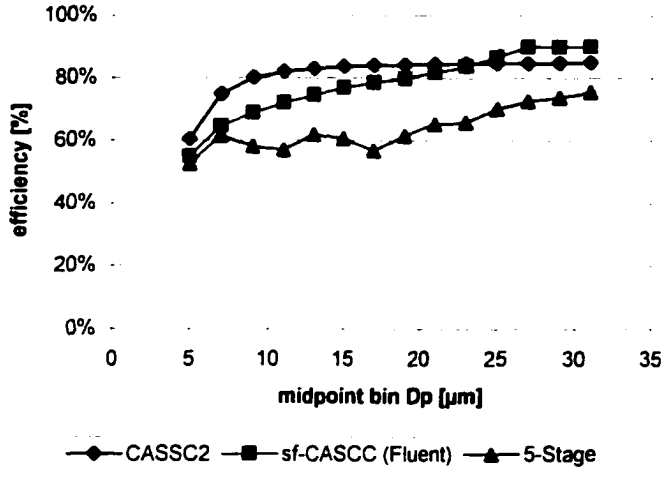

Figure 4-19: Overall collection efficiency curves for the CASCC2, sf-CASCC and the 5-Stage

4.4.2 5-Stage predicted and collected mass performance

The most complete suite of data exist for the W198 event as drop size distributions exist for three of the time periods the 5-Stage was operating : 6 – 7 a. m., 8 – 9 a. m., and 10 – 11 a. m.. Davis collected mass measurements are also available. The Whiteface data will be used to predict individual stage collection. Whiteface and Davis mass data will be used to assess aggregate performance.

4.4.2.1 Results

Qualitatively, one hour averages of the LWC measured by the PVM-100 during the W198 event indicated a rise from approximately 450 mg m^{-3} at the start of the event to a peak of 780 mg m^{-3} during the 9 – 10 a.m. time period. The total amount of water sampled in each cloud collector increased similarly. Additionally, at the start of the event there was relatively more mass collected in the small drop fraction of the sf-CASCC and the smaller stages of the CSU 5-Stage. As the event progressed, a shift in the size distribution resulted in most of the mass being

Reproduced with permission of the copyright owner. Further reproduction prohibited without permission.

collected in the large drop fraction of the sf-CASCC and the larger stages of the CSU 5-Stage. The trend in the effective diameter of the drops provided by the PVM-100 (see Appendix G) is also consistent with this observation.

Figures 4-20 and 4-21 focus on the Whiteface sampling periods. The first figure shows the results of the predicted/collected mass calculations for the 5-Stage. This calculation is the same as those for FROSTY in Chapter 3, although here transmission losses are specifically calculated too. Data points have been removed where sample was known to be lost prior to collection. The comparison with the sf-CASCC is used to illustrate that the 5-Stage can simulate the sf-CASCC collected water mass distribution and thus their size-resolving performance can be compared (figure 4-21). Figure 4-22 is a total mass collected comparison between the 3 collectors. All three collectors are included to highlight their mutually similar performance.

In addition to the factors included in the error analysis previously discussed for the CASCC2 and the sf-CASCC, the uncertainty associated with the 5-Stage collection efficiency curves is incorporated into the error bars shown. The 5-Stage residual uncollected mass was estimated as a function of collection surface area and varies from 2.4 – 0.5 g from Stage 1 (V1) through Stage 5 (V5). The 5-Stage flow rate uncertainty based upon measured field data is 4%.

4.4.2.2 Discussion

Although water loss prior to weighing makes figure 4-20 incomplete, predicted and collected masses are consistent with each other for the three time periods available. The experimental collection efficiency curves adequately predict the observed water distribution within the collector. The calculations tend to under-predict the collected mass on Stage 1 and over-predict it on Stage 2, although within the observational uncertainty. To explore this result, the Stage 1 collection efficiency curve was modified by adding its uncertainty to it and the Stage 2 collection efficiency

Reproduced with permission of the copyright owner. Further reproduction prohibited without permission.

curve was decreased similarly. This effectively increases and decreases their respective D_{p50}s. Better overall agreement is obtained for both Stage 1 and Stage 2 (Stage 1 predicted/collected

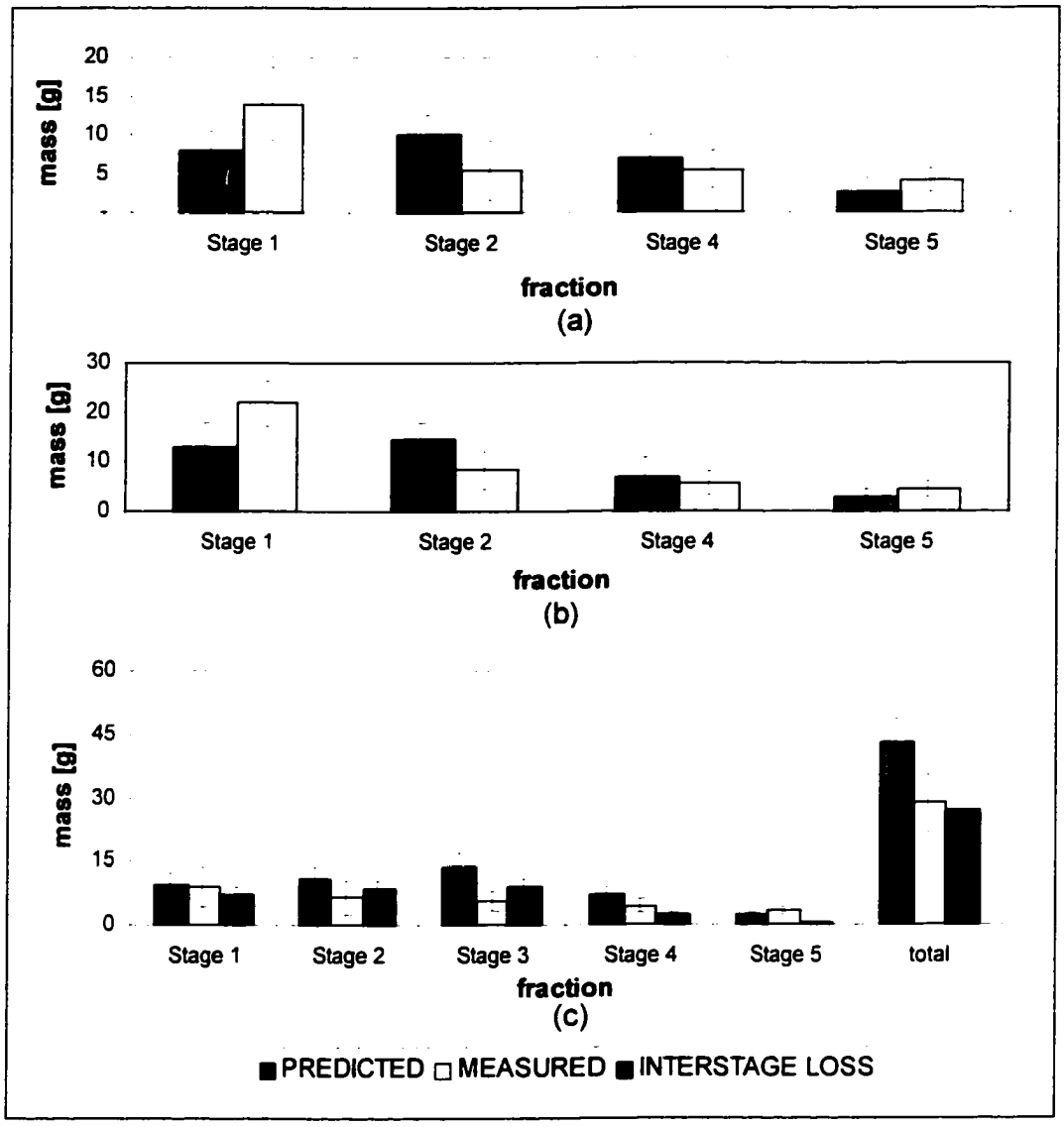

Figure 4-20: 5-Stage predicted and collected mass for the W198 event (a) 6 – 7 a. m., (b) 8 – 9 a. m., and (c) 10 – 11 a. m. Predicted interstage losses are shown only in (c) for clarity

mass becomes 70 – 129% from 50 – 103% and Stage 2 over-prediction is reduced to < 50%) without significantly impacting the results for the downstream stages. If similar patterns result from the analyses of future observations, it may be necessary to re-visit the Stage 1 and 2

Reproduced with permission of the copyright owner. Further reproduction prohibited without permission.

experimental calibration, particularly with regard to where drops are introduced into the collector (see Appendix B).

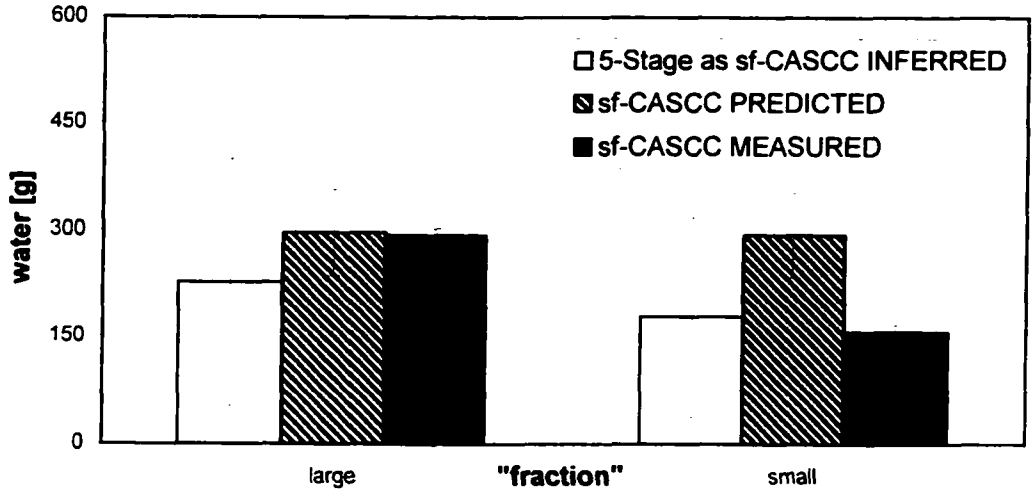

Figure 4-21: 5-Stage simulation of the sf-CASCC's collected mass performance (W198, 10 – 11 a. m.)

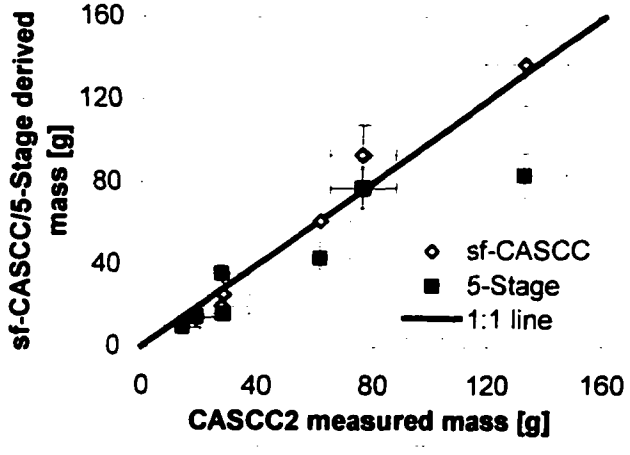

Figure 4-22: 5-Stage and sf-CASCC total mass compared to the CASCC2 for validated time periods. 5-Stage and sf-CASCC masses have been adjusted to reflect varying flow rates

During the 10 – 11 a.m. time period, Stage 3 has a predicted mass (13 g) approximately double the collected mass (5.6 g) and is responsible for most of the discrepancy between predicted and collected total mass (figure 4-20). One possible reason for this discrepancy may be an unrecorded loss of mass prior to weighing (the measured weight is near the vial's capacity).

Reproduced with permission of the copyright owner. Further reproduction prohibited without permission.

Another may be CSASP data limitations as many of the simulated size distribution points would be collected on Stage 3 (see Appendix G). However, the CASCCs' performances during this time period do not differ from those for other time periods (not shown). No data are available to resolve this discrepancy.

Interstage losses appear to be both real and uncollected in the sample vials (figure 4-20). They are of sufficient volume due to the relatively high LWCs and sequential sampling periods that any substantial re-entrainment should be readily apparent in the sampled masses. Minor migrations cannot be ruled out, albeit unlikely based upon prototype testing in the lab (Chapter 2). Quantitative prediction of internal losses by drop size based upon collector calibration curves is an advantage of this evaluation technique compared to others (Hoffmann and Metzig, 1991), and is necessary for multi-stage collectors.

The 5-Stage's aspiration efficiency is not predicted to measurably change the sampled distribution for in these conditions. That appears to be true as the very largest drops would be most affected and the collected amounts were largely as predicted (theoretical aspiration calculations cannot account for the shift in Stage 1 predicted/collected mass between time periods). It is not known if the windshield improved aspiration efficiency, but it did not appear to adversely impact it either.

Adjusting for differences in collection efficiency curves and flow rates, the CSU 5-Stage does a reasonable job of reproducing the sf-CASCC's results for the time period shown, although the predicted mass on the small fraction of the sf-CASCC is over-estimated (figure 4-21). This result suggests that comparing size-resolved chemical measurements between the two collectors is valid at Whiteface. However, this result must be tempered by the results of section 4.3, particularly with regards to Small fraction prediction.

Reproduced with permission of the copyright owner. Further reproduction prohibited without permission.

Figure 4-22 is derived strictly from measured masses. Inherent in this approach is the assumption that the collection efficiency for each collector is approximately constant across the range of drop sizes present. Neglecting any aspiration efficiency effects, this is approximately true – the CASCCs theoretically are at ≈ 85 – 90% efficiency and the sum of the CSU 5-Stage's curves are ≈ 60 – 65% for most drop sizes (figure 4-18). Variations exist at low drop diameter (< 10 μm) suggesting the CASCC2 collects more drops in this range, but that should not impact collected mass calculations appreciably. While this analysis is limited, it gives some measure of whether the collectors are, in fact, sampling the same drop populations and operating at their theoretical efficiencies. For the data shown in figure 4-22, the sf-CASCC derived mass is 97% on average (range 70 – 123%) of the CASCC2 and the CSU 5-Stage is 83% on average (range 55 – 127%). The CSU 5-Stage's result corresponds to a collection efficiency of ≈ 71% in absolute terms, consistent with its collection efficiency curves and additional data from all sampling periods (not shown). The CSU 5-Stage and the sf-CASCC exhibit similar variability. In Davis the sf-CASCC and CASCC2 were vertically co-located at 3 m, while the CSU 5-Stage was operated at ≈ 1 m so some variation in collected mass is not unexpected, particularly given the small-scale heterogeneity in radiation fogs.

This quantitative assessment could be improved if measurement uncertainties could be reduced. The CSASP data and the assumptions made to produce them are a major source of measurement uncertainty (Appendix G). Another significant contributor to the uncertainty is the standard deviation for large drops in the experimental collection efficiency curves (Straub and Collett, 2001a). This value was based upon limited replicate measurements in another collector of different configuration which itself introduces an unquantifiable error. Additional measurements using the CSU 5-Stage itself could potentially improve upon this uncertainty. Further, the Stage 5 lip and drop input location should be evaluated to determine if they modify the curves. Much of the CSU 5-Stage uncertainty in figures 4-20 and 4-21 derives from the low sample volumes measured. Increased attention must be made to both field mass measurements and the quantification of residual/uncollected mass in all collectors.

Reproduced with permission of the copyright owner. Further reproduction prohibited without permission.

4.5 *Derived "bulk" vs. bulk cloud water composition*

Here the chemical composition is compared species-by-species between the collectors. Bulk and derived "bulk" composition, based solely on measured compositions and masses, are compared between the collectors as the continuous drop size-dependent composition is not known. Derived "bulk" concentrations are the volume-weighted averages calculated acros all drop fractions and the associated error bars refelct both mass and chemical measurement uncertainty. I have neglected mixing issues which may affect the volatile species (Pandis and Seinfeld, 1991; Perdue and Beck, 1988) (see Chapter 9 for a discussion). Both multi-stage collectors will be compared to the CASCC2. The sf-CASCC and CASCC2 will be compared first for all the data available followed by the comparison with the eight 5-Stage sample sets. The eight 5-Stage sample sets are from: Whiteface (1 sample set (W198 event)), and Davis (7 sample sets from three events (D004 (3), D009 (2), and D010 (2)). The 5-Stage samples will be shown with the concurrent sf-CASCC and CASCC2 comparisons broken out. Only one Whiteface sample is available due to unknown amounts of mass lost in some stages (see figure 4-20, for example). Inherent in this approach is that the collectors are sampling representatively. Finally, as a "proof of concept" the 5-Stage composition data will be used to derive a continuous drop size-dependent composition profile which, in combination with the drop size distribution, can be used to explore whether we can obtain the drop fraction composition we observed.

For all the comparisons, data points were removed where collector or collector fraction/stage concentrations reported were not above an approximate Level of Quantitation derived from the calculated 95% Confidence Limit MDL (Chapter 5). For the modeling, a drop size distribution was derived for the Davis samples (see Chapter 9).

Reproduced with permission of the copyright owner. Further reproduction prohibited without permission.

4.5.1 Results

Table 4-5 contains the consolidated sf-CASCC to CASCC2 comparisons for all species separated by LWC – "low" (< 120 mg m^{-3}) and "high" (> 120 mg m^{-3}). Table 4-6 presents the same results for the 5-Stage and sf-CASCC for the same time periods, shown graphically in figures 4-23 and 4-24 for selected species. The error bars shown in these figures represent the cumulative analytical and mass measurement uncertainty. Figures 4-25 and 4-26 show two results from the "proof of concept" investigation to explore if an assumed concentration profile derived from the 5-Stage data could reproduce collector concentrations. The collector concentration data are plotted as measured in each fraction as a function of the volume median diameter collected on that stage/fraction. Data not included in the tables are not available.

Table 4-5: sf-CASCC to CASCC2 derived "bulk" to bulk concentration comparison for all data

collectors/ conditions/ results	derived "bulk" to measured bulk concentration ratios											
	Nitrate	Sulfate	Ammonium	pH	Nitrite	Chloride	Sodium ion	Potassium ion	Magnesium ion	Calcium ion	Iron	Manganese
sf-CASCC/CASCC2 (filter: >LOQ & >120 mg m^{-3} LWC)												
n	75	75	75	75	30	20	53	33	1	4	30	52
mean±std. dev.	**0.94** ±0.19	**0.95** ±0.19	**0.93** ±0.13	**1.0** ±0.02	**1.04** ±0.06	**1.06** ±0.24	**0.92** ±0.54	**1.0** ±0.41	**0.49**	**1.07** ±0.43	**1.11** ±0.33	**1.07** ±0.37
range	0.47 - 1.32	0.50 - 1.9	0.55 - 1.22	0.95 - 1.06	0.96 - 1.16	0.60 - 1.55	0.04 - 2.77	0.48 - 2.52	0.49	0.64 - 1.57	0.51 - 1.77	0 - 2.01
sf-CASCC/CASCC2 (filter: >LOQ & <120 mg m^{-3} LWC)												
n	25	25	25	25	23	16	25	23	1	16	20	21
mean±std. dev.	**0.66** ±0.20	**0.73** ±0.22	**0.71** ±0.20	**1.02** ±0.03	**1.12** ±0.17	**0.65** ±0.2	**0.76** ±0.32	**0.74** ±0.26	**0.72**	**0.97** ±0.32	**1.04** ±0.35	**0.98** ±0.28
range	0.36 - 1.01	0.4 - 1.41	0.36 - 1.08	0.97 - 1.09	0.94 - 1.70	0.29 - 1.0	0.38 - 2.01	0.39 - 1.48	0.72	0.37 - 1.54	0.37 - 1.72	0.59 - 1.6

Reproduced with permission of the copyright owner. Further reproduction prohibited without permission.

Table 4-6: 5-Stage and sf-CASCC to CASCC2 derived "bulk" to bulk concentration comparison for 5-Stage sampling periods only. Blank values are not available.

collectors/ conditions/ results	derived "bulk" to measured bulk concentration ratios											
	Nitrate	Sulfate	Ammonium	pH	Nitrite	Chloride	Sodium ion	Potassium ion	Magnesium ion	Calcium ion	Iron	Manganese
5-Stage/CASCC2 (filter >LOQ & >120 mg m^{-3} LWC)												
n	3	3	3	3	2	1					2	
mean ±std. dev.	**0.97** ±0.26	**1.01** ±0.14	**0.98** ±0.02	**1.01** ±0.01	**1.19** ±0.03	**1.99**					**1.50** ±0.82	
range	0.77 - 1.27	0.92 - 1.17	0.96 - 1.01	1.01 - 1.02	1.17 - 1.20	1.99					0.92 - 2.08	
sf-CASCC/CASCC2 (filter: >LOQ & >120 mg m^{-3} LWC)												
n	3	3	3	3	2						2	
mean ±std. dev.	**0.99** ±0.04	**0.94** ±0.06	**0.97** ±0.14	**1.00** ±0.005	**1.00** ±0.02						**1.58** ±0.23	
range	0.95 - 1.03	0.90 - 1.01	0.85 - 1.12	0.99 - 1.00	0.99 - 1.01						1.42 - 1.74	
5-Stage/CASCC2 (filter >LOQ & <120 mg m^{-3} LWC)												
n	3	3	3	4	3	3	2	3		2	1	
mean ±std. dev.	**0.56** ±0.15	**0.67** ±0.17	**0.64** ±0.20	**1.02** ±0.05	**1.25** ±0.39	**0.93** ±0.32	**7.36** ±8.63	**1.68** ±1.56		**6.02** ±6.89	**2.12**	
range	0.41 - 0.71	0.49 - 0.82	0.41 - 0.76	0.99 - 1.09	0.99 - 1.70	0.73 - 1.29	1.26 - 13.5	.49 - 3.45		1.15 - 10.9	2.12	
sf-CASCC/CASCC2 (filter: >LOQ & <120 mg m^{-3} LWC)												
n	4	4	4	4	4	4	3	4		3	2	1
mean ±std. dev.	**0.56** ±0.18	**0.63** ±0.16	**0.65** ±0.16	**1.02** ±0.02	**1.15** ±0.18	**0.61** ±0.18	**0.70** ±0.09	**0.62** ±0.20		**1.27** ±0.20	**1.14** ±0.31	**0.95**
range	0.38 - 0.72	0.46 - 0.78	0.44 - 0.78	1.00 - 1.05	1.00 - 1.37	0.42 - 0.82	0.60 - 0.79	0.46 - 0.91		1.03 - 1.40	0.92 - 1.36	0.95

4.5.2 Discussion

Interpreting these composition ratio results requires some knowledge of the drop size-dependent composition observations during the campaigns. The campaign chapters contain the details. Briefly, at both Whiteface and Davis, the major (high concentration) inorganic ions were ammonium, nitrate, and sulfate. The hydrogen ion was also important at Whiteface (low pH). Other "minor" species (e.g. calcium, iron) were measured generally at significantly lower concentrations. At Whiteface, drop size-dependent variations in concentration for the major species were muted, although calcium and the metals tended to be found in greater concentrations in larger drops. By contrast, in Davis the major species exhibited a strong drop size-dependence during all events and were found predominantly in the smaller drops. This was true for many of the minor species as well.

Reproduced with permission of the copyright owner. Further reproduction prohibited without permission.

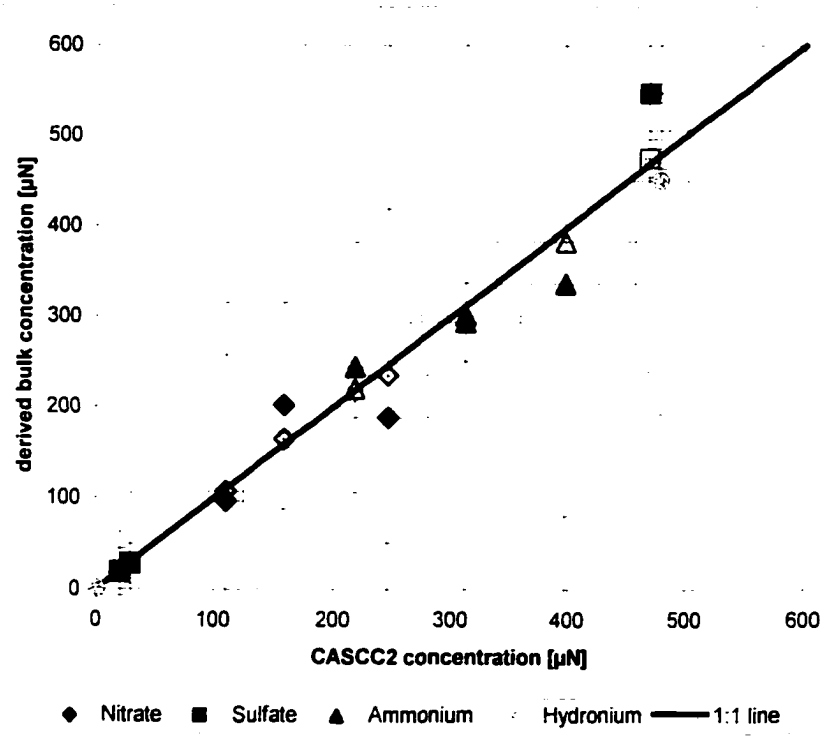

Figure 4-23: sf-CASCC (open) and 5-Stage (solid) derived bulk concentrations for major species compared to the CASCC2 – filtered for >LOQ and >120 mg m^{-3} LWC

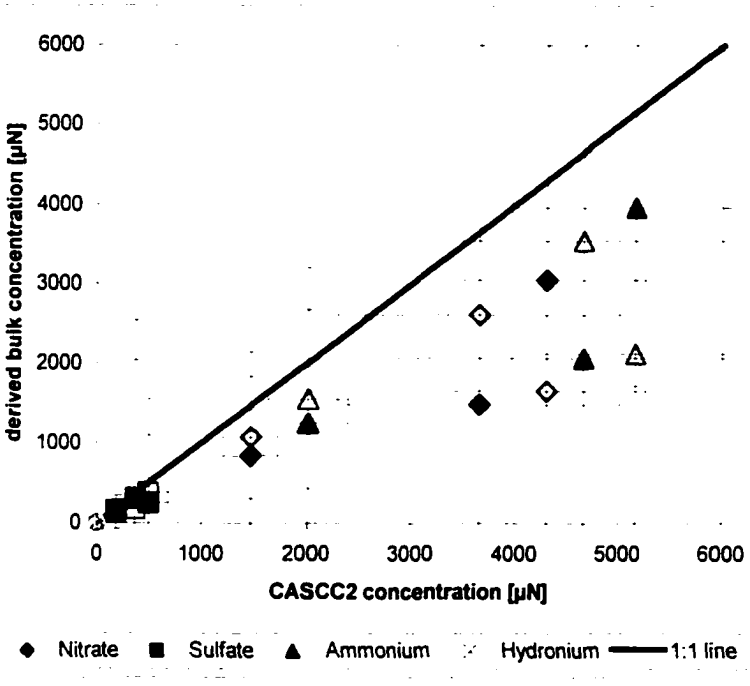

Figure 4-24: sf-CASCC (open) and 5-Stage (solid) derived bulk concentrations vs. CASCC2 concentration for selected species – filtered data > LOQ and < 120 mg m^{-3} LWC

Reproduced with permission of the copyright owner. Further reproduction prohibited without permission.

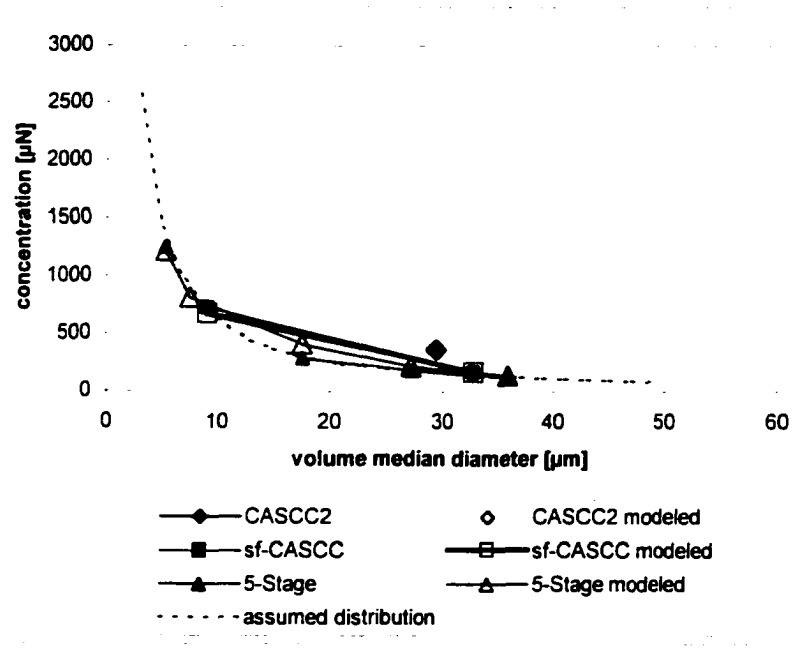

Figure 4-25: Sulfate distribution – observed and modeled (D010 event, 4 – 6 a. m.)

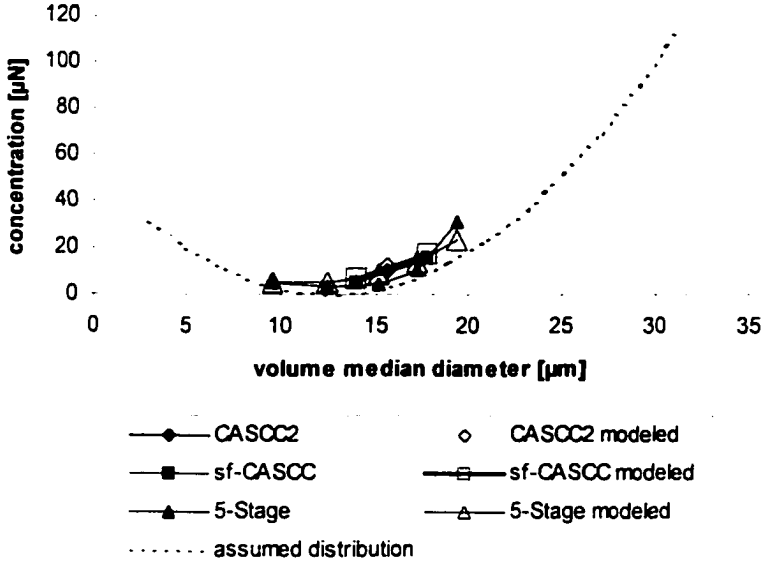

Figure 4-26: Manganese concentration – observed and modeled (W198 event, 6 – 7 a. m.)

Reproduced with permission of the copyright owner. Further reproduction prohibited without permission.

The LWC separation point (120 mg m^{-3}) chosen principally separates two events (D009 and D010) at Davis from the rest of the data set. Chemical "performance" of the multi-stage collectors compared to the CASCC2 varied on average during these two events compared to the others for the major inorganic ions and most of the minor species as well. Considering the sf-CASCC to CASCC2 evaluation first, derived bulk concentrations were ≈ 60 – 65% on average of the measured bulk during D009 and D010 compared to the other events where virtually 1:1 agreement was found (table 4-5). Variability was 15 – 20% for the major species which is reasonable for co-located collectors (Appendix B and references therein), although for the minor species, agreement was within ± 30% at high LWC. For low LWC, variability for the major ions reaches approximately 30% and for the other species the range also increases slightly to 30 – 40% (table 4-5). Some of the minor species (e.g. iron) have ratios still in the 1:1 range, but some do not (e.g. chloride). Table 4-5 suggests this result is relatively robust for all sf-CASCC and CASCC2 data. While a broad range of ratios for all species in all conditions is observed, these lower ratios were predominantly clustered in these two events.

The 5-Stage results mirror the sf-CASCC's during the time periods it was operating (table 4-6, figures 4-23 and 4-24), with somewhat higher variability for some of the major species. The 5-Stage results cover a somewhat broader range than the sf-CASCC, but, given the propagated uncertainties, this is not unexpected. Agreement is somewhat worse for the species measured in much lower concentrations (e.g. chloride, metal ions, Metals), and somewhat worse in the 5-Stage compared to the sf-CASCC. As many of these species were measured at trace concentration levels, slight sample handling contamination could have altered the 5-Stage concentrations.

It is interesting that the nitrite comparisons (based upon Davis data only) indicate relative over-prediction by the multi-stage collectors during the low LWC periods, with somewhat higher relative over-prediction in the 5-Stage. This is interesting because several investigators have

Reproduced with permission of the copyright owner. Further reproduction prohibited without permission.

suggested a significant ground source exists for HONO (see Chapter 9), and the 5-Stage was located closer to the ground than the other collectors (1 m instead of 3 m).

There are several possible reasons why a difference in collector performance may have been observed, although the data available do not permit resolution. The D009 and D010 events at Davis had the highest observed concentrations and the lowest overall average LWCs. Other events at Davis showed similar drop size-dependent chemistry but the concentration gradients appeared to be sharpest during D009 and D010. The elevated concentrations observed in the CASCC2 compared to the other collectors may stem from three factors – collection and aspiration efficiency differences for the CASCC2, and multi-stage collector performance problems. The theoretical D_{p50} for the CASCC2 is 3.5 μm, while the sf-CASCC Small D_{p50} is 4.0 μm and the 5-Stage's V5 D_{p50} is 4.5 μm. As the highest major ion concentrations were observed in V5, if the CASCC2 collected slightly more small drops its concentrations would be relatively larger. In fact, the collection curves (figure 4-19) suggest that the CASCC2 may do better in the 5 – 10 μm range than the other two collectors. In the very light winds experienced at Davis, the 5-Stage alone samples at near the correct isokinetic velocity. The other collectors are both sampling super-isokinetically and aspiration efficiency issues can become important for large drops. The sf-CASCC, for example, should collect 86% of the 49 μm drops during the D010 4 – 6 a. m. sampling period, but the CASCC2 with its higher velocity should only collect 72%. While 49 μm is an extreme drop size, 30 – 40 μm drops seem likely during these sampling periods. The water mass comparison (figure 4-22) is good, but some under-sampling of large drops could have occurred. The smaller inlet and higher sampling velocity of the CASCC2 (appendix E) should not affect sampling once the drops are aspirated.

Apart from the CASCC2, the two multi-stage collectors' performance limitations could affect these results. For example, the results of section 4.3 suggest the sf-CASCC collects fewer small drops than predicted. On D009 and D010, the sharp concentration gradient producing very high concentration in the smallest drops means that the under-sampling of small drops could result in

Reproduced with permission of the copyright owner. Further reproduction prohibited without permission.

a lower derived bulk concentration. However, the 5-Stage predicted/collected mass comparison is very good for V5 (figure 4-20). Therefore, its derived composition should match the CASCC2's better relative to the sf-CASCC, which is not the case.

To summarize, the CASCC2 may be relatively over-sampling the very smallest drops and under-sampling the very largest compared to the multi-stage collectors. The composition difference may also result from the multi-stage collectors' performance. The conditions observed during the D009 and D010 events likely factor in the observations as well. One collector's "representative" sample may not be the same as another's. "Bulking" the composition across several drop fractions is not the best way to perform a composition comparison, but is the only observational method available. Modeling can also help to understand these observations/discrepancies.

In order to explore how the drop size-dependent chemistry affected the bulk and derived bulk chemical comparisons, curves were fit for selected species and time periods to the 5-Stage data to obtain continuous concentration distributions. Several different types of curves were tested including power law, exponential, and quadratic and higher-order polynomial fits. The range of 5-Stage data fit spanned all the different "types" of profiles observed in the cloud (see Chapters 8 and 9). The "best" fit was chosen based upon the r^2 value, but also on equation behaviour extrapolated past the VMD's of the 5-Stage data to the diameter endpoints used in the simulation (2 – 50 μm for Davis). The same procedure used to predict mass (section 4.3 and 4.4) was used but here solute mass was carried through the calculations, too. The key assumptions in performing this calculation were how to model the collection efficiency curves of the collectors (principally the Large fraction of the sf-CASCC and the 5-Stage) where data did not exist (< 4 or > 34 μm) and what the extrapolated concentration size dependence was beyond the V1 and V5 volume median diameters. However, as figures 4-25 and 4-26 illustrate it is possible to obtain reasonable results for both species with strong size dependencies (sulfate at Davis) and weaker ones (manganese at Whiteface). Typically (as clearly seen for manganese) the continuous concentration derived from the 5-Stage needed to be offset to lower concentrations so the

Reproduced with permission of the copyright owner. Further reproduction prohibited without permission.

resulting "mix" obtained in the collectors would have the right concentration. For Davis, the D009 and D010 sampling periods were investigated to determine if differential collection efficiencies between the collectors could produced varying bulk and derived bulk sulfate concentrations. It was possible to obtain part of the relative concentration differences observed in tables 4-5 and 4-6. In the simulations, the presence of large (> 30 μm) drops and variations in collection efficiency differences for small drops appeared to be responsible for varying "bulk" concentrations between collectors. This investigation was neither definitive nor exhaustive and relied upon many assumptions of unknown validity. Still, it does suggest given 5-Stage and other data that continuous concentration profiles can be derived.

4.6 Summarizing discussion

This chapter evaluated several aspects of the performance of the warm cloud collectors. Co-located sf-CASCCs perform virtually identically on both a mass and composition basis. Co-located CASCC2 and sf-CASCCs perform consistently compared to each other in terms of collected total mass. Their performance relative to the PVM-100 adds further evidence to the known PVM negative LWC bias at large drop sizes. The modeled sf-CASCC Large fraction collection efficiency curve is an improvement to the theoretical curve, and the theoretical Small fraction curve does not appear to predict mass collection well. In contrast, the theoretical CASCC2 collection efficiency curve predicts mass collection within the measurement uncertainty suggesting that drop passage through the Large stage in the sf-CASCC may affect downstream collection. While the 5-Stage data are limited, the first results are encouraging as its mass collection appears predictable and it performs similarly to the sf-CASCC for both mass and composition. The range of and average composition ratios for the sf-CASCC and the 5-Stage compared to the CASCC2 are approximately identical. The 5-Stage performs similarly to the CASCC2 for mass, but varies for composition during some specific conditions. The 5-Stage interstage losses appear to be both real and uncollected. 5-Stage mass collection efficiency is about 70% overall, consistent with its overall collection efficiency curve (figure 4-19). While

Reproduced with permission of the copyright owner. Further reproduction prohibited without permission.

overlap between drop sizes collected by the stages of the 5-Stage is large, fraction composition clearly varies between stages (figures 4-25 and 4-26).

It is possible to derive a continuous drop size-dependent concentration profile from the 5-Stage data, although many assumptions must be made to perform the calculation. The 5-Stage yields a better measure of size-dependent drop chemistry than previously possible for our group. However, the "proof of concept" investigation suggests that the 5-Stage still may not quite yield the true profile of size-dependent drop composition, although this is confounded by the assumptions required to perform the calculations.

To improve this analysis more high quality data sets are needed. The residual mass left behind in the collectors needs to be quantified experimentally, improved attention to weight measurements/sample collection in the field needs to be taken, and the uncertainty inherent to drop size distribution measurement needs to be reduced. If future data and results warrant, the experimental efficiency curves of the 5-Stage may need to be re-visited to minimize uncertainty, investigate the effects of the Stage 5 lip, assess collection efficiency for a wider range of drop sizes and, perhaps most importantly, determine how drop introduction at the inlet impacts the Stage 1 and Stage 2 collection efficiency curves. Further, all the 5-Stage comparisons which involve the sf-CASCC and CASCC2 would be improved with better knowledge of those collectors' efficiency curves.

Finally, the results of this chapter emphasize that:

- analytical uncertainty may not necessarily capture the true uncertainty between concentrations observed in co-located collectors or duplicate samples from the same one
- collected mass comparison consistency does not necessarily imply bulk and derived bulk composition comparisons will be consistent

Reproduced with permission of the copyright owner. Further reproduction prohibited without permission.

- different collectors may obtain varying "representative" cloud water samples from the same cloud as they can have different overall sampling efficiencies in some ambient conditions
- theoretical collection efficiency curves may not necessarily capture actual efficiency (assuming aspiration can be accounted for),
- as a result, field performance must be evaluated for all conditions and events in several ways for all collectors, and
- it must be recognized that in-cloud sampling conditions may be quite different from those experienced in laboratory calibration studies possibly affecting their applicability

Reproduced with permission of the copyright owner. Further reproduction prohibited without permission.

5. Sampling and analytical protocol

The goal of this section is to briefly describe the sampling and analytical methods used in the field and in the laboratory to obtain the results presented. Many of the methods are described in varying detail in other sources: if an adequate description exists, it will only be summarized briefly here.

In particular, the "Red cloud water manual" (RCWM) developed as a set of Standard Operating Procedures written for the Integrated Monitoring Study 1995 (IMS95) campaign covers much of the basics of sf-CASCC and CASCC2 cleaning and field operation. The RCWM includes brief descriptions of some of the cloud water aliquot protocols and analytical procedures (which may also be found in Rao (1997)). Appendices C and D describe in detail protocols for cleaning and using both the 5-Stage and the FROSTY collectors. I wrote and compiled two additional documents regarding the use of the two Dionex DX-500 Ion Chromatographs (ICs), and the Varian SpectrAA 800 Graphite Furnace Atomic Absorption Spectrophotometer (GFAAS). "The World of the IC" is in three volumes – Practical Overview of the IC (revision 2, June 13, 1999), Step-by-Step IC (revision 2, June 2, 1999), and Troubleshooting and Set-up of the IC (revision 0, June 11, 1999) (Moore, 1999a). "Using the GFAAS" (revision 3, November 9, 1999) is in one volume only (Moore, 1999b). Together these two documents exceed 150 pages in length and therefore have not been included here.

The statistical analysis of the results for the various campaigns is included. The focus is on the chemical analytical results, but physical measurement uncertainty, if not discussed elsewhere, will also be included.

Reproduced with permission of the copyright owner. Further reproduction prohibited without permission.

5.1 Field sampling

5.1.1 Preparation

5.1.1.1 Collectors

All of the plastic and primarily plastic cloud water collectors (and related accessories) are thoroughly cleaned in the lab prior to going to the field. Once clean, DI blanks are taken. After the collectors have dried, they are sealed in clean plastic bags to prevent contamination in transit. (See the RCWM and Appendices C and D).

5.1.1.2 Aliquot Chemicals

As many of the species of interest in the cloud water are unstable, preservation reagents are added to separated portions (i.e. aliquots) of the sampled water in the field for later analysis in the lab. For all field campaigns described herein, except Storm Peak, I made up the reagent chemicals, the sole exception being some of the H_2O_2 (both for the aqueous-phase and gas-phase analysis) reagents which Eli Sherman made in some instances. Depending upon the field campaign, the following reagents may have been used: $CHCl_3$ (chloroform), HCHO Preservative, S(IV) Preservative, Catalase solution, H_2O_2 Conditioning reagent, H_2O_2 Fluorescence reagent, and 9.73% HNO_3 (for preserving the Metals aliquot).

The RCWM and the Collett Group "Recipes" binder contain much of the reagent formulation information. I standardized the initial make-up to 250 ml in order to fill 3 sets of bottles with aliquot chemicals, with a few exceptions. The Catalase solution is only made-up in two 100 ml

Reproduced with permission of the copyright owner. Further reproduction prohibited without permission.

batches, and only 10 – 25 ml of chloroform was taken to the field. The nitric acid dilution from trace metal grade concentrated nitric acid was only performed in 1 liter increments when necessary, but always before a field campaign and the standard reagent bottles continued to be used. Two aliquot sets were taken into the field.

Some of the laboratory analyses of the field samples require the use of the preservative reagents. It is a good idea to conduct the subsequent laboratory analysis with the third reagent chemical bottle to minimize the impact of switching reagents "mid-analysis". Where making up new reagents is unavoidable, this at least yields a measure of the additional variability (if any) added. This is particularly relevant to the trace metal analysis and, in fact, is necessary (Moore, 1999b).

5.1.2 Field Installation

5.1.2.1 Equipment

A description of each sampling site will be given in the appropriate chapter. However, the collectors should be reasonably co-located, particularly vertically, with the other equipment. Further, no obstructions should exist upstream which could either influence cloud drop availability or otherwise be a potential source of contamination. There are some limitations based upon power and space constraints.

5.1.3 Field Measurements

5.1.3.1 Cloud water

Reproduced with permission of the copyright owner. Further reproduction prohibited without permission.

Cloud water samples were collected in half-hour to two-hour increments depending upon the collectors in use, the liquid water content (LWC) and the size distribution. Minimum LWC to commence sampling was approximately 0.04 g m^{-3}.

5.1.3.2 Cloud physics and meteorological measurements

A Gerber Particle Volume Monitor Model 100 (PVM-100)(Gerber Scientific, Inc., Reston, VA) which is used to measure both cloud LWC and drop surface area was operated during all campaigns. Drop size distributions were obtained during the SPL, Horsetooth, Whiteface, and ACE-2 campaigns. For Whiteface and Horsetooth, this data was obtained from the CSU Classical Scattering Aerosol Spectrophotometer Probe Model 100, High Volume (CSASP-100-HV)(Particle Measurement Systems, Inc., Boulder, CO). For ACE-2 and SPL, drop size distributions were obtained from two different Forward Scattering Spectrophotometer Probe Model 100s (FSSP-100)(Particle Measurement Systems, Inc., Boulder, CO). Descriptions and uncertainty associated with this equipment are discussed in Appendix G. Ambient wind speed, wind direction, temperature, relative humidity, and pressure were measured at all locations.

These measurements were made at varying temporal resolution, but were generally logged and saved at no greater than 5 minute averages and the standard deviations for the time interval reported.

5.1.3.3 Gas-phase species

5.1.3.3.1 SO_2 and H_2O_2

Reproduced with permission of the copyright owner. Further reproduction prohibited without permission.

For Whiteface and Davis, SO_2 was continually measured using Thermo Environmental Co. (TECO) Model 43S pulsed fluorescent analyzers. At Whiteface, SUNY Albany/New York State Department of Health investigators reported half-hour averages to us. In Davis, we logged SO_2 as one minute averages.

For the $H_2O_{2(g)}$ data reported here, both the Collett and Husain groups use similar instruments. They are dual channel fluorometric analyzers, which measure $H_2O_{2(g)}$ based upon the horseradish peroxidase method (Lazrus *et al.*, 1986). Both channels (one for organic peroxides and one for total peroxides) are not always used. The Davis data is for total peroxides, although previous work in the Collett Group during IMS 95 suggests that organic peroxides are negligible in this type of environment. For Whiteface and Davis, 5 minute averages were logged, although only half hour averages have been reported.

Some ACE2 gas concentration data are available (see (Bower *et al.*, 2000) and references therein).

5.1.3.3.2 NH_3 and HNO_3

During the Davis campaign from 7:30 pm on January 6th through 7:12 pm on January 11, 1999, NH_3 and HNO_3 were continuously measured using pairs of coated glass ETH annular denuders (Oberholzer *et al.*, 1992). The coatings used were 0.05 M NaF for HNO_3 and 0.2M H_3PO_4 for NH_3. Twelve pairs of denuders were used, thus time resolution is relatively poor (on the order of eight – twelve hours). The intention was to match measurements with cloud event and pre- and post-event MOUDI aerosol samples. The denuders were coated in the field in January. The coating procedure involves swirling 5 ml of coating solution inside the annulus, discarding the waste, swirling another 5 ml of the coating solution, discarding the waste and then drying with N_2. Coated and "clean" (uncoated) denuders were kept capped and inside prior to outside installation. The denuder stand was capable of holding two pairs of denuders in parallel (one for HNO_3 and

Reproduced with permission of the copyright owner. Further reproduction prohibited without permission.

one for NH_3) vertically. Typically, two sets were kept installed (one "in-use" and one waiting) during operation. Subsequent tests suggested that keeping the denuders installed, but without gas flow in both dry and wet (foggy) conditions did not affect the blanks appreciably. This allowed for rapid switching between denuder sets when a fog event started or ended. Flow rates through the denuders were controlled by critical orifices. Each denuder was extracted with 3 ml of DI within hours (usually < 1 hour) of being removed from the stand. Both "clean" and coated, but unused, denuders were extracted for blanks. At every step, clean caps were used on the denuders to prevent contamination. The denuders and caps were thoroughly cleaned prior to use.

The denuders were operated with Teflon impactors at the inlet to minimize contamination by aspirated drops (Oberholzer *et al.*, 1992). The inlet height was approximately vertically co-located with the 5-Stage collector.

5.1.3.3.3 Additional gas phase measurements

O_3, NO, NO_x, and CO concentrations (reported as hourly averages) were obtained for Davis from the California-EPA's Air Resources Board web-site (http://arbis.arb.ca.gov/aqd/aqd.htm). Their sampling location was on the UC Davis campus, within a few kilometers of the fog sampling site over level terrain. According to Cal-EPA personnel, O_3 was measured photometrically, and NO and NO_x via chemiluminescent techniques.

5.1.3.4 Aerosol measurements

During the Davis campaign, size-resolved aerosol measurements were obtained before and after three cloud events using the MOUDI impactor (Marple *et al.*, 1991). Appendix J contains the MOUDI sampling protocol. The MOUDI inlet was vertically co-located with the 5-Stage.

Reproduced with permission of the copyright owner. Further reproduction prohibited without permission.

5.1.4 Field aliquot preparation

At every site, recovered cloud/fog sample was immediately brought to a small field lab area for processing. Samples were weighed first. Then small volumes of sample were pipetted into individual vials for either immediate analysis (pH) or subsequent analysis in the lab (see Table 5-1 (the Davis version)).

The standard sample size is LARGE (1 ml). In some instances, particularly in the 5-Stage and the small fraction of the sf-CASCC, sufficient sample volume was not recovered to permit LARGE aliquots, and SMALL (0.1 ml) sample volumes were used instead. LARGE are preferred, but the use of SMALL samples does not always introduce additional uncertainty in the results. Aliquot type priority varies both between and within campaigns and events. pH measurements have first priority, followed by IC. Then HCHO, H_2O_2, S(IV) and Metals aliquots may or may not be performed subsequently. Metals aliquots were usually high priority during 5-Stage operation.

The "NH_4^+" aliquot is not a standard aliquot, but was included in both the Davis and Whiteface campaigns to investigate the potential for biological degradation of NH_4^+ in solution. Additionally, in Davis some IC, Metals and NH_4^+ aliquots were made from filtered sample (Whatman ANOTOP IC syringe filter (0.2 μm pore size) and Nalgene 25 mm cellulose acetate membrane syringe filter (0.45 μm pore size)). The original intent was to investigate any impact on NH_4^+ concentrations by any colloidal material including bacteria in storage prior to analysis, but it was extended to Metals.

During ACE2, Whiteface, and Davis, duplicate aliquots were made occasionally (chiefly determined by available cloud water). These are parallel samples treated similarly to the "official" aliquot in all ways. The goal was to determine if the differences between duplicates and "official"

Reproduced with permission of the copyright owner. Further reproduction prohibited without permission.

samples exceeded the difference between replicate analyses of the "official" sample – the usual method used to determine the results' precision.

At Horsetooth, a few collected rime samples were kept frozen until returning to the lab to determine if the standard procedure of melting in the field produced any artifacts (discussed in Chapter 6).

Peroxidase and catalase reagent checks were performed during each cloud event. These solutions may be unstable, hence the checks to verify stability.

Samples are kept refrigerated prior to analysis. The RCWM and Rao (1997) describe the aliquot procedure in more detail than is presented here, and Table 5-1 is a summary.

5.2 Chemical analysis

5.2.1 pH

The pH measurements were made with an Orion Model 290A or 250A pH meter and a Microelectrodes, Inc. Model MI-710 combination pH electrode which was first calibrated with standard pH 4 and pH 7 buffers. The pH probe's calibration was periodically checked during an event and if it varied by more than ± 0.03 units the probe was re-calibrated.

5.2.2 IC (Inorganic ions)

"The World of the IC" contains a complete protocol description with particular comments for each campaign that I performed the analysis for (Moore, 1999a). Briefly, inorganic anions (Cl^-, NO_2^-, NO_3^-, $SO_4^=$) were determined using the AS4A-SC/AG4A-SC analytical and guard columns, a 25 µl standard injection, 1.8 mM Na_2CO_3/1.7 mM $NaHCO_3$ eluent with conductivity suppression, and

Reproduced with permission of the copyright owner. Further reproduction prohibited without permission.

Table 5-1: Davis campaign aliquot protocol (abridged)

Aliquot	Sample amount	9.7% HNO_3 SOLUTION	S(IV) PRESERVATIVE SOLUTION	CATALASE SOLUTION	H_2O_2 CONDITIONING REAGENT	H_2O_2 FLUORESCENT REAGENT	HCHO PRESERVATIVE SOLUTION	1.0 mM H_2O_2 SOLUTION	CHLOROFORM	Preferred vial
pH	40 µl*									0.5 ml microcentrifuge tube
IC	500 µl**									plastic IC vial (lid w/septum)
HCHO:										
LARGE	1 ml						100 µl			1.5 ml glass vial
SMALL	100 µl						10 µl			glass insert vial
S(IV):										
LARGE	1 ml		100 µl	100 µl						1.5 ml glass vial
SMALL	100 µl		10 µl	10 µl						glass insert vial
Metals:										
LARGE	1 ml	100 µl								1.2 ml cryovial
SMALL	100 µl	10 µl								plastic IC vial (lid w/o septum)
H_2O_2:										
LARGE	1 ml				200 µl	200 µl				1.5 ml glass vial
SMALL	100 µl				20 µl	20 µl				glass insert vial
NH_4^+:	500 µl†								25 µl	plastic IC vial (lid w/septum)
Per. CHECK	1 ml DI				200 µl	200 µl		100 µl		1.5 ml glass vial
Cat. CHECK	1 ml DI			100µl	200µl	200µl		100 µl		1.5 ml glass vial

**"condition" probe with 20 µl and then measure 20 µl of sample in new tube*
***small volume (300 µl) vials available if needed for SMALL volume aliquots (5-Stage)*
†KFM only

a 2 ml min^{-1} flow rate. Inorganic cations (Na^+, NH_4^+, K^+, Mg^{2+}, Ca^{2+}) were determined using the CS12A/CG12A analytical and guard columns, a 50 µl standard injection, 20 mM methanesulfonic acid eluent with conductivity suppression, and a 1 ml min^{-1} flow rate. Both SMALL and LARGE aliquots are measured similarly. For the Davis IC samples, the MOUDI cation analysis used a larger standard injection (100 µl) and the samples with very high concentrations of ammonium used a smaller standard injection (10 µl).

Standard calibration standards typically ranged from 2 – 1600 µN and were made from ACS-grade salts and de-ionized water (DI). The calibration standards were stored in sealed Nalgene

Reproduced with permission of the copyright owner. Further reproduction prohibited without permission.

bottles in the refrigerator and were stable for months. New calibration standards were made-up for every campaign. Every IC run had at least two, but usually three, NIST-traceable accuracy check standards for the relevant species which were analyzed at least twice each during the analysis of each set of samples. The accuracy check solutions for anions and cations were purchased from Dionex and then diluted with DI into the range of our IC. For nitrite, two different ACS-grade solutions were used to double-check the calibration make-up. It is very important that a range of accuracy check solutions be used as system response can vary between concentrations and calibration curves are not necessarily linear (see "The World of the IC" for details) (Moore, 1999a).

The denuder and aerosol substrate extracts were measured using the IC.

5.2.3 GFAAS (Metals)

"Using the GFAAS" contains a complete protocol description with particular comments for each campaign that I performed the analysis for (Moore, 1999b). Briefly, Fe, Mn, and occasionally Cu were determined using methods derived from the Varian-recommended analytical procedure described in the manuals. SMALL aliquots must be diluted for measurement, but are otherwise measured similarly.

The calibration standards for each species are made-up from ACS-grade 1000 ppm solutions in acid-washed glass labware. NIST-traceable accuracy check standards were purchased and measured without dilution. Two Fe/Mn combined standards were purchased, and later a Cu standard was also purchased.

Reproduced with permission of the copyright owner. Further reproduction prohibited without permission.

5.2.4 $H_2O_{2(aq)}$

Aliquots, stabilized by the addition of p-hydroxyphenylacetic acid solution in the field to form a dimer, are measured using the fluorescence spectrophotometer (Shimadzu RF-1501). SMALL and LARGE samples are analyzed similarly (only 80 µl of stabilized cloud water is used). This aliquot is not as stable as the others and is measured immediately upon return from the field. Details of the protocol are in the RCWM and Rao (1997), and the underlying method is based upon Lazrus *et al.* (1985).

5.2.5 $S(IV)_{(aq)}$

Stabilized aliquots (by the addition of catalase (to remove excess $H_2O_{2(aq)}$) and HCHO (to form hydroxymethanesulfonate (HMS))), are measured colorimetrically using a spectrophotometer (Hach DR/4000V). This is both a time-sensitive and reagent-order sensitive method. SMALL and LARGE samples are measured separately, and may have different statistical results. Details of the Collett Group protocol are in the RCWM and Rao (1997), and the underlying method is based upon the work of Dasgupta *et al.* (1980).

5.2.6 $HCHO_{(aq)}$

The HCHO aliquot is stabilized by the addition of bisulfite to form HMS. In the lab, reagents (2,4-pentanedione and ammonia) are added to form diacetyldihydrolutidine which is measured in the spectrofluorimeter (Shimadzu RF-1501). SMALL and LARGE samples are analyzed similarly (only 70 µl of stabilized cloud water is used). Details of the protocol are in the RCWM and Rao (1997), and the underlying method is based upon the work of Dong and Dasgupta (1987).

Reproduced with permission of the copyright owner. Further reproduction prohibited without permission.

5.3 Analytical uncertainty

The chemical analytical uncertainty includes the minimum detection limit, measured precision and accuracy (for IC and GFAAS only). The minimum detection limit (MDL) is calculated at the 95% confidence level (CL). The data used to calculate the MDL varies between instruments, and methods and will be included in the sub-sections that follow. The precision calculations are based upon the analysis of replicate pairs – samples for the IC and GFAAS and often calibration standards for the others.

Sample blanks are generally of low enough concentration – at or near the detection limit for all analyses other than via the GFAAS – that no blank correction is applied to the reported values. Some of the metals blanks were high enough to warrant minor correction, although the need for this step is arguable (see section 5.5.2.4).

5.3.1 pH

Although no repeat measurements were made in the field, subsequent repeat measurements in the lab indicated that both "low pH" (Whiteface), "high pH" (Davis), and selected Horsetooth samples could be measured within 1 – 2% (pH units) on average by a single investigator under varying laboratory conditions. However, field conditions are assumed to be more random and a larger uncertainty (± 5%) is used.

5.3.2 IC

The compiled results from the four campaigns are presented in detail in Appendix K. Minimum detection limit (MDL), precision, accuracy and any duplicate sample data are presented there. In

Reproduced with permission of the copyright owner. Further reproduction prohibited without permission.

general, the detection limits are very low (< 5 μN), accuracy is very good (± 10% or better), and so is precision expressed as the relative standard deviation (RSD) (< 5% for concentrations > 10 – 20 μN). As concentrations increase, both precision and accuracy can improve to within 2%. Precision is usually calculated for two concentration ranges: low (near the MDL) and high. The motivation behind this approach is to not swamp the relatively higher uncertainty associated with measurements near the detection limit with the relatively lower uncertainty for high concentration measurements (the data presented in Appendix K show that most species have much higher RSDs for measured concentrations < 10 – 20 μN than at larger concentrations). Calculations using IC data consider the uncertainty associated with precision only. The divalent cations, magnesium and calcium, are the most difficult to quantify at low (< 100 μN) concentrations and this issue is addressed in section 5.5.

Where they exist, duplicate sample data are typically not statistically different from the reported samples, although calculated precision tends to be worse via the duplicates. A smaller number of duplicate sample pairs is partly responsible.

It is important to recognize that the signal (peak) associated with a particular species in the IC must reach a threshold area level in order to be recognized (indicated in the tables in Appendix K). For example, no sodium is detected if the "measured" area is 450 units and the threshold area required is 500 units. For several species, particularly the early-eluting ones, this threshold area can correspond to a 1 – 1.5 μN peak. Therefore, calculating the minimum detection limit based upon a combination of the mean of the DI blanks (which invariably are less than the threshold) and replicate measurements of a low standard (2 μN) (which invariably are higher than the threshold) can yield misleading results. This was "standard practice" in our group. For example, if the DI blank mean is 0.0 μN and the standard deviation of the low standard is 0.2 μN then the calculated 95% confidence limit MDL might be 0.7 μN. The standard deviation from the low standard was used because the DI blank always measured 0.0 μN. However, this MDL is meaningless if it is less than the threshold value (e.g. the MDL corresponds to 450 area units, but

Reproduced with permission of the copyright owner. Further reproduction prohibited without permission.

the IC will not recognize any value less than 500 units). An improved approach is to use each calibration equation and the threshold area to calculate the MDL. For however many IC calibrations were required for the particular campaign, each species' calibration equation is multiplied by its threshold area to obtain the minimum (threshold) concentration. In this manner, the minimum recognizable concentration for each calibration and species is determined. These threshold concentrations are collectively used to determine a mean and standard deviation which in turn are used to calculate the 95% confidence limit MDL. This method is preferred and should be used in lieu of the DI blank/low standard approach where applicable (although both are reported in Appendix K). While the absolute difference between the two approaches is small, it can be significant if low concentrations are being considered. Reilly (2000) is incorrect in her assessment of this point. "The World of the IC" contains further information regarding the different calculation methods (Moore, 1999a).

Aerosol extract concentrations are assumed to have the same precision as the individual species' IC results. The ethanol used in the extraction did not affect the results for the species reported.

5.3.3 GFAAS

All GFAAS sample injections are performed in replicate which serve as the basis for the precision calculations. Tables 5 – 2, 5 – 3, and 5 – 4 contain the Fe, Mn, and Cu data, respectively. Reilly (2000) mis-reports Fe precision. Duplicate analyses are available for ACE-2 only and they indicate that roughly 15 of the 17 duplicates were within the 95% confidence level of the replicate sample. However, these bounds can be relatively large. The higher variation calculated using duplicates may indicate inconsistently aliquoted colloidal material in the sample.

5.3.4 $H_2O_{2(aq)}$

Reproduced with permission of the copyright owner. Further reproduction prohibited without permission.

Table 5 – 5 contains the aqueous-phase H_2O_2 data. Precision of the Whiteface duplicates are markedly worse, but still acceptable, than via the replicates. No accuracy data exist, and the verification of the concentration of the H_2O_2 primary 30% solution may not have occurred for the Davis campaign, but was completed for the other two.

Table 5-2: Fe compiled statistics

Fe				
Minimum Detection Limit (@ 95% CL)				
	ACE2	3.6	[µg/l]	
	Whiteface & Davis	2.4	[µg/l]	
Precision (relative standard deviation)				
		RSD	*RSD range*	*supporting information*
	ACE2*	10.2%	< 10 µg/l	(18 samples, 0.54 – 9.71 µg/l, mean 4.48 µg/l)
		3.5%	> 10 µg/l	(64 samples, 10.6 – 216.7 µg/l, mean 60.9 µg/l)
	Whiteface & Davis	6.2%	< 10 µg/l	(140 samples, -0.01 – 9.99 µg/l, mean 4.26 µg/l)
		2.8%	> 10 µg/l	(495 samples, 10.0 – 268.0 µg/l, mean 74.4 µg/l)
Accuracy (Whiteface & Davis only)				
	nominal [µg/l]	190	30	
	measured/nominal	104.4%	104.8%	
	std. dev./measured	5.7%	3.9%	
	# of measurements	31	36	
	**dilution adds 1% more uncertainty to some samples*			

Table 5-3: Mn compiled statistics

Mn				
Minimum Detection Limit (@ 95% CL)				
	ACE2	0.21	[µg/l]	
	Whiteface & Davis	0.16	[µg/l]	
Precision (relative standard deviation)				
		RSD	*RSD range*	*supporting information*
	ACE2*	6.5%	< 3.3 µg/l	(39 samples, 0.025 – 2.93 µg/l, mean 0.96 µg/l)
		2.0%	> 3.3 µg/l	(51 samples, 3.38 – 63.0 µg/l, mean 18.8 µg/l)
	Whiteface & Davis	11.3%	< 2 µg/l	(364 samples, -0.11 – 2.0 µg/l, mean 0.51 µg/l)
		2.6%	> 2 µg/l	(364 samples, 2.0 – 40.2 µg/l, mean 7.55 µg/l)
Accuracy (Whiteface & Davis only)				
	nominal [µg/l]	30		
	measured/nominal	106.2%		
	std. dev./measured	5.4%		
	# of measurements	69		
	**dilution adds 1% more uncertainty to some samples*			

Reproduced with permission of the copyright owner. Further reproduction prohibited without permission.

Table 5-4: Cu compiled statistics

Cu (selected samples only)				
Minimum Detection Limit (@ 95% CL)				
Whiteface & Davis		0.46	[µg/l]	
Precision (relative standard deviation)				
		RSD	*RSD range*	*supporting information*
	Whiteface & Davis	19.8%	< 1.5 µg/l	(108 samples, -0.53 – 1.49 µg/l, mean 0.43 µg/l)
		6.7%	> 1.5 µg/l	(223 samples, 1.52 – 192.0 µg/l, mean 7.52 µg/l)
Accuracy (Whiteface & Davis only)				
	nominal [µg/l]	30		
	measured/nominal	95.6%		
	std. dev./measured	6.7%		
	# of measurements	38		

The minimum detection limit calculations were based upon DI blanks for ACE2 and collector blanks for Davis and Whiteface. DI and collector blanks yield indistinguishable concentrations.

Table 5-5: Compiled $H_2O_{2(aq)}$ statistics

$H_2O_{2(aq)}$				
Minimum Detection Limit (@ 95% CL)				
	ACE2	0.23	[µM]	
	Whiteface	0.18	[µM]	
	Davis	0.05	[µM]	
Precision (relative standard deviation)				
		RSD	*method*	*supporting information*
	ACE2	1.9%	replicates	(8 samples, 62.1 – 75.3 µM, mean 68.1 µM)
	Whiteface	2.0%	replicates	(29 samples, -0.34 – 78.5 µM, mean 16.2 µM)
		10.3%	duplicates	(11 samples, 0.13 – 28.6 µM, mean 8.53 µM)
	Davis	9.3%	replicates	(12 samples, -0.12 – 30.2 µM, mean 7.65 µM)

5.3.5 $S(IV)_{(aq)}$

The compiled S(IV) statistics are in Table 5 – 6. SMALL and LARGE volume samples have different MDLs at Whiteface. Precision data are not reported for ACE2 and Whiteface because virtually all samples were at or below the MDL. The MDL is calculated based upon collector blanks. In Davis, while several samples had 10 – 15 µM concentrations, the precision calculations included many low concentration samples yielding a relatively high RSD (the median

Reproduced with permission of the copyright owner. Further reproduction prohibited without permission.

value of the sample pairs used to calculate the RSD is less than the reported 95% CL MDL (2.4 μM)). No accuracy information is available. In absolute terms the standard deviation is approximately 1.6 μM. The S(IV) method is very noisy at low concentrations which is reflected in the RSD – standards less than 5 μM in concentration overlap each other significantly.

Table 5-6: Compiled S(IV) statistics

S(IV)				
Minimum Detection Limit (@ 95% CL)				
	ACE-2	1.8	[μM]	
	Whiteface	3.1	[μM] SMALL	
		4.9	[μM] LARGE	
	Davis	2.9	[μM]	
Precision (relative standard deviation)				
		RSD	*method*	*supporting information*
	ACE-2	not reported	replicates	
	Whiteface	not reported	replicates	
	Davis	50%	replicates	(28 samples, -0.14 – 10.5 μM, mean 3.2 μM)

5.3.6 $HCHO_{(aq)}$

The compiled HCHO data is in Table 5 – 7. The minimum detection limit was calculated at Whiteface from collector and field blanks and from DI blanks at Davis. Duplicate pairs again give a higher calculated precision uncertainty than replicate pairs. No accuracy information is available.

5.3.7 Gas data

SO_2 (TECO) information is reported in Rattigan *et al.* (2001) for Whiteface, and Collett *et al.* (1999) for Davis-type conditions. At Whiteface, the SO_2 MDL was 0.06 ppbv with 1% precision (during calibration), and the H_2O_2 MDL was 0.05 ppbv. The Whiteface H_2O_2 precision was not clearly indicated, but Dr. Husain's group suggests the calibration is good to ± 10% at a 95% CL.

Reproduced with permission of the copyright owner. Further reproduction prohibited without permission.

Due to the low quantities measured, the H_2O_2 precision in Davis is estimated to be ± 20%. The Davis H_2O_2 MDL varied but was always < 0.1 ppbv. The Davis SO_2 MDL was 0.06 ppbv and the calculated precision was < 1%. ACE-2 information is not available, but as the same type of equipment was used for H_2O_2, it is assumed to be similar.

Table 5-7: Compiled HCHO statistics

HCHO				
Minimum Detection Limit (@ 95% CL)				
	Whiteface	1.4	[µM]	
	Davis	2.3	[µM]	
Precision (relative standard deviation)				
		RSD	*method*	*supporting information*
	Whiteface	1.2%	replicates	(27 samples, 0.36 – 21.1 µM, mean 9.1 µM)
		18.6%	duplicates	(10 samples, 3.3 – 12.2 µM, mean 7.8 µM)
	Davis	11.1%	< 20 µM (replicates)	(7 samples, 0.51 – 22.8 µM, mean 11.5 µM)
		7.3%	> 20 µM (replicates)	(27 samples, 20.7 – 143.2 µM, mean 67.1 µM)

Denuder concentrations were corrected using the parameters given in AT560 (Fall 1996) and the standard Gormley-Kennedy equation. Data obtained during AT560 (Fall 1996) indicated that the theoretical calculations fit the experimental results (approximately 96% efficiency). HNO_3 was no more than a factor of 2 – 3 greater than the MDL for NO_3^- (converted to a gas-phase concentration). Taking flow rate uncertainty into account (2%, measured), the RSD was 14%. The uncertainty in NH_3 calculated similarly is approximately 7%.

Gas data obtained from Cal-EPA are good to the reported resolution of the instrument (1 ppbv) (Bloudoff, 2001).

5.4 Other measurement uncertainty

Reproduced with permission of the copyright owner. Further reproduction prohibited without permission.

5.4.1 Meteorological measurements

Our weather station has not been officially calibrated since its original purchase. The operator's manual contains its original uncertainties. Wind direction was was verified in Davis using a compass. Whiteface wind direction data are consistent with the field notes. The other parameter measurements provided are assumed to be good relative to each other, but it is unknown how accurate they are in absolute terms. However, ASOS station data obtained at two nearby sites – the Sacramento Executive Airport, Sacramento, CA (approximately 5 miles W) and Travis Air Force Base (approximately 30 miles SSE) – are in general agreement with the Davis data. The relative humidity sensor's performance is questionable as it does not exceed 93 – 95% even during cloud events.

Ambient pressure data are required to compute gas concentrations (e.g. Davis NH_3 and HNO_3), and ambient wind speed data are required to make corrections for anisokinetic sampling conditions in some collectors and the drop size distribution measurements. In both instances, any uncertainty is neglected and is assumed to have a negligible impact upon the results. Ambient temperature measurements are assumed to be good to ±1°C, which is consistent with their treatment by other investigators (particularly relevant to gas/liquid partitioning calculations in Chapter 9, Appendix L).

At ACE2, UMIST performed the meteorological measurements (Bower *et al.*, 2000). Estimated uncertainties are treated similarly to our measurements.

5.4.2 Flow rates

The flow rates in the Caltech collectors are not measured and are assumed to be ± 5% from design as reported by Demoz *et al.* (1996) if the correct voltage is applied to the fans (13.7 V to

Reproduced with permission of the copyright owner. Further reproduction prohibited without permission.

the sf-CASCC). Combining repeat measurements of the flow rate through the 5-Stage at Whiteface and Davis gives a standard deviation of 4%. The relative standard deviation in the denuder flow rate measurements was 2%. For the MOUDI, the uncertainty in the flow rate is assumed to be ± 5% (consistent with repeat lab measurements).

5.5 Analytical data validation

5.5.1 Charge balance

The ratio of measured anions to cations was calculated for all cloud water IC samples. The calculation includes H^+, OH^- (derived from pH data and temperature) and the carbonate system. The carbonate system was included for completeness and assumed to be at equilibrium, although reportedly earlier measurements at another location suggested the assumption of equilibrium may not be accurate. However, the carbonate system was estimated to be of very minor influence (always < 10% of the anions on average and usually < 1%) in this data set. The preferred range of anions/cations is 80 – 120% which suggests that all charged species were reasonably measured given the uncertainty. As organic acid concentrations were not rigourously quantified in the samples, it is expected that an anion deficit (< 100%) is more likely to occur than a cation deficit. If the charge balance is outside these limits, the sample will be excluded unless concurrent samples (e.g. from other collectors) indicate that there is a systematic bias. For example, if high concentrations of unmeasured organic acids are present, the charge balance could be < 80%, but the observation must hold for across all collectors. Blanks are not included in this calculation as the total ionic concentrations are low. All the percentages that follow are the ratio of measured anions to cations.

Reproduced with permission of the copyright owner. Further reproduction prohibited without permission.

At Horsetooth, virtually all samples were within the 80 – 120% range. There were two exceptions – samples with 180% and 30% ratios were excluded from the data interpretation. At ACE-2, all samples were within 81 – 98% (92% mean). At Whiteface, the W185 data for all collectors showed very poor agreement (on the order of 50%) which is not surprising given the low total concentrations (the sum of the total charges was often < 200 μN). However, as the collectors were not oriented into the wind (see Chapter 4) these data are excluded. For the subsequent events, the mean ratio is estimated to be approximately 85%. A few individual samples had agreement as poor as 65%. However, as this was observed across all the collectors operated, these samples were accepted. In particular, the larger fractions of the 5-Stage for the first sample on W198 were about 70%. It is not clear what the source of this discrepancy at Whiteface is, and pH values are low enough that organic acids should not be occur in solution in their charged forms. In Davis, the collectors and collector fractions yielded somewhat different results. The small fraction of the sf-CASCC and the smaller fractions of the 5-Stage had results generally > 85% (with one or two exceptions). The large fraction of the sf-CASCC, CASCC2, and larger fractions of the 5-Stage had worse results that typically ranged from 60 – 70% up to 90%. However, on D004 the range was 40 – 70%. Formate and acetate were identified in some samples and the presence of the organic acid ions would be greater in the larger drops due to their higher pH. As the collectors and collector fractions yielded similar results, none were excluded.

5.5.2 Comments specific to particular analyses/campaigns

5.5.2.1 Low concentrations of divalent cations

Our cation system has persistent low-level peaks of both magnesium and calcium (< 5 – 7 μN). Attempts to eliminate this contamination failed. However, attempts to adjust for these peaks in

Reproduced with permission of the copyright owner. Further reproduction prohibited without permission.

the numerical processing of the chromatograms revealed that the pre-existing calibration method for magnesium and calcium had significant (and unquantified) accuracy issues at concentrations less than approximately 50 – 100 μN. While the method was subsequently improved (and is reflected in the data reported here), it is important to consider this factor when comparing these results to earlier ones. A full description of the method may be found in Moore (1999a).

Additionally, during the Whiteface IC runs it became apparent that the cation column was having difficulty with the magnesium and calcium peaks. Repeat injections of the same sample vial could yield a factor of 2 difference in the reported concentrations (if less than approximately 50 μN). Replacing the column, which was several years old, appeared to fix this problem which had not been previously observed.

The two identified problems with the divalent cation analysis – poor accuracy at low concentrations and column age yielding non-reproducible results – are independent of each other. The accuracy issue resulted from the then-current practice of accepting very poor calibration curve fits at low concentrations. While the system response to calcium concentrations is somewhat non-linear, most of the low level quantification problems stem from the persistent non-zero levels of the divalent cations.

5.5.2.2 GFAAS methods

It became apparent during the ACE-2 analysis that both the existing Fe and Mn methods were inadequate and had the potential to provide mis-leading results. (The Cu method was developed specifically for the Whiteface and Davis campaigns). Carryover contamination between samples in the furnace tube was a significant problem for Fe: blanks that were known to contain little/no Fe were interspersed with ACE-2 samples of moderate Fe levels and the blank levels steadily rose throughout the analysis (not shown). The Mn method attempted to calibrate well beyond the

Reproduced with permission of the copyright owner. Further reproduction prohibited without permission.

quantifiable range for the particular wavelength selected. Both of these methods and the GFAAS operating procedure were substantially revised (see Moore (1999b) for details). Calibration problems improved following method modification. Further, separate NIST-traceable accuracy standards were purchased which suggest that the Fe, Mn and Cu methods currently in use are acceptable. Previously reported MDLs may be much too low, although this partly stems from very poor methodology in measuring blanks (see Moore (1999b) for details). Further, the accuracy of the results may be very poor due to both to inadequate equipment operation methods, sample handling (see below), and a lack of a systematic methodology for its evaluation (see Moore (1999b) for details).

During the revision of the Fe and Mn methods, it became apparent that sample analysis (and re-analysis) had the potential to result in a previously unidentified evaporation problem. This effect was investigated and quantified using standards, and is a particular issue for SMALL volume samples (see Moore (1999b) for details). As a result, the Horsetooth Fe and Mn data are not reported.

5.5.2.3 5-Stage HCHO and S(IV) aliquots

The usual 5-Stage blank procedure suggested that HCHO and S(IV) could be measured without contamination. However, it became apparent after reviewing the Whiteface and Davis cloud data that low level contamination was occurring on the order of a few μM. There was a pronounced bias compared to the results reported by the other collectors. The 5-Stage body is composed of Delrin™ which is polymerized HCHO. It appears that for longer exposure times than typically used while taking blanks, some leaching may occur. Therefore, the 5-Stage should not be used for HCHO and S(IV) measurements. HCHO is used in the preservation of S(IV). Therefore, HCHO leaching into the collected water in an uncontrolled manner results in inconsistent results at least as compared to the data obtained from the Caltech collectors. It can be argued that the

Reproduced with permission of the copyright owner. Further reproduction prohibited without permission.

HCHO leaching may provide an "improved" value of S(IV) in solution but as the amount added may vary it is difficult to assess this quantitatively.

5.5.2.4 Whiteface DI contamination

Analytical work after the Whiteface campaign indicated that the DI used at Whiteface to clean the collectors contained on average 30 – 50 µg/l of Fe. Reported concentrations have not been blank-corrected, and the "operational detection limit" (as concentrations are well above the MDL) is assumed to be the background concentration. It is interesting to note that side-by-side operation of the "old" sf-CASCC (cleaned at CSU) and the "new" sf-CASCC (cleaned at Whiteface) on W188 yielded virtually identical results for Fe (see Chapter 4).

5.5.2.5 Sample stability

The stability of the S(IV) standards and the effect of using different batches of reagents on the reported results was investigated. No discernable difference was found between standards 6 – 9 months old and freshly made-up ones.

The stability of the ions in solution was a particular concern. While pH likely will change between field and later lab measurements, it is not clear if other species will change or not. The pH change is often attributed to the consumption of organic acids by biological material in the sample as the pH routinely increases. Work by others suggests that sodium, potassium, magnesium, calcium, chloride, nitrate and sulfate are reasonably stable once sampled (Karlsson *et al.*, 2000; Ramundo and Seastedt, 1990; Miller *et al.*, 1987). Nitrite in fog and rain samples has also been reported to be stable (Kieber *et al.*, 1999; Miller *et al.*, 1987). Of particular concern are ammonium concentrations which have been observed to decrease substantially within as little as

Reproduced with permission of the copyright owner. Further reproduction prohibited without permission.

a week depending upon sample handling (Karlsson *et al.*, 2000; Lamb and Comrie, 1993; Ramundo and Seastedt, 1990).

A comparison of the analytical results for a few common samples between our lab and another at ACE-2 prompted some of this work. All ions measured agreed within 10% except for ammonium which was closer to 20%. Given these results, approximately 30 selected IC vials were re-analyzed at 6 – 9 months following their initial quantification. For the "stable" species (e.g. chloride, nitrate) virtually no change was observed in concentration, although there is some suggestion (well within the uncertainty) of slight evaporation during IC vial storage. The IC vials, while stored in the refrigerator, have pierced septa following initial analysis so some loss of water is not surprising. Ammonium concentrations were slightly lower where samples needed to be diluted for sodium re-analysis and also after storage compared to their original values. In neither case, however, were the results outside the analytical uncertainty (not shown). Sample dilution should have raised the pH of the ACE-2 samples so some loss of ammonium from solution is not unexpected.

At Whiteface, selected additional IC vials were prepared with $CHCl_3$ added as a preservative to prevent biological activity. Subsequent analysis during the regular analysis suggested that biological activity was likely not important in changing refrigerated ammonium concentrations while waiting for analysis (at least for 1 – 2 months). Several authors have suggested it may be a factor in some situations (Lamb and Comrie, 1993; Ramundo and Seastedt, 1990).

At Davis, where ammonium is the principal cation in the samples, $CHCl_3$ was again added to some filtered and unfiltered samples. Comparisons between samples suggested that filtered, filtered and preserved, and unfiltered samples were within ± 15%. Most were within ± 5% which is within the uncertainty associated with the precision and variations in accuracy for ammonium (the ammonium RSD can be less than 5%, however accuracy can vary 5% from IC analysis-to-IC analysis). The reported ammonium concentration in the regular samples did tend to be lower

Reproduced with permission of the copyright owner. Further reproduction prohibited without permission.

than the other three, however. When all the cation analyses had been completed, a selected number of IC vials were re-analyzed for ammonium. There was approximately a month between the first analysis and the subsequent one. The results are shown in figure 5-1.

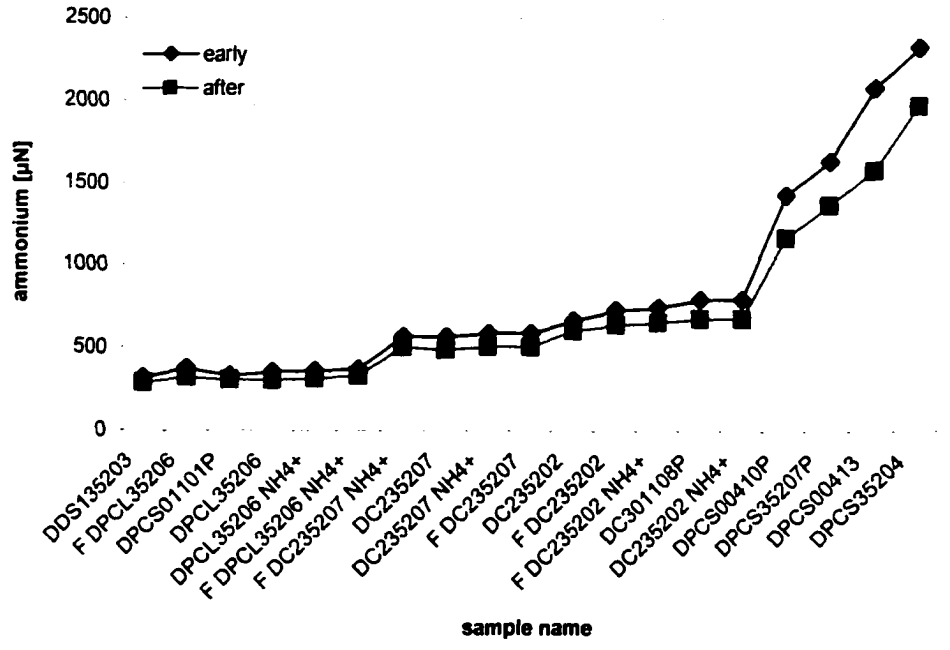

Figure 5-1: Davis: ammonium stability in IC vials after approximately 1 month of storage

For the cloud water samples selected which include filtered ("F"), filtered and preserved ("F" and "NH4+"), unfiltered and preserved ("NH4+" only), and regular (occasionally followed by a "P"), there does appear to be a bias in the results (up to a 25% loss at higher concentrations, although 10% is more typical). The analytical precision is < 3%, and a change in accuracy between sample runs does not appear to be able to account for this result. This should be investigated further.

In particular, the loss of ammonium was observed across all samples, regardless of field treatment. This suggests that whatever factor or factors are responsible may result from laboratory processing. A few items to consider are (a) ammonium appears to be indefinitely

Reproduced with permission of the copyright owner. Further reproduction prohibited without permission.

stable in the sealed Nalgene vials used to store the calibration standards, (b) the IC lids are not considered "gas-tight" by the manufacturer prior to septum puncture, (c) ambient lab NH_3 concentrations can be appreciably lower than in the field, and (d) the internal temperature of the IC autosampler often exceeds 30°C. As the standards are stable, this suggests that it is possible to handle the samples appropriately to mitigate losses. As NH_3 is a relatively small molecule it may be important that even the un-pierced IC lids are not gas-tight, particularly if ambient NH_3 concentrations are low in the lab or refrigerator. There is likely a concentration gradient between the headspace in the vial and the ambient lab (or refrigerator) atmosphere. Further, the Davis fog samples were collected near freezing temperatures. While the relative percentage of ammonium expected to be in solution for a given pH does not change, the overall solubility is very much reduced at 30°C in the autosampler and vials may stay loaded for extended periods (20 hours or more) of time.

Finally, selected samples were also re-analyzed for nitrite and no change was detected.

Reproduced with permission of the copyright owner. Further reproduction prohibited without permission.

6. Horsetooth

This section contains selected results from a supercooled cloud water sampling campaign conducted on Horsetooth Mountain in Fort Collins, CO during April 1998. The campaign's sampling site will first be described followed by a review of the motivation behind studying mixed-phase clouds and the results of an earlier campaign at Storm Peak Lab (SPL) the previous winter. The size-dependent drop composition results from FROSTY will then be presented. While the campaign itself was quite limited (only one event was sampled), we gained useful insights into our then-current analytical and sampling protocols. Although FROSTY has not been used in the field since, the Horsetooth results have benefited our other campaigns and have raised questions that should be investigated when FROSTY is used again.

6.1 The Horsetooth Mountain site

Horsetooth Mountain is located within Horsetooth Mountain State Park located to the east of the City of Fort Collins. We used a site on one of the mountain ridges where power and facilities were available. Based upon topographic maps, the elevation of the sampling site was approximately 2100 – 2150 m asl. While some trees and metal towers containing radio, television and police equipment surrounded the general sampling site, the immediate vicinity of the cloud water sampling location (on top of a small building) was relatively clear. The CSU PVM-100 had previously been installed on one of the towers.

One goal of the Horsetooth campaign was to obtain additional size-dependent cloud drop composition data via FROSTY to determine if the conclusions reached based upon its SPL measurements could be generalized. Further, most ground-based cloud composition

Reproduced with permission of the copyright owner. Further reproduction prohibited without permission.

measurements in Colorado have been conducted at SPL which is on the western side of the Rocky Mountains and not the eastern side as Horsetooth is. Measurements of "upslope" clouds at Horsetooth might be different from those observed at SPL because the air mass source regions and sampling elevation vary between the two sites. The Horsetooth site was also reasonably accessible from the Department of Atmospheric Science and provided a good location to attempt to obtain additional data using FROSTY. To my knowledge, no ground-based cloud water composition measurements have been reported for the Front Range of Colorado, although there has been at least one aircraft-based study several years ago near Denver (Parungo *et al.*, 1989).

6.2 Why study mixed-phase clouds?

Snow crystals grow by aggregation (with other crystals), vapor deposition and accretion (or riming) of supercooled cloud drops. Growth by vapor deposition results in very clean crystals and cloud drops have relatively higher solute concentrations. Collected rime generally is more concentrated than concurrent snow crystals (Berg *et al.*, 1991). Accretion can be an effective removal mechanism for cloud drops from the atmosphere in some mixed-phase clouds. For example, in a recent study of moderately rimed snowfall, thirty to forty percent of the deposited snow was accreted cloud water (Mitchell *et al.*, 1990). If substantial snow crystal riming occurs, the resulting precipitation can contain high solute concentrations. Several investigators have studied mixed-phase clouds and winter precipitation chemistry. Their analyses indicate that the degree of riming can be correlated with observed snow chemistry (Devulapalli and Collett, 1994; Kalina and Puxbaum, 1994; Collett *et al.*, 1993b; Collett *et al.*, 1991a; Mitchell and Lamb, 1989). In heavy riming conditions, precipitation and cloud composition converge (Borys *et al.*, 2000; Collett *et al.*, 1993a). Conversely, the snow and cloud composition may diverge if only light riming occurs (Borys *et al.*, 2000). Thus, variable riming impacts the snow chemistry (Voisin *et al.*, 2000; Baltensperger *et al.*, 1998). For these types of studies (typically at mountain sites) care must be taken not to confuse an air mass change for pollutant removal (Poulida *et al.*, 1998;

Reproduced with permission of the copyright owner. Further reproduction prohibited without permission.

Devulapalli and Collett, 1994; Collett *et al.*, 1991a). Riming tends to increase with cloud LWC, but drops with diameters < 10 μm are not efficiently collected on snow crystals (Wagenbach, 1997; Mosimann *et al.*, 1993). In a study in Bondville, IL, accreted ice crystal mass was dominated by drops in the 20 – 40 μm diameter range (Devulapalli and Collett, 1994). Therefore cloud and precipitation chemistry investigations should ideally be able to discern drop size-dependent chemical composition.

6.3 The Storm Peak Laboratory Winter 1996/7 Results

A brief discussion of the site and the measurements made at the Storm Peak Laboratory (SPL) is included in Chapter 3 accompanying the field performance evaluation of the two collectors operated there – FROSTY and the Caltech Heated Rod Cloud water Collector (CHRCC). Selected tabulated data from this campaign are in Appendix H.

The SPL campaign investigated both precipitation and cloud chemistry. Replicas of falling crystals were made to investigate the degree of riming. Forty cloud samples were collected over the six events sampled. H^+, $SO_4^=$, NO_3^-, NH_4^+, Ca^{2+}, Fe and Mn were all found to have size-dependent cloud drop composition, although the degree of the variation changed between and within events. In many instances, a "U-shaped" profile was observed across the 3 FROSTY stages (e.g. LARGE and SMALL drops were both more concentrated than drops from the MEDIUM stage). For some species, concentrations increased from SMALL to LARGE, while for others (e.g. Ca^{2+}) the opposite trend was observed. Some species showed little drop size variation. Nitrate, ammonium, and sulfate concentrations all tended to be higher in the smaller drops. Drop pH varied from 3.6 – 7.7 and the difference between the large and more acidic small drops was up to 1 pH unit. Sulfate, calcium, ammonium and nitrate concentrations varied from 7 – 376 μN, less than the detection limit – 229 μN, 13 – 438 μN, and 11 – 254 μN, respectively. HCHO (5 – 110 μM), Fe (50 – 500 μg l^{-1}) and Mn (typically < 5.0 μg l^{-1}) were also measured in the cloud water. A positive correlation was found in two of the four case studies presented in Xu *et*

Reproduced with permission of the copyright owner. Further reproduction prohibited without permission.

al. (1999) between degree of riming and the precipitation composition. As the drops in the FROSTY SMALL stage (D_{p50} < 11 μm) were the most concentrated for the species of interest (H^+, NO_3^-, $SO_4^=$), calculations indicated that neglecting size-dependent cloud composition when investigating the effect of riming on precipitation chemistry would yield acceptable results (± 15%). Although precipitation composition measurements were not performed at Horsetooth, the goal of sampling there was to see if the same kind of drop size-dependent composition was observed.

Xu *et al.* (1999) and references therein should be consulted for further details of the SPL campaign.

6.4 Results

On April 14, 1998 conditions suitable for the formation of an "upslope" cloud occurred (winds from the NE – E). The sampling site went into cloud and sampling commenced at 17:15 (local time). Winds were light (approximately 1 – 2 m s^{-1}) and, critically, the temperature remained > 1°C on average until after approximately 22:00. The cloud was patchy until 23:00. Then the cloud thickened and the site remained in cloud until it lifted at approximately 4:00 on April 15.

Eight sets of samples were collected from FROSTY during the event. The CSASP-HV-100 was operated from 22:21 through the end of the event. Inexplicably, no CSASP data was logged from approximately 23:50 to 0:52 on April 15, 1998. Our weather station was co-located with FROSTY and the CSASP. After the event, a data logging failure was discovered in the PVM system and no direct LWC data are available for the campaign (results from the later Whiteface campaign suggest CSASP-derived LWC is unreliable (see Appendix G)).

Sample volumes were extremely small, consistent with observations that the cloud was not thick. Collected masses rarely exceeded 1 g on the MEDIUM and SMALL stages. In some instances

Reproduced with permission of the copyright owner. Further reproduction prohibited without permission.

only sufficient sample existed to perform pH measurements. The complete aliquot set for the event included pH, IC, and Metals, although the latter are not reported (see Chapter 5).

In the figures that follow, the vertical and horizontal error bars represent plus and minus one combined "standard deviation" including all the quantified/estimated sources of uncertainty as described in previous chapters. The exception is for the horizontal axis when concentrations are plotted as a function of median mass diameter. Median mass diameter is calculated for FROSTY as described in Chapter 3. All figures, unless otherwise indicated, have both vertical and horizontal error bars. The vertical errors bars represent analytical uncertainty only. In some instances the analytical uncertainty is small enough that it does not show in the figures. Concentration values plotted are as measured for each FROSTY stage.

6.4.1 Data Validation

Validated data are tabulated in Appendix H.

6.4.1.1 FROSTY Operation in non-freezing conditions

If FROSTY is operated at non-freezing temperatures, drops do not freeze upon impact on the collection surfaces. Instead, they impact, coalesce, and migrate across the impaction surface under the influence of the impinging jet. They then flow over the lip of the impaction surface where they appear to collect. As drop collection is inconsistent, data where this was observed to occur were discarded (samples #1 and #2). During sampling, it was obvious that the drops were not freezing.

6.4.1.2 Charge balance

Reproduced with permission of the copyright owner. Further reproduction prohibited without permission.

Some stages from samples #4 and #8 failed the charge balance criterion (see Chapter 5). For both samples, the cloud was lifting which may have affected observations. The IC analysis suggested that low molecular weight organic acids were present and unquantified in the samples. However, in the absence of supporting measurements, the 30% and 180% measured anion/cation ratios calculated were unacceptable.

6.4.1.3 Drop size distributions

Complete CSASP data were available for samples #6 (April 15, 1:00 – 2:00) and #7 (April 15, 2:00 – 3:00). Therefore the plots that appear below will focus on these two periods, although the composition measured in samples #3 (April 14, 21:04 – 22:00) and #5 (April 14 23:02 – April 15 1:00) appear to be valid.

6.4.2 Drop size-dependent composition

Chloride, sodium, magnesium, and potassium ions were measured in concentrations near or at their detection limits and are not further discussed. The principal species observed were ammonium, calcium, nitrate, sulfate and H^+ as seen at SPL.

Drop pH measurements indicated that the pH generally increased with drop size (SMALL pH < MEDIUM pH < LARGE pH)(figure 6-1). The pH range in field measurements was from 3.6 (SMALL, sample #7) to 6.9 (LARGE, sample #3). Differences up to 3 pH units were observed (3.6 (SMALL) to 6.6 (LARGE) in sample #7), but for the other samples, 1.5 units were the maximum difference observed. In sample #6, the MEDIUM pH exceeded the LARGE pH which was similar to the observed SMALL pH (6.7 versus 5.4 and 5.5). This feature will be discussed in the context of the calcium ion concentrations (figure 6-3). Sample #7, where the lowest pH value

Reproduced with permission of the copyright owner. Further reproduction prohibited without permission.

was observed occurred when the cloud was beginning to lift. The MEDIUM pH also reached its lowest value during that time period (approximately 4.0).

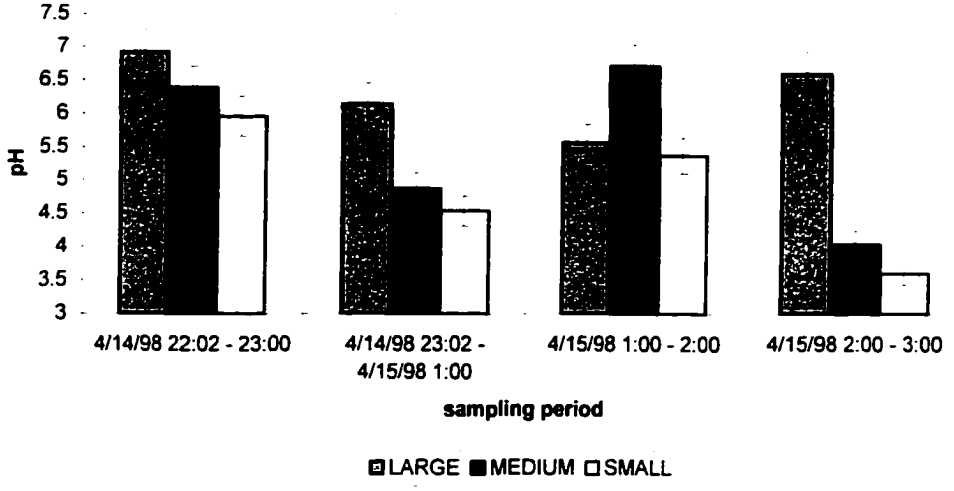

Figure 6-1: pH in all validated Horsetooth samples (4/14/98). Vertical error bars represent analytical uncertainty only.

Nitrate, sulfate and ammonium exhibited similar patterns for the four valid sample sets (nitrate is shown in figure 6-2). Concentrations on all stages generally increase as the event progresses and as the drop size decreased. Similar to observations at SPL, the SMALL fraction was 1.3 to 1.7 times more concentrated than the MEDIUM and LARGE fractions. Nitrate, sulfate and ammonium varied between 51 – 640 μN, 53 – 690 μN, and 61 – 1000 μN, respectively. While these concentrations were higher than those observed at SPL, collection volumes were lower which, regardless of the uncertainty (Chapter 3), suggests a lower cloud LWC may be at least partly responsible.

Calcium ion showed a more variable pattern (figure 6-3). Bigger drops were more concentrated than smaller drops, but the LARGE fraction concentration was not always higher than the MEDIUM fraction concentration. In fact, high pH observations correspond to peak Ca^{2+} concentrations (MEDIUM #6 and LARGE #7). Calcium's concentration ranged from 24 – 420 μN.

Reproduced with permission of the copyright owner. Further reproduction prohibited without permission.

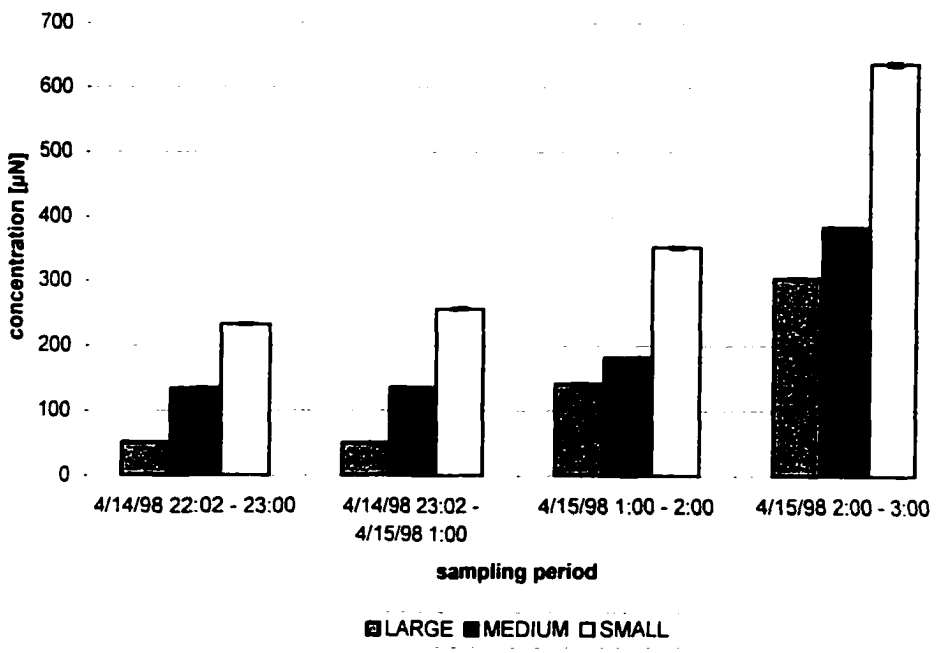

Figure 6-2: Nitrate concentrations in all validated Horsetooth samples (4/14/98). Vertical error bars represent analytical uncertainty only.

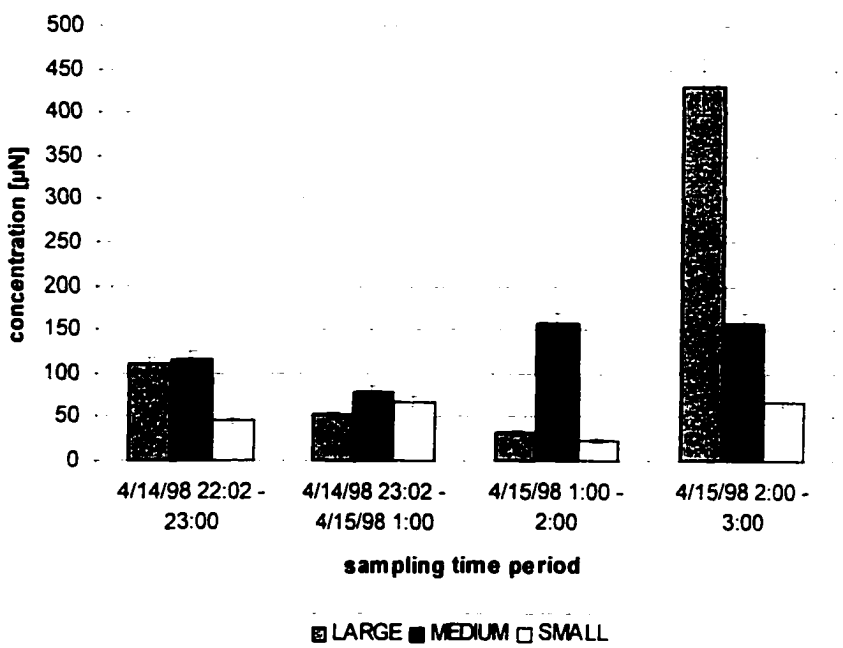

Figure 6-3: Calcium ion concentrations in all validated data at Horsetooth (4/14/98). Vertical error bars represent the analytical uncertainty only.

Reproduced with permission of the copyright owner. Further reproduction prohibited without permission.

Figures 6-4 through 6-8 are size-dependent concentration plots for calcium, sulfate, nitrate, ammonium and pH. The vertical error bars represent analytical uncertainty only (7.5%, 1.3%, 0.5%, 1.3% and 1.5%, respectively). The horizontal error bars represent volume median diameters corresponding to 16% and 84% of the predicted volume collected on that stage. Note that the volume median diameters are approximately 13.6, 10.9 and 8.4 μm for sample #6 and 11.7, 9.0, and 7 μm for sample #7 (LARGE, MEDIUM and SMALL), which is consistent with the decrease in calculated effective diameter from 10.2 to 7.7 μm. Recall that the FROSTY 50% cut-sizes for the stages are 17, 11 and 4.5 μm, respectively. Plotting the concentrations observed as a function of the stage cut-sizes obscures the fact that the observed concentrations are a function of the drop size distribution as well. It is not surprising that the SMALL volume median diameter was greater than 4.5 μm. However, for the MEDIUM and LARGE stages, the volume median diameters were less than the reported cut-sizes. This was also observed at SPL. The volume median diameter can be less than the reported 50% cut-size diameter because the volume median diameter reflects the drop distribution which is not considered in the D_{p50}. Further, the D_{p50} is usually calculated based upon the number of drops, not upon their volume. This emphasizes the importance of obtaining drop size distribution measurements while the multi-stage collectors are in use. Observed changes in concentration may result primarily from variations in the drop sizes.

Nitrate and sulfate (figures 6-5 and 6-6) have similar patterns. The effect of cloud drop distribution changes is evident in the shift to smaller drop sizes between sampling periods. Consequently, solute concentrations increase. While it is not shown, normalizing the PMS probe's dV concentrations to the 23:00 – 23:50 time period also indicates a reduction in relative LWC between the two sampling periods. The somewhat steeper gradient in sulfate concentrations compared to nitrate concentrations between the MEDIUM and LARGE fractions was also observed at SPL. We did not make sufficient additional measurements to attribute this to a particular cause.

Reproduced with permission of the copyright owner. Further reproduction prohibited without permission.

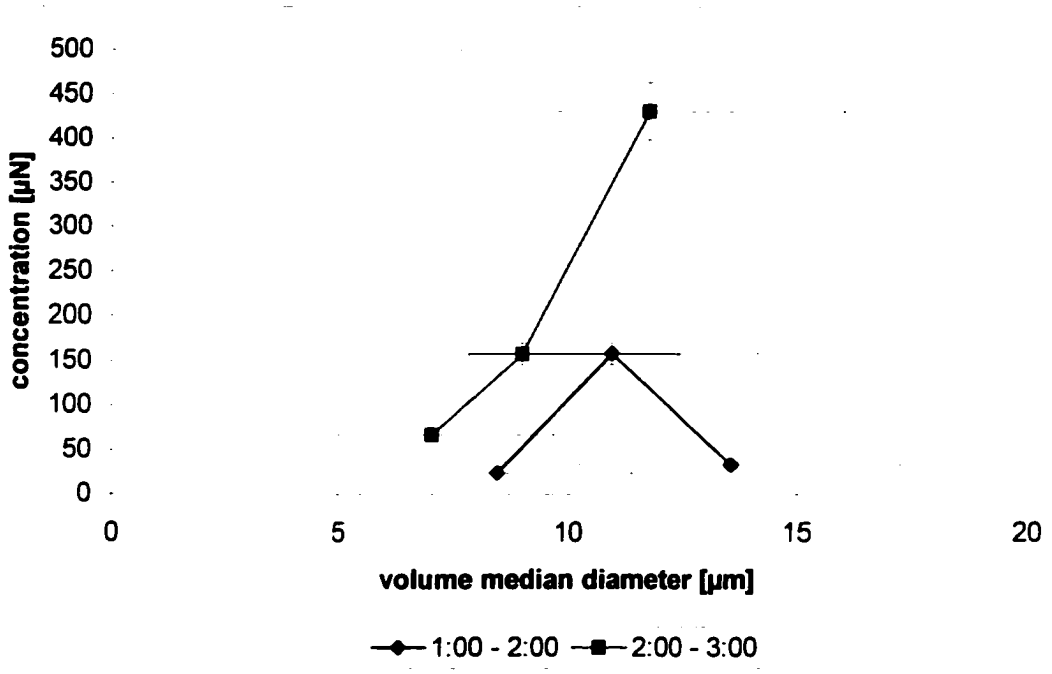

Figure 6-4: Horsetooth temporal evolution in calcium ion (April 15, 1998)

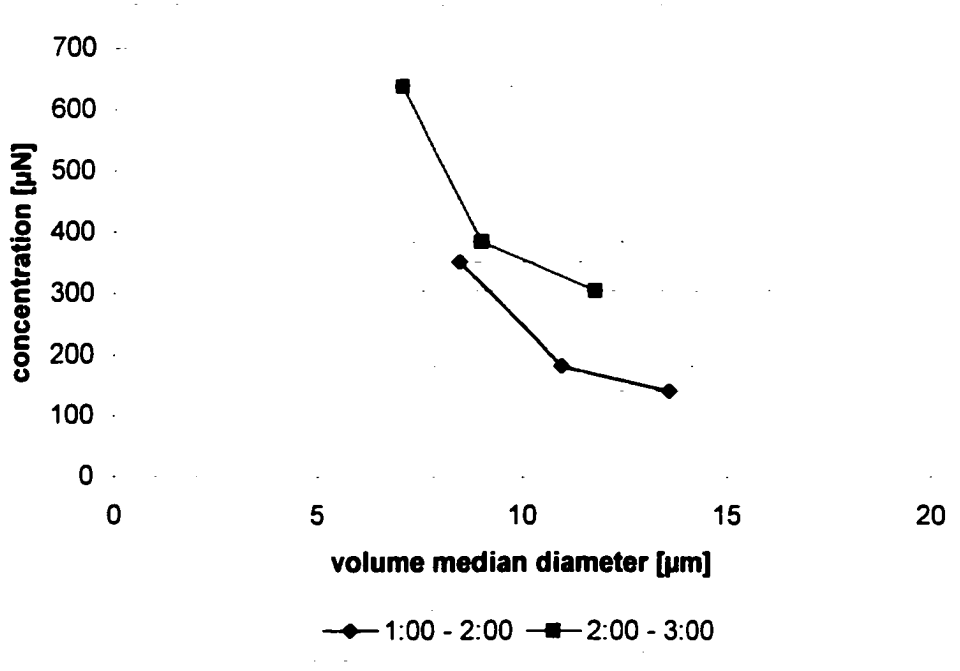

Figure 6-5: Horsetooth temporal evolution in nitrate (April 15, 1998).

Reproduced with permission of the copyright owner. Further reproduction prohibited without permission.

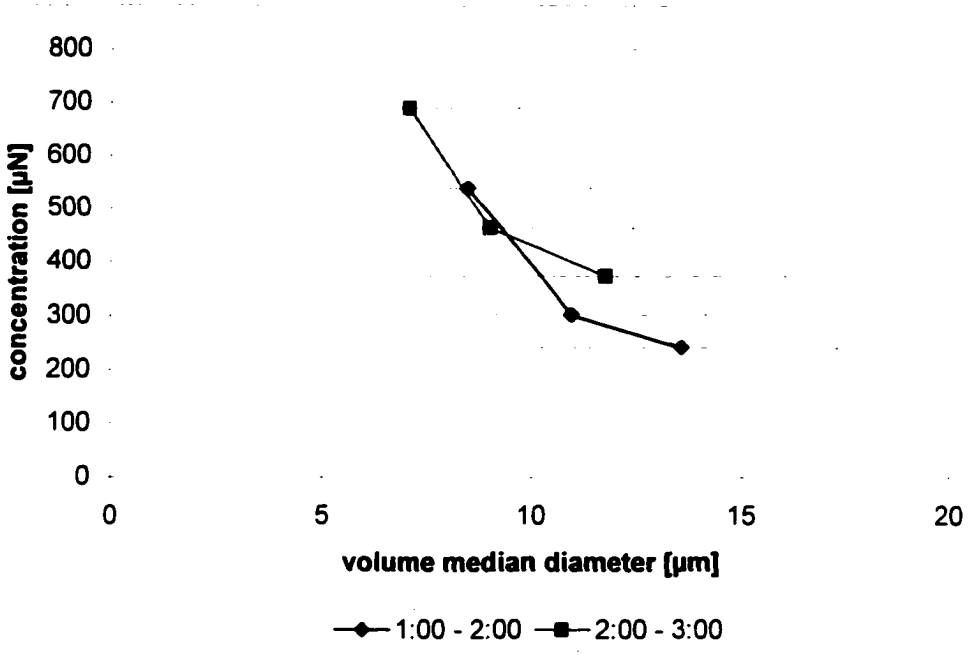

Figure 6-6: Horsetooth temporal evolution in sulfate (April 15, 1998).

Calcium ion (figure 6-4) shows a different concentration pattern from sulfate and nitrate. While there may be some low concentration accuracy issues not reflected in the use of the analytical precision to express the error bars, the MEDIUM concentration is clearly greater than either the LARGE or SMALL concentrations in sample #6. This "humped" pattern for calcium has also been observed elsewhere. What is interesting is how this affects ammonium (figure 6-7) and pH (figure 6-8) during the same time period. The MEDIUM ammonium concentration is reduced and the pH has risen due to the alkaline input in an effort to achieve equilibrium. The volatile species respond to the change imposed by calcium. It is possible that the cloud drops were a source of $NH_{3(g)}$ during that time period if it was also present in the CCN along with calcium. In sample #7, consistent with the change in the calcium pattern the LARGE fraction pH increases and the ammonium in the fraction is marginally reduced. Note how the MEDIUM ammonium concentration increases by approximately 200 µN between time periods.

Reproduced with permission of the copyright owner. Further reproduction prohibited without permission.

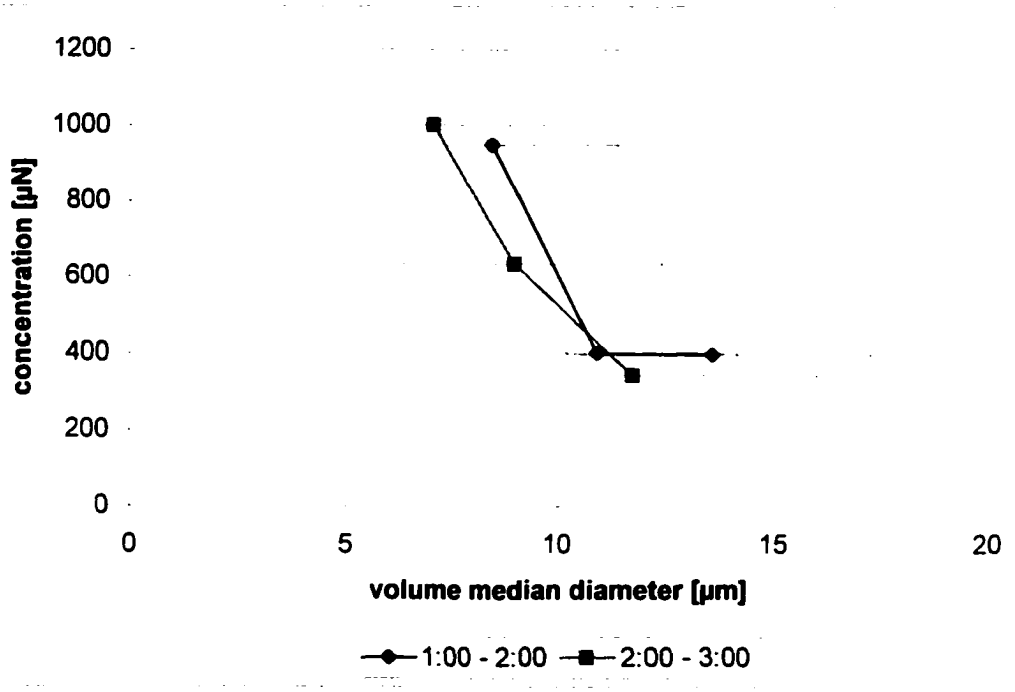

Figure 6-7: Horsetooth temporal evolution in ammonium (April 15, 1998)

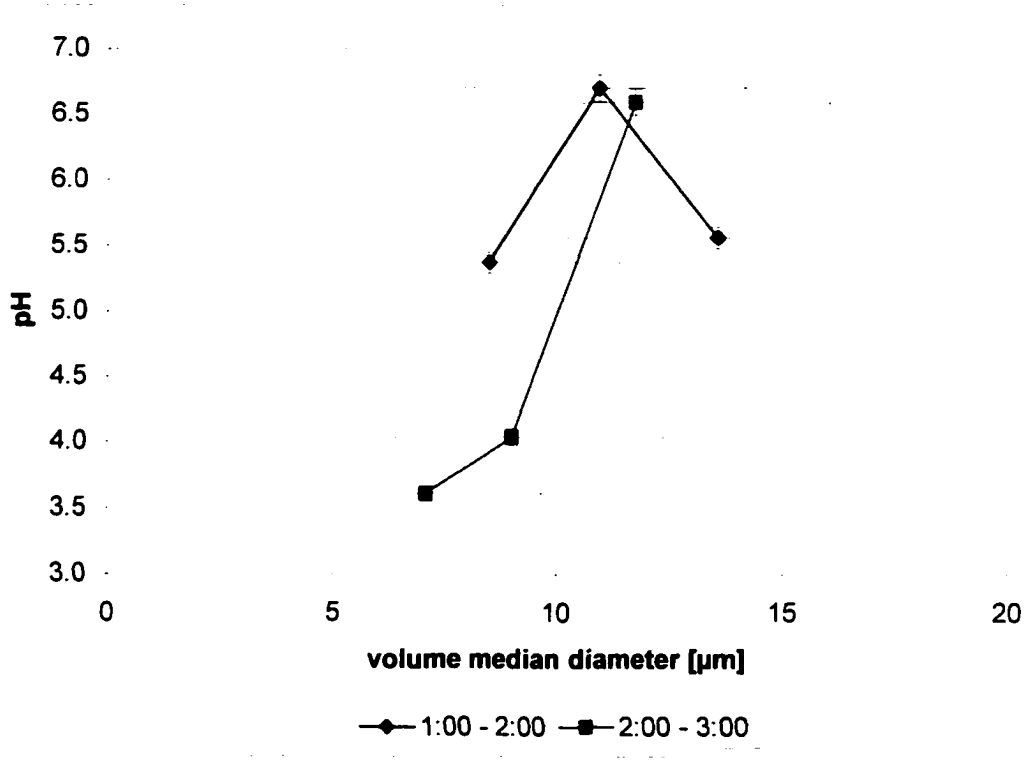

Figure 6-8: Horsetooth temporal evolution in pH (April 15, 1998)

Reproduced with permission of the copyright owner. Further reproduction prohibited without permission.

6.4.3 Sampling protocol

Many investigators (e.g. (Houdier *et al.*, 2000; Brantner *et al.*, 1994; Winkler, 1984) among others) do not melt collected rime (or snow (Gunz and Hoffmann, 1990)) samples until returning to the laboratory where they can be melted under controlled conditions. Where one sampler was melted in the field, it was bagged (Schemenauer *et al.*, 1995). Our procedure of melting the samples immediately (often in a crowded room as at SPL) may introduce artifacts, particularly for volatile species. Absorbing relatively high levels of CO_2 while the drops melt may alter the reported concentrations of low-molecular weight organic acids, ammonium, and pH.

For the LARGE fraction only, part of the rime collected during sampling periods #5, #6 and #7 was scraped off the collection surface using a Teflon-coated spatula into Ziploc bags. The rest of the sample was treated according to the usual protocol. The bags were sealed with minimal headspace and the samples were kept frozen. The sealed bags were melted in the lab, the pH measurement quickly repeated and an IC aliquot made.

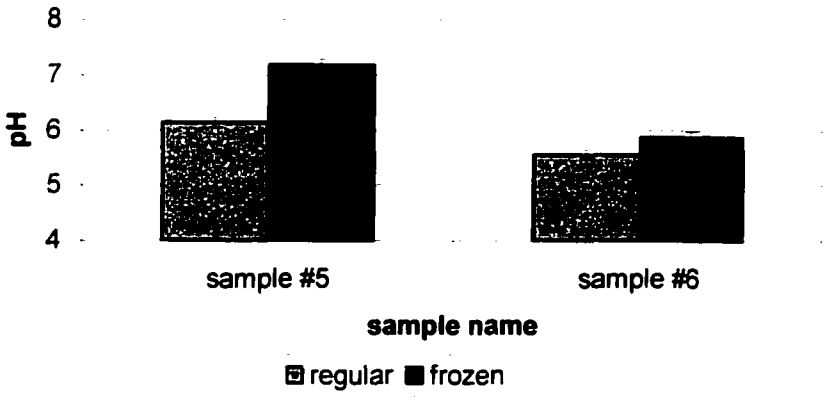

Figure 6-9: Horsetooth comparison of pH measurements for samples melted in the field and kept frozen until measurement in the lab. The frozen values reported are the mean of eight and six measurements respectively.

Reproduced with permission of the copyright owner. Further reproduction prohibited without permission.

A comparison of the pH measurements for two of the LARGE samples between the field and the laboratory is shown in figure 6-9. The differences between the field and laboratory (frozen) pH values were statistically significant at the 95% confidence level using the ± 1.5% precision estimate associated with a single investigator. Both frozen pH values were higher, consistent with acid uptake affecting the field measurements.

A comparison of the frozen vs. melted IC measurements for the three sample pairs indicate no change for chloride, sulfate, sodium, potassium and magnesium. Nitrate, ammonium and calcium show some differences (figure 6-10). Nitrate is only different (about 50 μN each) for one of the three samples. Calcium has somewhat more variation, but for some of the concentrations measured (e. g. < 50 μN), additional uncertainty due to poor accuracy may be partly responsible. Where the calcium concentration is larger, it may just be a measure of the heterogeneity between cloud drops collected on the same sampling surface. Ammonium had uniformly lower frozen than "regular" concentrations. This is consistent with the measured difference in pH reported above.

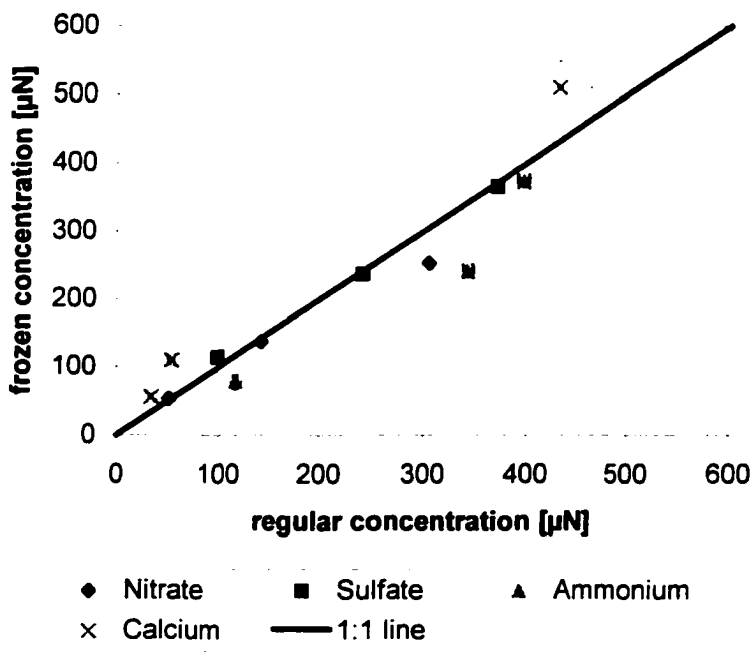

Figure 6-10: Frozen vs. "regular" concentrations for selected species in the three LARGE sample pairs. Error bars reflect component analytical uncertainty.

Reproduced with permission of the copyright owner. Further reproduction prohibited without permission.

6.5 Discussion

These results are limited as only four samples from one event can be validated. Given this, however, the drop size-dependent concentration patterns are similar to those at SPL which tends to support the conclusion of that study that adequate estimates of the effect of accretion on composition could ignore size-dependent drop composition. Accretion calculations based upon CHRCC bulk composition did not vary significantly from those using FROSTY's size-resolved composition data.

The behaviour of calcium is interesting. Its concentration can rise and fall substantially between individual sample periods – exhibiting much more variability than the other species present in high concentrations (if it is considered that some of the pH and ammonium variability observed is directly related to calcium content). High calcium measurements on one stage were often followed by very low concentrations. Although two sets of collection surfaces are used in FROSTY the fact that sodium and chloride remain low suggests that calcium observations do not result from contamination. It has been observed in many locations that calcium is enhanced in larger drops (see Chapters 7 – 9), and the "hump" profile has also been observed for this (and other species) in the 5-Stage. While insufficient concurrent observations exist to make a definitive conclusion about the behaviour of calcium ion, it is worth remarking that metals can have appreciably different concentration patterns in the same drops than the "big three" (nitrate, sulfate, ammonium) or "big four" (including pH). Conceivably, this may be a reflection of an external CCN mixture or, as is likely in some of these samples, the volatile species reacting to changes in non-volatile concentrations to maintain aqueous equilibrium.

The chemical comparison of samples melted and kept frozen in the field should be considered anecdotal given the small number of comparisons possible. However, the ammonium and pH results indicate that there may be a sampling artifact for the volatile species following our current standard protocol. This should be investigated further in the future. Our goal, after all, is to report

Reproduced with permission of the copyright owner. Further reproduction prohibited without permission.

cloud water concentrations as they exist naturally. Ziploc bags are not an ideal sample container, but the blanks were very clean and the "frozen sampling" technique itself is easy to perform.

One advantage of the CHRCC collector is that it can be operated at conditions both above and below freezing. FROSTY cannot. It should not be operated unless consistent drop freezing on the impaction surfaces can be ensured. The Rotating Multi Cylinder needs 4 or 5°C below freezing to avoid run-off (Howe, 1981), but it is unclear what the rime loading situation was there. Based upon this data set, no problem is observed as long as < 0 °C.

As indicated in the discussion of the 5-Stage (see Chapters 8 and 9), the advantage of the multi-stage collectors if drop size distribution data are available is that the link between changes in composition and drop size can be clearly observed. The concentration reported for each stage is not formed from a uniform drop population, but one that changes between sampling periods. While the same drop size range may be collected on a given stage, the "mix" of drops sizes within that range changes between sampling periods as do the reported concentrations. The interpretation of size-dependent composition and its evolution in-cloud must take the microphysical changes into consideration.

Finally, these results must be considered in view of the field performance evaluation (Chapter 3). Relative predicted and collected volumes for the two time periods with sufficient data to evaluate it at Horsetooth do not agree. This was generally true for SPL as well. Therefore, the assumptions inherent in the preceding discussion that drop collection can be predicted and that the collected drops are representative of the cloud sampled may not necessarily be true.

Reproduced with permission of the copyright owner. Further reproduction prohibited without permission.

7. ACE2

7.1 Project overview and site description

The second Aerosol Characterization Experiment (ACE2) was conducted during June – July 1997 in an extensive region of the sub-tropical northeast Atlantic encompassing both Tenerife, the Canary Islands, and Sagrès, Portugal. The ACE experiments are intended to intensively measure atmospheric properties at selected sites around the world to characterize the radiative and climate effects of atmospheric aerosol. ACE2 was designed to look at the impacts of African dust outflow and anthropogenic pollution from the European/Iberian peninsula on the marine boundary layer and free troposphere in this area. ACE2's scope is reviewed by Raes *et al.* (2000).

One component of ACE2 was the HILLCLOUD project. HILLCLOUD was intended to use measurements upstream, in and downstream of a hill cap cloud to investigate cloud processing of atmospheric species. Figure 7-1 is a diagram of the island of Tenerife where HILLCLOUD was located.

The upwind site is Taganana (TG1) where pre-cloud gas and aerosol measurements were performed. The cloud sampling equipment was located at El Bailadero (site TG2) on the ridge itself (elevation 660 m asl). Paiba is the downwind, post-cloud site (TG3). Figure 7-2 shows Taganana viewed from the El Bailadero site, and Figure 7-3 depicts the view from Taganana (site TG1 is on top of one of the buildings in the foreground) looking up to El Bailadero. The green building visible near the left side of the photograph is located on the ridge. From this direction, the scaffolding where the cloud sampling equipment was installed is faintly visible to the right.

Reproduced with permission of the copyright owner. Further reproduction prohibited without permission.

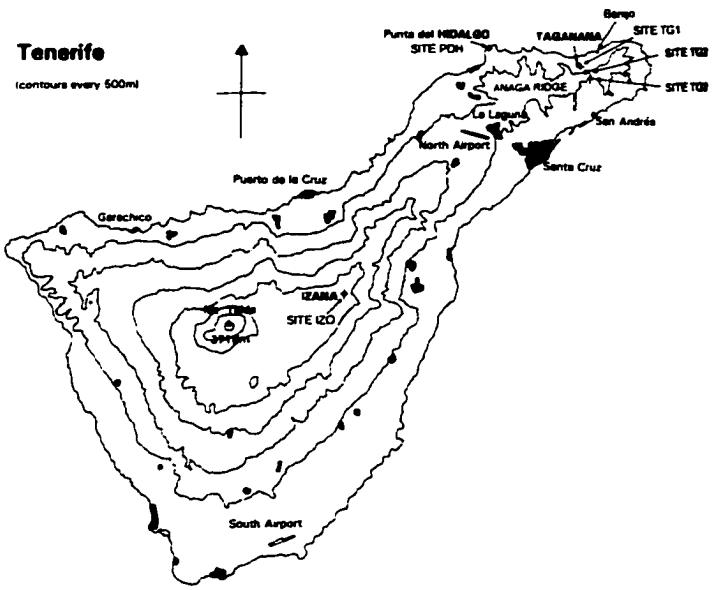

Figure 7-1: Map of Tenerife. HILLCLOUD sites surrounded the Anaga Ridge in the NE section of the island. (Bower *et al.*, 2000, figure 1).

Figure 7-4 shows the view towards Paiba from El Bailadero. These photographs indicate the steep terrain around the sampling site and the proximity to the coast.

Figure 7-2: Taganana as seen from El Bailadero (July 1997)

Reproduced with permission of the copyright owner. Further reproduction prohibited without permission.

Figure 7-3: Looking up to El Bailadero from Taganana (July 1997) The two white arrows indicate site TG1 (Taganana) and site (TG2) El Bailadero.

Figure 7-4: The view of Paiba from El Bailadero (July 1997)

A complete list of the measurements performed and investigators at these three sites can be found in Bower *et al.* (2000). The sf-CASCC and 5-Stage were installed next to the other cloud sampling equipment (approximately both horizontally and vertically co-located) (figures 7-5 and 7-6).

Reproduced with permission of the copyright owner. Further reproduction prohibited without permission.

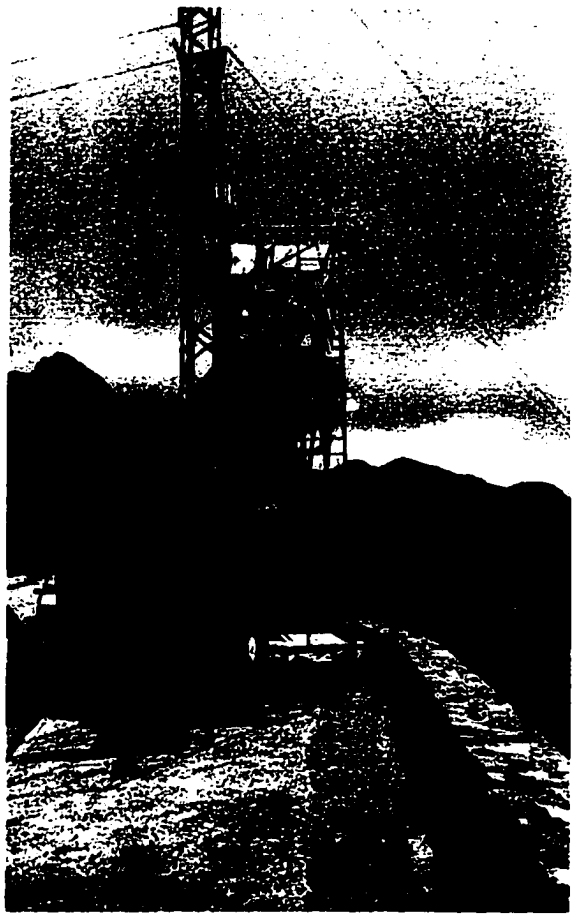

Figure 7-5: Cloud sampling equipment installation at El Bailadero. The sf-CASCC is in the foreground (July 1997)

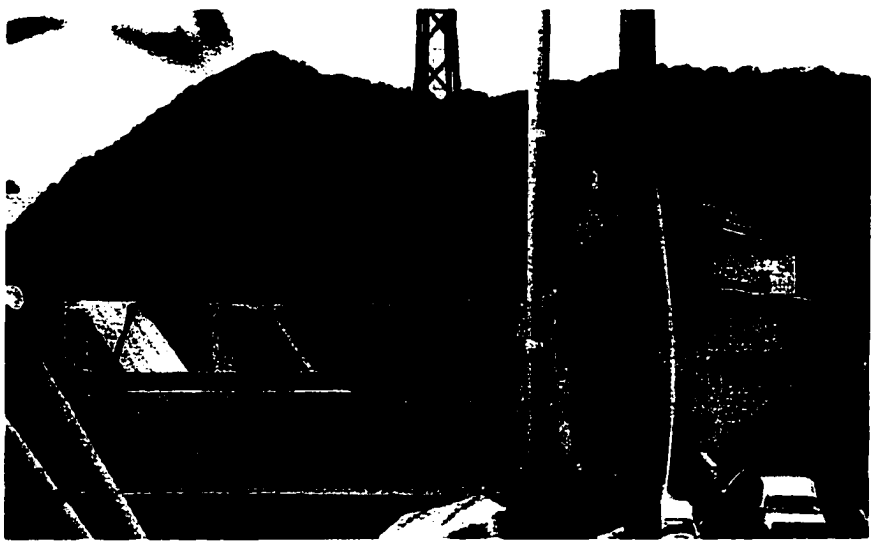

Figure 7-6: The sf-CASCC installed at El Bailadero (without attached sampling lines/bottles). The 5-Stage (not shown) was located immediately below (July 1997)

Reproduced with permission of the copyright owner. Further reproduction prohibited without permission.

7.2 *Summary of first reported results*

The first results from both ACE2 and HILLCLOUD were published in a special issue of Tellus in early 2000. Relevant composition results are summarized here and provide a framework for the interpretation of our results which follow. (Selected cloud measurements have been discussed previously (Chapter 4) and are not included here.)

During ACE2 HILLCLOUD, the eight cloud events sampled could be roughly divided into three categories – "polluted", "clean", and "intermediate". An analysis of the air masses' back-trajectories suggested the polluted air traveled over Europe and the Iberian Peninsula before reaching the Canary Islands in contrast to the clean air which was maritime in origin. The "intermediate" events were in air masses of less distinct history and the observed cloud water composition and cloud microphysical parameters were within the bounds established by the two extremes. The polluted air had high levels of O_3 (> 50 ppbv), and H_2O_2 and O_3 concentrations were higher than SO_2 throughout – "oxidant-rich" conditions. The fine mode (< 2.5 μm)/coarse mode concentration ratio of aerosol particles upwind at Taganana for selected species was 24 (ammonium), 4.26 (non-sea salt sulfate), 1.27 (sulfate), 0.18 (nitrate), and 0.06 (chloride) ("non-sea salt" concentrations are described below). The large (> 1.6 μm) aerosol particles at Taganana were mostly sea salt, while the small (< 0.15 μm) were a mix of ammonium, sulfate, sodium, and chloride particles (Bower *et al.*, 2000). Virtually all (97%) of fine aerosol sulfate was non-sea salt sulfate, decreasing to 29% in the coarse fraction (Bower *et al.*, 2000). At Punta del Hidalgo (site PDH, figure 7-1), non-sea salt calcium and magnesium concentrations in the sub-micron aerosol were reported as "dust". High dust concentrations were reported on 7/7 and 7/8, but were lower on 7/17/97 (Putaud *et al.*, 2000).

Cloud composition data from the two parallel three-stage IEP cloud collectors (Appendix B) indicate that the polluted and clean events had different drop size-dependent profiles. In polluted

Reproduced with permission of the copyright owner. Further reproduction prohibited without permission.

conditions (where total measured solute concentrations varied from 100 – 1700 mg l^{-1}), drops > 33 μm had the highest concentrations, and the observed pH range for all sizes was low (3.5 – 4.5). During the clean event, the pH range was higher (4.5 – 6) and relatively larger concentrations were observed in the 7 – 11 μm and 17 – 23 μm size ranges. Total clean event solute concentrations ranged from 50 – 350 mg l^{-1} (Bower *et al.*, 2000; Fuzzi *et al.*, 1998b).

Modeling of the cloud events indicated that aerosol particles as small as 40 – 55 nm activated during the clean event, while the lower bound was larger (65 – 80 nm) in polluted conditions. It does not appear that the aerosol spectra were modified significantly in the cap cloud. The H_2O_2 pathway dominated S(IV)-to-S(VI) conversion, but residence times were too short for substantial oxidation to occur. The results, however, suggest that driven by composition differences between the drops HNO_3, HCl, and NH_3 may re-partition from large drops to small drops. Large drops in particular may be a source of NH_3 to the air (Flynn *et al.*, 2000), although persistent sub-ppb NH_3 background concentrations were observed, (Bower *et al.*, 2000).

7.3 CSU's contribution to HILLCLOUD

Tabulated data from ACE2 are in Appendix H.

7.3.1 sf-CASCC data

We sampled during 5 of the 8 total sampling periods (table 7.1). Our T188, T189, T195, T201 and T203 events correspond to HILLCLOUD's #2, #3, #5, #7, and #8 (see (Bower *et al.*, 2000)). We did not sample during all the reported in-cloud periods. T188 and T189 are the polluted events and T203 is the clean one. T195 and T201 – intermediate events – have only one sample each and were more similar to the polluted rather than the clean events. A black film was observed in the Teflon trough after sampling during T188, consistent with its polluted designation. The 31 sf-CASCC sample pairs (Large and Small drop fractions) were analyzed for pH and major

Reproduced with permission of the copyright owner. Further reproduction prohibited without permission.

inorganic ions. Most sample pairs also had aliquots preserved for total S(IV), total peroxides, Fe, and Mn analyses. This duplicates many of the measurements performed by other investigators. However, our equipment and temporal resolution varied from theirs, and we alone measured Metals (Fe and Mn). Sampling periods were generally one hour in length, but ranged from one-half to 2 hours. The longer sampling periods were used to match 5-Stage samples.

Table 7-1: ACE2 event and sampling period summary

Event	Cloud sampling period [local time]	sf-CASCC sample pairs obtained
T188	7/7/97 19:28 -- 7/8/97 08:00	15
T189	7/8/97 23:02 -- 7/9/97 08:00	9
T195	7/14/97 06:04 -- 07:55	1
T201	7/20/97 20:00 -- 20:30	1
T203	7/22/97 17:30 -- 23:00	5

7.3.2 5-Stage data

HILLCLOUD was the first time the 5-Stage was used in the field. It became apparent during the course of the campaign that the initial sampling protocol was inadequate. On-site 5-Stage pH measurements were consistently high compared to the sf-CASCC. Subsequent additional analyses revealed what appear to be substantial contamination problems with the 5-Stage data. There are several possible reasons why this occurred:

- The sampling conditions at El Bailadero were "extreme": the ambient wind was often 14 – 15 m s^{-1} (see below) and high ambient concentrations of sea spray aerosol were probable at all times. Covering the 5-Stage between events with plastic bags apparently gave insufficient protection in these conditions.
- During sample recovery, a single Teflon scraper was used for more than one stage occasionally. The scrapers themselves may have become contaminated during storage/handling prior to sample recovery. Used scrapers may not have been separated from clean ones, and operator handling was not minimized. The

Reproduced with permission of the copyright owner. Further reproduction prohibited without permission.

two scraper ends were not always clearly differentiated, and "handles" may have come in contact with sample. Scrapers varied between stages and all were not easy to use.

- Opening the stage lids in high winds with the pumps not attached resulted in sample migration between stages (as is observed for similar velocities during operation in Stage 5). It was not possible to turn the pumps off during sample recovery due to power limitations.

Several changes were made in the sampling protocol (Appendix D) following ACE2:

- There is now a cover for the collector inlet ("Jet 1 Cover"). It is made of clear Plexiglas and fits snugly onto the inlet to prevent the aspiration of any "new" drops and sample migration during collection.
- Modifications to the Teflon scrapers did not improve their performance. The scrapers were replaced by commercial food-grade rubber-bladed spatulas. The spatulas are much easier to use and improve sample recovery. The spatulas themselves may contaminate more easily than if they were composed of Teflon, but no blank problems have been observed over the subsequent campaigns. In particular, rubber spatulas need to be kept clean to prevent permanent contamination. If the current protocol is followed, sample contamination should not result from spatula use. There are sufficient spatulas that no re-use should be necessary during any one event. Finally, spatulas are readily available, inexpensive, and thus easily replaced.

Implementing these changes in subsequent campaigns appears to have solved these problems. No 5-Stage data are reported for ACE2.

Reproduced with permission of the copyright owner. Further reproduction prohibited without permission.

7.4 Ambient conditions during cloud events

Wind came up the ridge from Taganana and the direction varied little. Mean pressure at El Bailadero was 935 – 940 mb approximately. Temperature and wind speed were both reasonably constant (table 7.2). As mentioned earlier, the ambient wind speed was relatively high throughout the campaign.

Table 7-2: ACE2 wind speed and temperature means/standard deviations by event

Event	wind speed [m s^{-1}]	Temperature [°C]
T188	11.7 ± 0.3	16.0 ± 0.1
T189	13.7 ± 0.3	15.4 ± 0.1
T195	8.8 ± 0.7	15.9 ± 0.2
T201	14.5 ± 0.4	16.2 ± 0.2
T203	14.3 ± 0.5	16.3 ± 0.1

Cloud liquid water content (LWC) ranged from as low as 82 mg m^{-3} to 305 mg m^{-3} (see Chapter 4 for additional information). Field notes indicate that there may have been some drizzle during the clean event, but the drop size distribution was considerably larger on that day (Chapter 4). It may also have drizzled during the single T195 sample.

7.5 Results and discussion

Figures 7-7 through 7-10 show representative Large and Small drop fraction composition data for the polluted and clean events. A series of Large vs. Small fraction comparisons for all the samples follow: pH (figure 7-11), sampled water mass (figure 7-12), cations (figures 7-13 and 7-14), anions (figures 7-15 and 7-16), peroxides (figures 7-17), and Fe and Mn (figures 7-18 and 7-19). In the Large vs. Small fraction plots, the error bars represent the analytical RSD only. Data are presented by event (e.g. T188) or by event type (e.g. polluted) as needed. Many studies in marine locations investigate the effect of anthropogenic or other influences on aerosol or cloud water components by comparing observations to the mean composition of sea water scaled by a stable species assumed to have no other sources (e.g. (Reynolds *et al.*, 1996; Jacob *et al.*,

Reproduced with permission of the copyright owner. Further reproduction prohibited without permission.

1985b) among others). Here sodium ion was used as the reference component to investigate possible chloride loss (figure 7-20), and the "non-sea salt" (or excess) concentrations of sulfate (figure 7-21) and selected cations (table 7-3). Mean seawater composition was taken from Stumm and Morgan (1996, p. 899). No temporal evolution of cloud water concentrations are shown as the major features generally tracked changes in LWC. All error bars represent analytical (chemical composition) or weight measurement (sample mass) uncertainty only, and some are not large enough to show in the figures (see Chapter 5). Supporting data tables are in Appendix H.

In the polluted Large fraction sample (figure 7-7) ionic composition is dominated by sodium and chloride (approximately 70% of the total). In polluted clouds, the Large drop sodium and chloride concentrations were uniformly on the order of mN. Their dominance is not surprising as the large aerosol particles were predominantly sea salt (section 7.2), and large drops typically form on large aerosol particles. Sulfate and magnesium comprise 8 – 9% each of the total measured charge (about 12,900 μN), while the rest of the species are minor contributors. By contrast, in the Small fraction (figure 7-8), sodium and chloride together represent 30% of the total charge (about 2,200 μN) which is approximately equal (27%) to the contribution from sulfate alone. Hydrogen ion and ammonium contribute 15% each, and the rest of the species are present in smaller relative concentrations. The increased importance of sulfate and ammonium is consistent with the size-dependent aerosol composition reported at Taganana (section 7.2). The sum of charges in the Large drop fraction is about a factor of 6 greater than in the Small. The two clean event fractions (figures 7-9 and 7-10) have very similar relative compositions to each other, although the Large fraction is approximately two times more concentrated (1,005 μN total) than the Small (476 μN). The absolute concentrations are much lower than in polluted clouds. The relative concentrations of sodium, chloride, sulfate and magnesium are the same as in the Large polluted fraction. Assuming nucleation scavenging is the predominant source for most species in solution, the precursor CCN appear to be similar for the Large polluted and both clean fractions suggesting a common maritime source or sources. Based upon these two sample pairs, composition

Reproduced with permission of the copyright owner. Further reproduction prohibited without permission.

differences are expected between the Large and Small drop fractions. However, it is important to remember that in the sf-CASCC some large drops are collected in the Small fraction.

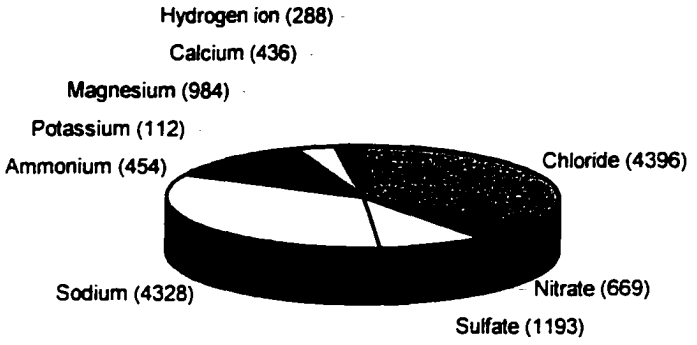

Figure 7-7: T189 3 – 4 a. m. Large fraction sf-CASCC sample (polluted). Concentration reported in μN for each species (12,859 total).

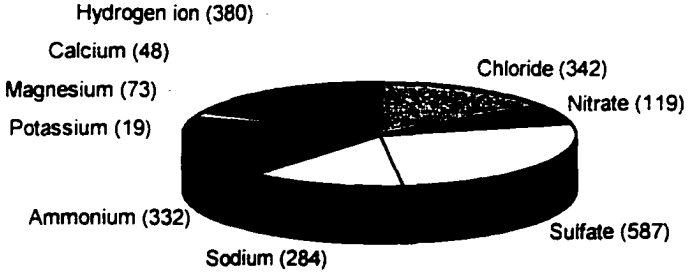

Figure 7-8: T189 3 – 4 a. m. Small fraction sf-CASCC sample (polluted). Concentration reported in μN for each species (2,183 total).

Reproduced with permission of the copyright owner. Further reproduction prohibited without permission.

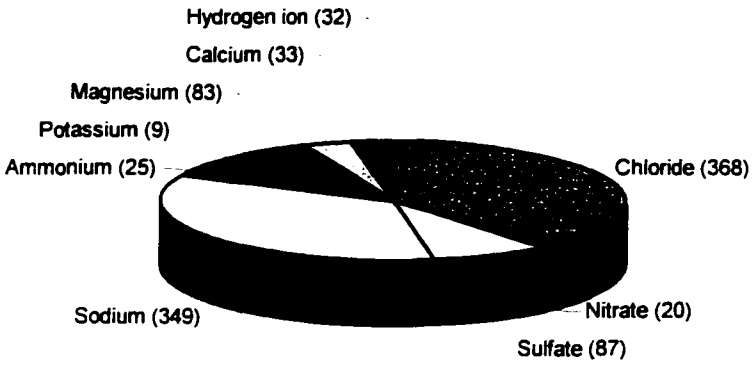

Figure 7-9: T203 9 – 10 p. m. Large sf-CASCC fraction sample (clean). Concentrations reported in μN for each species (1,005 total).

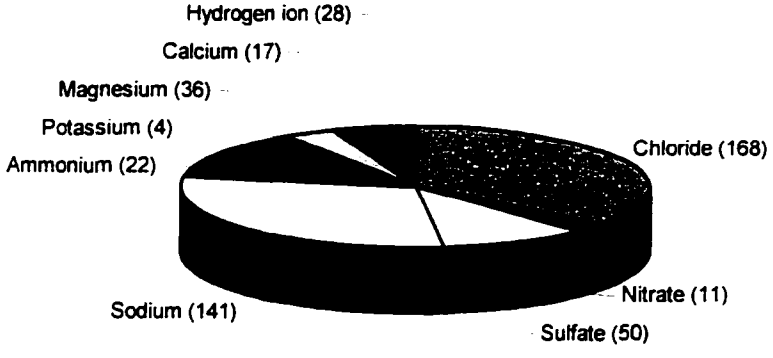

Figure 7-10: T203 9 – 10 p. m. Small fraction sf-CASCC sample (clean). Concentrations reported in μN for each species (476 total).

The pH data are consistent with observations at other locations (Bator and Collett, 1997; Collett *et al.*, 1994). Large drops tend to be less acidic than Small drops and while the differences are usually on the order of 0.5 pH units or less, up to a 2.1 unit difference has been observed. Polluted and intermediate event data are more acidic than the clean data which shows little pH size dependence and varies from approximately 4.5 – 5.

Reproduced with permission of the copyright owner. Further reproduction prohibited without permission.

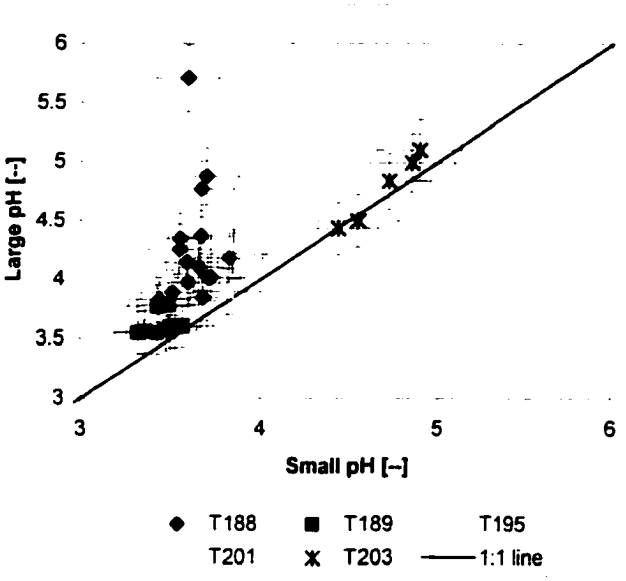

Figure 7-11: Large vs. Small sf-CASCC – pH for all events

The sampled water mass data are shown (figure 7-12) to illustrate the profound difference between water collection in the two fractions during the polluted/intermediate and clean events. The data are consistent with the effective drop diameters (Chapter 4). These data, in combination with the concentration data shown in the pie charts, indicate that total solute mass in the aqueous-phase varied between polluted and clean conditions and between Large and Small drops. The precursor aerosol particles the two cloud drop fractions formed on were distinct mixes of varying composition (polluted) and amount (polluted and clean).

In the polluted and intermediate event samples, sodium, potassium, magnesium and calcium ions have the same kind of sharp size dependence – approximately 5 – 10 times greater concentrations in the Large fraction (figure 7-13). Ammonium, by contrast, has a much weaker size-dependence and is present in only marginally higher concentrations in the Large fraction. This is consistent with ammonium's relative importance in the Small fraction. During the clean event (figure 7-14), there is about a 2:1 concentration difference for these cations between Large and Small, and some data suggest higher concentrations in the Small fraction. In the anion plots

Reproduced with permission of the copyright owner. Further reproduction prohibited without permission.

(figures 7-15 and 7-16) similar patterns are observed. Chloride concentrations are 5 – 10 times higher in the Large drops and nitrate has a similar size-dependence, although it is present at

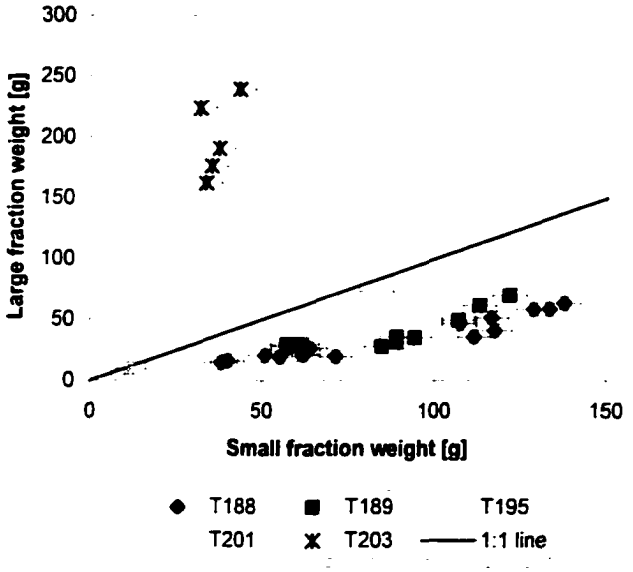

Figure 7-12: Large vs. Small sf-CASCC collected sample mass for all events

much lower concentrations. Sulfate and non-sea salt sulfate, like ammonium, have a much weaker size-dependence (< 2 (Large):1 (Small)) and are also relatively more important components of the Small fraction. Clean conditions exhibit more variable and weaker drop size-dependent cloud water composition.

Peroxide concentrations (figure 7-17) are largely independent of drop size as has been observed before (Appendix L). Clean event concentrations (about 60 μM) are within the range of polluted and intermediate concentrations (40 – 90 μM). The highest concentrations were actually observed at night. These high levels of aqueous-phase peroxide are consistent with the lack of measurable S(IV) in solution. Total aqueous-phase S(IV) concentrations were at or below detection levels and are not shown.

Reproduced with permission of the copyright owner. Further reproduction prohibited without permission.

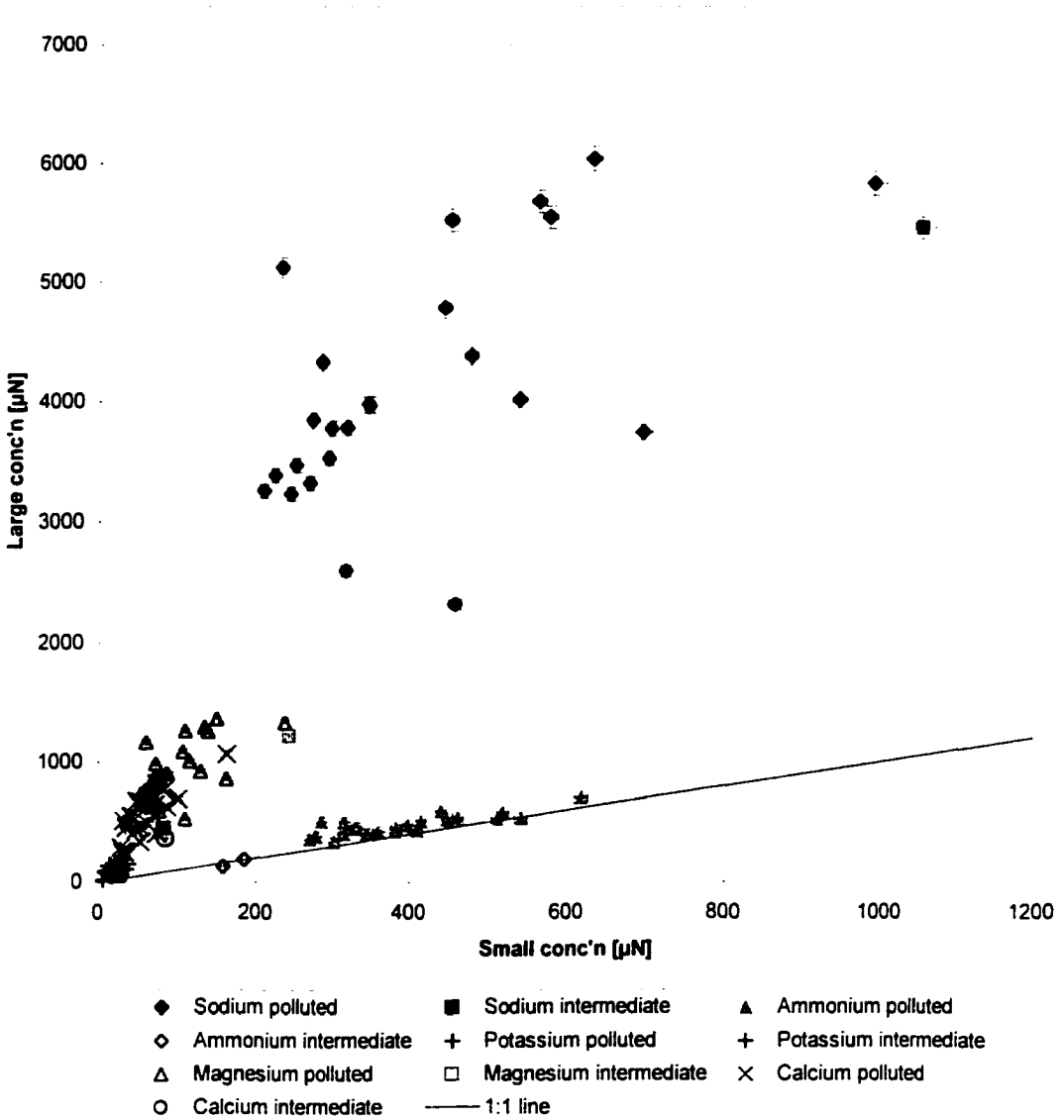

Figure 7-13: Large vs. Small sf-CASCC cation concentrations for polluted and intermediate events

Fe and Mn are both found in higher concentrations in larger drops in the polluted and intermediate events (figure 7-18). Fe varies from 50 – 900 µg/l and Mn from < 10 – 70 µg/l, but both evolve in roughly similar patterns within an event (i.e. the Fe/Mn ratio does not vary strongly). In contrast to most of the other species observed, in the clean event the Small fraction has higher concentrations of both metals (figure 7-19). While not shown, the clean event Fe and

Reproduced with permission of the copyright owner. Further reproduction prohibited without permission.

Mn concentrations are roughly factors of 3 and approximately 1.5 – 2 times greater than their respective MDLs.

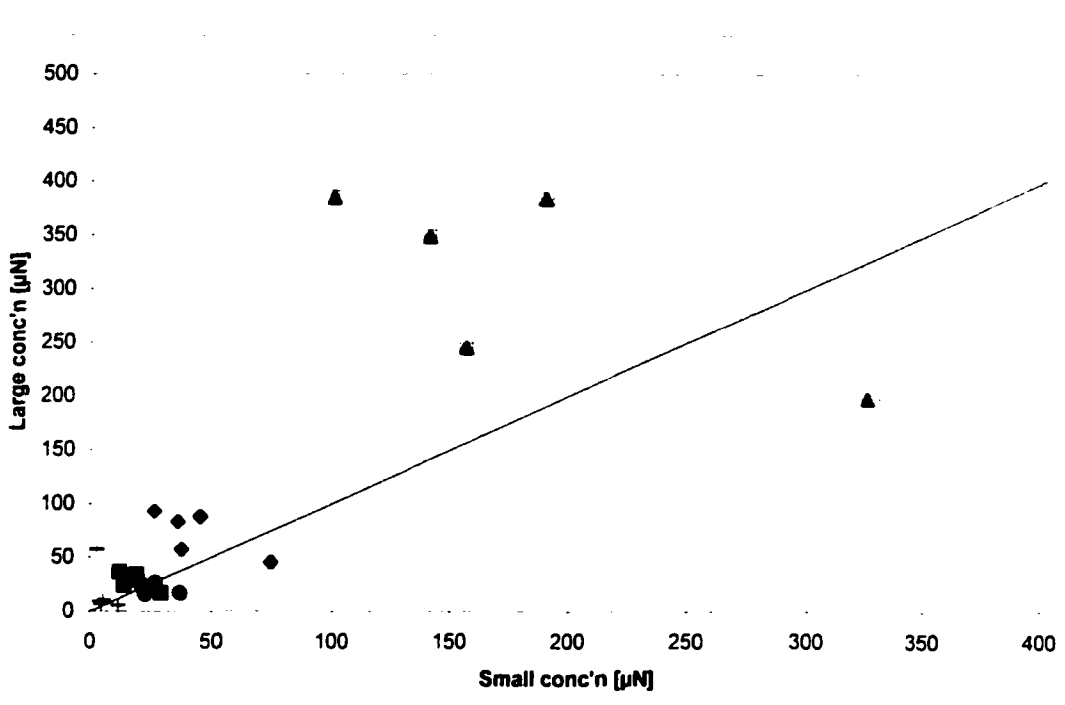

Figure 7-14: Large vs. Small sf-CASCC cation concentrations for the clean event

As the chloride loss and non-sea salt calculations are all based upon mean seawater composition, it is not known how much of a factor local sea water composition variations have in these results. The Large chloride concentration was 88% on average (81% - 96% range) of that predicted by mean seawater composition (figure 7-20). The Small fraction had a proportionately higher mean (94%) but a broader range (78% - 127%). During the clean event only, the predicted chloride loss was small – about 5% in both fractions. These results support the choice of sodium as the reference scaling component. Chloride loss from aerosol and in solution is well-established (Seinfeld and Pandis, 1998), and modeling (section 7.2) suggests HCl volatilization in these clouds. An earlier study at a nearby site during two previous summers (1995 and 1996) indicated that the Na/Cl ratio was approximately that for seawater and, given the uncertainties, our results are similar (Borys *et al.*, 1998). The Large/Small difference in the polluted clouds may

Reproduced with permission of the copyright owner. Further reproduction prohibited without permission.

be indicative of an additional source of chloride in the Small drops possibly from HCl re-partitioning or from the precursor aerosol. During ACE2, non-sea salt sulfate averaged 77%

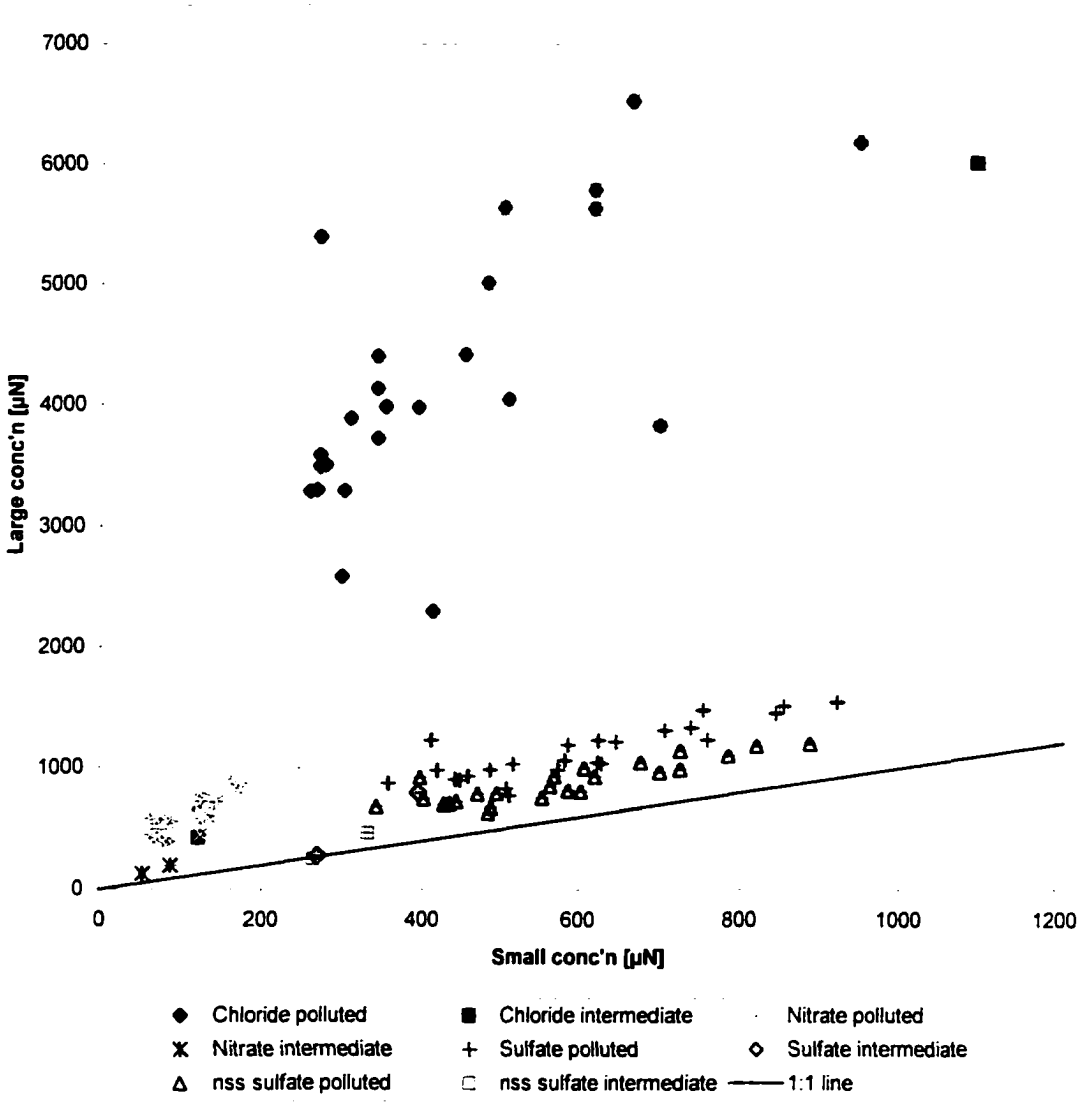

Figure 7-15: Large vs. Small sf-CASCC anion composition (including non-sea salt (nss) sulfate) for polluted and intermediate events

(56% - 90%) of the total sulfate concentrations in the Large drops and 93% of the total in Small drops (71% - 98%) (figure 7-21). During the clean event, this relative difference was retained – non-sea salt sulfate concentrations were approximately 70% and 80% of the Large and Small drop sulfate concentrations, respectively. The absolute amounts of non-sea salt sulfate are much

Reproduced with permission of the copyright owner. Further reproduction prohibited without permission.

different between the polluted and clean events, but its presence indicates it is available/produced by natural processes even in pristine marine conditions. This observation is

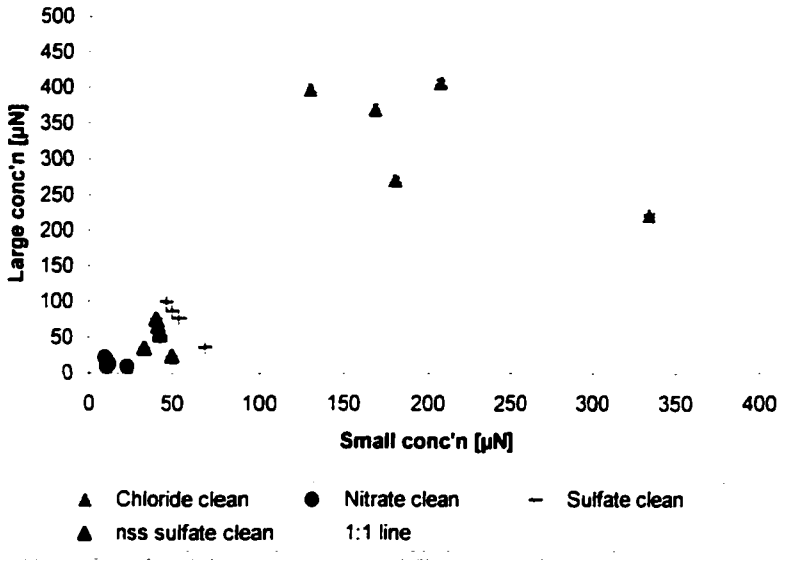

Figure 7-16: Large vs. Small sf-CASCC anion composition (including non-sea salt (nss) sulfate) for the clean event

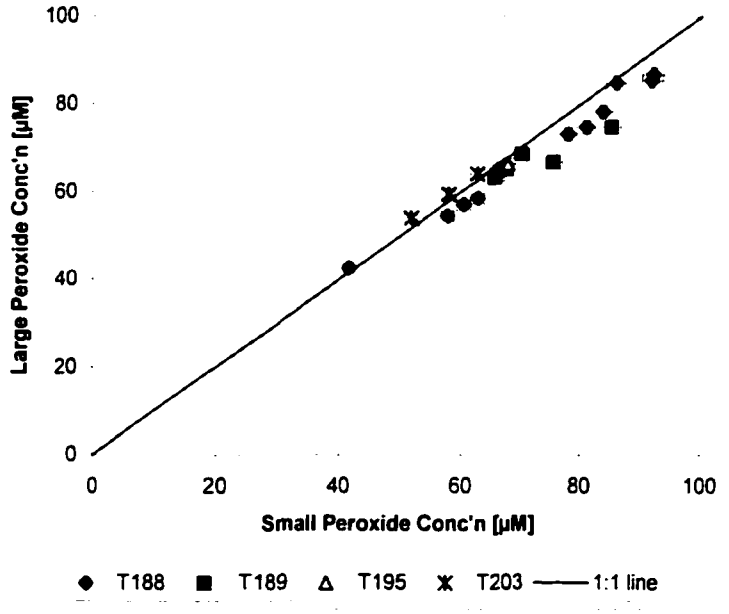

Figure 7-17: Large vs. Small sf-CASCC total peroxides for all events

Reproduced with permission of the copyright owner. Further reproduction prohibited without permission.

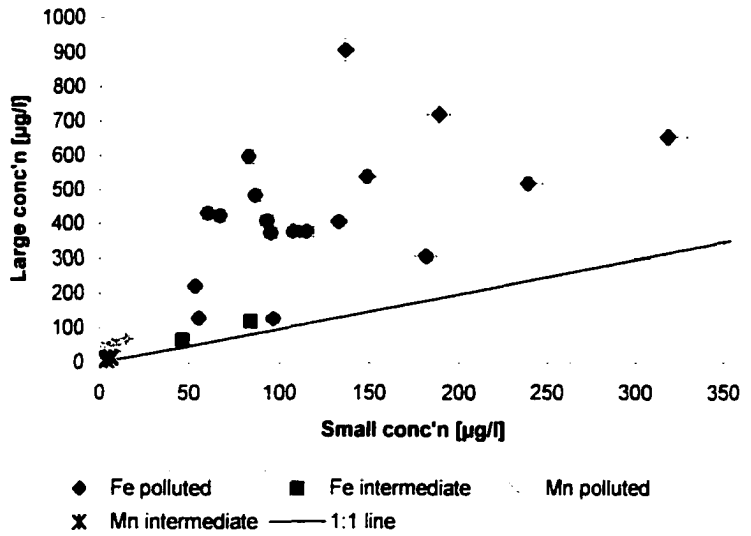

Figure 7-18: Large vs. Small sf-CASCC Fe and Mn for polluted and intermediate events

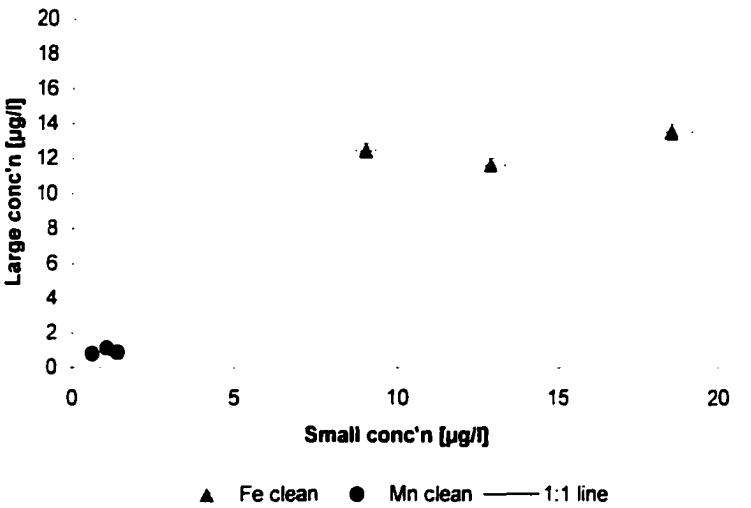

Figure 7-19: Large vs. Small sf-CASCC Fe and Mn for the clean event

consistent with a marine biogenic source of DMS (subsequently oxidized to sulfate in the atmosphere). The drop concentration differences are consistent with the fine/coarse mode aerosol composition observations (section 7.2) as some fine aerosol, once activated, will be sampled in the Large drop fraction. The significant amounts of excess calcium and magnesium

Reproduced with permission of the copyright owner. Further reproduction prohibited without permission.

observed in-cloud are consistent with the amount of dust observed at PDH around the T188 and T189 events (table 7-3). Excess calcium, sulfate and magnesium have been reported in many marine/coastal locations in cloud water and aerosol (Ogawa *et al.*, 1999; Sievering *et al.*, 1999; Reynolds *et al.*, 1996; Jacob *et al.*, 1985b; Sadasivan, 1980; Lazrus *et al.*, 1970). The drop size-dependent differences in the ratios are slight and little difference is observed on average between the clean event and the others. The similarity suggests that the source of both is the same and can occur in both types of air masses. The relative amounts of potassium in both clean fractions are approximately the same as the Large all or polluted fraction (20% – 25%) but the Small all or pollluted proportion (50%) is distinctly higher. These data are more variable than the other non-sea salt calculations. They suggest there may be an additional source of potassium in the fine polluted aerosol particles.

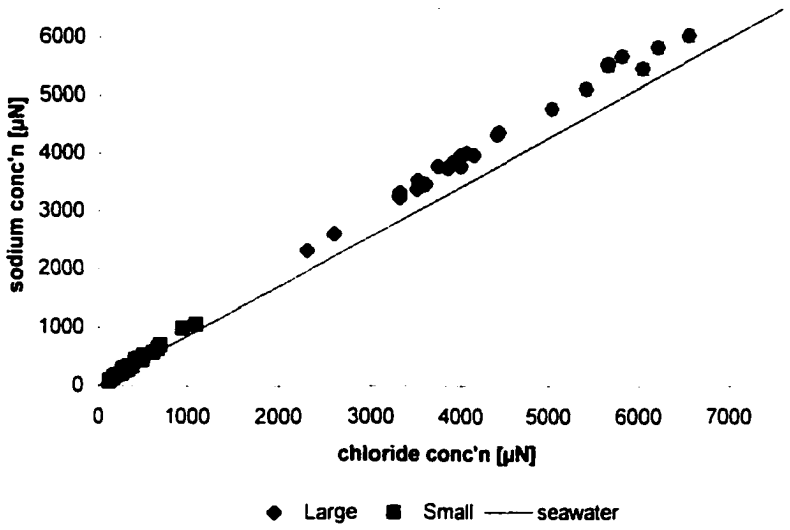

Figure 7-20: Sodium vs. chloride concentrations for all ACE2 data. The mean seawater ratio is shown for comparison

While non-sea salt sulfate can be produced by SO_2 oxidation, excess calcium and magnesium sources are more controversial. Possible natural sources include chemical fractionation in sea salt aerosol formation, enhanced concentrations in the ocean surface layer (or biological sources

Reproduced with permission of the copyright owner. Further reproduction prohibited without permission.

there), and dust (Sievering *et al.*, 1999; Jacob *et al.*, 1985b; Lazrus *et al.*, 1970). For calcium and magnesium, the results presented here suggest contributions from a single source or sources

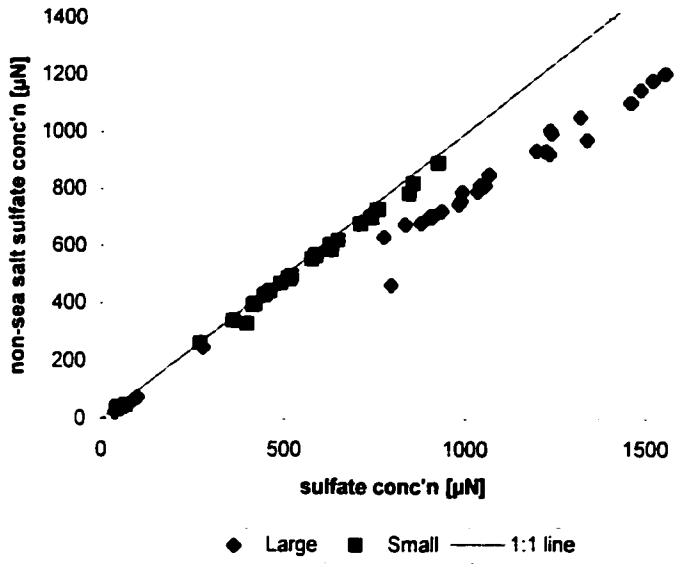

Figure 7-21: Non-sea salt vs. total sulfate concentrations for all ACE2 data

Table 7-3: Non-sea salt/total amount ratios by species for all data and clean event only

Species	ALL EVENTS				CLEAN EVENTS	
	Large		Small		Large	Small
	mean	range	mean	range	mean	mean
Calcium ion	81%	61% - 89%	84%	73% - 94%	76%	79%
Magnesium ion	50%	49% - 53%	54%	50% - 60%	51%	53%
Potassium ion	≈ 20%	-14% - 85%	52%	18% - 72%	33%*	24%

*if 85% data point excluded (final sample) then 20%

common to all the cloud events. This is consistent with the similar relative amounts of sodium and chloride observed between fractions (figures 7-7, 7-9 and 7-10). Different sources combined appropriately may yield what appears to be a single source, and our data cannot address that issue.

Reproduced with permission of the copyright owner. Further reproduction prohibited without permission.

Our results are consistent with the other measurements of size-resolved drop composition reported in section 7.2, as well as the difference in solute concentrations between types of events. The pH range and air mass source regions and their influence on observations are similar to those in the Summer 1995 and 1996 study previously discussed (Borys *et al.*, 1998).

Unlike the composition results presented in other chapters, these clouds are not uniformly dominated by nitrate, sulfate, and ammonium as observed in other locations and the observed size-dependence varies (see (Bator and Collett, 1997) for similar results at different locations). Different species also can exhibit varying drop size-dependencies. It is difficult to interpret the observations in terms of figure 1-1 with data from only two (somewhat overlapping) drop size fractions. However, to the first order, the generally higher concentrations observed in the Large drop fraction are consistent with condensational growth dominating (Region II). Air mass source region, not surprisingly, has an important influence on the observed drop composition. It appears that there are probably two types of precursor aerosol – sea salt or mixed sea salt/dust and ammonium, sulfate and nitrate particles found mostly in the polluted Small drop fraction. The sea salt or mixed sea salt/dust particles may be found in either the Large and/or Small drop fraction depending upon whether the event is polluted or clean.

Finally, while no 5-Stage data are available from this campaign, the problems experienced resulted in the development of a more robust sampling protocol that has been successfully used since.

Reproduced with permission of the copyright owner. Further reproduction prohibited without permission.

8. Whiteface

The July 1998 cloud sampling campaign at Whiteface Mountain, NY took place upon the mountain's summit in collaboration with L. Husain's group of SUNY Albany/New York Department of Health. The purpose of the campaign was two-fold: to use the 5-Stage in the field and to investigate size-dependent S(IV) oxidation in-cloud using a tracer technique (Husain, 1989). The results of the latter are described in Rattigan *et al.*, (2001) and Reilly (2000). Here I will focus on the chemical composition measurements made using the 5-Stage in comparison to those simultaneously obtained with the CASCC2 and sf-CASCC. Due to sample volume limitations, the 5-Stage was not useful to the tracer study.

8.1 Site description

At the summit of Whiteface (1483 m asl), the Atmospheric Sciences Research Center (ASRC) maintains a research facility. The CSU collectors, PVM-100, weather station and other equipment were installed on top of a building housing the summit elevator (figure 8-1). Our collectors were all vertically and horizontally co-located. The collectors were fixed in position along a railing oriented in the SW direction. The collectors' position relative to the wind could not be changed. However, the extensive studies at Whiteface have indicated that most air masses from this direction come from the Ohio Valley and are associated with higher, "polluted" species concentrations of most interest (e.g. low pH, high sulfate, high potential for in-cloud sulfate production) (Mohnen and Vong, 1993; Vong *et al.*, 1990). Air masses originating from Canada reach Whiteface from the north and typically are clean (Castillo and Jiusto, 1984). Dr. Husain's group occasionally used an ASRC-type passive collector (Appendix B) located on the laboratory tower to sample cloud water. Their collector is located at a higher (8 - 10 m) elevation than our

Reproduced with permission of the copyright owner. Further reproduction prohibited without permission.

collectors. According to Rattigan *et al.* (2001), the concentrations observed in the bulk collector were similar to those measured concurrently by CSU (Appendix B).

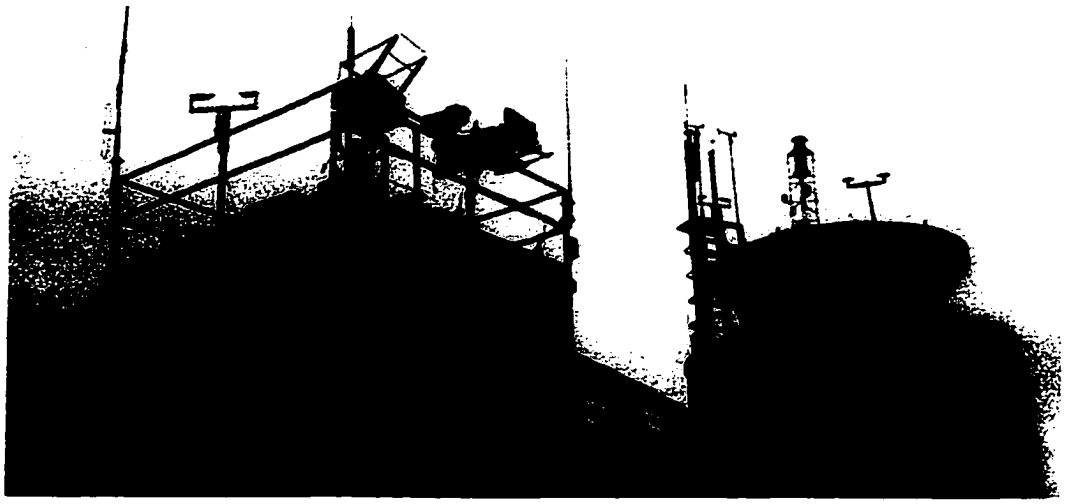

Figure 8-1: The Whiteface field site (July 1998). The bagged CSU collectors are in the foreground (5-Stage, CASCC2, sf-CASCC from left to right). The main laboratory building is to the right.

8.1.1 Equipment and protocols

The "new", all-plastic sf-CASCC was built for use at Whiteface and later Davis (see Chapter 4 for a comparison with the "old" (ACE2) sf-CASCC). Sample aliquot priority was essentially the same as at ACE2 – pH, IC, Metals*, total H_2O_2, total S(IV) – with some additions. A HCHO aliquot was preserved for most samples, and selected Metals aliquots were analyzed for Cu as well as Fe and Mn.

The post-campaign analytical work indicated that the DI water used to clean the collectors at Whiteface had a non-negligible concentration of Fe (30 – 50 μg l^{-1}) and that low concentrations of

*As in earlier chapters, "Metals" refers to metals quantified using the GFAAS (Chapter 5) and specifically refers to Fe, Mn and Cu (where measured).

Reproduced with permission of the copyright owner. Further reproduction prohibited without permission.

both Ca^{2+} and Mg^{2+} occasionally exhibited high variability. Both total S(IV) and HCHO suffer from sampling artifacts in the 5-Stage and are not reported from this device (Chapter 5).

8.1.1.1 Collector performance

While collector performance at Whiteface was very good to the extent that we can evaluate it (see Chapter 4), two operational points should be highlighted. The first is that the high LWC clouds in combination with hourly samples to match the 5-Stage resulted in some CASCC2 sample bottles falling off prior to collection. This is the reason there are more sf-CASCC sample pairs than CASCC2 samples. Further, the 5-Stage after the collection of the first sample set during the W185 event (section 8.2) was re-started with the Jet 1 Cover on. The error was noticed after 15 – 20 minutes of operation and the Cover removed. However, subsequent analytical work indicated that all three of the later sample sets contained evidence of contamination despite the relatively large (multi-ml) amounts of water collected. The 5-Stage, once contaminated, cannot "clean" itself during an event. Those data are not reported here.

8.2 Review of the sf-CASCC results

Selected sf-CASCC composition results are included here to assist the later presentation and interpretation of the 5-Stage results. These data (with the exception of Cu) can be found in Reilly (2000). Tabulated Cu data may be found in Appendix H.

At Whiteface, 59 sample pairs were collected using the sf-CASCC over six cloud events. The events were: July 4, 1998, 21:45 to July 5, 1998, 7:00 (the "W185" event); July 7, 1998, 13:00 to July 8, 1998, 0:50 (W188); July 16, 1998, 07:25 to 11:30 (W197); July 17, 1998, 01:30 to 11:00 (W198); July 20, 1998, 09:00 to 13:00 (W201); and July 22, 1998, 02:00 to 04:00 (W203). All times are local (EDT). Detailed descriptions of the ambient conditions are not included here (see Chapter 4 for selected events). In general, conditions were similar between events – wind

Reproduced with permission of the copyright owner. Further reproduction prohibited without permission.

velocities < 10 m s^{-1}, approximately 15°C, wind from the SW – with the exception of the W185 event. As the collectors were mis-aligned with the wind during that event and collection suffered (Chapter 4), W185 data are generally excluded from the following discussion.

Figures 8-2 through 8-7 present the sf-CASCC** Large vs. Small fraction concentration comparisons for pH, ammonium, nitrate, sulfate, calcium ion, and manganese. Figure 8-8 shows the same comparison for copper. All of the error bars represent analytical uncertainty only. All of these figures include a 1:1 concentration line for reference.

For the major ions – hydrogen ion (pH), ammonium, sulfate and nitrate (figures 8-2 through 8-5) – the cloud water composition as measured by the sf-CASCC is largely independent of drop size. These four species dominate the overall drop composition – on average they contribute greater than 90% of the total measured charge in the CASCC2, Large and Small fractions. The ratio of ammonium to the sum of nitrate and sulfate ranges from 20 – 60% (typically 30 – 40%); these drops are acidic. Some time periods occur where the concentrations of ammonium, sulfate and particularly nitrate are moderately drop size-dependent (figures 8-3 through 8-5). This Large/Small concentration divergence is strong at the end of the W197 event and the start of the W198 event (temporal resolution not shown). It is associated with elevated Large drop calcium ion concentrations (up to 10 times greater than during other event sampling periods). Calcium concentrations exhibit very strong size-dependency (Large/Small ratios up to 15) (figure 8-6). When calcium – and magnesium to a lesser degree – concentrations are lower and their respective Large/Small concentration ratios decrease to 3 – 4, then the major ion concentrations converge in the Large and Small fractions and appear to be independent of drop size. Occasionally the Large fraction calcium ion concentration may approach those observed for sulfate, nitrate, or ammonium. The change in calcium concentrations is associated with an increase in Large nitrate concentrations, but has varying relations to both ammonium and sulfate.

**As in earlier chapters, capitalized "Large" and "Small" refer specifically to the two sf-CASCC drop fractions.

Reproduced with permission of the copyright owner. Further reproduction prohibited without permission.

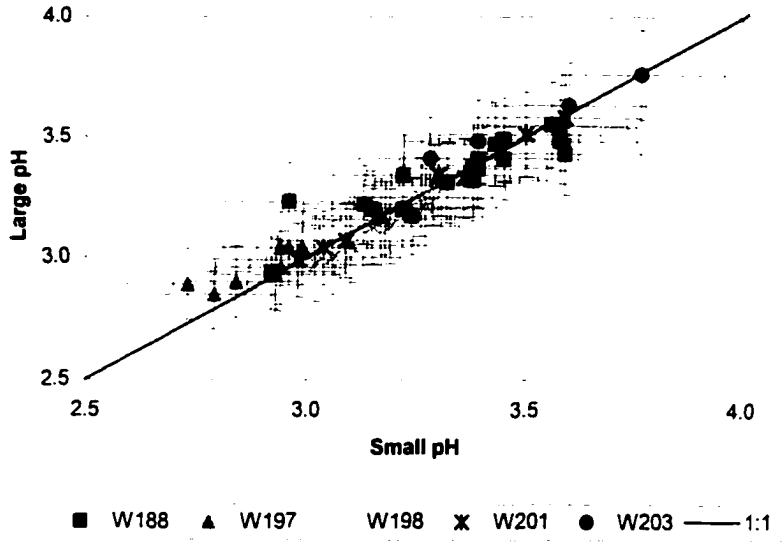

Figure 8-2: Large vs. Small sf-CASCC -- pH

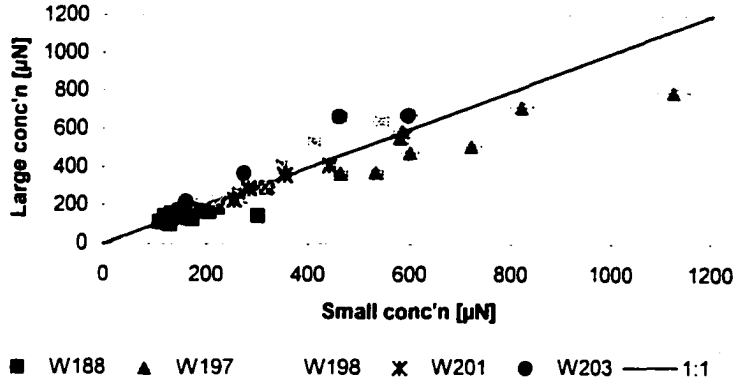

Figure 8-3: Large vs. Small sf-CASCC -- ammonium

Manganese (figure 8-7) is included because its Large vs. Small pattern is very similar to iron's (not shown), and some of the other species present in low (typically < 50 μN) concentrations in the drops (e.g. potassium ion). Manganese does not have as high a Large/Small concentration ratio as calcium and magnesium. Copper, iron and manganese, in fact, have higher

Reproduced with permission of the copyright owner. Further reproduction prohibited without permission.

concentrations in the Small fraction (figures 8-7 and 8-8) during the W188 event than in the Large.

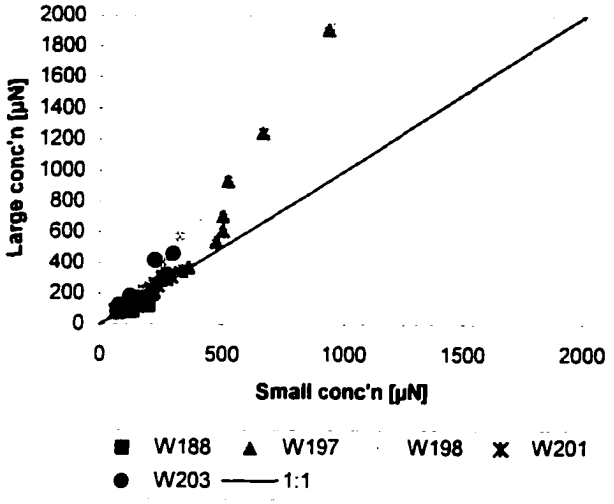

Figure 8-4: Large vs. Small sf-CASCC – nitrate

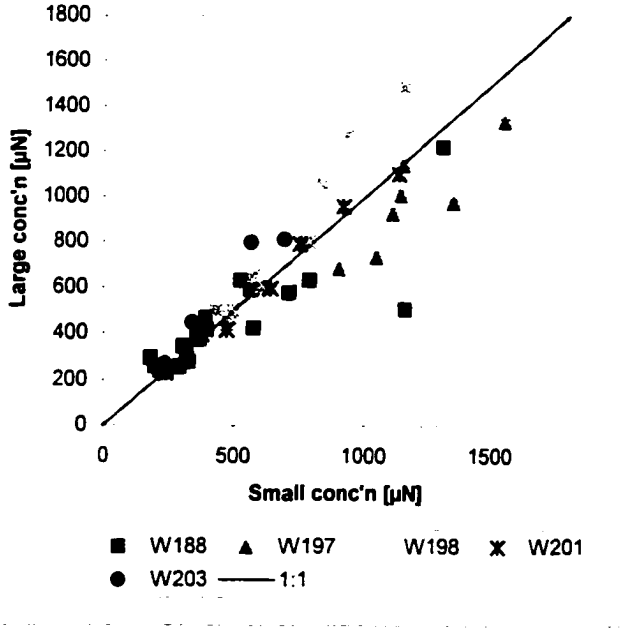

Figure 8-5: Large vs. Small sf-CASCC – sulfate

Reproduced with permission of the copyright owner. Further reproduction prohibited without permission.

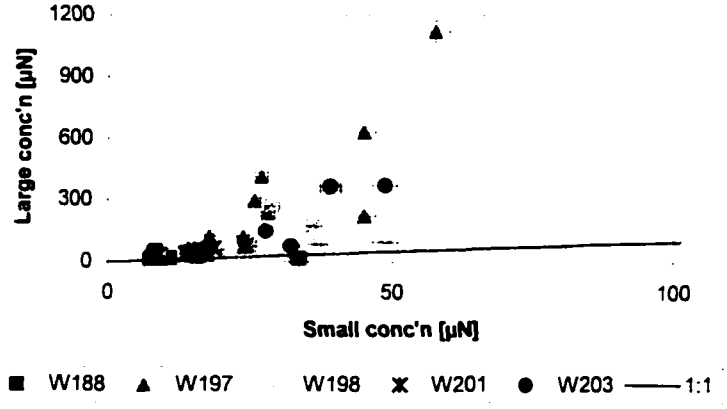

Figure 8-6: Large vs. Small sf-CASCC – calcium ion

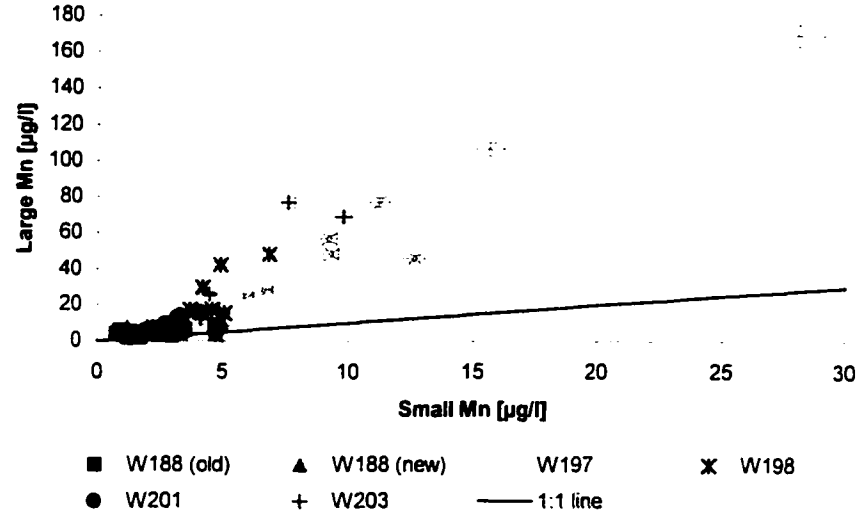

Figure 8-7: Large vs. Small sf-CASCC – manganese

Copper concentrations were measured in the W188, W197 and W198 Metals aliquots for comparison to the later Davis samples (Chapter 9). The motivation behind measuring copper is included in Chapter 9. At Whiteface, copper concentrations were generally near the detection limit (figure 8-7). Copper results are included in Table 8-1 which summarizes the Large and Small concentrations and Large/Small concentration ratios for selected species.

Reproduced with permission of the copyright owner. Further reproduction prohibited without permission.

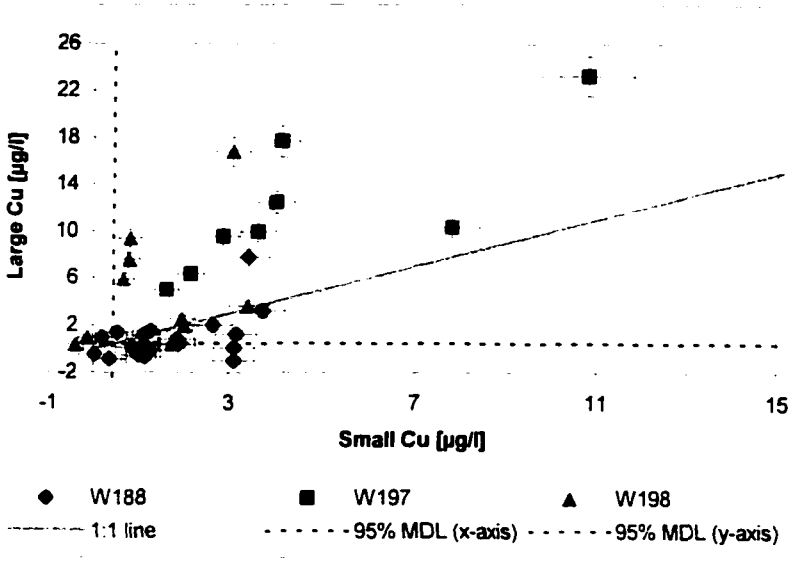

Figure 8-8: Large vs. Small sf-CASCC – copper

Table 8-1: sf-CASCC results from the Whiteface Campaign (July 1998)

Species	n	Large Concentration		Small Concentration		Large/Small		
		min	max	min	max	min	max	mean
S(IV) [µM]		DL	DL	DL	DL			
HCHO [µM]	38	3.3	18.6	3.6	19.5	0.5	1.3	0.9
H_2O_2 [µM]	31	DL	71.7	DL	61.5	0.5	3.3	1.0
NH_4^+ [µN]	59	8.7	793.2	12.9	1124.4	0.5	1.4	1.0
Mg^{2+} [µN]*	59	2.3	241.5	2.4	22.6	0.4	18.8	4.0
Ca^{2+} [µN]*	59	DL	1123.7	DL	57.3	0.3	19.6	3.8
NO_3^- [µN]	59	5.4	1908.7	8.7	926.9	0.6	2.1	1.2
$SO_4^=$ [µN]	59	14.3	1534.3	23.8	2192.6	0.4	1.6	1.0
pH	59	2.85	4.66	2.73	4.59	1.0	1.1	1.0
Cu [µg l^{-1}]#	37	DL	23.3	DL	10.8	0.4	11.5	3.1
Fe [µg l^{-1}]	77**	3.6	1159	4.5	467	0.3	7.8	2.5
Mn [µg l^{-1}]	77**	0.2	169.6	0.4	28.1	0.2	10.0	3.1

DL = at or below detection limit
n = number of sample pairs
*blank or variability issues at low levels (see text)
**sample pairs from both sf-CASCCs on W188 included
W188, W197 & W198 only – Large/Small ratio for 23 pairs only (omit < DL points)

The mean Large/Small ratios vary little for the major ions (1.0 – 1.2). Calcium and magnesium have mean ratios approximately equal to 4 (sodium, potassium, and chloride where data exist are similar, but not shown). The Metals (Fe, Mn and Cu) also tend to be higher in the Large fraction

Reproduced with permission of the copyright owner. Further reproduction prohibited without permission.

(Large/Small ratios average around 3), but not to as great a degree as calcium and the ions with calcium-like patterns and drop size-dependencies.

To summarize, the sf-CASCC data show some size-dependent drop composition for calcium ion, manganese and similar species. Ammonium, sulfate, nitrate and pH exhibit little concentration drop size-dependence. The 5-Stage data will be used to evaluate the validity of these observations.

8.3 5-Stage results and discussion

The 5-Stage was operated during the W185 (1 sample set), W188 (1 sample set), and W198 (5 sample sets) events. The W185 event data are excluded due to the reasons given above. On W188 only one set of samples was obtained at the end of the event when the cloud was dissipating. As one stage yielded no water and the sampling period varied slightly from the sf-CASCC and CASCC2, those data are also not presented. Therefore the focus will be on the five samples collected during the W198 event already described in terms of collector validation in Chapter 4.

Five complete sample sets were obtained from 02:00 – 03:00 (2 – 3 a. m.), 4 – 5 a. m., 6 – 7 a. m., 8 – 9 a. m., and 10 – 11 a. m.. Sf-CASCC data are available for all of these time periods and CASCC2 data are available for three. The LWC varied from 337 mg m^{-3} at the start of the event to a 741 mg m^{-3} peak during the 8 – 9 a. m. sample period. LWC declined in the last sample period. Winds were light (6 m s^{-1} at the start decreasing to 4 m s^{-1} during the last sample period).

The figures used to show the 5-Stage's observed size-dependent drop composition here and in Chapter 9 are all plotted the same way. The 5-Stage data are usually presented with both CASCC2 and sf-CASCC data. In some instances, the temporal evolution of a particular species' concentration is shown for a single collector, but figures for all three collectors are included. Both

Reproduced with permission of the copyright owner. Further reproduction prohibited without permission.

approaches are useful for interpreting the observations. All of the concentration data (y-axis) for a collector/collector stage during a sampling period are plotted against the calculated volume median diameter (VMD) (x-axis) for the appropriate collector/collector stage. Volume median diameters are calculated as described in Chapter 4. For the 2 – 3 a. m. and 4 – 5 a. m. sample periods, the drop distribution data failed validation (Appendix G and Chapter 4). For these two time periods, a dual-mode log normal drop distribution was modeled constrained by the measured PVM D_{eff} and the actual sf-CASCC sample volume (subject to Chapter 4). The resulting VMDs are highly uncertain and I have not included x-axis error bars for them. Despite this uncertainty, the modeled VMD data allow all of the concentration data to be plotted together. For the three later sample periods, the x-axis error bars represent the diameters corresponding to 16% and 84% of the volume. All of the y-axis (concentration) error bars represent analytical uncertainty only. The sf-CASCC and 5-Stage individual data points for a sample pair/set are joined by a straight line. The true distribution may be somewhat different (see Chapter 4). When interpreting these plots some idea of the cloud drop distribution can be gained without reference to Chapter 4 or Appendix G by locating the CASCC2 VMD. Finally, the 95% Confidence Level MDL is included where it is relevant to data interpretation. The 5-Stage concentration data are tabulated in Appendix H.

Table 8-2 compares the observed W198 concentration ranges for the major species from the three collectors. Figures 8–9 through 8–27 show the 5-Stage results for various species and time periods. "Minor" species are included to show that the observed drop size-dependent concentration patterns are robust – even at low concentrations and among many different species. Representative drop size-dependent concentration patterns for the 5-Stage were evaluated for all measured species. The data presented have not been filtered to show only the "best" results, but rather to minimize 5-Stage and sf-CASCC concentration pattern duplication. There are two kinds of figures or sets of figures – all the collector concentrations as a function of VMD for a particular time period and species are shown together, or three figures presenting the temporal evolution of drop size-dependent concentration as measured by each collector. Figures

Reproduced with permission of the copyright owner. Further reproduction prohibited without permission.

8-9 and 8-10 illustrate the drop size-dependent pH measurements for the 2 – 3 a. m. and 8 – 9 a. m. sample periods. Figures 8-11, 8-12 and 8-13 present the CASCC2, sf-CASCC and 5-Stage W198 profiles for ammonium to show the temporal evolution. While ammonium's patterns are broadly representative of those for nitrate and sulfate, some differences exist. Therefore, the 6 – 7 a. m. nitrate (figure 8-14), and 6 – 7 a. m., 8 – 9 a. m., and 10 – 11 a. m. sulfate (figures 8-15, 8-16, and 8-17) concentration patterns are shown. Figures 8-18, 8-19, and 8-20 show manganese concentrations. Manganese is broadly representative of the 5-Stage concentration profiles observed for minor species where sf-CASCC data show Large concentrations are relatively and consistently elevated compared to the Small (e.g. Fe, etc.). Figures 8-21 through 8-23 present calcium ion distributions which tend to have higher sf-CASCC Large/Small fraction concentration ratios than manganese. Figures 8-24 through 8-26 show potassium ion and chloride concentration profiles. Figure 8-27 presents the 10 – 11 a.m. concentration pattern for total peroxides. Table 8-3 summarizes the maximum variation in concentrations observed in the 5-Stage and the sf-CASCC for the different species for W198 and compares them to each other. The sf-CASCC data presented are a subset of those presented in table 8-1.

Recall for this discussion that Stage 1 (V1) of the 5-Stage is the largest and collects the largest drops, and Stage 5 (V5) is the smallest.

Table 8-2 is shown prior to the figures to emphasize two points. The first is that the 5-Stage is capable of resolving a wider range of concentrations for a given sampling period than the single-stage CASCC2 (bulk) or the two-stage sf-CASCC. While even the size-resolving collectors have substantial mixing between drops of different sizes collected by the individual stages (see Chapter 4), the 5-Stage successfully separates the very largest drops from the very smallest which the others do not. For the W198 event, the 5-Stage can resolve even higher concentrations in the first two (V1 and V2) stages where concurrent sf-CASCC sample pairs show Large/Small concentration ratios > 1. Second, the sf-CASCC measures a slightly lower concentration than the 5-Stage for some species which "should not" occur (e.g. if the 5-Stage

Reproduced with permission of the copyright owner. Further reproduction prohibited without permission.

data indicate some drop fraction concentrations are higher than the sf-CASCC does, it should concurrently measure some lower concentrations for the "bulk" volume-weighted average between the two collectors to match). While these concentration variations are generally within the analytical uncertainty, it is important to recognize that the collectors may sample slightly different drop populations which can result in somewhat different definitions of "representative" cloud drop samples (see Chapter 4). Therefore, while quantitative comparisons can be made, there is additional uncertainty in these measurements that is not captured by the analytical error bars shown. Field performance validation (Chapter 4) suggests that the collectors measured very similar drop populations.

Figures 8-9 and 8-10 were chosen to show the "extreme" pH values measured in the 5-Stage during this event, and how they compare to the other collectors. The sf-CASCC pH varied from 3.0 to 3.3 during this event and the 5-Stage from 2.9 – 3.5. Given the uncertainties (5% is shown), all three collectors measured essentially the same pH.

Table 8-2: W198 sample range by collector for selected species

Collector	Ammonium [μN]	Nitrate [μN]	Sulfate [μN]	Calcium [μN]
CASCC2*	218 - 442	159 - 383	469 - 1010	35 - 75
sf-CASCC**	172 - 533	161 - 569	429 - 1273	10 - 268
5-Stage**	193 - 716	153 - 1328	433 - 1355	29 - 1287

** 3 of 5 sampling periods*
***across all stages/fractions*

The ammonium results shown by collector (figures 8-11 through 8-13) are the first of many figures to clearly indicate the "extra" drop size-dependent composition information available from using the 5-Stage collector compared to the other collectors. The CASCC2 figure illustrates the change in D_{eff} to larger sizes during the event and (by inference as the concentration decreases) the increase in LWC from the first sample period to the last, but its utility compared to the next two figures in resolving size-dependent drop composition is limited. In the sf-CASCC figure, the

Reproduced with permission of the copyright owner. Further reproduction prohibited without permission.

first two sample periods have higher concentrations of ammonium in the Large fraction (there was a very high Large/Small calcium concentration during these time periods as discussed previously

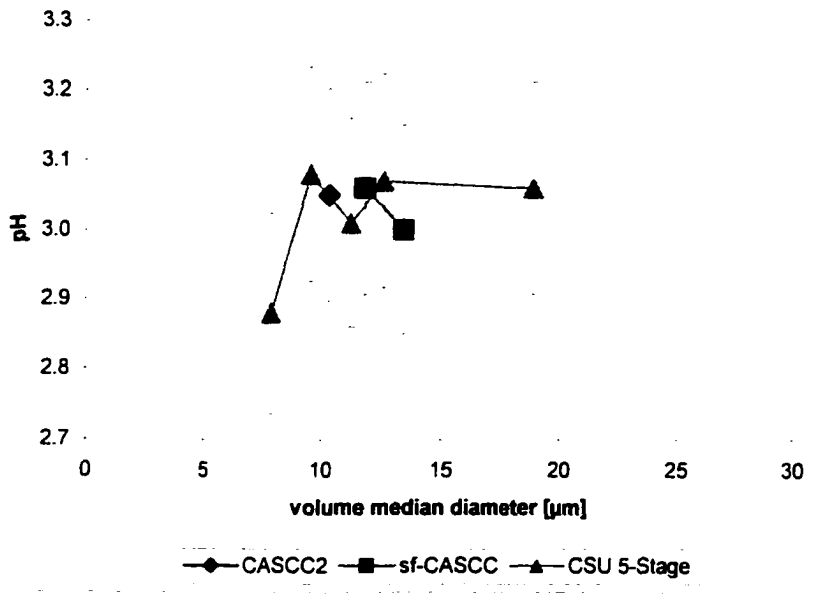

Figure 8-9: W198 2 – 3 a. m. pH (all collectors)

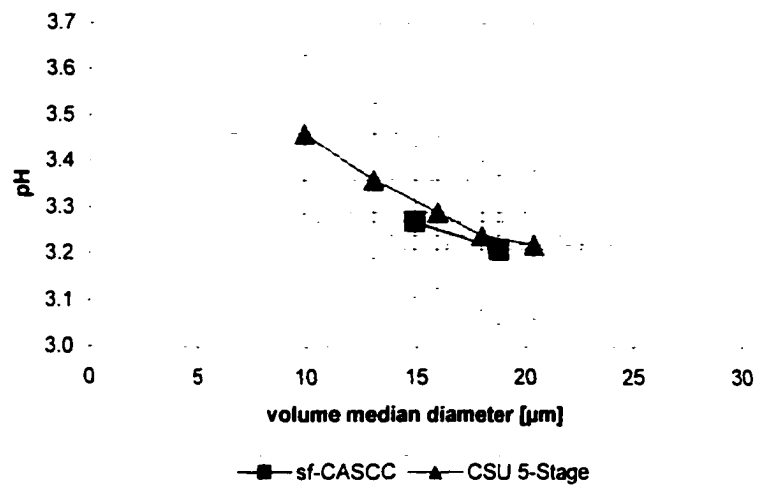

Figure 8-10: W198 8 – 9 a. m. pH (all collectors)

and shown below). As the event progresses, the gradient in concentration between the two stages of the sf-CASCC flattens out. The 5-Stage figure shows an even greater initial (2 – 3 a.

Reproduced with permission of the copyright owner. Further reproduction prohibited without permission.

m.) larger/smaller concentration gradient (approximately a factor of 1.8 from 716 μN (V1) to 403 μN in (V2)). During the 4 – 5 a. m. and 6 – 7 a. m. time periods the concentration profile is generally flat, although concentrations are somewhat higher in V1 than V5. For the last two time periods, a "U"-shaped curve develops. The V1 concentration is 274 μN and the concentration reaches a minimum of 207 μN (V4) before rising again to 261 μN (V5) during the 10 – 11 a. m. time period. There is a factor of approximately 1.3 difference between these concentrations while the 2 sf-CASCC fractions have essentially equal concentrations.

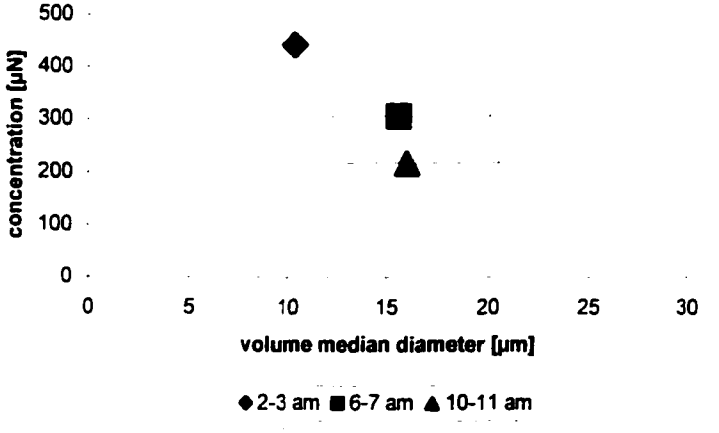

Figure 8-11: W198 CASCC2 temporal evolution -- ammonium

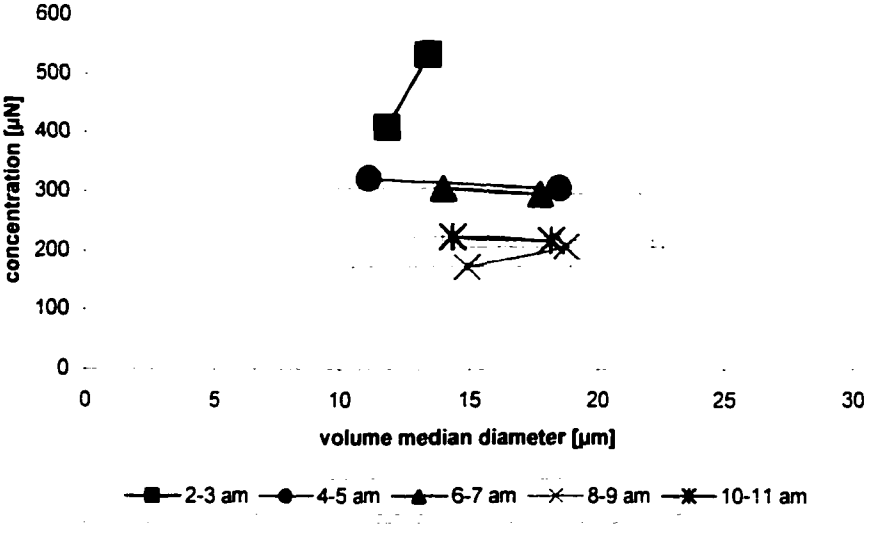

Figure 8-12: W198 sf-CASCC temporal evolution - ammonium

Reproduced with permission of the copyright owner. Further reproduction prohibited without permission.

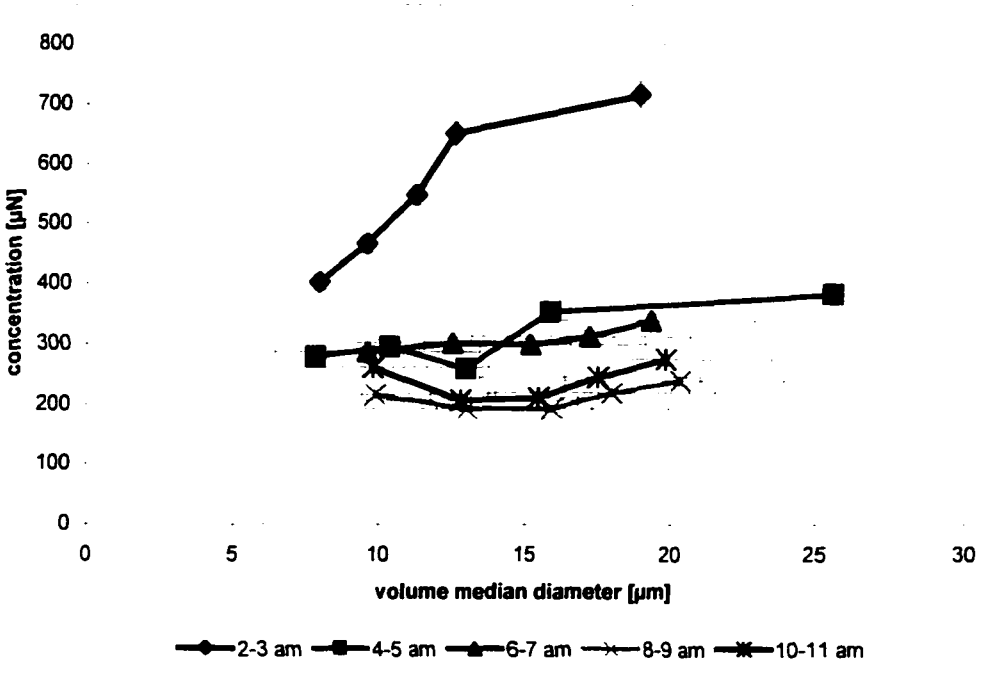

Figure 8-13: W198 5-Stage temporal evolution – ammonium

The nitrate concentration patterns for the 6 – 7 a. m. time period are shown (figure 8-14) because of the different size-dependent sf-CASCC results during this period compared to ammonium (figure 8-12). The Large nitrate concentration is greater than the Small instead of the reverse. The 5-Stage data suggest that this Large/Small difference is due to the very strong concentration gradient in nitrate between V1 (487 µN) and V2 (308 µN). The concentration decreases more gradually to smaller drop sizes (262 µN in V5). The difference between the V1 and V2 concentrations is approximately a factor of 1.6. Ammonium (figure 8-13) does not exhibit this strong change in the largest 5-Stage drop fraction concentrations.

The sulfate (figures 8-15 through 8-17) results are similar to those shown in figures 8-11 through 8-14 for ammonium and nitrate. During the 6 – 7 a. m. time period, the difference in sulfate concentration between V1 and V2 is only a factor of 1.1 (much less than for nitrate). The sf-CASCC profile for this time period is flat, but the 5-Stage reveals more variation. The V1/V5

Reproduced with permission of the copyright owner. Further reproduction prohibited without permission.

concentration ratio is approximately 1.4. During the last two time periods, the "U"-shaped profile is again evident and is strongest during the last time period.

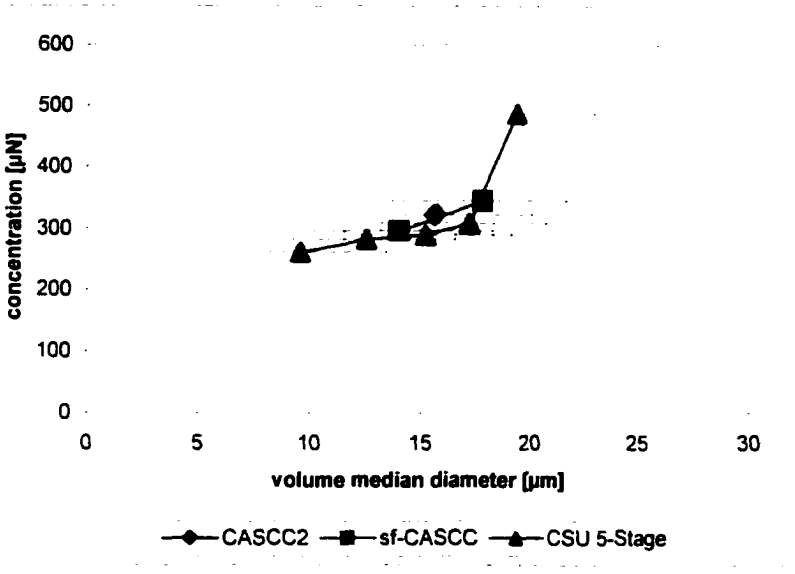

Figure 8-14: W198 6 – 7 a. m. nitrate (all collectors)

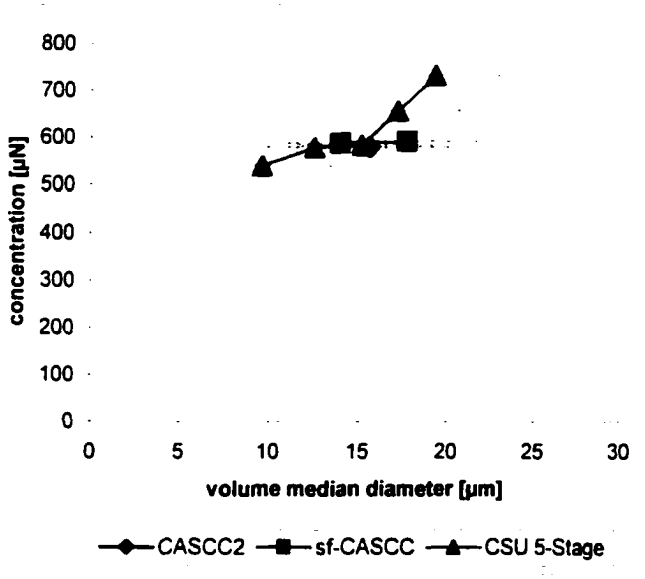

Figure 8-15: W198 6 – 7 a. m. sulfate (all collectors)

The 5-Stage data for ammonium, nitrate and sulfate illustrate that the size-dependent cloud drop composition is more varied than the sf-CASCC can resolve. Further, the concentrations

Reproduced with permission of the copyright owner. Further reproduction prohibited without permission.

measured in the different stages of the 5-Stage are consistent with whatever small variations in drop size-dependent composition the sf-CASCC shows. Multiple figures featuring these three dominant species are shown to illustrate that the patterns observed in the 5-Stage concentration

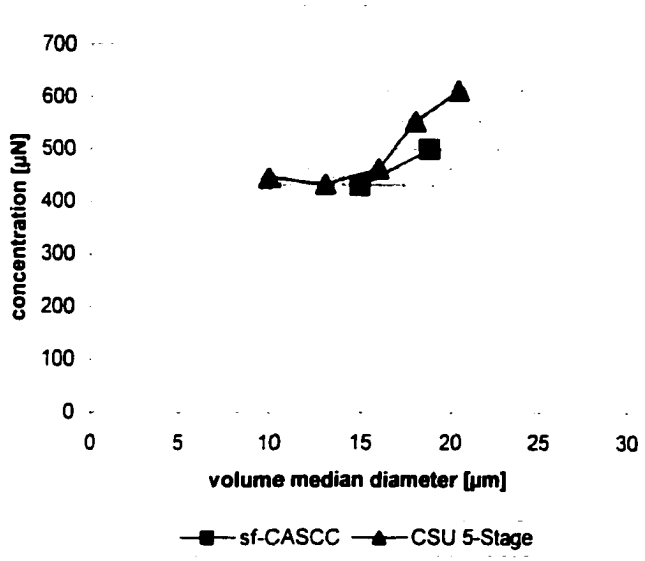

Figure 8-16: W198 8 – 9 a. m. sulfate (all collectors)

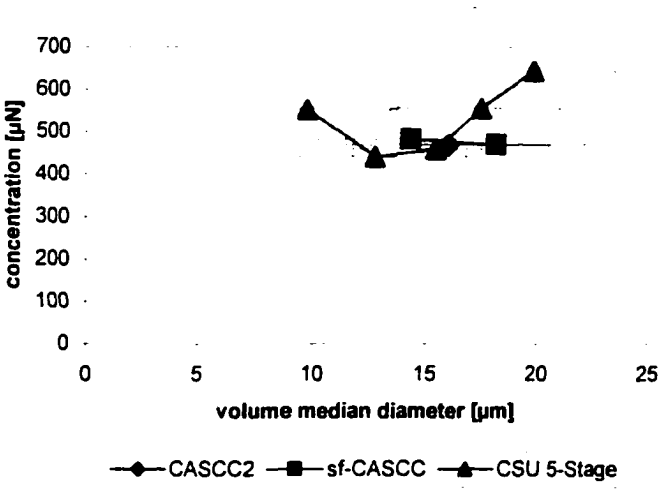

Figure 8-17: W198 10 – 11 a. m. sulfate (all collectors)

profiles are broadly consistent between them. While the 5-Stage data largely validate the sf-CASCC pH observations, they suggest that the lack of drop composition size-dependence for the other three species is more of a sf-CASCC sampling artifact.

Reproduced with permission of the copyright owner. Further reproduction prohibited without permission.

The Metals and the "minor" ions (Ca^{2+}, Mg^{2+}, K^{+}, Na^{+}, Cl^{-}) in the cloud water exhibit size-dependent composition in the sf-CASCC samples (section 8.2). Figures 8-18 through 8-20 illustrate again how limited the size-dependent drop composition information available from the CASCC2 and sf-CASCC is compared to the 5-Stage. As observed with ammonium, nitrate and sulfate, the larger drops are relatively more concentrated during the first sample period. Here the sf-CASCC Large concentration remains higher for all time periods instead of relaxing to the Small concentration. In the 5-Stage sample sets the minor ion profiles are similar to those for ammonium, nitrate and sulfate, but sharper concentration gradients are observed in the larger drop fractions. The "U"-shaped profile that develops is deeper with a broader range of concentrations observed. For example, the 10 – 11 a. m. manganese concentrations are 15.7 – 5.8 – 1.7 – 1.6 – 4.8 $\mu g\ l^{-1}$ for stages V1 through V5. The peak concentration ratio (V1/V4) is approximately 10, and a factor of 3 difference between the V4 and V5 concentrations produce the "small" arm of the "U". Figures 8–21 through 8–23 for calcium show broadly similar results to Mn, although in some instances there are steeper concentration gradients between stages producing sharper "U"-profiles. The minor species shown in figures 8–24 through 8–26 illustrate that these 5-Stage concentration profiles are consistent across many varying species. Where sf-CASCC Small fraction concentration measurements exceed Large ones, concurrent 5-Stage data (figure 8-24) again reflect it. The "W" pattern in the 5-Stage potassium profile (figure 8-25) was also observed for chloride and sodium, although all three are measured near their MDLs. The size-resolved IEP collector data from ACE-2 also exhibit "W"-type profiles for some species (Bower *et al.*, 2000). Figure 8-26 is interesting because a very strong "U"-shaped profile in the 5-Stage data yield virtually identical concentrations between the sf-CASCC Large and Small fractions.

Reproduced with permission of the copyright owner. Further reproduction prohibited without permission.

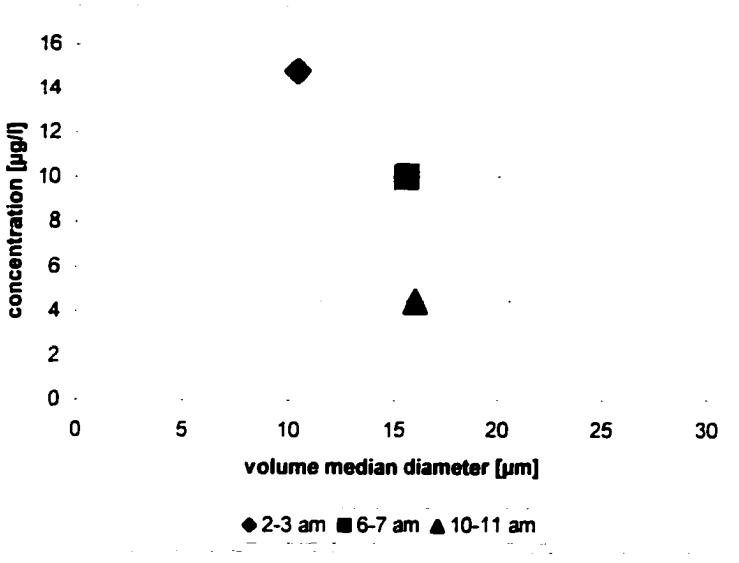

Figure 8-18: W198 CASCC2 temporal evolution -- manganese

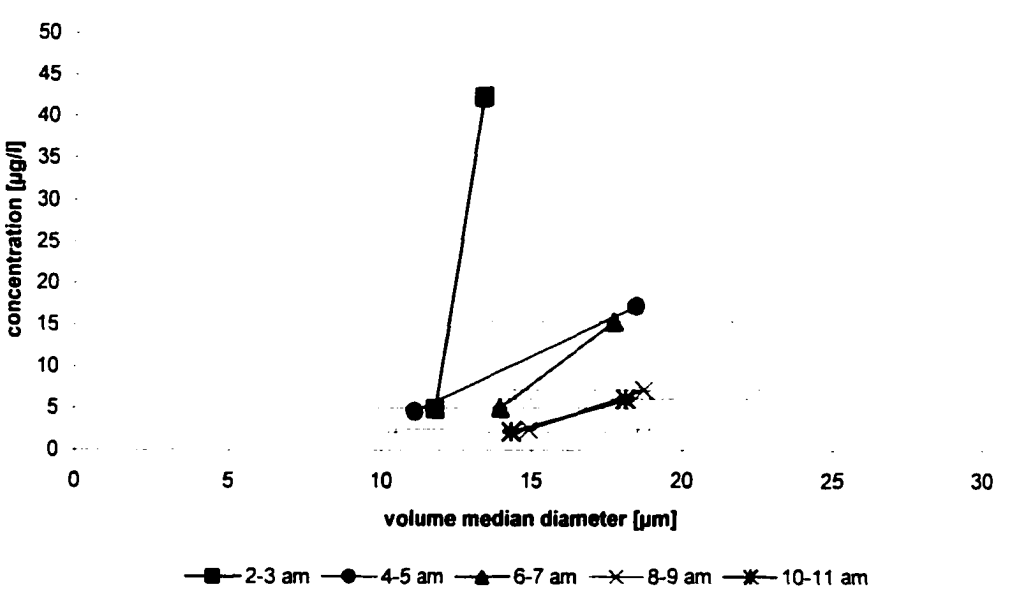

Figure 8-19: W198 sf-CASCC temporal evolution -- manganese

The total peroxide concentration profile is included for completeness (figure 8-27). The peroxide aliquot for the 5-Stage was usually preserved within 25 – 27 minutes after the end of the sampling

Reproduced with permission of the copyright owner. Further reproduction prohibited without permission.

period so any H_2O_2 in solution is subject to more degradation prior to preservation than either the sf-CASCC or CASCC's aliquot. The 5-Stage's results are "consistent" with the sf-CASCC's in the sense that little size-dependence is observed and the 5-Stage concentrations are generally lower.

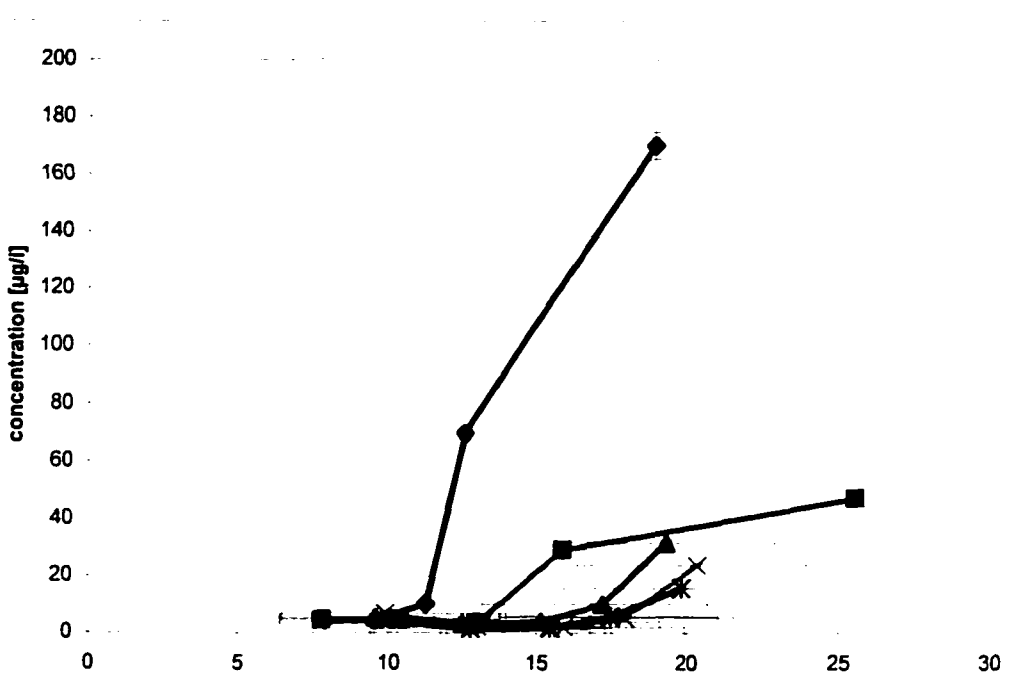

Figure 8-20: W198 5-Stage temporal evolution -- manganese

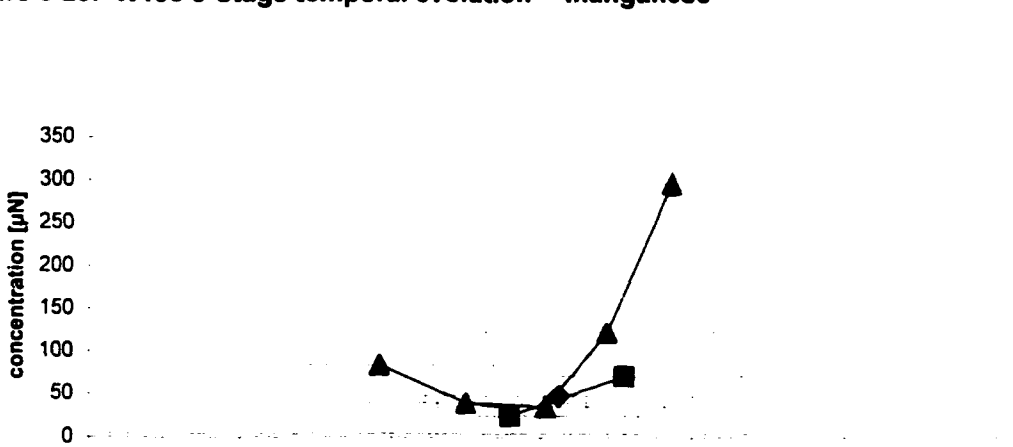

Figure 8-21: W198 6 – 7 a. m. calcium ion (all collectors)

Reproduced with permission of the copyright owner. Further reproduction prohibited without permission.

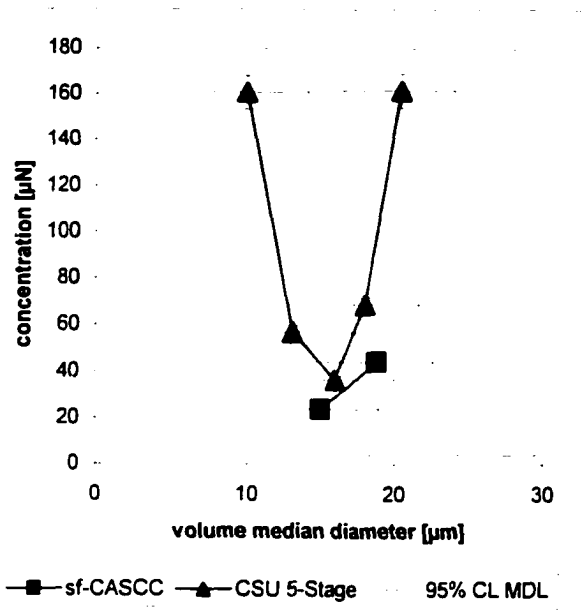

Figure 8-22: W198 8 – 9 a. m. calcium ion (all collectors)

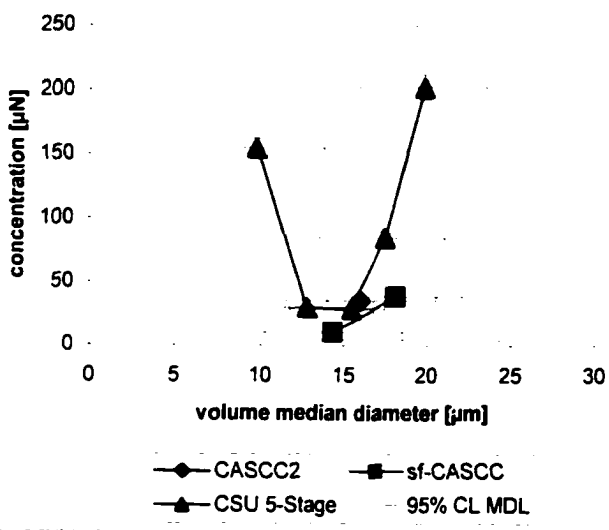

Figure 8-23: W198 10 – 11 a. m. calcium ion (all collectors)

If H_2O_2 measurements in the 5-Stage sample sets become a priority the aliquots will have to be collected and preserved within a shorter time frame.

Reproduced with permission of the copyright owner. Further reproduction prohibited without permission.

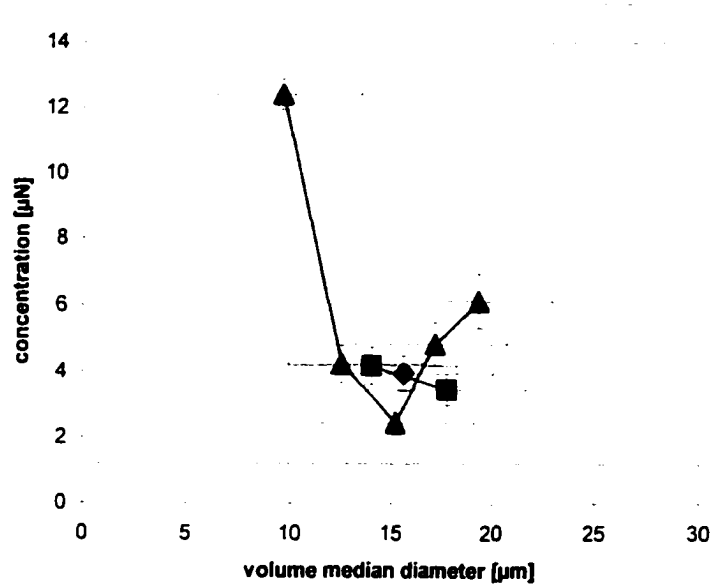

Figure 8-24: W198 6 – 7 a. m. potassium ion (all collectors)

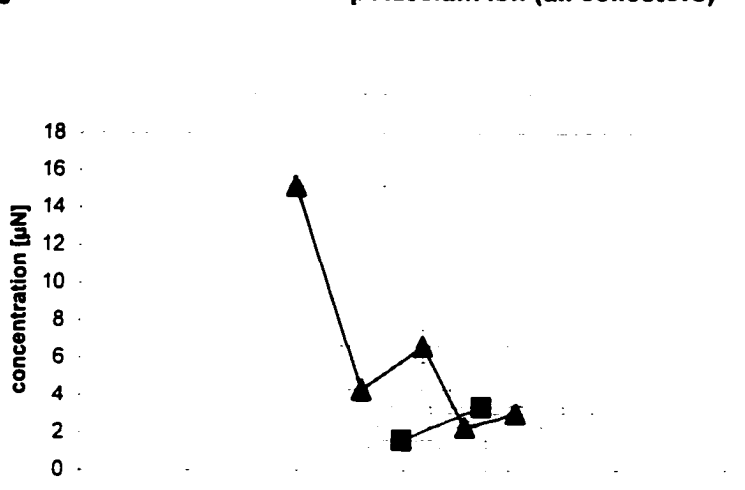

Figure 8-25: W198 8 – 9 a. m. potassium ion (all collectors)

Table 8-3 summarizes all of the available W198 data (copper is omitted as most 5-Stage concentrations were less than the MDL). The species are presented roughly in groups – the

Reproduced with permission of the copyright owner. Further reproduction prohibited without permission.

major inorganic ions are together, followed by the low concentration minor inorganic ions and then the Metals, calcium ion and magnesium ion. The last row in the table emphasizes the

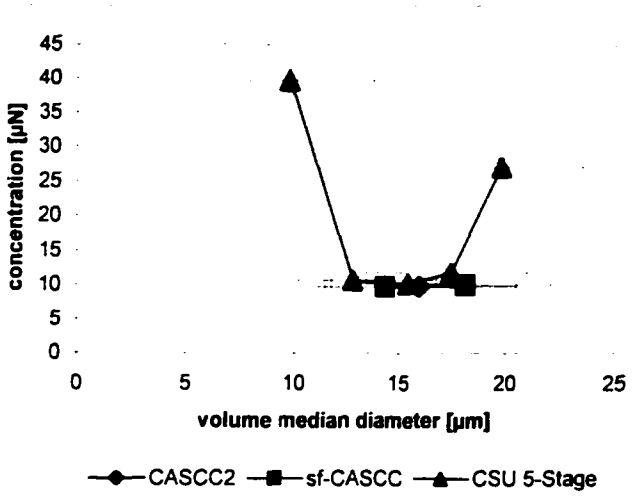

Figure 8-26: W198 10 – 11 a. m. chloride (all collectors)

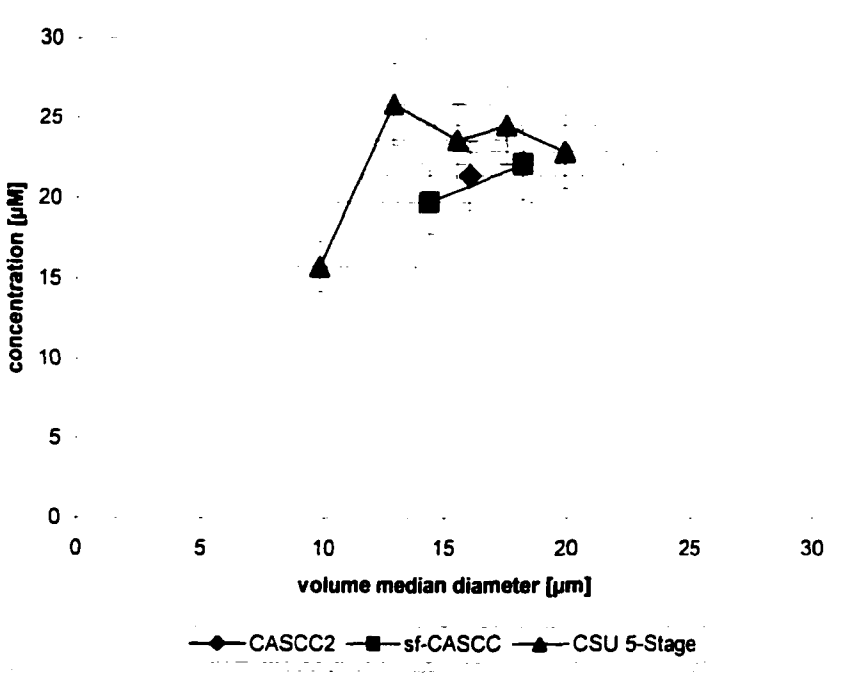

Figure 8-27: W198 10 – 11 a. m. total peroxides (all collectors)

broader variations in drop size-dependent composition the 5-Stage is able to measure compared to the sf-CASCC. For the species (e.g. calcium) with a strong sf-CASCC size-dependence, the

Reproduced with permission of the copyright owner. Further reproduction prohibited without permission.

difference between maximum and minimum concentrations can be up to a factor of 11 higher in the 5-Stage. Generally there is a 2 – 4 times wider range in the 5-Stage compared to the sf-CASCC. Where the sf-CASCC may have a maximum Large/Small ammonium concentration ratio of 1.3, the 5-Stage indicates a maximum of 1.8. For sulfate there can be as high as a 60% difference in sulfate concentrations between 5-Stage drop fractions compared to a maximum of 40% in the sf-CASCC. For calcium, a maximum Large/Small ratio of 9 in the sf-CASCC becomes up to a factor of 30 between fractions in the 5-Stage. Drop size-dependent composition is measured in the 5-Stage for virtually every measured sample and a broader range of concentrations is observed compared to the sf-CASCC or CASCC2.

Table 8-3: sf-CASCC and 5-Stage maximum/minimum concentration ratio for selected species on W198 and 5-Stage-to-sf-CASCC ratio comparison

maximum/ minimum concentration ratio*	pH	Ammonium	Nitrate	Sulfate	Sodium ion*	Potassium ion**	Chloride**	Magnesium ion*	Calcium ion	Manganese	Iron*
sf-CASCC	1.00 - 1.03	1.0 - 1.3	1.0 - 1.8	1.0 - 1.4	1.1 - 3.9	1.2 - 2.4	1.0 - 1.4	2.3 - 18.4	1.9 - 9.2	2.8 - 8.7	2.3 - 7.8
5-Stage	1.03 - 1.07	1.2 - 1.8	1.8 - 4.2	1.4 - 1.6	4.0 - 17.8	2.3 - 14.7	2.1 - 3.9	13.0 - 58.0	4.4 - 29.8	9.1 - 42.3	6.5 - 33.8
5-Stage/ sf-CASCC ratio***	1.02 - 1.05	1.0 - 1.4	1.4 - 2.4	1.1 - 1.6	1.5 - 8.5	2.3 - 11.2	1.9 - 3.8	2.4 - 5.6	1.8 - 4.4	3.0 - 4.9	2.6 - 4.3

** some data near MDL*

*** concentrations low (generally < 100 μN)*

** The minimum value possible is 1 indicating concentrations are independent of drop size.*

**** The 5-Stage's maximum/minimum concentration ratio for a given time period is divided by the sf-CASCC's maximum/minimum ratio to derive the values presented here.*

This analysis considers only one event at Whiteface and the 5-Stage data are limited. However, what exists illustrates the 5-Stage's promise at providing more information about the actual variation in size-dependent drop chemistry. Compared to the other events at Whiteface (table 8-1), the sf-CASCC W198 data (talbe 8-3) shows relatively little Large/Small concentration ratio variability. If the 5-Stage had been operated during these other events it is possible that an even wider size-dependent drop concentration range would have been observed. Contrary to observations obtained using the two-stage sf-CASCC, ammonium, sulfate and nitrate, which

Reproduced with permission of the copyright owner. Further reproduction prohibited without permission.

constitute a majority of the charged species in solution, exhibit size-dependent drop composition at Whiteface.

Given the theoretical basis for drop size-dependent cloud composition (Chapter 1), it appears that the Whiteface data are consistent with behaviour in both Regions I and II – the "growth to equilibrium" and "growth by condensation" regions which show decreasing concentrations as a function of drop size and then increasing concentrations, respectively. There are too many unmeasured factors to draw definitive conclusions about the evolution of the cloud. However, figure 8-28 shows the temporal evolution of the 5-Stage total inorganic ion concentration (the sum of the species measured by the IC (TIC)) profile which suggests Region II was strongly evident for the first time period and then as sampling progressed, Region I became visible too. Total (usually non-volatile) mass is the y-axis in the discussion of drop size-dependent composition in Chapter 1, and it is important to recognize that the sum of charged species is only an approximation. The mix of species, however, can vary between time periods. For example, both Regions I and II are evident for sulfate during the 10 – 11 a. m. sample, and, both are also evident for calcium ion in all the time periods shown. There are several possible explanations for this (e.g. different size-dependent aerosol composition profiles for the two species, an external aerosol mixture, in-cloud production of sulfate, among others). Earlier work at Whiteface using two sampling locations – the summit and the "slope" station (1250 m asl) – indicated that bulk cloud composition strongly depended upon location with respect to the cloud base. Near the cloud base, concentrations were higher (Vong *et al.*, 1990). Higher in the cloud as drops continued to grow by condensation and the LWC increased, species concentrations were lower due to dilution. Some of the size-dependence for ammonium, sulfate and nitrate observed at the start (W198) and end of an event (W197) may result from a shifting cloud base. We do not know where cloud base was, nor do we know the size-resolved composition of the input aerosol, gas-phase concentrations or the updraft strength.

Reproduced with permission of the copyright owner. Further reproduction prohibited without permission.

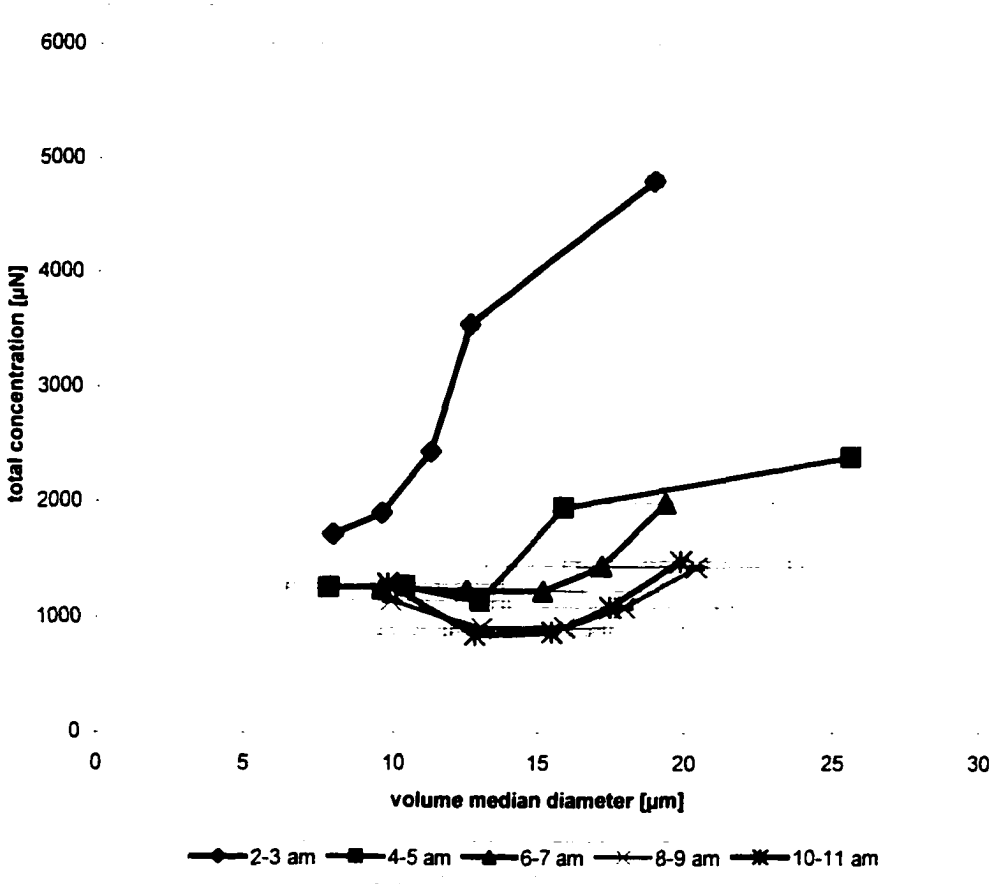

Figure 8-28: W198 5-Stage temporal evolution – total measured inorganic concentration

Data do not exist to resolve the association between elevated calcium and nitrate concentrations in the larger drops. However, these observations are consistent with some of the drops forming on coarse mode aerosol nitrate. A large proportion of the precursor CCN at Whiteface are likely to be aged aerosol where the potential exists for them to have experienced many cloud cycles. This would tend to homogenize the aerosol and dampen (but not eliminate) any size-dependent composition. Similar observations have been made at another mountain site, Kleiner Feldberg, where the aerosol also was not "fresh" (Wobrock *et al.*, 1994). However, part of the failure to observe size-dependent drop chemistry at Kleiner Feldberg may have been a measurement artifact given the size-resolving collector used and the ambient drop size distribution. The observation of Region II where drop concentrations increase with size has been observed at other mountain sampling sites (Heintzenberg *et al.*, 1989, among others), although the aerosol

Reproduced with permission of the copyright owner. Further reproduction prohibited without permission.

there may have been through fewer upstream cloud cycles. Sulfate, nitrate and ammonium have approximately similar concentration patterns in the 5-Stage which may suggest that their presence is tied to the same CCN source (but not necessarily first emission source into the atmosphere). This is possibly true for all of the species that can be grouped together by concentration pattern. Different species – as observed at ACE2 – have varying drop size-dependent concentration patterns within each sampling period.

As we have no upwind size-resolved aerosol- and gas-phase measurements, we cannot determine what the source of the species observed in the drops is. However, nucleation scavenging is the probable source for many of the species observed in-cloud, particularly the non-volatile ones. Much of the ammonium, sulfate and nitrate is probably from secondary aerosol production in the atmosphere upwind from Whiteface (which clouds encountered en route may affect); however, as indicated previously there may be some large calcium nitrate CCN. Due to the high acidity and LWC, any ammonia gas present at Whiteface would likely partition almost completely into the aqueous-phase as would any nitric acid (see Chapter 9). As the sulfate is not neutralized in the drops, nitrate may be volatilized upon evaporation. Evidence for in-cloud sulfate production from S(IV) oxidation at Whiteface is described by Rattigan *et al.* (2001)

All of the figures shown illustrate that the profiles observed in the 5-Stage were robust across many species. Sampling artifacts in one stage during one time period or for one species cannot account for the consistent drop size-dependent composition variations observed. The drop samples are integrated over one hour, but the drop size distributions were stable (where those data exist).

Several reasons explain why the sf-CASCC showed so little drop size-dependent chemistry. The first is that the size-dependent chemistry was not strong for the principal species (less than a factor of two according to the 5-Stage). Further, the D_{eff} was in the vicinity of the Large fraction D_{p50}. The broad collection efficiency curve smeared out the variation between stages as

Reproduced with permission of the copyright owner. Further reproduction prohibited without permission.

measured drop composition was dominated by the mean concentration associated with the effective diameter. Sulfate, for example, is not a good species to use for collector validation here because variations in concentration between drops are mostly within analytical uncertainty. A better measure would be calcium, for example, to investigate if common drop populations are being sampled. This is an important point to remember when considering collector validation comparisons (Appendix B).

The VMD is not the same as the D_{p50} for a particular stage during a sample period and, in fact, varies as a function of the drop size distribution. Therefore the D_{p50}, particularly for skewed distributions, is not necessarily representative of the actual drop population collected on a stage. As the VMDs shift between samples, they help to explain how the concentrations change. The interpretation of the drop size-dependent composition can not be separated from the cloud microphysics.

Reproduced with permission of the copyright owner. Further reproduction prohibited without permission.

9. Davis

The Davis radiation fog campaign was a companion project to the earlier Whiteface study during December 1998 – January 1999. This chapter focuses on the 5-Stage. The fog drop observations were complemented in Davis by some additional gas, aerosol, and deposition flux measurements which permit a broader interpretation of the fog and its effect on ambient chemistry. 5-Stage data are useful to this. Some aspects of this campaign have been previously reported (Collett *et al.*, 2001; Herckes *et al.*, 2001a; Reilly *et al.*, 2001; Reilly, 2000). Tabulated data for this campaign may be found in Appendix H. Notation introduced in this Chapter are defined in the List of Symbols.

9.1 Site description

The Davis site in the Sacramento Valley is located adjacent to the main University of California campus (NADP site #CA88, approximately 38.5°N, 121.75°W, and 50 m asl) (Anastasio and McGregor, 2001). The Sacramento Valley is roughly the northern third of California's Central Valley and is bounded to the west, northeast and east by mountains (the Coastal, Cascade and Sierra Nevada ranges, respectively), and to the south by the Carquinez Straits leading into the San Francisco Bay (Hayes *et al.*, 1992). During the winter, calm conditions can lead to poor ventilation and increased air pollution in the boundary layer and fog can be a common occurrence at night and in the early morning (Hayes *et al.*, 1992).

The sf-CASCC, CASCC2 and Gerber PVM-100 were all mounted on approximately 3 m poles in a field (figure 9-1). The 5-Stage was co-located on its approximately 1 m stand. The MOUDI impactorand the gas denuder inlets were at approximately 1 m, matching the 5-Stage. Square

Reproduced with permission of the copyright owner. Further reproduction prohibited without permission.

Teflon deposition plates were located on the ground at one side of the field to prevent contamination from investigators walking around the cloud collectors (figure 9-2). A small section of turf was removed so a scale could be placed at roughly ground surface level to measure the rate of water deposition flux during the cloud event. Both the deposition plates and the scale were not placed into position until a fog event had started. Co-location among the equipment was not as good as at Whiteface, although necessary to prevent possible interference among the collectors.

Figure 9-1: The Davis field site (December 1998). The 5-Stage was located to the left of the CASCC2 collector in the foreground. The collectors are normally aligned while sampling: this photograph was taken post-event during cleaning. The deposition plates were located to the right of the Gerber PVM-100 on the right side of the photograph. Additional collectors for organic analysis are shown.

9.2 Fog events and ambient conditions

9.2.1 Fog events

Seven fog events of varying duration were measured using the sf-CASCC and CASCC2 during this campaign (table 9-1) and a total of 53 samples and sample pairs were obtained. The 5-Stage was used exclusively during January and its 7 sampling periods are included in table 9-1.

Reproduced with permission of the copyright owner. Further reproduction prohibited without permission.

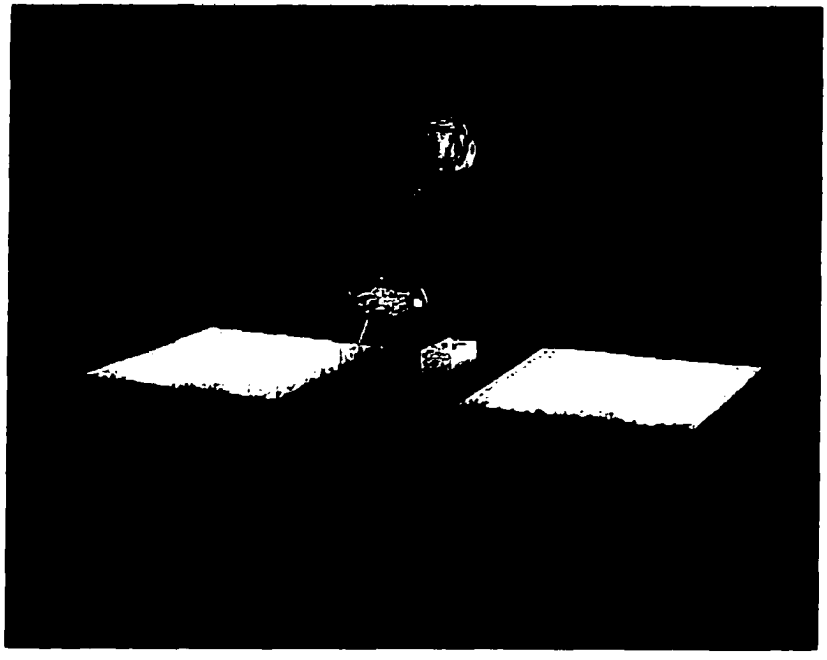

Figure 9-2: Eli Sherman collecting sample from the large Teflon deposition plates in Davis (December 1998).

All times are local (Pacific Standard Time). The fog typically lifted within a few hours of sunrise (approximately 7:20 a. m.) As the LWC was relatively low (section 9.2.2.2), the sampling periods for the Caltech collectors were typically one hour with two hours for the 5-Stage. Deposition plate measurements were synchronized with the fog water sampling and also used two hour sampling periods. Pairs of glass denuders were used to measure $NH_{3(g)}$ and $HNO_{3(g)}$ before, during and after the three consecutive events D009, D010, and D010B. The MOUDI was operated to obtain size-resolved inorganic aerosol measurements before and after those same events (table 9-2). There was up to a thirty-minute time lag during the transition out of or into a fog event for the denuders to be switched to the next pair and the MOUDI turned on or off. This was relatively short compared to the integrated sampling periods (> 8 hours).

9.2.2 Ambient conditions

During these seven fog events it was generally cold (2 - 3°C) and the wind speed was very light (< 1 – 1.5 m s^{-1} except for D011 and D013 where it increased up to 3 m s^{-1}). Wind direction

Reproduced with permission of the copyright owner. Further reproduction prohibited without permission.

tended to be highly variable (the standard deviation reported for wind direction often exceeded 180°) although the D011 and D013 events had relatively persistent and stable winds from the northerly direction. Ambient pressure in December was somewhat lower (1014 mb), but generally exceeded 1020 mb in January.

Table 9-1: Fog events and samples

EVENT	Event start and end	CASCC2 samples/ sf-CASCC sample pairs	5-Stage sample sets	5-Stage sampling periods
D352	12/18/98 03:22 - 12:00	9		
D004	1/4/99 20:08 - 1/5/99 10:00	13	3	20:08 - 22:00, 23:00 - 01:00, 02:00 - 0:400
D009	1/9/99 03:00 - 10:36	8	2	04:00 - 06:00, 07:00 - 09:00
D010	1/10/99 02:45 - 10:00	6	2	04:00 - 06:00, 06:52 - 09:00
D010B	1/10/99 22:50 - 1/11/99 09:42	8		
D011	1/11/99 23:00 - 1/12/99 09:42	8		
D013	1/13/99 05:50 - 09:17	1		

Table 9-2: MOUDI and denuder sampling periods between the D009, D010 and D010B events (denuders also sampled during events)

name	Sampling period
preD009	1/8/99 16:00 - 1/9/99 02:30
interD009/D010	1/9/99 11:00 - 1/10/99 02:21
interD010/D010B	1/10/99 10:33 - 1/10/99 22:28
postD010B	1/11/99 10:00 - 1/11/99 19:12

The synoptic weather charts from January show that a large high pressure region formed over NW Nevada. This "Great Basin High" is often associated with the formation of a cold pool of air in the Central Valley and widespread fog in the region. This pattern is occurred at the start of the 5 sequential events in January. From the D009 event through the D010B event, this was associated with overlying status through the day, although the fog cleared from the surface and temperatures peaked at < 5°C. During the afternoon of January 11th (between D010B and D011) the sky cleared due to a frontal passage. This is consistent with the wind shift to the N observed during D011 and D013 and earlier studies of the winter regional patterns (Holets and Swanson, 1981; Lorenzen, 1974). Automated weather (ASOS) data from two nearby locations – the

Reproduced with permission of the copyright owner. Further reproduction prohibited without permission.

Sacramento Executive airport (≈ 15 miles east) and Travis Air Force Base (≈ 30 miles south) – report mist and fog at the same times as our events and similar ambient conditions (low temperature, high pressure, low wind speed, generally variable wind direction). Fog was reported throughout the Central Valley on the synoptic charts.

9.2.2.1 Fog microphysics

Fog microphysics and dynamics are reviewed here as they are relevant to both the drop size distribution modeling and later consideration of in-fog observations including sedimentation and drop size-dependent chemistry.

Fog formation and life cycles are generally thought to depend upon radiative cooling, gravitational settling and turbulence (Roach, 1976b). While Roach and co-workers suggest that turbulence must be at a minimum for fog formation, later interpretations suggest that fog formation is tied to the turbulent mixing of near saturated eddies (Gerber, 1981; Brown and Roach, 1976; Roach, 1976a; b; Roach *et al.*, 1976). Updrafts tend to be weak in fogs (on the order of cm s^{-1}) so there is not a large driving force for drop activation. Observations and modeling work indicate that a quasi-periodic structure is often found in mature fogs affecting several parameters including LWC, temperature and relative humidity (Wendisch *et al.*, 1998; Bott, 1991; Duynkerke, 1991; Choularton *et al.*, 1981; Gerber, 1981; Roach *et al.*, 1976). The quasi-periodic structure has been observed to vary from as short as a few minutes to 40 minutes and has been attributed to gravity waves and the induction of small-scale circulation cells (e.g. (Duynkerke, 1991; Choularton *et al.*, 1981), among others). These fluctuations are associated with the large drops growing to a great enough size that they sediment out, leading to a decrease in LWC followed by an increase in relative humidity until more drops grow big enough to sediment out (Wendisch *et al.*, 1998; Bott and Carmichael, 1993; Bott *et al.*, 1990). As a result, the total water content of a fog is not constant (Brown and Roach, 1976). A bimodal drop distribution can result and has been observed in many locations (Wendisch *et al.*, 1998; Meyer *et al.*, 1980; Ludwig and Robinson,

Reproduced with permission of the copyright owner. Further reproduction prohibited without permission.

1970; May, 1961) and successfully modeled (Bott and Carmichael, 1993; Bott, 1991; Brown and Roach, 1976).

Gravitational settling of fog drops is an important feature in the life-cycle of fogs (Roach *et al.*, 1976). Field and modeling studies indicate that settling and the wet removal of solutes dissolved in the drops is a very important atmsopheric loss mechanism for these species (Lillis *et al.*, 1999; Bott, 1991; Forkel *et al.*, 1990; Pandis and Seinfeld, 1989; Waldman and Hoffmann, 1987; Jacob *et al.*, 1984b). Pollutant deposition rates for particular species can be elevated relative to their clear sky/dry values (Waldman and Hoffmann, 1987). In the aerosol-fog-aerosol cycle the production of new aerosol mass (source) competes with aerosol removal by deposition (sink) (Pandis *et al.*, 1990b). Large aerosol paticles can be depleted after fogs, although fine particles still remain (Ishizaka and Qian, 1994).

The bimodal drop distribution is thought to result from a mix of small unactivated and larger activated drops, although a recent study has identified the larger drops as a mix of activated, barely activated and unactivated drops (Frank *et al.*, 1998; Fuzzi *et al.*, 1998a; Wendisch *et al.*, 1998). As the fog event progresses, the larger drops continue to activate and the LWC maximum moves to the large drop mode as they scavenge water from the smaller drops (Wendisch *et al.*, 1998) The minimum drop diameter between these two peaks in a recent modeling study was between 8 – 12 μm (Bott, 1991) and consistent with observations in the recent Po Valley study (Wendisch *et al.*, 1998). While continuous drop size distribution data are not available from Davis, the collected mass distribution in the 5-Stage, although subject to considerable uncertainty, suggests the presence of a bimodal distribution during several time periods. The amount of water collected in Stage 5 (V5) often matched or exceeded that collected in Stage 4 (V4). Unpublished IMS95 drop size distribution spectra from the San Joaquin Valley also suggest bimodality.

Reproduced with permission of the copyright owner. Further reproduction prohibited without permission.

9.2.2.1.1 Bimodal drop distribution modeling

In order to plot the collected drop fraction composition as a function of size, drop size distribution spectra were required. A dual mode lognormal curve was fit based upon the mass diameter and geometric standard deviation for two modes from the Po Valley study. The small mode diameter was 8.4±1.8 μm, and the large mode diameter was 29.2±4.6 μm. The geometric standard deviations were 1.51±0.11 and 1.29±0.06, respectively (Wendisch *et al.*, 1998). Starting with the mean reported mode values, the procedure to predict the mass distribution between the stages/fractions of the collectors (Chapter 4) was followed. The fit parameters were then varied to improve the comparison between the predicted and actual sampled (normalized) masses in the collectors. Variations in the mode parameters were typically within the range of their standard deviations. As it was not possible to exactly fit the water distribution in both the 5-Stage and the sf-CASCC exactly and the mass measurements and collection efficiency curves (where known) are themselves subject to considerable error, it is not known how accurate the resulting drop distribution spectra are. However, they are at least generally representative and are useful for cloud drop composition comparisons between collectors. The collector/collector fraction volume median diameters were calculated using the collection efficiency curves for each modeled drop size distribution spectrum.

9.2.2.2 Davis LWC

The PVM-100 may not have been accurately reporting the ambient LWC due to the large drop sizes present (Chapter 4) and the LWC used is therefore primarily based upon the total mass collected in the CASCC2 and sf-CASCC via equations 4-1 and 4-2. These LWC data show consistent increases in both LWC and water deposition flux which has been observed before (Fitzjarrald and Lala, 1986), but was not indicated using the PVM LWC data.

Reproduced with permission of the copyright owner. Further reproduction prohibited without permission.

9.3 Review of the sf-CASCC data

In order to interpret the 5-Stage drop size-dependent composition shown in the next section, highlights of the sf-CASCC's results are reviewed here. Tabulated CASCC2 and sf-CASCC data for all the components except Cu and NO_2^- can be found in Reilly (2000).

9.3.1 Davis timelines

Of the six events where temporal resolution is possible, only D352 and D004 exhibited the classic "U"-shaped concentration profile associated with distinct fog formation, mature fog and dissipation stages (Jacob *et al.*, 1984b, among others) (not shown). The D010, D010B and D011 events typically exhibited very flat profiles with an occasional mild "hump" in solute concentration which usually was consistent across all of the major species. Some increased concentrations were exhibited at dissipation. The D009 event was somewhat different as the major ion concentrations (ammonium, sulfate, and nitrate) increased throughout the event. If fog onset was rapid, sampling may have started in the "mature" stage. For the D010B event, however, we were already on-site when the event "officially" started. Nitrite tended to have a sharper gradient during fog dissipation than, for example, sulfate or nitrate on D352 and D004. This may (in part) be a pH-driven effect and is discussed further in section 9.7.2. There did not appear to be a noticeable difference in nitrite concentrations after sunrise, except possibly on D009, although its photochemical degradation half-life in solution is on the order of hours for these conditions (Anastasio and McGregor, 2001). The partial pressure of $HONO_{(g)}$ – the assumed driving force for nitrite in solution – should be rapidly reduced even in foggy conditions after sunrise (see section 9.7.2).

Reproduced with permission of the copyright owner. Further reproduction prohibited without permission.

9.3.2 Large and Small Davis fog drop composition

9.3.2.1 Inorganic ions

In both the Large and Small drop fractions at Davis, the sum of ammonium, nitrate and sulfate exceeded 90% on average of the total measured inorganic charged species, as has been in observed in other fogs (Fuzzi *et al.*, 1998a). Ammonium represented 98% of the measured charged cations on average; the pH (figure 9-3) was high (> 5.5) so H^+ was not a significant component. Nitrate comprised about 76% of the total inorganic measured anions in the Large fraction (48 – 90% range), and 87% in the Small (63 – 92%). The ratio of nitrate to sulfate in the Large drops was about a factor of 8 on average increasing to a factor of 10 in the Small drops. Nitrite was, on average, about 15% of the nitrate charge in the Large drops (3 – 67% range), decreasing to only 1% of nitrate in the Small fraction. The ammonium/sulfate ratio (on a charge basis) was no less than 3 and typically 12 to 14. The ratio of ammonium to the sum of sulfate and nitrate was about 1.7 in the Large fraction and 1.2 in the Small. While neglected here, unquantified low molecular weight organic acids were present, particularly in the larger drops, which contribute to the total charge (Herckes *et al.*, 2001a) and the organic content of the fog water was high (Anastasio and McGregor, 2001).

Six Large vs. Small drop concentration figures are shown (figures 9-3 through 9-8) for pH, ammonium, nitrate, potassium, nitrite, iron, and copper All figures show a 1:1 lines and are plotted by event. The error bars shown represent analytical precision only.

In contrast to Whiteface, the pH in the Large drops was on average 0.4 units greater than in the more acidic Small drops (figure 9-3). The maximum difference observed was 0.9 units and the pH ranged from about 5.5 – 7.0. Both ammonium and nitrate (figures 9-4 and 9-5) are present in strongly elevated concentrations in the Small fraction with events D009 and D010 having the highest concentrations (and also the lowest mean LWC). Concentrations of ammonium reach on

Reproduced with permission of the copyright owner. Further reproduction prohibited without permission.

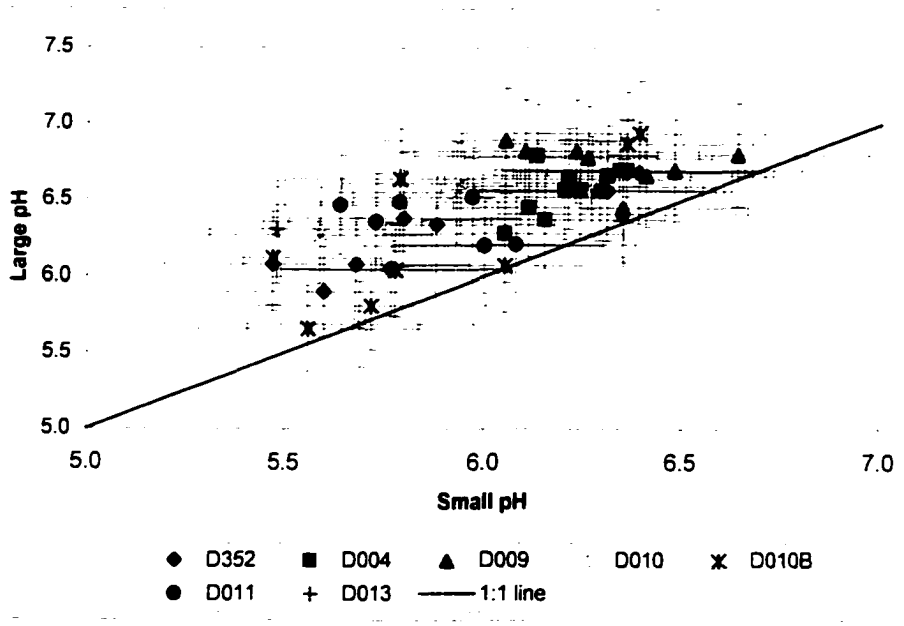

Figure 9-3: Large vs. Small sf-CASCC – pH

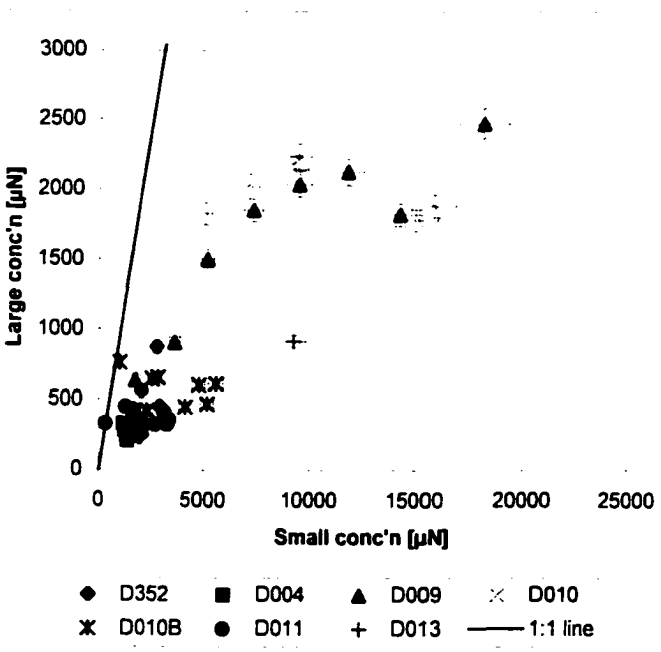

Figure 9-4: Large vs. Small sf-CASCC – ammonium

Reproduced with permission of the copyright owner. Further reproduction prohibited without permission.

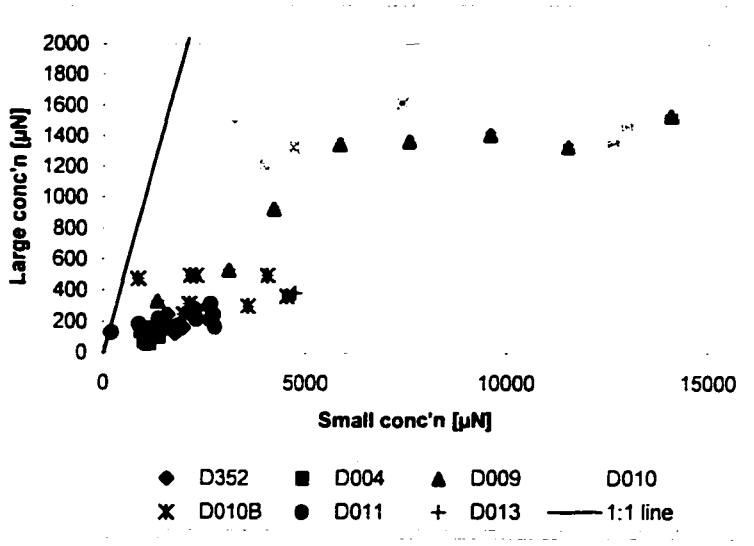

Figure 9-5: Large vs. Small sf-CASCC – nitrate

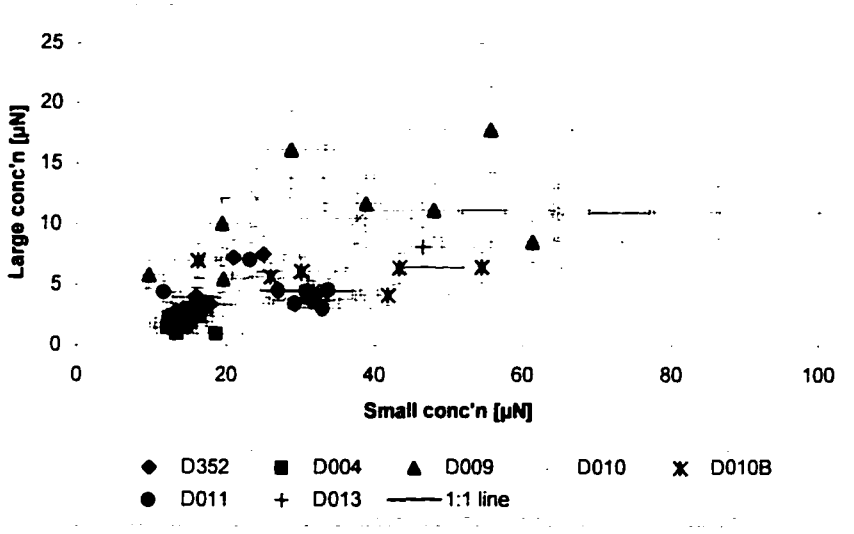

Figure 9-6: Large vs. Small sf-CASCC – potassium ion

the order of 18 mM and nitrate, up to 14 mM. Sulfate (not shown) exhibits a similar pattern. Potassium ion (figure 9-6) is present at much lower concentrations but also exhibits Small drop concentrations relatively elevated compared to the Large (consistent with the Chapter 4 results). Nitrite, by contrast, has a much different drop size-dependence and is present in relatively greater concentrations in the Large fraction. Nitrite is interesting for many reasons (section 9.7.2), and is

Reproduced with permission of the copyright owner. Further reproduction prohibited without permission.

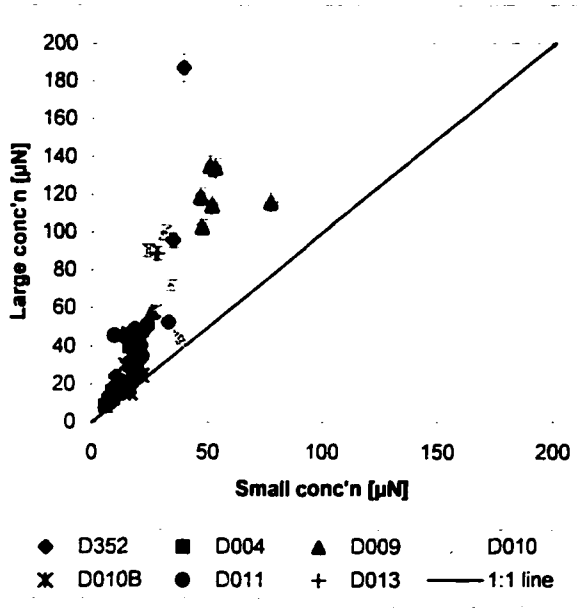

Figure 9-7: Large vs. Small sf-CASCC – nitrite

often present in concentrations on the order of sulfate's. This is the first large multi-event study of drop-size dependent nitrite concentrations in fog to my knowledge. An earlier study measured less than 5 pairs of "large" and "small" fog concentrations and some less-than-ideal assumptions were made to facilitate comparison (Lammel and Metzig, 1998). To the first order, these results are consistent with the difference in partitioning due to the pH variation between drop categories as HONO is a weak acid (pK_a = 3.44 at 2.5°C (Seinfeld and Pandis, 1998) (figure 9-37)). D352 showed the highest concentrations of nitrite, but D009 and D010 also had high concentrations.

Calcium, magnesium, sodium, and chloride ion concentrations typically represented a very small relative percentage of the charge (see the preceding discussion) and exhibit patterns similar to that shown for potassium (figure 9-6). Most magnesium measurements were at or below detection.

The largest concentration difference between Large and Small fractions could occur at the start, middle or end of the fog and varied by species (e.g. nitrate and nitrite behaved differently).

Reproduced with permission of the copyright owner. Further reproduction prohibited without permission.

9.3.2.2 Metals (Fe, Mn and Cu)

Fe and Mn are typically measured in cloud and fog water because of their potential to catalyze (as Fe(III) and Mn(II)) S(IV) auto-oxidation (Seinfeld and Pandis, 1998). At high pH (such as seen in these fogs) this pathway can occasionally be a very important production mechanism for sulfate. We routinely measure total Fe and Mn in cloud water, although "total" is usually not the value of most interest. Typically the observed total concentration is reduced by a factor estimated to represent the catalytically active forms to estimate the sulfur oxidation rates (Hoag, 1998).

Copper can interfere with the Fe(II)/Fe(III) redox cycle and S(IV) oxidation catalyzed by Fe, and can alter the drop HO_x cycle (Sedlak *et al.*, 1997; Warneck *et al.*, 1996; Sedlak and Hoigné, 1994; 1993; von Piechowski *et al.*, 1993). High concentrations of copper have been observed in San Joaquin Valley fogs – up to 82 μg l^{-1} using a RAC (Appendix B) – and have been attributed to agricultural pest control (Siefert *et al.*, 1997; Seiber *et al.*, 1993; Miller *et al.*, 1987; Jacob *et al.*, 1986). Varying copper concentrations have also been measured in fog and cloud water in the Po Valley, at Great Dun Fell, and at several sites around the United States (Schwanz *et al.*, 1998; Sedlak *et al.*, 1997; Siefert *et al.*, 1997). Barring complicating factors, if the Cu/Fe (expressed in various forms) ratio exceeds <1 to 2%, then Cu(I)/Cu(II) will be the dominant sink/oxidant of superoxide radical within the drop and will produce H_2O_2 (which itself can oxidize S(IV)) (Hoigné and Bühler, 1996; Hoigné *et al.*, 1994; von Piechowski *et al.*, 1993). Cu may inhibit the formation of Fe(III) complexes with oxalate (Sedlak and Hoigné, 1994), although Cu also can complex with organic ligands which can affect its ability to act as a catalyst.

Total copper was measured to investigate if sufficient quantities were present to affect drop HO_x chemistry. Three events were selected from each campaign – W188, W197, W198, D009, D010, and D011 – constituting "high" and "low" Fe concentration observations. While copper concentrations were negligible at Whiteface, Davis copper concentrations generally exceeded

Reproduced with permission of the copyright owner. Further reproduction prohibited without permission.

manganese on D009 and D010 (table 9-3) and were often greater than 2% of total Fe concentrations (on a molar basis). While the Davis organic content in the fog water was high (Herckes *et al.*, 2001a), these results suggest that copper may be a factor in fog drop redox chemistry.

Iron was consistently elevated in the Small drop fraction for only one event (D004), but otherwise varied between fractions within the other events measured (figure 9-8). Manganese exhibited a similar pattern (not shown), as does copper for the events it was measured (figure 9-9). Copper was measured in concentrations up to 80 $\mu g\ l^{-1}$, although there appear to be quantification issues at concentrations near the detection limit (approximately < 0.5 $\mu g\ l^{-1}$). The concentrations reported are not blank-corrected; some negative concentrations were measured.

9.3.2.3 Large vs. Small fraction concentration ratios

Table 9-3 contains the tabulated results for all Large and Small concentration and Large/Small concentration ratio data for all the events. In general, the major and most of the minor species are concentrated in the Small fraction. The Large/Small concentration ratio averages around 0.2 for the major species, but factors of up to 10 – 20 difference in concentration between Small and Large fractions are observed. By contrast, nitrite is about 2 times more concentrated in the Large fraction compared to the Small. Fe and Mn ratios are somewhat less than 1 on average, but exhibit a broad range. Cu's ratio is greater than 1, but only a small number of samples were included due to detection limit issues.

This pattern of drop size-dependent composition has been observed before in both the San Joaquin Valley and during several studies in the Po Valley (Collett *et al.*, 1999; Laj *et al.*, 1998; Bator and Collett, 1997; Heintzenberg, 1992; Ogren *et al.*, 1992, Chapter 1 and references therein). Using the Differential Fog Sampling System (DFSS) (Appendix B) in the Po Valley, the

Reproduced with permission of the copyright owner. Further reproduction prohibited without permission.

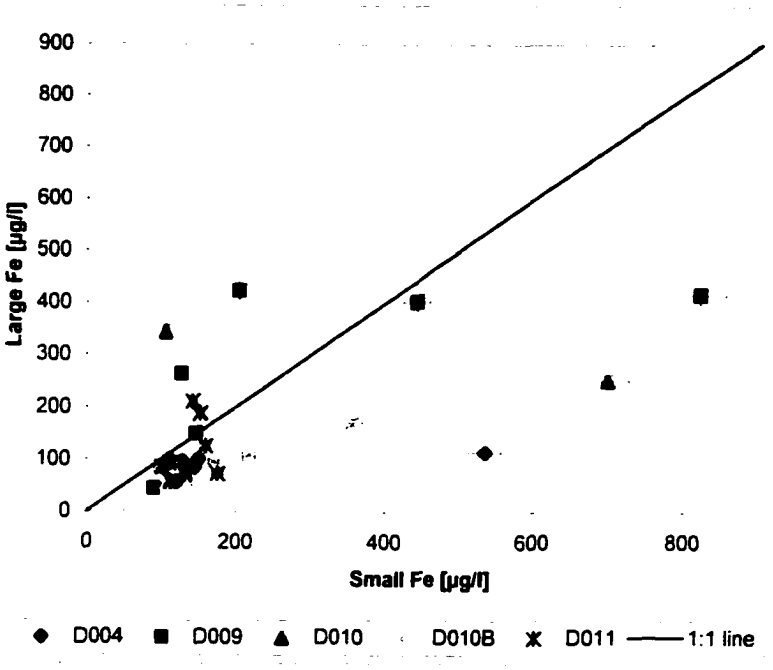

Figure 9-8: Large vs. Small sf-CASCC – iron

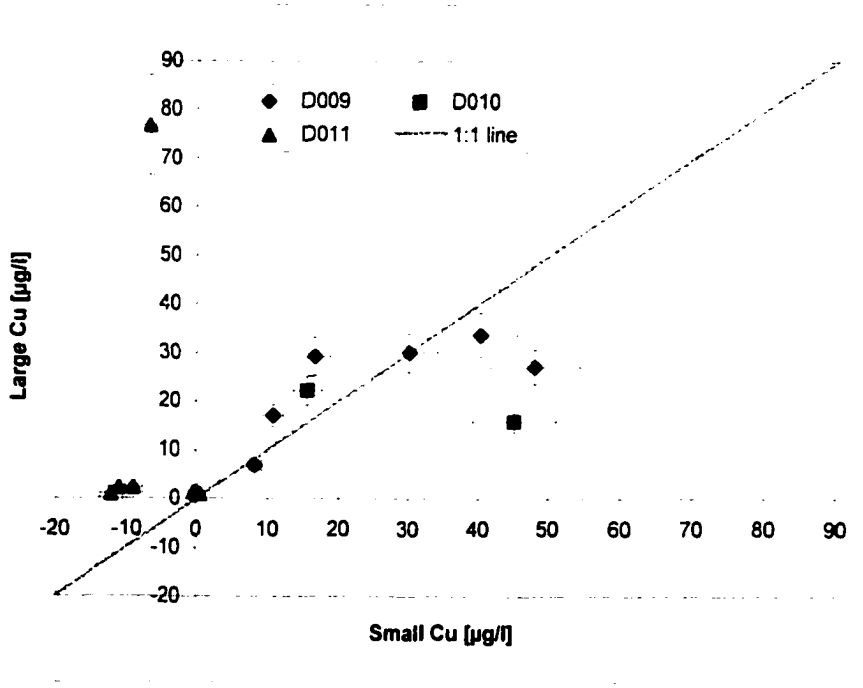

Figure 9-9: Large vs. Small sf-CASCC – copper

Reproduced with permission of the copyright owner. Further reproduction prohibited without permission.

major ion (ammonium, nitrate and sulfate) concentrations varied between drops fractions by up to an order of magnitude (Laj *et al.*, 1998), although in the Po Valley much higher concentrations of sulfate were observed. The Davis event occurred in a $NH_{3(g)}$-rich environment (section 9.5), and the LWC was predominantly associated with drops collected in the Large fraction consistent with mature Po Valley fog (Wendisch *et al.*, 1998). A bimodal drop distribution was likely to have occurred and the smallest drops were generally more characteristic of haze than cloud drops (e.g. very high concentrations). Ammonium and nitrate due to their high solubility were likely to be found in the smallest drops due to the competition between drop dilution and species mass transfer (Bott and Carmichael, 1993). Sufficient ammonia is present, however, to continually partition into the largest drops so ammonium will be present in both fractions. This has been observed and modeled for similar San Joaquin Valley fogs (Hoag *et al.*, 1999).

Table 9-3: Davis Campaign overall sf-CASCC composition results

Species	n	Large Concentration		Small Concentration		Large/Small		
		min	max	min	max	min	max	mean
S(IV) [μM]	22*	DL	7.1	2.1	14.3	0.02	0.77	0.25
HCHO [μM]	31	16.4	97.6	15.3	153.3	0.44	2.55	0.82
H_2O_2 [μM]	5*	3.9	13.9	3.8	8.4	0.7	3.71	1.71
Na^+ [μN]	45*	DL	27.9	4.71	68	0.05	0.67	0.27
NH_4^+ [μN]	51	210	2474	346	18,112	0.09	0.95	0.22
K^+ [μN]	51	0.94	17.85	9.6	86.3	0.05	0.6	0.22
Mg^{2+} [μN]	4*	DL	6.43	DL	26.17	0.23	0.67	0.48
Ca^{2+} [μN]	31*	DL	30	6.36	57.5	0.18	1.61	0.59
Cl^- [μN]	51	2.8	44.3	13.6	442	0.09	0.46	0.2
NO_3^- [μN]	51	56	1614	204	14,048	0.05	0.63	0.16
$SO_4^=$ [μN]	51	10.8	276.4	35.6	2285	0.08	0.59	0.2
NO_2^- [μN]	51	8.5	186.8	6	76.9	0.94	4.84	2.09
pH	51	5.66	6.94	5.47	6.64	0.94	1.15	1.07
Fe [μg l^{-1}]	29	43.8	424	89.9	822.1	0.21	3.28	0.87
Mn [μg l^{-1}]	29	2.4	25.9	4.3	39.7	0.16	1.4	0.62
Cu [μg l^{-1}]	10*	0.9	76.7	DL	47.9	0.35	22.7	3.29

DL = at or below detection limit
n = number of sample pairs
* Where DL values occur, the data are included in the reported concentration ranges shown, but excluded from the Large/Small calculations

Reproduced with permission of the copyright owner. Further reproduction prohibited without permission.

9.4 5-Stage in Davis

9.4.1 Results and discussion

As indicated in Table 9-2, the 5-Stage collected cloud water during the D004, D009 and D010 events. The results will be presented in a similar manner as in Chapter 8 – the concentration profiles have been culled for repeated or interesting patterns, and the focus will be primarily, but not exclusively, on the major ions. Figures are plotted as described in Chapter 8. Data from all three events will be shown to emphasize the robustness of some of the concentration patterns observed. The concentration profile figures show all three collectors. Their relevance to each other, given Chapter 4, should be considered. As only two 5-Stage sample sets were collected on D009 and D010, both are plotted on the same figure for the species that follow. Analytical uncertainty only is included in the y-axis (concentration) error bars. However, residual uncollected mass and measurement uncertainty are both included in the mass error bars where water distributions are shown. Selected 95% Confidence Limit MDLs are shown where relevant to the concentrations reported. All the concentrations are plotted against the volume median diameter derived from the modeled drop size distributions, thus no x-axis error bars are shown.

During the D004 event, ammonium, nitrate and sulfate exhibited virtually the same concentration profiles across the 5-Stage and the other collectors. This was also true for the two later events. As figures 9-10, 9-11, and 9-12 show, the sf-CASCC has a sharply higher Small fraction concentration for sulfate, while in the 5-Stage, the concentration gradient is sharpest from Stage 4 (V4) to Stage 5 (V5) – the very smallest drops are the most concentrated. This decreases somewhat in the last time period, but the sulfate concentration still more than doubles between V4 and V5. For ammonium during the last time period, the concentration decreased between V4 and V5, but that is associated with a strong spike of calcium (not shown). The sf-CASCC exhibits some of the size-dependent composition variation, but it is unable to show how the smallest

Reproduced with permission of the copyright owner. Further reproduction prohibited without permission.

drops (< 11 μm) are responsible for the high species concentrations. Although of small volume, the small drops disproportionately affect bulk concentrations.

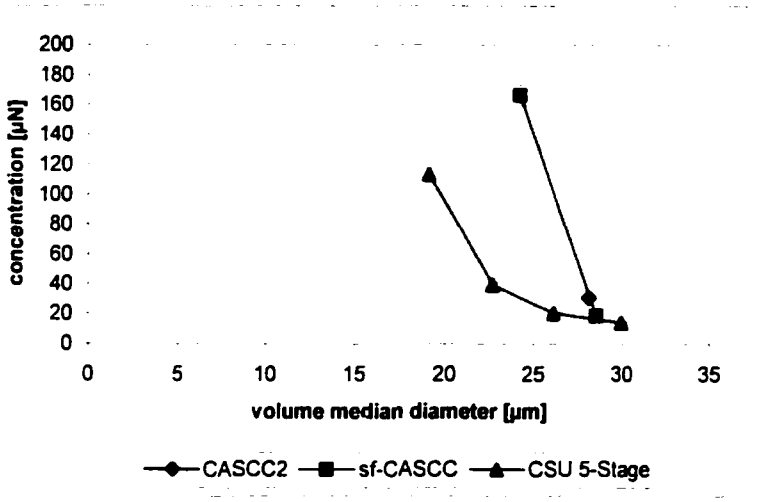

Figure 9-10: Sulfate – all three collectors (D004, 20:08 – 22:00). There is no V5 sample.

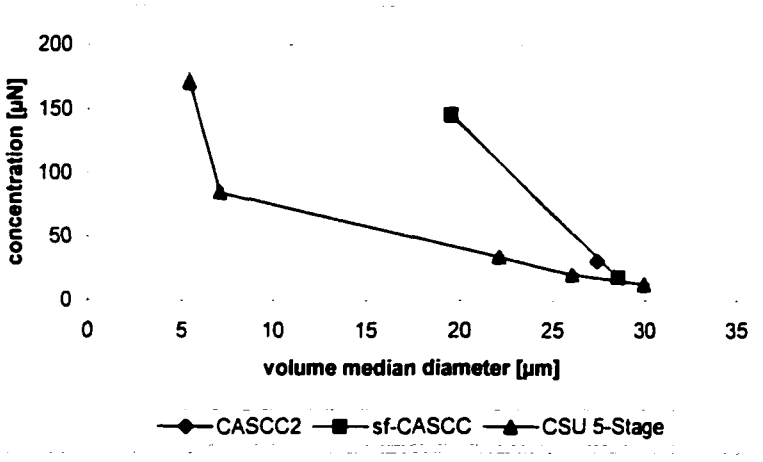

Figure 9-11: Sulfate – all three collectors (D004, 23:00 – 01:00)

The D004 chloride concentration during the last time period is used as a surrogate for all the minor ionic species (sodium, potassium, calcium, magnesium) where the gradient into the last fraction was very strong (over a factor of 10 in this instance). This was a fairly consistent feature during all sample sets for these species. Concentrations in the first 3 or 4 stages would be near

Reproduced with permission of the copyright owner. Further reproduction prohibited without permission.

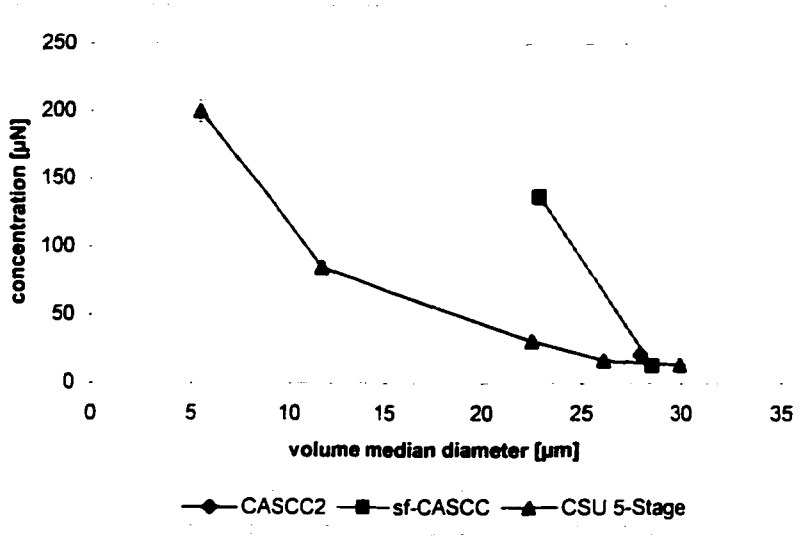

Figure 9-12: Sulfate – all three collectors (D004, 02:00 – 04:00)

the detection limit and then V5 (and occasionally V4) would be far greater. Manganese and iron exhibited a similar profile during this event, although manganese showed something of a "W" pattern and there was a large spike in the iron concentration.

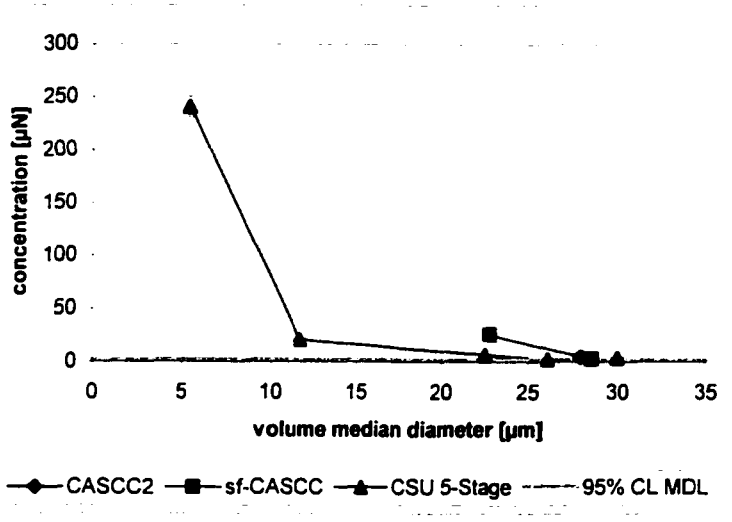

Figure 9-13: Chloride – all three collectors (D004, 02:00 – 04:00)

The pH concentration profiles (figures 9-14 and 9-15) and the nitrite concentration profiles (figures 9-16 and 9-17) virtually mirror each other during these two time periods. The pH tended to be somewhat higher in the 5-Stage compared to the other collectors (although within the

Reproduced with permission of the copyright owner. Further reproduction prohibited without permission.

analytical error) and there tends to be an increase from V4 to V5 in the two time periods shown. During the later time period, there is more of a pronounced "V" profile. Nitrite in these two time periods shows the highest concentration in the rear of the collector, in contrast to the sf-CASCC measurements which show lower concentrations. The pH difference can be explained (rising sharply in V5) due to the presence of reasonably large concentrations of calcium, magnesium and potassium. It may be that the sampling height difference of the collectors is reflected here. Small unactivated crustal aerosol particles may have entered the 5-Stage raising the pH in the back of the collector where they deposited. The sf-CASCC was not similarly affected. The concentration change in the nitrite is beyond the analytical uncertainty and at least partially explained by the change in pH. The collectors may be sampling from slightly different drop populations due to the sampling height differences. The 5-Stage is closer to fog base where a different drop population exists than at 3 m. There may also be a vertical gradient in the gas-phase species. However, on D004 the CASCC2, sf-CASCC and 5-Stage concentrations compare well (Chapter 4). It appears that the volatile species – ammonium, nitrite, hydrogen ion – are being affected by the changing composition of minor species on Stage 5.

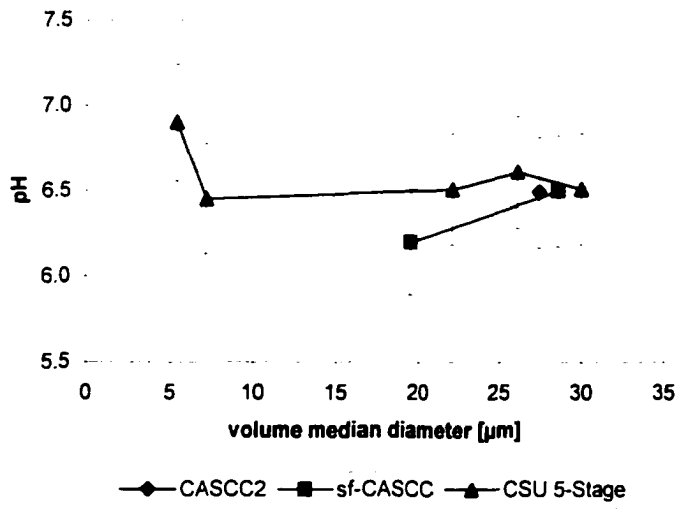

Figure 9-14: pH – all three collectors (D004, 23:00 – 01:00)

Reproduced with permission of the copyright owner. Further reproduction prohibited without permission.

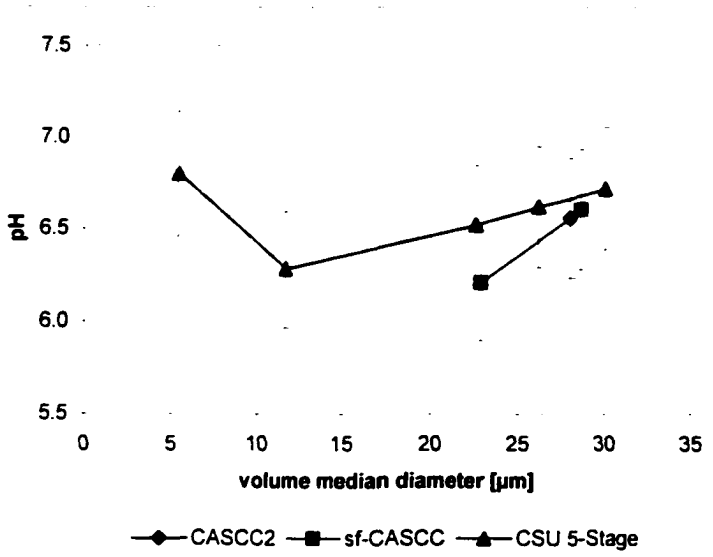

Figure 9-15: pH – all three collectors (D004, 02:00 – 04:00)

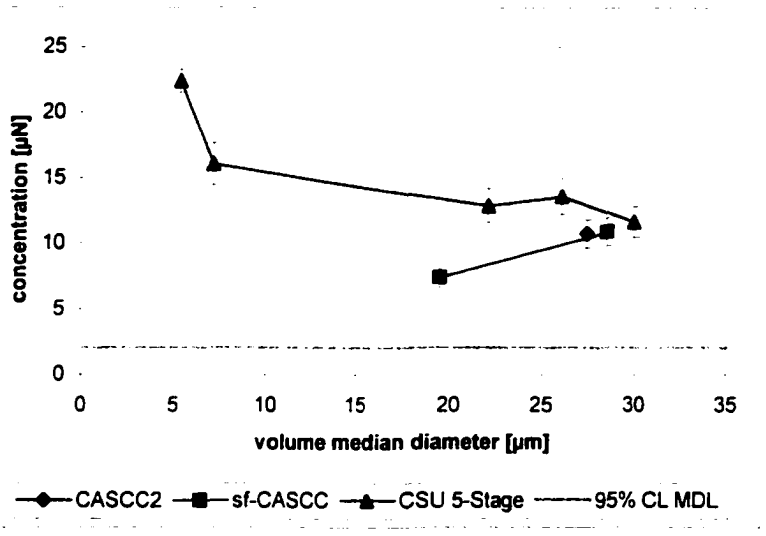

Figure 9-16: Nitrite – all three collectors (D004, 23:00 – 01:00)

The water distribution for D009 (figure 9-18) illustrates how much of the water volume was in the larger stages of the 5-Stage (about 80% in the first two stages) and in the Large fraction of the sf-CASCC (also about 80%). Due to the sharp difference in water, the high concentrations observed in the Small fraction and the smaller stages of the 5-Stage are not inconsistent with the relatively low concentrations observed in the bulk. The ammonium concentration profiles (figures

Reproduced with permission of the copyright owner. Further reproduction prohibited without permission.

9-19) illustrate major species behaviour during this event. Again, sharply higher concentrations are observed from Stage 4 to Stage 5, reaching almost 25,000 µN during the second time period.

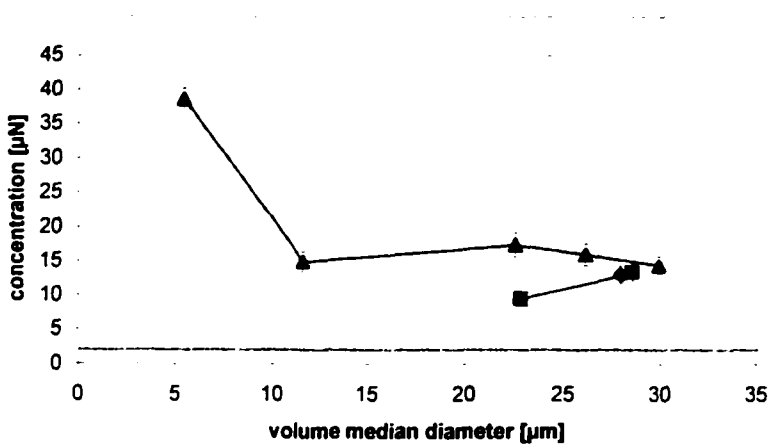

Figure 9-17: Nitrite – all three collectors (D004, 02:00 – 04:00)

Given this sharp gradient in concentration in the smallest drops, differential collection of these drops due to varying collector efficiency curves could affect observed bulk or derived "bulk" concentrations. Therefore, the D_{p50} difference between V5 of the 5-Stage, the Small fraction of the sf-CASCC and the CASCC2 could account for the difference in performance quantified in Chapter 4. The Stage 5 water volume decreases between the first and second sample set corresponding to the sharp concentration increase. The variation observed with the 5-Stage is far greater than that measured with the sf-CASCC. The pH and nitrite profiles are shown (figures 9-20 and 9-21), although in this instance the observed peak in pH in V5 during the first sampling period does not correspond to a peak in nitrite. A large peak is observed for the larger drops during the second sampling period, although the pH in the 5-Stage has not changed appreciably. It is not known why this occurred and this sample set exhibits high variability (see section 9.7.2 for more discussion).

Reproduced with permission of the copyright owner. Further reproduction prohibited without permission.

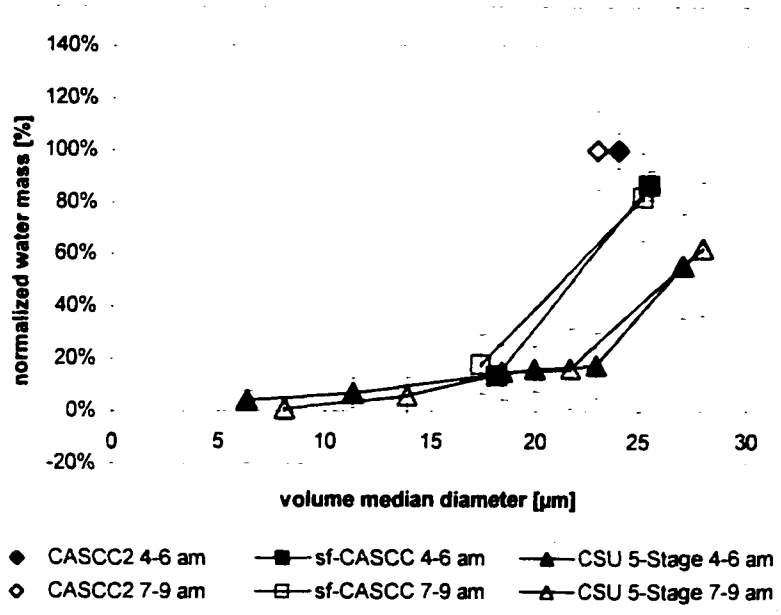

Figure 9-18: distributed water mass – all three collectors (D009)

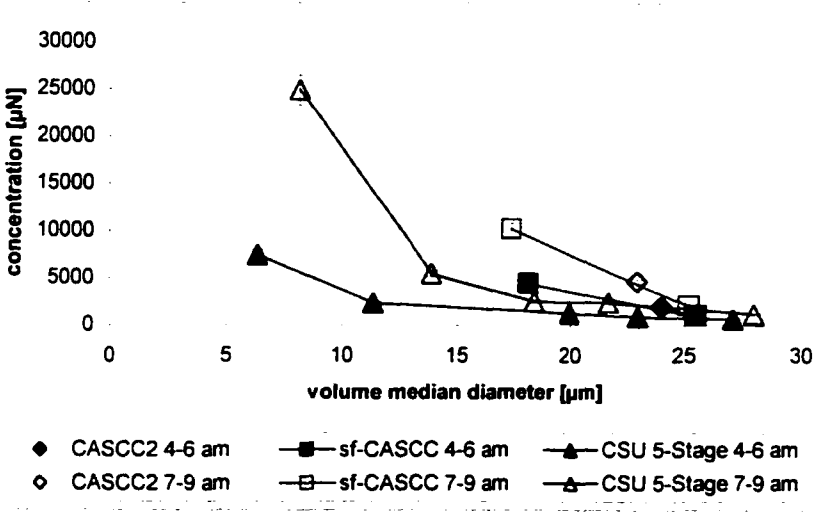

Figure 9-19: Ammonium – all three collectors (D009)

Reproduced with permission of the copyright owner. Further reproduction prohibited without permission.

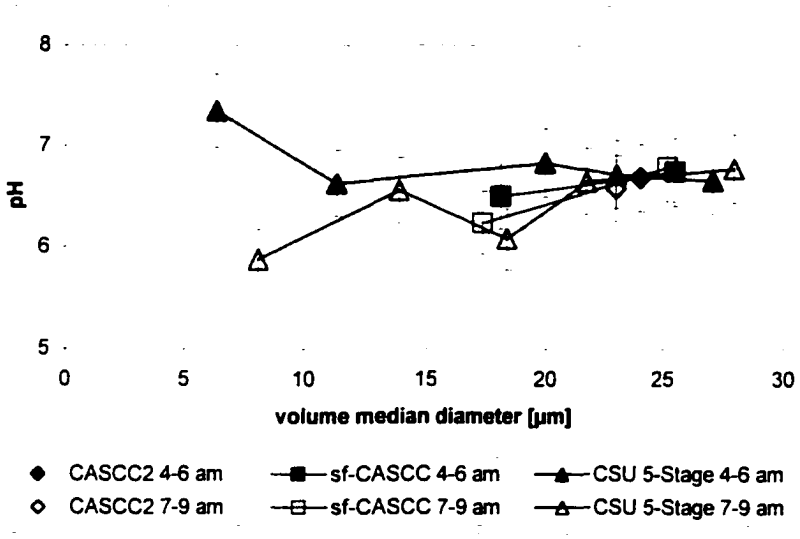

Figure 9-20: pH – all three collectors (D009)

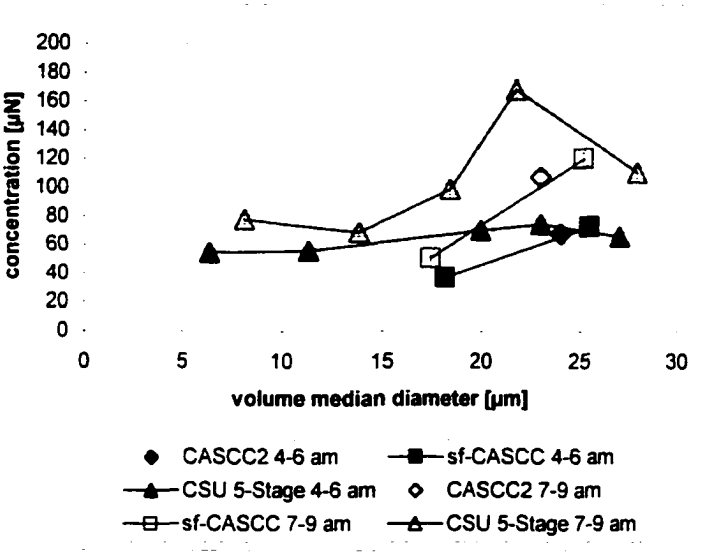

Figure 9-21: Nitrite – all three collectors (D009)

The copper profile (figure 9-22) has a "U"-shaped profile which it shares with manganese during this time period. The sf-CASCC shows little composition variation between fractions during this time period, while the 5-Stage shows a factor of 5 difference in concentration between stages. During the later time period, the Fe, Mn and Cu concentration profiles all generally exceed those

Reproduced with permission of the copyright owner. Further reproduction prohibited without permission.

in the sf-CASCC, although some of the concentrations are low. The profiles are more complicated, and possible differences in sampled drop populations as a function of height may explain the observations. As at Whiteface, the Metals (in this case Fe, Mn and Cu) can have somewhat different concentration profiles than the other species.

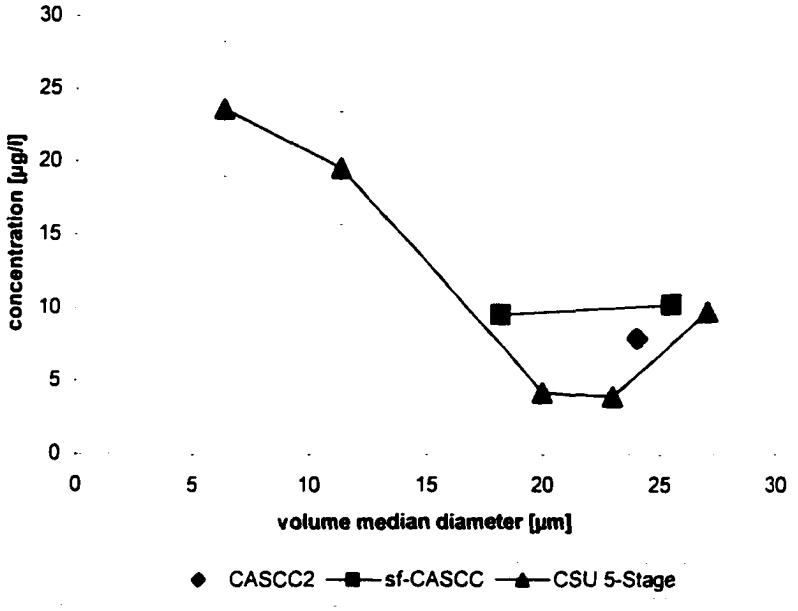

Figure 9-22: Copper – all three collectors (D009, 04:00 – 06:00)

The D010 water distribution profile is shown in figure 9-23 and illustrates how sharply favored the Large fraction of the sf-CASCC was for collecting drops (> 90% of the mass for both sampling periods here). The 5-Stage still collected over half of the mass on the first stage, but did obtain measurable amounts on each stage. In Stage 5 for both time periods, greater mass was collected than in the immediately preceding stage (Stage 4). Ammonium (figure 9-24) concentration gradients into the rear stages are very strong once again, as are the nitrate and sulfate concentrations (not shown). Peak concentrations in Stage 5 are lower than observed during D009 (about 13,000 µN). An even sharper gradient into the last stage is observed for some of the minor species; calcium is shown as an example (figure 9-25). Calcium ion concentrations are near the detection limit until Stage 5. The peaks in the pH (figure 9-26) in

Reproduced with permission of the copyright owner. Further reproduction prohibited without permission.

Stage 5 are likely associated with this increase in cations. While the differences observed between the pH measurements are within the uncertainty, given the water distribution, it is certainly possible to have high pHs in the smaller drops whose signature could be lost in mixing to yield the strict Large/Small concentration dependence observed in the sf-CASCC. Nitrite (figure 9-27) again shows a concentration that mimics the pH, but is more complicated than the sf-CASCC Large/Small profile suggests.

None of the Metals are shown for this event as not every stage of the 5-Stage could be aliquoted for them. However, where data exist, the 5-Stage is generally consistent (e.g. Large/Small concentration gradient is observed). Iron again has an observed concentration hump that the other species do not show.

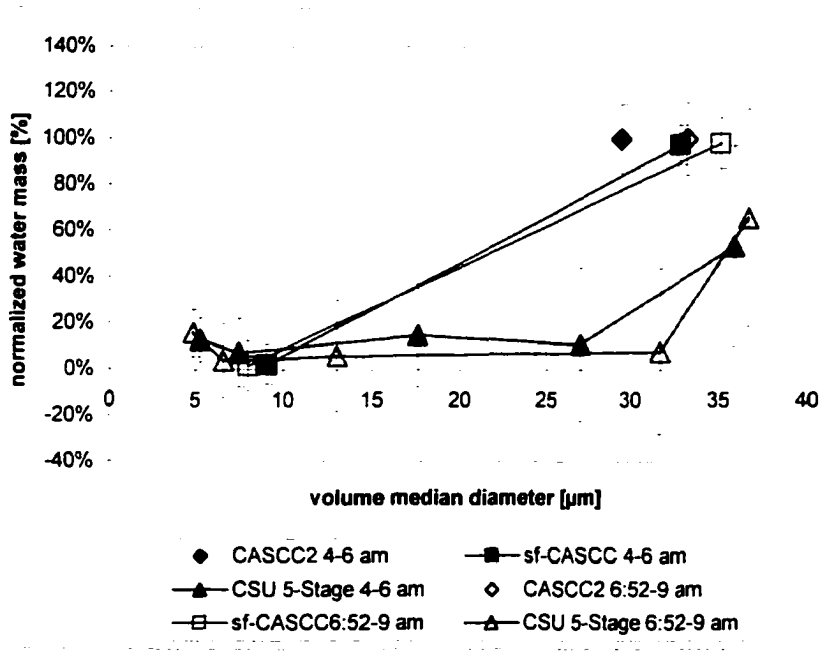

Figure 9-23: Distributed water mass – all three collectors (D010)

Table 9-4 illustrates that for a given sampling period the 5-Stage shows up to 4 – 5 times more variation in concentration than the sf-CASCC does for major species. At Whiteface, there was benefit from separating the largest and smallest drops from each other to get the "U" profile in the major species. Here, no "U" is found, but separating the largest drops from the very smallest

Reproduced with permission of the copyright owner. Further reproduction prohibited without permission.

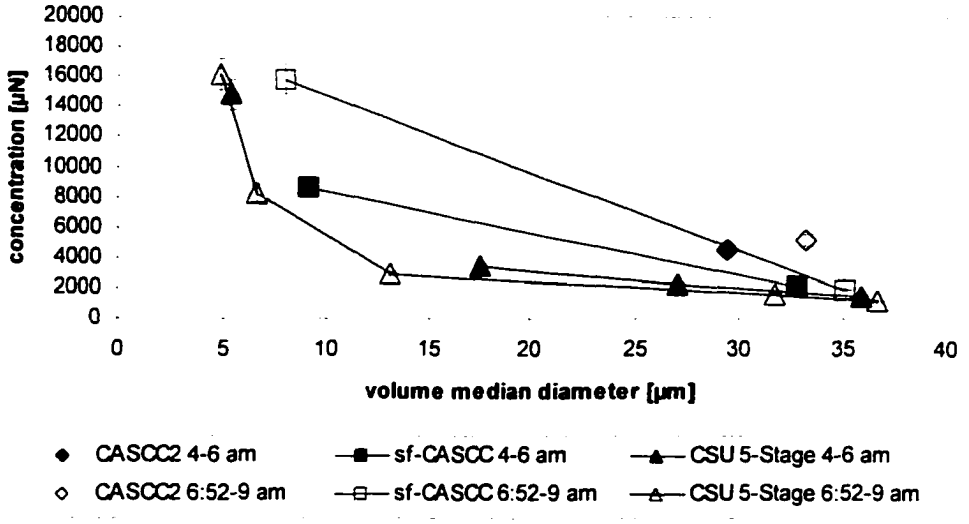

Figure 9-24: Ammonium – all three collectors (D010) V4 is not available during the first time period

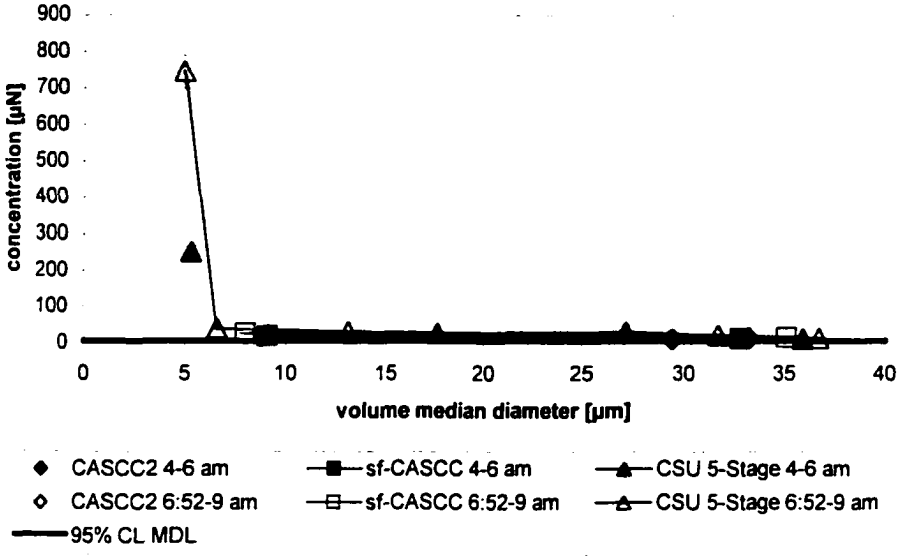

Figure 9-25: Calcium ion – all three collectors (D010). V4 is not available during the first time period

resolves the very high concentrations in the latter. Nitrite (not shown) may exhibit up to 50% more variation than in the sf-CASCC, but the pH differences observed are largely with the analytical uncertainty (up to 7% more variation in the 5-Stage comparatively, but the pH ranges itself varies somewhat). The minor species have been omitted from Table 9-4 due to detection

Reproduced with permission of the copyright owner. Further reproduction prohibited without permission.

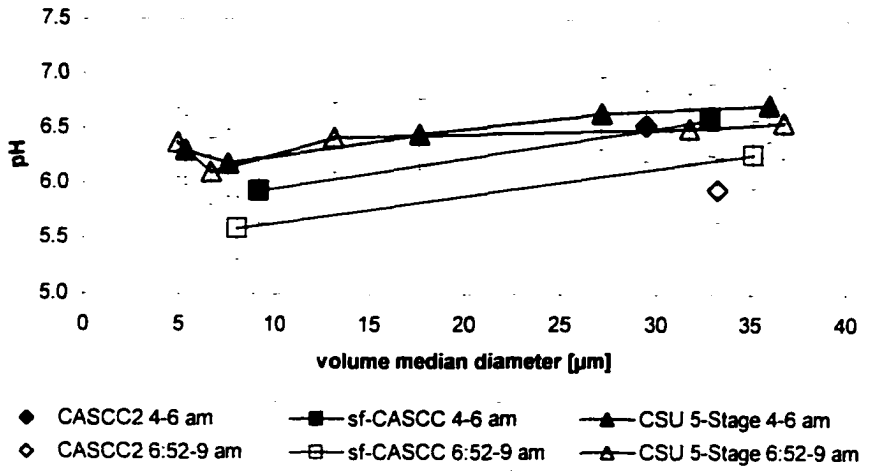

Figure 9-26: pH – all three collectors (D010)

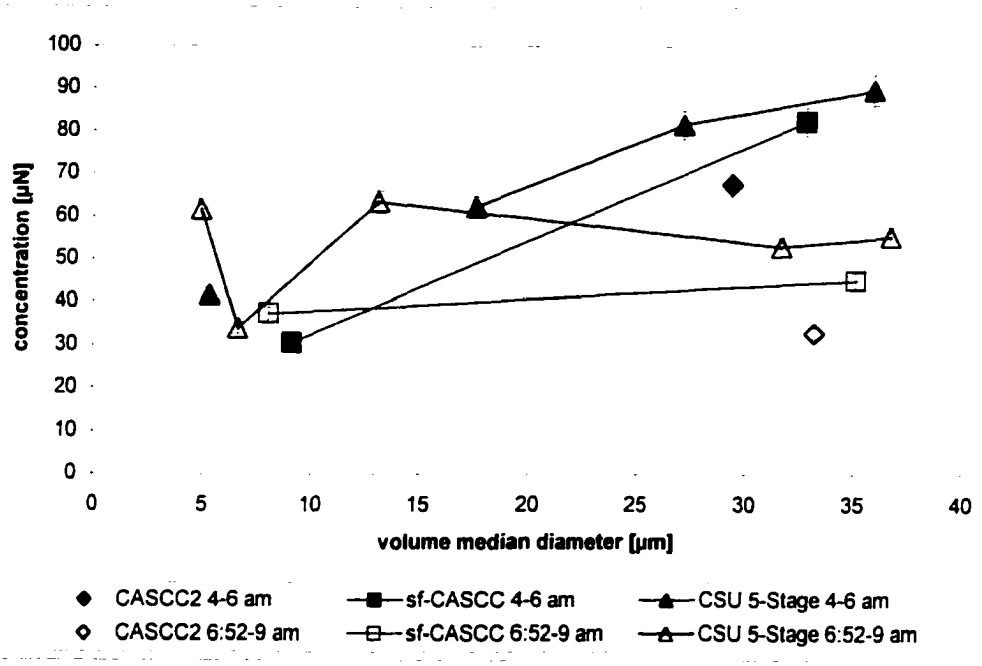

Figure 9-27: Nitrite – all three collectors (D010). V4 is not available during the first time period

limit issues for many of them, and the brief discussion that follows is intended only to provide some suggestion of what the limited observations suggest. For Fe, Mn, Cu and similar species, Table 9-3 indicates that up to a factor of 2 difference might be observed via the sf-CASCC.

Reproduced with permission of the copyright owner. Further reproduction prohibited without permission.

However, data from the 5-Stage easily shows factors exceeding 10 regularly and up to a factor of 50 has been observed. This is complicated by some of possible sampling problems described above, but the "minor" species appear to exhibit comparatively more variation than the major ones

Table 9-4: sf-CASCC, 5-Stage, and 5-Stage to sf-CASCC maximum/minimum concentration ratios for the major species

maximum/minimum concentration ratio	nitrate	sulfate	ammonium
sf-CASCC	2.6 - 16.7	3.8 - 10.6	4 - 8.4
5-Stage	>10.1 - 29.7	>8.1 - 19.3	>3.9 - 20.2
5-Stage to sf-CASCC	up to 5.1	up to 4.4	up to 4.2

The concentration profiles observed are very similar to those observed in the Po Valley (Laj *et al.*, 1998). Explaining the observed drop composition size-dependence there has been a focus of major effort (see Chapter 1). It has been proposed that there are very few large crustal aerosol particles so activation quickly leads to their dilution. The input aerosol are aged or at least are a soluble mixture of ammonium, nitrate and sulfate, but modeling work suggests that a large (unmeasured) fraction may be insoluble (Schell *et al.*, 1997b). The sharp concentration gradient in the smallest drops likely reflect collection of haze or haze-like drops that are not activated (see Chapter 1 regarding how a cloud "drop" is defined). Thus only one side of the "U" is observed (Region I). The Davis results are consistent with theirs and again show the utility of the 5-Stage collector – despite its limitations – to measure size-resolved drop composition. The total measured inorganic ion concentration (figure 9-28) shows essentially the same profile as the major ions and adds less insight to the discussion than at Whiteface (Chapter 8). While little variation between time periods is evident in the 5-Stage, that may just be a function of the assumed drop distributions and that fact that the Stage 4 sample is missing in the first time period. Compared to the sf-CASCC, the results suggest the relative importance of the small drops to determining the total inorganic charge.

Reproduced with permission of the copyright owner. Further reproduction prohibited without permission.

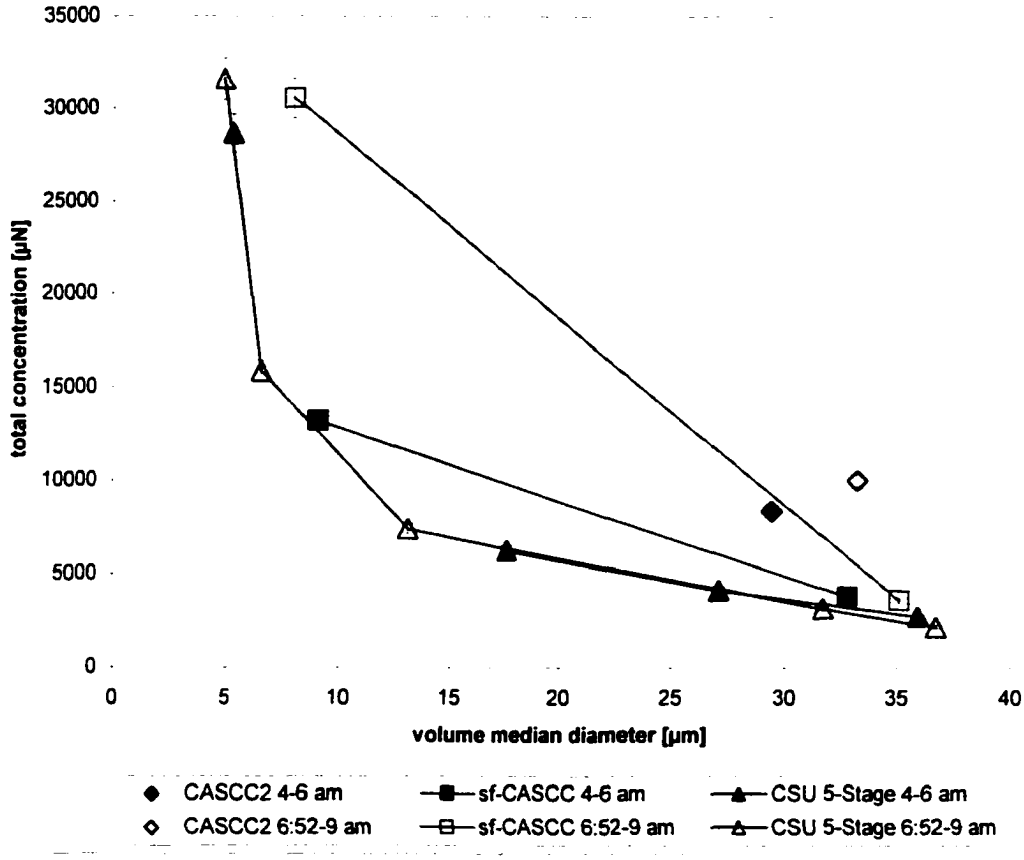

Figure 9-28: Total measured inorganic ion concentration (as defined in Chapter 8) for the two 5-Stage sampling periods on D010. In sample #1, V4 is missing.

As indicated earlier, several modeling studies (e.g. (Hoag *et al.*, 1999; Bott and Carmichael, 1993), among others) suggest that the most soluble species will be in the smallest drops and the least soluble in the larger ones. Figure 9-29 illustrates that in the 5-Stage on average there is proportionately more nitrate in each stage as the drops get smaller. Relative amounts vary from about 74% to about 84% of the measured anions. Ammonium starts relatively higher in the larger drops, declining marginally through the collector to Stage 5 where the sharp increase in calcium, magnesium, and other species cause it to decrease to only 77% of the total cations (from 97%).

As the water distribution profiles show, the observed drop-size dependent concentrations depend profoundly upon it. Cloud drop composition observations can not be explained without some consideration of drop size.

Reproduced with permission of the copyright owner. Further reproduction prohibited without permission.

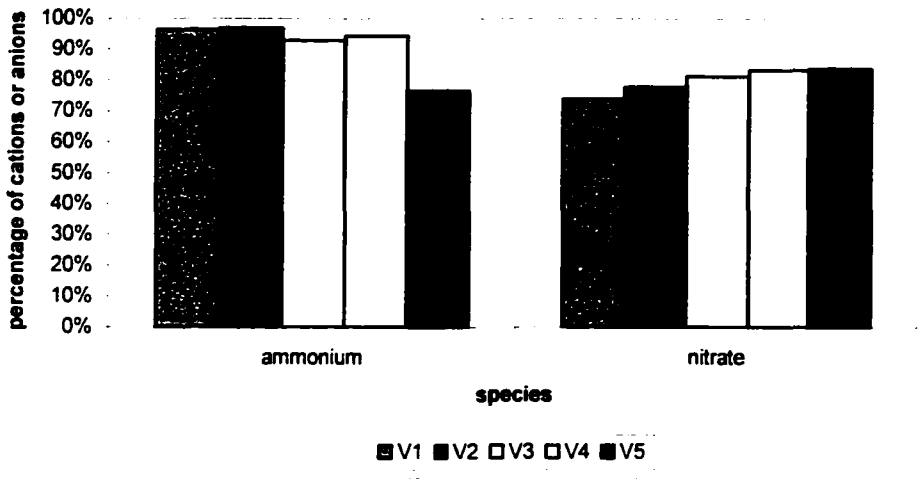

Figure 9-29: 5-Stage ammonium and nitrate ratios by stage to the respective sum of measured cations or anions (mean of all sample sets)

The varying sampling height may have affected these results, particularly as additional crustal species evident in the 5-Stage appear to have affected collected pH and other volatile species. This may just be a sampling artifact from the collection of different drop fractions, not contamination. Differences larger than the analytical uncertainty were observed.

This fog was discolored (the small fractions were often yellowish in color) and black particulate was observed which has often been seen in fogs (Berner, 1988; Fuzzi *et al.*, 1988; Weathers *et al.*, 1988). It is not known how the high organic loading affected these observations(Anastasio and McGregor, 2001).

9.5 Gas and aerosol measurements

The goal of the gas and aerosol measurements was to try to understand what fog impacts on the ambient aerosol and gas concentrations of some of the principal inorganic species were.

Reproduced with permission of the copyright owner. Further reproduction prohibited without permission.

9.5.1 Results and discussion

Figures 9-30 and 9-31 show the ammonia and nitric acid gas measurements performed during January. The events are labeled and the denuders were operated for two days prior to the events. Figures 9-32 through 9-35 show the size-resolved aerosol particle measurements for the three species present above the detection limit – ammonium, nitrate, and sulfate. The first two figures are before and after the D009 event and are shown on an absolute and relative mass basis. The second two are the same for D010.

The reported denuder concentrations have been adjusted using the Gormley-Kennedy equation for efficiency (approximately 96%). The combination of the denuder flow rate uncertainty (2%, measured), collection/extraction efficiency (5%, estimated), and the analytical uncertainty give a relative standard deviation for ammonia of approximately 7%. Ammonia's blank and MDL concentrations were uniformly < 2% of the measured value. Nitric acid has a 14% calculated relative standard deviation, but its blank and MDL concentrations were from 17% to 42% of the measured ambient concentration. Therefore the measured HNO_3 concentrations (0.025 – 0.064 ppbv) should be treated with caution. For the MOUDI concentrations, the error bars shown reflect flow rate (5%, estimated) and analytical uncertainty. Due to the high humidity conditions, conditions should be very poor for the loss of nitrate during MOUDI sampling (Zhang and McMurry, 1992). The Teflon filters used as substrates showed evidence of an insoluble black material that was not extractable using the method chosen, and there was no evidence of internal condensation on the jets.

Reproduced with permission of the copyright owner. Further reproduction prohibited without permission.

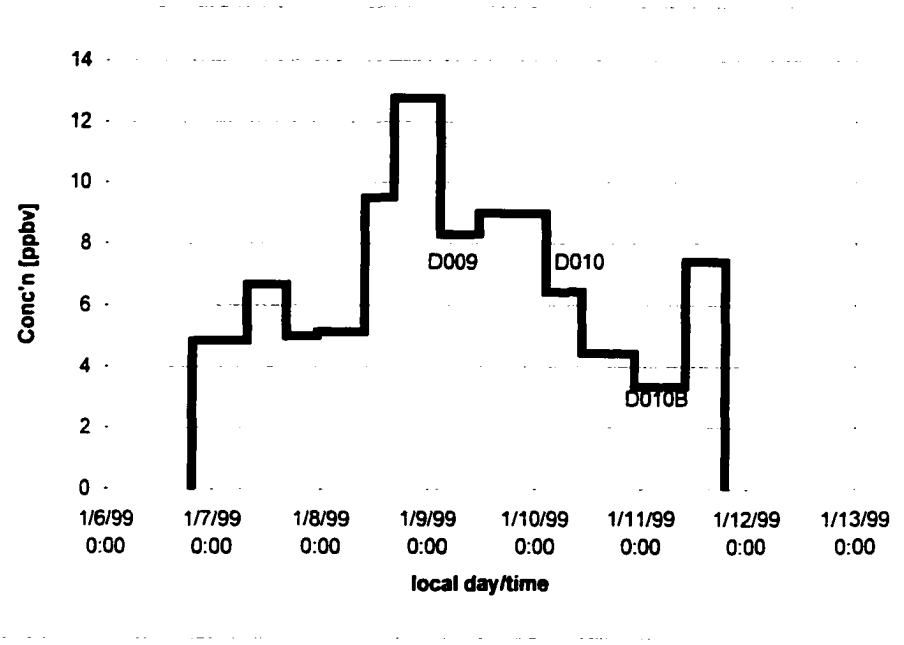

Figure 9-30: Ammonia concentrations in Davis (January). In-fog events are noted

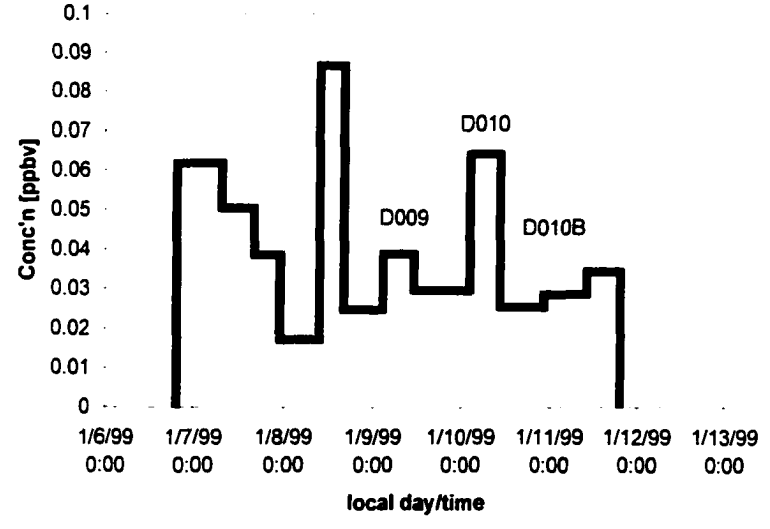

Figure 9-31: Nitric acid gas concentrations in Davis (January). In-fog events are noted

Reproduced with permission of the copyright owner. Further reproduction prohibited without permission.

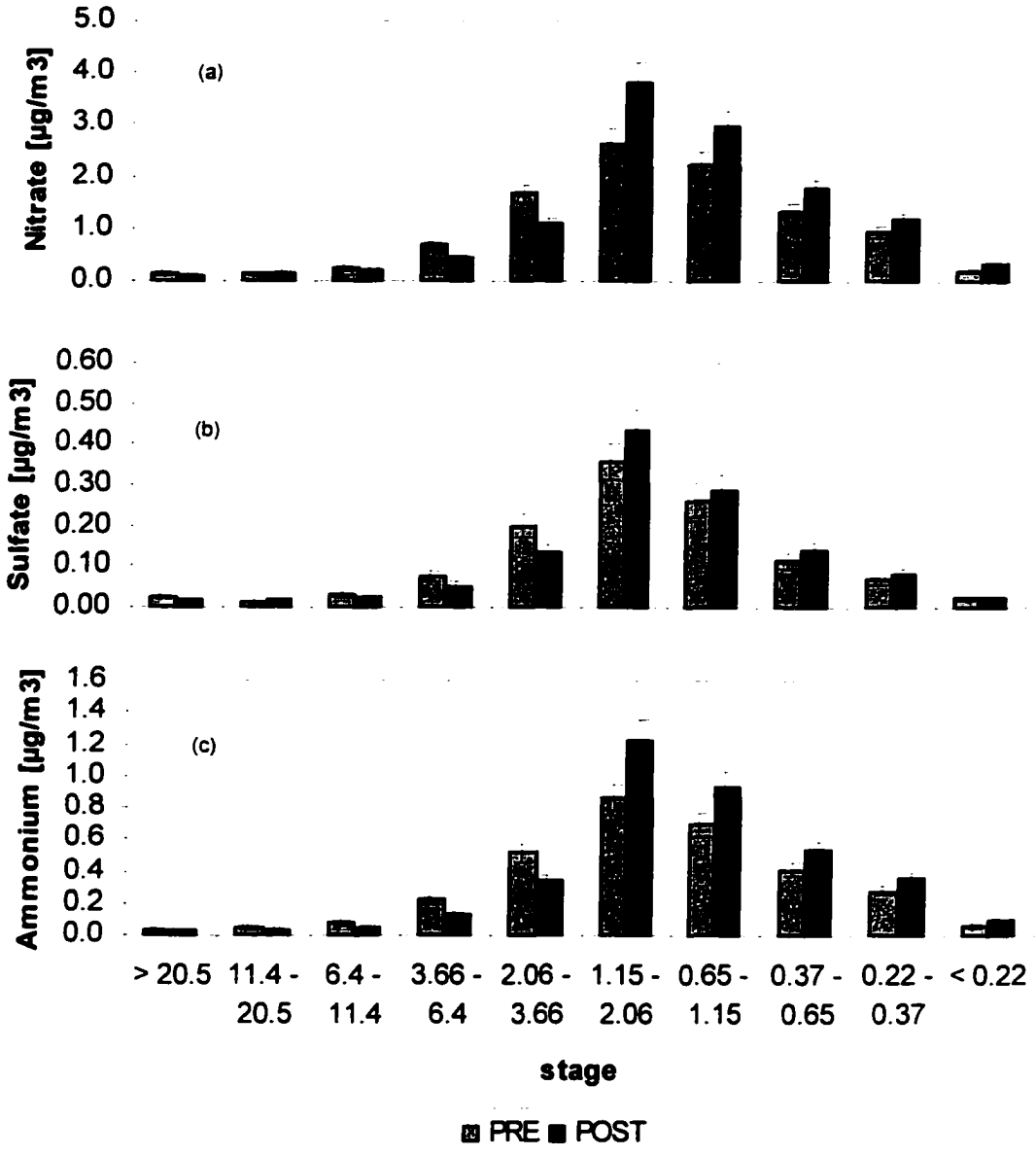

Figure 9-32: Size-resolved aerosol mass measurements before and after the D009 event for (a) nitrate, (b) sulfate, and (c) ammonium. The diameter range collected (in µm) is indicated.

Reproduced with permission of the copyright owner. Further reproduction prohibited without permission.

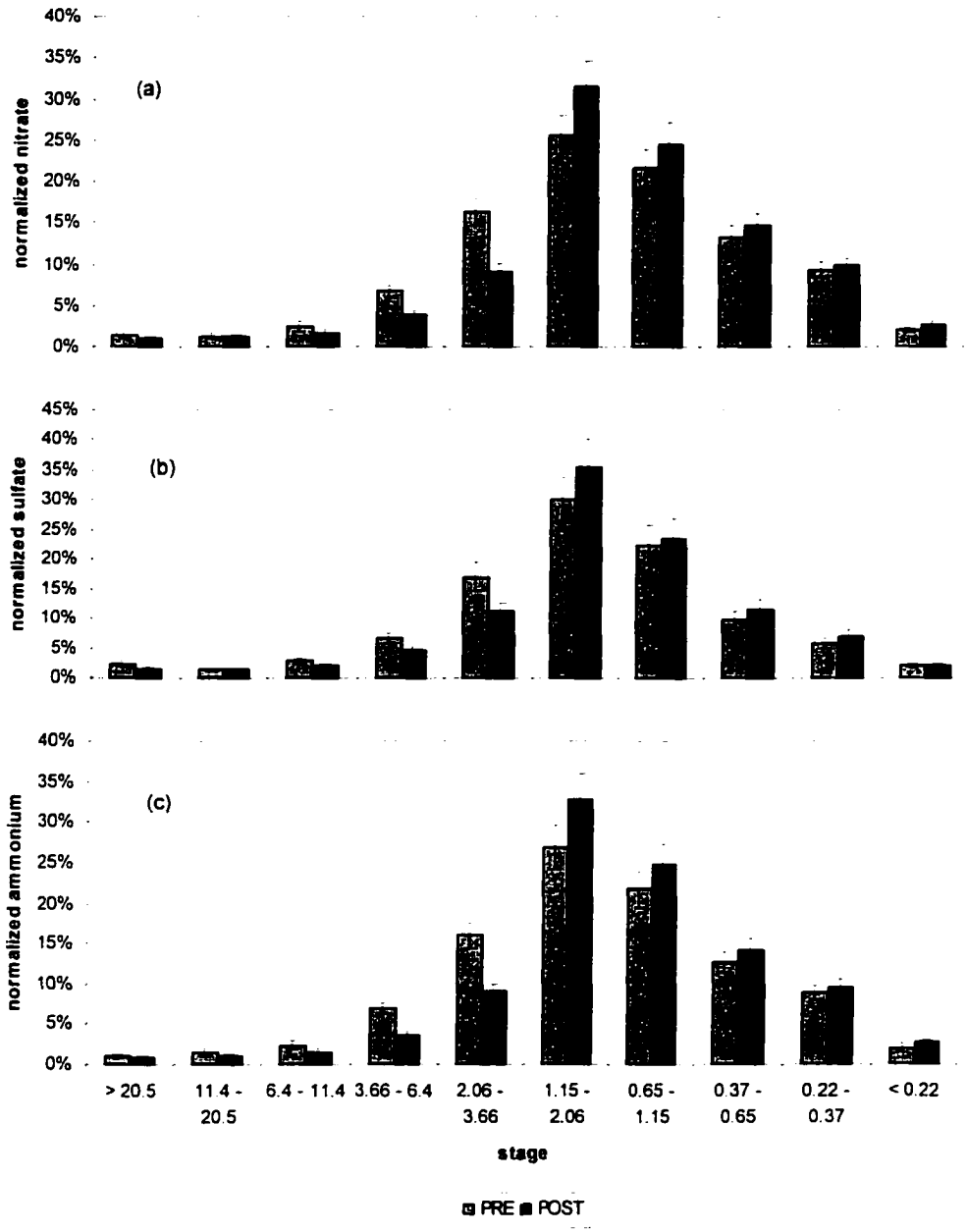

Figure 9-33: Same as figure 9-32, except mass is now normalized to show the relative change

Reproduced with permission of the copyright owner. Further reproduction prohibited without permission.

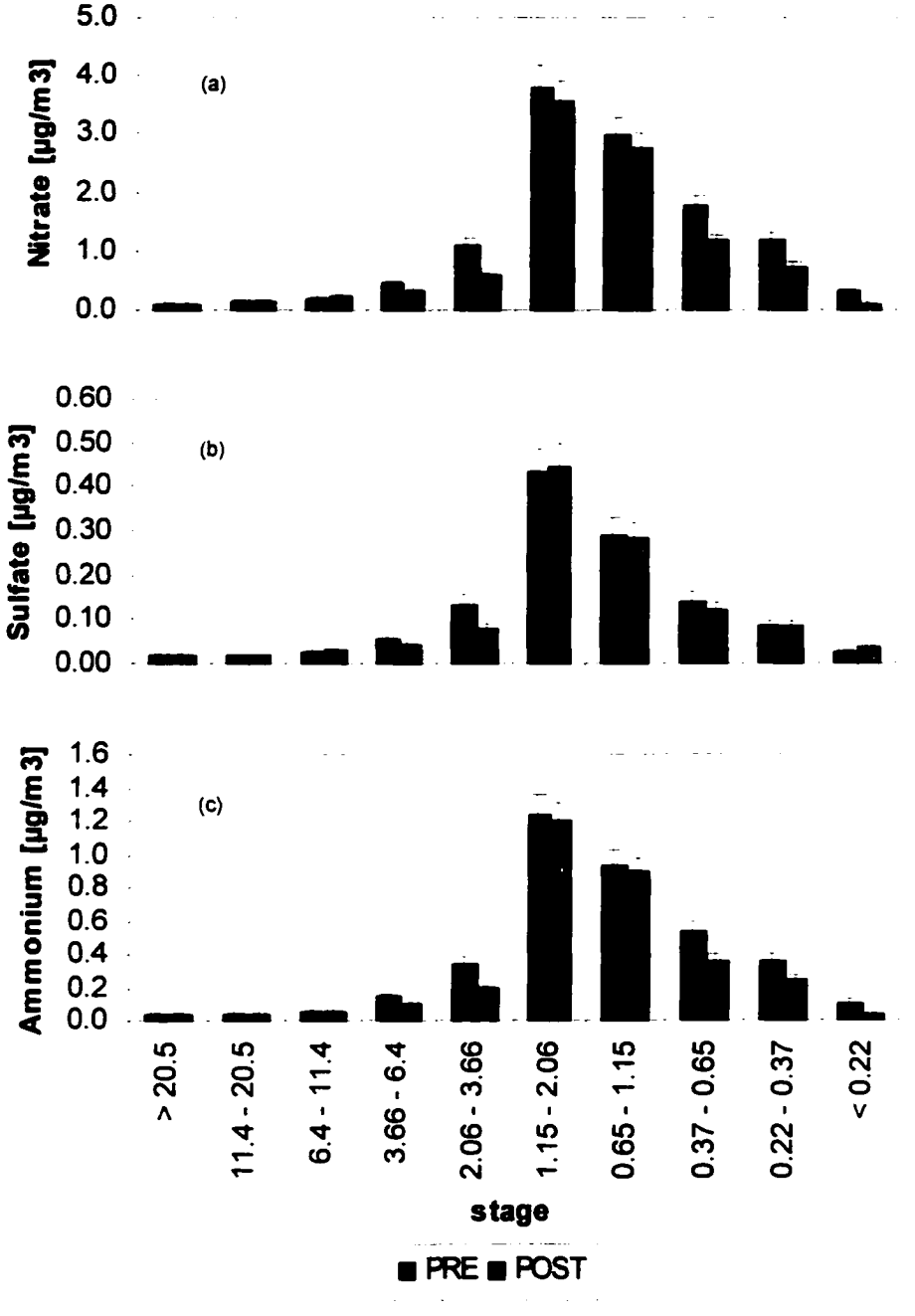

Figure 9-34: same as figure 9-32 except before and after the D010 event. The "POST" D009 measurement is the same as the "PRE" D010 measurement so the same color is used.

Reproduced with permission of the copyright owner. Further reproduction prohibited without permission.

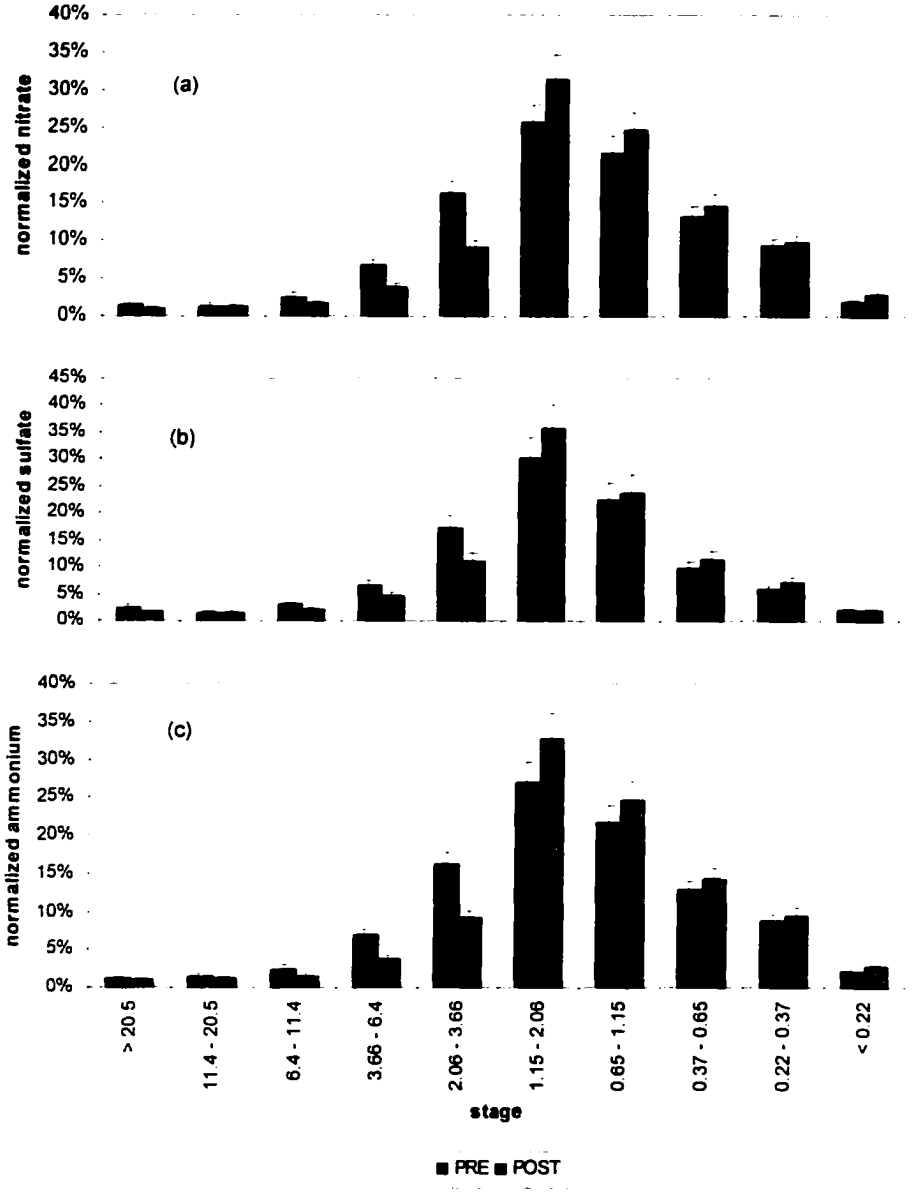

Figure 9-35: Same as figure 9-33, except normalized mass concentrations are shown

This is an ammonia-rich environment (figure 9-30). The presence of ammonia gas during the in-fog periods is consistent with the low LWC and the partitioning of ammonia between phases (Seinfeld and Pandis, 1998) (figure 9-37). The very low HNO_3 observations are also consistent

Reproduced with permission of the copyright owner. Further reproduction prohibited without permission.

with its very high solubility. It is usually not observed in the gas-phase in fogs (e.g. (Colvile *et al.*, 1994; Waldman and Hoffmann, 1987), among others).

Interpreting the MOUDI data is confounded by the fact that emissions, advection, and losses are constantly occurring and are not easy to control for given that the time resolution must be poor in order to gather enough sample to measure. However, over and between the D009 and D010 events the surrounding air mass seems to have remained reasonably the same, winds were typically light and other nearby locations experienced similar foggy conditions. The D010B data are not presented due to the frontal passage while sampling aerosol after the event. Most of the observed changes are within the known measurement error. Before D009, the sum of the reported concentrations was approximately 14.7 μg m^{-3}, increasing to 17.1 μg m^{-3} after the event, and decreasing to 13.9 μg m^{-3} after D010. It may appear that the fog may have contributed to an aerosol mass increase, although sulfate concentrations remained low. However, the change in observed concentration is likely due to a change in the mixing height between periods. Before the D009 event, surface temperatures were as high as 10°C, but the next MOUDI sampling periods had peak temperatures of < 5°C. We did not measure the mixing height and attempts to derive it from various sources did not yield satisfactory results. Of potentially more relevance is the relative change in the mass distribution before and after the fog events. Aerosol particles greater than 2 μm in diameter were uniformly found in lower relative concentrations after fog (figures 9-33 and 9-35) compared to particles of smaller diameter. This is consistent with the loss of large particles via sedimentation (section 9.2). In a Po Valley study, aerosols < 0.3 μm in diameter gained mass from advection and entrainment between pre- and in-cloud measurements, but large aerosol were nucleated into drops and lost. Advection and entrainment were on-going features of their fogs (Noone *et al.*, 1992) and may be responsible for some of the observed features here.

For the three matched gas- and aerosol-phase measurements, the initial ammonia/ammonium atmospheric concentration was approximately 0.7 μ-moles m^{-3} of which 25% were aerosol. The

Reproduced with permission of the copyright owner. Further reproduction prohibited without permission.

relative proportion of aerosol ammonium increased and the total amount of ambient ammonia/ammonium decreased to 0.37 μ-moles m^{-3} of which 47% were aerosol particles after the D010 event. Nitrate was virtually all in the solid phase, and the change between the three periods was 0.17 to 0.16 μ-moles m^{-3}, although concentrations were slightly elevated in the 2nd period (possibly from changes in the boundary layer height). Dissolved ammonium will stay in the aerosol phase if there are salts available, and a recent Po Valley study found that 20 – 70% of the ammonium and 5 – 60% of the nitric acid mass from the aqueous-phase remained in the aerosol (Laj *et al.*, 1998; Laj *et al.*, 1997a). Some modeling studies at Great Dun Fell suggest the orographic clouds themselves can be a source of ammonia upon evaporation, although the ammonia can get fixed with the nitrate and remain in the aerosol phase without S(IV) production being important (Bower *et al.*, 1999b). These results appear to be consistent with ammonia fixing in the solid-phase but there are many confounding factors as previously discussed.

There was no discernible difference between the relative charge concentrations in the aerosol for ammonium, nitrate and sulfate and those observed in the cloud water. While some previous studies observe obvious differences in the ratio of species such as nitrate and sulfate between fog and (for their case) interstitial aerosol (Fuzzi *et al.*, 1988), others have not (Laj *et al.*, 1998) which was attributed to minimal activation. These effects would also depend upon gas-phase concentrations.

According to the MOUDI measurements there were very low concentrations of large aerosol (figures 9-32 and 9-34) which are consistent with no evidence of the Region II drop size-dependent cloud concentration regime (Chapter 1) in the 5-Stage data.

While these results are interesting and consistent, it must be emphasized that they are limited and subject to many unquantified processes that may affect them.

Reproduced with permission of the copyright owner. Further reproduction prohibited without permission.

9.6 *In-fog deposition*

As discussed previously, loss of species via drop deposition can be an important removal mechanism from the atmosphere. In lieu of measuring species flux, investigators have measured the water flux and then multiplied that by the bulk cloud composition (e.g. (Fuzzi *et al.*, 1991; Pierson *et al.*, 1987), among others). However, if the composition of the drops varies with size and removal rate varies with size due to sedimentation then this may yield a misleading result. That approach can be evaluated by calculating the deposition velocity for the species:

$$v_{d,i} = {}^{F_i}\!/_{C_i} \qquad (9\text{-}1).$$

F_i is the measured material flux collected on the deposition plates and C_i is the concentration measured at 3 m in height. C_i is usually based upon the bulk cloud chemistry as the most representative and comprehensive.

The deposition velocity for water based upon equation 9-1 is:

$$v_{d,H_2O} = {}^{F_{H_2O}}\!/_{LWC} \qquad (9\text{-}2).$$

The deposition velocity for species A is similar and is calculated via:

$$v_{d,A} = \left({}^{F_A}\!/_{LWC}\right) \times \frac{1}{C_{bc,A}} \qquad (9\text{-}3).$$

The assumptions implicit in this approach to calculating the deposition velocity must be recognized. No derived deposition velocity is independent of the way it was measured. They are:

Reproduced with permission of the copyright owner. Further reproduction prohibited without permission.

- No evaporation/condensation on the deposition plates
- The deposition plates represent a "realistic" surface
- Constant LWC and bulk cloud composition (independent of height)
- The measured chemistry is not affected by drop mixing prior to collection

The first assumption is likely to be satisfied as long as conditions remain "in-cloud". Evaporation appears to affect the shiny metal plate on the scale used for more highly time-resolved deposition information (section 9.9), but the Teflon plates did not appear to be affected. We do not have the equipment to address whether or not the surfaces are realistic compared to natural grass, however at least they are flush with the ground. Sampling artifacts may be induced in volatile species whose gas/liquid partitioning is impacted by changes in the pH due to mixing (Pandis and Seinfeld, 1991; Perdue and Beck, 1988). This is difficult to evaluate without modeling. Due to the highly variable and transient state of these fogs, the two worst assumptions are probably that the LWC and bulk cloud chemistry are independent of height, particularly on low LWC days. This height independence is likely not to hold for all events, and the CASCC2 and sf-CASCC yield different results for what "bulk" composition is (Chapter 4). However, given the data available, these two assumptions cannot be avoided, and the CASCC2 must be used for consistency with earlier measurements. These calculations also presume that there is no ground source of the particular species (Wesely and Hrcko, 2000).

The calculations included here are a revision to those in Collett *et al.*, (2001) which were based upon only PVM LWC measurements (see Chapter 4).

9.6.1 Results and discussion

Figure 9-36 shows the calculated deposition velocity based upon measurements of species flux, derived LWC, and bulk cloud water composition for all of the Davis data. Nitrite, water, ammonium, nitrate and sulfate are shown. No uncertainty bars are shown for clarity, but based

Reproduced with permission of the copyright owner. Further reproduction prohibited without permission.

upon the relative standard deviation between pairs of the large plates (used in these calculations) the RSD for nitrite, water, ammonium, nitrate and sulfate are 5%, 5%, 4%, 5% and 9% respectively. These are generally on the order of the analytical uncertainty for the species. Table 9-5 shows the calculated size of the drops, assuming sedimentation was the only removal mechanism based upon non-Stokes flow where applicable. The drop diameters were calculated by matching the derived water deposition velocity.

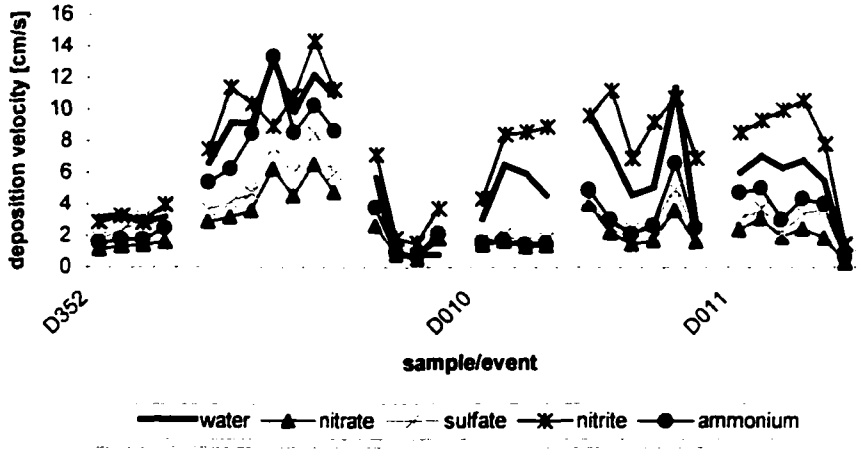

Figure 9-36: Davis deposition velocities for selected species

Table 9-5: Deposition drop diameters

event	mean diameter [μm]	diameter range [μm]
D352	29	28 - 31
D004	37	35 - 40
D009	18	14 - 26
D010	39	31 - 44
D010B	35	26 - 46
D011	37	13 - 27

Figure 9-36 shows that the deposition velocity for nitrite (mean 7.5 cm s^{-1}, range 1.5 – 14.3 cm s^{-1}) generally exceeds that for water (mean 6.0 cm s^{-1}, range 0.8 – 13.1 cm s^{-1}). In contrast, ammonium (mean 4.1 cm s^{-1}, range 0.6 – 13.4 cm s^{-1}) has a somewhat lower deposition velocity than water, followed by sulfate (mean 3.3, range 0.6 – 8.5 cm s^{-1}) and nitrate (mean 2.4 cm s^{-1},

Reproduced with permission of the copyright owner. Further reproduction prohibited without permission.

range 0.2 – 6.5 cm s^{-1}). This distribution of velocities (nitrite > water > ammonium > sulfate > nitrate) is consistent with their composition drop size-dependencies observed in the fog (sections 9.3 and 9.4). Similar results have been found previously and are a function of the species' solubility and their interaction with the fog (Collett *et al.*, 2001; Collett *et al.*, 1998). These species' averages represent a decline of about 40% from the previously reported values (Collett *et al.*, 2001) due to the change in LWC (which increased by approximately a factor of 2 and is located in the denominator in equations 9-2 and 9-3). These are very similar to results reported previously based upon RAC cloud water measurements in the southern San Joaquin Valley (Waldman and Hoffmann, 1987). They illustrate that the assumption that water and species have the same deposition velocity may sometimes be in error by as much as a factor of 2.

While the assumption that all deposition is via sedimentation is not uniformly true, several studies in a variety of locations) indicate that sedimentation dominates turbulent flux where wind speeds are less than 2 m s^{-1} in fogs (Eugster *et al.*, 2001; Burkhard *et al.*, 2000; Vong *et al.*, 1991; Fitzjarrald and Lala, 1986; Dollard and Unsworth, 1983). The importance of turbulent flux varied from negligible (Burkhard *et al.*, 2000) to 30 – 40% of the total (Dollard and Unsworth, 1983), so the drop sizes reported in Table 9-5 are likely overestimates. Despite this limitation, these results do lend credence to the drop size distribution spectra used to plot the figures in section 9.4 and that the very large drop sizes (up to approximately 70 μm) previously calculated were likely due to the inordinately low LWC reported by the PVM.

HONO's dry deposition velocity is estimated to be on the order of 2 cm s^{-1} (Harrison *et al.*, 1996), the same as HNO_3 (1 – 5+ cm s^{-1}) (Finlayson-Pitts and Pitts, 2000; Wesely and Hrcko, 2000), and may become as low as 0.4 cm s^{-1} at night in summer conditions (Staffelbach *et al.*, 1997). The wet deposition velocity calculated here suggests that fog water can provide an important removal mechanism for the species from the atmosphere to the ground. During the D004 event, when nitrite concentrations were occasionally elevated in the smaller drops according to the 5-Stage, the only time period occurs where the nitrite deposition velocity falls below that for water. This

Reproduced with permission of the copyright owner. Further reproduction prohibited without permission.

suggests that the gradient in nitrite concentrations observed in the 5-Stage may not be a sampling artifact, but may instead reflect real variations of unknown source.

For the large aerosol particles that end up in the largest drops, these calculated deposition velocities suggest they should be more efficiency removed than they would otherwise be which is consistent with the size-resolved MOUDI figures.

9.7 Gas/Liquid equilibria in-fog

In this section, measurements of in-fog concentrations from the three collectors and gas-phase measurements (where available) are used to explore whether or not gas/liquid equilibrium exists for the NH_4^+/NH_3, NO_3^-/HNO_3 and $NO_2^-/HONO$ systems.

Species that partition between the gas- and aqueous-phase may not be at equilibrium with each other for many reasons. Dis-equilibrium may be caused by rapid variations in LWC, whether measurements are at the center or edge of the cloud (related to LWC variations), species' solubility, liquid-phase reactions, and associated mass transport limitations (Voisin *et al.*, 2000; Audiffren *et al.*, 1998; Ricci *et al.*, 1998; Winiwarter *et al.*, 1994; Heintzenberg, 1992; Pandis and Seinfeld, 1992; Winiwarter *et al.*, 1992). The characteristic time for drop growth and/or evaporation can be much faster than the time needed for partitioning to achieve equilibrium (Leriche *et al.*, 2000). Organic films in polluted fogs may also limit the ability of species to achieve equilibrium across the gas/liquid/organic interface (Facchini *et al.*, 1992a). Species that are less soluble are less likely to become "trapped" in rapidly growing or evaporating drops and thus are more likely to be at equilibrium (Bower *et al.*, 1991). A modeling study has also suggested that vertical in-cloud gas-phase concentration gradients may also cause apparent deviations from equilibrium in the composition of the settling drops (Bott and Carmichael, 1993). Finally, the act of sampling drops while mixing them together may also introduce a supersaturation in H^+ which will affect partitioning of many of the weak acids and bases of interest

Reproduced with permission of the copyright owner. Further reproduction prohibited without permission.

(Winiwarter *et al.*, 1992; Pandis and Seinfeld, 1991; Perdue and Beck, 1988). Drops of the same size may not be composed of the same species due to the external mixture of CCN that they form on. Therefore these mixing effects may occur even if drop separation by size between cloud water collector stages are improved.

Several field studies have investigated gas-/aqueous-phase equilibria for species such as the low molecular weight organic acids, ammonia, nitric acid, formaldehyde, H_2O_2, and S(IV) among others (Lüttke *et al.*, 1999; Fuzzi *et al.*, 1998a; Ricci *et al.*, 1998; Jaeschke *et al.*, 1997; Laj *et al.*, 1997b; Keene *et al.*, 1995; Munger *et al.*, 1995; Colvile *et al.*, 1994; Seyffer and Helas, 1994; Facchini *et al.*, 1992b; Facchini *et al.*, 1992a; Sanhueza *et al.*, 1992; Glotfelty *et al.*, 1990; Radojevic *et al.*, 1990; Munger *et al.*, 1989b; Winiwarter *et al.*, 1988; Glotfelty *et al.*, 1987; Munger *et al.*, 1986; Richards *et al.*, 1983). While it is not always known why the deviations occur, pH-, LWC- and drop size-dependencies have all been suggested as possible reasons in addition to time-integrated sampling, the occurrence of in-cloud reactions – particularly S (IV) and H_2O_2 – and the presence of species absorbed to colloidal particles in the drop. Species may exhibit equilibrium in some conditions and not in others (e.g. (Munger *et al.*, 1995; Munger *et al.*, 1989b)).

There are different calculation techniques to assess if aqueous-phase species are in equilibrium with the gas-phase. The approach used here is to calculate the theoretical (equilibrium) and actual species distribution factors which are used to derive the respective mole fractions in the aqueous-phase. The ratio of actual to theoretical aqueous-phase mole fractions is > 1 if there is aqueous-phase supersaturation, and < 1 if subsaturation occurs. Following Seinfeld and Pandis (1998, p. 343):

$$f_{act} = \frac{c_{aq}}{c_g} \qquad (9\text{-}4),$$

Reproduced with permission of the copyright owner. Further reproduction prohibited without permission.

$$f_{equil} = H_{eff} RT(LWC) \quad \text{(9-5), and}$$

$$X_j = \frac{f_j}{1 + f_j} \quad \text{(9-6)}$$

where the index j is for either "act" (measured) or "equil" (theoretical). As the distribution factors are dimensionless, appropriate conversion factors are implied. In particular, LWC is imbedded in C_{aq}. The effective Henry's constant has been substituted in the equation which implies a pH-dependence to these calculations. Figures 9-37 and 9-38 show X_{equil} calculated for the NH_4^+/NH_3 and NO_2^-/HONO systems for Davis-type conditions. For the high pH and low LWC conditions of the Davis fogs, both species are expected to be in both phases. The pH-dependence varies, however, as NH_4^+ increases with decreasing pH and the opposite behavior occurs for NO_2^-. For both HONO and NH_3 the effective Henry's constants are > 10^5 M atm^{-1} so both are highly soluble in these conditions. The HNO_3/NO_3^- system is not shown as it is expected to partition virtually entirely to the aqueous-phase (H_{eff} > 10^{12} M atm^{-1}).

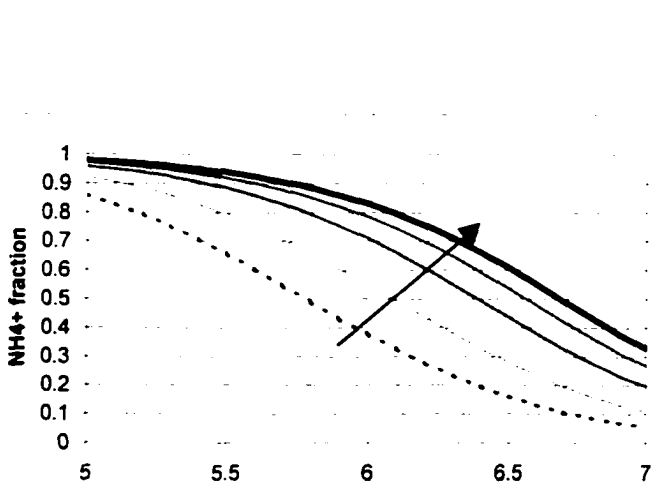

Figure 9-37: Equilibrium fraction of NH_4^+ predicted for varying pH and LWC. Arrow shows the direction of increasing LWC.

Reproduced with permission of the copyright owner. Further reproduction prohibited without permission.

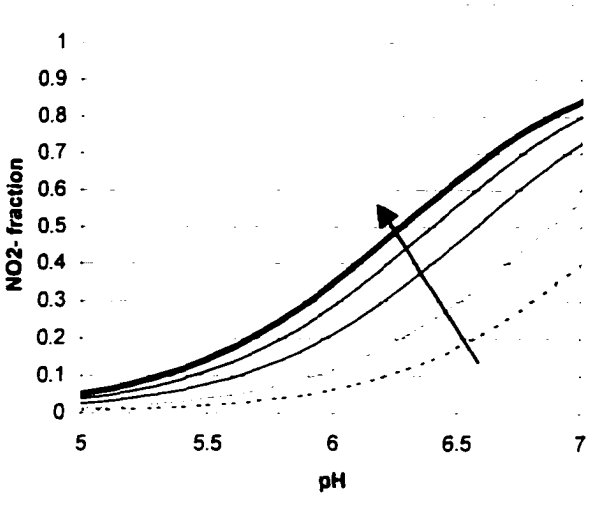

Figure 9-38: Equilibrium partitioning of NO_2^- in the aqueous-phase as a function of LWC and pH. Arrow shows the direction of increasing LWC.

9.7.1 NH_4^+/NH_3 and NO_3^-/HNO_3 results and discussion

As the denuder measurements were integrated over the entire D009, D010 and D010B events, a weighted average concentration for NH_4^+ and NO_3^- were calculated for the CASCC2, and sf-CASCC fractions. As HNO_3 was measured in concentrations near the detection limit and concentrations of aqueous-phase nitrate were very high, the HNO_3/NO_3^- system appears to be in equilibrium within the measurement uncertainty (not shown). Ricci and co-workers in a recent Po Valley study found nitrate to be subsaturated during some time periods, but nitric acid was measured in-fog (Ricci *et al.*, 1998). Figure 9-39 shows the results for the ammonia/ammonium system.

Reproduced with permission of the copyright owner. Further reproduction prohibited without permission.

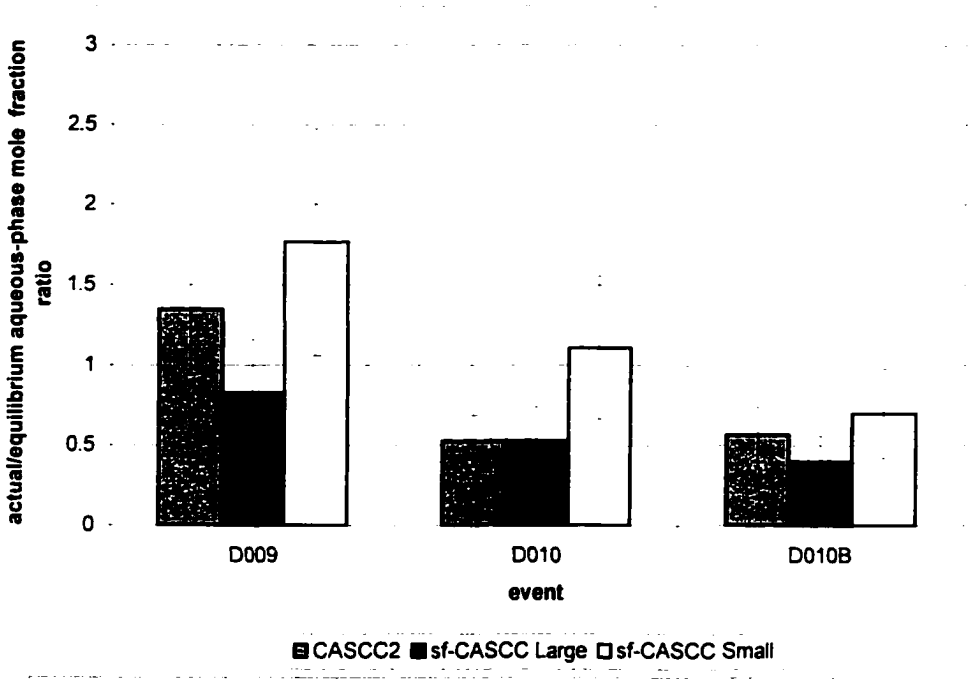

Figure 9-39: Actual/equilibrium aqueous-phase mole fraction ratio for ammonium by event mean.

The error bars shown reflect the cumulative uncertainty in H_{eff} (as a function of both temperature and pH (approximately)), aqueous-phase concentrations, LWC and the denuder measurements. Calculations suggest the error is on the order of ± 30% for the CASCC2 and ± 40% for the sf-CASCC if the additional uncertainty associated with splitting the LWC into two portions based upon the results of Chapter 4 are included. Although within the error, the results suggest that there might be a tendency for a slight sub-saturation in the aqueous-phase for the CASCC2 and Large sf-CASCC fraction accompanied by a slight super-saturation in the Small fraction. Some recent modeling work by Dr. C.-H. Kim suggested that likely in-cloud LWC variations could be responsible for some of the drop size-dependence observed. However, these model results consider the instantaneous concentrations (not the hourly sample average) and suggest that the nitric acid/nitrate system should also be out-of-equilibrium which the data does not indicate. Pandis and Seinfeld (1991), however, suggest that up to a factor of 3 supersaturation may occur due to drop mixing. The 5-Stage data from the D009 and D010 events are useful here, although

Reproduced with permission of the copyright owner. Further reproduction prohibited without permission.

no error bars are shown as it is not known how appropriate the event mean ammonia concentration used to calculate the ratios is. The 5-Stage's drop fractions, however, should be subject to less mixing than the other collectors, and relative differences between the collectors appear to be robust after experimenting with likely ammonia concentrations. If vertical gradients in the ammonia concentration do not exist, all three collectors should be subject to the same gas-phase concentration. Figures 9-40 and 9-41 show CASCC2, sf-CASCC and 5-Stage data selected from each event.

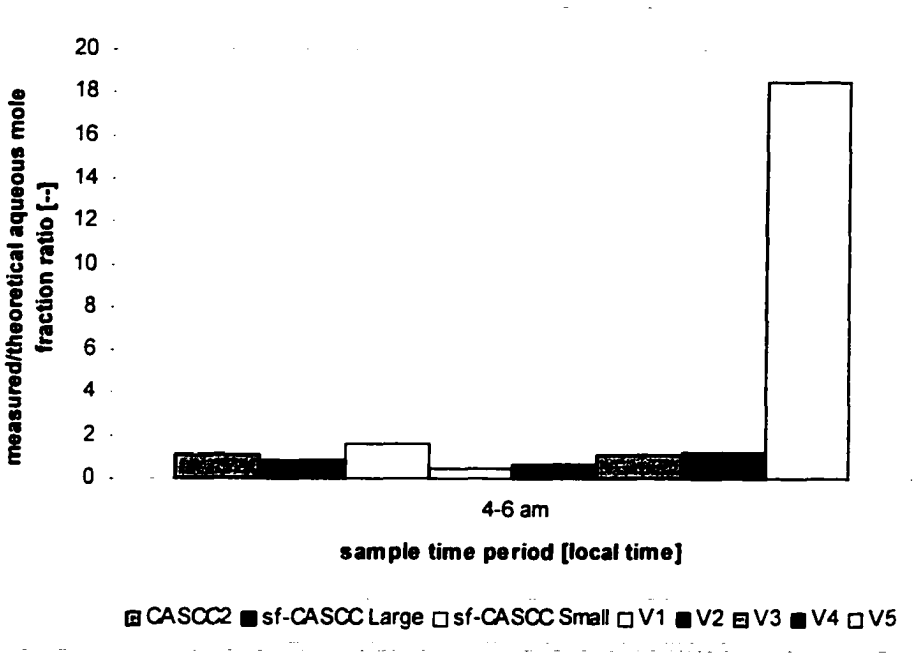

Figure 9-40: Measured/equilibrium aqueous-phase ammonium mole fraction ratio for a 5-Stage sampling period (D009, 4 – 6 a. m.). Gas-phase concentration assumed to be the event mean.

The other two time periods available showed similar results, although figure 9-40 was chosen as it represents the extreme range of calculated values. The 5-Stage data suggest that the supersaturation indicated by the Small fraction results on D009 and D010 may be real. The supersaturation shown for Stage 5 in the 4 – 6 a. m. sampling period exceeds the factor of 3 for mixing cited above. For all data the Stage 5 fraction result suggests substantial supersaturation,

Reproduced with permission of the copyright owner. Further reproduction prohibited without permission.

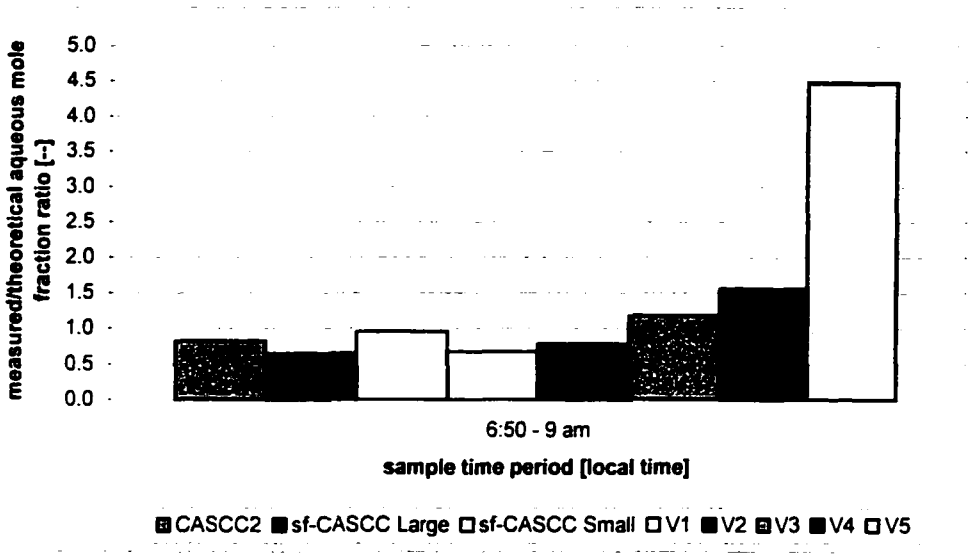

Figure 9-41: Measured/equilibrium aqueous-phase ammonium mole fraction ratio for a 5-Stage sampling period (D010, 6:52 – 9 a. m.). Gas-phase concentration assumed to be the event mean.

decreasing to values generally near equilibrium for the larger stages and drops. These results can be interpreted similarly to those in the recent Po Valley study – drops are formed on ammoniated particles and dilute much faster than the ammonium can partition (Ricci *et al.*, 1998). Drops are a potential source of ammonia to the atmosphere. The range of sub-/supersaturation values is very low compared to other studies (up to orders of magnitude have been observed (e.g. (Ricci *et al.*, 1998; Facchini *et al.*, 1992b)), and determining the appropriate error bounds are difficult so the trends observed are most useful.

In order to determine if large supersaturations from mixing might be expected, the calculation procedure outlined in Pandis and Seinfeld (1991) was used for both some sf-CASCC sample pairs and the 5-Stage sample sets. The results (not shown) suggested little effect, although the authors (correctly) point out that the calculations can be misleading if drop separation between stages is poor. Due to the problems with the PVM, only limited high time resolution LWC data are available, but calculations suggest that the LWC effect may not be large (Pandis and Seinfeld, 1992; Winiwarter *et al.*, 1992). Higher time resolution in all of the data would improve this evaluation in the future. However, that will not address all the difficulties.

Reproduced with permission of the copyright owner. Further reproduction prohibited without permission.

In particular, the CASCC2, sf-CASCC and 5-Stage bulk/derived "bulk" concentrations vary on D009 and D010 (Chapter 4). It is not known which collector has the more "representative" concentration. If the CASCC2 concentrations are reduced by 40%, its results more closely resemble the Large fraction's results in figure 9-39. The additional uncertainty introduced by the collectors themselves is an additional factor to take into consideration when evaluating reported results.

9.7.2 HONO/NO_2^- results and discussion

In-drop nitrite photolysis can be a major source of OH radical in the Davis fog drops (Anastasio and McGregor, 2001). Nitrite was not measured in the Davis aerosol, and our detection limit was approximately 30 ng m^{-3}. Very few studies have reported nitrite in the solid-phase (Lammel and Perner, 1988). Unfortunately, the NaF coating used for the nitric acid denuder is indeterminate for HONO (Perrino *et al.*, 1990), but evidence for the presence of HONO was found in all denuders that operated at least in part during night-time conditions; no "daylight-only" denuders contained any nitrite. Therefore, the nitrite observed in the drops is assumed to come entirely from HONO, consistent with other studies (Cape *et al.*, 1992). The source of HONO is highly controversial, but heterogeneous and/or surface reactions are likely to be involved and some studies have suggested that water (or at least water vapor) is important (Finlayson-Pitts and Pitts, 2000; Lammel and Cape, 1996; Calvert *et al.*, 1994; Notholt *et al.*, 1992). Nitrite can be produced in-drop from some aqueous-phase reactions, but evidence suggests that some of the most likely ones are not important (e.g. (McFadyen and Cape, 1999) among others). In-fog concentrations of nitrite are widely reported (e.g. (Acker *et al.*, 2001, Lammel, 1988 #394; Anastasio and McGregor, 2001; McFadyen and Cape, 1999; Fuzzi *et al.*, 1998a; Jaeschke *et al.*, 1998; Lammel and Metzig, 1998; Cape *et al.*, 1997; Lammel and Cape, 1996; Cape *et al.*, 1992; Sigg *et al.*, 1987) among others), and are typically low (< 10 μN). Concentrations on the order of 200 μN have been reported in polluted, high pH conditions (Fuzzi *et al.*, 1998a).

Reproduced with permission of the copyright owner. Further reproduction prohibited without permission.

As only aqueous-phase measurements were available, the HONO concentration can be derived using Henry's law for the CASCC2 and sf-CASCC fractions. If the nitrite concentration is at equilibrium, each collector/collector fraction should produce the same gas-phase concentration (figure 9-42).

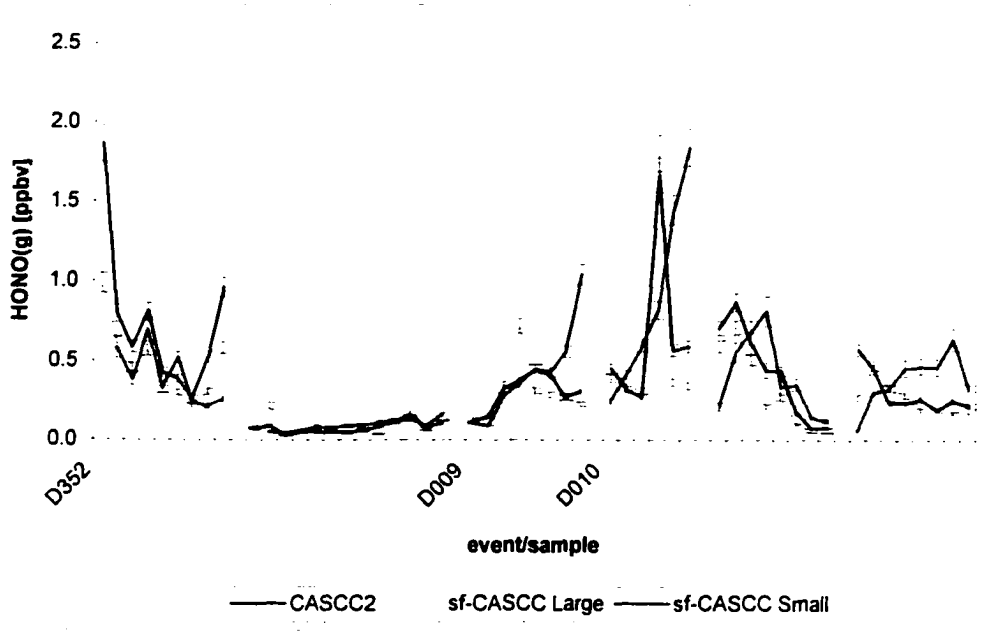

Figure 9-42: HONO(g) derived from aqueous-phase measurements plotted by event/sample.

The error bars shown include the cumulative uncertainty associated with analytical precision, temperature and pH. In general, the 3 collectors agree well and up to 2 ppbv HONO is determined, which is consistent with previously observed in-fog values (Harrison *et al.*, 1996; Lammel and Cape, 1996). There are noticeable deviations, however, particularly at the beginning and ends of events. As figure 9-43 shows, this is often associated with very low LWC (< 50 mg m^{-3}).

Reproduced with permission of the copyright owner. Further reproduction prohibited without permission.

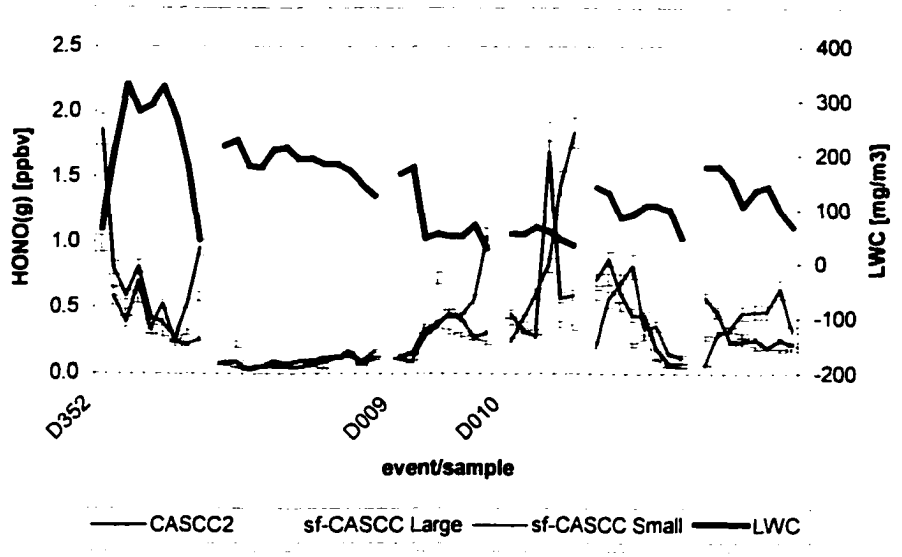

Figure 9-43: Same as figure 9-42 with LWC added on the secondary axis.

There is some association with diverging pH values between the Large and Small fractions, but not always, and the derived gas concentration can vary with and without sunlight. Concurrent 5-Stage data for the seven sample sets are shown in figure 9-44.

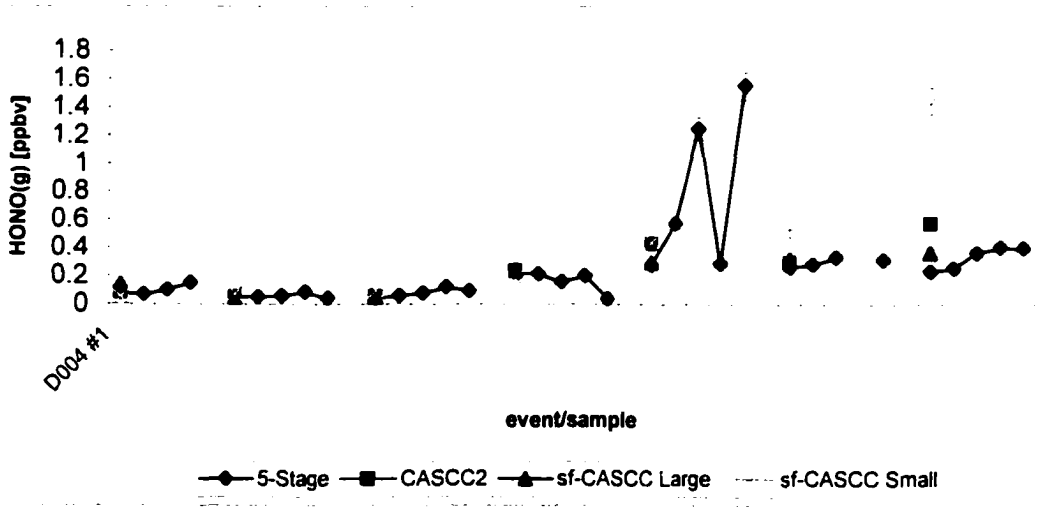

Figure 9-44: $HONO_{(g)}$ derived from the 5-Stage for all seven samples (data plotted from left to right, Stage 1 through Stage 5) and the other collectors (plotted with Stage 1). There are no D004 #1 V5 or D010 #1 V4 data.

Reproduced with permission of the copyright owner. Further reproduction prohibited without permission.

The 5-Stage data are plotted Stage 1 through Stage 5 for each time period and the other two collectors' results are printed with Stage 1. Where the LWC > 100 mg m^{-3} (the first four sample periods shown), the 5-Stage agreement with the other data is reasonably good. There is some variation on Stage 5, but recall the elevated pH there. Nitrite is often higher in the 5-Stage, but this is balanced by changes in the pH to yield generally similar nitrous acid concentrations to the other collectors. For the last three sample periods, agreement between the three collectors is poorer, particularly during the second sample sets on both D009 and D010. These may be sampling artifacts or due to the inhomogeneity in the sampled cloud water.

Data are not available to resolve the differences observed in figures 9-42 and 9-44, but they are consistent with changing pH and LWC leading to mass transfer delays into or out of the drops. At the low LWC (figure 9-38), small changes in pH of less than 0.5 pH unit can have a big effect on the equilibrium aqueous-phase mole fraction.

In sunny conditions, the ground has been found to be a source of HONO to the atmosphere when NO_2 concentrations exceed 10 ppb (Harrison and Kitto, 1994). The NO_2 concentrations reported for Davis are approximately of that order. However, the 5-Stage, which was located 2 m closer to the ground than the other two collectors, generally yields consistent results with the other two collectors.

Overall, gas-phase concentrations derived from the Large fraction were approximately 88% of the bulk-derived concentration and the Small fraction was 129% of it. Both the Large and Small fractions compared to the CASCC2's results yielded a broad range. As with the earlier results presented for ammonia/ammonium, the one hour time resolution available from the collector averages over some of the true atmospheric variation. The reported gas-phase HONO concentration is probably accurate to within ± 30%.

Reproduced with permission of the copyright owner. Further reproduction prohibited without permission.

While correlation of HONO with other species in order to shed light into the production mechanism has been questioned (Febo, 1994), several authors report the presence of some positive correlation with several species including CO, NO, NO_2, water vapor, and aerosol surface area, among others. No correlation was observed between CO, NO, NO_2 and LWC (as a surrogate species) in this data set (not shown). One problem may be the poor resolution of the CO, NO and NO_2 data obtained from Cal-EPA as the derived HONO concentrations tended to stack in columns over specific concentrations. For this data set, the $HONO/NO_2$ ratio varies from 0.2% to 17% with a mean of 3%. This is within the range of values previously reported, although measurements of this ratio are often made in clear sky, sunny and hot conditions (Lammel and Cape, 1996) where HONO concentrations have been studied most.

The last two or three samples from each event were after local sunrise and the nitrite levels appeared to persist in the drops despite, presumably the rapid loss of $HONO_{(g)}$ from the atmosphere. Drop release of HONO may keep replenishing concentrations and there is some evidence of low-level persistent HONO concentrations during day-time in some conditions (Vecera and Dasgupta, 1991).

9.8 Equivalent air concentrations

Cloud water concentrations are often expressed as equivalent air concentrations as changes in LWC can mask changes in the underlying solute concentrations. For fogs where sedimentation results in species removal, the equivalent air concentrations are typically lower at the end of an event (Fuzzi *et al.*, 1988). The equivalent air concentrations were calculated for ammonium, nitrate and sulfate for the Davis events. As the patterns were similar across the species, only nitrate's are shown (figure 9-45) for both the CASCC2 and the sf-CASCC fractions.

Reproduced with permission of the copyright owner. Further reproduction prohibited without permission.

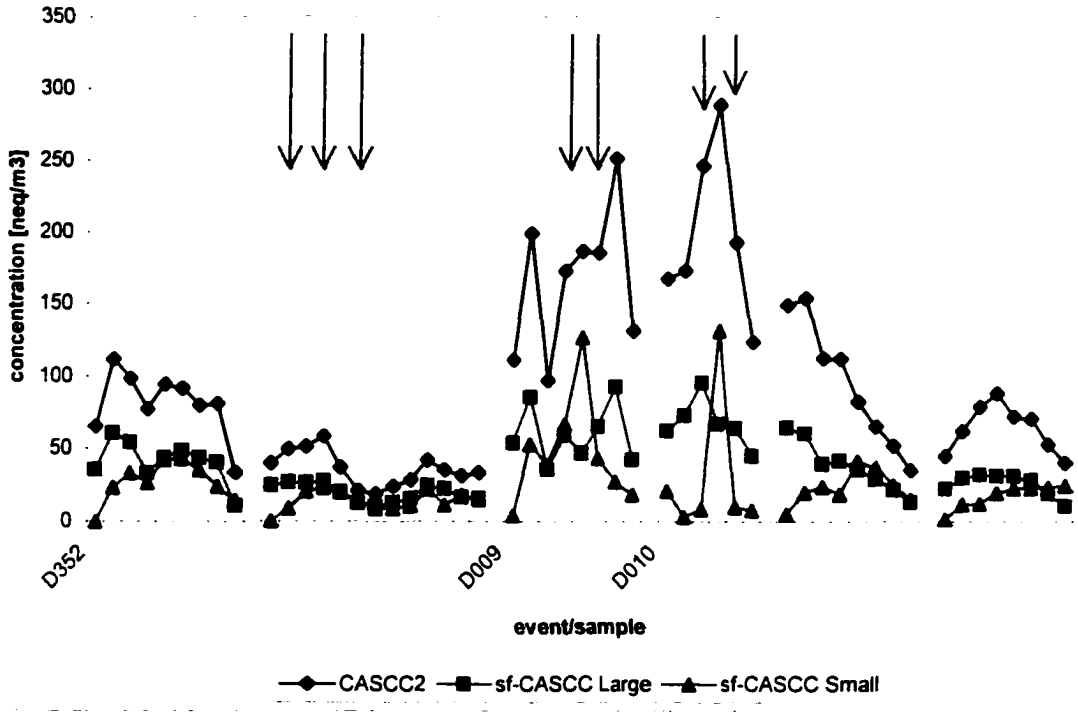

Figure 9-45: Equivalent nitrate air concentrations plotted by event and collector. The red arrows roughly correspond to 5-Stage sampling periods (figure 9-46).

For the D352, D010, D010B and D011 events, CASCC2-derived concentrations are lower at the end of the events than at the beginning. Only during the D010B event do concentrations consistently fall throughout the event. Large fraction-derived concentrations decrease or stay level throughout these same events, although Small fraction concentrations can increase at the same time. This is consistent with the Large fraction drops being responsible for most deposited drops. For the D004 event, concentrations fall and then rebound. D009 and D010 again present a different picture, and oscillate during the event. The oscillations cross PVM LWC and collector-derived LWC data so disagreement between the two are not responsible for all of the variation. During both of those events, there are noticeable spikes in the equivalent air concentration associated with the Small fraction, representing possibly the impact of Large drops evaporating into Small drops although the total increase suggests the incorporation of new mass. These features are observed in the CASCC2 concentrations, so mis-allocating LWC using the sf-CASCC collected water data is not solely responsible.

Reproduced with permission of the copyright owner. Further reproduction prohibited without permission.

5-Stage data for nitrate and nitrite can be plotted similarly for several of the time periods (figure 9-46) and are generally consistent with the first four of the time periods shown in figure 9-45. The later three time periods (D009 7 – 9 a. m., D010 4 – 6 a. m., and 6:52 – 9:00 a. m.) yield much more variation. The 5-Stage data there predicts smaller (D009) or larger (both D010) concentrations in the Small fraction should occur, than actually are observed. The difference is in part attributable to LWC variations as the D010 5-Stage collected water distribution has relatively high mass collected on Stage 5. Given the uncertain mass measurements (Chapter 4), particularly in the 5-Stage, at least part of the difference may be within the uncertainty due to the mass measurements. This discrepancy may just be a product of differences in sampler collection efficiency, but cannot be resolved with the data available. However, these results are consistent with thei high nitrite deposition velocity as nitrite is concentrated in Stage 1. Nitrate, in contrast, is present in high concentrations in both Stage 1 and Stage 5 so the overall deposition velocity is comparatively smaller.. 5-Stage data are useful to help explain observations made in addition to cloud drop composition. The relative advantage of the 5-Stage is that is can separate the smallest drops from the largest successfully.

In figure 9-46, the CASCC2 concentration is 40% higher than what the sum of the Large and Small fractions is for the D009 and D010 events (see Chapter 4). A recurring problem in this data analysis is where to assign the error or uncertainty when the collectors disagree. Although this cannot be resolved for this data set, future field studies can address this at least in part by more care in mass measurements and in resolving some of the sources of sampling variations between the collectors.

Reproduced with permission of the copyright owner. Further reproduction prohibited without permission.

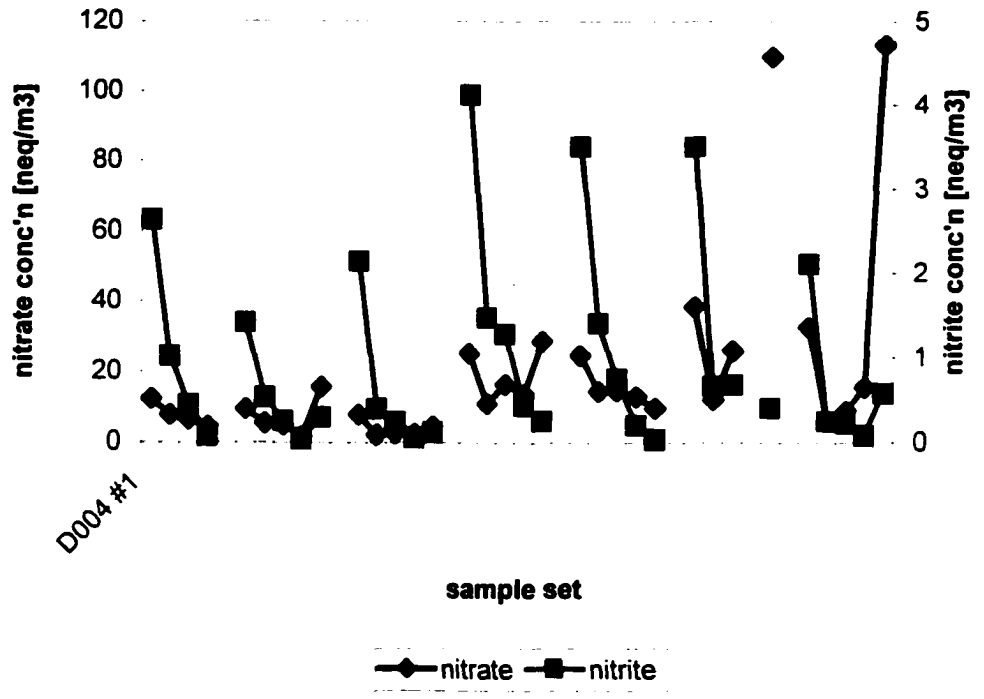

Figure 9-46: Equivalent nitrate and nitrite air concentrations derived from 5-Stage data plotted by event sample set (Stage 1 through Stage 5). Time periods correspond to the time periods indicated in figure 9-44. No data for D004 #1 V5 and D010 #1 V4 are available.

9.9 Scale data

The scale data was initially processed and validated by Mike Hannigan. Nine validated periods with paired measurements remain from 3 events: D352 (plate #2), D004 (plates #2 – 6), and D010B (plates #2 – 4). The RSD between water mass measurements was approximately 7.8%.

As much of the Gerber PVM-100 data is not useful in the Davis fogs, the change in water flux at the high temporal resolution of the scale allows some interpretation of the physical processes in the fogs. The D004 event data are shown in figure 9-47 and are representative of the others not shown. There are two points of particular interest. First, note that in general there is a periodicity of fluctuations in the water flux on the order of 20 minutes to about an hour as observed in earlier

Reproduced with permission of the copyright owner. Further reproduction prohibited without permission.

studies (see section 9.2) and is thought to correspond to the loss of very large drops from the fog followed by growth of new drops. While the water flux is only a surrogate for LWC (and, of course, the drop size distribution is important) our observations are not inconsistent with this interpretation. Modeling suggests that fog drop deposition is a discontinuous process (Bott *et al.*, 1990). Second, the time scale of physical fluctuations in the fogs is much smaller than our ability to sample fog chemistry. Therefore, it is important to recognize that our chemical measurements average over what may be substantial variations in the drop (size-dependent) chemistry.

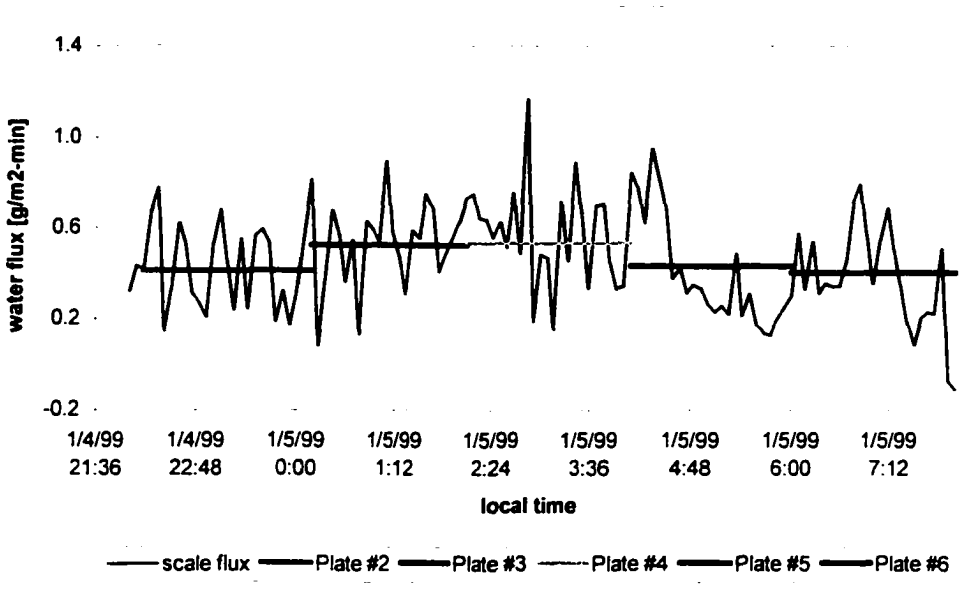

Figure 9-47: D004: 1/4/99 10:10 p.m. to 1/5/99 8:00 a.m. scale (4 minute average every five minutes) vs. deposition plate flux (2 hour sampling periods)

9.10 Summarizing remarks

In this chapter, the drop size-dependent fog composition observations from the 5-Stage are compared to other collectors and measurements to provide insight into the drop size-dependent composition and the effect of fog processes on ambient species. The sf-CASCC data suggests there is drop size-dependent chemistry in Davis and factors of up to 10 – 20 between Large and Small drop concentrations may occur, although 5 is more typical (table 9-3). The 5-Stage data

Reproduced with permission of the copyright owner. Further reproduction prohibited without permission.

suggests the true variation can be up to a factor of 4 – 5 times larger than the sf-CASCC suggests for ammonium, sulfate and nitrate. This variation may be even greater in the minor species measured, although many were close to detection limits and variations in sampling height between the collectors may have affected this result. This is a somewhat larger, but comparable, composition difference than observed by the DFSS in the Po Valley (Laj *et al.*, 1998). Fe, Mn (and Cu) have different drop size-dependent composition patterns from the other species, but still highly similar between them. Copper concentrations in Davis appear to be large enough that they have the potential to impact the drop redox chemistry. The 5-Stage data supports evidence for a bimodal drop distribution in the fogs and large (> 30 μm in diameter) drops.

The relative change in the size-resolved aerosol distribution between fogs is consistent with the loss of larger aerosol by nucleation into drops and subsequent deposition during fog. The derived deposition velocities illustrate how important a removal mechanism for many species occult deposition is. Virtually all of the nitric acid gas appears to have partitioned to the drops as equilibrium predicts, but ammonium/ammonia may not be at equilibrium in this environment. Gas-phase nitrous acid appears to be present in concentrations up to 2 ppbv during the fog events, and some data suggests that equilibrium partitioning may not be achieved across all drop fractions particularly during low LWC events with variable pH across the drop size spectrum and in time. The 5-Stage data, although limited, help to interpret these features due to its improved measurements of drop size-dependent chemistry.

In the presentation and discussion of the results, the variation in derived "bulk" and bulk concentrations between the three collectors for the D009 and D010 events repeatedly had some impact on the interpretation. As the scale data suggests, fogs are very inhomogeneous on both temporal and spatial scales. The lack of vertical co-location may have affected the observations between the collectors. However, it cannot account for all of it (Chapter 4). More attention to measurement – particularly mass weighing – uncertainty would improve these results. It is invariable that there are many uncontrolled factors while making measurements in fog which may

Reproduced with permission of the copyright owner. Further reproduction prohibited without permission.

affect the results and are difficult to quantify in terms of the error, particularly when making point measurements at long sampling intervals in a rapidly changing environment. The differences between collectors and the drops they sample should be considered in the evaluation of whether or not gas/liquid equilibria exist. This returns to the idea of what actually constitutes a "representative" drop sample.

Reproduced with permission of the copyright owner. Further reproduction prohibited without permission.

10. Conclusions and recommendations

10.1 Conclusions

In a recent "state of the science" review of the Atmospheric Sciences, the National Research Council indicated that priority should be placed upon improving observations and developing tools to improve observations of atmospheric chemistry (NRC, 1998). That is also the goal of the work described in preceding chapters – to develop new cloud water collectors to improve measurements of the drop size-dependent composition. Active, multi-stage cascade impactor designs were used to improve the ability of the collectors to separate drops into distinct fractions not possible with strand or passive designs.

The FROSTY collector for size-resolved sampling of super-cooled drops in mixed-phase clouds has been used twice in the field. Field performance validation indicates that FROSTY appears to operate more successfully than the Caltech Heated Rod Cloud water Collector (CHRCC) in extreme conditions. However, while the data available are limited, there appear to be one or more factors that inhibit its ability to collect the drop volume predicted on each stage. A likely candidate is that the aspiration efficiency for the collectors may not be 100% for the sampling conditions. This is consistent with the variation in collected mass results observed for the different ambient conditions at Horsetooth and Storm Peak Laboratory. Despite this, it does appear to collect three distinct fractions of varying composition that compare reasonably well to the bulk composition measured by the CHRCC. The reasonable comparison for composition and mass between FROSTY and the CHRCC should not obscure the fact that the drop populations sampled may not necessarily be the same. Similar size-dependent super-cooled drop composition was observed on both the Eastern and Western slopes of the Rockies with the

Reproduced with permission of the copyright owner. Further reproduction prohibited without permission.

smaller drops tending to be more concentrated for most species. The "U-shaped" composition profiles for non-precipitating cloud drops described in the Introduction with Region I ("growth to equilibrium") and Region II ("growth by condensation") are observed for many species. FROSTY provides super-cooled drop size-dependent chemical composition not previously achievable in our group, although optimal sample handling after collection may require further investigation. In the future, FROSTY must also be limited to use in clouds where drops will freeze upon impaction.

The 5-Stage collector for measuring size-resolved composition of warm clouds is unique in that it is the only single collector designed to separate drops into five fractions with reasonable temporal resolution. Its first results are promising. While only limited data are available, it appears in the field to collect drops on the stages predicted. The predicted interstage losses appear to be both real and remain uncollected. In order to facilitate comparison to the 5-Stage, the field performance of both the sf-CASCC and the CASCC2 were evaluated. Collected mass and bulk/derived "bulk" composition comparisons for all of the data available between the sf-CASCC and CASCC2 were consistent with the sub-set of data corresponding to 5-Stage sampling periods. The collected water masses from the CASCC2 and sf-CASCC were used to revise the LWC measurements provided by the PVM in large drop fogs at Davis. The results suggest that the CASCC2's collected water mass may be over-predicted by about 20%. They also indicate that a Fluent modeled collection efficiency curve for the sf-CASCC appears to be more representative of actual collection than a collection efficiency curve derived from simple theory. There appear to be significant unexplained mass losses in the Small drop fraction of the sf-CASCC. Total collected mass and derived "bulk" composition compare well between the 5-Stage and the sf-CASCC for conditions ranging from radiation fogs to "moderate" (e.g. wind speeds < 10 m s^{-1}) orographic clouds. Both comparisons to the CASCC2 are also generally good. However, for low LWC fogs with strongly size-dependent composition, the sf-CASCC and 5-Stage derived "bulk" compositions agree, but differ from the CASCC2's. The reasons for this cannot be resolved with the data available.

Reproduced with permission of the copyright owner. Further reproduction prohibited without permission.

Data from the sf-CASCC are reported for the ACE2 HILLCLOUD project. Our data is consistent with the results reported by other investigators. The data can be generally separated into four groups – Large and Small fractions for both polluted and clean events. The Large polluted and both fractions in clean events have similar relative compositions and are dominated by sodium and chloride ions. The Small polluted fraction has a different signature and high concentrations of ammonium and sulfate, too. The polluted events show some evidence of atmospheric processing and the influence of anthropogenic activity. Cloud composition ratios between selected species vary from those predicted based solely upon mean sea water. As only two drop size fractions were obtained, we cannot describe our observations in terms of the interpretative Region I and Region II model of size-dependent cloud drop composition.

At both Whiteface Mtn., NY and Davis, CA, the 5-Stage collector provides a better measure of the actual drop size-dependent composition than previously available with the two-stage sf-CASCC. While the sf-CASCC suggests the drop composition at Whiteface for sulfate, nitrate and ammonium is largely independent of drop size, the 5-Stage data indicate that there can be up to at least a factor of two difference between the maximum and minimum observed drop concentrations for a given species. For Davis, the concentration difference for the major ions between the Large and Small sf-CASCC fractions is typically a factor of 5, but the 5-Stage data suggest that the variation actually can exceed a factor of 15 – 20.

Both Whiteface and Davis 5-Stage composition profiles can be interpreted using the Region I and Region II size-dependent drop composition model. While insufficient data were gathered to make definitive conclusions possible, the Whiteface results show evidence for both regions. Distinct "U-shaped" profiles are observed for most major and minor measured species. This result is consistent with the modeling results and observations reported for "fresh" orographic clouds (Schell *et al.*, 1997b), although the CCN upstream of Whiteface have probably been activated several times prior to reaching the site. The aging of the CCN may minimize drop size-dependent composition at Whiteface. The Davis concentration profiles from the 5-Stage are consistent with

Reproduced with permission of the copyright owner. Further reproduction prohibited without permission.

those reported for Po Valley fogs showing a sharply decreasing concentration gradient for most species from the smallest drops (approximately < 11 μm) into the larger ones. No evidence for Region II was observed. The absence of high concentrations of coarse mode aerosol can account for this observation which is consistent with aerosol measurements between the fogs and modeling results (Schell *et al.*, 1997b). High concentrations of insoluble species are also a factor in these results. For both locations, the patterns observed in the 5-Stage data were consistent although they varied between species. It is important to emphasize that the detailed modeling efforts supporting the concept of the "growth to equilibrium" and "growth by condensation" regions do generally not include all the heterogeneity in CCN size and composition possible in the clouds measured, and also all of the possible physical processes occurring in-cloud. Therefore, it is not surprising that there is a rich variation in size-dependent drop composition observed for both volatile and non-volatile species. While nitrate, sulfate, ammonium and the hydrogen ion dominate the observed 5-Stage drop composition at Whiteface, calcium ion may also be an important component of the larger drops. Modeling work using these data sets may improve the interpretation of the observations.

The 5-Stage data also proved useful for interpreting observations of the Davis fog and its impact on ambient species concentrations. Observations of size-resolved nitrite and copper drop concentrations in Davis suggest that copper is present in high enough concentrations to affect drop redox chemistry and that HONO may be present in concentrations up to 2 ppbv during the fog events studied. Nitric acid and nitrate appear to be at equilibrium between the gas- and aqueous--phases in the fog, but ammonia and ammonium may not be. Larger drops may be sub-saturated in ammonium and smaller drops may be super-saturated. Some evidence suggests that nitrite and nitrous acid are not at equilibrium between phases for all conditions, but that cannot be resolved with the data available. For all of these observations, data available from the 5-Stage provided insights not available from the other collectors or equipment.

Reproduced with permission of the copyright owner. Further reproduction prohibited without permission.

While the 5-Stage provides increased resolution of the drop size-dependent chemical composition which varies between locations and species, using the 5-Stage data to derive continuous drop size-dependent composition profiles suggests that additional variation may exist but remains uncaptured. While mixing between drop sizes is relatively limited in the 5-Stage compared to other collectors, the five measured fractions still represent the mean composition of a group of drops of varying sizes. The observed composition may, in fact, reflect some sampling artifact from the mixing, although if cloud drops are externally mixed (as evidence suggests) this cannot be resolved at any level less than single-drop resolution. In addition, the sampling periods required to obtain sample, particularly in radiation fogs, are longer than the time scales of change in the fog's microphysical structure. While the time necessary to obtain sufficient sample has been reduced from some of the earlier multi-stage collectors, the 5-Stage still averages over microphysical changes that may produce sampling artifacts in the measured drop fractions.

Many of the comparisons between the three collectors or between duplicate aliquots obtained from the same collector suggest that analytical uncertainty alone – although easily quantifiable – is not necessarily representative of the actual variability. This raises again the difficulty in determining based upon the measured data how "representative" a drop sample actually is. The observations of drop composition are not independent of the collector, sampling and handling methodology, or ambient conditions used to obtain them. It is necessary to resolve the collected mass prediction problems for some collectors and sampling conditions to understand this effect further. Size-dependent drop composition cannot be interpreted without knowledge of the cloud microphysics as well.

10.2 Recommendations

The preceding chapters suggest that field work is sometimes very successful. At other times equipment malfunction or other problems limit the ability to both collect and/or interpret data. It cannot be emphasized enough that each cloud event represents only one unique sampling

Reproduced with permission of the copyright owner. Further reproduction prohibited without permission.

opportunity. As data from only five of the seven campaigns described in the Acknowledgements are included here, some campaigns did not even present one "good" opportunity to sample cloud water. Therefore, every preparatory step possible to ensure successful sampling must be taken which includes adequate training, documentation, oversight, and proven/tested sampling and analytical protocols (including methodology, calibration, and accuracy checks). Cloud sampling techniques and the development of analytical protocols should not be left to the biases of each new investigator. In particular, collector set-up and orientation must not be neglected and analytical methodology and data evaluation must be carefully reviewed. That does not mean to imply that there is not ample room for improvement in existing protocols and techniques including those described herein, but that a common ground must be clearly established, documented and maintained as it evolves. The data produced cannot be correctly interpreted if the underlying details of how it was gathered are unknown. In my opinion, this does not "average out" between investigators and the assumption that the underlying details can be neglected is not necessarily justified. While there is no substitute for experience and we all make mistakes, we all should be able to benefit from the lessons learned, and every step taken to minimize the unquantifiable uncertainty. The goal is to make consistent and accurate observations.

The interpretation of future cloud observations would be improved if the collection efficiency curves of the Caltech family of cloud water collectors were investigated further either numerically or experimentally in the laboratory. There appear to be deficiencies in some of the theoretical curves which compromise the ability to predict collected mass, particularly in the Small fraction of the sf-CASCC. The aspiration and transmission efficiency of all of the collectors – including the 5-Stage and particularly FROSTY – may benefit from being modeled numerically. While sampling in ambient conditions will always present challenges, some insight into the collectors' overall performance will be gained. The isokinetic inlets used by other investigators (see Appendix B) are not the only solution and, in particular, as they are converging nozzles some transmission losses are likely to still occur. It would be useful to extend this analysis to the aspiration and transmission efficiency of the CSASP in order to improve interpretation of its drop

Reproduced with permission of the copyright owner. Further reproduction prohibited without permission.

size-distribution measurements. It may be useful to more thoroughly review the drop shattering literature available in the cloud physics literature to improve our understanding of the important parameter values for drop shattering.

Observations in radiation fogs would be improved by a thorough investigation of calm air sampling and how the overall sampling efficiencies of the 5-Stage, sf-CASCC, CASCC2, and CSASP are affected. The performance of the PVM-100 should continue to be evaluated carefully in radiation fogs. While it is not possible to resolve the differences in composition observed between the collectors during the D009 and D010 events, the conditions that produced these results (e.g. low LWC and strongly size-dependent drop composition) may be common in fogs. The possible reasons behind the discrepancies should be determined. The 5-Stage collection efficiency curves should be extended beyond their current experimental limits of 4 – 34 μm to enhance the ability to evaluate its performance in radiation fogs. At the same time it would be useful to evaluate if any of the collectors have an "upper limit" for successfully aspirated, transmitted and sampled drops. The current fog sampling stands for the CASCC2, sf-CASCC and 5-Stage used in radiation fogs vary in elevation by approximately 2 m. It would be useful in future fog campaigns to co-locate a CASCC2, sf-CASCC (or both) vertically with the 5-Stage to investigate if variations in drop composition or collected dust occur.

Interpretation of the uncertainty inherent in field measurements would be aided by a greater emphasis on preparing duplicate aliquots in the field – particularly for the Metals (Fe, Mn and Cu). The variation in field pH measurements should also be evaluated as it may vary from laboratory evaluations. An increased emphasis should be placed upon the quantification of residual collected mass within the collectors and minimizing the uncertainty in collected mass measurements in the field. Because of the limited mass usually collected in the 5-Stage in fogs, it may be better to extend the length of its sampling period to obtain only one size-resolved drop composition sample per event. The flow rate through the sf-CASCC and CASCC2 should not be estimated, but rather measured while sampling. Due to the high degree of turbulence within the

Reproduced with permission of the copyright owner. Further reproduction prohibited without permission.

collectors, pitot tubes and hot-wire anemometers placed in poorly-located ports on the collector body are likely inadequate for this task.

As the results indicate, collector performance can vary between locations. Therefore collector performance validation must be determined for each event within each campaign to the degree possible. Field project planning should always incorporate this as one of the goals. As up to a factor of 2 difference in major ion concentration is observed in the same cloud (D009 and D010) by two reasonably well-characterized and maintained collectors (CASCC2 and sf-CASCC), this raises issues about what kind of difference must be observed between clouds at different locations and times to constitute "trends" in concentration. Many poorly-characterized features of the cloud water collectors or collection techniques (e.g. the flow rate; the tautness, alignment and thickness of the collection strands; dry deposition; among others), and the fact that single location drop collection data is generally only available suggest, in my opinion, that consistent differences may need to exceed an order of magnitude to have defensibly "different" composition between clouds. While it is difficult to determine an absolute composition difference needed in this hypothetical case, our Davis results suggest at least a factor of 2 is not enough. Further, as indicated in the Conclusions, drop composition needs to be considered in the context of cloud microphysics.

In future campaigns, size-resolved aerosol composition may be better measured more coarsely (e.g. < 1 μm and > 1 μm in diameter) at a higher volumetric flow rate in order to limit sampling periods. These data could be supplemented by more finely size-resolved MOUDI data gathered over a longer sampling period. Gas-phase HONO measurements at high time resolution would usefully complement aqueous-phase measurements of nitrite in Davis (or similar) fogs, and measurements of copper may also be warranted. If gas/liquid equilibria are going to be investigated further, higher resolution measurements of gas-phase ammonia are also warranted. It would also be useful to measure the fog (or cloud) physical parameters. For example, the exact location of fog (or cloud) height, the collectors' position relative to fog (or cloud) base and

Reproduced with permission of the copyright owner. Further reproduction prohibited without permission.

improved characterization of the fog (or cloud) microphysical structure would assist the interpretation of drop composition and deposition measurements. However, it must be remembered that the fog is not a closed system and advection/entrainment of gas- and solid-phase species into the fog are likely (and difficult to quantify). Modeling has the potential to lend some insight here, but many important parameters must be assumed as measurements remain inadequate.

To understand size-dependent cloud drop composition, observations and modeling complement each other and are both needed. The time-averaged data provided by field studies is not, in many cases, ideal for modeling where "instantaneous" values are required. It would be useful to extend the capabilities of models to include the effects of drop sampling on observations (e.g. mixing effects, non-ideal aspiration of the drop population into the collector). Improving observations for modeling probably requires enhancing the temporal resolution of the measurements while at the same time obtaining enough sample to achieve minimal analytical uncertainty. While the differences between data requirements for modeling and possible observations are in many ways intractable, there is some margin for improvement from both. Each approach provides insight into understanding the chemistry of clouds.

Reproduced with permission of the copyright owner. Further reproduction prohibited without permission.

11. References

Acker, K., Möller, D., Wieprecht, W., Auel, R. and Kalaß, D., 2001. Results of cloud physical and chemical measurements in low clouds observed at Mt. Brocken, Germany. In: R.S. Schemenauer and H. Puxbaum (Editors), 2nd International Conference on Fog and Fog Collection, St. John's, Newfoundland, Canada, pp. 117 - 120.

Acker, K., Möller, D., Wieprecht, W., Kalaß, D. and Auel, R., 1998. Investigations of ground-based clouds at the Mt. Brocken. *Fresenius Journal of Analytical Chemistry*, 361: 59 - 64.

Adzuhata, T., Okamura, T., Inotsume, J., Kikuchi, R., Ozeki, T., Kajikawa, M. and Ogawa, N., 2001. A proposed fog uptake mechanism of air pollutant in Northern Japan using oblique rotational factor analysis. In: R.S. Schemenauer and H. Puxbaum (Editors), 2nd International Conference on Fog and Fog Collection, St. John's, Newfoundland, Canada, pp. 25 - 28.

Agarwal, J.K. and Liu, B.Y.H., 1980. A criterion for accurate aerosol sampling in calm air. *American Industrial Hygiene Association Journal*, 41: 191-197.

Anastasio, C. and McGregor, K.G., 2001. Chemistry of fog water in California's Central Valley: 1. in situ photoformation of hydroxyl radical and singlet molecular oxygen. *Atmospheric Environment*, 35: 1079 - 1089.

Anderson, D.E. and Landsberg, H.E., 1979. Detailed structure of pH in hydrometeors. *Environmental Science and Technology*, 13(8): 992 - 994.

Anderson, J.B., Baumgardner, R.E., Mohnen, V.A. and Bowser, J.J., 1999. Cloud chemistry in the eastern United States, as sampled from three high-elevation sites along the Appalachian mountains. *Atmospheric Environment*, 33: 5105 - 5114.

Anderson, T.L., Charlson, R.J. and Covert, D.S., 1993. Calibration of a Counterflow Virtual Impactor at aerodynamic diameters from 1 to 15 µm. *Aerosol Science and Technology*, 19: 317 - 329.

Andre, K., Dlugi, R. and Schnatz, G., 1981. Absorption of visible radiation by atmospheric aerosol particles, fog and cloud water residues. *Journal of the Atmospheric Sciences*, 38: 141 - 155.

Arends, B.G., Kos, G.P.A. and Möls, H.J., 1997. Field and wind tunnel experiments in clouds and fog by ECN. In: S. Fuzzi and D. Wagenbach (Editors), Cloud multi-phase processes and high alpine air and snow chemistry. Springer-Verlag, Berlin, pp. 61 - 67.

Arends, B.G., Kos, G.P.A., Wobrock, W., Schell, D., Noone, K.J., Fuzzi, S. and Pahl, S., 1992. Comparison of techniques for measurements of fog liquid water content. *Tellus*, 44B: 604-611.

Reproduced with permission of the copyright owner. Further reproduction prohibited without permission.

Arnulf, A., Bricard, J., Curé, E. and Véret, C., 1957. Transmission by haze and fog in the spectral region 0.35 to 10 microns. *Journal of the Optical Society of America*, 47(6): 491 - 498.

Audiffren, N., Renard, M., Buisson, E. and Chaumerliac, N., 1998. Deviations from Henry's law equilibrium during cloud events: a numerical approach of the mass transfer between phases and its specific numerical effects. *Atmospheric Research*, 49: 139 - 161.

Ayers, G.P. and Larson, T.V., 1990. Numerical study of droplet size dependent chemistry in oceanic, wintertime stratus cloud at southern mid-latitudes. *Journal of Atmospheric Chemistry*, 11: 143 - 167.

Azevado, J. and Morgan, D.L., 1974. Fog precipitation in coastal California forests. *Ecology*, 55: 1135 - 1141.

Baechmann, K., Ebert, P., Haag, I., Prokop, T. and Steigerwald, K., 1996. The chemical composition of raindrops as a function of drop radius -- II. field experimental study on the scavenging of marked aerosol particles by raindrops sampled as a function of drop size. *Atmospheric Environment*, 30(7): 1027 - 1033.

Baker, B., Baker, M.B., Jayaratne, E.R., Latham, J. and Saunders, C.P.R., 1987. The influence of diffusional growth rates on the charge transfer accompanying rebounding collisions between the ice crystal and soft hailstones. *Quarterly Journal of the Royal Meteorological Society*, 113: 1193 - 1215.

Baltensperger, U., Schwitkowski, M., Jost, D.T., Nyeki, S., Gäggeler, H.W. and Poulida, O., 1998. Scavenging of atmospheric constituents in mixed phase clouds at the high-alpine site Jungfraujoch Part 1: basic concept and aerosol scavenging by clouds. *Atmospheric Environment*, 32(23): 3975 - 3983.

Basabe, F.A., Edmonds, R.L., Chang, W.L. and Larson, T.V., 1989. Fog and cloud water chemistry in Western Washington. In: R.K. Olson and A.S. Lefohn (Editors), Effects of air pollution on Western Forests. Air and Waste Management Association, Anaheim, CA, pp. 33 - 49.

Bator, A. and Collett, J.L., Jr., 1997. Cloud chemistry varies with drop size. *Journal of Geophysical Research: Atmospheres*, 102: 28,071 - 28,078.

Baumgardner, D., 1995. Status of in-situ cloud microphysical measurements, ETL/CSU Cloud-related Process Modeling and Measurement Workshop, Boulder, CO, pp. 67-102.

Baumgardner, D. and Spowart, M., 1990. Evaluation of the Forward Scattering Spectrometer Probe. Part III: Time response and laser inhomogeneity limitations. *Journal of Atmospheric and Oceanic Technology*, 7: 666-672.

Baumgardner, D., Strapp, W. and Dye, J.E., 1985. Evaluation of the Forward Scattering Spectrometer Probe. Part II: Corrections for coincidence and dead-time losses. *Journal of Atmospheric and Oceanic Technology*, 2: 626-632.

Baumgardner, D., 1983. An analysis of five water droplet measuring instruments. *Journal of Applied Meteorology*, 22: 891-910.

Behra, P. and Sigg, L., 1990. Evidence for redox cycling of iron in atmospheric water droplets. *Nature*, 344: 419 - 421.

Reproduced with permission of the copyright owner. Further reproduction prohibited without permission.

Behra, P., Sigg, L. and Stumm, W., 1989. Dominating influence of NH_3 on the oxidation of aqueous SO_2: the coupling of NH_3 and SO_2 in atmospheric water. *Atmospheric Environment*, 23(12): 2691 - 2707.

Berg, N., Dunn, P. and Fenn, M., 1991. Spatial and temporal variability of rime ice and snow chemistry at fives sites in California. *Atmospheric Environment*, 25A(5/6): 915 - 926.

Berner, A., Dusek, U., Galambos, Z. and Kruisz, C., 1998. Sampling of fog droplets by cascade impactors. *Contributions to Atmospheric Physics*, 71(1): 101-114.

Berner, A. and Kruisz, C., 1997. High alpine air, aerosol, and cloud chemistry. In: S. Fuzzi and D. Wagenbach (Editors), Cloud Multi-phase Processes and High Alpine Air and Snow Chemistry. Springer-Verlag, Berlin, pp. 235 - 240.

Berner, A., 1996. personal communication

Berner, A., 1988. The collection of fog droplets by a jet impaction stage. *The Science of the Total Environment*, 73: 217 - 228.

Berner, A., Reischl, G., Enderle, K.H., Jaeschke, W., Fuzzi, S., Orsi, G. and Facchini, M.-C., 1988. The liquid water content of a radiation fog measured by an FSSP-100 optical probe and a fog impactor. *The Science of the Total Environment*, 77: 133 - 140.

Bin, L. and Wenquan, S., 1996. Analyses of several chemical composition of the stratus in north along Mt. Tianshan in Xinjiang in winter, 12th International Conference on Clouds and Precipitation, Zurich, Switzerland, pp. 1125 - 1127.

Bird, R.B., Stewart, W.E. and Lightfoot, E.L., 1960. Transport Phenomena. John Wiley & Sons, New York, 780 pp.

Bloudoff, D., 2001. Cal-EPA. personal communication

Borys, R.D., Lowenthal, D.H. and Mitchell, D.L., 2000. The relationships among cloud microphysics, chemistry, and precipitation rate in cold mountain clouds. *Atmospheric Environment*, 34: 2593 - 2602.

Borys, R.D., Lowenthal, D.H., Wetzel, M.A., Herrera, F., Gonzalez, A. and Harris, J., 1998. Chemical and microphysical properties of marine stratiform cloud in the north Atlantic. *Journal of Geophysical Research*, 103(D17): 22,073 - 22,085.

Borys, R.D., Hindman, E.E. and DeMott, P.J., 1988. The chemical fractionation of atmospheric aerosol as a result of snow crystal formation and growth. *Journal of Atmospheric Chemistry*, 7: 213 - 239.

Bott, A., 1999. A numerical model of the cloud-topped boundary-layer: chemistry in marine stratus and the effects on aerosol particles. *Atmospheric Environment*, 33: 1921 - 1936.

Bott, A. and Carmichael, G.R., 1993. Multiphase chemistry in a microphysical radiation fog model - a numerical study. *Atmospheric Environment*, 27A: 503 - 522.

Bott, A., 1991. On the influence of the physico-chemical properties of aerosols on the life cycle of radiation fogs. *Boundary Layer Meteorology*, 56: 1 - 31.

Reproduced with permission of the copyright owner. Further reproduction prohibited without permission.

Bott, A., Sievers, U. and Zdunkowski, W., 1990. A radiation fog model with a detailed treament of the interaction between radiative transfer and fog microphysics. *Journal of the Atmospheric Sciences*, 47(18): 2153 - 2166.

Bower, K.N., Choularton, T.W., Gallagher, M.W., Beswick, K.M., Flynn, M.J., Allen, A.G., Davison, B.M., James, J.D., Robertson, L., Harrison, R.M., Hewitt, C.N., Cape, J.N., McFadyen, G.G., Milford, C., Sutton, M.A., Martinsson, B.G., Frank, G., Swietlicki, E., Zhou, J., Berg, O.H., Mentes, B., Papaspiropoulos, G., Hansson, H.-C., Leck, C., Kulmala, M., Aalto, P., Väkevä, M., Berner, A., Bizjak, M., Fuzzi, S., Laj, P., Facchini, M.-C., Orsi, G., Ricci, L., Nielsen, M., Allan, B.J., Coe, H., McFiggans, G., Plane, J.M.C., Collett, J.L., Jr., Moore, K.F. and Sherman, D.E., 2000. ACE-2 HILLCLOUD. An overview of the ACE-2 ground-based cloud experiment. *Tellus*, 52B(2): 750-778.

Bower, K.N., Jones, A. and Choularton, T.W., 1999a. A modelling study of aerosol processing by stratocumulous clouds and its impact on general circulation model parameterizations of cloud and aerosol. *Atmospheric Research*, 50: 317 - 344.

Bower, K.N., Choularton, T.W., Gallagher, M.W., Colville, R.N., Beswick, K.M., Inglis, D.W.F., Bradbury, C., Martinsson, B.G., Swietlicki, E., Berg, O.H., Cederfelt, S.-I., Frank, G., Zhou, J., Cape, J.N., Sutton, M.A., McFadyen, G.G., Milford, C., Birmili, W., Yuskiewicz, B., Wiedensohler, A., Stratmann, F., Wendisch, M., Berner, A., Ctyroky, P., Galambos, Z., Mesfin, S.H., Dusek, U., Dore, C.J., Lee, D.S., Pepler, S.A., Bizjak, M. and Divjak, B., 1999b. The Great Dun Fell Experiment 1995: an overview. *Atmospheric Research*, 50: 151 - 184.

Bower, K.N., Choularton, T.W., Gallagher, M.W., Colvile, R., Wells, M., Beswick, K.M., Wiedensohler, A., Hansson, H.-C., Svenningsson, B., Swietlicki, E., Wendisch, M., Berner, A., Kruisz, C., Laj, P., Facchini, M.-C., Fuzzi, S., Bizjak, B., Dollard, G.J., Jones, B., Acker, K., Wieprecht, W., Preiss, M., Sutton, M.A., Hargreaves, K.J., Storeton-West, R.L., Cape, J.N. and Arends, B.G., 1997. Observations and modelling of the processing of aerosol by a hill cap cloud. *Atmospheric Environment*, 31(16): 2527 - 2544.

Bower, K.N., Hill, T.A., Coe, H. and Choularton, T.W., 1991. SO_2 oxidation in an entraining cloud model with explicit microphysics. *Atmospheric Environment*, 25A(10): 2401 - 2418.

Bradbury, C., Bower, K.N., Choularton, T.W., Swietlicki, E., Birmili, W., Wiedensohler, A., Yuskiewicz, B., Berner, A., Dusek, U., Dore, C. and McFadyen, G.G., 1999. Modelling of aerosol modification resulting from passage through a hillcap cloud. *Atmospheric Research*, 50: 185 - 204.

Brantner, B., Fierlinger, H., Puxbaum, H. and Berner, A., 1994. Cloudwater chemistry in the subcooled droplet regime at Mount Sonnblick (3106 m asl, Salzburg, Austria). *Water, Air and Soil Pollution*, 74: 363 - 384.

Brenguier, J.L., Baumgardner, D. and Baker, B., 1994. A review and discussion of processing algorithms for FSSP concentration measurements. *Journal of Atmospheric and Oceanic Technology*, 11: 1409-1414.

Brenguier, J.L., 1989. Coincidence and dead-time corrections for particle counters. Part II: high concentration measurements with an FSSP. *Journal of Atmospheric and Oceanic Technology*, 6: 585-598.

Brenguier, J.L. and Amodei, L., 1989. Coincidence and dead-time corrections for particle counters. Part I: a general mathematical formalism. *Journal of Atmospheric and Oceanic Technology*, 6: 575-584.

Reproduced with permission of the copyright owner. Further reproduction prohibited without permission.

Brenguier, J.-L., Bourrianne, T., de Araujo Coelho, A., Isbert, J., Peytavi, R., Trevarin, D. and Weschler, P., 1998. Improvements of droplet size distribution measurements with the Fast-FSSP (Forward Scattering Spectrometer Probe). *Journal of Atmospheric and Oceanic Technology*, 15: 1077-1090.

Bressan, D.J. and Larson, R.E., 1979. The history of air forming various marine fogs of Nova Scotia in August 1975. *Journal of Geophysical Research*, 84(C4): 1746 - 1754.

Brewer, R.L., Gordon, R.J., Shepard, L.S. and Ellis, E.C., 1983. Chemistry of mist and fog from the Los Angeles urban area. *Atmospheric Environment*, 17(11): 2267 - 2270.

Bridges, K.S., 1998. Deposition processes and their impact on a heavily industrialized region of the northern Czech Republic. Ph.D. Dissertation, School of Environmental Sciences, University of East Anglia.

Brockmann, J.E., 1993. Sampling and transport of aerosols. In: K. Willeke and P.A. Baron (Editors), Aerosol Sampling: Principles, Techniques, and Applications. Van Nostrand Reinhold, New York, NY, pp. 77-111.

Brown, R. and Roach, W.T., 1976. The physics of radiation fog: II - a numerical study. *Quarterly Journal of the Royal Meteorological Society*, 102: 335 - 354.

Brun, R.J., Lewis, W., Perkins, P.J. and Serafini, J.S., 1955. Impingement of cloud droplets on a cylinder and procedure for measuring liquid-water content and droplet sizes in supercooled clouds by rotating multicylinder method. Report #1215, National Advisory Committee for Aeronautics, Washington, D.C.

Burkhard, R., Eugster, W. and Thalmann, E., 2000. A direct method for fog and cloud droplet deposition flux measurements. *EOS, transactions*, 81(48): F64 - F65.

Bytnerowicz, A., Carroll, J.J., Takemoto, B.K., Miller, P.R., Fenn, M.E. and Musselman, R.C., 2000. Distribution and transport of air pollutants to vulnerable California ecosystems. In: K.M. Scow, G.E. Fogg, D.E. Hinton and M.L. Johnson (Editors), Integrated assessment of ecosystem health. Lewis Publishers, Boca Raton, FL, pp. 93 - 118.

Calvert, J.G., Yarwood, G. and Dunker, A.M., 1994. An evaluation of the mechanism of HONO formation in the urban atmosphere. *Res. Chemical Intermediates*, 20(3/4/5): 463 - 502.

Cape, J.N., Hargreaves, K.J., Storeton-West, R.L., Jones, B., Davies, T., Colvile, R., Gallagher, M.W., Choularton, T.W., Pahl, S., Berner, A., Kruisz, C., Bizjak, M., Laj, P., Facchini, M.-C., Fuzzi, S., Arends, B.G., Acker, K., Wieprecht, W., Harrison, R.M. and Peak, J.D., 1997. The budge of oxidized nitrogen species in orographic clouds. *Atmospheric Environment*, 31(16): 2625 - 2636.

Cape, J.N., Hargreaves, K.J., Storeton-West, R.L., Fowler, D., Colvile, R., Choularton, T.W. and Gallagher, M.W., 1992. Nitrite in orographic cloud as an indicator of nitrous acid in rural air. *Atmospheric Environment*, 26A(13): 2301 - 2307.

Carter, E.J. and Borys, R.D., 1993. Aerosol-cloud chemical fractionation: enrichment factor analysis of cloud water. *Journal of Atmospheric Chemistry*, 17: 277 - 292.

Castillo, R.A. and Jiusto, J.E., 1984. A preliminary study of the chemical modification of cloud condensation nuclei in stratiform clouds at Whiteface Mountain, NY. *Atmospheric Environment*, 18(9): 1933 - 1937.

Reproduced with permission of the copyright owner. Further reproduction prohibited without permission.

Castillo, R.A., Jiusto, J.E. and McLaren, E., 1983. The pH and ionic composition of stratiform cloud water. *Atmospheric Environment*, 17(8): 1497 - 1505.

Castillo, R.A. and Jiusto, J.E., 1983. Characteristics of non-precipitating stratiform clouds. In: H.R. Pruppacher, R.G. Semonin and W.G.N. Slinn (Editors), Precipitation Scavenging, Dry Deposition, and Resuspension. Elsevier, New York, NY, pp. 115 - 122.

Cerni, T.A., 1983. Determination of the size and concentration of cloud drops with an FSSP. *Journal of Climate and Applied Meteorology*, 22: 1346-1355.

Chang, W.-L., 1989. Characterization of cloud and fog water in the mountains of western Washington. M. S. Thesis, Department of Civil Engineering, University of Washington. Seattle, WA.

Charlson, R.J., Seinfeld, J.H., Nenes, A., Kulmala, M., Laaksonen, A. and Facchini, M.-C., 2001. Reshaping the theory of cloud formation. *Science*, 292: 2025 - 2026.

Chérif, S., Millet, M., Sanusi, A., Herckes, P. and Wortham, H., 1998. Protocol for analysis of trace metals and other ions in filtered and unfiltered fog water. *Environmental Pollution*, 103: 301 - 308.

Choularton, T.W., Colvile, R., Bower, K.N., Gallagher, M.W., Wells, M., Beswick, K.M., Arends, B.G., Möls, J.J., Kos, G.P.A., Fuzzi, S., Lind, J., Orsi, G., Facchini, M.-C., Laj, P., Gieray, R., Wieser, P., Engelhardt, T., Berner, A., Kruisz, C., Möller, D., Acker, K., Wieprecht, W., Lüttke, J., Levsen, K., Bizjak, B., Hansson, H.-C., Cederfelt, S.-I., Frank, G., Mentes, B., Martinsson, B.G., Orsini, D., Svenningsson, B., Swietlicki, E., Wiedensohler, A., Noone, K.J., Pahl, S., Winkler, P., Seyffer, E., Helas, G., Jaeschke, W., Georgii, H.-W., Wobrock, W., Preiss, M., Maser, R., Schell, D., Dollard, G.J., Jones, B., Davies, T., Sedlak, D.L., David, M.M., Wendisch, M., Cape, J.N., Hargreaves, K.J., Sutton, M.A., Storeton-West, R.L., Fowler, D., Hallberg, A., Harrison, R.M. and Peak, J.D., 1997. The Great Dun Fell Cloud Experiment 1993: an overview. *Atmospheric Environment*, 31(16): 2393 - 2407.

Choularton, T.W., Consterdine, I.E., Gardiner, B.A., Gay, M.J., Hill, M.K., Latham, J. and Stromberg, I.M., 1986. Field studies of the optical and microphysical characteristics of clouds enveloping Great Dun Fell. *Quarterly Journal of the Royal Meteorological Society*, 112: 131-148.

Choularton, T.W., Fullarton, G., Latham, J., Mill, C.S., Smith, M.H. and Stromberg, I.M., 1981. A field study of radiation fog in Meppen, West Germany. *Quarterly Journal of the Royal Meteorological Society*, 107: 381 - 394.

Chow, J.C., Watson, J.G., Lu, Z., Lowenthal, D.H., Frazier, C.A., Solomon, P.A., Thuillier, R.H. and Magliano, K., 1996. Descriptive analysis on $PM_{2.5}$ and PM_{10} at regionally representative locations during SJVAQS/AUSPEX. *Atmospheric Environment*, 30(12): 2079 - 2112.

Chow, J.C., Watson, J.G., Lowenthal, D.H., Solomon, P.A., Magliano, K., Ziman, S.D. and Richards, L.W., 1993. PM_{10} and $PM_{2.5}$ composition in California's San Joaquin Valley. *Aerosol Science and Technology*, 18: 105 - 128.

Chuang, P.Y., Charlson, R.J. and Seinfeld, J.H., 1997. Kinetic limitations on droplet formation in clouds. *Nature*, 390: 594 - 596.

Reproduced with permission of the copyright owner. Further reproduction prohibited without permission.

Chung, Y.S., Kim, H.S. and Yoon, M.B., 1999. Observations of visibility and chemical composition related to fog, mist and haze in South Korea. *Water, Air and Soil Pollution*, 111: 139 - 157.

Collett, J.L., Jr., Sherman, D.E., Moore, K.F., Hannigan, M.P. and Lee, T., 2001. Aerosol particle processing and removal by fogs: observations in chemically heterogeneous central California radiation fogs. *Water, Air and Soil Pollution (in press)*.

Collett, J.L., Jr., Hoag, K.J., Sherman, D.E., Bator, A. and Richards, L.W., 1999. Spatial and temporal variations in San Joaquin Valley fog chemistry. *Atmospheric Environment*, 33: 129 - 140.

Collett, J.L., Jr., Iovinelli, R.J. and Demoz, B.B., 1995. A three-stage cloud impactor for size-resolved measurement of cloud drop chemistry. *Atmospheric Environment*, 29(10): 1145 - 1154.

Collett, J.L., Jr., Oberholzer, B. and Staehelin, J., 1993a. Cloud chemistry at Mt. Rigi Switzerland: dependence on drop size and relationship to precipitation chemistry. *Atmospheric Environment*, 27A: 33 - 42.

Collett, J.L., Jr., Daube, B.C., Jr., Munger, J.W. and Hoffmann, M.R., 1990. A comparison of two cloudwater/fogwater collectors: the rotating arm collector and the Caltech active strand cloudwater collector. *Atmospheric Environment*, 24A(7): 1685 - 1692.

Collett, J.L., Jr., Hoag, K.J. and Pandis, S.N., 1998. The influence of drop size-dependent fog chemistry on aerosol production and deposition in San Joaquin Valley fogs, Department of Atmospheric Science, Colorado State University, Fort Collins, CO.

Collett, J.L., Jr., Bator, A., Rao, X. and Demoz, B.B., 1994. Acidity variations across the cloud drop size spectrum and their influence on rates of atmospheric sulfate production. *Geophysical Research Letters*, 21(22): 2393 - 2396.

Collett, J.L., Jr., Oberholzer, B., Mosimann, L., Staehelin, J. and Waldvogel, A., 1993b. Contributions of cloud processes to precipitation chemistry in mixed phase clouds. *Water, Air and Soil Pollution*, 68: 43 - 57.

Collett, J.L., Jr., Prévôt, A.S.H., Staehelin, J. and Waldvogel, A., 1991a. Physical factors influencing winter precipitation chemistry. *Environmental Science and Technology*, 25: 782 - 788.

Collett, J.L., Jr., Daube, B.C., Jr. and Hoffmann, M.R., 1991b. Spatial and temporal variations in precipitation and cloud interception in the Sierra Nevada of central California. *Tellus*, 43B: 390 - 400.

Collett, J.L., Jr., Daube, B.C., Jr., Munger, J.W. and Hoffmann, M.R., 1989. Cloudwater chemistry in Sequoia National Park. *Atmospheric Environment*, 23(5): 999 - 1007.

Colvile, R.H., Sander, R., Choularton, T.W., Bower, K.N., Inglis, D.W.F., Wobrock, W., Schell, D., Svenningsson, B., Wiedensohler, A., Hansson, H.-C., Hallberg, A., Ogren, J.A., Noone, K.J., Facchini, M.-C., Fuzzi, S., Orsi, G., Arends, B.G., Winiwarter, W., Schneider, T. and Berner, A., 1994. Computer modelling of clouds at Kleiner Feldberg. *Journal of Atmospheric Chemistry*, 19: 189 - 229.

Cooper, W.A., 1988. Effects of coincidence on measurements with a Forward Scattering Spectrometer Probe. *Journal of Atmospheric and Oceanic Technology*, 5: 823-832.

Reproduced with permission of the copyright owner. Further reproduction prohibited without permission.

Cossali, G.E., Coghe, A. and Marengo, M., 1997. The impact of a single drop on a wetted solid surface. *Experiments in Fluids*, 22: 463-472.

Crossley, A., Wilson, D.B. and Milne, R., 1992. Pollution in the upland environment. *Environmental Pollution*, 75: 81 - 87.

Crossley, A., 1988. Particles in orographic cloud and implications of their transfer to plant surfaces. In: M.H. Unsworth and D. Fowler (Editors), Acid deposition at high elevation sites. Kluwer Academic Publishers, Dordrecht, pp. 453 - 464.

Dasgupta, P.K., DeCesare, K. and Ullrey, J.C., 1980. Determination of atmospheric sulfur dioxide without tetrachloromercurate(II) and the mechanism of the Schiff reaction. *Analytical Chemistry*, 52: 1912 - 1922.

Daube, B.C., Jr., Kimball, K.D., Lamar, P.A. and Weathers, K.C., 1987. Two new ground-level cloud water sampler designs which reduce rain contamination. *Atmospheric Environment*, 21(4): 893 - 900.

Däumer, B., Niessner, R. and Klockow, D., 1988. Design and calibration of a low volume fog sampler. *Journal of Aerosol Science*, 19(2): 175 - 181.

Davidson, C.I. and Friedlander, S.K., 1978. A filtration model for aerosol dry deposition: application to trace metal deposition from the atmosphere., *Journal of Geophysical Research*, 83(C5): 2343 - 2352.

Davies, C.N., 1968. The entry of aerosols into sampling tubes and heads. *British Journal of Applied Physics (J. Phys. D.) Ser.* 2,(1): 921 - 932.

Dawson, W., 2001. DMT, personal communication

deFelice, T.P., 1997. Investigation of wet acidic deposition episodes capable of damaging red spruce in the Mt. Mitchell State Park. *Atmospheric Research*, 43: 325 - 344.

deFelice, T.P. and Saxena, V.K., 1990. Mechanisms for the operation of 3 cloud water collectors: comparison of mountain-top results. *Atmospheric Research*, 25: 277 - 292.

Del Monte, M. and Rossi, P., 1997. Fog and gypsum crystals on building materials. *Atmospheric Environment*, 31: 1637 - 1646.

Demoz, B.B., Collett, J.L., Jr. and Daube, B.C., Jr., 1996. On the Caltech Active Strand Cloudwater Collectors. *Atmospheric Research*, 41: 47-62.

Dessens, H., 1949. The use of spiders' threads in the study of condensation nuclei. *Quarterly Journal of the Royal Meteorological Society*, 75: 23 - 26.

Devulapalli, S.S.N. and Collett, J.L., Jr., 1994. The influence of riming and frontal dynamics on winter precipitation chemistry in level terrain. *Atmospheric Research*, 32: 203 - 213.

Dixon, R.M. and Charlson, R.J., 1994. Development of a new real-time method for measuring S(IV) in cloud water using a counter-flow virtual impactor. *Tellus*, 46B: 193 - 204.

Dockery, D.W., Schwarz, J. and Spengler, J.D., 1992. Air pollution and daily mortality: associations with particulates and acid aerosols. *Environmental Research*, 59: 362 - 373.

Reproduced with permission of the copyright owner. Further reproduction prohibited without permission.

Dollard, G.J. and Unsworth, M.H., 1983. Field measurements of turbulent fluxes of wind-driven fog drops to a grass surface. *Atmospheric Environment*, 17(4): 775 - 780.

Dong, S. and Dasgupta, P.K., 1987. Fast fluorometric flow injection analysis of formaldehyde in atmospheric water. *Environmental Science and Technology*, 21: 581 - 588.

Dröscher, F., 1986. Design of a fog water collector for chemical analysis. In: H.-W. Georgii (Editor), Atmospheric Pollutants in Forest Areas: Their Deposition and Interception. D. Reidel Publishing Company, Dordrecht, pp. 111 - 128.

Duncan, L.C., 1992. Chemistry of rime and snow collected at a site in the central Washington Cascades. *Environmental Science and Technology*, 26(1): 61 - 66.

Dunnett, S.J. and Ingham, D.B., 1988. An empirical model for the aspiration efficiencies of blunt aerosol samplers oriented at an angle to the oncoming flow. *Aerosol Science and Technology*, 8: 245-264.

Duynkerke, P.G., 1991. Observations of a quasi-periodic oscillation due to gravity waves in a shallow radiation fog. *Quarterly Journal of the Royal Meteorological Society*, 117: 1207 - 1224.

Dye, J.E. and Baumgardner, D., 1984. Evaluation of the Forward Scattering Spectrometer Probe. Part I: Electronic and optical studies. *Journal of Atmospheric and Oceanic Technology*, 1: 329-344.

Eckardt, F.D. and Schemenauer, R.S., 1998. Fog water chemistry in the Namib Desert, Namibia. *Atmospheric Environment*, 32(14/15): 2595 - 2599.

Ekern, P.C., 1979. Direct interception of cloud and fog water, Rain Cistern Symposium, Monterey, CA.

Elbert, W., Hoffmann, M.R., Krämer, M., Schmitt, G. and Andreae, M.O., 2000. Control of solute concentrations in cloud and fog water by liquid water content. *Atmospheric Environment*, 34: 1109 - 1122.

Eliáš, V., Tesar, M. and Buchtele, J., 1995. Occult precipitation: sampling, chemical analysis and process modelling in the Sumava Mts. (Czech Republic) and in the Taunus Mts. (Germany). *Journal of Hydrology*, 166: 409 - 420.

Eriksson, E., 1952a. Composition of atmospheric precipitation I. Nitrogen compounds. *Tellus*, 4: 215 - 232.

Eriksson, E., 1952b. Composition of atmospheric precipitation II. Sulfur, chloride, iodine compounds. Bibliography. *Tellus*, 4: 280 - 303.

Eugster, W., Burkhard, R., Klemm, O. and Wrzesinsky, T., 2001. Fog deposition measurements with the eddy covariance method. In: R.S. Schemenauer and H. Puxbaum (Editors), 2nd International Conference on Fog and Fog Collection, St. John's, Newfoundland, Canada, pp. 193 - 196.

Facchini, M.-C., Fuzzi, S., Lind, J.A., Fierlinger, H., Kalina, M., Puxbaum, H., Winiwarter, W., Arends, B.G., Wobrock, W., Jaeschke, W., Berner, A. and Kruisz, C., 1992a. Phase-partitioning and chemical reactions of low molecular weight organic compounds in fog. *Tellus*, 44B: 533 - 544.

Reproduced with permission of the copyright owner. Further reproduction prohibited without permission.

Facchini, M.-C., Fuzzi, S., Kessel, M., Wobrock, W., Jaeschke, W., Arends, B.G., Möls, J.J., Berner, A., Solly, I., Kruisz, C., Reischl, G., Pahl, S., Hallberg, A., Ogren, J.A., Fierlinger-Oberlinninger, H., Marzorati, A. and Schell, D., 1992b. The chemistry of sulfur and nitrogen species in a fog system - a multiphase approach. *Tellus*, 44B: 505 - 521.

Fairall, C.W., 1984. Interpretation of eddy-correlation measurements of particulate deposition and flux. *Atmospheric Environment*, 18(7): 1329-1337.

Falconer, R.E. and Falconer, P.D., 1980. Determination of cloud water acidity at a mountain observatory in the Adirondack Mountains of New York state. *Journal of Geophysical Research*, 85(C12): 7465 - 7470.

Fang, C.P., Marple, V.A. and Rubow, K.L., 1991. Influence of cross-flow on particle collection characteristics of multi-nozzle impactors. *Journal of Aerosol Science*, 22(4): 403 - 415.

Febo, A., 1994. Nitrous acid in the oxidation processes in urban areas. In: G. Angeletti and G. Restelli (Editors), Physico-chemical Behaviour of Atmospheric Pollutants. European Commission, Luxembourg, pp. 277 - 286.

Fenn, M.E., Poth, M.A., Schilling, S.L. and Grainger, D.B., 2000. Throughfall and fog deposition of nitrogen and sulfur at an N-limited and N-saturated site in the San Bernardino Mountains, southern California. *Canadian Journal of Forest Research*, 30: 1476 - 1488.

Fenn, M.E. and Bytnerowicz, A., 1997. Summer throughfall and winter deposition in the San Bernardino mountains in southern California. *Atmospheric Environment*, 31(5): 673 - 683.

Finlayson-Pitts, B.J. and Pitts, J.N., Jr., 2000. Chemistry of the Upper and Lower Atmosphere: Theory, Experiments, and Applications. Academic Press, San Diego, CA, 969 pp.

Fitzjarrald, D.R. and Lala, G.G., 1986. Observed fine structure in radiation fog, 23rd conference on radiation meteorology and conference on cloud physics. American Meteorological Society, Snowmass, CO, pp. P226 - P228.

Fletcher, N.H., 1969. The Physics of Rain Clouds. Cambridge University Press, Cambridge.

Flossmann, A.I., Pruppacher, H.R. and Topalian, J.H., 1987. A theoretical study of the wet removal of atmospheric pollutants. Part II: the uptake and redistribution of $(NH_4)_2SO_4$ particles and SO_2 gas simultaneously scavenged by growing cloud drops. *Journal of the Atmospheric Sciences*, 44(20): 2912 - 2923.

Flossmann, A.I., Hall, W.D. and Pruppacher, H.R., 1985. A theoretical study of the wet removal of atmospheric pollutants. Part I: the redistribution of aerosol particles captured through nucleation and impaction scavenging by growing cloud drops. *Journal of the Atmospheric Sciences*, 42(6): 583 - 606.

Flynn, M.J., Bower, K.N., Choularton, T.W., Wobrock, W., Mäkelä, J.M., Martinsson, B.G., Frank, G., Hansson, H.-C., Karlsson, H. and Laj, P., 2000. Modelling cloud processing of aerosol during the ACE-2 HILLCLOUD experiment. *Tellus*, 52B(2): 779-800.

Forkel, R., Seidl, W., Dlugi, R. and Deigele, E., 1990. A one dimensional numerical model to simulate formation and balance of sulfate during radiation fog events. *Journal of Geophysical Research*, 95(D11): 18,501 - 18,515.

Reproduced with permission of the copyright owner. Further reproduction prohibited without permission.

Fowler, D., Cape, J.N., Leith, I.D., Choularton, T.W., Gay, M.J. and Jones, A., 1988a. The influence of altitude on rainfall composition at Great Dun Fell. *Atmospheric Environment*, 22(7): 1355 - 1362.

Fowler, D., Cape, J.N., Leith, I.D., Choularton, T.W., Gay, M.J. and Jones, A., 1988b. Wet deposition and altitude, the role of orographic cloud. In: M.H. Unsworth and D. Fowler (Editors), Acid deposition at high elevation sites. Kluwer Academic Publishers, Dordrecht, pp. 231 - 257.

Frank, G., Martinsson, B.G., Cederfelt, S.-I., Berg, O.H., Swietlicki, E., Wendisch, M., Yuskiewicz, B., Heintzenberg, J., Wiedensohler, A., Orsini, D., Stratmann, F., Laj, P. and Ricci, L., 1998. Droplet Formation and Growth in Polluted Fogs. *Contributions to Atmospheric Physics*, 71(1): 65-85.

Fricke, W., Georgii, H.-W. and Gravenhorst, G., 1978. Application of a new sampling device for cloud-water analysis. In: I.P. Mazin and A.K. Khrgian (Editors), Some problems of cloud physics: collected papers. Gidrometeoizdat, Leningrad, USSR, pp. 200 - 212.

Friedlander, S.K., 2000. Smoke, Dust, and Haze: Fundamentals of Aerosol Dynamics. Oxford University Press, New York, 407 pp.

Fuchs, N.A., 1964. The Mechanics of Aerosols. Dover Publications, Inc., New York, 408 pp.

Fuhrer, J., 1986. Chemistry of fogwater and estimated rates of occult deposition in an agricultural area of central Switzerland. *Agriculture, Ecosystems and Environment*, 17: 153 - 164.

Fuzzi, S., Laj, P., Ricci, L., Orsi, G., Heintzenberg, J., Wendisch, M., Yuskiewicz, B., Mertes, S., Orsini, D., Schwanz, M., Wiedensohler, A., Stratmann, F., Berg, O.H., Swietlicki, E., Frank, G., Martinsson, B.G., Günther, A., Dierssen, J.P., Schell, D., Jaeschke, W., Berner, A., Dusek, U., Galambos, Z., Kruisz, C., Mesfin, N.S., Wobrock, W., Arends, B. and ten Brink, H., 1998a. Overview of the Po Valley Fog Experiment 1994 (CHEMDROP). *Contributions to Atmospheric Physics*, 71(1): 3-19.

Fuzzi, S., Laj, P., Facchini, M.-C., Ricci, L. and Berner, A., 1998b. Size-dependent chemistry of fog and cloud droplets, 1st International conference on fog and fog collection, Vancouver, Canada, pp. 203 - 206.

Fuzzi, S., Orsi, G., Bonforte, G., Zardini, B. and Franchini, P.L., 1997. An automated fog water collector suitable for deposition networks: design, operation and field tests. *Water, Air and Soil Pollution*, 93: 383 - 394.

Fuzzi, S. (Editor), 1997a. Cloud multi-phase processes and high alpine air and snow chemistry, 5. Springer-Verlag, Berlin, 3 - 59 pp.

Fuzzi, S. and Zappoli, S., 1997. The organic component of fog droplets. In: B. Larsen, B. Versino and G. Angeletti (Editors), The Oxidizing Capacity of the Troposphere. European Commission, Luxembourg, pp. 566 - 569.

Fuzzi, S., 1997b. Aerosols, clouds and multiphase tropospheric processes. In: B. Larsen, B. Versino and G. Angeletti (Editors), The Oxidizing Capacity of the Troposphere. European Commission, Luxembourg, pp. 476 - 483.

Fuzzi, S., Laj, P., Ricci, L., Berner, A., Schell, D., Wendisch, M. and Wobrock, W., 1996. The size-dependent chemistry of fog droplets, 12th International Conference on Clouds and Precipitation, Zurich, Switzerland, pp. 1034 - 1037.

Reproduced with permission of the copyright owner. Further reproduction prohibited without permission.

Fuzzi, S., Facchini, M.-C., Schell, D., Wobrock, W., Winkler, P., Arends, B.G., Kessel, M., Möls, J.J., Pahl, S., Schneider, T., Berner, A., Solly, I., Kruisz, C., Kalina, M., Fierlinger, H., Hallberg, A., Vitali, P., Santoli, L. and Tigli, G., 1994. Multiphase chemistry and acidity of clouds at Kleiner Feldberg. *Journal of Atmospheric Chemistry*, 19: 87 - 106.

Fuzzi, S., Facchini, M.-C., Orsi, G. and Ferri, D., 1991. Seasonal trend in fog water chemical composition in the Po Valley. *Environmental Pollution*, 75: 75 - 80.

Fuzzi, S., Cesari, G., Evangelisti, F., Facchini, M.-C. and Orsi, G., 1990. An automatic station for fog water collection. *Atmospheric Environment*, 24A(10): 2609 - 2614.

Fuzzi, S., Orsi, G., Nardini, G., Facchini, M.-C., McLaren, S., McLaren, E. and Mariotti, M., 1988. Heterogeneous processes in the Po Valley radiation fog. *Journal of Geophysical Research*, 93(D9): 11,141 - 11,151.

Fuzzi, S., 1988. Fog chemistry and deposition in the Po Valley, Italy. In: M.H. Unsworth and D. Fowler (Editors), Acid deposition at high elevations. Kluwer Academic Publishers, Dordrecht, pp. 443 - 452.

Fuzzi, S., Castillo, R.A., Jiusto, J.E. and Lala, G.G., 1984. Chemical composition of radiation fog water at Albany, NY, and its relationship to fog microphysics. *Journal of Geophysical Research*, 89(D5): 7159 - 7164.

Fuzzi, S., Gazzi, M., Pesci, C. and Vicenti, V., 1980. A linear impactor for fog droplet sampling. *Atmospheric Environment*, 14: 797 - 801.

Galvin, P.J., 1983. Cloud chemistry studies at the Whiteface Mountain field station. Ph.D. Dissertation, Department of Atmospheric Science, State University of New York at Albany, Albany, NY.

Ganor, E., Levin, Z. and Pardess, D., 1993. Determining the acidity and chemical composition of fog, haze and cloud droplets in Israel. *Atmospheric Environment*, 27A(12): 1821 - 1832.

Garland, J.A., Branson, J.R. and Cox, L.C., 1973. A study of the contribution of visibility in a radiation fog. *Atmospheric Environment*, 7: 1079 - 1092.

Garland, J.A., 1971. Some fog droplet size distributions obtained by an impaction method. *Quarterly Journal of the Royal Meteorological Society*, 97: 483 - 494.

Gerber, H., 2001. personal communication

Gerber, H., Frick, G. and Rodi, A.R., 1999. Ground-based FSSP and PVM measurements of liquid water content. *Journal of Atmospheric and Oceanic Technology*, 16: 1143-1149.

Gerber, H., Arends, B.G. and Ackerman, A.S., 1994. New microphysics sensor for aircraft use. *Atmospheric Research*, 31: 235-252.

Gerber, H., 1991. Direct measurement of suspended particulate volume concentration and far-infrared extinction coefficient with a laser-diffraction instrument. *Applied Optics*, 30(33): 4824 - 4831.

Gerber, H., 1981. Microstructure of a radiation fog. *Journal of the Atmospheric Sciences*, 38: 454 - 458.

Reproduced with permission of the copyright owner. Further reproduction prohibited without permission.

Gertler, A., Miller, D.F., Lamb, D. and Katz, U., 1984. Studies of sulfur dioxide and nitrogen dioxide reactions in haze and cloud. In: J.L. Durham (Editor), Chemistry of Particles, Fogs and Rain. Butterworth Publishers, Boston, MA, pp. 131 - 160.

Gertler, A., 1983. A comparison study of fog collectors in the Los Angeles basin. CAPA-21-80 (7/83), Desert Research Institute, Reno, NV.

Gervat, G.P., Clark, P.A., Marsh, A.R.W., Teasdale, I., Chandler, A.S., Choularton, T.W., Gay, M.J., Hill, M.K. and Hill, T.A., 1988. Field evidence for the oxidation of SO_2 by H_2O_2 in cap clouds. *Nature*, 333: 241 - 243.

Gibson, H. and Ogden, T.L., 1977. Some entry efficiencies for sharp-edged samplers in calm air. *Journal of Aerosol Science*, 8: 361-365.

Gieray, R., Lammel, G., Metzig, G. and Wieser, P., 1993. Size dependent single particle and chemical bulk analysis of droplets and interstitial particles in an orographic cloud. *Atmospheric Research*, 30: 263 - 293.

Glotfelty, D.E., Majewski, M.S. and Seiber, J.N., 1990. Distribution of several organophosphorus insecticides and their oxygen analogues in a foggy atmosphere. *Environmental Science and Technology*, 24: 353 - 357.

Glotfelty, D.E., Seiber, J.N. and Liljedahl, L.A., 1987. Pesticides in fog. *Nature*, 325: 602 - 605.

Glotfelty, D.E., Seiber, J.N. and Liljedahl, L.A., 1986. Pesticides and other organics in fog, 1986 EPA/APCA Symposium on Measurement of Toxic Air Pollutants, Raleigh, N. C., pp. 168 - 175.

Golovin, M.N. and Putnam, A.A., 1962. Inertial impaction on single elements. *Industrial and Engineering Chemistry Fundamentals*, 1(4): 264 - 273.

Goodman, J., 1985. The collection of fog drip. *Water Resources Research*, 21(3): 392 - 394.

Graedel, T.E., Hawkins, D.T. and Claxton, L.D., 1986. Atmospheric Chemical Compounds: Sources, Occurrence, and Bioassay. Academic Press, Inc., Orlando, FL, 647 pp.

Grasserbauer, M., Paleczek, S., Rendl, J., Kasper, A. and Puxbaum, H., 1994. Inorganic constituents in aerosols, cloudwater and precipitation collected at the high-alpine measurement station Sonnblick: sampling, analysis and exemplary results. *Fresenius Journal of Analytical Chemistry*, 350: 431 - 439.

Grinshpun, S.A., Willeke, K. and Kalatoor, S., 1993. A general equation for aerosol aspiration by thin-walled sampling probes in calm and moving air. *Atmospheric Environment*, 27A(9): 1459-1470.

Grinshpun, S.A., Lipatov, G.N. and Sutugin, A.G., 1990. Sampling errors in cylindrical nozzles. *Aerosol Science and Technology*, 12(716-740).

Grunow, J., 1960. The productiveness of fog precipitation in relation to the cloud droplet spectrum. In: H. Weikmann (Editor), Proceedings of the Cloud Physics conference. American Geophysical Union, Woods Hole, MA, pp. 110 - 117.

Gundel, L.A., Benner, W.H. and Hansen, A.D.A., 1994. Chemical composition of fog water and interstitial aerosol in Berkeley, CA. *Atmospheric Environment*, 28(16): 2715 - 2725.

Reproduced with permission of the copyright owner. Further reproduction prohibited without permission.

Gunz, D.W. and Hoffmann, M.R., 1990. Field investigations on the snow chemistry in central and sourthern California - I. inorganic ions and hydrogen peroxide. *Atmospheric Environment*, 24A(7): 1661 - 1671.

Gurciullo, C.S. and Pandis, S.N., 1997. Effect of composition variations in cloud droplet populations of aqueous-phase chemistry. *Journal of Geophysical Research*, 102(D8): 9375-9385.

Hallberg, A., Noone, K.J. and Ogren, J.A., 1998. Aerosol particles and clouds: which particles form cloud droplets? *Tellus*, 50B: 59 - 75.

Hallberg, A., Ogren, J.A., Noone, K.J., Okada, K., Heintzenberg, J. and Svenningsson, B., 1994a. The influence of aerosol particle composition on cloud droplet formation. *Journal of Atmospheric Chemistry*, 19: 153 - 171.

Hallberg, A., Noone, K.J., Ogren, J.A., Svenningsson, I.B., Flossmann, A., Wiedensohler, A., Hansson, H.-C., Heintzenberg, J., Anderson, T.L., Arends, B.G. and Maser, R., 1994b. Phase partitioning of aerosol particles in clouds at Kleiner Feldberg. *Journal of Atmospheric Chemistry*, 19: 107 - 127.

Hallberg, A., Ogren, J.A., Noone, K.J., Heintzenberg, J., Berner, A., Solly, I., Kruisz, C., Reischl, G., Fuzzi, S., Facchini, M.-C., Hansson, H.-C., Wiedensohler, A. and Svenningsson, I.B., 1992. Phase partitioning for different aerosol species in fog. *Tellus*, 44B: 545 - 555.

Hallett, J. and Christensen, J., 1984. Splash and penetration of drops in water. *Journal de Recherches Atmosphériques*, 18(4): 225-242.

Harrison, R.M., Peak, J.D. and Collins, G.M., 1996. Tropospheric cycle of nitrous acid. *Journal of Geophysical Research*, 101(D9): 14,429 - 14,439.

Harrison, R.M. and Kitto, A.-M.N., 1994. Evidence for a surface course of atmospheric nitrous acid. *Atmospheric Environment*, 28(6): 1089 - 1094.

Hayes, T.P., Kinney, J.J.R. and Wheeler, N.J.M., 1992. California Surface Wind Climatology, California Air Resources Board, Technical Support Division, Modeling and Meteorology Branch,.

Hegg, D.A., Yuen, P.F. and Larson, T.V., 1992. Modeling the effect of heterogeneous cloud chemistry on the marine particle size distribution. *Journal of Geophysical Research*, 97(D12): 12,927 - 12,933.

Hegg, D.A. and Larson, T.V., 1990. The effects of microphysical parameterization on model predictions of sulfate production in clouds. *Tellus*, 42B: 272 - 284.

Hegg, D.A. and Hobbs, P.V., 1988. Comparisons of sulfate and nitrate production in clouds on the mid-Atlantic and Pacific northwest coasts of the United States. *Journal of Atmospheric Chemistry*, 7: 325 - 333.

Hegg, D.A. and Hobbs, P.V., 1986. Sulfate and nitrate chemistry in cumuliform clouds. *Atmospheric Environment*, 20(5): 901 - 909.

Hegg, D.A., Hobbs, P.V. and Radke, L.F., 1984. Measurements of the scavenging of sulfate and nitrate in clouds. *Atmospheric Environment*, 18(9): 1939 - 1946.

Reproduced with permission of the copyright owner. Further reproduction prohibited without permission.

Hegg, D.A. and Hobbs, P.V., 1983. Preliminary measurements on the scavenging of sulfate and nitrate by clouds. In: H.R. Pruppacher, R.G. Semonin and W.G.N. Slinn (Editors), Precipitation Scavenging, Dry Deposition, and Resuspension. Elsevier, New York, NY, pp. 79 - 87.

Hegg, D.A. and Hobbs, P.V., 1982. Measurements of sulfate production in natural clouds. *Atmospheric Environment*, 16(11): 2663 - 2668.

Hegg, D.A. and Hobbs, P.V., 1981. Cloud water chemistry and the production of sulfates in clouds. *Atmospheric Environment*, 15(9): 1597 - 1604.

Heintzenberg, J., 1992. The Po Valley Fog Experiment 1989. What have we learned, where do we go from here? *Tellus*, 44B: 443 - 447.

Heintzenberg, J., Ogren, J.A., Noone, K.J. and Gärdneus, L., 1989. The size distribution of submicrometer particles within and about stratocumulus cloud droplets on Mt. Åreskutan, Sweden. *Atmospheric Research*, 24: 89 - 101.

Hemmerlein, M.T. and Perkins, T.D., 1993. Techniques for pollution monitoring in remote sites: III. near real-time monitoring of cloudwater conductivity and pH. *Water, Air and Soil Pollution*, 71: 43 - 50.

Henterich, R. and Herrmann, R., 1990. Comparing the distribution of nitrated phenols in the atmosphere of two german hill sites. *Environmental Technology*, VII: 961 - 972.

Herckes, P., Hannigan, M.P., Trenary, L., Lee, T. and Collett, J.L., Jr., 2001a. The organic composition of radiation fog in Davis (California). *submitted to Atmospheric Research.*

Herckes, P., Mirabel, P.H. and Wortham, H., 2001b. Fogwater studies in the Vosges Mountains (France). In: R.S. Schemenauer and H. Puxbaum (Editors), 2nd International Conference on Fog and Fog Collection, St. John's, Newfoundland, Canada, pp. 145 - 148.

Hering, S.V., Blumenthal, D.L., Brewer, R.L., Gertler, A., Hoffmann, M.R., Kadlecek, J.A. and Pettus, K., 1987. Field intercomparison of five types of fogwater collectors. *Environmental Science and Technology*, 21: 654 - 663.

Hileman, B., 1983. Acid Fog. *Environmental Science and Technology*, 17(3): 117A - 120A.

Hindman, E.E., Campbell, M.A. and Borys, R.D., 1994. A ten-winter record of cloud-droplet physical and chemical properties at a mountaintop site in Colorado. *Journal of Applied Meteorology*, 33: 797 - 807.

Hindman, E.E., Carter, E.J., Borys, R.D. and Mitchell, D.L., 1992. Collecting supercooled cloud droplets as a function of droplet size. *Journal of Atmospheric and Oceanic Technology*, 9(4): 337 - 353.

Hindman, E.E., 1988. Airborne "cloud sieving". *Annalen der Meteorologie*, 25(1): 229 - 231.

Hinds, W.C., 1999. Aerosol Technology: Properties, Behavior, and Measurement of Airborne Particles. Wiley-Interscience, New York, 483 pp.

Hoag, K.J., Collett, J.L., Jr. and Pandis, S.N., 1999. The influence of drop size-dependent fog chemistry on aerosol processing by San Joaquin Valley fogs. *Atmospheric Environment*, 33: 4817-4832.

Reproduced with permission of the copyright owner. Further reproduction prohibited without permission.

Hoag, K.J., 1998. Heterogeneous fog chemistry and S(IV) oxidation in the San Joaquin Valley. M. S. Thesis, Department of Atmospheric Science, Colorado State University, Fort Collins, CO.

Hobbs, P.V., 1986. Field studies of cloud chemistry and the relative importance of various mechanisms of the incorporation of sulfate and nitrate into cloud water. In: W. Jaeschke (Editor), Chemistry of multiphase atmospheric systems. Springer-Verlag, Berlin, pp. 191 - 211.

Hoffmann, J. and Metzig, G., 1991. Calibration of fog water collectors. *Journal of Aerosol Science*, 22(S1): S291-S294.

Hoigné, J. and Bühler, R., 1996. Kinetics of ozonation processes in cloud and fogwater: effect of transition metal ions on free radical reactions. In: P. Warneck (Editor), Heterogeneous and Liquid-Phase Processes. Springer-Verlag, Berlin, pp. 110 - 115.

Hoigné, J., Zuo, Y. and Nowell, L., 1994. Photochemical reactions in atmospheric waters: role of dissolved iron species. In: G.R. Helz, R.G. Zepp and D.G. Crosby (Editors), Aquatic and Surface Photochemistry. Lewis Publishers, Boca Raton, FL, pp. 75 - 84.

Holets, S. and Swanson, R.N., 1981. High inversion fog episodes in central California. *Journal of Applied Meteorology*, 20: 890 - 899.

Houdier, S., Perrier, S., Defrancq, E. and Legrand, M., 2000. A new fluorescent probe for sensitive detection of carbonyl compounds: sensitivity improvement and application to environmental water samples. *Analytica Chimica Acta*, 412: 221 - 233.

Houghton, H.G., 1955. On the chemical composition of fog and cloud water. *Journal of Meteorology*, 12: 355 - 357.

Houghton, H.G. and Radford, W.H., 1938. On the measurement of drop size and liquid water content in fogs and clouds, Papers in Physical Oceanography and Meteorology, 6(4). Massachusetts Institute of Technology and Woods Hole Oceanographic Institution, Cambridge, MA, 31 pp.

Howe, J.B., 1991. Rotating Multicylinder Method for the measurement of cloud liquid water content and droplet size, Cold Regions Research and Engineering Laboratory.

Howe, J.B., 1981. The rotating multicylinder method for measuring cloud liquid-water content and droplet size: a re-examination, 2nd conference on Mountain Meteorology. American Meteorology Society, Steamboat Springs, CO, pp. 401 - 403.

Huang, S., Mo, T. and Wang, M., 1991. Observation of chemical composition of supercooled cloud and snow. *Acta Meteorologica Sinica*, 5(1): 123 - 127.

Huebert, B.J., Vanbramer, S. and Tschudy, K.L., 1988. Liquid cloudwater collection using modified Mohnen slotted rods. *Journal of Atmospheric Chemistry*, 6: 251 - 263.

Huebert, B.J. and Baumgardner, D., 1985. A preliminary evaluation of the Mohnen slotted-rod cloud water collector. *Atmospheric Environment*, 19(5): 843 - 846.

Husain, L., 1989. A technique for determining in-cloud formation of SO_4. *Geophysical Research Letters*, 16(1): 57 - 60.

Reproduced with permission of the copyright owner. Further reproduction prohibited without permission.

Igawa, M., Tsutsumi, Y., Mori, T. and Okuchi, H., 1998. Fogwater chemistry at a mountainside forest and the estimation of the air pollutant deposition via fog droplets based on the atmospheric quality at the mountain base. *Environmental Science and Technology*, 32: 1566 - 1572.

IPCC, 2001. Climate Change 2001: Summary for Policymakers. Intergovernmental Panel on Climate Change, http://www.ipcc.ch, pp. 1 - 83.

Iribarne, J.V. and Cho, H.R., 1989. Models of cloud chemistry. *Tellus*, 41B: 2 - 23.

Ishizaka, Y. and Qian, G.-W., 1994. Mixtures of nitrate and sulfate in individual particles in acidic fogs. *Atmospheric Research*, 31: 147 - 156.

Jacob, D.J., 2000. Heterogeneous chemistry and tropospheric ozone. *Atmospheric Environment*, 34: 2131 - 2159.

Jacob, D.J., Munger, J.W., Waldman, J.M. and Hoffmann, M.R., 1986. The H_2SO_4-HNO_3-NH_3 system at high humidities and in fogs 1. spatial and temporal patterns in the San Joaquin Valley of California. *Journal of Geophysical Research*, 91(D1): 1073 - 1088.

Jacob, D.J., Waldman, J.M., Haghi, M., Hoffmann, M.R. and Flagan, R.C., 1985a. Instrument to collect fogwater for chemical analysis. *Review of Scientific Instruments*, 56(6): 1291-1293.

Jacob, D.J., Waldman, J.M., Munger, J.W. and Hoffmann, M.R., 1985b. Chemical composition of fogwater collected along the California coast. *Environmental Science and Technology*, 19: 730 - 736.

Jacob, D.J., Wang, R.-F.T. and Flagan, R.C., 1984a. Fogwater collector design and characterization. *Environmental Science and Technology*, 18(11): 827 - 833.

Jacob, D.J., Waldman, J.M., Munger, J.W. and Hoffmann, M.R., 1984b. A field investigation of physical and chemical mechanisms affecting pollutant concentrations in fog droplets. *Tellus*, 36B: 272 - 285.

Jacob, D.J., Flagan, R.C., Waldman, J.M. and Hoffmann, M.R., 1983. Design and calibration of a rotating arm collector for ambient fog sampling. In: H.R. Pruppacher, R.G. Semonin and W.G.N. Slinn (Editors), Precipitation Scavenging, Dry Deposition, and Resuspension. Elsevier, New York, NY, pp. 125 - 134.

Jaeschke, W. and Günther, A., 2001. Chemical composition of size segregated cloud drops collected with an airborne two stage impactor. In: R.S. Schemenauer and H. Puxbaum (Editors), 2nd International Conference on Fog and Fog Collection, St. John's, Newfoundland, Canada, pp. 65 - 68.

Jaeschke, W., Dierssen, J.P., Günther, A., Schickedanz, U., Wolf, A., Ricci, L. and Arends, B.G., 1998. Mass Fluxes and Chemical Pathways During a Fog Event. *Contributions to Atmospheric Physics*, 71(1): 145-157.

Jaeschke, W., Georgii, H.-W., Schell, D., Preiss, M., Maser, R. and Wobrock, W., 1997. The dynamic behaviour of pollutants in fog and captive clouds. In: S. Fuzzi and D. Wagenbach (Editors), Cloud multi-phase processes and high alpine air and snow chemistry. Springer-Verlag, Berlin, pp. 113 - 122.

Reproduced with permission of the copyright owner. Further reproduction prohibited without permission.

Jaeschke, W., Enderle, K.H., Fuzzi, S., Orsi, G., Facchini, M.-C., Berner, A. and Reischl, G., 1990. Ground based cloud and fog experiments. In: G. Restelli and G. Angeletti (Editors), Physico-chemical Behaviour of Atmospheric Pollutants. Kluwer Academic Publishing, Dordrecht, pp. 57 - 62.

Jaeschke, W., 1986. Multiphase atmospheric chemistry. In: W. Jaeschke (Editor), Chemistry of multiphase atmospheric systems. Springer-Verlag, Berline, pp. 3 - 40.

Jagels, R., Carlisle, J., Cunningham, R., Serreze, S. and Tsai, P., 1989. Impact of acid fog and ozone on coastal red spruce. *Water, Air and Soil Pollution*, 48: 193 - 208.

Jiusto, J.E., 1981. Fog structure. In: P.V. Hobbs and A. Deepak (Editors), Clouds: Their Formation, Optical Properties, and Effects. Academic Press, Inc., New York, pp. 187 - 239.

Jiusto, J.E., 1967. Aerosol and cloud microphysics measurements in Hawaii. *Tellus*, 19: 359 - 368.

Johnson, C.A., Sigg, L. and Zobrist, J., 1987. Case studies on the chemical composition of fogwater: the influence of local gaseous emissions. *Atmospheric Environment*, 21(11): 2365 - 2374.

Joslin, J.D., Mueller, S.F. and Wolfe, M.H., 1990. Tests of models of cloudwater deposition to forest canopies using artificial and living collectors. *Atmospheric Environment*, 24A(12): 3007 - 3019.

Juvik, J.O. and Perreira, D.J., 1973. The interception of fog and cloudwater of windward Mauna Loa, Hawaii, Department of Botany, University of Hawaii, Honolulu, HI.

Kalina, M., Zambo, E. and Puxbaum, H., 1998. Cloud water chemistry and impact on total deposition of sulfur and nitrogen at different elevational levels in an alpine valley (Achkenkirch, 930 - 1758 m a.s.l., Tyrol, Austria), 1st International conference on fog and fog collection, Vancouver, Canada, pp. 57 - 60.

Kalina, M. and Puxbaum, H., 1994. A study of the influence of riming of ice crystals on snow chemistry during different seasons in precipitating continental clouds. *Atmospheric Environment*, 28(20): 3311 - 3328.

Karlsson, V., Lauren, M. and Peltoniemi, S., 2000. Stability of major ions and sampling variability in daily bulk precipitation samples. *Atmospheric Environment*, 34: 4859 - 4865.

Kasahara, M., Ma, C.-J. and Tohno, S., 2001. Physical and chemical properties of single fog droplets applying fixation techniques. In: R.S. Schemenauer and H. Puxbaum (Editors), 2nd International Conference on Fog and Fog Collection, St. John's, Newfoundland, Canada, pp. 69 - 72.

Kaslow, D.E. and Emrich, R.J., 1974. Particle sampling efficiencies for an aspirating blunk, thick-walled tube in calm air, Technical Report #25. Department of Physics, Lehigh University, PA.

Katz, U., 1980. A droplet impactor to collect liquid water from laboratory clouds for chemical analysis, 8th International Conference on Cloud Physics, Clermont-Ferrand, France, pp. V.17 - 20.

Reproduced with permission of the copyright owner. Further reproduction prohibited without permission.

Keene, W.C., Mosher, B.W., Jacob, D.J., Munger, J.W., Talbot, R.W., Artz, R.C., Maben, J.R., Daube, B.C., Jr. and Galloway, J.N., 1995. Carboxylic acids in clouds at a high-elevation forested site in central Virginia. *Journal of Geophysical Research*, 100(D5): 9345 - 9357.

Khemani, L.T., Momin, G.A., Naik, M.S., Prakasa Rao, P.S., Safai, P.D. and Murty, A.S.R., 1987. Influence of alkaline particulates on pH of cloud and rain water in India. *Atmospheric Environment*, 21(5): 1137 - 1145.

Khemani, L.T., Sharma, S.K., Murty, A.S.R. and Ramana Murty, B.V., 1982. A simple gadget for collection of cloud/rain water from aircraft, Conference on Cloud Physics. American Meteorological Society, Chicago, IL, pp. 303 - 305.

Khemani, L.T., Momin, G.A. and Ramana Murty, B.V., 1981. Chemical composition of cloud water at a hill station. In: A.F. Roddy and T.C. O'Connor (Editors), 9th International conference on Atmospheric Aerosols, Condensation and Ice Nuclei. Galway University Press, Galway, Ireland, pp. 233 - 238.

Kieber, R.J., Rhines, M.F., Willey, J.D. and Avery, G.B.J., 1999. Nitrite variability in coastal North Carolina rainwater and its impact on the nitrogen cycle in rain. *Environmental Science and Technology*, 33(3): 374 - 377.

Kim, Y.J. and Boatman, J.F., 1992. The collection efficiency of a modified Mohnen slotted-rod cloudwater collector in summer clouds. *Journal of Atmospheric and Oceanic Technology*, 9: 36 - 41.

Kins, L., Müller, K.P., Enhalt, D.H. and Meixner, F.X., 1988. Experiment ALSDAN (1985): some preliminary results of the height resolved measurements of trace gases, aerosol composition, cloud- and precipitation water. In: M.H. Unsworth and D. Fowler (Editors), Acid deposition at high elevation sites. Kluwer Academic Publishers, Dordrecht, pp. 375 - 394.

Kins, L., Junkermann, W., Meixner, F.X., Müller, K.P. and Enhalt, D.H., 1986. Development and calibration of a ground-based active collector for cloud- and fogwater, American Chemical Society, Petroleum Chemistry Division. American Chemical Society, New York, pp. 527 - 532.

Klemm, O., 2001. Trends in fog composition at a site in NE Bavaria. In: R.S. Schemenauer and H. Puxbaum (Editors), 2nd International Conference on Fog and Fog Collection, St. John's, Newfoundland, Canada, pp. 73 - 76.

Klemm, O., Talbot, R.W. and Klemm, K., 1991. Sulfur dioxide in coastal New England fog. *Atmospheric Environment*, 26A(11): 2063 - 2075.

Kmiec, G., Kacperczyk, K., Zwozdziak, A. and Zwozdziak, J., 1995. Acid pollutants in air and precipitation/deposition at the Sudetan Mountains, Poland. *Water, Air and Soil Pollution*, 85: 2131 - 2136.

Kowalski, A.S., Anthoni, P.M., Vong, R.J., Delany, A.C. and MacLean, G.D., 1997. Deployment and evaluation of a system for ground-based measurement of cloud liquid water turbulent fluxes. *Journal of Atmospheric and Oceanic Technology*, 14: 468-479.

Kozima, K., Ono, T. and Yamaji, K., 1953. The size distribution of fog particles. In: T. Hori (Editor), Studies on Fog. Tanne Trading Company, Sapporo, pp. 303 - 309.

Reproduced with permission of the copyright owner. Further reproduction prohibited without permission.

Krämer, M., Beltz, N., Schell, D., Schütz, L., Sprengard-Eichel, C. and Wurzler, S., 2000. Cloud processing of continental aerosol particles: experimental investigations of different drop sizes. *Journal of Geophysical Research*, 105(D9): 11,739 - 11,752.

Krämer, M. and Schütz, L., 1994. On the collection efficiency of a rotating arm collector and its applicability to cloud- and fogwater sampling. *Journal of Aerosol Science*, 25(1): 137 - 148.

Krämer, M., Schütz, L., Svenningsson, B. and Wiedensohler, A., 1991. Number size distribution of insoluble atmospheric aerosol particles in fog/cloud-water. *Journal of Aerosol Science*, 22(Supplement 1): S525 - S528.

Krämer, M. and Schütz, L., 1990. Collection efficiency of the Mainz rotating-arm-collector. *Journal of Aerosol Science*, 21(Supplement 1): S653 - S656.

Kroll, G. and Winkler, P., 1988. Estimation of wet deposition in fog. In: K. Grefen and J. Löbel (Editors), Environmental Meteorology. Kluwer Academic Publishing, Dordrecht, pp. 227 - 236.

Kruisz, C., Berner, A. and Brandner, B., 1992. A cloud water sampler for high wind speeds. In: P.M.e.a. Borrell (Editor), EUROTRAC Symposium '92. SPB Academic Publishing, pp. 523 - 525.

Kulmala, M., Laaksonen, A., Charlson, R.J. and Korhonen, P., 1997. Clouds without supersaturation. *Nature*, 388: 336 - 337.

Kulmala, M., Laaksonen, A., Korhonen, P., Vesala, T., Ahonen, T. and Barrett, J.C., 1993. The effect of atmospheric nitric acid vapor on cloud condensation nucleus activation. *Journal of Geophysical Research*, 98(D12): 22,949 - 22,958.

Kuriowa, D., 1956. The composition of sea-fog nuclei as identified by electron microscope. *Journal of Meteorology*, 13: 408 - 410.

Kuriowa, D., 1953. Electron-microscope study of atmospheric condensation nuclei. In: T. Hori (Editor), Studies on Fog. Tanne Trading Company, Sapporo, pp. 349 - 382.

Kuriowa, D., 1951. Electron-microscope study of fog nuclei. *Journal of Meteorology*, 8: 157 - 160.

Laaksonen, A., Korhonen, P., Kulmala, M. and Charlson, R.J., 1998. Modification of the Kohler equation to include soluble trace gases and slightly soluble substances. *Journal of the Atmospheric Sciences*, 55: 853 - 862.

Lai, H.-C., Tanner, P.A., Huang, M.-Y., Shen, Z.-L. and Wu, Y.-X., 1997. The acidification process under the cloud in southwest China: observation results and simulation. *Atmospheric Environment*, 31(6): 851 - 861.

Laj, P., Fuzzi, S., Lazzari, A., Ricci, L., Orsi, G., Berner, A., Dusek, U., Schell, D., Günther, A., Wendisch, M., Wobrock, W., Frank, G., Martinsson, B.G. and Hillamo, R., 1998. The Size Dependent Composition of Fog Droplets. *Contributions to Atmospheric Physics*, 71(1): 115-130.

Laj, P., Fuzzi, S., Facchini, M.-C., Orsi, G., Berner, A., Kruisz, C., Wobrock, W., Hallberg, A., Bower, K.N., Gallagher, M.W., Beswick, K.M., Colvile, R., Choularton, T.W., Nason, P. and Jones, B., 1997a. Experimental evidence for in-cloud production of aerosol sulfate. *Atmospheric Environment*, 31(16): 2503 - 2514.

Reproduced with permission of the copyright owner. Further reproduction prohibited without permission.

Laj, P., Fuzzi, S., Facchini, M.-C., Lind, J., Orsi, G., Preiss, M., Maser, R., Jaeschke, W., Seyffer, E., Helas, G., Acker, K., Wieprecht, W., Möller, D., Arends, B.G., Möls, J.J., Colvile, R., Gallagher, M.W., Beswick, K.M., Hargreaves, K.J., Storeton-West, R.L. and Sutton, M.A., 1997b. Cloud processing of soluble gases. *Atmospheric Environment*, 31(16): 2589 - 2598.

Lamb, D. and Comrie, L., 1993. Comparability and precision of MAP3S and NADP/NTN precipitation chemistry data at an acidic site in eastern North America. *Atmospheric Environment*, 27A: 1993 - 2008.

Lammel, G. and Metzig, G., 1998. On the occurrence of nitrite in urban fogwater. *Chemosphere*, 37(8): 1603 - 1614.

Lammel, G. and Cape, J.N., 1996. Nitrous acid and nitrite in the atmosphere. *Chemical Society Reviews*: 361 - 369.

Lammel, G. and Perner, D., 1988. The atmospheric aerosol as a source of nitrous acid in the polluted atmosphere. *Journal of Aerosol Science*, 19(7): 1199 - 1202.

Langmuir, I. and Blodgett, K.B., 1946. A Mathematical investigation of water droplet trajectories. 5418, Army Air Forces Technical Report #5418, Washington, DC.

Lazrus, A.L., Kok, G.L., Lind, J.A., Gitlin, S.N., Heikes, B.G. and Shetter, R.E., 1986. Automated fluorometric method for H_2O_2 in air. *Analytical Chemistry*, 58: 594 - 597.

Lazrus, A.L., Kok, G.L., Gitlin, S.N. and Lind, J.A., 1985. Automated fluorometric method for hydrogen peroxide in atmospheric precipitation. *Analytical Chemistry*, 57: 917 - 922.

Lazrus, A.L., Baynton, H.W. and Lodge, J.P.J., 1970. Trace constituents in oceanic cloud water and their origin. *Tellus*, 22: 106 - 113.

Lelieveld, J. and Heintzenberg, J., 1992. Sulfate cooling effect on climate through in-cloud oxidation of anthropogenic SO_2. *Science*, 258: 117 - 120.

Lelieveld, J. and Crutzen, P.J., 1991. The role of clouds in tropospheric chemistry. *Journal of Atmospheric Chemistry*, 12: 229 - 267.

Lelieveld, J. and Crutzen, P.J., 1990. Influences of cloud photochemical processes on tropospheric ozone. *Nature*, 343: 227 - 233.

Leriche, M., Voisin, D., Chaumerliac, N., Monod, A. and Aumont, B., 2000. A model for tropospheric multiphase chemistry: application to one cloudy event during the CIME experiment. *Atmospheric Environment*, 34: 5015 - 5036.

Lesnic, D., Elliott, L. and Ingham, D.B., 1993. A mathematical model for predicting the collection efficiency of the rotating arm collector. *Journal of Aerosol Science*, 24(2): 163 - 180.

Levin, Z., Price, C. and Ganor, E., 1990. The contribution of sulfate and desert aerosols to the acidification of clouds and rain in Israel. *Atmospheric Environment*, 24A(5): 1143 - 1151.

Levsen, K., Behnert, S., Mußmann, P., Raabe, M. and Prieß, B., 1993. Organic compounds in cloud and rainwater. *International Journal of Environmental Analytical Chemistry*, 52: 87 - 97.

Reproduced with permission of the copyright owner. Further reproduction prohibited without permission.

Lide, D.R. (Editor), 1998. CRC Handbook of Chemistry and Physics. CRC Press, Boca Raton, FL, 14-16 - 14-22 pp.

Lillis, D., Cruz, C.N., Collett, J.L., Jr., Richards, L.W. and Pandis, S.N., 1999. Production and removal of aerosol in a polluted fog layer: model evaluation and fog effect on PM. *Atmospheric Environment*, 33: 4797 - 4816.

Lin, N.-H. and Saxena, V.K., 1991. Interannual variability in acidic deposition on the Mt. Mitchell area forest. *Atmospheric Environment*, 25A(2): 517 - 524.

Liu, P.S.K., Leaitch, W.R., MacDonald, A.M., Isaac, G.A., Strapp, J.W. and Wiebe, H.A., 1993. Sulfate production in summer cloud over Ontario, Canada. *Tellus*, 45B: 368 - 389.

Lorenzen, A. (Editor), 1974. Climate of the Sacramento Valley Air Basin. Air Basin Climatology Series. California Air Resources Board, Division of Technical Services, 1 - 28 pp.

Ludwig, F.L. and Robinson, E., 1970. Observations of aerosols and droplets in California stratus. *Tellus*, 22: 94 - 105.

Lüttke, J., Levsen, K., Acker, K., Wieprecht, W. and Möller, D., 1999. Phenols and nitrated phenols in clouds at Mt. Brocken. *International Journal of Environmental Analytical Chemistry*, 74(1-4): 69 - 89.

Lüttke, J., Scheer, V., Levsen, K., Wünsch, G., Cape, J.N., Hargreaves, K.J., Storeton-West, R.L., Acker, K., Wieprecht, W. and Jones, B., 1997. Occurrence and formation of nitrated phenols in and out of cloud. *Atmospheric Environment*, 31(16): 2637 - 2648.

Lüttke, J. and Levsen, K., 1997. Phase partitioning of phenol and nitrophenols in clouds. *Atmospheric Environment*, 31(16): 2649 - 2656.

Lüttke, J., Koch, C., Mußmann, P. and Levsen, K., 1994. Organic compounds in clouds. In: G. Angeletti and G. Restelli (Editors), Physico-chemical Behaviour of Atmospheric Pollutants. European Commission, Luxembourg, pp. 982 - 988.

Ma, C.-J., Kasahara, M., Tohno, S., Kamiya, T. and Sakai, T., 2001. Sampling of individual fog droplets and its chemical analysis. In: R.S. Schemenauer and H. Puxbaum (Editors), 2nd International Conference on Fog and Fog Collection, St. John's, Newfoundland, Canada, pp. 45 - 48.

Mack, E.J., Pilie, R.J. and Kocmond, W.C., 1973. An investigation of the microphysical and micrometeorological properties of sea fog, Calspan Corporation, Buffalo, NY.

Majeed, M.A. and Wexler, A.S., 2001. Microphysics of aqueous droplets in clouds and fogs as applied to PM-fine modeling. *Atmospheric Environment*, 35: 1639 - 1653.

Mallant, R.K.A.M., 1988. A fog chamber and wind tunnel facility for calibration of cloud water collectors. In: M.H. Unsworth and D. Fowler (Editors), Acid deposition at high elevation sites. Kluwer Academic Publishers, Dordrecht, the Netherlands, pp. 479-490.

Marple, V.A., Rubow, K.L. and Behm, S.M., 1991. A Microorifice Uniform Deposit Impactor (MOUDI): description, calibration and use. *Aerosol Science and Technology*, 14: 424 - 446.

Reproduced with permission of the copyright owner. Further reproduction prohibited without permission.

Marple, V.A. and Rubow, K.L., 1986. Theory and design guidelines. In: J.P. Lodge, Jr. and T.L. Chan (Editors), Cascade Impactor: Sampling and Data Analysis. American Industrial Hygiene Association, Akron, OH, pp. 79-102.

Marple, V.A. and Willeke, K., 1975. Inertial impactors: theory, design and use. In: B.Y.H. Liu (Editor), Symposium on Fine Particles. US EPA Office of Research and Development, Minneapolis, MN, pp. 411 - 446.

Marple, V.A., 1970. A fundamental study of inertial impactors. Ph.D. Thesis, University of Minnesota, Minneapolis, MN, 186 pp.

Martens, C.S. and Harris, R.C., 1973. Chemistry of aerosols, cloud droplets, and rain in Puerto Rican marine atmosphere. *Journal of Geophysical Research*, 78(6): 949 - 957.

Martinsson, B.G., Frank, G., Cederfelt, S.-I., Berg, O.H., Mentes, B., Papaspiropoulos, G., Swietlicki, E., Zhou, J., Flynn, M., Bower, K.N., Choularton, T.W., Mäkelä, J.M., Virkkula, A. and van Dingenen, R., 2000. Validation of very high cloud droplet number concentrations in air masses transported thousands of kilometres over the ocean. *Tellus*, 52B(2): 801-814.

Martinsson, B.G., Frank, G., Cederfelt, S.-I., Swietlicki, E., Berg, O.H., Zhou, J., Bower, K.N., Bradbury, C., Birmili, W., Stratmann, F., Wendisch, M., Wiedensohler, A. and Yuskiewicz, B., 1999. Droplet nucleation and growth in orographic clouds in relation to the aerosol population. *Atmospheric Research*, 50: 289 - 315.

Martinsson, B.G., Cederfelt, S.-I., Svenningsson, B., Frank, G., Hansson, H.-C., Swietlicki, E., Wiedensohler, A., Wendisch, M., Gallagher, M.W., Colvile, R., Beswick, K.M., Choularton, T.W. and Bower, K.N., 1997a. Experimental determination of the connection between cloud droplet size and its dry residue. *Atmospheric Environment*, 31(16): 2477 - 2490.

Martinsson, B.G., Cederfelt, S.-I., Hansson, H.-C. and Frank, G., 1997b. A droplet aerosol analysing system for cloud studies. In: S. Fuzzi and D. Wagenbach (Editors), Cloud multi-phase processes and high alpine air and snow chemistry. Springer-Verlag, Berlin, pp. 130 - 137.

Maser, R., Franke, H., Preiss, M. and Jaeschke, W., 1994. Methods provided and applied in a research aircraft for the study of cloud physics and chemistry. *Contributions to Atmospheric Physics*, 67(4): 321 - 334.

Mauldin, R.L.I., Madronich, S., Flocke, S.J., Eisele, F.L., Frost, G.J. and Prévôt, A.S.H., 1997. New insights on OH: measurements around and in clouds. *Geophysical Research Letters*, 24(23): 3033 - 3036.

May, K.R. and Clifford, R., 1967. The impaction of aerosol particles on cylinders, spheres, ribbons and discs. *Annals of Occupational Hygiene*, 19: 83 - 95.

May, K.R., 1961. Fog-droplet sampling using a modified impactor technique. *Quarterly Journal of the Royal Meteorological Society*, 87: 535 - 548.

May, K.R., 1945. The cascade impactor: an instrument for sampling coarse aerosols. *Journal of Scientific Instruments*, 22: 187-195.

Reproduced with permission of the copyright owner. Further reproduction prohibited without permission.

McFadyen, G.G. and Cape, J.N., 1999. Springtime sources and sinks of peroxyacetyl nitrate in the UK and its contribution to acidification and nitrification of cloud water. *Atmospheric Research*, 50: 359 - 371.

McFarland, A.R. and Ortiz, C.A., 1984. Characterization of the mesh impaction fog sampler. Texas Engineering Experiment Station Project 32525-1107, Air Quality Laboratory, Department of Civil Engineering, Texas A & M University, College Station, TX.

Menon, S., Saxena, V.K. and Logie, B.D., 2000. Chemical heterogeneity across cloud droplet size spectra in continental and marine air masses. *Journal of Applied Meteorology*, 39: 887 - 903.

Mercer, T.T., 1973. Aerosol Technology in Hazard Evaluation. Academic Press, New York, pp. p 41 in Mercer.

Mercer, T.T. and Chow, H.Y., 1968. Impaction from rectangular jets. *Journal of Colloid and Interface Science*, 27(1): 75 - 83.

Meyer, M.B., Jiusto, J.E. and Lala, G.G., 1980. Measurements of visual range and radiation-fog (haze) microphysics. *Journal of the Atmospheric Sciences*, 37: 622 - 629.

Miller, D.R., Byrd, J.E. and Perona, M.J., 1987. The source of Pb, Cu and Zn in fog water. *Water, Air and Soil Pollution*, 32: 329 - 340.

Miller, E.K., Panek, J.A., Friedland, A.J., Kadlecek, J.A. and Mohnen, V.A., 1993. Atmospheric deposition to a high-elevation forest at Whiteface Mountain, New York, USA. *Tellus*, 45B: 209 - 227.

Miller, R.L. and Kahn, J.S., 1962. Statistical Analyses in the Geological Sciences. John Wiley and Sons, Inc., New York.

Millet, M., Wortham, H., Sanusi, A. and Mirabel, P.H., 1997. Low molecular weight organic acids in fogwater in an urban area: Strasbourg (France). *The Science of the Total Environment*, 206: 57 - 65.

Millet, M., Sanusi, A. and Wortham, H., 1996. Chemical composition of fogwater in an urban area: Strasbourg (France). *Environmental Pollution*, 94(3): 345 - 354.

Millet, M., Worthan, H. and Mirabel, P.H., 1995. Solubility of polyvalent cations in fogwater at an urban site in Strasbourg (France). *Atmospheric Environment*, 29(19): 2625 - 2631.

Milne, R., Crossley, A. and Unsworth, M.H., 1988. Physics of cloudwater deposition and evaporation at Castlelaw, SE Scotland. In: M.H. Unsworth and D. Fowler (Editors), Acid deposition at high elevation sites. Kluwer Academic Publishers, Dordrecht, pp. 299 - 307.

Minami, Y. and Ishizaka, Y., 1996. Evaluation of chemical composition of fog water near the summit of a high mountain in Japan. *Atmospheric Environment*, 30(19): 3363 - 3376.

Mitchell, D.L., Zhang, R. and Pitter, R.L., 1990. Mass-dimensional relationships for ice particles and the influence of riming on snowfall rates. *Journal of Applied Meteorology*, 29: 153 - 163.

Mitchell, D.L. and Lamb, D., 1989. Influence of riming on the chemical composition of snow in winter orographic storms. *Journal of Geophysical Research*, 94(D12): 14,831 - 14,840.

Reproduced with permission of the copyright owner. Further reproduction prohibited without permission.

Mohnen, A.J., 1980. Cloud water collector from aircraft. *Atmospheric Technology*, 12: 20 - 25.

Mohnen, V.A. and Vong, R.J., 1993. A climatology of cloud chemistry for the eastern United States derived from the Mountain Cloud Chemistry Project. *Environmental Review*, 1: 38 - 54.

Mohnen, V.A. and Kadlecek, J.A., 1989. Cloud chemistry research at Whiteface Mountain. *Tellus*, 41B: 79 - 91.

Moore, K.F., 1999a. The World of the IC, Department of Atmospheric Science, Colorado State University, Fort Collins, CO.

Moore, K.F., 1999b. Using the GFAAS, Department of Atmospheric Science, Colorado State University, Fort Collins, CO.

Mosimann, L., Steiner, M., Collett, J.L., Jr., Henrich, W., Schmid, W. and Waldvogel, A., 1993. Ice crystal observations and the degree of riming in winter precipitation. *Water, Air and Soil Pollution*, 68: 29 - 42.

Mossop, S.C., 1983. Intercomparison of instruments used for measurement of cloud drop concentration and size distribution. *Journal of Climate and Applied Meteorology*, 22: 419-428.

Mrose, H., 1966. Measurements of pH, and chemical analyses of rain-, snow-, and fog-water. *Tellus*, 18: 266 - 270.

Mueller, S.F. and Weatherford, F.P., 1988. Chemical deposition to a high elevation red spruce forest. *Water, Air and Soil Pollution*, 38: 345 - 363.

Müller, F. and Mauersberger, G., 1994. Case study on the interaction of size dependent multiphase chemistry and detailed microphysics. *Atmospheric Research*, 32: 273 - 288.

Mundo, C., Sommerfeld, M. and Tropea, C., 1995. Droplet wall collisions: experimental studies of the deformation and break-up process. *International Journal of Multiphase Flow*, 21(2): 151-173.

Munger, J.W., Jacob, D.J., Daube, B.C., Jr., Horowitz, L.W., Keene, W.C. and Heikes, B.G., 1995. Formaldehyde, glyoxal and methylglyoxal in air and cloud water at a rural mountain site in central Virginia. *Journal of Geophysical Research*, 100(D5): 9325 - 9333.

Munger, J.W., Collett, J.L., Jr., Daube, B.C., Jr. and Hoffmann, M.R., 1989a. Chemical composition of coastal stratus clouds: dependence on drop size and distance from the coast. *Atmospheric Environment*, 23(10): 2305 - 2320.

Munger, J.W., Collett, J.L., Jr., Daube, B.C., Jr. and Hoffmann, M.R., 1989b. Carboxylic acids and carbonyl compounds in southern California clouds and fogs. *Tellus*, 41B: 230 - 242.

Munger, J.W., Tiller, C. and Hoffmann, M.R., 1986. Identification of hydroxymethanesulfonate in fog water. *Science*, 231: 247 - 249.

Munger, J.W., Jacob, D.J., Waldman, J.M. and Hoffmann, M.R., 1983. Fogwater chemistry in an urban atmosphere. *Journal of Geophysical Research*, 88(C9): 5109 - 5121.

Reproduced with permission of the copyright owner. Further reproduction prohibited without permission.

Munzert, K., 1988. Chemistry of cloud water and precipitation at an alpine mountain station. In: M.H. Unsworth and D. Fowler (Editors), Acid deposition at high elevation sites. Kluwer Academic Publishers, Dordrecht, pp. 395 - 401.

Nagel, J.F., 1956. Fog precipitation on Table Mountain. *Quarterly Journal of the Royal Meteorological Society*, 82: 452 - 460.

Nenes, A., Ghan, S., Abdul-razzak, H., Chuang, P.Y. and Seinfeld, J.H., 2001. Kinetic limitations on cloud droplet formation and impact on cloud albedo. *Tellus*, 53B: 133 - 149.

Noone, K.J., Ogren, J.A., Hallberg, A., Heintzenberg, J., Ström, J., Hansson, H.-C., Svenningsson, B., Wiedensohler, A., Fuzzi, S., Facchini, M.-C., Arends, B.G. and Berner, A., 1992. Changes in aerosol size- and phase distributions due to physical and chemical processes in fog. *Tellus*, 44B: 489 - 504.

Noone, K.J., Ogren, J.A., Heintzenberg, J., Charlson, R.J. and Covert, D.S., 1988a. Design and calibration of a counterflow virtual impactor for sampling of atmospheric fog and cloud droplets. *Aerosol Science and Technology*, 8: 235 - 244.

Noone, K.J., Charlson, R.J., Covert, D.S., Ogren, J.A. and Heintzenberg, J., 1988b. Cloud droplets: solute concentration is size-dependent. *Journal of Geophysical Research*, 93(D8): 9477 - 9482.

Noone, K.J., Hansson, H.-C. and Mallant, R.K.A.M., 1988c. Droplet sampling from crosswinds: an inlet efficiency calibration. *Journal of Aerosol Science*, 23(2): 153 - 164.

Norment, H.G., 1987. Numerical studies of sampling efficiencies of the ASCME and PMS aspirator hydrometeor measurement instruments. *Journal of Atmospheric and Oceanic Technology*, 4(2): 253-263.

Noruse, H. and Maruyama, H., 1971. On the hygroscopic nuclei in cloud droplets. *Papers in Meteorology and Geophysics*, 22(1): 1 - 21.

Notholt, J., Hjorth, J. and Raes, F., 1992. Formation of HONO on aerosol surfaces during foggy periods in the presence of NO and NO_2. *Atmospheric Environment*, 26A: 211 - 217.

Novakov, T., Rivera-Carpio, C., Penner, J.E. and Rogers, C.F., 1994. The effect of anthropogenic sulfate aerosols on marine cloud droplet concentrations. *Tellus*, 46B: 132 - 141.

NRC, 1998. The Atmospheric Sciences: Entering the 21st Century. National Academy Press, Washington, DC, 337 pp.

Oberholzer, B., Collett, J.L., Jr., Staehelin, J. and Waldvogel, A., 1992. In-cloud scavenging of gases and aerosols at a mountain site in central Switzerland. *Journal of Atmospheric Chemistry*, 14: 61 - 71.

Oddie, B.C.V., 1962. The chemical composition of precipitation at cloud levels. *Quarterly Journal of the Royal Meteorological Society*, 88: 535 - 538.

O'Dowd, C.D., Lower, J.A., Clegg, N., Smith, M.H. and Clegg, S.L., 2000. Modeling heterogeneous sulphate production in maritime stratiform clouds. *Journal of Geophysical Research*, 105(D6): 7143 - 7160.

Reproduced with permission of the copyright owner. Further reproduction prohibited without permission.

Ogawa, N., Kikuchi, R., Okamura, T., Adzuhata, T., Kajikawa, M. and Ozeki, T., 1999. Cloud droplet size dependence of the concentrations of various ions in cloud water at a mountain ridge in northern Japan. *Atmospheric Research*, 51: 77 - 80.

Ogiwara, S. and Okita, T., 1952. Electron-Microscope study of cloud and fog nuclei. *Tellus*, 4: 233 - 240.

Ogren, J.A., Noone, K.J., Hallberg, A., Heintzenberg, J., Schell, D., Berner, A., Solly, I., Kruisz, C., Reischl, G., Arends, B.G. and Wobrock, W., 1992. Measurements of the size dependence of the concentration of non-volatile material in fog droplets. *Tellus*, 44B: 570-580.

Ogren, J.A. and Charlson, R.J., 1992. Implications for models and measurements of chemical inhomogeneities among cloud droplets. *Tellus*, 44B: 208 - 225.

Ogren, J.A., Heintzenberg, J., Zuber, Z., Noone, K.J. and Charlson, R.J., 1989. Measurements of the size-dependence of solute concentrations in cloud droplets. *Tellus*, 41B: 24 - 31.

Ogren, J.A. and Rodhe, H., 1986. Measurements of the chemical composition of cloudwater at a clean air site in central Scandinavia. *Tellus*, 38B: 190 - 196.

Okita, T. and Ota, S., 1981. The concentrations of trace constituents in the atmosphere and in cloud water in relation to meteorological conditions and oxidant level. In: A.F. Roddy and T.C. O'Connor (Editors), 9th International Conference on Atmospheric Aerosols, Condensation and Ice Nuclei. Galway University Press, Galway, Ireland, pp. 239 - 243.

Okita, T., 1968. Concentration of sulfate and other inorganic materials in fog and cloud water. *Journal of the Meteorological Society of Japan*, 42(2): 120 - 126.

Okita, T., 1965. Some chemical and meteorological measurements of air pollution in Asahikawa. *International Journal of Air and Water Pollution*, 9: 323 - 332.

Okita, T., 1961. Size distribution of large droplets in precipitating clouds. *Tellus*, 13: 509 - 521.

Osborne, S.R., Johnson, D.W., Bower, K.N. and Wood, R., 2001. Modification of aerosol size distribution within exhaust plumes produced by diesel-powered ships. *Journal of Geophysical Research*, 106(D9): 9827 - 9842.

Oura, H., 1953. On the capture of fog particles by a forest (I). In: T. Hori (Editor), Studies on Fog. Tanne Trading Company, Sapporo, pp. 239 - 252.

Pade, G., Covert, D.S. and Larson, T.V., 1987. Design and calibration of a high volume fogwater collector. *Journal of Atmospheric and Oceanic Technology*, 4: 340 - 344.

Pandis, S.N. and Seinfeld, J.H., 1992. Reply. *Journal of Geophysical Research*, D97: 6078 - 6080.

Pandis, S.N. and Seinfeld, J.H., 1991. Should bulk cloud water samples obey Henry's law? *Journal of Geophysical Research*, D96: 10,791 - 10,798.

Pandis, S.N., Seinfeld, J.H. and Pilinis, C., 1990a. Chemical composition differences in fog and cloud droplets of different sizes. *Atmospheric Environment*, 24A: 1957 - 1969.

Pandis, S.N., Seinfeld, J.H. and Pilinis, C., 1990b. The smog-fog-smog cycle and acid deposition. *Journal of Geophysical Research*, 95(D11): 18,489 - 18,500.

Reproduced with permission of the copyright owner. Further reproduction prohibited without permission.

Pandis, S.N. and Seinfeld, J.H., 1989. Mathematical modeling of acid deposition due to radiation fog. *Journal of Geophysical Research*, 94(D10): 12,911 - 12,923.

Parungo, F., Nagamoto, C. and Kopcewicz, B., 1989. Front range acidic clouds and precipitation. In: R.K. Olson and A.S. Lefohn (Editors), Effects of air pollution on western forests. Air and Waste Management Association, Anaheim, CA, pp. 15 - 31.

Perdue, E.M. and Beck, K.C., 1988. Chemical consequences of mixing atmospheric droplets of varied pH. *Journal of Geophysical Research*, 93: 691 – 698.

Perrino, C., DeSantis, F. and Febo, A., 1990. Criteria for the choice of a denuder sampling technique devoted to the measurement of atmospheric nitrous and nitric acids. *Atmospheric Environment*, 24A: 617 - 626.

Pierson, W.R., Brachaczek, W.W., Gorse, R.A.J., Japar, S.M., Norbeck, J.M. and Keeler, G.J., 1987. Acid deposition and atmospheric chemistry at Allegheny Mountain. In: R.W. Johnson, G.E. Gordon, W. Calkins and A.Z. Elzerman (Editors), The Chemistry of Acid Rain: Sources and Atmospheric Processes. American Chemical Society, Washington, D. C., pp. 28 - 38.

Pilie, R.J. and Mack, E.J., 1975. Fog Water Collector, U. S. A. Patent 3,889,532.

Pinnick, R.G., Garvey, D.M. and Duncan, L.D., 1981. Calibration of Knollenberg FSSP light-scattering counters for measurement of cloud droplets. *Journal of Climate and Applied Meteorology*, 20: 1049-1057.

Pinnick, R.G. and Auvermann, H.J., 1979. Response characteristics of Knollenberg light-scattering aerosol counters. *Journal of Aerosol Science*, 10: 55-74.

Politovich, M.K., 1993. A Study of the Broadening of the Droplet Size Distributions in Cumuli. *Journal of the Atmospheric Sciences*, 50(14): 2230 - 2244.

Poulida, O., Schwitkowski, M., Baltensperger, U., Staehelin, J. and Gaeggeler, H.W., 1998. Scavenging of atmospheric constituents in mixed phase clouds at the high-alpine site Jungfraujoch - Part II. influence of riming on the scavenging of particulates and gaseous chemical species. *Atmospheric Environment*, 32(23): 3985 - 4000.

Pruppacher, H.R. and Klett, J.D., 1997. Microphysics of Clouds and Precipitation. Kluwer Academic Publishers, Dordrecht, the Netherlands, 954 pp.

Putaud, J.-P., van Dingenen, R., Mangoni, M., Virkkula, A., Raes, F., Maring, H., Prospero, J.M., Swietlicki, E., Berg, O.H., Hillamo, R. and Mäkelä, T., 2000. Chemical mass closure and assessment of the origin of the submicron aerosol in the marine boundary layer and the free troposphere at Tenerife during ACE-2. *Tellus*, 52B: 141 - 168.

Puxbaum, H. and Tscherwenka, W., 1998. Relationships of major ions in snow fall and rime at Sonnblick observatory (SBO, 3106 m) and implications for scavenging processes in mixed clouds. *Atmospheric Environment*, 32(23): 4011 - 4020.

Qian, G.-W., Ishizaka, Y., Minami, Y., Kurahashi, Y., Tjandradewi, B.I. and Takenaka, C., 1992. Transformation of individual aerosol particles in acidic fog evolution. *Journal of the Meteorological Society of Japan*, 70(2): 711 - 721.

Radojevic, M., Tyler, B.J., Wicks, A.J., Gay, M.J. and Choularton, T.W., 1990. Field studies of SO_2/aqueous S(IV) equilibrium in clouds. *Atmospheric Environment*, 24A(2): 323 - 328.

Reproduced with permission of the copyright owner. Further reproduction prohibited without permission.

Raes, F., Bates, T., McGovern, F. and van Liedekerke, M., 2000. The 2nd Aerosol Characterization Experiment (ACE-2): general overview and main results. *Tellus*, 52B(2): 111 - 125.

Ramundo, R.A. and Seastedt, T.R., 1990. Site-specific underestimation of wetfall NH_4^+ using NADP data. *Atmospheric Environment*, 24A(12): 3093 - 3095.

Rancourt, K.L. and Howe, J.B., 1987. On the distribution of acidity within clouds as a function of droplet size, Mt. Washington Observatory News Bulletin, pp. 48 - 52.

Ranz, W.E. and Wong, J.B., 1952. Impaction of dust and smoke particles on surface and body collectors. *Industrial and Engineering Chemistry*, 44(6): 1371 - 1380.

Rao, X. and Collett, J.L., Jr., 1998. The drop size-dependence of iron and manganese concentrations in clouds and fogs: implications for sulfate production. *Journal of Atmospheric Chemistry*, 30: 273 - 289.

Rao, X., 1997. Cloud chemical heterogeneity and its influence on aqueous Sulfur(IV) oxidation. Ph.D. Dissertation, Department of Civil and Environmental Engineering, University of Illinois at Urbana-Champaign, Urbana-Champaign, IL, 231 pp.

Rao, X. and Collett, J.L., Jr., 1995. Behaviour of S(IV) and formaldehyde in a chemically heterogeneous cloud. *Environmental Science and Technology*, 29: 1023 - 1031.

Rattigan, O.V., Reilly, J.E., Judd, C., Moore, K.F., Das, M., Sherman, D.E., Dutkiewicz, V.A., Collett, J.L., Jr. and Husain, L., 2001. Sulfur dioxide oxidation in clouds at Whiteface Mountain as a function of drop size. *Journal of Geophysical Research: Atmospheres*, 106(D15): 17,347 - 17,358.

Ravishankara, A.R., 1997. Heterogeneous and multi-phase chemistry in the troposphere. *Science*, 276: 1058 - 1065.

Reilly, J.E., Rattigan, O.V., Moore, K.F., Judd, C., Sherman, D.E., Dutkiewicz, V.A., Kreidenweis, S.M., Husain, L. and Collett, J.L., Jr., 2001. Drop size-dependent S(IV) oxidation in chemically heterogeneous radiation fogs. *Atmospheric Environment*, 35(33): 5717 - 5728.

Reilly, J.E., 2000. Application of a tracer technique to study sulfur dioxide oxidation in cloud drops as a function of drop size. M.S. Thesis, Department of Atmospheric Science, Colorado State University, Fort Collins, CO.

Reim, M., 1993. Phenomena of liquid drop impact on solid and liquid surfaces. *Fluid Dynamics Research*, 12: 61-93.

Reynolds, B., Fowler, D. and Thomas, S., 1996. Chemistry of cloud water at an upland site in mid-Wales. *The Science of the Total Environment*, 188: 115 - 125.

Ricci, L., Fuzzi, S., Laj, P., Lazzari, A., Orsi, G., Berner, A., Günther, A., Jaeschke, W., Wendisch, M. and Arends, B.G., 1998. Gas-Liquid Equilibria in Polluted Fog. *Contributions to Atmospheric Physics*, 71(1): 159-170.

Richards, L.W., Anderson, J.A., Blumenthal, D.L., McDonald, J.A., Kok, G.L. and Lazrus, A.L., 1983. Hydrogen peroxide and sulfur(IV) in Los Angeles cloud water. *Atmospheric Environment*, 17(4): 911 - 914.

Reproduced with permission of the copyright owner. Further reproduction prohibited without permission.

Richartz, H., Reischl, A., Trautner, F. and Hutzinger, O., 1990. Nitrated phenols in fog. *Atmospheric Environment*, 24A(12): 3067 - 3071.

Roach, W.T., 1976a. On the effect of radiative exchange on the growth by condensation of a cloud or fog droplet. *Quarterly Journal of the Royal Meteorological Society*, 102: 361 - 372.

Roach, W.T., 1976b. On some quasi-periodic oscillations observed during a field investigation of radiation fog. *Quarterly Journal of the Royal Meteorological Society*, 102: 355 - 359.

Roach, W.T., Brown, R., Caughey, S.J., Garland, J.A. and Readings, C.J., 1976. The physics of radiation fog: I - a field study. *Quarterly Journal of the Royal Meteorological Society*, 102: 313 - 333.

Roelofs, G.J.H., 1993. A cloud chemistry sensitivity study and comparison of explicit and bulk cloud model performance. *Atmospheric Environment*, 27A(15): 2255 - 2264.

Roelofs, G.J.H., 1992a. On the drop and aerosol size dependence of aqueous sulfate formation in a continental cumulous cloud. *Atmospheric Environment*, 26A(13): 2309 - 2321.

Roelofs, G.J.H., 1992b. Drop size dependent sulfate distribution in a growing cloud. *Journal of Atmospheric Chemistry*, 14: 109 - 118.

Rogers, D.C., Baumgardner, D. and Vali, G., 1983. Determination of supercooled liquid water content by measuring rime rate. *Journal of Climate and Applied Meteorology*, 22: 153 - 162.

Sadasivan, S., 1980. Trace constituents in cloud water, rain water, and aerosol sampled collected near the west coast on India during the southwest monsoon. *Atmospheric Environment*, 14: 33 - 38.

Sanhueza, E., Santana, M. and Hermoso, M., 1992. Gas- and aqueous-phase formic and acetic acids at a tropical cloud forest site. *Atmospheric Environment*, 26A(8): 1421 - 1426.

Saxena, V.K., Stogner, R.E., Hendler, A.H., deFelice, T.P., Yeh, R.J.-Y. and Lin, N.-H., 1989. Monitoring the chemical climate of the Mt. Mitchell State Park for evaluation of its impact on forest decline. *Tellus*, 41B: 92 - 109.

Saxena, V.K. and Yeh, R.J.-Y., 1988. Temporal variability in cloud water acidity: physico-chemical characteristic of atmospheric aerosols and windfield. *Journal of Aerosol Science*, 19(7): 1207 - 1210.

Schell, D., Maser, R., Wobrock, W., Jaeschke, W., Georgii, H.-W., Kos, G.P.A., Arends, B.G., Beswick, K.M., Bower, K.N. and Gallagher, M.W., 1997a. A two-stage impactor for fog droplet collection: design and performance. *Atmospheric Environment*, 31(16): 2671 - 2679.

Schell, D., Wobrock, W., Maser, R., Preiss, M., Jaeschke, W., Georgii, H.-W., Gallagher, M.W., Bower, K.N., Beswick, K.M., Pahl, S., Facchini, M.-C., Fuzzi, S., Wiedensohler, A., Hansson, H.-C. and Wendisch, M., 1997b. The size-dependent chemical composition of cloud droplets. *Atmospheric Environment*, 31(16): 2561 - 2576.

Schell, D., Georgii, H.-W., Maser, R., Jaeschke, W., Arends, B.G., Kos, G.P.A., Winkler, P., Schneider, T., Berner, A. and Kruisz, C., 1992. Intercomparison of fog water samplers. *Tellus*, 44B: 612-631.

Reproduced with permission of the copyright owner. Further reproduction prohibited without permission.

Schell, D. and Georgii, H.-W., 1989. Design and operation of a two-stage fogwater collector. In: H.-W. Georgii (Editor), Mechanisms and Effects of Pollutant-Transfer into Forests. Kluwer Academic Publishers, Dordrecht, pp. 221 - 229.

Schemenauer, R.S., Banic, C.M. and Urquizo, N., 1995. High elevation fog and precipitation chemistry in southern Quebec, Canada. *Atmospheric Environment*, 29(17): 2235 - 2252.

Schemenauer, R.S. and Cereceda, P., 1994. A proposed standard fog collector for use in high-elevation regions. *Journal of Applied Meteorology*, 33: 1313 - 1322.

Schemenauer, R.S. and Cereceda, P., 1992. The quality of fog water collected for domestic and agricultural use in Chile. *Journal of Applied Meteorology*, 31: 275 - 290.

Schemenauer, R.S. and Joe, P.I., 1989. The collection efficiency of a massive fog collector. *Atmospheric Research*, 24: 53 - 69.

Schemenauer, R.S. and Winston, C., 1988. The 1986 Chemistry of High Elevation Fog Project, 81st annual meeting of the Air Pollution Control Association. Air Pollution Control Association, Dallas, TX, pp. 88-129.6.

Schemenauer, R.S. and Joe, P.I., 1988. The collection efficiency of a massive fog collector. *Annalen der Meteorologie*, 25(1): 135 - 137.

Schemenauer, R.S., Cereceda, P. and Carvajal, N., 1987. Measurements of fog water deposition and their relationships to terrain features. *Journal of Climate and Applied Meteorology*, 26: 1285 - 1291.

Scherbatskoy, T. and Bliss, M., 1984. Occurrence of acidic rain and cloud water in high elevations ecosystems in the Green Mountains of Vermont. In: P.J. Samson (Editor), The Meteorology of Acid Deposition. Air Pollution Control Association, Pittsburgh, PA, pp. 449 - 463.

Schlesinger, W.H. and Reiners, W.A., 1974. Deposition of water and cations on artificial foliar collectors in Fir Krummholz of New England mountains. *Ecology*, 55: 378 - 386.

Schmitt, G., 1988. Measurements of the chemical composition in cloud and fogwater. In: M.H. Unsworth and D. Fowler (Editors), Acid deposition at high elevation sites. Kluwer Academic Publishers, Dordrecht, pp. 403 - 417.

Schmitt, G., 1986. The temporal distribution of trace element concentrations in fog water during individual fog events. In: H.-W. Georgii (Editor), Atmospheric Pollutants in Forest Areas: Their Deposition and Interception. D. Reidel Publishing Company, Dordrecht, pp. 129 - 141.

Schomburg, C.J., Glotfelty, D.E. and Seiber, J.N., 1991. Pesticide occurrence and distribution in fog collected near Monterey, California. *Environmental Science and Technology*, 25: 155 - 160.

Schwanz, M., Warneck, P., Preiss, M. and Hoffmann, P., 1998. Chemical Speciation of Iron in Fog Water. *Contributions to Atmospheric Physics*, 71(1): 131-143.

Schwarzenböck, A. and Heintzenberg, J., 2000. Cut size minimization and cloud element break-up in a ground-based CVI. *Journal of Aerosol Science*, 31(4): 477 - 489.

Reproduced with permission of the copyright owner. Further reproduction prohibited without permission.

Schwitkowski, M., Baltensperger, U., Gaeggeler, H.W. and Poulida, O., 1998. Scavenging of atmospheric constituents in mixed phase clouds at the high-alpine site Jungfraujoch Part III: quantification of the removal of chemical species by precipitating snow. *Atmospheric Environment*, 32(23): 4001 - 4010.

Scott, B.C. and Laulainen, N.S., 1979. On the concentration of sulfate in precipitation. *Journal of Applied Meteorology*, 18: 138 - 147.

Scott, W.D., 1978. The pH of cloud water and the production of sulfate. *Atmospheric Environment*, 12: 917 - 921.

Sedlak, D.L., Hoigné, J., David, M.M., Colvile, R., Seyffer, E., Acker, K., Wieprecht, W., Lind, J. and Fuzzi, S., 1997. The cloudwater chemistry of iron and copper at Great Dun Fell, U. K. *Atmospheric Environment*, 31(16): 2515 - 2526.

Sedlak, D.L. and Hoigné, J., 1994. Oxidation of S(IV) in atmospheric water by photooxidants and iron in the presence of copper. *Environmental Science and Technology*, 28: 1898 - 1906.

Sedlak, D.L. and Hoigné, J., 1993. The role of copper and oxalate in the redox cycling of iron in atmospheric waters. *Atmospheric Environment*, 27A(14): 2173 - 2185.

Seiber, J.N., Wilson, B.W. and McChesney, M.M., 1993. Air and fog deposition residues of four organophosphate insecticides used on dormant orchards in the San Joaquin Valley, California. *Environmental Science and Technology*, 27: 2236 - 2243.

Seidl, W., 1989. Ionic concentrations and initial S(IV) oxidation rates in droplets during the condensational stage of cloud. *Tellus*, 41B(1): 32 - 50.

Seinfeld, J.H. and Pandis, S.N., 1998. Atmospheric chemistry and physics: from air pollution to climate change. Wiley-Interscience, New York, NY, 1326 pp.

Self, S.A., 2001. personal communication.

Self, S.A., 1980. Diagnostic techniques for combusion MHD systems, American Institute of Aeronautics and Astronautics International Meeting "Global Technology 2000", Baltimore, MD, pp. 20.

Sethi, V. and John, W., 1993. Particle impaction patterns from a circular jet. *Aerosol Science and Technology*, 18: 1 - 10.

Seyffer, E. and Helas, G., 1994. The balance of concentrations of formic and acetic acids in the gas and liquid phase of hydrometeors. In: G. Angeletti and G. Restelli (Editors), Physico-chemical Behaviour of Atmospheric Pollutants. European Commission, Luxembourg, pp. 989 - 994.

Sherman, D.E., 1998. personal communication.

Siefert, R.L., Johansen, A.M., Hoffmann, M.R. and Pehkonen, S.O., 1997. Measurements of trace metal (Fe, Cu, Mn, Cr) oxidation states in fog and stratus clouds. *Journal of the Air and Water Management Association*, 48: 128 - 143.

Sievering, H., Lerner, B., Slavich, J., Anderson, J., Posfai, M. and Cainey, J., 1999. O_3 oxidation of SO_2 in sea-salt aerosol water: size distribution of non-sea-salt sulfate during the First Aerosol Characterization Experiment (ACE-1). *Journal of Geophysical Research*, 104(D17): 21,707 - 21,717.

Reproduced with permission of the copyright owner. Further reproduction prohibited without permission.

Sigg, L., Stumm, W., Zobrist, J. and Zürcher, F., 1987. The chemistry of fog: factors regulating its composition. *Chimia*, 41(5): 159 - 165.

Snider, J.R. and Huang, J., 1998. Factors influencing the retention of hydrogen peroxide and molecular oxygen in rime ice. *Journal of Geophysical Research*, 103(D1): 1405 - 1415.

Snider, J.R., Montague, D.C. and Vali, G., 1992. Hydrogen peroxide retention in rime ice. *Journal of Geophysical Research*, 97(D7): 7569 - 7578.

Staffelbach, T., Neftel, A. and Horotwitz, L.W., 1997. Photochemical oxidant formation over southern Switzerland 2. model results. *Journal of Geophysical Research*, 102(D19): 23,363 - 23,373.

Straub, D.J. and Collett, J.L., Jr., 2001a. Development of a multi-stage cloud water collector: 2. Numerical and experimental calibration. *accepted by Atmospheric Environment.*

Straub, D.J. and Collett, J.L., Jr., 2001b. Numerical and experimental performance evaluation of the 3-Stage FROSTY supercooled cloud collector. *Aerosol Science and Technology*, 34: 247 - 261.

Straub, D.J. and Collett, J.L., Jr., 1999. Numerical and experimental performance evaluation of two multi-stage cloud collectors. 676, Department of Atmospheric Science, Colorado State University, Fort Collins, CO.

Stumm, W. and Morgan, J.J., 1996. Aquatic Chemistry: Chemical Equilibria and Rates in Natural Waters. Wiley-Interscience, New York, NY, 1022 pp.

Svenningsson, B., Hansson, H.-C., Wiedensohler, A., Noone, K.J., Ogren, J.A., Hallberg, A. and Colvile, R., 1994. Hygroscopic growth of aerosol particles and its influence on nucleation scavenging in cloud: experimental results from Kleiner Feldberg. *Journal of Atmospheric Chemistry*, 19: 129 - 152.

Tabata, T., Huzioka, T. and Matsumura, N., 1953. On a recording fog meter. In: T. Hori (Editor), Studies on Fog. Tanne Publishing Company, Sapporo, pp. 169 - 173.

Tanner, R.L., 1987. Chemical instrumentation of atmospheric wet deposition processes. In: R.W. Johnson, G.E. Gordon, W. Calkins and A.Z. Elzerman (Editors), The chemistry of acid rain: sources and atmospheric processes. American Chemical Society, Washington, D.C., pp. 289 - 302.

Tenberken, B. and Bächmann, K., 1998. Sampling and analysis of single cloud and fog drops. *Atmospheric Environment*, 32(10): 1757 - 1763.

Tesar, M., Sir, M., Fottova, D., Fišák, J. and Eliáš, V., 2001. Cloud and fog water deposition and its hydrological and ecological importance in selected regions of the Czech Republic. In: R.S. Schemenauer and H. Puxbaum (Editors), 2nd International Conference on Fog and Fog Collection, St. John's, Newfoundland, Canada, pp. 153 - 156.

Tomlinson, G.H., Brouzes, R.J.P., McLean, R.A.N. and Kadlecek, J.A., 1980. The role of clouds in atmospheric transport of mercury and other pollutants 2. the role of cloudwater in atmospheric transport. In: D. Drabløs and A. Tollan (Editors), Ecological impact of acid precipitation, Sandefjord, Norway, pp. 135 - 137.

Reproduced with permission of the copyright owner. Further reproduction prohibited without permission.

Tsai, P.-J. and Vincent, J.H., 1993. Impaction model for the aspiration efficiencies of aerosol samplers at large angles with respect to the wind. *Journal of Aerosol Science*, 24(7): 919-928.

Twohy, C.H., Austin, P.H. and Charlson, R.J., 1989a. Chemical consequences of the initial diffusional growth of cloud droplets: a clean marine case. *Tellus*, 41B: 51 - 60.

Twohy, C.H., Clarke, A.D., Warren, S.G., Radke, L.F. and Charlson, R.J., 1989b. Light-absorbing material extracted from cloud droplets and its effects on cloud albedo. *Journal of Geophysical Research*, 94(D6): 8623 - 8631.

Valente, R.J., Mallant, R.K.A.M., McLaren, S.E., Schemenauer, R.S. and Stogner, R.E., 1989. Field intercomparison of ground-based cloud physics instruments at Whitetop Mountain, Virginia. *Journal of Atmospheric and Oceanic Technology*, 6: 396 - 406.

van Valin, C.C., Wellman, D.L. and Stearns, L.P., 1987. Aerosol and cloudwater properties and Whiteface Mtn., NY. *Water, Air and Soil Pollution*, 34: 369 - 383.

Vecera, Z. and Dasgupta, P.K., 1991. Measurement of ambient nitrous acid and a reliable calibration source for gaseous nitrous acid. *Environmental Science and Technology*, 25: 255 - 260.

Verhoeven, W., Herrmann, R., Eiden, R. and Klemm, O., 1987. A comparison of the chemical composition of fog and rainwater collected in the Fichtelgebirge, Federal Republic of Germany, and the South Island of New Zealand. *Theoretical and Applied Climatology*, 38: 210 - 221.

Vincent, J.H., 1989. Aerosol Sampling: Science and Practice. John Wiley & Sons, Ltd., Chichester, England, 390 pp.

Vincent, J.H., 1987. Recent advances in aspiration theory for thin-walled and blunt aerosol sampling probes. *Journal of Aerosol Science*, 18(5): 487-498.

Vincent, J.H. and Mark, D., 1982. Applications of blunt sampler theory to the definition and measurement of inhalable dust. *Annals of Occupational Hygiene*, 26(1-4): 3-19.

Vincent, J.H., Hutson, D. and Mark, D., 1982. The nature of air flow near the inlets of blunt dust sampling probes. *Atmospheric Environment*, 16(5): 1243-1249.

Voisin, D., Legrand, M. and Chaumerliac, N., 2000. Scavenging of acidic gases (HCOOH, CH_3COOH, HNO_3, HCl, and SO_2) and ammonia in mixed liquid-solid water clouds at the Puy de Dôme Mountain (France). *Journal of Geophysical Research*, 105(D5): 6817 - 6835.

von Piechowski, M., Nouser, T., Hoigné, J. and Bühler, R.E., 1993. O_2^- decay catalyzed by Cu^{2+} and Cu^+ ions in aqueous solutions: a pulse radiolysis study for atmospheric chemistry. *Ber. Bunsenges. Phys. Chem.*, 97(6): 762 - 771.

Vong, R.J., Baker, B.M., Brechtel, F.J., Collier, R.T., Harris, J.M., Kowalski, A.S., McDonald, N.C. and McInnes, L.M., 1997. Ionic and trace element composition of cloud water collected on the Olympic peninsula of Washington state. *Atmospheric Environment*, 31(13): 1991 - 2001.

Vong, R.J. and Kowalski, A.S., 1995. Eddy correlation measurements of size-dependent cloud droplet turbulent fluxes to complex terrain. *Tellus*, 47B: 331-352.

Reproduced with permission of the copyright owner. Further reproduction prohibited without permission.

Vong, R.J., Sigmon, J.T. and Mueller, S.F., 1991. Cloudwater deposition to Appalachian forests. *Environmental Science and Technology*, 25(6): 1014 - 1021.

Vong, R.J., Bailey, B.H., Markus, M.J. and Mohnen, V.A., 1990. Factors governing cloud water composition in the Appalachian mountains. *Tellus*, 42B: 435 - 453.

Wagenbach, D. (Editor), 1997. High Alpine Air and Snow chemistry. Springer-Verlag, Berlin, 165 - 199 pp.

Waldman, J.M. and Hoffmann, M.R., 1987. Depositional aspects of pollutant behaviour in fog and intercepted clouds. In: R.A. Hites and S.J. Eisenreich (Editors), Sources and Fates of Aquatic Pollutants. Advances in Chemistry Series #216. American Chemical Society, pp. 79 - 129.

Walters, P.T., Moore, M.J. and Webb, A.H., 1983. A separator for obtaining samples of cloudwater in aircraft. *Atmospheric Environment*, 17(6): 1083 - 1091.

Warneck, P., Mirabel, P.H., Salmon, G.A., van Eldik, R., Vinckier, C., Wannowius, K.J. and Zetzsch, C., 1996. Review of the activites and achievements of the EUROTRAC subproject HALIPP. In: P. Warneck (Editor), Heterogeneous and Liquid-Phase Processes. Springer-Verlag, Berlin, pp. 7 - 74.

Watanabe, K., Ishizaka, Y. and Takenaka, C., 2001. Chemical characteristics of cloud water over the Japan Sea and the Northwestern Pacific Ocean near the central part of Japan: airborne measurements. *Atmospheric Environment*, 35: 645 - 655.

Weathers, K.C., Likens, G.E., Bormann, F.H., Bicknell, S.H., Bormann, B.T., Daube, B.C., Jr., Eaton, J.S., Galloway, J.N., Keene, W.C., Kimball, K.D., McDowell, W.H., Siccama, T.G., Smiley, D. and Tarrant, R.A., 1988. Cloudwater chemistry from ten sites in North America. *Environmental Science and Technology*, 22: 1018 - 1026.

Wen, X. and Ingham, D.B., 2000. Aspiration efficiency of a thin-walled cylindrical aerosol sampler at yaw orientations with respect to the wind. *Journal of Aerosol Science*, 31(11): 1355-1365.

Wendisch, M., Garrett, T., Hobbs, P.V. and Strapp, J.W., 2000. PVM-100A performance tests in the NASA and NRC wind tunnels, 13th International Conference on Clouds and Precipitation, Reno, NV, pp. 194 - 198.

Wendisch, M., Mertes, S., Heintzenberg, J., Wiedensohler, A., Schell, D., Wobrock, W., Frank, G., Martinsson, B.G., Fuzzi, S., Orsi, G., Kos, G. and Berner, A., 1998. Drop Size Distribution and LWC in Po Valley Fog. *Contributions to Atmospheric Physics*, 71(1): 87-100.

Wendisch, M., 1998. A quantitative comparison of ground-based FSSP and PVM measurements. *Journal of Atmospheric and Oceanic Technology*, 15: 887-900.

Wendisch, M., Keil, A. and Korolev, A.V., 1996. FSSP characterization with monodisperse water droplets. *Journal of Atmospheric and Oceanic Technology*, 13: 1152-1165.

Wesely, M.L. and Hrcko, B.B., 2000. A review of the current status of knowledge on dry deposition. *Atmospheric Environment*, 34: 2261 - 2282.

Wilkins, E.T., 1956. Air pollution aspects of the London fog of December 1952. *Quarterly Journal of the Royal Meteorological Society*, 80: 267 - 278.

Reproduced with permission of the copyright owner. Further reproduction prohibited without permission.

Winiwarter, W., Fierlinger, H., Puxbaum, H., Facchini, M.-C., Arends, B.G., Fuzzi, S., Schell, D., Kaminski, U., Pahl, S., Schneider, T., Berner, A., Solly, I. and Kruisz, C., 1994. Henry's law and the behavior of weak acids and bases in fog and cloud. *Journal of Atmospheric Chemistry*, 19: 173 - 188.

Winiwarter, W., Brantner, B. and Puxbaum, H., 1992. Comments on: Should bulk cloud water samples obey Henry's law? *Journal of Geophysical Research*, D97: 6075 - 6078.

Winiwarter, W., Puxbaum, H., Fuzzi, S., Facchini, M.-C., Orsi, G., Beltz, N., Enderle, K.H. and Jaeschke, W., 1988. Organic acid gas and liquid-phase measurements in Po Valley fall-winter conditions in the presence of fog. *Tellus*, 40B: 348 - 357.

Winkler, P. and Pahl, S., 1997. Input of trace substances to high elevation forests by cloud water interception. In: S. Fuzzi and D. Wagenbach (Editors), Cloud multi-phase processes and high alpine air and snow chemistry. Springer-Verlag, Berlin, pp. 146 - 152.

Winkler, P., 1992. Design and calibration of a fogwater collector, WMO Technical Conference on Instruments and Methods of Observation (TECO-92). World Meteorological Organization, Vienna, Austria, pp. 17 - 21.

Winkler, P. and Kroll, G., 1987. Preliminary results on fog deposition. In: G. Angeletti and G. Restelli (Editors), Physico-chemical Behaviour of Atmospheric Pollutants. D. Reidel Publishing, Co., Dordrecht, pp. 579 - 587.

Winkler, P., 1986. Observation of fog water composition in Hamburg. In: H.-W. Georgii (Editor), Atmospheric Pollutants in Forest Areas: Their Deposition and Interception. D. Reidel Publishing Company, Dordrecht, pp. 143 - 151.

Winkler, P., 1984. Observations on acid particles and droplets in the atmosphere. In: J.L. Durham (Editor), Chemistry of particles, fogs and rain. Butterworth Publishers, Boston, MA, pp. 161 - 196.

Wobrock, W., Schell, D., Maser, R., Jaeschke, W., Georgii, H.-W., Wieprecht, W., Arends, B.G., Mols, J.J., Kos, G.P.A., Fuzzi, S., Facchini, M.-C., Orsi, G., Berner, A., Solly, I., Kruisz, C., Svenningsson, B., Wiedensohler, A., Hansson, H.-C., Ogren, J.A., Noone, K.J., Hallberg, A., Pahl, S., Schneider, T., Winkler, P., Winiwarter, W., Colvile, R., Choularton, T.W., Flossmann, A. and Borrmann, S., 1994. The Kleiner Feldberg Cloud experiment 1990. An overview. *Journal of Atmospheric Chemistry*, 19: 3 - 35.

Wong, J.B., Ranz, W.E. and Johnstone, H.F., 1955. Inertial impaction of aerosol particles on cylinders. *Journal of Applied Physics*, 26(2): 244 - 249.

Woodcock, A.H., Blanchard, D.C. and Jiusto, J.E., 1981. Marine fog droplets and salt nuclei - part II. *Journal of the Atmospheric Sciences*, 38: 129 - 140.

Wrzesinsky, T., 2001. personal communication.

Wrzesinsky, T., Thalmann, E., Burkhard, R., Eugster, W. and Klemm, O., 2001. Fog deposition of nutrients and pollutants to a montane forest site. In: R.S. Schemenauer and H. Puxbaum (Editors), 2nd International Conference on Fog and Fog Collection, St. John's, Newfoundland, Canada, pp. 169 - 172.

Wrzesinsky, T. and Klemm, O., 2000. Summertime fog chemistry at a mountainous site in Central Europe. *Atmospheric Environment*, 34: 1487 - 1496.

Reproduced with permission of the copyright owner. Further reproduction prohibited without permission.

Wujcik, C.E., Cahill, T.M. and Seiber, J.N., 1999. Determination of trifluoroacetic acid in 1997-1997 precipitation and surface waters in California and Nevada. *Environmental Science and Technology*, 33: 1747 - 1751.

Wurzler, S., Reisin, T.G. and Levin, Z., 2000. Modification of mineral dust particles by cloud processing and subsequent effects on drop size distributions. *Journal of Geophysical Research*, 105(D4): 4501 - 4512.

Wurzler, S., 1998. The scavenging of nitrogen compounds by clouds and precipitation: Part II. the effects of cloud microphysical parameterization on model precitions of nitric acid scavenging by clouds. *Atmospheric Research*, 47-48: 219 - 233.

Wurzler, S., Flossmann, A.I., Pruppacher, H.R. and Schwartz, S.E., 1995. The scavenging of nitrate by clouds and precipitation. *Journal of Atmospheric Chemistry*, 20: 259 - 280.

Xu, G., Sherman, D.E., Andrews, E., Moore, K.F., Straub, D.J., Hoag, K.J. and Collett, J.L., Jr., 1999. The influence of chemical heterogeneity among cloud drop populations on processing of chemical species in winter clouds. *Atmospheric Research*, 51: 119 - 140.

Zhang, X. and McMurry, P.H., 1992. Evaporative losses of fine particulate nitrates during sampling. *Atmospheric Environment*, 26A(18): 3305 - 3312.

Zhang, Y., Kreidenweis, S.M. and Feingold, G., 1999. Stratocumulus processing of gases and cloud condensation nuclei 2: chemistry sensitivity analysis. *Journal of Geophysical Research*, 104(D13): 16,061 - 16,080.

Zhang, Y., Kreidenweis, S.M. and Taylor, G.R., 1998. The effects of clouds on aerosol and chemical species production and distribution. part III: aerosol model description and sensitivity analysis. *Journal of the Atmospheric Sciences*, 55(6): 921 - 939.

Reproduced with permission of the copyright owner. Further reproduction prohibited without permission.

Reproduced with permission of the copyright owner. Further reproduction prohibited without permission.

DISSERTATION

DROP SIZE-DEPENDENT CHEMICAL COMPOSITION IN CLOUDS AND FOGS

VOLUME II: APPENDICES

Submitted by

Katharine F. Moore

Department of Atmospheric Science

In partial fulfullment of the requirements

for the Degree of Doctor of Philosophy

Colorado State University

Fort Collins, Colorado

Spring 2002

Reproduced with permission of the copyright owner. Further reproduction prohibited without permission.

Table of Contents

Volume II

A. Appendix: Review of Cloud Chemistry Measurements 309

B. Appendix: Cloud water collectors – review, characterization and reported field comparisons 345

C. Appendix: The FROSTY Collector: Cleaning, Assembly and Sampling Protocol ... 411

D. Appendix: The CSU 5-Stage Collector: Cleaning & Sampling Protocol 419

E. Appendix: Drop stopping distance and characteristic times for varying ambient conditions 429

F. Appendix: the wind shield (baffle) 437

G. Appendix: Drop size distributions – instruments, problems and processing 444

H. Appendix: Data tables 474

I. Appendix: Performance of the Gerber PVM-100 510

J. Appendix: Microorifice Uniform Deposit Impactor (MOUDI) protocol 515

K. Appendix: Compiled IC statistics 518

Reproduced with permission of the copyright owner. Further reproduction prohibited without permission.

A. Appendix: Review of Cloud Chemistry Measurements

This appendix contains a brief review of the identified cloud water species in the literature. Its goal is to emphasize the large number of species that have been identified by different investigators at a variety of locations around the Earth. It is important to recognize that the discussion in the main text, while comprehensive in many regards, does not include all solutes relevant to the aqueous-phase chemistry.

A.1 Species identified in-cloud

Bulk cloud chemistry measurements have been reported for six of the seven continents: Asia (Watanabe *et al.*, 2001; Qian *et al.*, 1992; Khemani *et al.*, 1987; Okita and Ota, 1981; Petrenchuk and Selezneva, 1970), Australia and New Zealand (Ayers and Gillett, 1988; Verhoeven *et al.*, 1987; Scott, 1978), North America (Anderson *et al.*, 1999; Collett *et al.*, 1999a; Schemenauer, 1986), South America (Eklund *et al.*, 1997; Sanhueza *et al.*, 1992; Schemenauer and Cereceda, 1992a), Europe (Acker *et al.*, 1998b; Fuzzi *et al.*, 1998a; Choularton *et al.*, 1997), and Africa (Eckardt and Schemenauer, 1998; Schemenauer and Cereceda, 1992b; Levin *et al.*, 1990). A few individual drop measurements have been reported for the South Pole as well (Ohtake, 1981). Several major cloud observation field campaigns in Europe, North America, and the North Atlantic have been completed in the last 15 years as the importance of clouds to atmospheric chemistry has become increasingly recognized (Bower *et al.*, 2000; Anderson *et al.*, 1999; Collett *et al.*, 1999a; Acker *et al.*, 1998a; Fuzzi *et al.*, 1998a; Choularton *et al.*, 1997; Wagenbach, 1997; Preiss *et al.*, 1994; Wobrock *et al.*, 1994; Heintzenberg, 1992; Weathers *et al.*, 1988a; Schemenauer,

Reproduced with permission of the copyright owner. Further reproduction prohibited without permission.

1986). These campaigns, in addition to the specific interests of individual investigators working in their own locales, have generated a large number of cloud composition data sets.

As indicated in the main text, pH values < 2 and > 10 have been reported, but 3 – 7 is a more typical range for the observations. Other inorganic ions that have been reported include: chloride, nitrate, nitrite, sulfate, sulfite, bromide, iodide, sodium, ammonium, potassium, magnesium, calcium, phosphate, non-sea-salt calcium, non-sea-salt sulfate, bicarbonate, and fluoride. It should be noted that low molecular weight organic acids can be easily mis-identified as fluoride in some ion chromatographic analyses, which raises questions about some measurements. Total, dissolved, and occasionally the speciation of some of the following metals have been reported: Fe, Mn, Cu, Pb, Si, Zn, Ni, Al, S, Ti, P, V, Te, Th, Pd, Hg, Sr, Cd, Ba, As, Sb, Se, Cr, Rb, Li, Be, Ag, Tl, U, Ga, Ge, Y, Zr, Nb, Cs, La, Ce, Pr, Nd, Sm, Eu, Gd, Tb, Dy, Ho, Er, Tm, Yb, Lu, Hf, Bi, B, Mo, and Sn. Hydrogen peroxide and "organic" peroxides have also been identified as have total S(IV), hydroxymethanesulfonate (HMS), and methane sulfonic acid (MSA) which are relevant to S(IV)-to-S(VI) aqueous-phase oxidation. Carbon-based compounds have been identified and constitute an area of active research. The simplest quantification is as elemental, total organic or dissolved organic carbon. One avenue of organic cloud water research attempts to primarily distinguish compounds by their general functionality (neutral species, high molecular weight aromatic polycarboxylic acids, etc.), because current techniques for individual identification leave much of the organic mass unidentified. Given this limitation, however, a wide variety of classes and/or individual compounds have been successfully identified: mono- and dicarboxylic acids (no less than 17), carbonyls (principally HCHO, but at least 10 aldehydes and ketones), aliphatic alcohols, phenols (no less than 20 – mostly methyoxylated or nitrated), n-alkanes, aromatics, polycyclic aromatic compounds (not less than 20 in addition to polychlorinated biphenyls and dioxins and furans), pesticides and their break-down products (as distinct from the previous categories), proteins and their break-down products, bacteria, yeast, molds, and "biological debris". While there is some overlap between the organic categories identified above, it is evident that there is a rich organic chemistry in clouds co-existing and

Reproduced with permission of the copyright owner. Further reproduction prohibited without permission.

interacting with the more widely reported mainly inorganic species. Citations for this work are found in the next section.

A.2 Cloud chemistry literature

The observations discussed in the citations that follow have been made by a variety of methods on both the ground and in the air. They are primarily "bulk" cloud composition measurements, but size-resolved, individual drop, and drop residue citations are also included. They have not been filtered for poor sampling and analytical protocols as the relevant information has not always been reported. It is important to recognize that no measurement is independent of either the method, equipment and/or investigator. It is not uncommon for field data to be repeatedly reported in a variety of formats (e.g. annual average, individual case study), but no attempt has been made to remove papers that duplicate results presented elsewhere. Modeling studies that draw on field measurements have been included as sometimes the observational data is not otherwise reported, and/or the study is cited as a data source. Selected conference proceedings have been included because they are either widely cited, peer-reviewed, or not otherwise available in the English language. Studies focusing solely on measurements of fog water volume, precipitation chemistry, weather modification and isotopic composition have been omitted.

While these studies represent an extensive amount of effort, there are some limitations. Cloud sampling is generally limited (for ground-based studies) to specific time periods of the year, and collected water volume generally does not permit extensive analysis for all species in every sample. Therefore, while much has been done, there is still much to do.

Reproduced with permission of the copyright owner. Further reproduction prohibited without permission.

A.3 References for this Appendix

Acker, K., Möller, D., Wieprecht, W., Auel, R. and Kalaß, D., 2001. Results of cloud physical and chemical measurements in low clouds observed at Mt. Brocken, Germany. In: R.S. Schemenauer and H. Puxbaum (Editors), 2nd International Conference on Fog and Fog Collection, St. John's, Newfoundland, Canada, pp. 117 - 120.

Acker, K., Möller, D., Marquardt, W., Brüggemann, E., Wieprecht, W., Auel, R. and Kalaß, D., 1998a. Atmospheric research program for studying changing emission patterns after German unification. *Atmospheric Environment*, **32**(20): 3435 - 3443.

Acker, K., Möller, D., Wieprecht, W., Kalaß, D. and Auel, R., 1998b. Investigations of ground-based clouds at the Mt. Brocken. *Fresenius Journal of Analytical Chemistry*, **361**: 59 - 64.

Acker, K., Möller, D., Wieprecht, W. and Naumann, S., 1995a. Mt. Brocken, a site for a cloud chemistry measurement programme in central Europe. *Water, Air and Soil Pollution*, **85**: 1979 - 1984.

Acker, K., Wieprecht, W., Möller, D., Mauersberger, G., Naumann, S. and Oestreich, A., 1995b. Evidence of ozone destruction in clouds. *Naturwissenschaften*, **82**: 86 - 89.

Adzuhata, T., Okamura, T., Inotsume, J., Kikuchi, R., Ozeki, T., Kajikawa, M. and Ogawa, N., 2001. A proposed fog uptake mechanism of air pollutant in Northern Japan using oblique rotational factor analysis. In: R.S. Schemenauer and H. Puxbaum (Editors), 2nd International Conference on Fog and Fog Collection, St. John's, Newfoundland, Canada, pp. 25 - 28.

Aggarwal, S.G., Tiwari, K.K., Patel, R., Agarwal, S., Gupta, V.K. and Mundhara, G.L., 2001. Pesticide contamination in fog-water of middle-east part of India. In: R.S. Schemenauer and H. Puxbaum (Editors), 2nd International Conference on Fog and Fog Collection, St. John's, Newfoundland, Canada, pp. 81 - 84.

Ali, K., Tiwari, S., Momin, G.A., Rao, P.S.P., Safai, P.D., Naik, M.S. and Chate, D.M., 2001. Chemical composition of fog water at Delhi, North India. In: R.S. Schemenauer and H. Puxbaum (Editors), 2nd International Conference on Fog and Fog Collection, St. John's, Newfoundland, Canada, pp. 97 - 100.

Anastasio, C. and McGregor, K.G., 2001. Chemistry of fog water in California's Central Valley: 1. in situ photoformation of hydroxyl radical and singlet molecular oxygen. *Atmospheric Environment*, **35**: 1079 - 1089.

Anastasio, C. and McGregor, K.G., 2000. Photodestruction of dissolved organic nitrogen species in fog waters. *Aerosol Science and Technology*, **32**(2): 106 - 119.

Anderson, D.E. and Landsberg, H.E., 1979. Detailed structure of pH in hydrometeors. *Environmental Science and Technology*, **13**(8): 992 - 994.

Anderson, J.B., Baumgardner, R.E., Mohnen, V.A. and Bowser, J.J., 1999. Cloud chemistry in the eastern United States, as sampled from three high-elevation sites along the Appalachian mountains. *Atmospheric Environment*, **33**: 5105 - 5114.

Andre, K., Dlugi, R. and Schnatz, G., 1981. Absorption of visible radiation by atmospheric aerosol particles, fog and cloud water residues. *Journal of the Atmospheric Sciences*, **38**: 141 - 155.

Reproduced with permission of the copyright owner. Further reproduction prohibited without permission.

Aneja, V.P., Claiborn, C.S., Chiswell, S.R. and Bradow, R.L., 1988. Dynamic chemical characterization of montane clouds, 81st annual meeting of the Air Pollution Control Association. Air Pollution Control Association, Dallas, TX, pp. 88-129.2.

Ayers, G.P. and Gillett, R.W., 1988. Acidification in Australia. In: H. Rodhe and R. Herrera (Editors), Acidification in Tropical Countries. John Wiley and Sons, Ltd., Chichester, pp. 347 - 398.

Azevado, J. and Morgan, D.L., 1974. Fog precipitation in coastal California forests. *Ecology*, **55**: 1135 - 1141.

Baechmann, K., Ebert, P., Haag, I. and Prokop, T., 1996. The chemical composition of raindrops as a function of drop radius - I. field measurements at the cloud base and below the cloud. *Atmospheric Environment*, **30**(7): 1019 - 1025.

Baltensperger, U., Schwitkowski, M., Jost, D.T., Nyeki, S., Gäggeler, H.W. and Poulida, O., 1998. Scavenging of atmospheric constituents in mixed phase clouds at the high-alpine site Jungfraujoch Part 1: basic concept and aerosol scavenging by clouds. *Atmospheric Environment*, **32**(23): 3975 - 3983.

Banic, C.M., Schemenauer, R.S. and Anlauf, K.G., 1991. Continuous high elevation surface chemical measurements in Quebec during the 1988 and 1990 EMEFS intensives, 7th joint conference on applications of air pollution meteorology with the Air and Waste Management Association. American Meteorological Society and the Air and Waste Management Association, New Orleans, LA, pp. 242 - 245.

Banic, C.M., Isaac, G.A., Cho, H.R. and Iribarne, J.V., 1986. The distribution of pollutants near a frontal surface: a comparison between field experiments and modeling. *Water, Air and Soil Pollution*, **30**: 171 - 177.

Bank, S. and Castillo, R.A., 1987. Analysis of organic matter from cloud particles. *Geophysical Research Letters*, **14**(3): 210 - 212.

Barth, M.C., Hegg, D.A., Hobbs, P.V., Walega, J.G., Kok, G.L., Heikes, B.G. and Lazrus, A.L., 1989. Measurements of atmospheric gas-phase and aqueous-phase hydrogen peroxide concentrations in winter on the east coast of the United States. *Tellus*, **41B**: 61 - 69.

Basabe, F.A., Edmonds, R.L., Chang, W.L. and Larson, T.V., 1989. Fog and cloud water chemistry in Western Washington. In: R.K. Olson and A.S. Lefohn (Editors), Effects of air pollution on Western Forests. Air and Waste Management Association, Anaheim, CA, pp. 33 - 49.

Bator, A. and Collett, J.L., Jr., 1997. Cloud chemistry varies with drop size. *Journal of Geophysical Research: Atmospheres*, **102**: 28,071 - 28,078.

Bauer, H., Giebl, H., Kasper-Giebl, A., Löflund, M., Schuster, B., Zibuschka, F., Hitzenberger, R., Reischl, G. and Puxbaum, H., 2001. Bacteria and fungi in aerosols and clouds. In: R.S. Schemenauer and H. Puxbaum (Editors), 2nd International Conference on Fog and Fog Collection, St. John's, Newfoundland, Canada, pp. 5 - 8.

Behra, P. and Sigg, L., 1990. Evidence for redox cycling of iron in atmospheric water droplets. *Nature*, **344**: 419 - 421.

Reproduced with permission of the copyright owner. Further reproduction prohibited without permission.

Behra, P., Sigg, L. and Stumm, W., 1989. Dominating influence of NH_3 on the oxidation of aqueous SO_2: the coupling of NH_3 and SO_2 in atmospheric water. *Atmospheric Environment*, **23**(12): 2691 - 2707.

Beltz, N., Jaeschke, W., Kok, G.L., Gitlin, S.N., Lazrus, A.L., McLaren, S., Shakespeare, D. and Mohnen, V.A., 1987. A comparison of the enzyme fluorometric and the peroxyoxalate chemiluminescence methods for measuring H_2O_2. *Journal of Atmospheric Chemistry*, **5**: 311 - 322.

Berg, N., Dunn, P. and Fenn, M., 1991. Spatial and temporal variability of rime ice and snow chemistry at fives sites in California. *Atmospheric Environment*, **25A**(5/6): 915 - 926.

Bicknell, S.H., 1989. Fog and rain chemistry in Northern California. In: R.K. Olson and A.S. Lefohn (Editors), Effects of air pollution on western forests. Air and Waste Management Association, Anaheim, CA, pp. 147 - 167.

Bin, L. and Wenquan, S., 1996. Analyses of several chemical composition of the stratus in north along Mt. Tianshan in Xinjiang in winter, 12th International Conference on Clouds and Precipitation, Zurich, Switzerland, pp. 1125 - 1127.

Boatman, J.F., van Valin, C.C., Ray, J.D. and Gunter, R.L., 1991. The physical and chemical characteristics of clouds sampled during the 1988 ACID-MODES experiment, 7th joint conference on applications of Air Pollution Meteorology with the Air and Waste Management Association. American Meteorological Society and the Air and Waste Management Association, New Orleans, LA, pp. 238 - 241.

Bormann, B.T., Tarrant, R.F., McClellan, M.H. and Savage, T., 1989. Chemistry of rainwater and cloud water at remote sites in Alaska and Oregon. *Journal of Environmental Quality*, **18**: 149 - 152.

Borys, R.D., Lowenthal, D.H. and Mitchell, D.L., 2000. The relationships among cloud microphysics, chemistry, and precipitation rate in cold mountain clouds. *Atmospheric Environment*, **34**: 2593 - 2602.

Borys, R.D., Lowenthal, D.H., Wetzel, M.A., Herrera, F., Gonzalez, A. and Harris, J., 1998. Chemical and microphysical properties of marine stratiform cloud in the north Atlantic. *Journal of Geophysical Research*, **103**(D17): 22,073 - 22,085.

Borys, R.D., Hindman, E.E. and DeMott, P.J., 1988. The chemical fractionation of atmospheric aerosol as a result of snow crystal formation and growth. *Journal of Atmospheric Chemistry*, **7**: 213 - 239.

Bower, K.N., Choularton, T.W., Gallagher, M.W., Beswick, K.M., Flynn, M.J., Allen, A.G., Davison, B.M., James, J.D., Robertson, L., Harrison, R.M., Hewitt, C.N., Cape, J.N., McFadyen, G.G., Milford, C., Sutton, M.A., Martinsson, B.G., Frank, G., Swietlicki, E., Zhou, J., Berg, O.H., Mentes, B., Papaspiropoulos, G., Hansson, H.-C., Leck, C., Kulmala, M., Aalto, P., Väkevä, M., Berner, A., Bizjak, M., Fuzzi, S., Laj, P., Facchini, M.-C., Orsi, G., Ricci, L., Nielsen, M., Allan, B.J., Coe, H., McFiggans, G., Plane, J.M.C., Collett, J.L., Jr., Moore, K.F. and Sherman, D.E., 2000. ACE-2 HILLCLOUD. An overview of the ACE-2 ground-based cloud experiment. *Tellus*, **52B**(2): 750-778.

Bower, K.N., Choularton, T.W., Gallagher, M.W., Colville, R.N., Beswick, K.M., Inglis, D.W.F., Bradbury, C., Martinsson, B.G., Swietlicki, E., Berg, O.H., Cederfelt, S.-I., Frank, G., Zhou, J., Cape, J.N., Sutton, M.A., McFadyen, G.G., Milford, C., Birmili, W., Yuskiewicz, B., Wiedensohler, A., Stratmann, F., Wendisch, M., Berner, A., Ctyroky, P., Galambos, Z., Mesfin, S.H., Dusek, U., Dore, C.J., Lee, D.S., Pepler, S.A., Bizjak, M. and Divjak, B.,

Reproduced with permission of the copyright owner. Further reproduction prohibited without permission.

1999. The Great Dun Fell Experiment 1995: an overview. *Atmospheric Research*, **50**: 151 - 184.

Bradbury, C., Bower, K.N., Choularton, T.W., Swietlicki, E., Birmili, W., Wiedensohler, A., Yuskiewicz, B., Berner, A., Dusek, U., Dore, C. and McFadyen, G.G., 1999. Modelling of aerosol modification resulting from passage through a hillcap cloud. *Atmospheric Research*, **50**: 185 - 204.

Brantner, B., Fierlinger, H., Puxbaum, H. and Berner, A., 1994. Cloudwater chemistry in the subcooled droplet regime at Mount Sonnblick (3106 m asl, Salzburg, Austria). *Water, Air and Soil Pollution*, **74**: 363 - 384.

Bressan, D.J. and Larson, R.E., 1979. The history of air forming various marine fogs of Nova Scotia in August 1975. *Journal of Geophysical Research*, **84**(C4): 1746 - 1754.

Brewer, R.L., Gordon, R.J., Shepard, L.S. and Ellis, E.C., 1983. Chemistry of mist and fog from the Los Angeles urban area. *Atmospheric Environment*, **17**(11): 2267 - 2270.

Bridges, K.S., 1998. Deposition processes and their impact on a heavily industrialized region of the northern Czech Republic. Ph.D. Dissertation, School of Environmental Sciences, University of East Anglia.

Bridges, K.S., Davies, T.D., Jickells, T.D., Zeman, Z. and Hunova, I., 1998. Cloudwater observations on the Czech Krusne Hory Mountain plateau, overlooking a heavily-industrialized valley, 1st International conference on fog and fog collection, Vancouver, Canada, pp. 65 - 68.

Brown, R.M., Daum, P.H., Schwartz, S.E. and Hjemfelt, M.F., 1984. Variations in the chemical composition of clouds during frontal passage. In: P.J. Samson (Editor), The Meteorology of Acid Deposition. Air Pollution Control Association, Pittsburgh, PA, pp. 202 - 212.

Burkhard, E.G., Ghauri, B.M., Dutkiewicz, V.A. and Husain, L., 1995. A multielement tracer technique for the determination of SO_2 oxidation in clouds. *Journal of Geophysical Research*, **100**(D12): 26,051 - 26,059.

Burkhard, E.G., Dutkiewicz, V.A. and Husain, L., 1994. A study of SO_2, $SO_4^=$ and trace elements in clear air and clouds above the midwestern United States. *Atmospheric Environment*, **28**(8): 1521 - 1533.

Cape, J.N., Hargreaves, K.J., Storeton-West, R.L., Jones, B., Davies, T., Colvile, R., Gallagher, M.W., Choularton, T.W., Pahl, S., Berner, A., Kruisz, C., Bizjak, M., Laj, P., Facchini, M.-C., Fuzzi, S., Arends, B.G., Acker, K., Wieprecht, W., Harrison, R.M. and Peak, J.D., 1997. The budge of oxidized nitrogen species in orographic clouds. *Atmospheric Environment*, **31**(16): 2625 - 2636.

Cape, J.N., Hargreaves, K.J., Storeton-West, R.L., Fowler, D., Colvile, R., Choularton, T.W. and Gallagher, M.W., 1992. Nitrite in orographic cloud as an indicator of nitrous acid in rural air. *Atmospheric Environment*, **26A**(13): 2301 - 2307.

Capel, P.D., Gunde, R., Zürcher, F. and Giger, W., 1990. Carbon speciation and surface tension of fog. *Environmental Science and Technology*, **24**(5): 722 - 727.

Carter, E.J. and Borys, R.D., 1993. Aerosol-cloud chemical fractionation: enrichment factor analysis of cloud water. *Journal of Atmospheric Chemistry*, **17**: 277 - 292.

Reproduced with permission of the copyright owner. Further reproduction prohibited without permission.

Castillo, R.A., Kadlecek, J.A. and McLaren, S., 1985. Selected Whiteface Mountain cloud water concentrations Summers 1981 and 1982. *Water, Air and Soil Pollution*, **24**: 323 - 328.

Castillo, R.A. and Jiusto, J.E., 1984. A preliminary study of the chemical modification of cloud condensation nuclei in stratiform clouds at Whiteface Mountain, NY. *Atmospheric Environment*, **18**(9): 1933 - 1937.

Castillo, R.A., Jiusto, J.E. and McLaren, E., 1983. The pH and ionic composition of stratiform cloud water. *Atmospheric Environment*, **17**(8): 1497 - 1505.

Castillo, R.A. and Jiusto, J.E., 1983. Characteristics of non-precipitating stratiform clouds. In: H.R. Pruppacher, R.G. Semonin and W.G.N. Slinn (Editors), Precipitation Scavenging, Dry Deposition, and Resuspension. Elsevier, New York, NY, pp. 115 - 122.

Chandler, A.S., Choularton, T.W., Dollard, G.J., Eggleton, A.E.J., Gay, M.J., Hill, T.A., Jones, B.M.R., Tyler, B.J., Bandy, B.J. and Penkett, S.A., 1988a. Measurements of H_2O_2 and SO_2 in clouds and estimates of their reaction rate. *Nature*, **336**: 562 - 565.

Chandler, A.S., Choularton, T.W., Dollard, G.J., Gay, M.J., Hill, T.A., Jones, A., Jones, B.M.R., Morse, A.P., Penkett, S.A. and Tyler, B.J., 1988b. A field study of the cloud chemistry and cloud microphysics at Great Dun Fell. *Atmospheric Environment*, **22**(4): 683 - 694.

Chang, W.-L., 1989. Characterization of cloud and fog water in the mountains of western Washington. M. S. Thesis, Department of Civil Engineering, University of Washington, Seattle, WA.

Chérif, S., Millet, M., Sanusi, A., Herckes, P. and Wortham, H., 1998. Protocol for analysis of trace metals and other ions in filtered and unfiltered fog water. *Environmental Pollution*, **103**: 301 - 308.

Choularton, T.W., Colvile, R., Bower, K.N., Gallagher, M.W., Wells, M., Beswick, K.M., Arends, B.G., Möls, J.J., Kos, G.P.A., Fuzzi, S., Lind, J., Orsi, G., Facchini, M.-C., Laj, P., Gieray, R., Wieser, P., Engelhardt, T., Berner, A., Kruisz, C., Möller, D., Acker, K., Wieprecht, W., Lüttke, J., Levsen, K., Bizjak, B., Hansson, H.-C., Cederfelt, S.-I., Frank, G., Mentes, B., Martinsson, B.G., Orsini, D., Svenningsson, B., Swietlicki, E., Wiedensohler, A., Noone, K.J., Pahl, S., Winkler, P., Seyffer, E., Helas, G., Jaeschke, W., Georgii, H.-W., Wobrock, W., Preiss, M., Maser, R., Schell, D., Dollard, G.J., Jones, B., Davies, T., Sedlak, D.L., David, M.M., Wendisch, M., Cape, J.N., Hargreaves, K.J., Sutton, M.A., Storeton-West, R.L., Fowler, D., Hallberg, A., Harrison, R.M. and Peak, J.D., 1997. The Great Dun Fell Cloud Experiment 1993: an overview. *Atmospheric Environment*, **31**(16): 2393 - 2407.

Chung, Y.S., Kim, H.S. and Yoon, M.B., 1999. Observations of visibility and chemical composition related to fog, mist and haze in South Korea. *Water, Air and Soil Pollution*, **111**: 139 - 157.

Chýlek, P., Banic, C.M., Johnson, B., Damiano, P.A., Isaac, G.A., Leaitch, W.R., Liu, P.S.K., Boudala, F.S., Winter, B. and Ngo, D., 1996. Black carbon: atmospheric concentrations and cloudwater content measurements over southern Nova Scotia. *Journal of Geophysical Research*, **101**(D22): 29,105 - 29,110.

Claiborn, C.S. and Aneja, V.P., 1991. Measurements of atmospheric hydrogen peroxide in the gas phase and in cloud water. *Journal of Geophysical Research*, **96**(D10): 18,771 - 18,787.

Reproduced with permission of the copyright owner. Further reproduction prohibited without permission.

Clark, P.A., Fletcher, I.S., Kallend, A.S., McElroy, W.J., Marsh, A.R.W. and Webb, A.H., 1984. Observations of cloud chemistry during long-range transport of power plant plumes. *Atmospheric Environment*, **18**(9): 1849 - 1858.

Collett, J.L., Jr., Hoag, K.J., Sherman, D.E., Bator, A. and Richards, L.W., 1999a. Spatial and temporal variations in San Joaquin Valley fog chemistry. *Atmospheric Environment*, **33**: 129 - 140.

Collett, J.L., Jr., Iovinelli, R.J. and Demoz, B.B., 1995. A three-stage cloud impactor for size-resolved measurement of cloud drop chemistry. *Atmospheric Environment*, **29**(10): 1145 - 1154.

Collett, J.L., Jr., Oberholzer, B. and Staehelin, J., 1993a. Cloud chemistry at Mt. Rigi Switzerland: dependence on drop size and relationship to precipitation chemistry. *Atmospheric Environment*, **27A**: 33 - 42.

Collett, J.L., Jr., Daube, B.C., Jr., Munger, J.W. and Hoffmann, M.R., 1990a. A comparison of two cloudwater/fogwater collectors: the rotating arm collector and the Caltech active strand cloudwater collector. *Atmospheric Environment*, **24A**(7): 1685 - 1692.

Collett, J.L., Jr., Hoag, K.J., Rao, X. and Pandis, S.N., 1999b. Internal acid buffering in San Joaquin Valley fog drops and its influence on aerosol processing. *Atmospheric Environment*, **33**: 4833 - 4847.

Collett, J.L., Jr., Bator, A., Rao, X. and Demoz, B.B., 1994. Acidity variations across the cloud drop size spectrum and their influence on rates of atmospheric sulfate production. *Geophysical Research Letters*, **21**(22): 2393 - 2396.

Collett, J.L., Jr., Oberholzer, B., Mosimann, L., Staehelin, J. and Waldvogel, A., 1993b. Contributions of cloud processes to precipitation chemistry in mixed phase clouds. *Water, Air and Soil Pollution*, **68**: 43 - 57.

Collett, J.L., Jr., Daube, B.C., Jr., Gunz, D.W. and Hoffmann, M.R., 1990b. Intensive studies of Sierra Nevada cloudwater chemistry and its relationship to precursor aerosol and gas concentrations. *Atmospheric Environment*, **24A**(7): 1741 - 1757.

Collett, J.L., Jr., Daube, B.C., Jr. and Hoffmann, M.R., 1990c. The chemical composition of intercepted cloud water in the Sierra Nevada. *Atmospheric Environment*, **24A**: 959 - 972.

Collett, J.L., Jr., Daube, B.C., Jr., Munger, J.W. and Hoffmann, M.R., 1989. Cloudwater chemistry in Sequoia National Park. *Atmospheric Environment*, **23**(5): 999 - 1007.

Crossley, A., Harvey, F.J., Cape, J.N., Guillevic, C., Binnie, J., Wilson, D.B. and Fowler, D., 1998. Long-term measurements of cloud frequency and chemical composition in an upland forest in Scotland, 1st international conference on fog and fog collection, Vancouver, Canada, pp. 321 - 324.

Crossley, A., Wilson, D.B. and Milne, R., 1992. Pollution in the upland environment. *Environmental Pollution*, **75**: 81 - 87.

Crossley, A., 1988. Particles in orographic cloud and implications of their transfer to plant surfaces. In: M.H. Unsworth and D. Fowler (Editors), Acid deposition at high elevation sites. Kluwer Academic Publishers, Dordrecht, pp. 453 - 464.

Cunningham, R., 1998. Fog studies in the Bay of Fundy over a span of 60 years, 1st international conference on fog and fog collection, Vancouver, Canada, pp. 153 - 156.

Reproduced with permission of the copyright owner. Further reproduction prohibited without permission.

Cunningham, R.H., 1941. Chloride content of fog water in relation to air trajectory. *Bulletin of the American Meteorology Society*, **22**: 17 - 20.

Dasch, J.M., 1988a. Chemical inputs to fir trees from rain and clouds at Clingmans Peak, North Carolina, 81st annual meeting of the Air Pollution Control Association. Air Pollution Control Association, Dallas, TX, pp. 88-129.3.

Dasch, J.M., 1988b. Hydrological and chemical inputs to fir trees from rain and clouds during a 1-month study at Clingmans Peak, NC. *Atmospheric Environment*, **22**(10): 2255 - 2262.

Daum, P.H., Kelly, T.J., Schwartz, S.E. and Newman, L., 1984a. Measurements of the chemical composition of stratiform clouds. *Atmospheric Environment*, **18**(12): 2671 - 2684.

Daum, P.H., Schwartz, S.E. and Newman, L., 1984b. Acidic and related constituents in liquid water stratiform clouds. *Journal of Geophysical Research*, **89**(D1): 1447 - 1458.

Daum, P.H., Schwartz, S.E. and Newman, L., 1983. Studies of the gas- and aqueous-phase composition of stratiform clouds. In: H.R. Pruppacher, R.G. Semonin and W.G.N. Slinn (Editors), Precipitation Scavenging, Dry Deposition, and Resuspension. Elsevier, New York, NY, pp. 31 - 44.

Däumer, B., Niessner, R. and Klockow, D., 1988. Design and calibration of a low volume fog sampler. *Journal of Aerosol Science*, **19**(2): 175 - 181.

Decesari, S., Facchini, M.-C., Fuzzi, S. and Tagliarini, E., 2000. Characterization of water-soluble organic compounds in atmospheric aerosol: a new approach. *Journal of Geophysical Research*, **105**(D1): 1481 - 1489.

deFelice, T.P., 1997. Investigation of wet acidic deposition episodes capable of damaging red spruce in the Mt. Mitchell State Park. *Atmospheric Research*, **43**: 325 - 344.

deFelice, T.P. and Saxena, V.K., 1990a. Mechanisms for the operation of 3 cloud water collectors: comparison of mountain-top results. *Atmospheric Research*, **25**: 277 - 292.

deFelice, T.P. and Saxena, V.K., 1990b. Temporal and vertical distribution of acidity and ionic composition in clouds: comparison between modeling results and observations. *Journal of the Atmospheric Sciences*, **47**(9): 1117 - 1126.

Del Monte, M. and Rossi, P., 1997. Fog and gypsum crystals on building materials. *Atmospheric Environment*, **31**: 1637 - 1646.

Derexel, P. and Masniere, P., 1990. Study of rain and fogs collected in the Vosges Region (1986 - 1988). In: G. Restelli and G. Angeletti (Editors), Physico-Chemical Behaviour of Atmospheric Pollutants. Kluwer Academic Publishers, Dordrecht, pp. 431 - 438.

Dixon, R.M. and Charlson, R.J., 1994. Development of a new real-time method for measuring S(IV) in cloud water using a counter-flow virtual impactor. *Tellus*, **46B**: 193 - 204.

Dlugi, R., 1989. Chemistry and deposition of soot particles in moist air and fog. *Aerosol Science and Technology*, **10**: 93 - 105.

Dollard, G.J., Jones, B.M.R., Chandler, A.S. and Gay, M.J., 1988. Measurements of ambient SO_2 and H_2O_2 at Great Dun Fell and evidence of their reaction in cloud. In: M.H. Unsworth and D. Fowler (Editors), Acid deposition at high elevation sites. Kluwer Academic Publishers, Dordrecht, pp. 215 - 229.

Reproduced with permission of the copyright owner. Further reproduction prohibited without permission.

Dollard, G.J., Unsworth, M.H. and Harve, M.J., 1983. Pollutant transfer in upland regions by occult deposition. *Nature*, **302**(241 - 243).

Dollard, G.J. and Unsworth, M.H., 1983. Pollutant deposition as a result of interception of wind-driven cloud - measurements made at a site in northern England. In: H.R. Pruppacher, R.G. Semonin and W.G.N. Slinn (Editors), Precipitation Scavenging, Dry Deposition, and Resuspension. Elsevier, New York, pp. 161 - 169.

Dröscher, F., 1986. Design of a fog water collector for chemical analysis. In: H.-W. Georgii (Editor), Atmospheric Pollutants in Forest Areas: Their Deposition and Interception. D. Reidel Publishing Company, Dordrecht, pp. 111 - 128.

Duncan, L.C., 1992. Chemistry of rime and snow collected at a site in the central Washington Cascades. *Environmental Science and Technology*, **26**(1): 61 - 66.

Dutkiewicz, V.A. and Husain, L., 1998. Inefficient scavenging of aerosol sulfate by non-precipitating clouds in polluted air. *Atmospheric Environment*, **32**(16): 2793 - 2801.

Dutkiewicz, V.A., Burkhard, E.G., Hussain, M.M. and Husain, L., 1996. Scavenging and solubility of trace element bearing aerosols in frontal clouds at Whiteface Mountain, NY. *Atmospheric Research*, **41**: 337 - 348.

Dutkiewicz, V.A., Burkhard, E.G. and Husain, L., 1995. Availability of H_2O_2 for oxidation of SO_2 in clouds in the northeastern United States. *Atmospheric Environment*, **29**(22): 3281 - 3292.

Eckardt, F.D. and Schemenauer, R.S., 1998. Fog water chemistry in the Namib Desert, Namibia. *Atmospheric Environment*, **32**(14/15): 2595 - 2599.

Eklund, T.J., McDowell, W.H. and Pringle, C.M., 1997. Seasonal variation of tropical precipitation chemistry: La Selva, Costa Rica. *Atmospheric Environment*, **31**(23): 3903 - 3910.

Elbert, W., Hoffmann, M.R., Krämer, M., Schmitt, G. and Andreae, M.O., 2000. Control of solute concentrations in cloud and fog water by liquid water content. *Atmospheric Environment*, **34**: 1109 - 1122.

Eliáš, V., Tesar, M. and Buchtele, J., 1995. Occult precipitation: sampling, chemical analysis and process modelling in the Sumava Mts. (Czech Republic) and in the Taunus Mts. (Germany). *Journal of Hydrology*, **166**: 409 - 420.

Erel, Y., Pehkonen, S.O. and Hoffmann, M.R., 1993. Redox chemistry of iron in fog and stratus clouds. *Journal of Geophysical Research*, **98**(D10): 18,423 - 18,434.

Eriksson, E., 1952a. Composition of atmospheric precipitation I. Nitrogen compounds. *Tellus*, **4**: 215 - 232.

Eriksson, E., 1952b. Composition of atmospheric precipitation II. Sulfur, chloride, iodine compounds. Bibliography. *Tellus*, **4**: 280 - 303.

Facchini, M.-C., Decesari, S., Mircea, M., Fuzzi, S. and Loglio, G., 2000. Surface tension of atmospheric wet aerosol and cloud/fog droplets in relation to their organic carbon content and chemical composition. *Atmospheric Environment*, **34**: 4853 - 4857.

Facchini, M.-C., Fuzzi, S., Zappoli, S., Andracchio, A., Gelencsér, A., Kiss, G., Krivácsy, Z., Mészáros, E., Hansson, H.-C., Alsberg, T. and Zebühr, Y., 1999a. Partitioning of the

Reproduced with permission of the copyright owner. Further reproduction prohibited without permission.

organic aerosol component between fog droplets and interstitial air. *Journal of Geophysical Research*, **104**(D21): 26,821 - 26,832.

Facchini, M.-C., Mircea, M., Fuzzi, S. and Charlson, R.J., 1999b. Cloud albedo enhancement by surface-active organic solutes in growing drops. *Nature*, **401**: 257 - 259.

Facchini, M.-C., Fuzzi, S., Lind, J.A., Fierlinger, H., Kalina, M., Puxbaum, H., Winiwarter, W., Arends, B.G., Wobrock, W., Jaeschke, W., Berner, A. and Kruisz, C., 1992a. Phase-partitioning and chemical reactions of low molecular weight organic compounds in fog. *Tellus*, **44B**: 533 - 544.

Facchini, M.-C., Fuzzi, S., Kessel, M., Wobrock, W., Jaeschke, W., Arends, B.G., Möls, J.J., Berner, A., Solly, I., Kruisz, C., Reischl, G., Pahl, S., Hallberg, A., Ogren, J.A., Fierlinger-Oberlinninger, H., Marzorati, A. and Schell, D., 1992b. The chemistry of sulfur and nitrogen species in a fog system - a multiphase approach. *Tellus*, **44B**: 505 - 521.

Facchini, M.-C., Lind, J., Orsi, G. and Fuzzi, S., 1990a. Chemistry of carbonyl compounds in Po Valley fog water. *The Science of the Total Environment*, **91**: 79 - 86.

Facchini, M.-C., Fuzzi, S., Lind, J. and Orsi, G., 1990b. Low molecular weight organic compounds in the Po Valley fog water. In: G. Restelli and G. Angeletti (Editors), Physico-Chemical Behaviour of Atmospheric Pollutants. Kluwer Academic Publishers, Dordrecht, pp. 505 - 509.

Facchini, M.-C. and Chiavari, G., 1987. Analysis of carbonyl compounds in the atmospheric liquid phase. In: G. Angeletti and G. Restelli (Editors), Physico-Chemical Behaviour of Atmospheric Pollutants. D. Reidel Publishing, Co., Dordrecht, pp. 188 - 197.

Falconer, R.E. and Falconer, P.D., 1980. Determination of cloud water acidity at a mountain observatory in the Adirondack Mountains of New York state. *Journal of Geophysical Research*, **85**(C12): 7465 - 7470.

Faust, B.C., Anastasio, C., Allen, J.M. and Arakaki, T., 1993. Aqueous-phase photochemical formation of peroxides in authentic cloud and fog water. *Science*, **260**: 73 - 75.

Fenn, M.E., Poth, M.A., Schilling, S.L. and Grainger, D.B., 2000. Throughfall and fog deposition of nitrogen and sulfur at an N-limited and N-saturated site in the San Bernardino Mountains, southern California. *Canadian Journal of Forest Research*, **30**: 1476 - 1488.

Ferek, R.J., Lazrus, A.L. and Winchester, J.W., 1983. Electron microscopy of acidic aerosols collected over the northeastern United States. *Atmospheric Environment*, **17**(8): 1545 - 1561.

Fišák, J., Rezácová, D., Eliáš, V. and Tesar, M., 2001. Comparison of polluted concentrations in fog (low cloud) water in North and South Bohemia. In: R.S. Schemenauer and H. Puxbaum (Editors), 2nd International Conference on Fog and Fog Collection, St. John's, Newfoundland, Canada, pp. 57 - 60.

Fowler, D., Cape, J.N., Leith, I.D., Choularton, T.W., Gay, M.J. and Jones, A., 1988a. The influence of altitude on rainfall composition at Great Dun Fell. *Atmospheric Environment*, **22**(7): 1355 - 1362.

Fowler, D., Cape, J.N., Leith, I.D., Choularton, T.W., Gay, M.J. and Jones, A., 1988b. Wet deposition and altitude, the role of orographic cloud. In: M.H. Unsworth and D. Fowler (Editors), Acid deposition at high elevation sites. Kluwer Academic Publishers, Dordrecht, pp. 231 - 257.

Reproduced with permission of the copyright owner. Further reproduction prohibited without permission.

Frank, G., Martinsson, B.G., Cederfelt, S.-I., Berg, O.H., Swietlicki, E., Wendisch, M., Yuskiewicz, B., Heintzenberg, J., Wiedensohler, A., Orsini, D., Stratmann, F., Laj, P. and Ricci, L., 1998. Droplet Formation and Growth in Polluted Fogs. *Contributions to Atmospheric Physics*, **71**(1): 65-85.

Fricke, W., Georgii, H.-W. and Gravenhorst, G., 1978. Application of a new sampling device for cloud-water analysis. In: I.P. Mazin and A.K. Khrgian (Editors), Some problems of cloud physics: collected papers. Gidrometeoizdat, Leningrad, USSR, pp. 200 - 212.

Fuhrer, J., 1986. Chemistry of fogwater and estimated rates of occult deposition in an agricultural area of central Switzerland. *Agriculture, Ecosystems and Environment*, **17**: 153 - 164.

Fuzzi, S., Laj, P., Ricci, L., Orsi, G., Heintzenberg, J., Wendisch, M., Yuskiewicz, B., Mertes, S., Orsini, D., Schwanz, M., Wiedensohler, A., Stratmann, F., Berg, O.H., Swietlicki, E., Frank, G., Martinsson, B.G., Günther, A., Dierssen, J.P., Schell, D., Jaeschke, W., Berner, A., Dusek, U., Galambos, Z., Kruisz, C., Mesfin, N.S., Wobrock, W., Arends, B. and ten Brink, H., 1998a. Overview of the Po Valley Fog Experiment 1994 (CHEMDROP). *Contributions to Atmospheric Physics*, **71**(1): 3-19.

Fuzzi, S., Laj, P., Facchini, M.-C., Ricci, L. and Berner, A., 1998b. Size-dependent chemistry of fog and cloud droplets, 1st International conference on fog and fog collection, Vancouver, Canada, pp. 203 - 206.

Fuzzi, S., Mandrioli, P. and Perfetto, A., 1997a. Fog droplets - an atmospheric source of secondary biological aerosol particles. *Atmospheric Environment*, **31**(2): 287 - 290.

Fuzzi, S. and Zappoli, S., 1997. The organic component of fog droplets. In: B. Larsen, B. Versino and G. Angeletti (Editors), The oxidizing capacity of the troposphere. European Commission, Luxembourg, pp. 566 - 569.

Fuzzi, S., Mandrioli, P. and Perfetto, A., 1997b. Fog droplets as a source of secondary biological aerosol particles. In: B. Larsen, B. Versino and G. Angeletti (Editors), The oxidizing capacity of the troposphere. European Commission, Luxembourg, pp. 562 - 566.

Fuzzi, S., Facchini, M.-C., Orsi, G., Bonforte, G., Martinotti, W., Ziliani, G., Mazzali, P., Rossi, P., Natale, P., Grosa, M.M., Rampado, E., Vitali, P., Raffaelli, R., Azzini, G. and Grotti, S., 1996a. The NEVALPA project: a regional network for fog chemical climatology over the Po Valley basin. *Atmospheric Environment*, **30**(2): 201 - 213.

Fuzzi, S., Laj, P., Ricci, L., Berner, A., Schell, D., Wendisch, M. and Wobrock, W., 1996b. The size-dependent chemistry of fog droplets, 12th International Conference on Clouds and Precipitation, Zurich, Switzerland, pp. 1034 - 1037.

Fuzzi, S., Facchini, M.-C., Schell, D., Wobrock, W., Winkler, P., Arends, B.G., Kessel, M., Möls, J.J., Pahl, S., Schneider, T., Berner, A., Solly, I., Kruisz, C., Kalina, M., Fierlinger, H., Hallberg, A., Vitali, P., Santoli, L. and Tigli, G., 1994. Multiphase chemistry and acidity of clouds at Kleiner Feldberg. *Journal of Atmospheric Chemistry*, **19**: 87 - 106.

Fuzzi, S., Facchini, M.-C., Orsi, G. and Ferri, D., 1991. Seasonal trend in fog water chemical composition in the Po Valley. *Environmental Pollution*, **75**: 75 - 80.

Fuzzi, S., Cesari, G., Evangelisti, F., Facchini, M.-C. and Orsi, G., 1990. An automatic station for fog water collection. *Atmospheric Environment*, **24A**(10): 2609 - 2614.

Reproduced with permission of the copyright owner. Further reproduction prohibited without permission.

Fuzzi, S., Orsi, G., Nardini, G., Facchini, M.-C., McLaren, S., McLaren, E. and Mariotti, M., 1988. Heterogeneous processes in the Po Valley radiation fog. *Journal of Geophysical Research*, **93**(D9): 11,141 - 11,151.

Fuzzi, S., 1988. Fog chemistry and deposition in the Po Valley, Italy. In: M.H. Unsworth and D. Fowler (Editors), Acid deposition at high elevations. Kluwer Academic Publishers, Dordrecht, pp. 443 - 452.

Fuzzi, S., Orsi, G., Nardini, G. and Facchini, M.-C., 1987. Physico-chemical properties of radiation fog in the Po Valley, Italy. In: G. Angeletti and G. Restelli (Editors), Physico-Chemical Behaviour of Atmospheric Pollutants. D. Reidel Publishing, Co., Dordrecht, pp. 677 - 684.

Fuzzi, S., Castillo, R.A., Jiusto, J.E. and Lala, G.G., 1984. Chemical composition of radiation fog water at Albany, NY, and its relationship to fog microphysics. *Journal of Geophysical Research*, **89**(D5): 7159 - 7164.

Fuzzi, S., Orsi, G. and Mariotti, M., 1983. Radiation fog liquid water acidity at a field station in the Po Valley. *Journal of Aerosol Science*, **14**(2): 135 - 138.

Gallagher, M.W., Beswick, K.M., Choularton, T.W., Coe, H., Fowler, D. and Hargreaves, K.J., 1992. Measurements and modelling of cloudwater deposition to moorland and forests. *Environmental Pollution*, **75**: 97 - 107.

Gallagher, M.W., Downer, R.M., Choularton, T.W., Gay, M.J., Stromberg, I., Mill, C.S., Radojevic, M., Tyler, B.J., Bandy, B.J., Penkett, S.A., Davies, T.J., Dollard, G.J. and Jones, B.M.R., 1990. Case studies of the oxidation of sulfur dioxide in a hill cap cloud using ground and aircraft based measurements. *Journal of Geophysical Research*, **95**(D11): 18,517 - 18,537.

Gallagher, M.W., Choularton, T.W., Morse, A.P. and Fowler, D., 1988. Measurements of the size-dependence of cloud droplet deposition at a hill site. *Quarterly Journal of the Royal Meteorological Society*, **114**: 1291 - 1303.

Galvin, P.J., Kadlecek, J.A., Mohnen, V.A., Kelly, T.J. and Tanner, R., 1984. Atmospheric chemistry measurements in cloud-free and cloudy air at Whiteface Mountain and evidence of the oxidation of sulfur dioxide in clouds. In: P.J. Samson (Editor), The Meteorology of Acid Deposition. Air Pollution Control Association, Pittsburgh, PA, pp. 3 - 16.

Galvin, P.J., 1983. Cloud chemistry studies at the Whiteface Mountain field station. Ph.D. Thesis, Department of Atmospheric Sciences, State University of New York at Albany, Albany, NY.

Ganor, E., 1999. A method for identifying sulfuric acid in single cloud and fog droplets. *Atmospheric Environment*, **33**: 4235 - 4242.

Ganor, E., 1998. The chemical and physical properties of individual fog droplets, 1st international conference on fog and fog collection, Vancouver, Canada, pp. 211 - 212.

Ganor, E., Levin, Z. and Pardess, D., 1993. Determining the acidity and chemical composition of fog, haze and cloud droplets in Israel. *Atmospheric Environment*, **27A**(12): 1821 - 1832.

Gelencsér, A., Sallai, M., Krivácsy, Z., Kiss, G. and Mészáros, E., 2000. Voltammetric evidence for the presence of humic-like substances in fog water. *Atmospheric Environment*, **34**: 157 - 165.

Reproduced with permission of the copyright owner. Further reproduction prohibited without permission.

Ghauri, B.M., Ishaq Mirza, M., Richter, R., Dutkiewicz, V.A., Rusheed, A., Khan, A.R. and Husain, L., 2001. Composition of aerosols and cloud water at a remote mountain site (2.8 kms) in Pakistan. *Chemosphere - Global Change Science*, **3**: 51 - 63.

Gieray, R., Wieser, P., Engelhardt, T., Swietlicki, E., Hansson, H.-C., Mentes, B., Orsini, D., Martinsson, B.G., Svenningsson, B., Noone, K.J. and Heintzenberg, J., 1997. Phase partitioning of aerosol constituents in cloud based on single-particle and bulk analysis. *Atmospheric Environment*, **31**(16): 2491 - 2502.

Gieray, R., Lammel, G., Metzig, G. and Wieser, P., 1993. Size dependent single particle and chemical bulk analysis of droplets and interstitial particles in an orographic cloud. *Atmospheric Research*, **30**: 263 - 293.

Gieray, R., Greiner, W. and Wieser, P., 1989. Laser microprobe mass analysis of fog droplet residues. *Journal of Aerosol Science*, **20**(8): 1209 - 1212.

Glotfelty, D.E., Majewski, M.S. and Seiber, J.N., 1990. Distribution of several organophosphorus insecticides and their oxygen analogues in a foggy atmosphere. *Environmental Science and Technology*, **24**: 353 - 357.

Glotfelty, D.E., Seiber, J.N. and Liljedahl, L.A., 1987. Pesticides in fog. *Nature*, **325**: 602 - 605.

Glotfelty, D.E., Seiber, J.N. and Liljedahl, L.A., 1986. Pesticides and other organics in fog, 1986 EPA/APCA Symposium on Measurement of Toxic Air Pollutants, Raleigh, N. C., pp. 168 - 175.

Grasserbauer, M., Paleczek, S., Rendl, J., Kasper, A. and Puxbaum, H., 1994. Inorganic constituents in aerosols, cloudwater and precipitation collected at the high-alpine measurement station Sonnblick: sampling, analysis and exemplary results. *Fresenius Journal of Analytical Chemistry*, **350**: 431 - 439.

Grosch, S. and Schmitt, G., 1988. Experimental investigations of the deposition of trace elements in forest areas. In: K. Grefen and J. Löbel (Editors), Environmental Meteorology. Kluwer Academic Publishing, Dordrecht, pp. 201 - 216.

Grosjean, D. and Wright, B., 1983. Carbonyls in urban fog, ice fog, cloud water and rain water. *Atmospheric Environment*, **17**(10): 2093 - 2096.

Gundel, L.A., Benner, W.H. and Hansen, A.D.A., 1994. Chemical composition of fog water and interstitial aerosol in Berkeley, CA. *Atmospheric Environment*, **28**(16): 2715 - 2725.

Hallberg, A., Ogren, J.A., Noone, K.J., Okada, K., Heintzenberg, J. and Svenningsson, B., 1994a. The influence of aerosol particle composition on cloud droplet formation. *Journal of Atmospheric Chemistry*, **19**: 153 - 171.

Hallberg, A., Noone, K.J., Ogren, J.A., Svenningsson, I.B., Flossmann, A., Wiedensohler, A., Hansson, H.-C., Heintzenberg, J., Anderson, T.L., Arends, B.G. and Maser, R., 1994b. Phase partitioning of aerosol particles in clouds at Kleiner Feldberg. *Journal of Atmospheric Chemistry*, **19**: 107 - 127.

Hansen, A.D.A. and Novakov, T., 1989. Real-time measurements of the size fractionation of ambient black carbon aerosols at elevated humidity. *Aerosol Science and Technology*, **10**: 106 - 110.

Reproduced with permission of the copyright owner. Further reproduction prohibited without permission.

Hart, K.M., Tremp, J., Molnar, E. and Giger, W., 1993. The occurrence and the fact of organic pollutants in the atmosphere. *Water, Air and Soil Pollution*, **68**: 91 - 112.

Hegg, D.A. and Hobbs, P.V., 1988. Comparisons of sulfate and nitrate production in clouds on the mid-Atlantic and Pacific northwest coasts of the United States. *Journal of Atmospheric Chemistry*, **7**: 325 - 333.

Hegg, D.A. and Hobbs, P.V., 1986. Sulfate and nitrate chemistry in cumuliform clouds. *Atmospheric Environment*, **20**(5): 901 - 909.

Hegg, D.A., Hobbs, P.V. and Radke, L.F., 1984a. Measurements of the scavenging of sulfate and nitrate in clouds. *Atmospheric Environment*, **18**(9): 1939 - 1946.

Hegg, D.A., Radke, L.F. and Hobbs, P.V., 1984b. Measurements of transformations in the physical and chemical properties of clouds associated with onshore flow in Washington state. *Journal of Climate and Applied Meteorology*, **23**: 979 - 984.

Hegg, D.A. and Hobbs, P.V., 1983. Preliminary measurements on the scavenging of sulfate and nitrate by clouds. In: H.R. Pruppacher, R.G. Semonin and W.G.N. Slinn (Editors), Precipitation Scavenging, Dry Deposition, and Resuspension. Elsevier, New York, NY, pp. 79 - 87.

Hegg, D.A. and Hobbs, P.V., 1982. Measurements of sulfate production in natural clouds. *Atmospheric Environment*, **16**(11): 2663 - 2668.

Hegg, D.A. and Hobbs, P.V., 1981. Cloud water chemistry and the production of sulfates in clouds. *Atmospheric Environment*, **15**(9): 1597 - 1604.

Hegg, D.A. and Hobbs, P.V., 1979. The homogeneous oxidation of sulfur dioxide in cloud droplets. *Atmospheric Environment*, **13**: 981 - 987.

Heintzenberg, J., 1992. The Po Valley Fog Experiment 1989. What have we learned, where do we go from here? *Tellus*, **44B**: 443 - 447.

Heintzenberg, J., Ogren, J.A., Noone, K.J. and Gärdneus, L., 1989. The size distribution of submicrometer particles within and about stratocumulus cloud droplets on Mt. Åreskutan, Sweden. *Atmospheric Research*, **24**: 89 - 101.

Hemmerlein, M.T. and Perkins, T.D., 1993. Techniques for pollution monitoring in remote sites: III. near real-time monitoring of cloudwater conductivity and pH. *Water, Air and Soil Pollution*, **71**: 43 - 50.

Henterich, R. and Herrmann, R., 1990. Comparing the distribution of nitrated phenols in the atmosphere of two german hill sites. *Environmental Technology*, **VII**: 961 - 972.

Herckes, P., Trenary, L., Hannigan, M.P., Lee, T. and Collett, J.L.J., 2001a. Cloud and fog processing of atmospheric organic compounds. In: R.S. Schemenauer and H. Puxbaum (Editors), 2nd International Conference on Fog and Fog Collection, St. John's, Newfoundland, Canada, pp. 13 - 16.

Herckes, P., Mirabel, P.H. and Wortham, H., 2001b. Fogwater studies in the Vosges Mountains (France). In: R.S. Schemenauer and H. Puxbaum (Editors), 2nd International Conference on Fog and Fog Collection, St. John's, Newfoundland, Canada, pp. 145 - 148.

Reproduced with permission of the copyright owner. Further reproduction prohibited without permission.

Hering, S.V., Blumenthal, D.L., Brewer, R.L., Gertler, A., Hoffmann, M.R., Kadlecek, J.A. and Pettus, K., 1987. Field intercomparison of five types of fogwater collectors. *Environmental Science and Technology*, **21**: 654 - 663.

Hindman, E.E., Campbell, M.A. and Borys, R.D., 1994. A ten-winter record of cloud-droplet physical and chemical properties at a mountaintop site in Colorado. *Journal of Applied Meteorology*, **33**: 797 - 807.

Hitzenberger, R., Berner, A., Kromp, R., Kasper-Giebl, A., Limbeck, A., Tscherwenka, W. and Puxbaum, H., 2000. Black carbon and other species at a high-elevation European site (Mount Sonnblick, 3106 m, Austria): concentrations and scavenging efficiencies. *Journal of Geophysical Research*, **105**(D20): 24,637 - 24,645.

Hitzenberger, R., Kromp, R., Tscherwenka, W. and Puxbaum, H., 1998. Wet scavenging of black carbon: black carbon and ionic species in Mt. Sonnblick cloud water. *Journal of Aerosol Science*, **29**(Supplement 1): S521 - S522.

Hoag, K.J., Collett, J.L., Jr. and Pandis, S.N., 1999. The influence of drop size-dependent fog chemistry on aerosol processing by San Joaquin Valley fogs. *Atmospheric Environment*, **33**: 4817-4832.

Hoag, K.J., 1998. Heterogeneous fog chemistry and S(IV) oxidation in the San Joaquin Valley. M. S. Thesis, Department of Atmospheric Science, Colorado State University, Fort Collins, CO.

Hoffmann, P., Sinner, T., Dedik, A.N., Karandashev, V.K., Malyshev, A.A., Weber, S. and Ortner, H.M., 1994. Iron in atmospheric aqueous and particulate samples. *Fresenius Journal of Analytical Chemistry*, **350**: 34 - 37.

Hottenroth, S., Römpp, A., Völkel, W., Wieprecht, W., Wrzesinsky, T., Klemm, O. and Frank, H., 2001. Nitrophenols and haloacetates in fog and rain. In: R.S. Schemenauer and H. Puxbaum (Editors), 2nd International Conference on Fog and Fog Collection, St. John's, Newfoundland, Canada, pp. 89 - 92.

Houdier, S., Perrier, S., Defrancq, E. and Legrand, M., 2000. A new fluorescent probe for sensitive detection of carbonyl compounds: sensitivity improvement and application to environmental water samples. *Analytica Chimica Acta*, **412**: 221 - 233.

Houghton, H.G., 1955. On the chemical composition of fog and cloud water. *Journal of Meteorology*, **12**: 355 - 357.

Houghton, H.G. and Bemis, A.C., 1939. Cloud particle studies on Mt. Washington. *Bulletin of the American Meteorology Society*, **20**: 400 - 402.

Houghton, H.G. and Radford, W.H., 1938. On the measurement of drop size and liquid water content in fogs and clouds, Papers in Physical Oceanography and Meteorology. Massachusetts Institute of Technology and Woods Hole Oceanographic Institution, Cambridge, MA, **6**(4): 31 pp.

Huang, S., Mo, T. and Wang, M., 1991. Observation of chemical composition of supercooled cloud and snow. *Acta Meteorologica Sinica*, **5**(1): 123 - 127.

Husain, L., Rattigan, O.V., Dutkiewicz, V.A., Das, M., Judd, C., Khan, A.R., Richter, R.C., Balasubramanian, R., Swami, K. and Walcek, C.J., 2000. Case studies of SO_2 and H_2O_2 reaction in clouds. *Journal of Geophysical Research*, **105**(D8): 9831 - 9841.

Reproduced with permission of the copyright owner. Further reproduction prohibited without permission.

Husain, L., 1989. A technique for determining in-cloud formation of SO_4. *Geophysical Research Letters*, **16**(1): 57 - 60.

Igawa, M., Tsutsumi, Y., Mori, T. and Okuchi, H., 1998. Fogwater chemistry at a mountainside forest and the estimation of the air pollutant deposition via fog droplets based on the atmospheric quality at the mountain base. *Environmental Science and Technology*, **32**: 1566 - 1572.

Igawa, M., Munger, J.W. and Hoffmann, M.R., 1989. Analysis of aldehydes in cloud- and fogwater samples by HPLC with a postcolumn reaction detector. *Environmental Science and Technology*, **23**: 556 - 561.

Ishizaka, Y. and Qian, G.-W., 1994. Mixtures of nitrate and sulfate in individual particles in acidic fogs. *Atmospheric Research*, **31**: 147 - 156.

Jacob, D.J., Munger, J.W., Waldman, J.M. and Hoffmann, M.R., 1986a. The H_2SO_4-HNO_3-NH_3 system at high humidities and in fogs 1. spatial and temporal patterns in the San Joaquin Valley of California. *Journal of Geophysical Research*, **91**(D1): 1073 - 1088.

Jacob, D.J., Waldman, J.M., Munger, J.W. and Hoffmann, M.R., 1986b. The H_2SO_4-HNO_3-NH_3 system at high humidities and in fogs 2. comparisons of field data with thermodynamic calculations. *Journal of Geophysical Research*, **91**(D1): 1089 - 1096.

Jacob, D.J., Waldman, J.M., Munger, J.W. and Hoffmann, M.R., 1985. Chemical composition of fogwater collected along the California coast. *Environmental Science and Technology*, **19**: 730 - 736.

Jacob, D.J., Waldman, J.M., Munger, J.W. and Hoffmann, M.R., 1984. A field investigation of physical and chemical mechanisms affecting pollutant concentrations in fog droplets. *Tellus*, **36B**: 272 - 285.

Jaeschke, W. and Günther, A., 2001. Chemical composition of size segregated cloud drops collected with an airborne two stage impactor. In: R.S. Schemenauer and H. Puxbaum (Editors), 2nd International Conference on Fog and Fog Collection, St. John's, Newfoundland, Canada, pp. 65 - 68.

Jaeschke, W., Dierssen, J.P., Günther, A., Schickedanz, U., Wolf, A., Ricci, L. and Arends, B.G., 1998. Mass Fluxes and Chemical Pathways During a Fog Event. *Contributions to Atmospheric Physics*, **71**(1): 145-157.

Jaeschke, W., Enderle, K.H., Fuzzi, S., Orsi, G., Facchini, M.-C., Berner, A. and Reischl, G., 1990. Ground based cloud and fog experiments. In: G. Restelli and G. Angeletti (Editors), Physico-chemical Behaviour of Atmospheric Pollutants. Kluwer Academic Publishing, Dordrecht, pp. 57 - 62.

Jagels, R., 2001. The pathways and effects of acidic fogs on and within conifer needles. In: R.S. Schemenauer and H. Puxbaum (Editors), 2nd International Conference on Fog and Fog Collection, St. John's, Newfoundland, Canada, pp. 137 - 140.

Jagels, R., Cunningham, R., Carlisle, J. and Day, M., 1998. Documented 50-year change in acidity and chemistry of New England fog, 1st International conference on fog and fog collection, Vancouver, Canada, pp. 5 - 8.

Jagels, R., Carlisle, J., Cunningham, R., Serreze, S. and Tsai, P., 1989. Impact of acid fog and ozone on coastal red spruce. *Water, Air and Soil Pollution*, **48**: 193 - 208.

Reproduced with permission of the copyright owner. Further reproduction prohibited without permission.

Johnson, C.A., Sigg, L. and Zobrist, J., 1987. Case studies on the chemical composition of fogwater: the influence of local gaseous emissions. *Atmospheric Environment*, **21**(11): 2365 - 2374.

Johnson, D.W. and Lindberg, S.E. (Editors), 1992. Atmospheric deposition and forest nutrient cycling: a synthesis of the Integrated Forest Study. Springer-Verlag, New York. Chapter 13 (495 - 570) and Appendices (610 - 688).

Jordan, C.E., Talbot, R.W. and Keim, B.D., 2000. Water-soluble nitrogen at the New Hampshire sea coast: HNO_3, aerosols, precipitation, and fog. *Journal of Geophysical Research*, **105**(D21): 26,403 - 26,431.

Joslin, J.D., McDuffie, C. and Brewer, P.F., 1988. Acidic cloud water and cation loss from red spruce foliage. *Water, Air and Soil Pollution*, **39**: 355 - 363.

Judd, C. and Husain, L., 2000. Determination of gas-phase nitric acid using a tracer technique. *Atmospheric Environment*, **34**: 2333 - 2341.

Junge, C.E., 1963. Air chemistry and radioactivity. Academic Press, New York.

Junge, C.E., 1954. The chemical composition of atmospheric aerosols, I: measurements at Round Hill field station, June-July 1953. *Journal of Meteorology*, **11**: 323 - 333.

Kadlecek, J.A., McLaren, S., Camarota, N., Mohnen, V.A. and Wilson, J., 1983. Cloud water chemistry at Whiteface Mountain. In: H.R. Pruppacher, R.G. Semonin and W.G.N. Slinn (Editors), Precipitation Scavenging, Dry Deposition and Resuspension. Elsevier, New York, NY, pp. 103 - 112.

Kalina, M., Zambo, E. and Puxbaum, H., 1998. Cloud water chemistry and impact on total deposition of sulfur and nitrogen at different elevational levels in an alpine valley (Achkenkirch, 930 - 1758 m a.s.l., Tyrol, Austria), 1st International conference on fog and fog collection, Vancouver, Canada, pp. 57 - 60.

Kalina, M. and Puxbaum, H., 1994. A study of the influence of riming of ice crystals on snow chemistry during different seasons in precipitating continental clouds. *Atmospheric Environment*, **28**(20): 3311 - 3328.

Kasahara, M., Ma, C.-J. and Tohno, S., 2001. Physical and chemical properties of single fog droplets applying fixation techniques. In: R.S. Schemenauer and H. Puxbaum (Editors), 2nd International Conference on Fog and Fog Collection, St. John's, Newfoundland, Canada, pp. 69 - 72.

Kasper, A., Puxbaum, H., Brantner, B. and Paleczek, S., 1998. Scavenging efficiency of lead and sulfate in supercooled clouds at Sonnblick, 3106 masl, Austria. *Atmospheric Environment*, **32**(23): 3967 - 3974.

Kasper-Giebl, A., Koch, A., Hitzenberger, R. and Puxbaum, H., 2000. Scavenging efficiency of "Aerosol Carbon" and sulfate in supercooled clouds at Mt. Sonnblick (3106 m a.s.l., Austria). *Journal of Atmospheric Chemistry*, **35**: 33 - 46.

Kawamura, K., Steinberg, S. and Kaplan, I.R., 1985. Capillary GC determination of short-chain dicarboxylic acids in rain, fog, and mist. *International Journal of Environmental Analytical Chemistry*, **19**: 175 - 188.

Kawamura, K. and Kaplan, I.R., 1984. Capillary GC determination of volatile organic acids in rain and fog samples. *Analytical Chemistry*, **56**: 1616 - 1620.

Reproduced with permission of the copyright owner. Further reproduction prohibited without permission.

Keene, W.C., Mosher, B.W., Jacob, D.J., Munger, J.W., Talbot, R.W., Artz, R.C., Maben, J.R., Daube, B.C.J. and Galloway, J.N., 1995. Carboxylic acids in clouds at a high-elevation forested site in central Virginia. *Journal of Geophysical Research*, **100**(D5): 9345 - 9357.

Kelly, T.J., Daum, P.H. and Schwartz, S.E., 1985. Measurements of peroxides in cloudwater and rain. *Journal of Geophysical Research*, **90**(D5): 7861 - 7871.

Keuken, M.P., Bakker, F.P., Lingerak, W.A. and Slanina, J., 1987. Flow injection analysis of hydrogen peroxide, sulfite, formaldehyde and hydroxymethanesulfonic acid in precipitation samples. *International Journal of Environmental Analytical Chemistry*, **31**: 263 - 279.

Khemani, L.T., Momin, G.A., Naik, M.S., Prakasa Rao, P.S., Safai, P.D. and Murty, A.S.R., 1987. Influence of alkaline particulates on pH of cloud and rain water in India. *Atmospheric Environment*, **21**(5): 1137 - 1145.

Khemani, L.T., Sharma, S.K., Murty, A.S.R. and Ramana Murty, B.V., 1982. A simple gadget for collection of cloud/rain water from aircraft, Conference on Cloud Physics. American Meteorological Society, Chicago, IL, pp. 303 - 305.

Khemani, L.T., Momin, G.A. and Ramana Murty, B.V., 1981. Chemical composition of cloud water at a hill station. In: A.F. Roddy and T.C. O'Connor (Editors), 9th International conference on Atmospheric Aerosols, Condensation and Ice Nuclei. Galway University Press, Galway, Ireland, pp. 233 - 238.

Kikuchi, R., Adzuhata, T., Okamura, T., Ozeki, T., Kajikawa, M. and Ogawa, N., 2001. Relationship among the element ratio of insoluble substances, ionic components in fog water and the back trajectory at Akita Hachimantai Mountain range in northern Japan. In: R.S. Schemenauer and H. Puxbaum (Editors), 2nd International Conference on Fog and Fog Collection, St. John's, Newfoundland, Canada, pp. 105 - 108.

Kimball, K.D., Jagels, R., Gordon, G.A., Weathers, K.C. and Carlisle, J., 1988. Differences between New England coastal fog and mountain cloud water chemistry. *Water, Air and Soil Pollution*, **39**: 383 - 393.

Kins, L., Müller, K.P., Enhalt, D.H. and Meixner, F.X., 1988. Experiment ALSDAN (1985): some preliminary results of the height resolved measurements of trace gases, aerosol composition, cloud- and precipitation water. In: M.H. Unsworth and D. Fowler (Editors), Acid deposition at high elevation sites. Kluwer Academic Publishers, Dordrecht, pp. 375 - 394.

Kins, L., Meixner, F.X., Enhalt, D.H., Müller, K.P., Slanina, J., Moels, J.J., Beltz, N., Jaeschke, W. and Rumpel, K.-J., 1986. Scavenging of trace substances by clouds and precipitation, American Chemical Society, Petroleum Chemistry Division. American Chemical Society, New York, pp. 457 - 463.

Kiss, G., Varga, B., Gelencsér, A., Krivácsy, Z., Molnár, Á., Alsberg, T., Persson, L., Hansson, H.-C. and Facchini, M.-C., 2001. Characterization of polar organic compounds in fog water. *Atmospheric Environment*, **35**: 2193 - 2200.

Klemm, O., 2001. Trends in fog composition at a site in NE Bavaria. In: R.S. Schemenauer and H. Puxbaum (Editors), 2nd International Conference on Fog and Fog Collection, St. John's, Newfoundland, Canada, pp. 73 - 76.

Reproduced with permission of the copyright owner. Further reproduction prohibited without permission.

Klemm, O., Bachmeier, A.S., Talbot, R.W. and Klemm, K., 1994. Fog chemistry at the New England coast: influence of air mass history. *Atmospheric Environment*, **28**(6): 1181 - 1188.

Klemm, O., Talbot, R.W. and Klemm, K., 1991. Sulfur dioxide in coastal New England fog. *Atmospheric Environment*, **26A**(11): 2063 - 2075.

Kmiec, G., Kacperczyk, K., Zwozdziak, A. and Zwozdziak, J., 1995. Acid pollutants in air and precipitation/deposition at the Sudetan Mountains, Poland. *Water, Air and Soil Pollution*, **85**: 2131 - 2136.

Kotronarou, A. and Sigg, L., 1993. SO_2 oxidation in atmospheric water: role of Fe(II) and effect of ligands. *Environmental Science and Technology*, **27**: 2725 - 2735.

Krämer, M., Beltz, N., Schell, D., Schütz, L., Sprengard-Eichel, C. and Wurzler, S., 2000. Cloud processing of continental aerosol particles: experimental investigations of different drop sizes. *Journal of Geophysical Research: Atmospheres*, **105**(D9): 11,739 - 11,752.

Krämer, M., Schütz, L., Svenningsson, B. and Wiedensohler, A., 1991. Number size distribution of insoluble atmospheric aerosol particles in fog/cloud-water. *Journal of Aerosol Science*, **22**(Supplement 1): S525 - S528.

Krivácsy, Z., Kiss, G., Varga, B., Galambos, I., Sárvári, Z., Gelencsér, A., Molnár, Á., Fuzzi, S., Facchini, M.-C., Zappoli, S., Andracchio, A., Alsberg, T., Hansson, H.-C. and Persson, L., 2000. Study of humic-like substances in fog and interstitial aerosol by size-exclusion chromatography and capillary electrophoresis. *Atmospheric Environment*, **34**: 4273 - 4281.

Kroll, G. and Winkler, P., 1990. Ion deposition due to fog water interception at high elevation. In: G. Restelli and G. Angeletti (Editors), Physico-chemical Behaviour of Atmospheric Pollutants. Kluwer Academic Publishing, Dordrecht, pp. 516 - 521.

Kroll, G. and Winkler, P., 1989a. Ion deposition due to fog water deposition at high elevations. In: G. Restelli and G. Angeletti (Editors), Physico-chemical behaviour of atmospheric pollutants. Kluwer Academic Publishers, Dordrecht, pp. 516 - 521.

Kroll, G. and Winkler, P., 1989b. Trace substance input to coniferous forests via cloud interception. In: H.-W. Georgii (Editor), Mechanisms and effects of pollutant-transfer into forests. Kluwer Academic Publishers, Dordrecht, pp. 205 - 211.

Kroll, G. and Winkler, P., 1988. Estimation of wet deposition in fog. In: K. Grefen and J. Löbel (Editors), Environmental Meteorology. Kluwer Academic Publishing, Dordrecht, pp. 227 - 236.

Kuriowa, D., 1956. The composition of sea-fog nuclei as identified by electron microscope. *Journal of Meteorology*, **13**: 408 - 410.

Kuriowa, D., 1953. Electron-microscope study of atmospheric condensation nuclei. In: T. Hori (Editor), Studies on Fog. Tanne Trading Company, Sapporo, pp. 349 - 382.

Kuriowa, D., 1951. Electron-microscope study of fog nuclei. *Journal of Meteorology*, **8**: 157 - 160.

Lai, H.-C., Tanner, P.A., Huang, M.-Y., Shen, Z.-L. and Wu, Y.-X., 1997. The acidification process under the cloud in southwest China: observation results and simulation. *Atmospheric Environment*, **31**(6): 851 - 861.

Reproduced with permission of the copyright owner. Further reproduction prohibited without permission.

Laj, P., Fuzzi, S., Lazzari, A., Ricci, L., Orsi, G., Berner, A., Dusek, U., Schell, D., Günther, A., Wendisch, M., Wobrock, W., Frank, G., Martinsson, B.G. and Hillamo, R., 1998. The size dependent composition of fog droplets. *Contributions to Atmospheric Physics*, **71**(1): 115-130.

Laj, P., Fuzzi, S., Facchini, M.-C., Orsi, G., Berner, A., Kruisz, C., Wobrock, W., Hallberg, A., Bower, K.N., Gallagher, M.W., Beswick, K.M., Colvile, R., Choularton, T.W., Nason, P. and Jones, B., 1997a. Experimental evidence for in-cloud production of aerosol sulfate. *Atmospheric Environment*, **31**(16): 2503 - 2514.

Laj, P., Fuzzi, S., Facchini, M.-C., Lind, J., Orsi, G., Preiss, M., Maser, R., Jaeschke, W., Seyffer, E., Helas, G., Acker, K., Wieprecht, W., Möller, D., Arends, B.G., Möls, J.J., Colvile, R., Gallagher, M.W., Beswick, K.M., Hargreaves, K.J., Storeton-West, R.L. and Sutton, M.A., 1997b. Cloud processing of soluble gases. *Atmospheric Environment*, **31**(16): 2589 - 2598.

Lammel, G. and Metzig, G., 1998. On the occurrence of nitrite in urban fogwater. *Chemosphere*, **37**(8): 1603 - 1614.

Lammel, G., 1996. Sensitive method for the determination of different S(IV) species in cloud and fog water. *Fresenius Journal of Analytical Chemistry*, **356**: 107 - 108.

Lammel, G. and Cape, J.N., 1996. Nitrous acid and nitrite in the atmosphere. *Chemical Society Reviews*: 361 - 369.

Lammel, G. and Gieray, R., 1994. Reduced species of sulfur and nitrogen in fog-water. In: G. Angeletti and G. Restelli (Editors), Physico-chemical Behaviour of Atmospheric Pollutants. European Commission, Luxembourg, pp. 975 - 981.

Lammel, G. and Metzig, G., 1991. Multiphase chemistry of orographic clouds: observations at subalpine mountain sites. *Fresenius Journal of Analytical Chemistry*, **340**: 564 - 574.

Lazrus, A.L., Baynton, H.W. and Lodge, J.P.J., 1970. Trace constituents in oceanic cloud water and their origin. *Tellus*, **22**: 106 - 113.

Leaitch, W.R., Isaac, G.A., Strapp, J.W., Banic, C.M. and Wiebe, H.A., 1992. The relationship between cloud droplet number concentrations and anthropogenic pollution: observations and climate implications. *Journal of Geophysical Research*, **97**(D2): 2463 - 2474.

Leaitch, W.R., Isaac, G.A., Strapp, J.W. and MacPherson, J.I., 1991. Chemical and microphysical case studies of towering cumuli in Ontario, 1988, 7th joint conference on applications of Air Pollution meteorology with the Air and Waste Management Association. American Meteorological Society and the Air and Waste Management Association, New Orleans, LA, pp. 232 - 237.

Leaitch, W.R., Strapp, J.W., Wiebe, H.A. and Isaac, G.A., 1983. Measurements of scavenging and transformation of aerosol inside cumulus. In: H.R. Pruppacher, R.G. Semonin and W.G.N. Slinn (Editors), Precipitation Scavenging, Dry Deposition, and Resuspension. Elsevier, New York, NY, pp. 53 - 66.

Leuenberger, C., Czuczwa, J., Heyerdahl, E. and Giger, W., 1988. Aliphatic and polycyclic aromatic hydrocarbons in urban rain, snow and fog. *Atmospheric Environment*, **22**(4): 695 - 705.

Levin, Z., Price, C. and Ganor, E., 1990. The contribution of sulfate and desert aerosols to the acidification of clouds and rain in Israel. *Atmospheric Environment*, **24A**(5): 1143 - 1151.

Reproduced with permission of the copyright owner. Further reproduction prohibited without permission.

Levsen, K. and Lüttke, J., 1997. The role of nitrophenols in cloud chemistry. In: S. Fuzzi and D. Wagenbach (Editors), Cloud multi-phase processes and high alpine air and snow chemistry. Springer-Verlag, Berlin, pp. 123 - 129.

Levsen, K., Behnert, S., Mußmann, P., Raabe, M. and Prieß, B., 1993. Organic compounds in cloud and rainwater. *International Journal of Environmental Analytical Chemistry*, **52**: 87 - 97.

Li, Z. and Aneja, V.P., 1992. Regional analysis of cloud chemistry at high elevations in the Eastern United States. *Atmospheric Environment*, **26A**(11): 2001 - 2017.

Lillis, D., Cruz, C.N., Collett, J.L.J., Richards, L.W. and Pandis, S.N., 1999. Production and removal of aerosol in a polluted fog layer: model evaluation and fog effect on PM. *Atmospheric Environment*, **33**: 4797 - 4816.

Limbeck, A. and Puxbaum, H., 2000. Dependence of in-cloud scavenging of polar organic aerosol compounds on the water solubility. *Journal of Geophysical Research*, **105**(D15): 19,857 - 19,867.

Lin, N.-H., 1994. A cloud chemistry model: simulation of cloud water acidity and its dependence on droplet size. *TAO*, **5**(1): 43 - 62.

Lin, N.-H. and Saxena, V.K., 1991. Interannual variability in acidic deposition on the Mt. Mitchell area forest. *Atmospheric Environment*, **25A**(2): 517 - 524.

Lindberg, S.E., Silsbee, D., Schaefer, D.A., Owens, J.G. and Petty, W., 1988. A comparison of atmospheric exposure conditions at high- and low-elevation forests in the southern Appalachian Mountain range. In: M.H. Unsworth and D. Fowler (Editors), Acid deposition at high elevation sites. Kluwer Academic Publishers, Dordrecht, pp. 321 - 344.

Liu, P.S.K., Leaitch, W.R., MacDonald, A.M., Isaac, G.A., Strapp, J.W. and Wiebe, H.A., 1993. Sulfate production in summer cloud over Ontario, Canada. *Tellus*, **45B**: 368 - 389.

Lovett, G.M. and Reiners, W.A., 1983. Cloud water: an important vector of atmospheric deposition. In: H.R. Pruppacher, R.G. Semonin and W.G.N. Slinn (Editors), Precipitation Scavenging, Dry Deposition, and Resuspension. Elsevier, New York, pp. 171 - 180.

Lovett, G.M., Reiners, W.A. and Olson, R.K., 1982. Cloud droplet deposition in subalpine balsam fir forests: hydrological and chemical inputs. *Science*, **218**: 1303 - 1304.

Lüttke, J., Levsen, K., Acker, K., Wieprecht, W. and Möller, D., 1999. Phenols and nitrated phenols in clouds at Mt. Brocken. *International Journal of Environmental Analytical Chemistry*, **74**(1-4): 69 - 89.

Lüttke, J., Scheer, V., Levsen, K., Wünsch, G., Cape, J.N., Hargreaves, K.J., Storeton-West, R.L., Acker, K., Wieprecht, W. and Jones, B., 1997. Occurrence and formation of nitrated phenols in and out of cloud. *Atmospheric Environment*, **31**(16): 2637 - 2648.

Lüttke, J. and Levsen, K., 1997. Phase partitioning of phenol and nitrophenols in clouds. *Atmospheric Environment*, **31**(16): 2649 - 2656.

Lüttke, J., Koch, C., Mußmann, P. and Levsen, K., 1994. Organic compounds in clouds. In: G. Angeletti and G. Restelli (Editors), Physico-chemical Behaviour of Atmospheric Pollutants. European Commission, Luxembourg, pp. 982 - 988.

Reproduced with permission of the copyright owner. Further reproduction prohibited without permission.

Ma, C.-J., Kasahara, M., Tohno, S., Kamiya, T. and Sakai, T., 2001. Sampling of individual fog droplets and its chemical analysis. In: R.S. Schemenauer and H. Puxbaum (Editors), 2nd International Conference on Fog and Fog Collection, St. John's, Newfoundland, Canada, pp. 45 - 48.

MacDonald, A.M., Anlauf, K.G., Wiebe, H.A., Leaitch, W.R., Banic, C.M., Watt, M.F., Puckett, K.J. and Bregman, B., 1991. Measurements of aqueous and gaseous hydrogen peroxide in central Ontario, 7th joint conference on applications of air pollution meteorology with the Air and Waste Management Association. American Meteorological Society and the Air and Waste Management Association, New Orleans, LA, pp. 77 - 80.

Marsh, A.R.W., 1983. Studies of the acidity and chemical composition of clouds. In: S. Beilke and A.J. Elshout (Editors), Acid Deposition. D. Reidel Publishing, Dordrecht, the Netherlands, pp. 185 - 194.

Martens, C.S. and Harriss, R.C., 1973. Chemistry of aerosols, cloud droplets, and rain in Puerto Rican marine atmosphere. *Journal of Geophysical Research*, **78**(6): 949 - 957.

Martinsson, B.G., Cederfelt, S.-I., Svenningsson, B., Frank, G., Hansson, H.-C., Swietlicki, E., Wiedensohler, A., Wendisch, M., Gallagher, M.W., Colvile, R., Beswick, K.M., Choularton, T.W. and Bower, K.N., 1997. Experimental determination of the connection between cloud droplet size and its dry residue. *Atmospheric Environment*, **31**(16): 2477 - 2490.

McFadyen, G.G. and Cape, J.N., 1999. Springtime sources and sinks of peroxyacetyl nitrate in the UK and its contribution to acidification and nitrification of cloud water. *Atmospheric Research*, **50**: 359 - 371.

McGregor, K.G. and Anastasio, C., 2001. Chemistry of fog waters in California's Central Valley: 2. photochemical transformations of amino acids and alkyl amines. *Atmospheric Environment*, **35**: 1091 - 1104.

McLaren, S.E., Kadlecek, J.A. and Mohnen, V.A., 1986. SO_2 oxidation in summertime cloudwater at Whiteface Mountain. In: D.D. Adams and W.P. Page (Editors), Acid Deposition: Environmental, Economic and Policy Issues. Plenum Press, New York, pp. 31 - 48.

Menon, S., Saxena, V.K. and Logie, B.D., 2000. Chemical heterogeneity across cloud droplet size spectra in continental and marine air masses. *Journal of Applied Meteorology*, **39**: 887 - 903.

Migala, K. and Liebersbach, J., 2001. Rime in the Karkonosze Mtns. (high Sudetes, Poland). In: R.S. Schemenauer and H. Puxbaum (Editors), 2nd International Conference on Fog and Fog Collection, St. John's, Newfoundland, Canada, pp. 197 - 200.

Miller, D.F., Borys, R.D. and Graw, R., 1989. Chemistry of summer cloud, precipitation and air at a Rocky Mountain-top location. In: R.K. Olson and A.S. Lefohn (Editors), Effects of air pollution on Western forests. Air and Waste Management Association, Anaheim, CA, pp. 105 - 115.

Miller, D.R., Byrd, J.E. and Perona, M.J., 1987. The source of Pb, Cu and Zn in fog water. *Water, Air and Soil Pollution*, **32**: 329 - 340.

Miller, E.K., Panek, J.A., Friedland, A.J., Kadlecek, J.A. and Mohnen, V.A., 1993. Atmospheric deposition to a high-elevation forest at Whiteface Mountain, New York, USA. *Tellus*, **45B**: 209 - 227.

Reproduced with permission of the copyright owner. Further reproduction prohibited without permission.

Millet, M., Wortham, H., Sanusi, A. and Mirabel, P.H., 1997. Low molecular weight organic acids in fogwater in an urban area: Strasbourg (France). *The Science of the Total Environment*, **206**: 57 - 65.

Millet, M., Sanusi, A. and Wortham, H., 1996. Chemical composition of fogwater in an urban area: Strasbourg (France). *Environmental Pollution*, **94**(3): 345 - 354.

Millet, M., Worthan, H. and Mirabel, P.H., 1995. Solubility of polyvalent cations in fogwater at an urban site in Strasbourg (France). *Atmospheric Environment*, **29**(19): 2625 - 2631.

Milne, R., Crossley, A. and Unsworth, M.H., 1988. Physics of cloudwater deposition and evaporation at Castlelaw, SE Scotland. In: M.H. Unsworth and D. Fowler (Editors), Acid deposition at high elevation sites. Kluwer Academic Publishers, Dordrecht, pp. 299 - 307.

Minami, Y. and Ishizaka, Y., 1996. Evaluation of chemical composition of fog water near the summit of a high mountain in Japan. *Atmospheric Environment*, **30**(19): 3363 - 3376.

Mindas, J., 2001. Fog/cloud deposition in the Polana Mtns. region (Slovakia). In: R.S. Schemenauer and H. Puxbaum (Editors), 2nd International Conference on Fog and Fog Collection, St. John's, Newfoundland, Canada, pp. 149 - 153.

Mindas, J. and Skvarenina, J., 1998. Fog occurrence and chemistry in mountainous regions of Slovakia, 1st International Conference on Fog and Fog Collection, Vancouver, Canada, pp. 361 - 364.

Mitchell, D.L. and Lamb, D., 1989. Influence of riming on the chemical composition of snow in winter orographic storms. *Journal of Geophysical Research*, **94**(D12): 14,831 - 14,840.

Mohnen, V.A. and Vong, R.J., 1993. A climatology of cloud chemistry for the eastern United States derived from the Mountain Cloud Chemistry Project. *Environmental Review*, **1**: 38 - 54.

Mohnen, V.A. and Kadlecek, J.A., 1989. Cloud chemistry research at Whiteface Mountain. *Tellus*, **41B**: 79 - 91.

Mohnen, V.A. and Kadlecek, J.A., 1988. Cloud chemistry research at Whiteface Mountain, 81st annual meeting Air Pollution Control Association. Air Pollution Control Association, Dallas, TX, pp. 88-129.1.

Möller, D., Acker, K., Wieprecht, W. and Auel, R., 1997. Study of the interaction of photo-oxidants and acidic components between gas and liquid phase. In: S. Fuzzi and D. Wagenbach (Editors), Cloud multi-phase processes and high alpine air and snow chemistry. Springer-Verlag, Berlin, pp. 138 - 145.

Möller, D., Acker, K. and Wieprecht, W., 1996. A relationship between liquid water content and chemical composition in clouds. *Atmospheric Research*, **41**: 321 - 335.

Möller, D., Acker, K. and Wieprecht, W., 1994. Cloud chemistry at Mt. Brocken/Harz (Germany). In: G. Angeletti and G. Restelli (Editors), Physico-Chemical Behaviour of Atmospheric Pollutants. European Commission, Luxembourg, pp. 968 - 974.

Mrose, H., 1966. Measurements of pH, and chemical analyses of rain-, snow-, and fog-water. *Tellus*, **18**: 266 - 270.

Mueller, S.F. and Weatherford, F.P., 1988. Chemical deposition to a high elevation red spruce forest. *Water, Air and Soil Pollution*, **38**: 345 - 363.

Reproduced with permission of the copyright owner. Further reproduction prohibited without permission.

Munger, J.W., Jacob, D.J., Daube, B.C., Jr., Horowitz, L.W., Keene, W.C. and Heikes, B.G., 1995. Formaldehyde, glyoxal and methylglyoxal in air and cloud water at a rural mountain site in central Virginia. *Journal of Geophysical Research*, **100**(D5): 9325 - 9333.

Munger, J.W., Collett, J.L., Jr., Daube, B.C., Jr. and Hoffmann, M.R., 1990. Fogwater chemistry at Riverside, California. *Atmospheric Environment*, **24B**(2): 185 - 205.

Munger, J.W., Collett, J.L., Jr., Daube, B.C., Jr. and Hoffmann, M.R., 1989. Carboxylic acids and carbonyl compounds in southern California clouds and fogs. *Tellus*, **41B**: 230 - 242.

Munger, J.W., Collett, J.L., Jr., Daube, B.C., Jr. and Hoffmann, M.R., 1989. Chemical composition of coastal stratus clouds: dependence upon drop size and distance from coast. *Atmospheric Environment*, **23**(10): 2305 - 2320.

Munger, J.W., 1989. The chemical composition of fogs and clouds in southern California. Ph.D. Thesis, Department of Environmental Engineering Science, California Institute of Technology, Pasadena, CA, 354 pp.

Munger, J.W., Tiller, C. and Hoffmann, M.R., 1986. Identification of hydroxymethanesulfonate in fog water. *Science*, **231**: 247 - 249.

Munger, J.W., Jacob, D.J. and Hoffmann, M.R., 1984. The occurrence of bisulfite-aldehyde addition products in fog- and cloudwater. *Journal of Atmospheric Chemistry*, **1**: 335 - 380.

Munger, J.W., Jacob, D.J., Waldman, J.M. and Hoffmann, M.R., 1983a. Fogwater chemistry in an urban atmosphere. *Journal of Geophysical Research*, **88**(C9): 5109 - 5121.

Munger, J.W., Waldman, J.M., Jacob, D.J. and Hoffmann, M.R., 1983b. Vertical variability and short-term temporal trends in precipitation chemistry. In: H.R. Pruppacher, R.G. Semonin and W.G.N. Slinn (Editors), Precipitation Scavenging, Dry Deposition, and Resuspension. Elsevier, New York, pp. 275 - 282.

Munzert, K., 1988. Chemistry of cloud water and precipitation at an alpine mountain station. In: M.H. Unsworth and D. Fowler (Editors), Acid deposition at high elevation sites. Kluwer Academic Publishers, Dordrecht, pp. 395 - 401.

Neftel, A., Sigg, A. and Jacob, P., 1987. H_2O_2 in solid precipitation. In: G. Angeletti and G. Restelli (Editors), Physico-chemical Behaviour of Atmospheric Pollutants. D. Reidel Publishing Co., Dordrecht, pp. 45 - 47.

Noone, K.J., Ostrom, E., Pockalny, R.A., De Bock, L. and Van Grieken, R., 1996. Chemical and microphysical properties of cloud droplet residual particles in marine stratocumulus clouds observed during the MAST experiment, 12th International Conference on Clouds and Precipitation, Zurich, Switzerland, pp. 1176 - 1178.

Noone, K.J., Ogren, J.A., Hallberg, A., Hansson, H.-C., Wiedensohler, A. and Swietlicki, E., 1992. A statistical examination of the chemical differences between interstitial and scavenged aerosol. *Tellus*, **44B**: 581 - 592.

Noone, K.J., Ogren, J.A., Noone, K.B., Hallberg, A., Fuzzi, S. and Lind, J.A., 1991. Measurements of the partitioning of hydrogen peroxide in a stratiform cloud. *Tellus*, **43B**: 280 - 290.

Reproduced with permission of the copyright owner. Further reproduction prohibited without permission.

Noone, K.J., Charlson, R.J., Covert, D.S., Ogren, J.A. and Heintzenberg, J., 1988. Cloud droplets: solute concentration is size-dependent. *Journal of Geophysical Research*, **93**(D8): 9477 - 9482.

Noruse, H. and Maruyama, H., 1971. On the hygroscopic nuclei in cloud droplets. *Papers in Meteorology and Geophysics*, **22**(1): 1 - 21.

Oberholzer, B., Collett, J.L., Jr., Staehelin, J. and Waldvogel, A., 1992. In-cloud scavenging of gases and aerosols at a mountain site in central Switzerland. *Journal of Atmospheric Chemistry*, **14**: 61 - 71.

Oddie, B.C.V., 1962. The chemical composition of precipitation at cloud levels. *Quarterly Journal of the Royal Meteorological Society*, **88**: 535 - 538.

Ogawa, N., Kikuchi, R., Okamura, T., Inotsume, J., Adzuhata, T., Ozeki, T. and Kajikawa, M., 2000. Evaluation of ionic pollutants in cloud droplets at a mountain ridge in northern Japan using constrained oblique rotational factor analysis. *Atmospheric Research*, **54**: 279 - 283.

Ogawa, N., Kikuchi, R., Okamura, T., Adzuhata, T., Kajikawa, M. and Ozeki, T., 1999. Cloud droplet size dependence of the concentrations of various ions in cloud water at a mountain ridge in northern Japan. *Atmospheric Research*, **51**: 77 - 80.

Ogiwara, S. and Okita, T., 1952. Electron-Microscope study of cloud and fog nuclei. *Tellus*, **4**: 233 - 240.

Ogren, J.A., Noone, K.J., Hallberg, A., Heintzenberg, J., Schell, D., Berner, A., Solly, I., Kruisz, C., Reischl, G., Arends, B.G. and Wobrock, W., 1992. Measurements of the size dependence of the concentration of non-volatile material in fog droplets. *Tellus*, **44B**: 570-580.

Ogren, J.A., Heintzenberg, J., Zuber, Z., Noone, K.J. and Charlson, R.J., 1989. Measurements of the size-dependence of solute concentrations in cloud droplets. *Tellus*, **41B**: 24 - 31.

Ogren, J.A., Heintzenberg, J., Zuber, A., Hansson, H.-C., Noone, K.J., Covert, D.S. and Charlson, R.J., 1988. Measurements of the short-term variability of aqueous-phase mass concentrations in cloud droplets. In: M.H. Unsworth and D. Fowler (Editors), Acid deposition at high elevation sites. Kluwer Academic Publishers, Dordrecht, pp. 125 - 137.

Ogren, J.A. and Rodhe, H., 1986. Measurements of the chemical composition of cloudwater at a clean air site in central Scandinavia. *Tellus*, **38B**: 190 - 196.

Ohta, S., Okita, T. and Kato, C., 1981. A numerical model of acidification of cloud water. *Journal of the Meteorological Society of Japan*, **59**(6): 892 - 901.

Ohtake, T., 1981. X-ray analyses of nuclei in individual fog droplets and nuclei. In: A.F. Roddy and T.C. O'Connor (Editors), 9th International Conference on Atmospheric Aerosols, Condensation and Ice Nuclei. Galway University Press, Galway, Ireland, pp. 213 - 217.

Okita, T. and Ota, S., 1981. The concentrations of trace constituents in the atmosphere and in cloud water in relation to meteorological conditions and oxidant level. In: A.F. Roddy and T.C. O'Connor (Editors), 9th International Conference on Atmospheric Aerosols, Condensation and Ice Nuclei. Galway University Press, Galway, Ireland, pp. 239 - 243.

Okita, T., 1968. Concentration of sulfate and other inorganic materials in fog and cloud water. *Journal of the Meteorological Society of Japan*, **42**(2): 120 - 126.

Reproduced with permission of the copyright owner. Further reproduction prohibited without permission.

Okita, T., 1965. Some chemical and meteorological measurements of air pollution in Asahikawa. *International Journal of Air and Water Pollution*, **9**: 323 - 332.

Pade, G., Covert, D.S. and Larson, T.V., 1987. Design and calibration of a high volume fogwater collector. *Journal of Atmospheric and Oceanic Technology*, **4**: 340 - 344.

Pahl, S., Winkler, P., Arends, B.G., Kos, G.P.A., Schell, D., Facchini, M.-C., Fuzzi, S., Gallagher, M.W., Colvile, R., Choularton, T.W., Berner, A., Kruisz, C., Bizjak, M., Acker, K. and Wieprecht, W., 1997. Vertical gradients of dissolved chemical constituents in evaporating clouds. *Atmospheric Environment*, **31**(16): 2577 - 2588.

Parungo, F., Nagamoto, C. and Kopcewicz, B., 1989. Front range acidic clouds and precipitation. In: R.K. Olson and A.S. Lefohn (Editors), Effects of air pollution on western forests. Air and Waste Management Association, Anaheim, CA, pp. 15 - 31.

Pehkonen, S.O., Erel, Y. and Hoffmann, M.R., 1992. Simultaneous spectrophotometric measurement of Fe(II) and Fe(III) in atmospheric water. *Environmental Science and Technology*, **26**: 1731 - 1736.

Penkett, S.A. and Tyler, B.J., 1988. A field study of the cloud chemistry and cloud microphysics at Great Dun Fell. *Atmospheric Environment*, **22**(4): 683 - 694.

Petrenchuk, O.P., 1975. Estimation of condensation nuclei chemical composition from the results of cloud water analysis. In: I.I. Gaivoronsky (Editor), Proceedings of the 8th International Conference on Nucleation. Gidrometeoizdat, Leningrad, USSR, pp. 445 - 449.

Petrenchuk, O.P. and Selezneva, E.S., 1970. Chemical composition of precipitation in regions of the Soviet Union. *Journal of Geophysical Research*, **75**(18): 3629 - 3634.

Petrenchuk, O.P. and Drozdova, V.M., 1966. On the chemical composition of cloud water. *Tellus*, **18**: 280 - 286.

Pierson, W.R., Brachaczek, W.W., Gorse, R.A.J., Japar, S.M., Norbeck, J.M. and Keeler, G.J., 1987. Acid deposition and atmospheric chemistry at Allegheny Mountain. In: R.W. Johnson, G.E. Gordon, W. Calkins and A.Z. Elzerman (Editors), The Chemistry of Acid Rain: Sources and Atmospheric Processes. American Chemical Society, Washington, D. C., pp. 28 - 38.

Plessow, K., Acker, K., Heinrichs, H. and Möller, D., 2001. Time study of trace elements and major ions during two cloud events at Mt. Brocken. *Atmospheric Environment*, **35**: 367 - 378.

Ponce, F.N. and Hindman, E.E., 2001. Wintertime cloud and snow pH increased between 1984 and 2000 in the northern Colorado Rockies. In: R.S. Schemenauer and H. Puxbaum (Editors), 2nd International Conference on Fog and Fog Collection, St. John's, Newfoundland, Canada, pp. 61 - 64.

Post, D., Bridgeman, H.A. and Ayers, G.P., 1991. Fog and rainwater composition in rural SE Australia. *Journal of Atmospheric Chemistry*, **13**: 83 - 95.

Poulida, O., Schwitkowski, M., Baltensperger, U., Staehelin, J. and Gaeggeler, H.W., 1998. Scavenging of atmospheric constituents in mixed phase clouds at the high-alpine site Jungfraujoch - Part II. influence of riming on the scavenging of particulates and gaseous chemical species. *Atmospheric Environment*, **32**(23): 3985 - 4000.

Reproduced with permission of the copyright owner. Further reproduction prohibited without permission.

Preiss, M., Maser, R., Franke, H., Jaeschke, W. and Graf, J., 1994. Distribution of trace substances inside and outside of clouds. *Contributions to Atmospheric Physics*, **67**(4): 341 - 351.

Pruppacher, H.R. and Klett, J.D., 1997. Microphysics of Clouds and Precipitation. Kluwer Academic Publishers, Dordrecht, the Netherlands, 954 pp.

Pueschel, R.F., van Valin, C.C., Castillo, R.C., Kadlecek, J.A. and Ganor, E., 1986. Aerosols in polluted vs. non-polluted air masses: long-range transport and effects on clouds. *Journal of Climate and Applied Meteorology*, **25**: 1908 - 1917.

Puxbaum, H. and Tscherwenka, W., 1998. Relationships of major ions in snow fall and rime at Sonnblick observatory (SBO, 3106 m) and implications for scavenging processes in mixed clouds. *Atmospheric Environment*, **32**(23): 4011 - 4020.

Qian, G.-W., Ishizaka, Y., Minami, Y., Kurahashi, Y., Tjandradewi, B.I. and Takenaka, C., 1992. Transformation of individual aerosol particles in acidic fog evolution. *Journal of the Meteorological Society of Japan*, **70**(2): 711 - 721.

Radojevic, M., Tyler, B.J., Hall, S. and Penderghest, N., 1995. Air oxidation of S(IV) in cloud-water samples. *Water, Air and Soil Pollution*, **85**: 1985 - 1990.

Radojevic, M., Tyler, B.J., Wicks, A.J., Gay, M.J. and Choularton, T.W., 1990. Field studies of SO_2/aqueous S(IV) equilibrium in clouds. *Atmospheric Environment*, **24A**(2): 323 - 328.

Rancourt, K.L. and Howe, J.B., 1987. On the distribution of acidity within clouds as a function of droplet size, Mt. Washington Observatory News Bulletin, pp. 48 - 52.

Rao, X. and Collett, J.L., Jr., 1998. The drop size-dependence of iron and manganese concentrations in clouds and fogs: implications for sulfate production. *Journal of Atmospheric Chemistry*, **30**: 273 - 289.

Rao, X., 1997. Cloud chemical heterogeneity and its influence on aqueous sulfur(IV) oxidation. Ph.D. Dissertation, Department of Civil Engineering. University of Illinois at Urbana-Champaign, Urbana-Champaign, IL.

Rao, X. and Collett, J.L., Jr., 1995. Behaviour of S(IV) and formaldehyde in a chemically heterogeneous cloud. *Environmental Science and Technology*, **29**: 1023 - 1031.

Reijnders, H.F.R., van Zijl, J., van Pul, W.A.J., Romer, F.G. and Slangewal, H.J., 1987. Characterization of cloud and rain water chemical composition. In: G. Angeletti and G. Restelli (Editors), Physico-chemical Behaviour of Atmospheric Pollutants. D. Reidel Publishing, Co., Dordrecht, pp. 451 - 459.

Reilly, J.E., 2000. Application of a tracer technique to study sulfur dioxide oxidation in cloud drops as a function of drop size. M.S. Thesis, Department of Atmospheric Science. Colorado State University, Fort Collins, CO.

Reisinger, L.M. and Imhoff, R.E., 1988. Source/receptor relationships in high elevation acidic deposition, 81st annual meeting of the Air Pollution Control Association. Air Pollution Control Association, Dallas, TX, pp. 88-129.7.

Reynolds, B., Fowler, D. and Thomas, S., 1996. Chemistry of cloud water at an upland site in mid-Wales. *The Science of the Total Environment*, **188**: 115 - 125.

Reproduced with permission of the copyright owner. Further reproduction prohibited without permission.

Ricci, L., Fuzzi, S., Laj, P., Lazzari, A., Orsi, G., Berner, A., Günther, A., Jaeschke, W., Wendisch, M. and Arends, B.G., 1998. Gas-liquid equilibria in polluted fog. *Contributions to Atmospheric Physics*, **71**(1): 159-170.

Richards, L.W., 1995. Airborne chemical measurements in night time stratus clouds in the Los Angeles basin. *Atmospheric Environment*, **29**(1): 27 - 46.

Richards, L.W., 1989. Airborne chemical measurements in night time stratus clouds in the Los Angeles basin. In: R.K. Olson and A.S. Lefohn (Editors), Effects of air pollution on Western Forests. Air and Waste Management Association, Anaheim, CA, pp. 51 - 72.

Richards, L.W., Anderson, J.A., Blumenthal, D.L., McDonald, J.A., Kok, G.L. and Lazrus, A.L., 1983. Hydrogen peroxide and sulfur(IV) in Los Angeles cloud water. *Atmospheric Environment*, **17**(4): 911 - 914.

Richartz, H., Reischl, A., Trautner, F. and Hutzinger, O., 1990. Nitrated phenols in fog. *Atmospheric Environment*, **24A**(12): 3067 - 3071.

Richter, R.C., Swami, K., Chace, S. and Husain, L., 1998. Determination of arsenic, selenium, and antimony in cloud water by inductively coupled plasma mass spectroscopy. *Fresenius Journal of Analytical Chemistry*, **361**: 168 - 173.

Römer, F.G., Viljeer, J.W., vandenBeld, L., Slangewal, H.J., Veldkamp, A.A. and Reijnders, H.F.R., 1985. The chemical composition of cloud and rainwater. Results of preliminary measurements from an aircraft. *Atmospheric Environment*, **19**(11): 1847 - 1858.

Römer, F.G., Viljeer, J.W., vandenBeld, L., Slangewal, H.J., Veldkamp, A.A., Kema, N.V. and Reijnders, H.F.R., 1983. Preliminary measurements from an aircraft into the chemical composition of clouds. In: S. Beilke and A.J. Elshout (Editors), Acid deposition. D. Reidel Publishing, Dordrecht, pp. 195 - 203.

Römpp, A., Klemm, O., Fricke, W. and Frank, H., 2001. Haloacetates in fog and rain. *Environmental Science and Technology*, **35**: 1294 - 1298.

Ruprecht, H. and Sigg, L., 1990. Interactions of aerosols (ammonium sulfate, ammonium nitrate, and ammonium chloride) and of gases (HCl, HNO_3) with fogwater. *Atmospheric Environment*, **24A**(3): 573 - 584.

Sadasivan, S., 1980. Trace constituents in cloud water, rain water, and aerosol sampled collected near the west coast on India during the southwest monsoon. *Atmospheric Environment*, **14**: 33 - 38.

Sagabiel, J.C. and Seiber, J.N., 1993. Studies on the occurrence and distribution of wood smoke marker compounds in foggy atmospheres. *Environmental Toxicology and Chemistry*, **12**: 813 - 822.

Sanhueza, E., Santana, M. and Hermoso, M., 1992. Gas- and aqueous-phase formic and acetic acids at a tropical cloud forest site. *Atmospheric Environment*, **26A**(8): 1421 - 1426.

Sattler, B., Puxbaum, H. and Psenner, R., 2001. Bacterial growth in supercooled cloud drops. *Geophysical Research Letters*, **28**(2): 239 - 242.

Saxena, V.K., Stogner, R.E., Hendler, A.H., deFelice, T.P., Yeh, R.J.-Y. and Lin, N.-H., 1989. Monitoring the chemical climate of the Mt. Mitchell State Park for evaluation of its impact on forest decline. *Tellus*, **41B**: 92 - 109.

Reproduced with permission of the copyright owner. Further reproduction prohibited without permission.

Saxena, V.K. and Yeh, R.J.-Y., 1988. Temporal variability in cloud water acidity: physico-chemical characteristic of atmospheric aerosols and windfield. *Journal of Aerosol Science*, **19**(7): 1207 - 1210.

Saxena, V.K. and Hendler, A.H., 1983. In-cloud scavenging and resuspension of cloud active aerosols during winter storms over Lake Michigan. In: H.R. Pruppacher, R.G. Semonin and W.G.N. Slinn (Editors), Precipitation Scavenging, Dry Deposition, and Resuspension. Elsevier, New York, NY, pp. 91 - 100.

Schell, D., Maser, R., Wobrock, W., Jaeschke, W., Georgii, H.-W., Kos, G.P.A., Arends, B.G., Beswick, K.M., Bower, K.N. and Gallagher, M.W., 1997a. A two-stage impactor for fog droplet collection: design and performance. *Atmospheric Environment*, **31**(16): 2671 - 2679.

Schell, D., Wobrock, W., Maser, R., Preiss, M., Jaeschke, W., Georgii, H.-W., Gallagher, M.W., Bower, K.N., Beswick, K.M., Pahl, S., Facchini, M.-C., Fuzzi, S., Wiedensohler, A., Hansson, H.-C. and Wendisch, M., 1997b. The size-dependent chemical composition of cloud droplets. *Atmospheric Environment*, **31**(16): 2561 - 2576.

Schell, D. and Georgii, H.-W., 1989. Design and operation of a two-stage fogwater collector. In: H.-W. Georgii (Editor), Mechanisms and Effects of Pollutant-Transfer into Forests. Kluwer Academic Publishers, Dordrecht, pp. 221 - 229.

Schemenauer, R.S., Banic, C.M. and Urquizo, N., 1995. High elevation fog and precipitation chemistry in southern Quebec, Canada. *Atmospheric Environment*, **29**(17): 2235 - 2252.

Schemenauer, R.S. and Cereceda, P., 1992a. The quality of fog water collected for domestic and agricultural use in Chile. *Journal of Applied Meteorology*, **31**: 275 - 290.

Schemenauer, R.S. and Cereceda, P., 1992b. Monsoon cloudwater chemistry on the Arabian peninsula. *Atmospheric Environment*, **26A**(9): 1583 - 1587.

Schemenauer, R.S. and Winston, C., 1988. The 1986 Chemistry of High Elevation Fog Project, 81st annual meeting of the Air Pollution Control Association. Air Pollution Control Association, Dallas, TX, pp. 88-129.6.

Schemenauer, R.S., Schuepp, P.H., Kermasha, S. and Cereceda, P., 1988. Measurements of the properties of high elevation fog in Quebec. In: M.H. Unsworth and D. Fowler (Editors), Acid deposition at high elevation sites. Kluwer Academic Publishers, Dordrecht, pp. 359 - 374.

Schemenauer, R.S., 1986. Acidic deposition to forests: the 1985 Chemistry of High Elevation Fog (CHIEF) project. *Atmosphere-Ocean*, **24**(4): 303 - 328.

Scherbatskoy, T. and Bliss, M., 1984. Occurrence of acidic rain and cloud water in high elevations ecosystems in the Green Mountains of Vermont. In: P.J. Samson (Editor), The Meteorology of Acid Deposition. Air Pollution Control Association, Pittsburgh, PA, pp. 449 - 463.

Schlesinger, W.H. and Reiners, W.A., 1974. Deposition of water and cations on artificial foliar collectors in Fir Krummholz of New England mountains. *Ecology*, **55**: 378 - 386.

Schmitt, G., 1989. Comparison of wet deposition inputs via rain and fog interception at a high elevated forest site. In: H.-W. Georgii (Editor), Mechanisms and effects of pollutant transfer into forests. Kluwer Academic Publishers, Dordrecht, pp. 213 - 220.

Reproduced with permission of the copyright owner. Further reproduction prohibited without permission.

Schmitt, G., 1988. Measurements of the chemical composition in cloud and fogwater. In: M.H. Unsworth and D. Fowler (Editors), Acid deposition at high elevation sites. Kluwer Academic Publishers, Dordrecht, pp. 403 - 417.

Schmitt, G., 1986. The temporal distribution of trace element concentrations in fog water during individual fog events. In: H.-W. Georgii (Editor), Atmospheric Pollutants in Forest Areas: Their Deposition and Interception. D. Reidel Publishing Company, Dordrecht, pp. 129 - 141.

Schomburg, C.J., Glotfelty, D.E. and Seiber, J.N., 1991. Pesticide occurrence and distribution in fog collected near Monterey, California. *Environmental Science and Technology*, **25**: 155 - 160.

Schwanz, M., Warneck, P., Preiss, M. and Hoffmann, P., 1998. Chemical speciation of iron in fog water. *Contributions to Atmospheric Physics*, **71**(1): 131-143.

Scott, B.C. and Laulainen, N.S., 1979. On the concentration of sulfate in precipitation. *Journal of Applied Meteorology*, **18**: 138 - 147.

Scott, W.D., 1978. The pH of cloud water and the production of sulfate. *Atmospheric Environment*, **12**: 917 - 921.

Sedlak, D.L., Hoigné, J., David, M.M., Colvile, R., Seyffer, E., Acker, K., Wieprecht, W., Lind, J. and Fuzzi, S., 1997. The cloudwater chemistry of iron and copper at Great Dun Fell, U. K. *Atmospheric Environment*, **31**(16): 2515 - 2526.

Sedlak, D.L. and Hoigné, J., 1993. The role of copper and oxalate in the redox cycling of iron in atmospheric waters. *Atmospheric Environment*, **27A**(14): 2173 - 2185.

Seiber, J.N., Wilson, B.W. and McChesney, M.M., 1993. Air and fog deposition residues of four organophosphate insecticides used on dormant orchards in the San Joaquin Valley, California. *Environmental Science and Technology*, **27**: 2236 - 2243.

Seyffer, E. and Helas, G., 1994. The balance of concentrations of formic and acetic acids in the gas and liquid phase of hydrometeors. In: G. Angeletti and G. Restelli (Editors), Physico-chemical Behaviour of Atmospheric Pollutants. European Commission, Luxembourg, pp. 989 - 994.

Shen, Z., Wu, Y., Huang, M., Xiao, H. and Lei, H., 1996. Measurement and research on cloudwater chemistry over severe acid rain areas of China, 12th International Conference on Clouds and Precipitation, Zurich, Switzerland, pp. 1128 - 1129.

Shen, Z., Wu, Y., Xiao, H., Bai, C. and Huang, M., 1993. Some basic features of cloudwater chemistry in southwest China. *Scientia Atmospherica Sinica*, **17**(2): 195 - 205.

Siefert, R.L., Johansen, A.M., Hoffmann, M.R. and Pehkonen, S.O., 1997. Measurements of trace metal (Fe, Cu, Mn, Cr) oxidation states in fog and stratus clouds. *Journal of the Air and Water Management Association*, **48**: 128 - 143.

Sigg, L., Stumm, W., Zobrist, J. and Zürcher, F., 1987. The chemistry of fog: factors regulating its composition. *Chimia*, **41**(5): 159 - 165.

Sigmon, J.T. and Estes, M.J., 1988. Relationship between cloud chemistry and meteorology in central Virginia: a preliminary study, 81st annual meeting of the Air Pollution Control Association. Air Pollution Control Association, Dallas, TX, pp. 88-129.4.

Reproduced with permission of the copyright owner. Further reproduction prohibited without permission.

Sinner, T., Hoffmann, P. and Ortner, H.M., 1994. Determination of the pH-value, redox-potential, transition metals concentration and Fe(II)- and Fe(III)-content in cloud water samples. *Contributions to Atmospheric Physics*, **67**(4): 353 - 357.

Skvarenina, J. and Mindas, J., 2001. Long-term change in acidity and chemistry of fog/cloud water in high elevation sites in Slovakia. In: R.S. Schemenauer and H. Puxbaum (Editors), 2nd International Conference on Fog and Fog Collection, St. John's, Newfoundland, Canada, pp. 81 - 84.

Skybová, M., 2001. Chemical polluted icing and fog in the mountain regions of the Czech Republic. In: R.S. Schemenauer and H. Puxbaum (Editors), 2nd International Conference on Fog and Fog Collection, St. John's, Newfoundland, Canada, pp. 109 - 112.

Snider, J.R. and Huang, J., 1998. Factors influencing the retention of hydrogen peroxide and molecular oxygen in rime ice. *Journal of Geophysical Research*, **103**(D1): 1405 - 1415.

Snider, J.R. and Vali, G., 1994. Sulfur dioxide oxidation in winter orographic clouds. *Journal of Geophysical Research*, **99**(D9): 18,713 - 18,733.

Snider, J.R., Montague, D.C. and Vali, G., 1992. Hydrogen peroxide retention in rime ice. *Journal of Geophysical Research*, **97**(D7): 7569 - 7578.

Staudinger, M., Schöner, W., Puxbaum, H. and Böhm, R., 1997. Accumulation of acidic components in two snowfields in the Sonnblick region. In: S. Fuzzi and D. Wagenbach (Editors), Cloud multi-phase processes and high alpine air and snow chemistry. Springer-Verlag, Berlin, pp. 219 - 224.

Steinberg, S. and Kaplan, I.R., 1984. The determination of low molecular weight aldehydes in rain, fog and mist by reversed phase liquid chromatography of the 2,4-dinitrophenylhydrazone derivatives. *International Journal of Environmental Analytical Chemistry*, **18**: 253 - 266.

Svenningsson, B., Hansson, H.-C., Martinsson, B.G., Wiedensohler, A., Swietlicki, E., Cederfelt, S.-I., Wendisch, M., Bower, K.N., Choularton, T.W. and Colvile, R., 1997. Cloud droplet nucleation scavenging in relation to the size and hygroscopic behaviour of aerosol particles. *Atmospheric Environment*, **31**(16): 2463 - 2476.

Tenberken, B. and Bächmann, K., 1998. Sampling and analysis of single cloud and fog drops. *Atmospheric Environment*, **32**(10): 1757 - 1763.

Tesar, M., Sir, M., Fottova, D., Fišák, J. and Eliáš, V., 2001. Cloud and fog water deposition and its hydrological and ecological importance in selected regions of the Czech Republic. In: R.S. Schemenauer and H. Puxbaum (Editors), 2nd International Conference on Fog and Fog Collection, St. John's, Newfoundland, Canada, pp. 153 - 156.

Tomlinson, G.H., Brouzes, R.J.P., McLean, R.A.N. and Kadlecek, J.A., 1980. The role of clouds in atmospheric transport of mercury and other pollutants 2. the role of cloudwater in atmospheric transport. In: D. Drabløs and A. Tollan (Editors), Ecological impact of acid precipitation, Sandefjord, Norway, pp. 135 - 137.

Trautner, F. and Eiden, R., 1988. A measuring device to quantify deposition of fog water and ionic input by fog on small spruce trees. *Trees*, **2**: 92 - 95.

Tremp, J., 1992. Sources and fates of nitrated phenols in the atmospheric environment. Ph.D. Thesis, ETH, Zurich, Switzerland.

Reproduced with permission of the copyright owner. Further reproduction prohibited without permission.

Tripathi, A.N., Aggarwal, S.G. and Kamavisdar, A., 2001. Studies in heavy metal pollution in fog water samples from Raipur (Chattisgarh), India. In: R.S. Schemenauer and H. Puxbaum (Editors), 2nd International Conference on Fog and Fog Collection, St. John's, Newfoundland, Canada, pp. 93 - 96.

Twohy, C.H., Clarke, A.D., Warren, S.G., Radke, L.F. and Charlson, R.J., 1989. Light-absorbing material extracted from cloud droplets and its effects on cloud albedo. *Journal of Geophysical Research*, **94**(D6): 8623 - 8631.

Unsworth, M.H. and Wilshaw, J.C., 1989. Wet, occult and dry deposition of pollutants on forests. *Agricultural and Forest Meteorology*, **47**: 221 - 238.

van Valin, C.C., Wellman, D.L. and Stearns, L.P., 1987. Aerosol and cloudwater properties and Whiteface Mtn., NY. *Water, Air and Soil Pollution*, **34**: 369 - 383.

Verhoeven, W., Herrmann, R., Eiden, R. and Klemm, O., 1987. A comparison of the chemical composition of fog and rainwater collected in the Fichtelgebirge, Federal Republic of Germany, and the South Island of New Zealand. *Theoretical and Applied Climatology*, **38**: 210 - 221.

Voisin, D., Legrand, M. and Chaumerliac, N., 2000. Scavenging of acidic gases (HCOOH, CH_3COOH, HNO_3, HCl, and SO_2) and ammonia in mixed liquid-solid water clouds at the Puy de Dôme Mountain (France). *Journal of Geophysical Research*, **105**(D5): 6817 - 6835.

Vong, R.J., Baker, B.M., Brechtel, F.J., Collier, R.T., Harris, J.M., Kowalski, A.S., McDonald, N.C. and McInnes, L.M., 1997. Ionic and trace element composition of cloud water collected on the Olympic peninsula of Washington state. *Atmospheric Environment*, **31**(13): 1991 - 2001.

Vong, R.J. and Guttorp, P., 1991. Co-occurrence of ozone and acidic cloud water in high-elevation forests. *Environmental Science and Technology*, **25**: 1325 - 1329.

Vong, R.J., Bailey, B.H., Markus, M.J. and Mohnen, V.A., 1990. Factors governing cloud water composition in the Appalachian mountains. *Tellus*, **42B**: 435 - 453.

Wagenbach, D. (Editor), 1997. High Alpine Air and Snow chemistry. Springer-Verlag, Berlin, 165 - 199 pp.

Waldman, J.M. and Hoffmann, M.R., 1987. Depositional aspects of pollutant behaviour in fog and intercepted clouds. In: R.A. Hites and S.J. Eisenreich (Editors), Sources and Fates of Aquatic Pollutants. Advances in Chemistry Series #216. American Chemical Society, pp. 79 - 129.

Waldman, J.M., Munger, J.W., Jacob, D.J. and Hoffmann, M.R., 1985. Chemical characterization of stratus cloudwater and its role as a vector for pollutant deposition in a Los Angeles pine forest. *Tellus*, **37B**: 91 - 108.

Waldman, J.M., Munger, J.W., Jacob, D.J. and Hoffmann, M.R., 1983. Fogwater composition in Southern California. In: H.R. Pruppacher, R.G. Semonin and W.G.N. Slinn (Editors), Precipitation Scavenging, Dry Deposition, and Resuspension. Elsevier, New York, NY, pp. 137 - 145.

Waldman, J.M., Munger, J.W., Jacob, D.J., Flagan, R.C., Morgan, J.J. and Hoffmann, M.R., 1982. Chemical composition of acid fog. *Science*, **218**: 677 - 680.

Reproduced with permission of the copyright owner. Further reproduction prohibited without permission.

Watanabe, K., Ishizaka, Y. and Takenaka, C., 2001. Chemical characteristics of cloud water over the Japan Sea and the Northwestern Pacific Ocean near the central part of Japan: airborne measurements. *Atmospheric Environment*, **35**: 645 - 655.

Watanabe, K., Ishizaka, Y. and Takenaka, C., 1999. Chemical composition of fog water near the summit of Mt. Norikura in Japan. *Journal of the Meteorological Society of Japan*, **77**(5): 997 - 1006.

Weathers, K.C. and Likens, G.E., 1997. Clouds in Southern Chile: An important source of nitrogen to nitrogen-limited ecosystems? *Environmental Science and Technology*, **31**: 210 - 213.

Weathers, K.C., Likens, G.E., Bormann, F.H., Bicknell, S.H., Bormann, B.T., Daube, B.C., Jr., Eaton, J.S., Galloway, J.N., Keene, W.C., Kimball, K.D., McDowell, W.H., Siccama, T.G., Smiley, D. and Tarrant, R.A., 1988a. Cloudwater chemistry from ten sites in North America. *Environmental Science and Technology*, **22**: 1018 - 1026.

Weathers, K.C., Likens, G.E., Bormann, F.H., Eaton, J.S., Kimball, K.D., Galloway, J.N., Siccama, T.G. and Smiley, D., 1988b. Chemical concentrations in cloud water from four sites in the Eastern United States. In: M.H. Unsworth and D. Fowler (Editors), Acid deposition at high elevation sites. Kluwer Academic Publishing, Dordrecht, pp. 345 - 357.

Weathers, K.C., Likens, G.E., Bormann, F.H., Eaton, J.S., Bowden, W.B., Andersen, J.L., Cass, D.A., Galloway, J.N., Keene, W.C., Kimball, K.D., Huth, P. and Smiley, D., 1986. A regional acidic cloud/fog water event in the eastern United States. *Nature*, **319**: 657 - 658.

Winiwarter, W., Puxbaum, H., Fuzzi, S., Facchini, M.-C., Orsi, G., Beltz, N., Enderle, K.H. and Jaeschke, W., 1988. Organic acid gas and liquid-phase measurements in Po Valley fall-winter conditions in the presence of fog. *Tellus*, **40B**: 348 - 357.

Winkler, P., 1992. Design and calibration of a fogwater collector, WMO Technical Conference on Instruments and Methods of Observation (TECO-92). World Meteorological Organization, Vienna, Austria, pp. 17 - 21.

Winkler, P. and Kroll, G., 1987. Preliminary results on fog deposition. In: G. Angeletti and G. Restelli (Editors), Physico-chemical Behaviour of Atmospheric Pollutants. D. Reidel Publishing, Co., Dordrecht, pp. 579 - 587.

Winkler, P., 1986. Observation of fog water composition in Hamburg. In: H.-W. Georgii (Editor), Atmospheric Pollutants in Forest Areas: Their Deposition and Interception. D. Reidel Publishing Company, Dordrecht, pp. 143 - 151.

Winkler, P., 1984. Observations on acid particles and droplets in the atmosphere. In: J.L. Durham (Editor), Chemistry of particles, fogs and rain. Butterworth Publishers, Boston, MA, pp. 161 - 196.

Wisniewski, J., 1982. The potential acidity associated with dews, frosts, and fogs. *Water, Air and Soil Pollution*, **17**: 361 - 377.

Wobrock, W., Schell, D., Maser, R., Jaeschke, W., Georgii, H.-W., Wieprecht, W., Arends, B.G., Mols, J.J., Kos, G.P.A., Fuzzi, S., Facchini, M.-C., Orsi, G., Berner, A., Solly, I., Kruisz, C., Svenningsson, B., Wiedensohler, A., Hansson, H.-C., Ogren, J.A., Noone, K.J., Hallberg, A., Pahl, S., Schneider, T., Winkler, P., Winiwarter, W., Colvile, R., Choularton, T.W., Flossmann, A. and Borrmann, S., 1994. The Kleiner Feldberg Cloud experiment 1990. An overview. *Journal of Atmospheric Chemistry*, **19**: 3 - 35.

Reproduced with permission of the copyright owner. Further reproduction prohibited without permission.

Woodcock, A.H., Blanchard, D.C. and Jiusto, J.E., 1981. Marine fog droplets and salt nuclei - part II. *Journal of the Atmospheric Sciences*, **38**: 129 - 140.

Wrzesinsky, T., Thalmann, E., Burkhard, R., Eugster, W. and Klemm, O., 2001. Fog deposition of nutrients and pollutants to a montane forest site. In: R.S. Schemenauer and H. Puxbaum (Editors), 2nd International Conference on Fog and Fog Collection, St. John's, Newfoundland, Canada, pp. 169 - 172.

Wrzesinsky, T. and Klemm, O., 2000. Summertime fog chemistry at a mountainous site in Central Europe. *Atmospheric Environment*, **34**: 1487 - 1496.

Wujcik, C.E., Cahill, T.M. and Seiber, J.N., 1999. Determination of trifluoroacetic acid in 1997-1997 precipitation and surface waters in California and Nevada. *Environmental Science and Technology*, **33**: 1747 - 1751.

Wujcik, C.E., Zehavi, D. and Seiber, J.N., 1998. Trifluoroacetic acid levels in 1994 - 1996 fog, rain, snow and surface waters from California and Nevada. *Chemosphere*, **36**(6): 1233 - 1245.

Xue, H., de Lurdes, M., Gonçalves, S., Reutlinger, M., Sigg, L. and Stumm, W., 1991. Copper(I) in fogwater: determination and interactions with sulfite. *Environmental Science and Technology*, **25**: 1716 - 1722.

Yu, X., 2001. The collection effect of trees on fog water. In: R.S. Schemenauer and H. Puxbaum (Editors), 2nd International Conference on Fog and Fog Collection, St. John's, Newfoundland, Canada, pp. 201 - 203.

Zehavi, D. and Seiber, J.N., 1996. An analytical method for trifluoracetic acid in water and air samples using headspace gas chromatographic determination of the methyl ester. *Analytical Chemistry*, **68**: 3450 - 3459.

Zhu, B., Li, Z., Huang, J., Yang, J., Huang, Y. and Huang, Y., 2001. Chemical composition of the urban and suburban fogs in Xishuangbanna. In: R.S. Schemenauer and H. Puxbaum (Editors), 2nd International Conference on Fog and Fog Collection, St. John's, Newfoundland, Canada, pp. 113 - 116.

Zimmermann, F. and Zimmermann, L., 2001. Fog deposition on Norway spruce stands at high-elevations sites in the eastern Erzgebirge. In: R.S. Schemenauer and H. Puxbaum (Editors), 2nd International Conference on Fog and Fog Collection, St. John's, Newfoundland, Canada, pp. 173 - 176.

Zuo, Y., 1994. Light-induced oxidation of bisulfite-aldehyde adducts in real fog water. *Naturwissenschaften*, **81**: 505 - 507.

Zuo, Y. and Hoigné, J., 1993. Evidence for photochemical formation of H_2O_2 and oxidation of SO_2 in authentic fog water. *Science*, **260**: 71 - 73.

Zuo, Y., 1992. Photochemistry of Iron(III)/Iron(II) complexes in atmospheric liquid phases and its environmental significance. Ph.D. Thesis, ETH, Zurich, Switzerland.

Reproduced with permission of the copyright owner. Further reproduction prohibited without permission.

B. Appendix: Cloud water collectors – review, characterization and reported field comparisons

This appendix has multiple goals. The first is to review the different methods reported in the literature to collect cloud water. This starts with the earliest collectors as many current ones are clearly derivative. The review motivates the question of how the collectors are characterized theoretically and/or experimentally, as a method's utility is limited if its biases are unknown. Side-by-side collector comparisons are then reviewed. A discussion of the material presented and its implications comprise the final section.

This review is limited to ground-based collectors in the readily-available (English language) literature. There are a wide variety of airborne collectors, but they are not included (Jaeschke and Günther, 2001; Watanabe *et al.*, 2001; Lai *et al.*, 1997; Bin and Wenquan, 1996; Dixon and Charlson, 1994; Maser *et al.*, 1994; Liu *et al.*, 1993; Kim and Boatman, 1992; Parungo *et al.*, 1989; Hindman, 1988; Huebert *et al.*, 1988; Khemani *et al.*, 1987; Tanner, 1987; Hobbs, 1986; Huebert and Baumgardner, 1985; Hegg and Hobbs, 1983; Walters *et al.*, 1983; Khemani *et al.*, 1982; Hegg and Hobbs, 1981; Mohnen, 1980, and references therein; Tomlinson *et al.*, 1980; Scott and Laulainen, 1979; Fricke *et al.*, 1978; Scott, 1978; Jiusto, 1967; Oddie, 1962). All cloud water chemistry studies are not discussed individually (see Appendix A), and not all authors indicate how their reported cloud water composition measurements were made. Some of the collectors presented have, to my knowledge, only been used to collect water to gauge occult deposition. However, they have been included if relevant.

Reproduced with permission of the copyright owner. Further reproduction prohibited without permission.

B.1 Review of ground-based cloud water collectors

The collectors described in this review are divided into the following categories: "early" collectors (roughly through the early 1970s or before the considerable activity later associated with acid rain studies), passive string collectors, passive string collectors for potable water, (active) rotating arm collectors, active string collectors, active impactors, super-cooled drop (rime) collectors, methods for individual drops, drop residue methods, alternate approaches, and some final ambiguous references. Some of the collectors presented can be included in multiple categories. Many of the collectors that follow appear in the literature only once or twice; the most routinely-used collectors are indicated in section B.4.

B.1.1 Early cloud water collectors

Many of the early cloud water collector developers identified collection problems that remain unresolved (e.g. aspiration efficiency, representative drop sampling, sample evaporation, among others), although some of the theoretical development widely used today had not yet been formalized (Grunow, 1960; Nagel, 1956; May, 1945; Houghton and Radford, 1938). Understanding cloud physical properties such as drop size distributions, liquid water content (LWC), visibility impacts and occult deposition rates motivated much of the development.

The simplest approach was actually to use spiders' webs as they were of small enough diameter (< 0.01 μm) to collect haze drops (figure B-1) (Arnulf *et al.*, 1957; Dessens, 1949). The use of fine strands to collect drops carried by the ambient wind continues to the present. More formal cylindrical arrangements of parallel fine strands strung on a frame include several Japanese passive collectors (Okita, 1961; Tabata *et al.*, 1953), which both feature 0.12 mm diameter enameled copper wires spaced at 1 mm intervals, collecting funnels underneath the strands and an overhanging rain shelter above to prevent contamination (figures B-2 and B-3). Alternatively a wire mesh could be attached to a cylindrical frame subsequently placed on top of a rain gauge. Grunow and Nagel used 0.1 mm and 0.25 mm diameter wire, respectively, and Grunow indicated

Reproduced with permission of the copyright owner. Further reproduction prohibited without permission.

that the collection efficiency improved as the wire diameter decreased (figures B-4 and B-5) (Grunow, 1960; Nagel, 1956). Grunow (1960) suggested that 20 μm drops were collected with roughly constant efficiency for winds up to 10 m s^{-1} winds, and that earlier collectors had featured gauze or grass blades attached over funnels. The advantage of cylindrical arrangements is omni-directional sampling. Several "flat" arrangements of either parallel wires or mesh are also reported. The "harp" was formed when several wires were hung from a common rod whose lower ends form a "V" shape once attached to a common base (collection) wire (figure B-6) (May, 1961). Large flat sheets of stainless steel or nickel mesh (figure B-7) (Houghton and Radford, 1938) or "pervious cloth" stretched over a wood frame (Mrose, 1966) were also used. Oura (1953) hung sheets of wire mesh at right angles to each other under louvers in a forest to investigate wind-driven deposition while avoiding precipitation (figure B-8).

Houghton and Radford (1938) developed an active screen collector featuring a wind tunnel to minimize distortion of the sampled drop size distribution and a rear fan to pull the fog through their collector (figure B-9). They observed drop blow-off if the ambient wind exceeded 9 m s^{-1}. Measurements of fog drops were actually reported with the first cascade impactor (May, 1945). This was a 4 stage (D_{p50}s: 12, 4, 1.5, 0.5 μm) rectangular slot impactor (which became the Casella impactor) where the impaction surfaces were glass slides (figure B-10). The impactor was hung from a wind vane initially to orient itself into the wind (figure B-11), but later work suggested that a wind tunnel was needed to avoid biasing the collected drop size distribution (figure B-12) (May, 1961). Drop evaporation within the collector was observed and only Stages 1 and 3 were subsequently used. Garland and co-workers followed a similar approach, although the impaction surfaces were modified to films fitted around rotating cylinders (figure B-13) (Garland *et al.*, 1973; Garland, 1971). Finally, glass impingers and filter packs were also used to collect drops (figure B-14) (Garland *et al.*, 1973; May, 1961).

These collection techniques – passive collectors with mesh or strands hung on flat or cylindrical frames, active screen collectors, active impactors – continue to be used, as do wind vanes and

Reproduced with permission of the copyright owner. Further reproduction prohibited without permission.

other steps to optimize aspiration. Drop blow-off and other collection non-idealities also hinder more current equipment.

Figure B-1: Drops on spider threads (Arnulf *et al.*, 1957, figure 3)

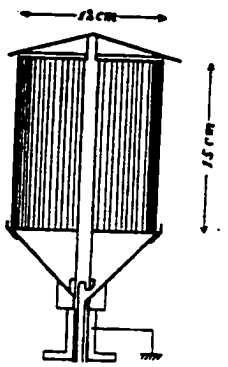

Figure B-2: Passive cylindrical drop collector (Tabata *et al.*, 1953, figure 1)

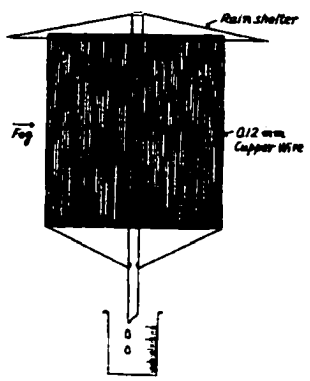

Figure B-3: Passive cylindrical drop collector (Okita, 1961, figure 5)

Reproduced with permission of the copyright owner. Further reproduction prohibited without permission.

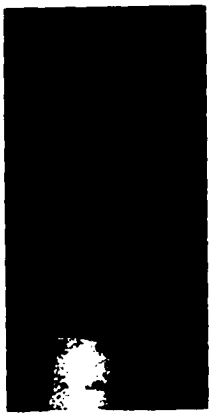

Figure B-4: Cylindrical mesh over a rain gauge (Grunow, 1960, figure 1)

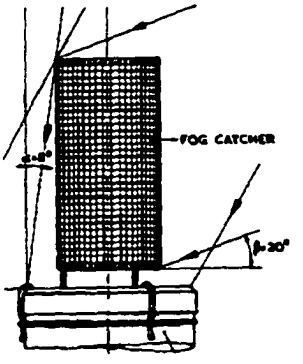

Figure B-5: Cylindrical mesh collector on a rain gauge (Nagel, 1956, figure 1)

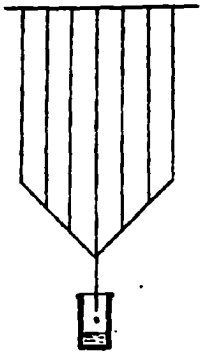

Figure B-6: The "harp" collector (May, 1961, figure 4)

Reproduced with permission of the copyright owner. Further reproduction prohibited without permission.

Figure B-7: Flat passive mesh collector (Houghton and Radford, 1938, figure 1)

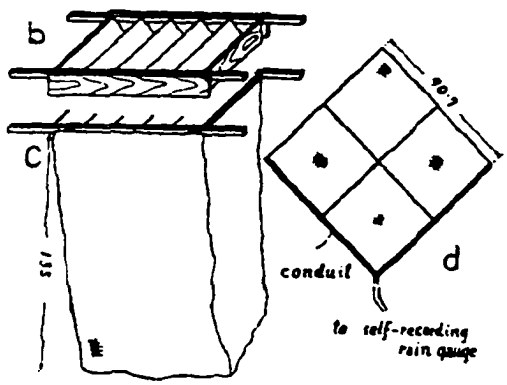

Figure B-8: Flat passive mesh collectors (Oura, 1953, figure 2)

Figure B-9: Active screen collector (collecting area is within the small central area) (Houghton and Radford, 1938, figure 2)

Reproduced with permission of the copyright owner. Further reproduction prohibited without permission.

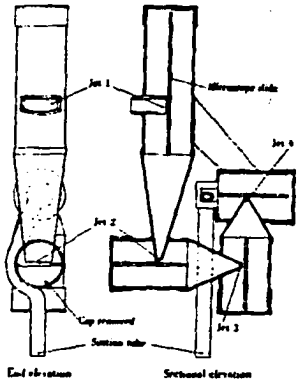

Figure B-10: Casella impactor (May, 1945, figure 2)

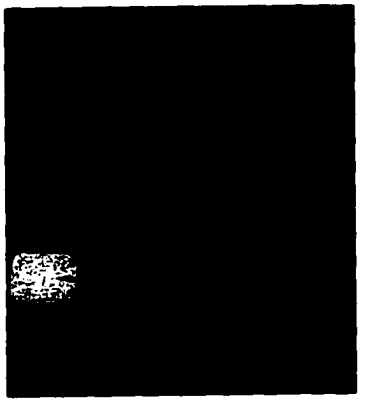

Figure B-11: Installed Casella impactor (May, 1945, figure 3)

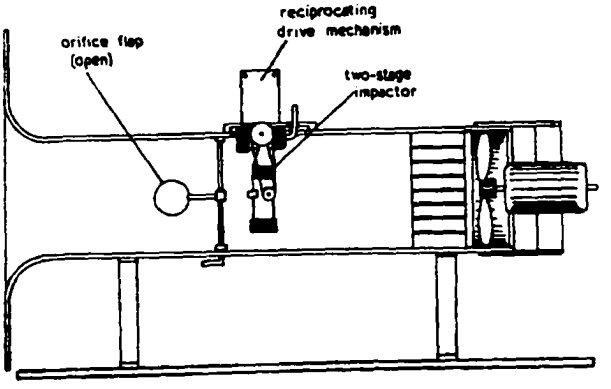

Figure B-12: Portable wind tunnel to promote aspiration with modified Casella impactor installed (May, 1961, figure 1)

Reproduced with permission of the copyright owner. Further reproduction prohibited without permission.

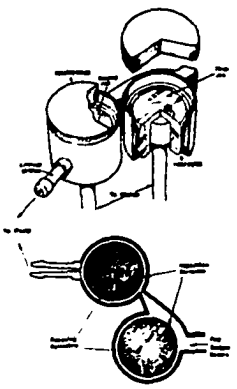

Figure B-13: Two-stage modified impactor heads (used in a portable wind tunnel) (Garland, 1971, figure 2)

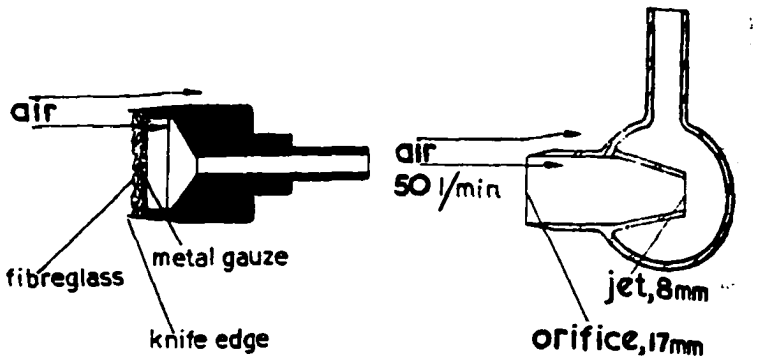

Figure B-14: Filter (left) and impinger (right) for fog drop sampling (May, 1961, figures 2 and 3)

B.1.2 Passive string collectors

There are over thirty different versions of passive string- or mesh-type collectors* reported in the literature since the collectors described in section B.1.1. They are made from many different materials (enameled or ETFE-coated copper, Teflon, stainless steel, aluminum, nylon, polypropylene, Tefzel, polyethylene, acrylic, among others). These collectors have widely varying dimensions (strand diameters from 0.1 mm to 1.12 mm, strand spacing from approximately 1 mm to 3 mm, varying mesh wire diameters and spacing, 100 to > 700 strands, single and multiple strand or mesh layers, 0.15 to 1 m strand length, varying overall collecting cylinder diameter and

* "String" and "strand" are used to describe arrangements of parallel collecting cylinders and "mesh" is used to describe woven or non-parallel ones.

Reproduced with permission of the copyright owner. Further reproduction prohibited without permission.

length, and varying overall collection screen height and width). The collectors are installed via multiple techniques with or without precipitation covers (Adzuhata *et al.*, 2001; Tesar *et al.*, 2001; Bytnerowicz *et al.*, 2000; Elbert *et al.*, 2000; Fenn *et al.*, 2000; Acker *et al.*, 1998; Bridges, 1998; Eckardt and Schemenauer, 1998; deFelice, 1997; Fenn and Bytnerowicz, 1997; Reynolds *et al.*, 1996; Kmiec *et al.*, 1995; Schemenauer *et al.*, 1995; Levsen *et al.*, 1993; Crossley *et al.*, 1992; Sanhueza *et al.*, 1992; Collett *et al.*, 1991b; Henterich and Herrmann, 1990; Joslin *et al.*, 1990; Basabe *et al.*, 1989; Chang, 1989; Jagels *et al.*, 1989; Mohnen and Kadlecek, 1989; Crossley, 1988; Fowler *et al.*, 1988b; a; Milne *et al.*, 1988; Mueller and Weatherford, 1988; Munzert, 1988; Schemenauer and Winston, 1988; Schmitt, 1988; Daube *et al.*, 1987; Verhoeven *et al.*, 1987; Schmitt, 1986; Goodman, 1985; Scherbatskoy and Bliss, 1984; Castillo and Jiusto, 1983; Galvin, 1983; Falconer and Falconer, 1980; Sadasivan, 1980; Anderson and Landsberg, 1979; Ekern, 1979; Azevado and Morgan, 1974; Juvik and Perreira, 1973; Lazrus *et al.*, 1970; Okita, 1968). However, they can be generally separated into cylindrical collectors with strings or mesh, harp-type collectors, combinations of flat mesh screens or strands, and a few that are somewhat different.

Drop impaction is driven by the ambient wind and wind speeds > 3 m s^{-1} are required for adequate sampling by passive collectors (Jaeschke, 1986). Thus, these collectors may not be optimal for sampling in all environments (e.g. radiation fogs). Drop sizes collected are theoretically a function of the ambient wind speed and the diameter of the string (smaller drop sizes are collected as the wind increases and the diameter decreases) (see section B.2). Therefore one location's observed collection efficiencies may not be applicable to another if the wind speed, drop distribution or collector dimensions vary. After impaction, drops coalesce and drip by gravity into attached bottles/vials. None of the collectors in this section are capable of size-resolved drop sampling as currently configured. The advantage, of course, is that no power is required. These collectors are often operated "remotely" and the cloud water collected only weekly or bi-weekly. Infrequent sample retrieval raises the potential for contamination by either precipitation or dry deposition. Most of these collectors are omni-directional so mis-alignment

Reproduced with permission of the copyright owner. Further reproduction prohibited without permission.

with ambient wind is not problematic and sampling periods < 15 minutes are possible due to the high collection rates achieved in some conditions.

The ASRC passive collector (figure B-15) (Mohnen and Kadlecek, 1989; Falconer and Falconer, 1980) appears to be directly descended from earlier collectors (figures B-2, B-3, and B-16) (Scherbatskoy and Bliss, 1984). While this collector is widely cited, many investigators have freely modified the string diameter (0.4 mm), string material (Teflon), string spacing (3 mm), string length (1 m), overall cylinder diameter (25 cm), and used multiple string layers instead of one (Falconer and Falconer, 1980; Mohnen, 1980). Figure B-15 does not show a precipitation cover: passive collectors may be kept in a protected housing during clear periods and then can be raised into the cloud when a minimum cloud LWC has been reached. A schematic of one of these systems with a small precipitation cover is shown in figure B-17 (Schmitt, 1986). A remote system (figure B-18) is hung from a tree and features a large precipitation cover (Fenn *et al.*, 2000). Another variation for remote operation is to use an extremely truncated collection region that does not extend far below the precipitation cover. A pole-mounted version is shown in Figure B-19 (Tesar *et al.*, 2001). Henterich et al. (1990) may have used an ASRC-type passive collector composed of glass and stainless steel to measure organics. Goodman (1985) utilizes three concentric cylinders, all hung with varying numbers of strands to facilitate collection (figure B-20). A commercial version of the ASRC-type passive collector is available in Japan (Model #FWP-500, Usui Kogyo Kenkyusho, Inc.) whose cited reference is the collector in figure B-3.

Three cylindrical collectors hung with mesh have been reported (Munzert, 1988; Verhoeven *et al.*, 1987; Azevado and Morgan, 1974). While I was unable to obtain a complete description, the automated pH measurement apparatus described by Anderson and Landsberg (1979) may be of this type.

The collector shown in figure B-6 has been the inspiration for a series of harp-type collectors (Bridges, 1998; Reynolds *et al.*, 1996; Kmiec *et al.*, 1995; Crossley *et al.*, 1992; Crossley, 1988; Fowler *et al.*, 1988b; a; Milne *et al.*, 1988). In the newer versions, the collection strands appear to

Reproduced with permission of the copyright owner. Further reproduction prohibited without permission.

come to a point or near-point inside the collecting funnel. A schematic of one with an extensive precipitation/dry deposition cover is shown in figure B-21 and a photo of one without is in figure B-22 (Bridges, 1998; Reynolds *et al.*, 1996).

The AMC/WPI passive collector is very similar to and preceded the Caltech family of active strand collectors (Chapter 2), but uses no fan. It has an upstream baffle to help protect the strands from contamination by precipitation and is mounted with a wind-vane (figures B-23 and B-24) (Daube *et al.*, 1987). Several more "traditional" flat collectors similar to figure B-7 use either parallel strings (figure B-25) (Goodman, 1985; Okita, 1968) or mesh (Jagels *et al.*, 1989; Lazrus *et al.*, 1970).

A few investigators primarily interested in fog drop interception by trees report using vertically-oriented louvers and mesh/louver combinations (Ekern, 1979; Juvik and Perreira, 1973). Sadasivan (1980) indicates a nylon net was used to collect cloud water, but it is unclear what the collector arrangement was.

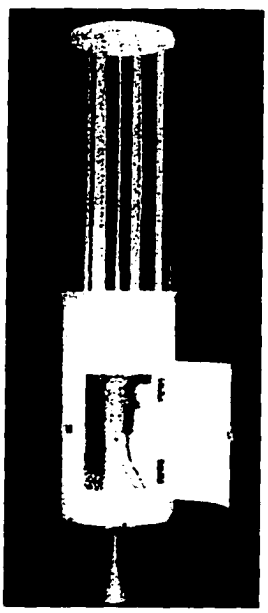

Figure B-15: The ASRC passive collector (Falconer and Falconer, 1980, figure 1)

Reproduced with permission of the copyright owner. Further reproduction prohibited without permission.

Figure B-16: Rain (left) and cloud water collectors (Scherbatskoy and Bliss, 1984, figure 1)

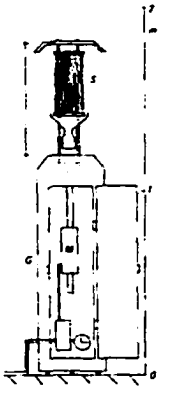

Figure B-17: Motorized passive collector (fog sensor removed from the figure) (Schmitt, 1986, figure 1)

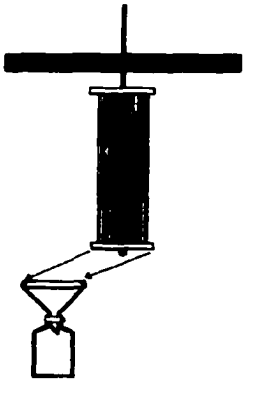

Figure B-18: Passive collector mounted from the top (Fenn *et al.*, 2000)

Reproduced with permission of the copyright owner. Further reproduction prohibited without permission.

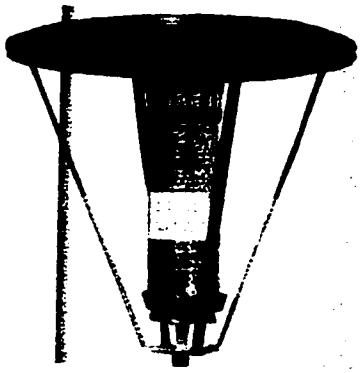

Figure B-19: Passive collector with limited sampling area (Tesar *et al.*, 2001)

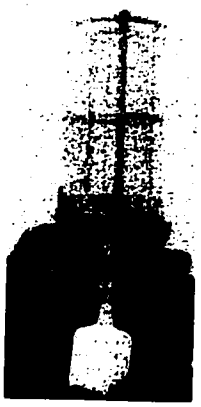

Figure B-20: Concentric cylinder passive collector (Goodman, 1985, figure 2)

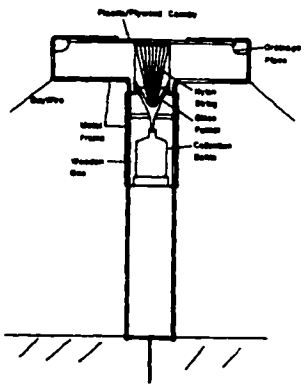

Figure B-21: Protected harp collector (Reynolds *et al.*, 1996)

Reproduced with permission of the copyright owner. Further reproduction prohibited without permission.

Figure B-22: Harp collector in the field (Bridges, 1998)

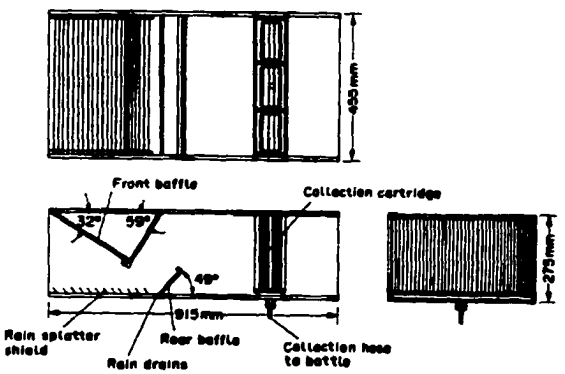

Figure B-23: Schematic of AMC/WPI passive collector (Daube *et al.*, 1987, figure 2)

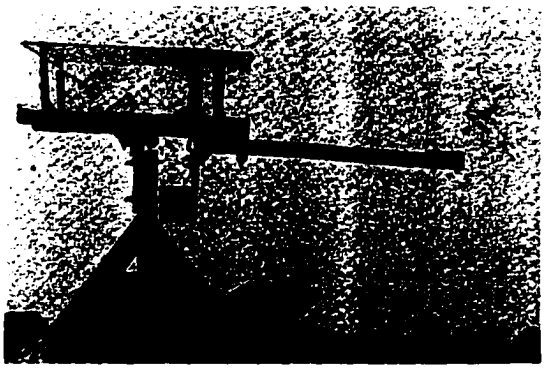

Figure B-24: AMC/WPI passive collector in the field (wind vane to the right) (Daube *et al.*, 1987, figure 1)

Reproduced with permission of the copyright owner. Further reproduction prohibited without permission.

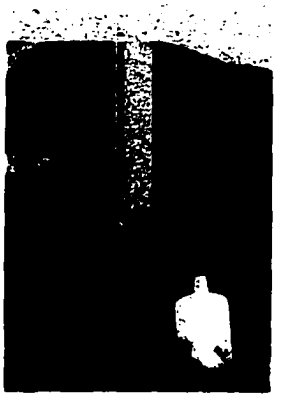

Figure B-25: Flat string collector (Goodman, 1985, figure 1)

B.1.3 Passive collectors for potable water

This brief section is devoted to the cloud water collectors designed for obtaining potable water in otherwise arid environments. Their development has been spearheaded by Schemenauer and co-workers. The designs are descended from Houghton and Radford's passive collector (figure B-7) with the additional restriction that the materials be locally available. Water has to meet certain health-based chemical composition standards to be considered potable. This motivates several of the measurements reported (Eckardt and Schemenauer, 1998, among others), although they also represent drop composition data where it was previously unavailable.

The first collector reported was mounted with a wind vane so the 0.5 m by 0.5 m collection area is perpendicular to the ambient wind (figure B-26) (Schemenauer *et al.*, 1987). This was used to evaluate whether the location chosen was adequate for multiple arrays of the larger 10 m long by 4 m high (Schemenauer and Joe, 1988) or 12 m by 4 m (Schemenauer and Joe, 1989) (figure B-27) collectors to be installed to provide a remote village's water. Double layers of polypropylene mesh are strung from the frames (figure B-28) (Schemenauer and Joe, 1989). All of these collectors are installed 2 or more meters above the ground to help prevent contamination. Water drips off the mesh into a collecting trough where it can then flow to attached storage tanks and be chemically-treated or filtered if needed. A revised version of figure B-26 with a larger (1.0 m by 1.0 m) collection area is the proposed "standard fog collector" (figures B-29 and B-30).

Reproduced with permission of the copyright owner. Further reproduction prohibited without permission.

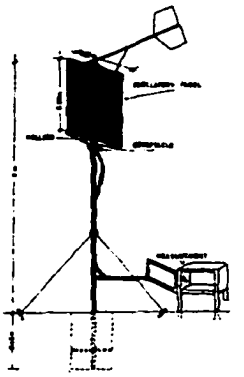

Figure B-26: Neblinómetro collector (Schemenauer *et al.*, 1987, figure 3)

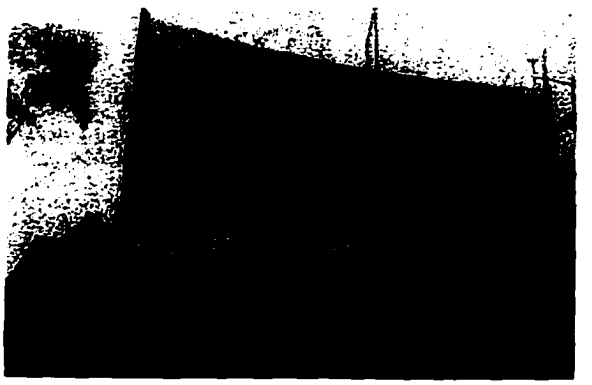

Figure B-27: Massive fog collector (Camanchaca project) installed in El Tofo, Chile. A FSSP is installed near the center of the collector for calibration (Schemenauer and Joe, 1989, figure 1)

Figure B-28: The mesh used (1 mm wide by 0.1 mm thick) for the massive fog collector (Schemenauer and Joe, 1989, figure 2)

Reproduced with permission of the copyright owner. Further reproduction prohibited without permission.

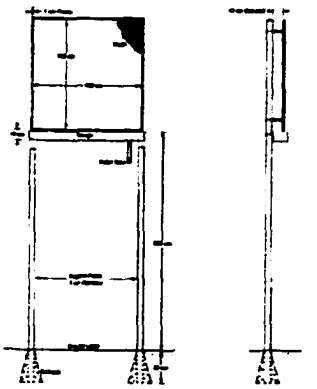

Figure B-29: Schematic of the proposed standard fog collector (Schemenauer and Cereceda, 1994, figure 2)

Figure B-30: Proposed standard fog collector. Guywires are installed to support the collector (Schemenauer and Cereceda, 1994, figure 1)

B.1.4 Rotating arm collectors

The rotating arm collectors were thought to have similar collection characteristics to single strands when they were first developed. A rod of approximately 1 m in overall length and 0.9 – 1.4 cm in diameter is rotated around its center point at high speed (0 – 3450 rpm, although those still in use operate at < 500 rpm) (Krämer *et al.*, 1991; Hering *et al.*, 1987; Schmitt, 1986; Mack *et al.*, 1973). Incident drops impact and are sampled along a section of the rod with a central milled slot. In most cases the drops flow by centrifugal force into collection vials attached at the ends of the rod. The presumed advantage of these collectors was that the lack of an inlet would preclude anisokinetic sampling (Jacob *et al.*, 1984a), but later development suggests that single cylinder theoretical collection in isokinetic conditions may not be applicable (Krämer and Schütz, 1994;

Reproduced with permission of the copyright owner. Further reproduction prohibited without permission.

Lesnic *et al.*, 1993; Krämer and Schütz, 1990). These collectors are not widely used today. Presumably safety issues are one factor, although the reported D_{p50}s tend to be higher (14 – 20 μm) than most other active collectors (Krämer and Schütz, 1994; Jacob *et al.*, 1984a).

The first version was developed to measure cloud LWC, although later chemical composition measurements were reported (figures B-31 and B-32) (Pilie and Mack, 1975; Mack *et al.*, 1973). The milled slot extends almost the entire length of the arm (the patent drawing is not-to-scale). Castillo and co-workers report using a collector based upon this version, but no details are given (Castillo *et al.*, 1983). The Caltech Rotating Arm Collector (RAC) was subsequently developed and widely used in the mid-1980s (figures B-33 and B-34) (Jacob *et al.*, 1984a). It was expressly designed for chemical composition measurements (Teflon-coated stainless steel rod) and the slot length is limited. At least one modified version of the RAC has been reported (Miller *et al.*, 1987). Significant theoretical and experimental work has gone into the development of the still-used Mainz RAC (MRAC) (figures B-35 and B-36) (Krämer *et al.*, 2000; Krämer and Schütz, 1994; Lesnic *et al.*, 1993; Krämer *et al.*, 1991; Krämer and Schütz, 1990). The MRAC differs from the RAC by operating at lower speeds (< 480 vs 1750 rpm), having a modified collection surface, and different mounting and adjustment schemes.

It is not clear if the AeroVironment rotating collector (figure B-37) has a milled collection slot, although the use of two different collection lengths to obtain two size fractions is intriguing. It is also not clear that this collector was ever operated in the field with the exception of one side-by-side collector validation study (Hering *et al.*, 1987). According to Schell *et al.* (1997a) this idea was pursued by Schmitt. Another version of a rotating collector uses multiple slotted rods (similar to the ASRC airborne slotted rod collector (Mohnen, 1980)) and a somewhat longer (2.4 m) arm (figure B-38) (Schmitt, 1986). It is not known if this collector was modified to use two different arm lengths, and its drop collection may be hindered by the same factors that affect the airborne slotted rod collectors (see (Huebert *et al.*, 1988; Huebert and Baumgardner, 1985)).

Reproduced with permission of the copyright owner. Further reproduction prohibited without permission.

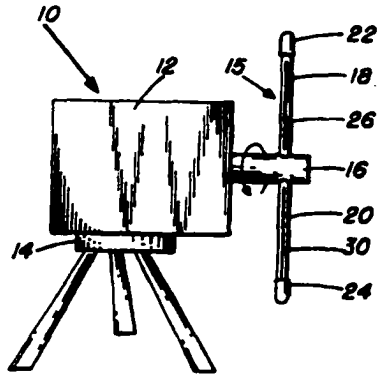

Figure B-31: First rotating arm collector (Pilie and Mack, 1975, figure 1 (numbers correspond to details in the patent)). Note that the collecting slot extends to the hub.

Figure B-32: First rotating arm collector installed in the field (Mack *et al.*, 1973, figure 1)

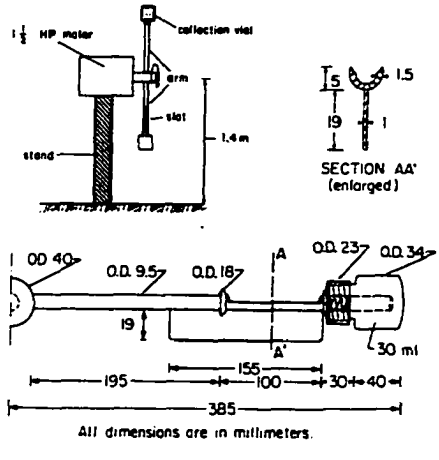

Figure B-33: The Caltech RAC: overall schematic (top left), cross-section (top right) and arm detail (bottom) (Jacob *et al.*, 1983, figure 2)

Reproduced with permission of the copyright owner. Further reproduction prohibited without permission.

Figure B-34: The Caltech RAC (Jacob *et al.*, 1983)

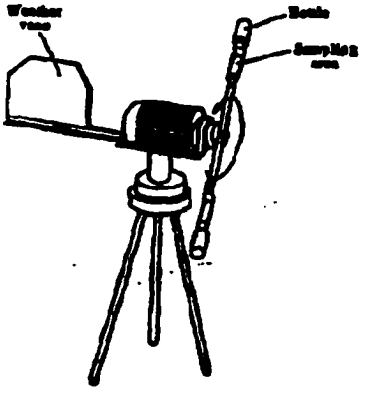

Figure B-35: The Mainz RAC (MRAC) (Krämer and Schütz, 1994, figure 2)

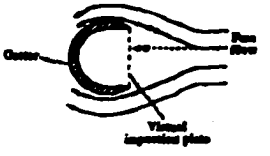

Figure B-36: The Mainz RAC collection surface (Krämer and Schütz, 1994, figure 3)

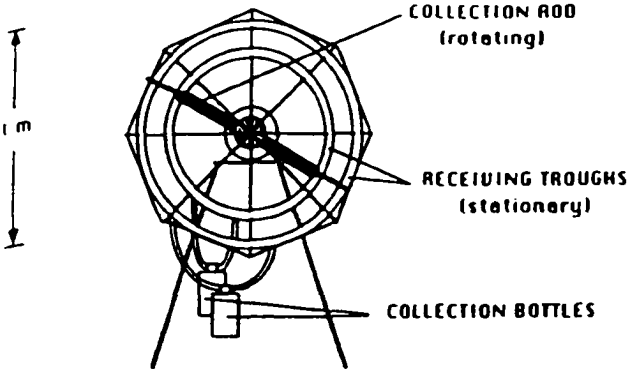

Figure B-37: The AeroVironment rotating arm collector (Hering *et al.*, 1987, figure 1)

Reproduced with permission of the copyright owner. Further reproduction prohibited without permission.

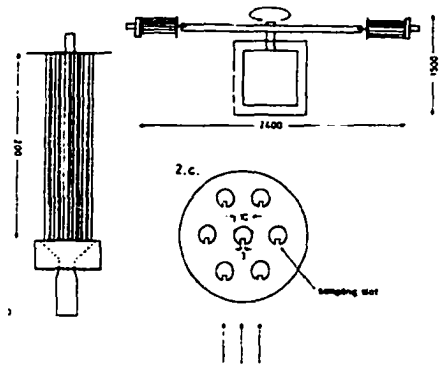

Figure B-38: A horizontal rotating arm collector with multiple impaction surfaces: overview (top right), collecting end detail (left), and slotted rod arrangement (bottom right) (Schmitt, 1986, figure 2)

B.1.5 Active string collectors

This section describes samplers that depend upon drop collection via forced flow past multiple cylinders. A wide variety of collectors result due to the multiple design approaches possible. The current Caltech family of active strand collectors is included in Chapter 2, and is not presented here, although recently several uncharacterized stainless steel versions have been developed for organic sampling. Taking active flow past cylinders to the limit, filter methods are included. Like the passive string collectors, a wide variety of collecting strand diameters (sub-mm filter threads to 1.27 cm), woven or parallel strand arrangements, overall collector dimensions, flow rates (up to 73 m^3 min^{-1}), cut-sizes (down to 2 µm, although ≈ 5 µm is more typical), materials, internal velocities (1.4 – 25 m s^{-1}), collection efficiencies (up to 100% for some drop sizes), and mounting options are described (Tesar *et al.*, 2001; Bytnerowicz *et al.*, 2000; Fenn *et al.*, 2000; Menon *et al.*, 2000; Wujcik *et al.*, 1999; Schwitkowski *et al.*, 1998; Fuzzi *et al.*, 1997; Fuzzi and Zappoli, 1997; Vong *et al.*, 1997; Demoz *et al.*, 1996; Minami and Ishizaka, 1996; Munger *et al.*, 1995; Gundel *et al.*, 1994; Hemmerlein and Perkins, 1993; Klemm *et al.*, 1991; Schomburg *et al.*, 1991; Glotfelty *et al.*, 1990; Richartz *et al.*, 1990; Chang, 1989; Schell and Georgii, 1989; Fuzzi, 1988; Kins *et al.*, 1988; Weathers *et al.*, 1988; Daube *et al.*, 1987; Pade *et al.*, 1987; Dröscher, 1986; Jaeschke, 1986; Kins *et al.*, 1986; Jacob *et al.*, 1985a; Fuzzi *et al.*, 1984; McFarland and Ortiz,

Reproduced with permission of the copyright owner. Further reproduction prohibited without permission.

1984; Brewer *et al.*, 1983; Andre *et al.*, 1981; Bressan and Larson, 1979; Okita, 1968; May, 1961).

Some of the more unusual designs are the collectors described by Pade *et al.*, (1987) (figures B-39 and B-40) and by Fuzzi and co-workers (figures B-41 and B-42) (Fuzzi *et al.*, 1990; Fuzzi *et al.*, 1988). The University of Washington collector is a radial array of upward slanting rods housed within a vertically-oriented sampling tunnel. A pump pulls the air down across the rods and impacted drops flow down to the central hub for collection (Pade *et al.*, 1987). Although no figure is available, rods of a larger size were added in a later version above the smaller rods to make size-resolved measurements (Vong *et al.*, 1997). The ASRC rotating string collector is also a radial array of strands, but instead they form a "lampshade" shape that rotates at approximately 100 rpm. Centrifugal force encourages the sampled drops to flow to a collecting ring. Jaeschke (1986) used a version with smaller diameter elements (0.1 mm instead of 0.4 mm). The FISBAT rotating harp (figure B-42) rotates at 15 rpm horizontally and features a double layer of strands (Fuzzi, 1988).

Two cylindrical collectors are highly similar to the CASCCs (Dröscher, 1986; Andre *et al.*, 1981). One may be oriented into the wind (figure B-43) and one is vertically-oriented and protected from precipitation (figure B-44). In both instances, the cartridges holding the parallel strands are installed at an angle to promote drop run-off and subsequent collection. An active collector using pentagonal frames strung with nylon threads has been reported (Minami and Ishizaka, 1996). The Cloud Water Project (CWP) collector has a vertically-oriented collection cartridge with a downward-facing inlet to prevent precipitation contamination (figure B-45) (Daube *et al.*, 1987). Several versions of the CWP have been used, including for remote sites figures B-46 (Hemmerlein and Perkins, 1993) and B-47 (Bytnerowicz *et al.*, 2000; Fenn *et al.*, 2000), among others (Tesar *et al.*, 2001; Chang, 1989; Weathers *et al.*, 1988). Strand widths used vary from 0.5 to 0.87 mm in diameter although 0.78 mm is specified (Tesar *et al.*, 2001; Chang, 1989; Daube *et al.*, 1987). In figure B-47, the louvers used to seal the inlet and exhaust are lifted by the

Reproduced with permission of the copyright owner. Further reproduction prohibited without permission.

action of the fan which will affect the flow rate (potentially significantly) and thus the collection characteristics of this particular version. The first version of a Caltech active strand collection is shown in figure B-48 and has a more rudimentary trough and fewer cartridges of strands than later versions (Jacob *et al.*, 1985a), although variations are still used (Wujcik *et al.*, 1999). A truck-mounted version derived from the Jacob *et al.* paper has been reported for very high flow rate sampling (Schomberg *et al.*, 1991). Figures B-49 and B-50 are very similar to later CASCCs, although the first features a wind-vane and an inlet cover for remote operation (Kins *et al.*, 1986), and the second an anemometer and downward-facing inlet (Fuzzi *et al.*, 1997). There are two modified versions of the CASCCs (Demoz *et al.*, 1996): Klemm and co-workers (1991) sealed any internal metal surfaces of a single-stage CASCC with plastic, and an alternate arrangement of smaller (9.5 mm in diameter) rods was used to make the Large fraction of another sf-CASCC (Menon *et al.*, 2000; Munger *et al.*, 1995). Finally, Schell and Georgii (1989) use cartridges of strands as the first stage of their two-stage collector which features an impactor in the rear (figures B-51 and B-52).

Several cylindrical collectors work by impacting drops on one or more layers of mesh (figures B-53 through B-57) (Glotfelty *et al.*, 1990; Richartz *et al.*, 1990; Fuzzi *et al.*, 1984; McFarland and Ortiz, 1984; Okita, 1968). Most of these are very similar to Houghton and Radford's active collector (figure B-7). Two of the more interesting are the rotating version (Glotfelty *et al.*, 1990) (figure B-56) and the Global Geochemistry Corporation (GGC) mesh collector (figure B-57) (McFarland and Ortiz, 1984). The high volume rotating screen collector pulls drops on to the screen by the action of the rear fan and then uses rotation to force them into a surrounding collection channel. The GGC collector uses several layers of polypropylene mesh at the inlet and collected drops flow down the "V" formed by the Teflon-coated PVC pipe into an attached sample bottle. Another version of this collector has been used at the Lawrence Berkeley Laboratory (Gundel *et al.*, 1994). The multiple layers of mesh at the inlet are somewhat similar to drop collection using filters which several authors have used (figures B-58 and B-59) (Schwitkowski *et al.*, 1998; Bressan and Larson, 1979; May, 1961). While drop sampling with filters can be quite

Reproduced with permission of the copyright owner. Further reproduction prohibited without permission.

successful, drop interception is likely to play an important role and the flow rate may change during sampling due to an increasing pressure drop as the filter becomes loaded.

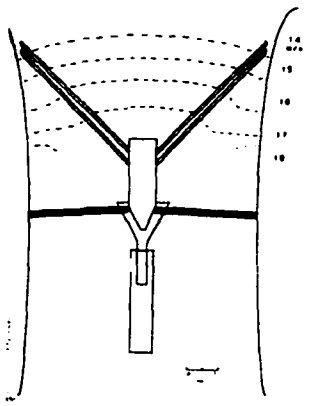

Figure B-39: University of Washington collector (side view). The dashed lines are isotachs (Pade *et al.*, 1987, figure 1)

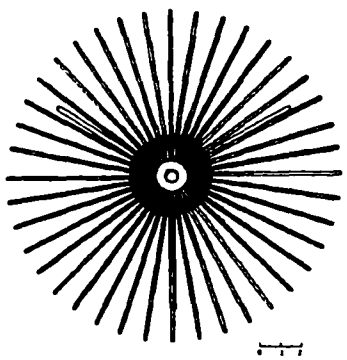

Figure B-40: University of Washington collector (top view) (Pade *et al.*, 1987, figure 2)

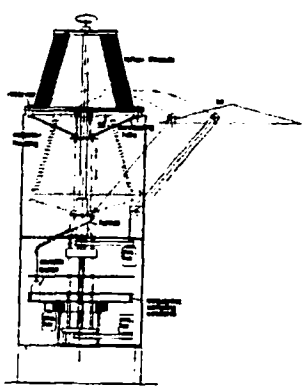

Figure B-41: Schematic of the ASRC rotating string collector (Fuzzi *et al.*, 1990, figure 2)

Reproduced with permission of the copyright owner. Further reproduction prohibited without permission.

Figure B-42: FISBAT rotating string collector (Fuzzi, 1988, figure 3)

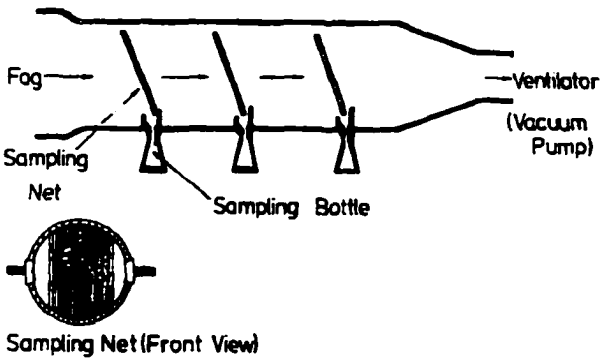

Figure B-43: Active string collector with cylindrical body (Andre *et al.*, 1981, figure 4)

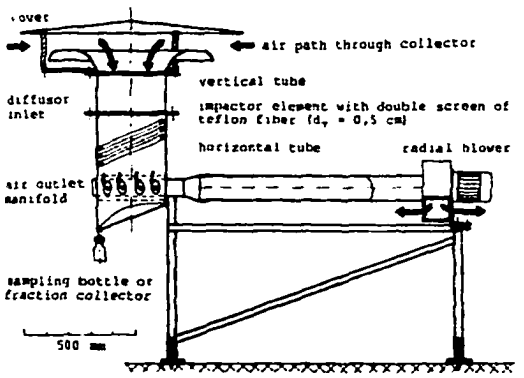

Figure B-44: The IVD collector (Dröscher, 1986, figure 6)

Reproduced with permission of the copyright owner. Further reproduction prohibited without permission.

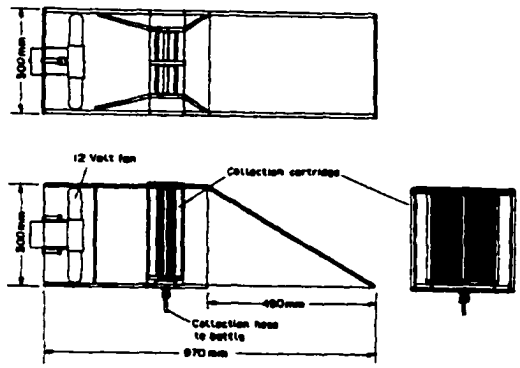

Figure B-45: The CWP active collector: top view (top left), side view (bottom left) and an upstream view of the cartridge (right) (Daube *et al.*, 1987, figure 5)

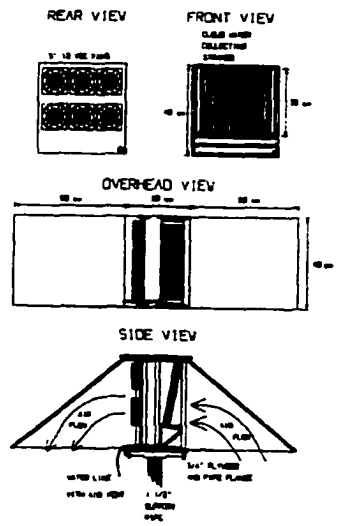

Figure B-46: The Forest Decline Project collector (Hemmerlein and Perkins, 1993, figure 1)

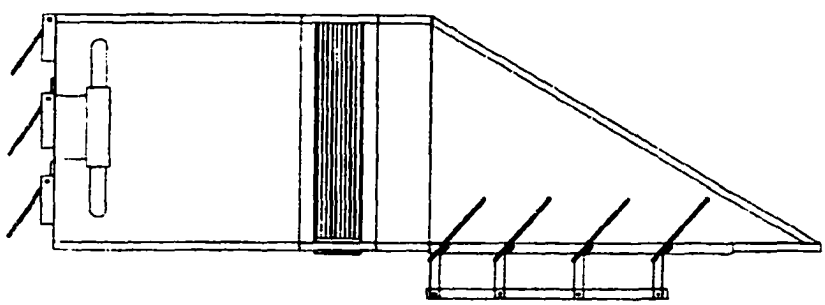

Figure B-47: Louvered version of the CWP (Fenn *et al.*, 2000)

Reproduced with permission of the copyright owner. Further reproduction prohibited without permission.

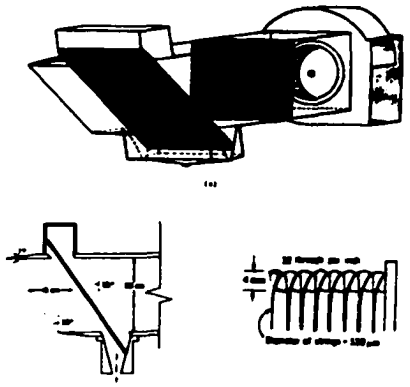

Figure B-48: The first version of the CASCC: overall (top), side view (bottom left), cartridge stringing pattern (bottom right) (Jacob *et al.*, 1985a, figure 1)

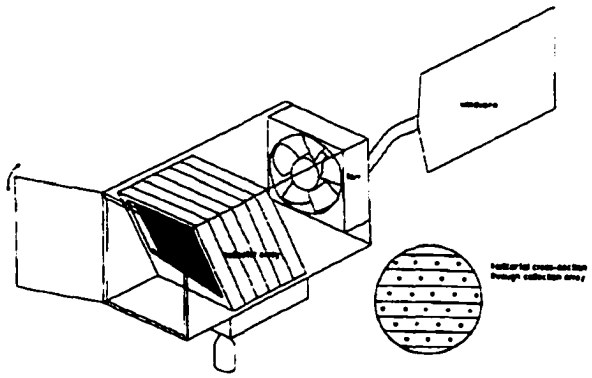

Figure B-49: TV tower cloud collector (Kins *et al.*, 1986, figure 1)

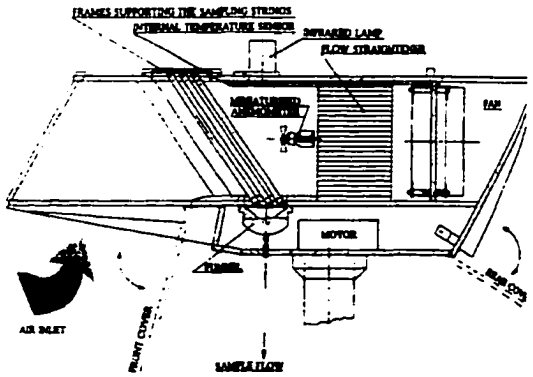

Figure B-50: Automated station collector (Fuzzi *et al.*, 1997, figure 3)

Reproduced with permission of the copyright owner. Further reproduction prohibited without permission.

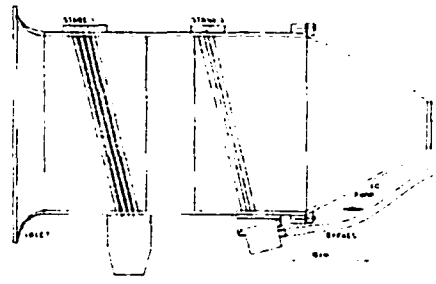

Figure B-51: Two-stage string/impactor collector (side view) (Schell and Georgii, 1989, figure 1)

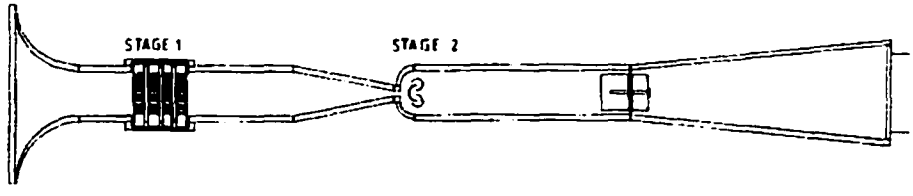

Figure B-52: Two-stage string/impactor collector (top view) (Schell and Georgii, 1989, figure 2)

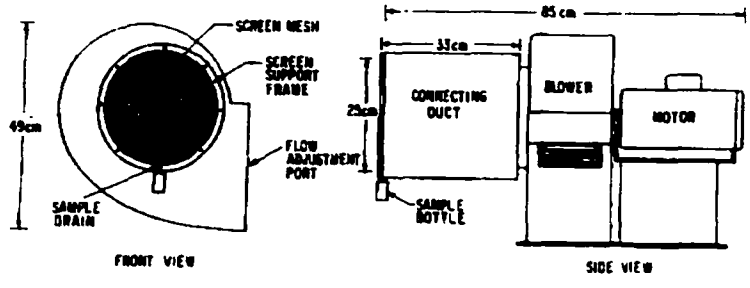

Figure B-53: Round screen/blower collector (Fuzzi *et al.*, 1984, figure 1)

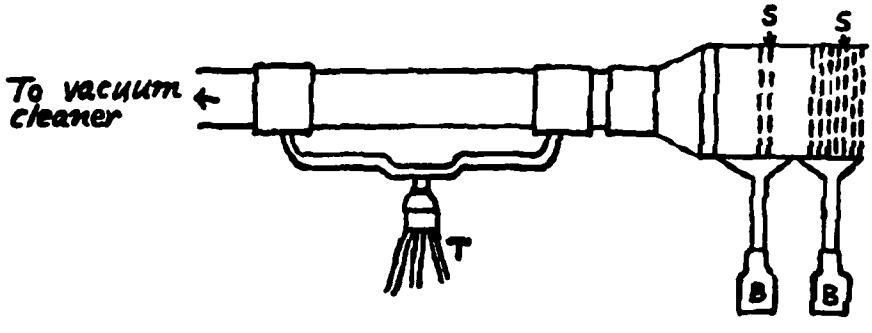

Figure B-54: Mesh multi-screen cylindrical active collector (Okita, 1968, figure 2)

Reproduced with permission of the copyright owner. Further reproduction prohibited without permission.

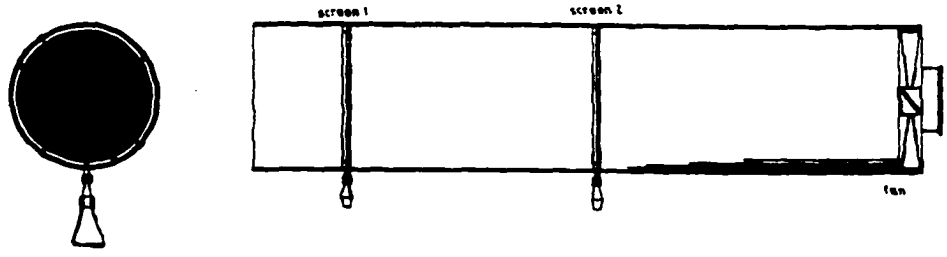

Figure B-55: Dual mesh screen active collector: front view (left) and side view (right) (Richartz *et al.*, 1990, figure 1)

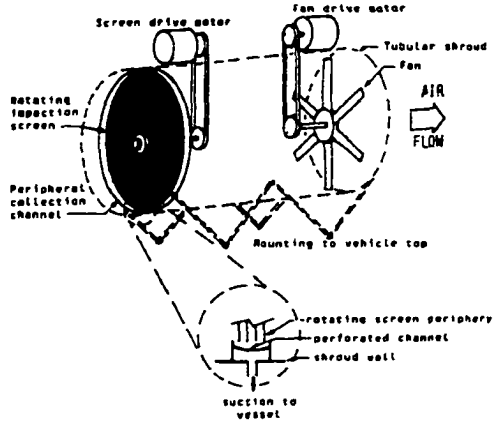

Figure B-56: Rotating high volume mesh active collector (Glotfelty *et al.*, 1986, figure 1)

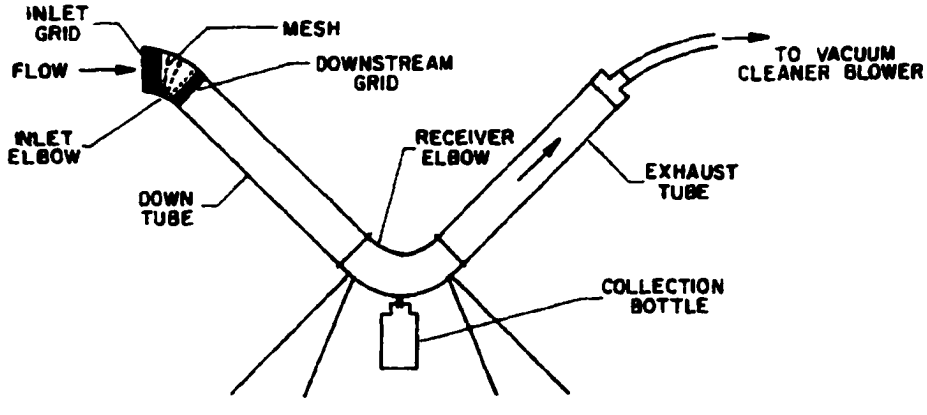

Figure B-57: The Global Geochemistry Corporation (GGC) active mesh collector (McFarland and Ortiz, 1984, figure 1)

Reproduced with permission of the copyright owner. Further reproduction prohibited without permission.

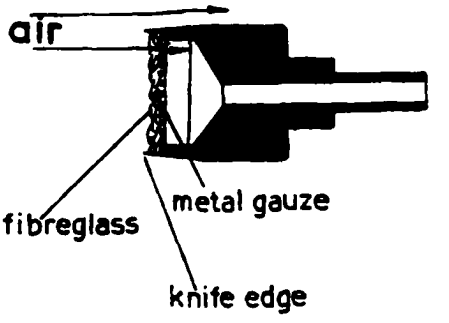

Figure B-58: Active filter collector (May, 1961, figure 2)

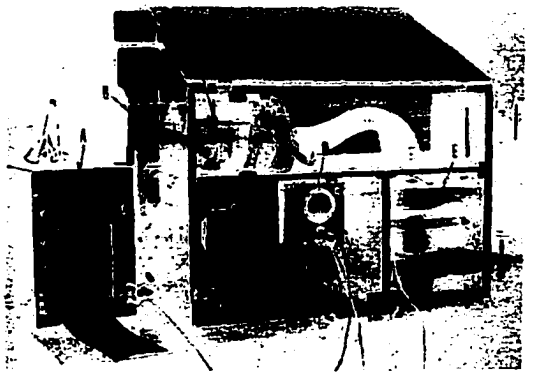

Figure B-59: "Fog conductivity meter" (an active filter collector) (Bressan and Larson, 1979)

B.1.6 Active impactor collectors

One of the drawbacks of active string collectors is the broad collection efficiency curve possible for relatively high inertia drops and large strand diameters (see figure B-92). There has been an increasing use of jet impactors to collect fog and cloud drops as sharper efficiency curves are theoretically possible. Designers typically cite the impactor guidelines developed by Marple and co-workers, although some also cite earlier work (see the references in Chapter 2, and section B.1.1). Unlike the rotating arm collectors, D_{p50}s as low as 2 and 3 μm are readily achievable, although 4 – 5 μm for single-stage or the smallest stage of multi-stage impactors are more typical (e.g. (Schell *et al.*, 1997a; Winkler and Pahl, 1997; Collett *et al.*, 1995; Millet *et al.*, 1995), among others). The primary disadvantage of these collectors is that far lower flow rates (≈ 2 m^3 min^{-1}) for single-jet impactors are usually used due to Re restrictions. Poorer sample temporal resolution

Reproduced with permission of the copyright owner. Further reproduction prohibited without permission.

results, although it can be partially mitigated by sampling in parallel. At relatively high Re (up to and exceeding 20,000), the efficiency curves are much broader than ideal (see the 5-Stage and FROSTY efficiency curves in Chapters 3 and 4, for example) (Schell *et al.*, 1997a; Winkler and Pahl, 1997; Schell and Georgii, 1989, among others). Round or rectangular jet active impactors have been developed in either single, parallel multi-single, or multi-stage versions. A somewhat different approach to impaction was used by Fuzzi and co-workers to collect drops to construct size distributions (figure B-60) (Fuzzi *et al.*, 1980) where film sections were accelerated through clouds. Typically, air, not the collector, is accelerated. Similar to the collectors described in the preceding sections, a variety of materials, flow rates, collector geometries and mounting configurations have been used.

Two early single-stage round jet impactors were apparently oriented into the wind and the sampled drops collected in the attached vials (figures B-61 and B-62). The flow rates reported were quite low (0.03 and 0.125 m^3 min^{-1}, respectively) suggesting that multi-hour sampling intervals were required (Däumer *et al.*, 1988; Andre *et al.*, 1981). Berner followed with a somewhat different arrangement where the inlet was vertically-oriented and perpendicular to the ambient wind (figure B-63) (Berner, 1988). In order to minimize sampling time, several investigators created samplers with multiple round heads in parallel – four ("IEP") (Schell *et al.*, 1992), eight (Millet *et al.*, 1995), and sixteen (Jaeschke *et al.*, 1990) (figures B-64, B-65, and B-66). A drop size upper-bound for collection (determined by calibration) is only explicitly indicated for one of these samplers, although the reported operating conditions suggest this might apply to all of them (Millet *et al.*, 1995, and references therein). Three multi-stage round jet impactors have been reported that are all similar in design to existing aerosol multi-stage impactors – the ETH two-stage (Collett *et al.*, 1993a), the IESL three-stage (Collett *et al.*, 1995), and the Vienna six-stage (Berner *et al.*, 1998) (figures B-67 through B-70). Unlike the Berner-type single-stage impactors, these collectors either have the sampled water pipetted out of the collection troughs (ETH and IESL), or sampling is onto removable foils (Vienna). Several different impaction stage combinations are possible with the IESL collector to provide different cut-sizes for varying

Reproduced with permission of the copyright owner. Further reproduction prohibited without permission.

conditions, although as handling is time-consuming it is not clear that they were ever changed in the field (Collett *et al.*, 1995).

Rectangular jet impactors have become increasingly popular for collecting cloud drops as compact designs are somewhat easier to achieve (see Chapter 2) than for round jet impactors. These collectors are typically oriented into the wind. Only the Isokinetic Cloud Probing System (ICPS) is a single jet, single stage design (figure B-71) (Jaeschke *et al.*, 1997, p. 116), although the rear fraction of the Schell and Georgii (1989) strand/impactor two-stage collector could be included here (figures B-51 and B-52). The ICPS has an "isokinetic" inlet which can be adjusted to match ambient wind speeds and the Schell and Georgii (1989) impaction surface is specifically designed to avoid drop re-entrainment (the velocity is approximately 46 m s^{-1}) and encourage flow to an attached collection bottle via the application of a slight reduction in pressure (figure B-72) (Schell and Georgii, 1989). More typically, parallel configurations of multiple rectangular jet/impaction surfaces are used. Winkler and co-workers use a parallel dual-jet approach and have spent considerable effort investigating the best impaction surface shape (figures B-73 through B-75) (Schell *et al.*, 1992; Winkler, 1992; Winkler and Kroll, 1987; Winkler, 1986). These "MOH" collectors are oriented into the wind during operation and the collected water drains into one or two bottles installed underneath the impaction surfaces. The Desert Research Institute (DRI) impactor uses 3 rectangular jets oriented at 120° from each other and while developed for cloud chamber use, has sampled "real" clouds with minor modification (figure B-76) (Gertler *et al.*, 1984; Gertler, 1983; Katz, 1980). Aspirated drops impact on rotating cylinders which deliver the drops to a central collecting cylinder that directs them into an attached test tube. A parallel configuration of six rectangular jet/impaction surface stages has been developed to maximize sample volume in order to study organics (figure B-77) (Lüttke and Levsen, 1997; Lüttke *et al.*, 1997). Many multi-stage impactors depend at least in part on sampling in parallel. The Two Stage Fog water Impactor (TFI2) has a single "isokinetic" inlet, but the flow downstream of the first impaction stage is split and two "small" drop fractions are simultaneously obtained (figures B-78 and B-79) (Jaeschke *et al.*, 1997, p. 114; Schell *et al.*, 1997a). During the CHEMDROP 94

Reproduced with permission of the copyright owner. Further reproduction prohibited without permission.

campaign, 5 two-stage collectors (of two different designs) were operated simultaneously and the drop-dependent chemistry determined by difference into six fractions: 6 – 12 μm, 9 – 16.2 μm, 16.2 – 19.6 μm, 19.6 – 23.2 μm, 23.2 – 32 μm, and 32 – 47 μm (figure B-80) (Fuzzi *et al.*, 1998a; Laj *et al.*, 1998). The five largest fractions were determined by collectors that did not sample into the wind, but instead used wind shields. During ACE-2, 2 three-stage collectors oriented into the wind produced five simultaneous fractions: 7 – 11 μm, 11 – 17 μm, 17 – 22 μm, 22 – 33 μm, and > 33 μm (figure B-81) (Fuzzi *et al.*, 1998b).

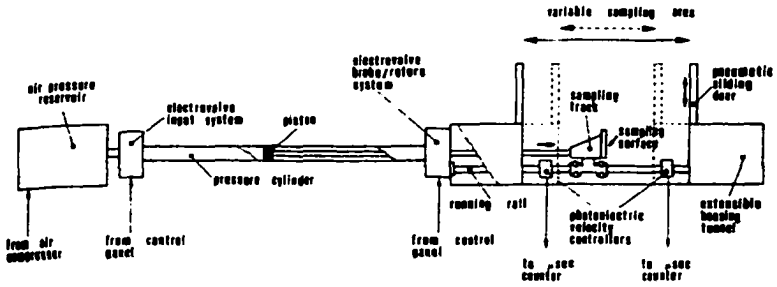

Figure B-60: Linear impactor for drop spectra (Fuzzi *et al.*, 1980, figure 3)

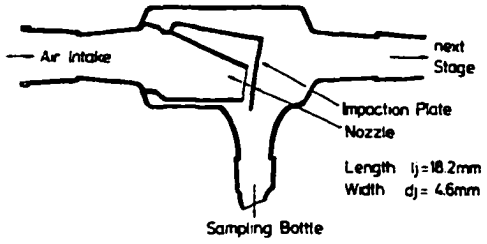

Figure B-61: Circular cross-section impactor (Andre *et al.*, 1981, figure 4)

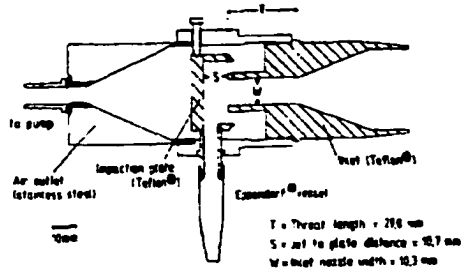

Figure B-62: Circular cross-section impactor (Däumer *et al.*, 1988, figure 1)

Reproduced with permission of the copyright owner. Further reproduction prohibited without permission.

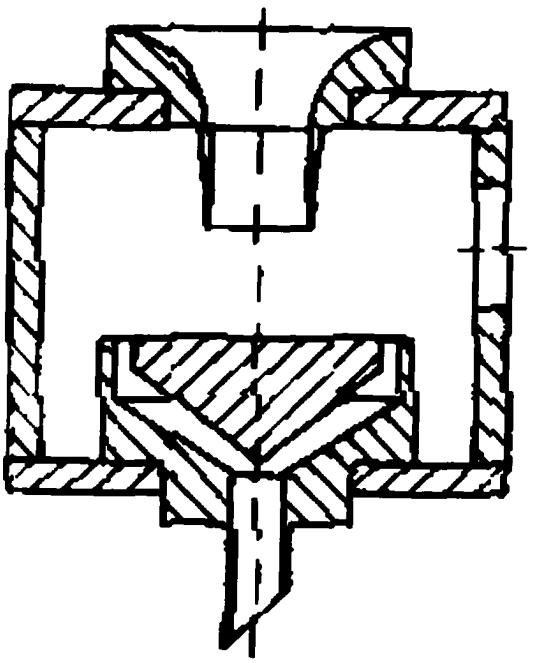

Figure B-63: Berner single circular jet, vertically-oriented impactor (Berner, 1988, figure 1)

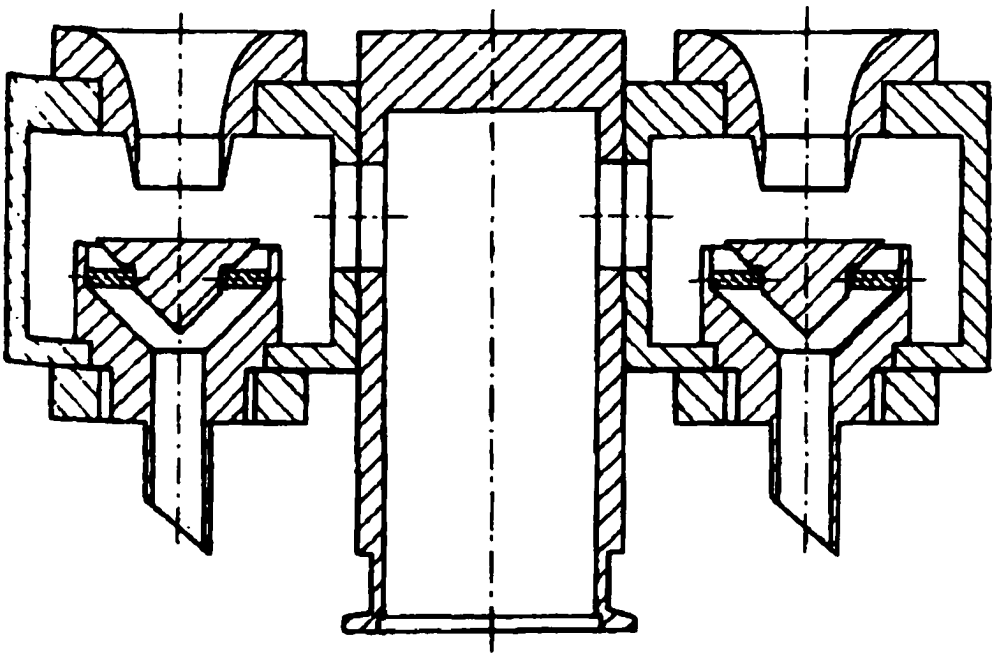

Figure B-64: IEP 4 (in parallel) round jet vertically-oriented impactor. Designed by A. Berner. Jets are located at the four corners of a square (Schell *et al.*, 1992, figure 2)

Reproduced with permission of the copyright owner. Further reproduction prohibited without permission.

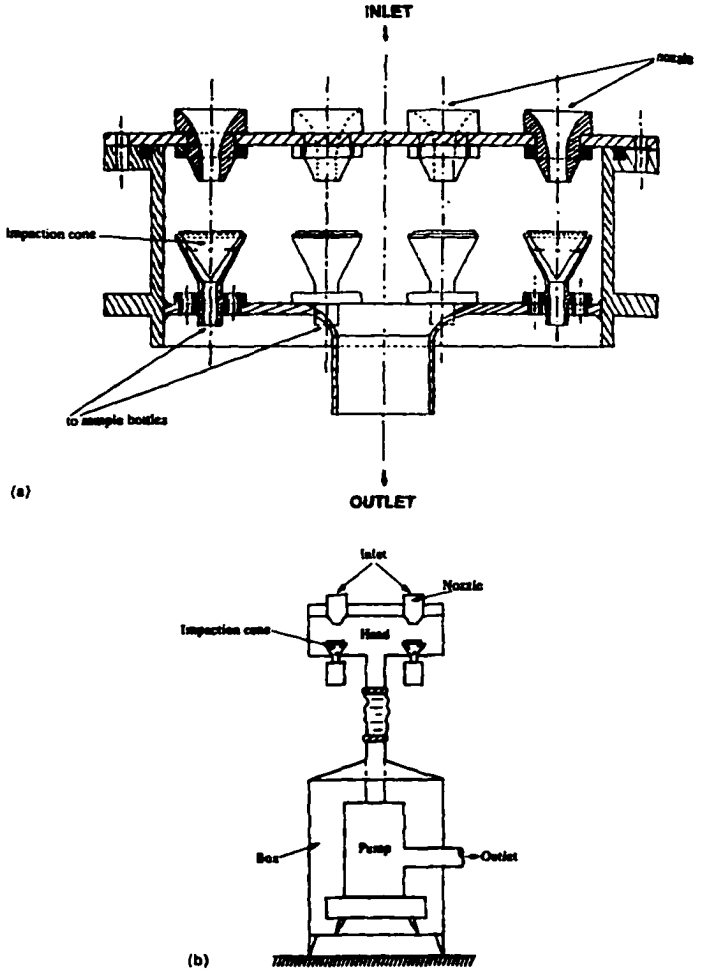

Figure B-65: 8 vertically-oriented round jet impactor: head (top), overall installation (bottom). Note that the head is not shown in actual cross-section (Millet *et al.*, 1995, figure 1)

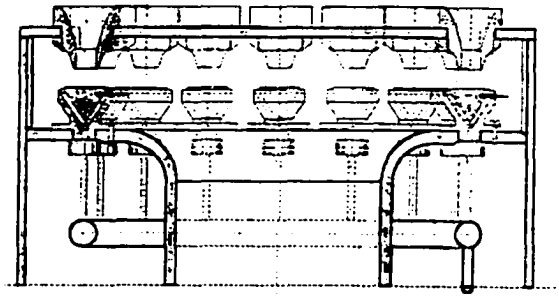

Figure B-66: 16 jet, vertically-oriented impactor (Jaeschke *et al.*, 1990, figure 1)

Reproduced with permission of the copyright owner. Further reproduction prohibited without permission.

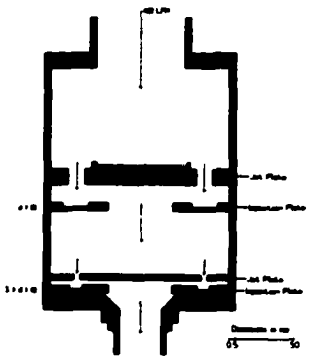

Figure B-67: The ETH two-stage round jet vertically-oriented impactor (side view schematic) (Collett *et al.*, 1993a, figure 1)

Figure B-68: The ETH collector (Collett *et al.*, 1995, figure 1)

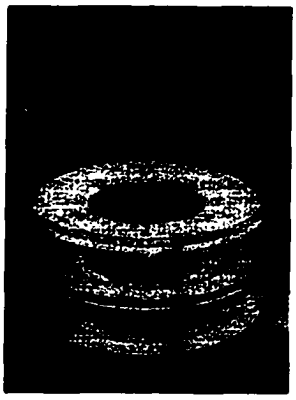

Figure B-69: The IESL three-stage vertically-oriented round jet impactor (Collett *et al.*, 1995, figure 2)

Reproduced with permission of the copyright owner. Further reproduction prohibited without permission.

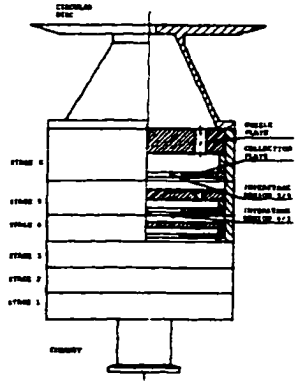

Figure B-70: Berner multi-stage, vertically-oriented round jet impactor (Berner *et al.*, 1998, figure 1)

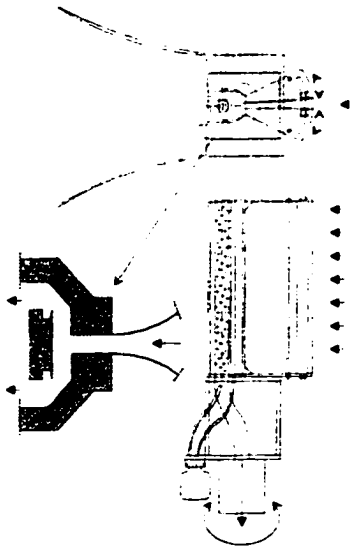

Figure B-71: Isokinetic Cloud Probing System (ICPS): top view (top), side view (lower right), and impaction surface detail (lower left) (Jaeschke *et al.*, 1997, figure 5.9.2, p. 116)

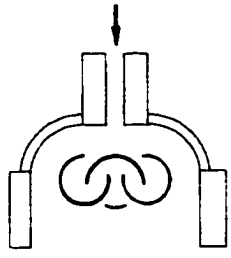

Figure B-72: Impaction surface detail for the two-stage active strand/rectangular impactor (figures B-52 and B-53) (Schell and Georgii, 1989, figure 3)

Reproduced with permission of the copyright owner. Further reproduction prohibited without permission.

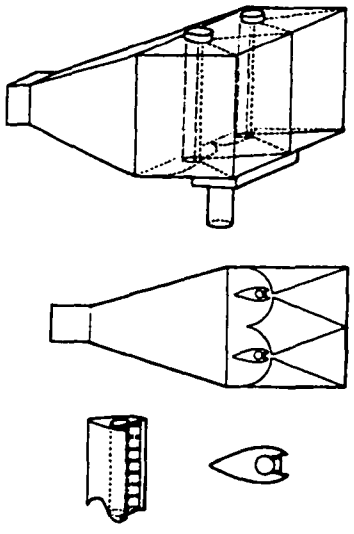

Figure B-73: Dual rectangular jet impactor: oblique view (top), top view (middle), detail of impaction surface (bottom) (Winkler and Kroll, 1987, figure 5)

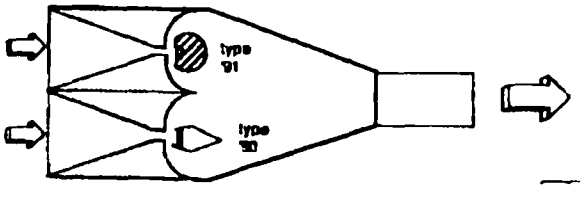

Figure B-74: Later version of the dual jet impactor with revised impaction surfaces (Winkler, 1992, figure 1)

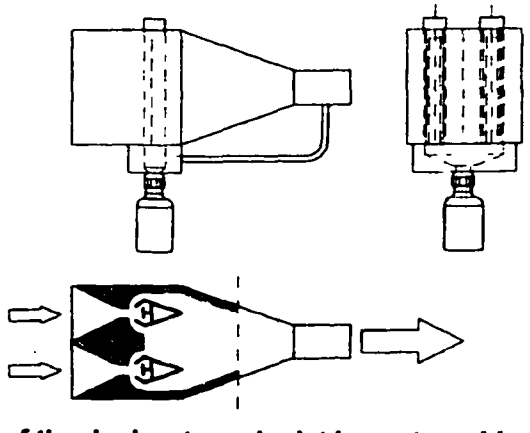

Figure B-75: Three view of the dual rectangular jet impactor: side view (top left), front view (top right), top view (bottom). The impaction surface is further modified (Schell *et al.*, 1992, figure 1)

Reproduced with permission of the copyright owner. Further reproduction prohibited without permission.

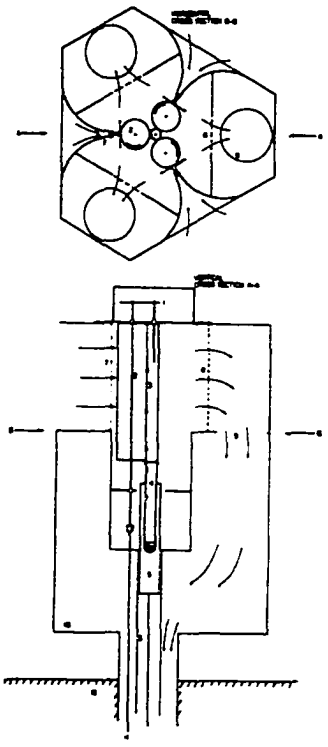

Figure B-76: Tri-rectangular jet DRI impactor: top view of the sampling head (top), side view schematic (bottom) (Katz, 1980, figure 1)

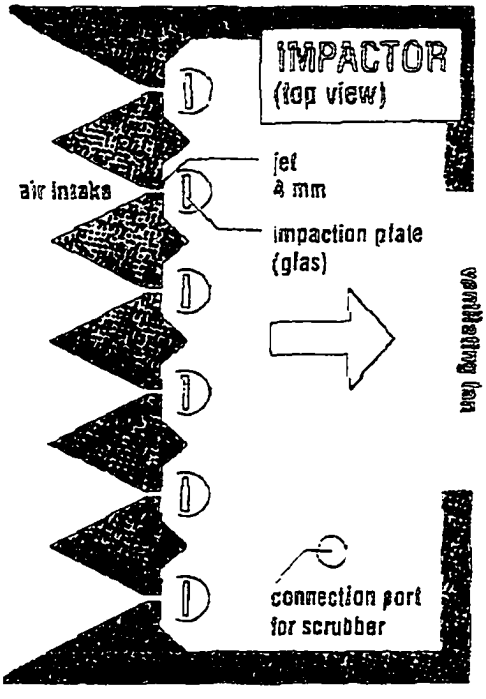

Figure B-77: High volume six rectangular jet impactor for organics (Lüttke and Levsen, 1997, figure 1)

Reproduced with permission of the copyright owner. Further reproduction prohibited without permission.

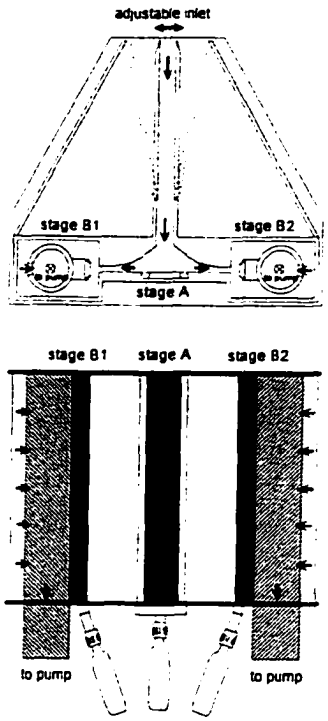

Figure B-78: Two-stage Fog water impactor (TFI2): top view (top), view from behind the instrument (bottom). Single rectangular jet front stage and then two parallel rear stages (Jaeschke *et al.*, 1997, figure 5.9.1, p. 114)

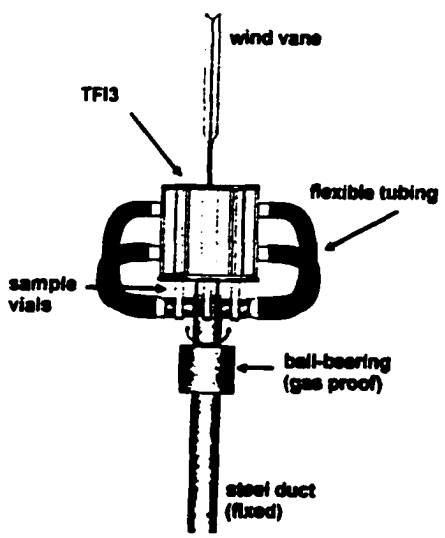

Figure B-79: The TFI3 installed in the field (same as the TFI2, but operated at a different flow rate) (Schell *et al.*, 1997a, figure 2)

Reproduced with permission of the copyright owner. Further reproduction prohibited without permission.

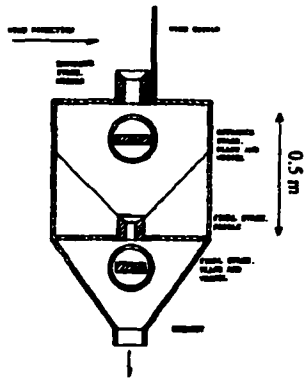

Figure B-80: Schematic of one of the Differential Fog Sampling System (DFSS) two-stage rectangular jet impactors. Designed by A. Berner (Laj *et al.*, 1998, figure 1a)

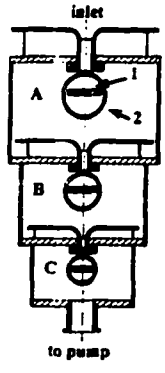

Figure B-81: Schematic of the ACE-2 HILLCLOUD three stage rectangular jet impactors. Designed by A. Berner (Fuzzi *et al.*, 1998b, figure 1)

B.1.7 Super-cooled cloud drop collectors

Many collectors in the previous sections can be used to sample super-cooled drops (e.g. (Bridges, 1998; Fuzzi *et al.*, 1997; Schemenauer *et al.*, 1995; Collett *et al.*, 1993a; Mohnen and Vong, 1993; Winkler, 1992; Anderson and Landsberg, 1979), among others), and several of the super-cooled drop collectors can also with little, if any, modification be used successfully in warm clouds (e.g. the CWS described below, the CHRCC, among others). The collectors included here are primarily, but not exclusively, intended for sampling super-cooled drops. Both passive and active string collectors, as well as active jet impactors have been used. Key differences with warm-cloud collectors are (a) the drops freeze so if collection is by an attached bottle a melting system must be used, and (b) the deposition of rime can alter the collection characteristics of the

Reproduced with permission of the copyright owner. Further reproduction prohibited without permission.

impaction surface (also true for warm cloud samplers but much less important). The effects of these factors on measured composition is difficult to accurately quantify, but it does suggest that heavy riming may result in a bare rod D_{p50} not necessarily being a relevant measure of drop collection. Additionally, the spacing between rods to prevent interference must be larger than for warm cloud collectors due to riming. These collectors are more likely to be composed of metal or plastic-coated metal due to the ambient conditions that they are used in, but like the other collectors a wide variety of materials and designs have been reported.

Several investigators have collected rime just by breaking it off an exposed railing (Puxbaum and Tscherwenka, 1998; Mrose, 1966). Several different flat passive arrays of parallel strands of varying diameter, spacing and number placed perpendicular to the ambient wind have also been used (Eliáš *et al.*, 1995; Duncan, 1992; Huang *et al.*, 1991; Mitchell and Lamb, 1989; Mohnen and Kadlecek, 1989 and references therein; Borys *et al.*, 1988). While details regarding these designs are scarce, the filament diameters used range from as little as 0.2 mm to 1.6 mm prior to riming (Duncan, 1992; Borys *et al.*, 1988). As with warm cloud designs, some investigators use mesh instead of parallel strands (Berg *et al.*, 1991; Scherbatskoy and Bliss, 1984; Okita, 1965).

Active strand collectors use either stationary or rotating arrays of rods. The CHRCC, BITÖK (derived from the CHRCC), and NESAI (also apparently derived from the Caltech family of collectors) collectors fall into the former category (Klemm, 2001; Wrzesinsky, 2001; Wrzesinsky *et al.*, 2001; Kalina *et al.*, 1998; Demoz *et al.*, 1996). One version of the CHRCC used in Europe operates at a lower flow rate than reported in Chapter 2 (Demoz *et al.*, 1996). Rotating collectors used for composition studies include the "Rotorod" (an "H"-shaped collector spun around a central axis), and two flat arrays of rods developed at the University of Wyoming (the latest, "CWI", is shown in figure B-82) (Snider and Huang, 1998; Snider *et al.*, 1992; Rogers *et al.*, 1983). The CWI features Teflon-coated stainless steel collection rods of two different diameters (9.5 mm and 3.2 mm) which potentially could provide size-dependent drop composition measurements.

Reproduced with permission of the copyright owner. Further reproduction prohibited without permission.

Size-resolved super-cooled drop composition measurements have been obtained by using either the Rotating MultiCylinder (RMC) collector (figure B-83) or the cloud sieves (figure B-84) which were developed in response to some perceived short-comings in the RMC (Hindman *et al.*, 1992; Howe, 1991). Both depend upon the ambient wind to impact drops onto cylinders and/or mesh (sieves) of different sizes. The RMC rotates to rime evenly along the entire surface. As the RMC is made of aluminum and bronze, a layer of ice is used as an effective barrier between the surface and the collected rime when chemical composition measurements are intended. Size-resolved composition can be derived by difference for both collectors. The cloud sieves use different lengths of strand/rod to permit sufficient riming on all sieves used for a given time period.

The CWS collector is the only impactor in addition to FROSTY almost exclusively used for rime collection (figure B-85) (Kruisz *et al.*, 1992). It is a single-stage rectangular jet impactor oriented perpendicular to the wind with an attached wind shield. The body is Teflon-coated aluminum and the impaction surface varies between Teflon and Plexiglas depending upon the investigator (Baltensperger *et al.*, 1998; Brantner *et al.*, 1994; Grasserbauer *et al.*, 1994). A different tray can be used for warm clouds.

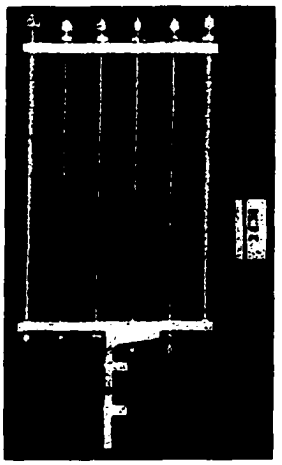

Figure B-82: The University of Wyoming Cloud Water Impactor (CWI) (Snider and Huang, 1998, figure 2)

Reproduced with permission of the copyright owner. Further reproduction prohibited without permission.

Figure B-83: The Rotating MultiCylinder (Howe, 1991, figure 1)

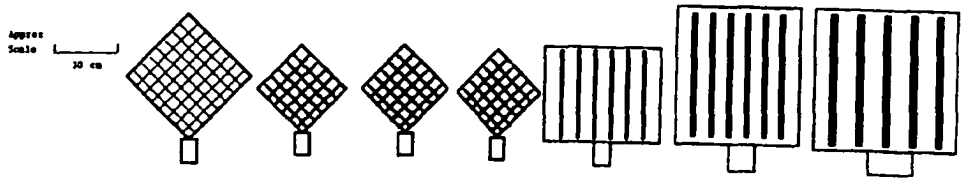

Figure B-84: The cloud sieves. The available D_{p50}s (unrimed) are >2, >3, >5, >7, >10, >14, >23 μm for a windspeed of 9.5 m s^{-1} (as at Storm Peak Laboratory) (Hindman *et al.*, 1992).

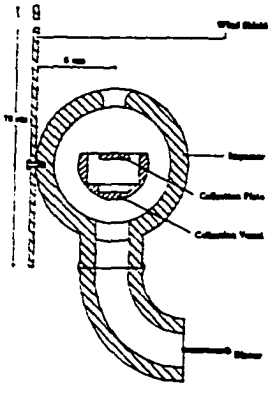

Figure B-85: The CWS rectangular jet impactor (cross-section) (Kruisz *et al.*, 1992, figure 1)

B.1.8 Individual cloud drop methods

Methods to collect individual drops for subsequent chemical investigation have not changed appreciably in the last fifty years. Individual drops are impacted onto thin colloidon or polymeric films or, increasingly, transmission electron microscope grids (Kasahara *et al.*, 2001; Ma *et al.*, 2001; Ishizaka and Qian, 1994; Qian *et al.*, 1992; Levin *et al.*, 1990; Kozima *et al.*, 1953; Kuriowa,

Reproduced with permission of the copyright owner. Further reproduction prohibited without permission.

1953; Ogiwara and Okita, 1952). Subsequent chemical identification is via microscopy. Silicon film-coated glass slides have also been used (Woodcock *et al.*, 1981). One group has recently captured individual drops under a layer of paraffin using electrostatic precipitation and then analyzed the ionic composition of the individual drops using capillary electrophoresis (Tenberken and Bächmann, 1998). Recently a cyanoacrylate method of drop fixation has been developed (Kasahara *et al.*, 2001). While only the latter technique does not evaporate the drop's water off prior to analysis, these methods are grouped separately from two distinct "drop residue only" methods.

B.1.9 Drop residue methods

The Counterflow Virtual Impactor (CVI) and the Differential Aerosol Analyzer (DAA) are two instruments used to collect drops based upon their ambient size (Martinsson *et al.*, 1997b; Noone *et al.*, 1988a). Both systems then dry the collected drops and the drop residues can be subsequently sized and analyzed. The CVI (figures B-86, B-87, and B-88) is a virtual impactor with variable D_{p50}. "Virtual" indicates that the impaction "surface" is actually a stagnation region created by two opposed air flows. The ground-based CVI is operated within a wind tunnel to prevent aspiration artifacts (figure B-88). Aspiration into the wind tunnel itself has been investigated and the results suggested that anisokinetic conditions result in the loss of some drops from the system (Noone *et al.*, 1988c). The DAA uses a series of differential mobility analyzers to size the drops and their residues. The CVI has been widely used to study cloud drop composition including its size-dependence, and the DAA, developed more recently, has focused primarily on cloud-related CCN changes, not drop composition itself (Martinsson *et al.*, 2000; Martinsson *et al.*, 1999; Hallberg *et al.*, 1998; Martinsson *et al.*, 1997b; Martinsson *et al.*, 1997a; Hallberg *et al.*, 1994b; Hallberg *et al.*, 1994a; Hallberg *et al.*, 1992; Ogren *et al.*, 1992; Heintzenberg *et al.*, 1989; Ogren *et al.*, 1989; Twohy *et al.*, 1989b; Noone *et al.*, 1988b; Ogren and Rodhe, 1986). Both systems use an operational definition of "non-volatile" which, while useful for many applications, may result in the loss of some ionic species present in the cloud

Reproduced with permission of the copyright owner. Further reproduction prohibited without permission.

drop (e.g. NH_4^+/NH_3). However, operational limits have been established to prevent residue shattering (e.g. one drop = one drop residue) (Schwarzenböck and Heintzenberg, 2000). They may be considered complementary techniques to the collection and analysis of liquid/rimed drops, but a full description of the drop chemistry cannot be "backed-out". One advantage of the CVI is it is very well characterized for a variety of sampling conditions (Anderson *et al.*, 1993; Noone *et al.*, 1988c; Noone *et al.*, 1988a).

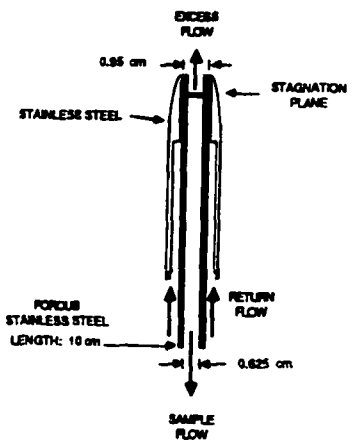

Figure B-86: Tip of the first version of the CVI (Noone *et al.*, 1988a, figure 2)

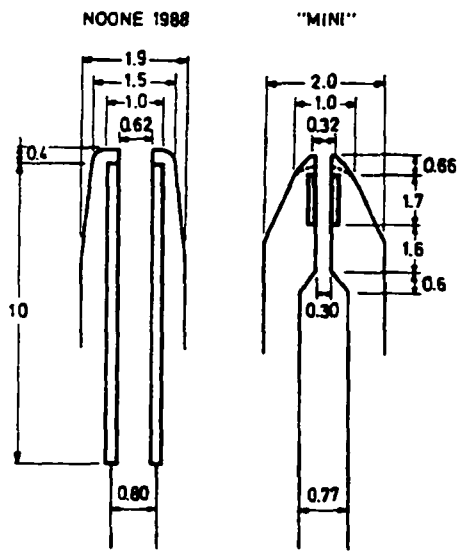

Figure B-87: "Sharp" CVI tip (width is exaggerated 2:1) for lower cut-sizes (Anderson *et al.*, 1993, figure 3)

Reproduced with permission of the copyright owner. Further reproduction prohibited without permission.

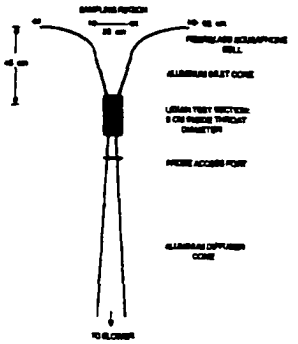

Figure B-88: Wind tunnel for ground-based CVI sampling (Noone *et al.*, 1988a, figure 1)

B.1.10 Alternate approaches to drop collection

Two investigators have used gravitational settling chambers upstream of cascade impactors to collect drop spectra information and drops for subsequent chemical analysis (Martens and Harriss, 1973; Ludwig and Robinson, 1970). As drop deposition to trees motivated many drop composition studies, one investigator actually used a small, primarily plastic, tree to collect drops, although the choice of materials (PVC) may have lead to sample artifacts (Schlesinger and Reiners, 1974). While Parungo and co-workers used liquid nitrogen to cool a metal rod for airborne sampling of cloud drops, a later investigator allows individual (relatively large) drops to sediment into liquid nitrogen and subsequently freeze (figure B-89) (Baechmann *et al.*, 1996; Parungo *et al.*, 1989). Finally, a fog "kite" (figure B-90) has been used for shipboard sampling, although it was subsequently found to be subject to substantial sea spray contamination (Bressan and Larson, 1979).

Reproduced with permission of the copyright owner. Further reproduction prohibited without permission.

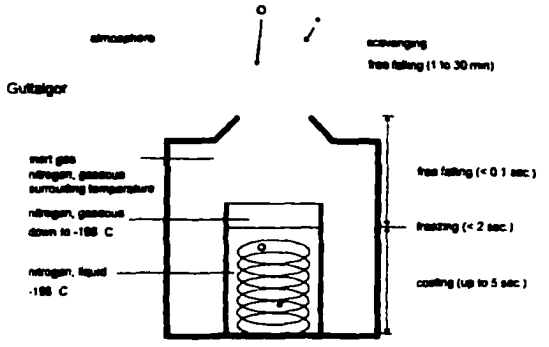

Figure B-89: The "Guttalgor" method for sedimenting drops into liquid nitrogen (Baechmann *et al.*, 1996, figure 2)

Figure B-90: The "fog kite". One end is attached to the bow sprit and the other to a pole (Bressan and Larson, 1979)

B.1.11 Ambiguous cloud drop collection methods

While many authors do not describe their drop collection methods, in several instances partial or ambiguous references are given. Behra and Sigg (1990) report using the "Mallant cyclone collector", although Mallant (1988) suggests that sample evaporation may be a problem for cyclone collectors. It is not known if this is a subsequently improved design. Two studies refer to special equipment but provide no references, and/or contradictory descriptions (Khemani *et al.*, 1981; Okita and Ota, 1981). Finally, Chung and co-workers cite the Hering *et al.* (1987) collector intercomparison paper but then describe the use of "cooling Al coils" to obtain cloud water (Chung *et al.*, 1999).

Reproduced with permission of the copyright owner. Further reproduction prohibited without permission.

B.2 Collector calibration

Ideally, detailed observation-based characterization of experimental equipment is performed. Otherwise, it is not necessarily clear what is being measured. In this section, the various theoretical and experimental techniques used to characterize cloud water collector performance are described. The advantages and disadvantages, where known, are included.

B.2.1 Theoretical characterization

B.2.1.1 Theoretical characterization – strand collectors

At the simplest level, the impaction of drops upon a single cylinder in cross-flow can be used to characterize both active and passive strand collectors. One of the first studies to develop predictive equations was by Langmuir and Blodgett (1946) and it has been cited (in various forms) in relation to many collectors (e.g. (Snider and Huang, 1998; Vong *et al.*, 1997; Minami and Ishizaka, 1996; Howe, 1991; Mohnen and Kadlecek, 1989; Schemenauer and Joe, 1989; Daube *et al.*, 1987; Kins *et al.*, 1986; Castillo *et al.*, 1983; Falconer and Falconer, 1980; Houghton, 1955), among others). Later studies/compilations by Ranz and Wong (1952), Brun (1955), Wong *et al.*, (1955), Golovin and Putnam (1962), May and Clifford (1967) and Fletcher (1969, p. 89) either reproduce the original Langmuir and Blodgett (1946) curves and/or provide additional experimental evidence that their original investigation was reasonable (within approximately ± 20%) at least where drop Stokes numbers (Stk) were < 2 (Wong *et al.*, 1955). Larger Stk may have sharper collection efficiency curves. Langmuir and Blodgett's equations are applicable for non-Stokes drops, but most of the experimental verification has been performed in the Stokes regime. The results from the later works are often cited in lieu of the original (as it can be difficult to obtain). However, some of the references (e.g. (Ranz and Wong, 1952)) are somewhat ambiguous unless specific figures/equations are included. Updated equations to calculate the efficiency curve for a cylinder in cross-flow based upon a least squares fit of the

Reproduced with permission of the copyright owner. Further reproduction prohibited without permission.

available data are provided in Davidson and Friedlander (1978) which is cited in Demoz *et al.*, (1996). Demoz and co-workers also include equations to calculate the cumulative efficiency of multiple rows of strands/rods (the first equation should be used in lieu of the later set of equations which approximate it) (Demoz *et al.*, 1996). These calculations consider impaction alone, but interception (at least theoretically and as measured in some investigations) is negligible (Wong *et al.*, 1955; Ranz and Wong, 1952; Langmuir and Blodgett, 1946). If these theoretical curves are used to define the collector's performance, the shapes of the curves are also defined.

Using the Langmuir and Blodgett (1946) method, the collection efficiency curves for a variety of cylinder diameters spanning the range often used for passive string collectors (0.12 – 1 mm) at 4 different speeds (1, 5, 10, 15 m s^{-1}) for conditions similar to those observed at Whiteface were calculated (see figure B-91 for an example (0.5 mm), and Table B-1 for the compilation). Additionally, the curves for the two fractions of the sf-CASCC and the CASCC2 were also calculated. As diameters decrease and the velocities increase, the sharpness of the collection efficiency curves improves. While this is a simplification, passive collectors would experience similar changes in theoretical collection efficiency as the ambient wind speed increased or decreased. Figure B-92 shows the calculated collection efficiency for the front/Large fraction of the sf-CASCC, and is included to illustrate how an "ambient" D_{p50} (about 25 μm) might differ from a "scaled" D_{p50} (about 21 μm) as mentioned in Chapter 2.

Of particular interest in these results is that for a range of cylinder diameters (0.35 – 0.6 mm), there is not a wide variety in the theoretical results. This suggests that it does not likely make a significant difference to collection efficiency where different investigators use varying strand widths (neglecting factors such as drop blow-off, and the potential for multiple strands interfering with the assumptions behind this calculation).

Reproduced with permission of the copyright owner. Further reproduction prohibited without permission.

Table B-1: Selected cut-sizes for cylinders after Langmuir and Blodgett (1946)

collection diameter [mm] or fraction	D_{p20} [μm]	D_{p50} [μm]	D_{p90} [μm]
0.12	1.5	2.8	8
0.35	2.5	5.5	14
0.4	2.8	5	14.5
0.45	3	5	16
0.5	3	5.2	16
0.55	3.2	5.2	17
0.6	3.5	5.5	18
0.8	4	7	21
1	4.5	7.5	24
CASCC2	2.5	4.2	13
sf-CASSC Large	3	4.5	14.5
sf-CASSC Small	15	25	49*

D_{p78} (@ 49 μm)

data inferred from plotted efficiency curves

for Whiteface conditions, 5 m s^{-1} velocity except for active collectors (@ nominal sampling velocity)

D_{p20}, D_{p50}, D_{p90} are not scaled

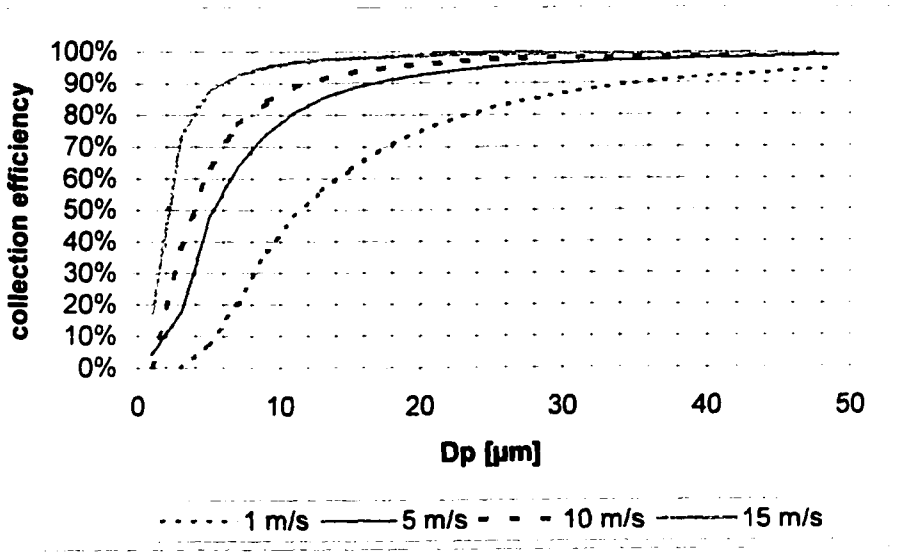

Figure B-91: Langmuir and Blodgett (1946) calculated efficiency curves for a single strand/cylinder (0.5 mm diameter) in cross-flow as a function of ambient velocity

Interaction between rods is not addressed by either the single cylinder treatment or by the extension to multiple rows of rods suggested by Demoz *et al.*, (1996). For many of the passive

Reproduced with permission of the copyright owner. Further reproduction prohibited without permission.

and active collectors with small diameter (< 1 mm) strands, the spacing between them is on the order 4 – 8 times the strand diameter (e.g. (Joslin *et al.*, 1990; Daube *et al.*, 1987; Falconer and Falconer, 1980), among others). For the Large fraction of the sf-CASCC the spacing is on the order of one rod diameter. As a result it appears that the flow around the rods and the resulting collection efficiency are both affected (see Chapter 4). Multiple rows of strands (some of the passive collectors are "double-strung") may also affect downstream collection due to induced turbulence.

B.2.1.2 Theoretical characterization – impactors

The design equations described in Chapter 2 for impactors permit calculation of the D_{p50} (Marple and Rubow, 1986; Marple and Willeke, 1975; Marple, 1970). If the design guidelines are followed, the resulting collection efficiency curves are expected to be "sharp", but equations for the shape are not provided. Most, if not all, collectors operate at significantly higher Re (> 3000) than is recommended which is expected to flatten the efficiency curves (see (Schell *et al.*, 1997a; Winkler, 1992), among others). Many investigators who use impactors also mention observations of losses within the impactor (see (Berner *et al.*, 1998; Millet *et al.*, 1995), among others).

B.2.1.3 Discussion of theoretical characterization

For both active impactors and strand collectors, calculated D_{p50}s are an improvement over the considerable uncertainties associated with passive collector D_{p50}s. However, as various investigations have indicated (see Chapter 4, section B.2.2, and (Straub and Collett, 2001a; b; Straub and Collett, 1999), among others), theory and observation do not necessarily coincide for many reasons. Assumptions used to derive the theory are often violated in practice (e.g. neglected factors may be important). Therefore, while active collectors are preferred to passive ones because of the known theoretical collection efficiencies, active collectors with experimentally-verified and reported collection efficiency curves are preferred to those without.

Reproduced with permission of the copyright owner. Further reproduction prohibited without permission.

Numerical modeling of cloud water collector performance has not been widely reported, although FROSTY and the 5-Stage both have been modeled (Straub and Collett, 2001a; b; Straub and Collett, 1999). While the results are promising, they reveal that not all the features observed experimentally can be verified numerically. It is a useful tool for investigating observations, but is not necessarily an ideal replacement for experimental collection investigations without some verification.

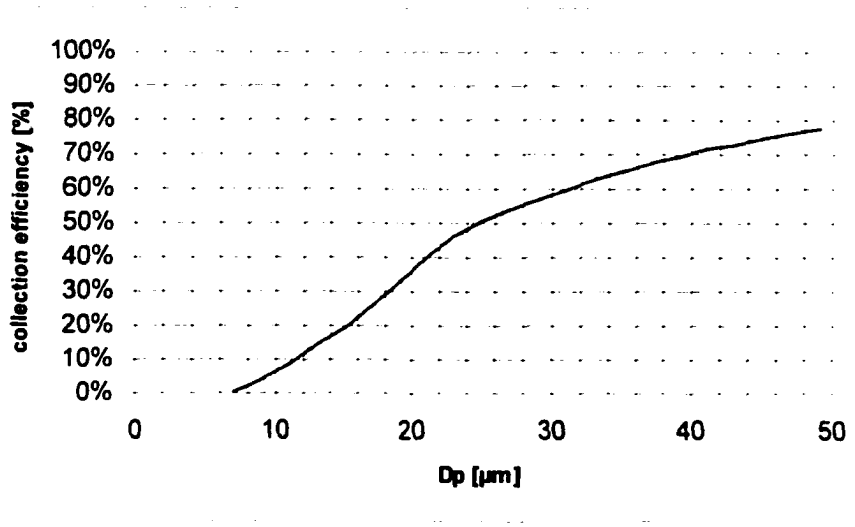

Figure B-92: Langmuir and Blodgett (1946) calculated collection efficiency for a single rod in the front/Large stage of the sf-CASCC at the nominal sampling velocity (6.7 m/s)

B.2.2 Experimental collector characterization

The CHIEF (Chamber for Investigation with Equilibrated Fog) facility is a wind tunnel specifically intended to evaluate the performance of cloud and fog measurement devices (Mallant, 1988). Capabilities include drop generation, stable fog, and drop size distribution and fog LWC measurements. Unfortunately not many cloud and fog water collectors have been validated there. While the CHIEF facility represents the closest controlled approximation to field conditions available, many other approaches – some similar to what is possible at CHIEF – have been used to experimentally confirm collector performance.

Reproduced with permission of the copyright owner. Further reproduction prohibited without permission.

This section will consider field observation techniques first, followed by different laboratory, or laboratory-inspired, techniques. A discussion specific to the laboratory techniques used for FROSTY and the 5-Stage is included.

The collector efficiency curves shown above and in Chapters 3 and 4 show the efficiency as a function of drop number concentration. While it is not always clear, many of the comparisons that follow are drop volume-based which is not the same. This distinction is largely irrelevant for single-stage collectors with sufficiently small D_{p50}s (e.g. 5 μm), but scenarios are possible where this may become important in multi-stage collectors (e.g. narrow drop spectra).

B.2.2.1 Field observation techniques

Collector validation via field observation generally consists of comparisons between the collector's sampled mass and an independent concurrent LWC measurement (see Chapters 3 and 4 for examples). Several authors report positive correlations between collected mass and LWC for active single-stage collectors (Fuzzi *et al.*, 1997; Demoz *et al.*, 1996; Brantner *et al.*, 1994; Gundel *et al.*, 1994; Lüttke *et al.*, 1994; Kruisz *et al.*, 1992; Berner, 1988; Jacob *et al.*, 1984a; Houghton and Radford, 1938). In general the collected mass is only a fraction (e.g. 60% (Jacob *et al.*, 1984a), 43 ± 12% (Fuzzi *et al.*, 1997), up to 70% (Lüttke *et al.*, 1994)) of that possible suggesting that either some drops are not being sampled, losses are occurring during sampling or "independent" measures of LWC are incorrect. Cloud LWC and drop size distribution are also important parameters that affect collector sampling. For example, varying correlations between the CWS (figure B-86) collected mass and LWC for two locations are attributed to different drop spectra. The correlation is poorer where many drops are smaller than the CWS' (unrimed) D_{p50} (Kruisz *et al.*, 1992). Positive correlations betweent collected volume and LWC for passive ASRC- or harp-type collectors (figures B-15 and B-22) as a function of ambient wind speed and other factors have also been reported (deFelice, 1997; Miller *et al.*, 1993; Fowler *et al.*,

Reproduced with permission of the copyright owner. Further reproduction prohibited without permission.

1988b). Compared to a co-located FSSP, Fowler and co-workers report their harp collector sampled 11 – 47% of the available water (mean ≈ 29%) (Fowler *et al.*, 1988b). Schemenauer and co-workers used a co-located FSSP upstream of their massive fog collector (figure B-27) to evaluate their collection efficiency (possibly as high as 60%) (Schemenauer and Joe, 1988).

For multi-stage collectors, comparing collected water to LWC in the applicable drop size range is also a useful technique, although it does depend upon drop size distribution measurements which are subject to considerable error (see Appendix G). This technique was used to validate the Differential Fog Sampling System (figure B-80) (Laj *et al.*, 1998). While there is a high correlation between stage collected mass and "stage LWC", a curve is actually fit to the data points – not a straight line which might be expected. No explanation is offered. If no drop size distribution data are available then the overall collected mass across all stages can be compared to the ambient LWC.

These techniques tend to "reward" the ability to collect larger drops which contribute more volume than the smaller ones. A collected mass vs. LWC comparison can also neglect consistent losses in water collection. Perfect correlation does not imply that water is being collected with 100% or theoretical efficiency. Predicted/derived vs. measured LWC comparisons may be a better measure of collector performance as collection inefficiencies are not generally obscured, although this method's utility is limited for low mass – small – drops. These techniques are useful, but they may be better at indicating collector sampling problems than unequivocally suggesting that the collectors work according to their design. For example, a Po Valley comparison of co-located FSSP and ASRC rotating harp collector (figure B-40) data indicated that the FSSP and the collector sampled different drop populations (Berner *et al.*, 1988, and references therein).

Reproduced with permission of the copyright owner. Further reproduction prohibited without permission.

B.2.2.2 Laboratory calibration techniques

One laboratory calibration technique is very similar to the techniques described in the preceding section. Drop size distribution measurements (and occasionally a separate LWC measurement) are performed upstream and downstream of a collector. Collected water and the changes in the drop size distribution can then be used to evaluate the collection efficiency (Schell *et al.*, 1997a; Schell *et al.*, 1992; Winkler, 1992; Hoffmann and Metzig, 1991; Krämer and Schütz, 1990; Kins *et al.*, 1986). This technique is particularly useful to investigate how changing cloud parameters (e.g. LWC, drop size distribution) can affect collector aspiration and overall collection efficiency (Schell *et al.*, 1992). Given the considerable uncertainty when all of the measurements are combined, it is difficult with this technique to produce collection efficiency curves. Rather, the results can be judged either consistent or inconsistent with the theoretical collection efficiency curves, and insights into the magnitude of non-idealities in collection performance can be gained (Schell *et al.*, 1997a; Winkler, 1992; Hoffmann and Metzig, 1991). For example, in the TFI2 (figure B-78), the first stage was 70 – 90% and the dual rear stages were 40 – 70% efficient for collected water mass according to this technique. Internal drop losses may be important upstream of the 2nd stages. In some instances, drops were produced from salt solution of varying composition, or two different drop spectra were produced from different solutions (e.g. "large" and "small" drops are of different composition) (Schell *et al.*, 1997a; Schell *et al.*, 1992; Winkler, 1992; Mallant, 1988). In addition to providing more information about collection characteristics than just measurements of water mass, this can suggest if evaporation is a problem.

Several authors calibrated their collectors by making inert (or relatively inert) drops and then determining how the drops were collected when introduced into the sampler. Noone and co-workers generated ammonium sulfate drops and aspirated them into the CVI in ambient conditions where evaporation should not have affected the results (> 80% relative humidity) (Noone *et al.*, 1988a). Drops composed of dibutyl phthalate, fluorescein, and oleic acid are more typically used (Straub and Collett, 2001a; b; Straub and Collett, 1999; Pade *et al.*, 1987; Jacob *et*

Reproduced with permission of the copyright owner. Further reproduction prohibited without permission.

al., 1985a; May, 1945). May (1945) could not control drop size well and instead measured the size of drop marks left on the glass collection surface slides in his impactor (figure B-10). Collett and co-workers used a similar technique for the IESL collector (figure B-69) (Collett *et al.*, 1995). Other calibration techniques consider the collected drops in aggregate, but the individual sizes still need to be verified (Straub and Collett, 1999). The advantage of these techniques is that they potentially permit evaluation of where losses may be occurring. However, one limitation of these techniques is that these drops once collected do not necessariy behave like water.

B.2.2.3 FROSTY and 5-Stage calibration techniques

The experimental collector efficiency curves for FROSTY and the 5-Stage are presented in Chapters 3 and 4 and the laboratory techniques are described in detail elsewhere (Straub and Collett, 2001a; b; Straub and Collett, 1999). This summary is included here as it is relevant to the interpretation of the results presented in Chapters 3 and 4.

For both FROSTY and the 5-Stage, the theoretical D_{p50}s and efficiency curve sharpness are discussed in Chapter 2.

The experimental calibration depended upon the generation and subsequent collection of fluorescein-tagged drops of known size (corrected for doublets and triplets). Drops were generated using a Vibrating Orifice Aerosol Generator (TSI, Inc., Minneapolis, MN). In 2 μm increments, essentially mono-disperse drops from 4 to 34 μm in diameter were individually introduced into the collectors and their collection efficiency on each stage or "loss" between each stage evaluated. The drops were introduced virtually directly into each collector's inlet, so aspiration efficiency is not evaluated. The drops did not spread out over the entire length of the jets until downstream of the first stage or stages. No drops < 4 μm or > 34 μm were used as their generation was very difficult. Due to the amount of time required to make a single drop size measurement (approximately 8 hours) in the 5-Stage, the uncertainties associated with repeated

Reproduced with permission of the copyright owner. Further reproduction prohibited without permission.

measurements of similar sizes in FROSTY were assumed to be applicable. The lip added to Stage 5 to prevent drop re-entrainment was not included in the experimental calibration.

B.2.3 Drop collection problems

While perfect collection efficiency for all drops may be impossible to achieve, 100% efficiency is not needed as long as a representative sample is collected in sufficient volume for analysis (Schell *et al.*, 1997a). Leaving aside the question of how to judge what "representative" is, non-idealities in drop collection due to a variety of mechanisms are widely reported and are usefully considered here. While some of the losses reported are a function of aspiration efficiency (see Chapter 2), many of the problems result from operational factors that are not necessarily amenable to either theoretical or experimental calibration under controlled conditions. Collected drop losses are more typical, but precipitation drops can be a positive artifact in some instances.

Non-ideal aspiration efficiencies and inlet losses (e.g. upstream of the collecting surfaces in active collectors) have been reported by many authors. Variations in aspiration efficiency between the vertically-oriented IEP (figure B-64) and one version of the MOH collector (figure B-75) as a function of LWC and drop distribution spectra resulted in substantially different drop composition measurements between the two collectors (Schell *et al.*, 1992). Although a wind shield was added which improved the collection efficiency of the IEP collector (Arends *et al.*, 1997), virtually calm wind speeds (< 1 m s^{-1}) must occur for similar volume and composition samples to be obtained (Fuzzi, 1997a). As mentioned previously, different studies report sampling in cross-winds affects sampler collection efficiency (Noone *et al.*, 1988c; Houghton and Radford, 1938). Inlet losses are separate from aspiration efficiency and can be considered as a form of "transmission" efficiency. Several authors report either inlet losses, the potential for them or emphasize that they must be reduced (Fenn *et al.*, 2000; Jaeschke *et al.*, 1997; Chang, 1989; Däumer *et al.*, 1988). The combination of aspiration and transmission efficiencies suggests that

Reproduced with permission of the copyright owner. Further reproduction prohibited without permission.

the actual drops incident on the collection surfaces can be different than the ambient drop distribution.

Sampled drops may also be lost before they are safely in the attached collection bottle. For the passive string collectors, many studies report drop losses due to blow-off in "high" ambient winds (> 12 m s^{-1} according to Galvin (1983), although other authors suggest it occurs at lower wind speeds) (Mohnen and Kadlecek, 1989; Fowler *et al.*, 1988a). Therefore while higher wind speeds will theoretically improve collection efficiency (see figure B-91) for the passive strand collectors, they may also worsen collection efficiency due to drop blow-off. Suspended passive collectors also may lose drops as they are buffeted by the wind. Galvin (1983) suggests that blown-off drops are collected by the thicker supporting rods used to separate the strands, however, their coverage is not uniform across the ASRC-passive collector's cross-section (figure B-15). Choularton and co-workers report an interesting phenomenon observed in the passive-string collectors deployed during the Great Dun Fell 1993 experiment. The relatively high winds experienced led to drops remaining suspended on the collection strands which affected the temporal resolution possible. They observed that the collection efficiency of the passive string collectors decreased as the wind speed increased (Choularton *et al.*, 1997). Several authors who use both passive and active string collectors indicate that drop blow-off/re-entrainment/loss is enhanced if the strings themselves are not taut (Schomburg *et al.*, 1991; Joslin *et al.*, 1990). For the CWP collector (figure B-45), three strand diameters – 0.38 mm, 0.64 mm, and 1.12 mm – were investigated. The 0.64 mm strands performed the best while the 0.38 mm ones had the worst blow-off problems (Daube *et al.*, 1987). Thus, while theoretically many different diameters ought to collect drops similarly, in actuality they may vary.

Drop blow-off or re-entrainment is a suspected or reported problem in many active impactors, too (Laj *et al.*, 1998; Winkler and Pahl, 1997; Lüttke *et al.*, 1994; Schell *et al.*, 1992). If the jet velocity is high (e.g. > 25 m s^{-1} (Laj *et al.*, 1998)) drops get carried off the impaction surface. This

Reproduced with permission of the copyright owner. Further reproduction prohibited without permission.

problem was observed in Stage 5 of the 5-Stage (see Chapter 2) and steps were taken to mitigate it. Experimental calibration using non-water drops does not necessarily observe this.

Finally, construction materials, particularly if not conditioned, may also affect collection efficiencies (Schell *et al.*, 1997a; Huebert and Baumgardner, 1985).

B.3 Collector comparison studies

Sections B.1 and B.2 illustrate both the wide variety of collectors available and the advantages/disadvantages of how each may or may not be characterized. Although not considered above, operational differences (e.g. variations between sampling protocols) may also lead to different drop composition measurements being made. Therefore, another useful way to evaluate collectors is to compare them to each other (see Chapters 3 and 4 for FROSTY, the CHRCC, the 5-Stage, CASCC2 and sf-CASCC comparisons). Collector intercomparison allows drop composition to be considered which is not the case for the sample volume-based field comparisons described in section B.2.2.1. Table B-2 contains the comparisons found in the literature (sorted by year and author).

While most of the comparisons are straight-forward (e.g. the collector with a higher flow rate sampled more water for a given time period), there are a few of particular interest. The results from the large-scale Great Dun Fell 1993 field campaign indicate the problems that become apparent when with using multiple collectors to measure the same cloud (Choularton *et al.*, 1997). It emphasizes the importance of being able to relate composition measurements between collectors (one of the goals of Chapters 3 and 4) as a function of ambient drop size distribution and collector overall sampling efficiency. The Schell *et al.* (1992) study may have prompted the effort that subsequently went into the development of wind shields for collectors that do not face into the wind and isokinetic inlets for those that do (Berner *et al.*, 1998; Berner and Kruisz, 1997; Schell *et al.*, 1997a; Jaeschke *et al.*, 1990). The first major collector intercomparison study

Reproduced with permission of the copyright owner. Further reproduction prohibited without permission.

yielded results, in part, similar to those observed at Great Dun Fell – different collectors can measure "different" clouds simultaneously (Hering *et al.*, 1987). This study also emphasized that horizontally co-located collectors of the same design could have consistently similar results and that theoretical performance may sharply differ from actual performance (e.g. the AeroVironment rotating collector) (Hering *et al.*, 1987). It is interesting that many dissimilar collectors make highly comparable drop composition measurements. However, if there is not a strong size-dependent drop composition, varying efficiencies for different-sized drops won't be reflected strongly in the measured composition (Wobrock *et al.*, 1994). Size-dependent drop composition is likely a factor in the Great Dun Fell results and some of the other studies included in Table B-2. One additional advantage of using co-located collector measurements is that contamination problems may be readily apparent (e.g. (Jagels *et al.*, 1989), among others).

B.4 Discussion

Cloud and fog water is collected using a variety of techniques (section B-1) of varying aspiration, transmission and collection (impaction) efficiencies (section B-2) and, while some collector intercomparisons yield very good results for both collected mass and drop composition, some do not (section B-3). Different investigators take into consideration or neglect different issues depending upon their own particular needs – all of these choices may be reflected in what is ultimately measured. Some of these are obvious from their choice of collectors, but some (e.g. sampling and handling protocols) are not readily apparent.

Of the collectors discussed, the ASRC passive, CWP passive, the Caltech family of active strand collectors, and moderate variations thereof are the mostly widely used for drop composition measurements. While jet impactors are used in many studies, they tend to be operated only by their developers.

Reproduced with permission of the copyright owner. Further reproduction prohibited without permission.

Table B-2: Collector comparisons in the literature

Collector comparisons			
Author/year	***Collectors***	***Cloud type/ location (if known)***	***Results***
(Rattigan *et al.*, 2001)	ASRC passive, sf-CASCC, CASCC2	Whiteface Mtn., NY (orographic)	good agreement for chemistry (major inorganic ions)
(Hoag, 1998)	5 CASCC2s	San Pedro Hill, CA	chemical variation between collectors (major inorganic ions) within 10% for three time periods (within analytical uncertainty)(performed by B. Daube, May 1989)
(Choularton *et al.*, 1997)	UMIST passive (cylindrical) string, MOH dual-jet impactor, EAWAG active strand, IEP 4 nozzle impactor, TFI2, six-jet impactor for organics, ICPS?, another collector?	orographic (Great Dun Fell 1993 campaign)	in high winds (> 13 m s^{-1}) the passive collectors had higher concentrations than the active ones, but passive collection efficiency went down. Composition variations between collectors were as high as a factor of 3 and sometimes exceeded that. NaCl showed worse agreement than ammonium sulfate.
(Fuzzi, 1997a)	MOH dual-jet impactor and IEP 4 nozzle impactor	3 Ground-based Cloud Experiments (GCE): Po Valley (fog), Kleiner Feldberg (orographic), Great Dun Fell (orographic)	Collection efficiency varied with the drop spectra and between the collectors. At low wind speeds (<1 m s^{-1}) similar collection rates were observed.
(Demoz *et al.*, 1996)	sf-CASCC and CASCC2	Mt. Mitchell, NC (orographic)	similar overall collection efficiencies
(Collett *et al.*, 1995)	IESL and ETH impactors		IESL collects more water than the ETH
(Millet *et al.*, 1995)	2 - 6 µm and 5 - 8 µm round impactors		these are actually two different collectors although I tend to treat them as one. Composition and collected volume differences obtained as a function of size, but consistent with each other.
(Schemenauer and Cereceda, 1994)	AES version/ASRC passive and "std. cloud water"		The larger standard cloud water collector collects more water
(Wobrock *et al.*, 1994)	MOH dual-jet impactor, two-stage strand/impactor, and IEP 4 nozzle impactor	Kleiner Feldberg (orographic)	The IEP was used with a wind shield and composition compared well between collectors. There was a 20 - 30% difference in collected water. There may not have been a strong size-dependence in drop composition.
(Levsen *et al.*, 1993)	"ICARE" passive and 1992 MOH dual-jet impactor		The passive collected 10 times more water. HCHO and CH_3CHO concentrations were similar between the two collectors, although HCHO was generally lower in the active collector.
(Schell *et al.*, 1992)	MOH dual-jet impactor and IEP 4 nozzle impactor	Po Valley (fog) and CHIEF facility	Different composition and collected water observed in the Po Valley. At CHIEF determined that the collection efficiencies for both collectors were a function of LWC and drop spectra. Part of the difference is attributed to aspiration efficiency differences between the two. The MOH collector lost large drops at the inlet, and the IEP collector lost similar amounts of large but also small drops. Up to and exceeding a 100% difference was observed between the two collectors for nitrate, ammonium and sulfate in the Po Valley, although 20 - 25% variation was the mean.
(Schemenauer and Cereceda, 1992)	AES version/ASRC passive, and massive fog water		differences in observed composition could be explained by dry deposition variations

Reproduced with permission of the copyright owner. Further reproduction prohibited without permission.

Author/year	*Collectors*	*Cloud type/ location (if known)*	*Results*
(Collett *et al.*, 1990; Collett *et al.*, 1989)	CASCC and RAC		The CASCC has relatively higher collected mass than predicted. Composition variations (more magnesium, calcium, sodium and chloride in the RAC, while nitrate, sulfate and ammonium were relatively similar) explained by higher collection efficiency of CASCC for smaller drops. Results suggest size-dependent drop chemistry
(deFelice and Saxena, 1990)	CASCC, DRI impactor and ASRC passive	Mt. Mitchell, NC (orographic)	DRI had a substantially lower sampling rate than the other two collectors
(Basabe *et al.*, 1989)	ASRC passive and CWP	western Washington	composition close enough that results reported together
(Chang, 1989)	CWP and ASRC passive	Cheeka Peak, WA and the Burley site (also WA?)	collected composition was similar but comparions between volumes was poor
(Jagels *et al.*, 1989)	flat screen	U.S. East coast and laboratory	pH raised by nickel collectors, stainless steel and teflon collectors gave similar results.
(Mohnen and Kadlecek, 1989)	CWP and ASRC passive	Whiteface Mtn.?	For 3 - 30 m s^{-1} winds, similar composition observed
(Munger *et al.*, 1989b)	CASCC and RAC		HCHO reported to be the same (based upon work by Collett)
(Ogren *et al.*, 1989)	CVI and ASRC passive		Concentration differences were within about a factor of 2 for comparable time periods. Possibly attributable to different size cuts.
(Saxena *et al.*, 1989)	CASCC(s?) and ASRC-passive(s?)	Mt. Mitchell, NC (orographic)	pH and collected volumes agree within 5% despite different inefficiencies
(Fuzzi *et al.*, 1988)	FISBAT rotating harp and ASRC rotating string	Po Valley (fog)	Limited data is available, but composition was within 15% for the species measured
(Daube *et al.*, 1987)	CWP, AMC/WPI passive and ASRC passive	Whiteface Mtn. or Mt. Washington, NH?	Some chemical difference observed between the AMC and the CWP. The ASRC collector aspirated rain. Differences generally within analytical capabilities
(Hering *et al.*, 1987)	RAC, GGC, AeroVironment rotating, Mack and Pilie rotating, DRI impactor	Henninger Flats, CA (stratus?)	5/5 collectors agreed for pH, 4/5 for other ions, 3/5 for LWC. Co-located RAC volumes within 2% (6% for GGCs). Horizontal variability was 10% for RACs (6% for GGCs). The coefficient of variation for LWC between all collectors was 109%. Results varied as a function of drop spectra (volume median diameter) and LWC. Soil dust may have been aspirated by some collectors. The coefficients of variation for nitrate, sulfate, and ammonium were 24%, 30% and 33%, respectively.
(Johnson *et al.*, 1987)	RAC and EAWAG screen (based upon 1st CASCC)	Dubendorf, Switzerland (fog)	Nitrate, chloride, sulfate, and ammonium were higher in the screen collector (attributed to differences in collection efficiency for small drops)
(van Valin *et al.*, 1987)	ASRC passive and ASRC rotating string	Whiteface Mtn. (orographic)	no statistical concentration differences
(Fuhrer, 1986)	CWP and ASRC passive	ground-based fog (< 1 m s^{-1})	concentration differences observed attributed to different collection efficiencies
(Goodman, 1985)	concentric cylinder and flat screen passive	CA	cylinders collected more water
(Jacob *et al.*, 1985a)	1st version of the CASCC and the RAC		Similar collected composition reported.
(Bressan and Larson, 1979)	fog kite and conductivity meter	offshore Nova Scotia	the fog kite picked up sea spray
(Schlesinger and Reiners, 1974)	plastic tree and open bucket		PVC tree "needles" may have been a source of contamination

Reproduced with permission of the copyright owner. Further reproduction prohibited without permission.

Both passive and active collectors can be successfully operated. The primary disadvantage of the passive collectors is that the drop sizes collected change as a function of wind speed and drop losses/blow-off also change. It is not known if the net amount collected is consistent and/or predictable but it is likely a function of at least wind speed, the drop spectra, LWC, strand diameter, strand length, strand number, strand condition, spacing of strands, collector orientation relative to the wind and collector mounting. Several investigators also use nylon filaments which promote the possibility of HNO_3/NO_3^- artifacts primarily via dry deposition between events. While nylon is sufficient for LWC-only measurements, it may not be suitable if composition information is required. While active collectors should perform consistently, the recent work cited above indicates that transmission, aspiration and internal losses occur under most sampling conditions and will likely alter the collected drop composition. In other words, the sampled drop spectrum may vary from the actual drop spectrum which has the potential to affect the measured composition. As a result, overall sampling efficiency for active collectors as a function of drop size is therefore dependent upon many of the same or similar parameters listed above for passive collectors. The advantage of active collectors compared to passive is that theoretically the losses in an active collector are consistent between time periods, assuming aspiration (and transmission) do not change. Given all of these factors, it is probably not surprising that theoretical collection efficiency curves do not necessarily adequately describe the overall collection efficiency for either strand collectors or impactors.

While laboratory experimental collection efficiency curve determination has its own limitations, it can indicate where deviations from ideal design conditions affect the results. The laboratory work, in conjunction with field observations (e.g. LWC/collected mass comparisons), and collector intercomparisons (if available) provide a better indication of collector performance. However, if there is little variation in size-dependent drop composition, composition comparisons may not yield additional information.

Reproduced with permission of the copyright owner. Further reproduction prohibited without permission.

Theoretically, jet impactors (and cascade impactors for size-resolved measurements) offer the possibility of sharp size cuts. However, the use of high Re flows, collector geometry and the difficulties of working with relatively large liquid drops appear to have significantly broadened the collection efficiency curves. Cloud and fog drops have relatively a lot of inertia compared to aerosol particles typically sampled with cascade impactors (see Appendix E). Sample time resolution remains poor compared to passive collectors in high ambient wind conditions. To achieve consistent sub-hourly sampling intervals (at least for the major ionic species) would require increasing the flow rate to >10 m^3 min^{-1} for a drop size-resolving impactor. For current designs, this would either result in very large impactors or potentially even flatter collection efficiency curves due to higher Re flows. Aspiration and transmission efficiency non-idealities may or may not be consistently improved by wind shields. The use of several impactors in parallel to determine size-resolved composition is complicated by the assumption that at the least all non-idealities in aspiration, transmission and/or the collection efficiency curves off-set each other.

The preceding discussion suggests that it may be difficult to quantitatively compare results between different investigators using different equipment and/or sampling and handling protocols at varying locations. General consistency may be (and has been) observed, particularly if drop spectra, cloud LWC, and ambient conditions are known and the collectors are highly similar although the propagated uncertainty may be large. However, the "right" answer may be observed for the "wrong" reasons. Collector and sampling protocol standardization has been used to mitigate variations (e.g. MADPro and CWP (Anderson *et al.*, 1999; Weathers *et al.*, 1988)). The best approach is to repeatedly use the same collectors and protocols, but even so composition variations may be obscured if the total uncertainty remains high. To interpret size-dependent composition measurements, the collection efficiency of the collector, cloud LWC, and drop distribution must be known (Jaeschke *et al.*, 1998; Fuzzi, 1997a; Vong *et al.*, 1997). Aspiration (and transmission if a problem and not included in the collection efficiency curve) should also be considered if they alter drop collection. Size-dependent drop composition cannot be separated

Reproduced with permission of the copyright owner. Further reproduction prohibited without permission.

from drop physics, at least above the level of individual drop measurements. Unfortunately, cloud drop collection in ambient conditions is affected by the fluctuating atmosphere. Multi-collector investigations help to discern if one or more collectors are not operating consistently. Field performance must always be evaluated with whatever data are available.

Implicit in much of the above is that the composition of all drop losses and all drops collected – whether size-resolved or not – are "representative". Current individual drop measurement techniques do not easily permit evaluation of this assumption. There is currently no alternative but to make this assumption, and it is uniformly made by all investigators.

Reproduced with permission of the copyright owner. Further reproduction prohibited without permission.

C. Appendix: The FROSTY Collector: Cleaning, Assembly and Sampling Protocol

This appendix describes the cleaning and assembly of the FROSTY collector and its use in the field. It is very important to remember while handling/using FROSTY that all steps must be taken to ensure the integrity of its collected samples. Further, the collector is designed primarily for the quantification of inorganic ions and trace metals in supercooled drops so all contact with metal (particularly on its internal surfaces) must be minimized. Do not use metal fasteners.

C.1 Major Cleaning and Collector Disassembly/Assembly

This section is for major cleaning before or after field campaigns. Collector disassembly and assembly is required for major cleaning and it is therefore included here.

1. Disassemble the collector
    - Remove the exit stage
    - For the main body, the best way to take it apart is to remove the nylon bolts holding the top or bottom plate onto the side walls/jet plates
        - Once the bolts are removed, tap gently on one end and gradually work it off
        - The thin side wall pieces will pop completely out eventually
        - Remove the rest of the bolts so all plastic components are separated
    - For the two sets of collection rods, remove the Teflon inserts from the Stage 1/LARGE and Stage 2/MEDIUM black Delrin holders (do not disassemble the Stage 3/SMALL rods)

Reproduced with permission of the copyright owner. Further reproduction prohibited without permission.

- There has occasionally been contamination trouble if the inserts are not removed for thorough cleaning of both the Delrin support rods and Teflon surfaces prior to a campaign

2. Cleaning
   - Put on gloves
   - All of the plastic parts (including the exit stage and any bolts) should be washed with the following sequence:
     - Dilute Triton-X, DI rinse, alcohol (usually methanol), DI rinse, Dilute Triton-X, thorough DI rinse
     - While some pieces of the collector are somewhat scratched, there should be no visible grime on any of the surfaces after cleaning
     - Use Q-tips, Kimwipes, plastic toothbrushes (etc.) for scrubbing and make sure that the grooves in the top and bottom plates are cleaned as well
     - Do NOT forget that Kimwipes, Q-tips and gloves are not necessarily "clean" themselves
   - As the parts complete the third washing/rinse, place them in clean plastic tubs filled with (fresh) DI to soak
     - Cover the tubs

3. Collector Assembly
   - FROSTY can be difficult to re-assemble, but the following procedure has worked well
     - Approximately 30 minutes is required (when skilled)
   - Obtain all needed screwdrivers and a plastic hammer/mallet
     - A rubber mallet can be used if its head is encased in a Ziploc (or similar)
       - The Ziploc will likely need replacing during assembly
       - The Ziploc is used because otherwise fine rubber particles are deposited on/in the collector

Reproduced with permission of the copyright owner. Further reproduction prohibited without permission.

- Prepare a clean work surface
  - Garbage bags work well
- Put on gloves
- Remove the FROSTY parts from the tubs and allow them to dry
- Loosely assemble the top and bottom plates with the Jet 1, Jet 2, and Jet 3 plates
  - Do not put on the Stage 3/SMALL walls yet (they prevent the Stage 2/MEDIUM sides from being inserted)
  - The bolts should be tight enough that the thin wall pieces for Stage 1/LARGE and Stage 2/MEDIUM can be inserted into the grooves without popping out, but not tight enough that their insertion is unduly restricted
  - Minimize handling/touching any part of the collector that it will be difficult to clean once it is assembled
    - Do not touch any pieces that will be internal to the collector once it is assembled
- Starting with one of the thin wall pieces for Stage 2/MEDIUM, insert it into its grooves from the rear of the collector
  - Make sure that the correct end of the side piece is inserted into the groove
  - Gently tap on the edge sticking out to feed the thin wall piece into its groove
    - Try to evenly feed the wall piece in
    - It helps to push on the center of the external surface of the wall piece with your hand to minimize bowing and assist the wall into place
    - The Stage 2/MEDIUM wall pieces are more difficult to insert than the Stage 1/LARGE ones so it is easier to work with them first
  - As the wall piece gets closer to its final position it becomes increasingly difficult to push the plastic in (hammer harder)
- Once the wall piece is in position, take one of the plastic pieces with the triangular cross-section and use it to "loosely" attach the wall to Jet 2/MEDIUM
  - It is easiest to start this off with longer bolts than will ultimately be used (they can be replaced with shorter ones when needed).

Reproduced with permission of the copyright owner. Further reproduction prohibited without permission.

- "loosely" is in quotation marks, because the plastic walls will be pushing against the triangular piece
- the two triangular cross-section pieces used for attaching to Jet 2/MEDIUM are interchangeable to my knowledge (as are the four with a different bolt pattern used for Jet 1/LARGE and Jet 3/SMALL)

- Use the appropriate plastic piece to attach the other end of the thin side piece to the Jet 3/SMALL plate "loosely"
  - Use longer bolts initially as above
- Repeat the above steps for the other Stage 2/MEDIUM thin wall piece
- Repeat the above steps for the Stage 1/LARGE thin wall pieces
- When the four thin wall pieces are "loosely" in place, insert the Stage 3/SMALL (thick, curved) wall pieces and loosely bolt them into position
- Tighten all the nylon bolts
- Attach the exit stage
  - There are markings to orient the manifold plate and the exit stage
- The collection rods can also be re-assembled
  - Use the bolts to attach the Teflon surfaces to the Delrin
    - The surfaces are threaded
    - Teflon and Delrin have different thermal expansion/contraction coefficients and the Teflon will pop out at sub-freezing temperatures otherwise
- The collector should be re-washed (external surfaces too) and then placed into the giant rectangular Nalgene tub filled with (fresh) DI to soak some more
  - The giant Nalgene tub usually needs to be washed and rinsed prior to filling it with DI.

4. Drying
   - Put on gloves (I sometimes use longer neoprene gloves)
   - After soaking, the entire collector is removed from the tank and placed on a clean work surface for drying

Reproduced with permission of the copyright owner. Further reproduction prohibited without permission.

- Large garbage bags are sufficient
- It may be stood on one end to facilitate drying

- Cover the collector with garbage bags to prevent deposition
- The collection rods should be "collection surface-down" while drying
- Once dry, all openings in the collector body should be covered with parafilm taped into position (do not use duct tape)
- The collection surfaces/rods should be grouped into two sets
  - They are labeled "O" and "1" at the top of the collection rod
- The collector can now be bagged for the field and blanks can be taken from the collection surfaces
- Do not use Kimwipes to dry off the collector or collection surfaces
- Do not forget to take a complete set of materials into the field to allow for any field disassembly, thorough cleaning, etc.

5. Blanks
   - Blanks must be taken from the collection surfaces only
   - Using a spray bottle, apply approximately 5 – 10 ml of DI to the surface
   - Pipette the blank off (use the tip for collection)
     - Include the junction of the Delrin holder and the Teflon piece if you will be including sample from there while in the field
   - After blanks, the rods should be allowed to dry and then are grouped into sets and bagged for transport into the field
     - Small garbage bags usually work well

C.2 Field Installation

Reproduced with permission of the copyright owner. Further reproduction prohibited without permission.

There is a dedicated stand for the FROSTY collector which includes a metal wind shield and is mounted on a sheet of plywood (currently). The bottom plate of the FROSTY collector has four threaded holes where bolts passing through the stand can be inserted (not all of these are correctly aligned). The main body of the collector can be installed and the blower (GAST Regenair #R4P115) attached prior to sampling. Be aware that the length and position of the flexible hosing used can affect the flow rate. Currently a Sierra Instruments, Inc. mass flow meter (#760-N5-VI-PS-EZ) is attached between the blower and the collector. The flow straightener must be installed for this model to operate properly. The mass flow meter is calibrated for sea level and 25°C. Therefore calculations should be performed prior to sampling to ensure that the flow rate set corresponds to an actual volumetric flow rate of 1.5 m^3 min^{-1} during operation. The flow rate is adjusted with an attached ball valve. The blower and flow meter should be kept protected from ambient conditions. Keep the collector bagged and do not install the collection surfaces until sampling (although they should be kept cold).

C.3 Sampling

1. Preparing to Sample/Sampling
    - It must remain below freezing for the collector to operate successfully
        - Drops that do not freeze upon impact migrate over the edge of the collection surfaces
    - Get some gloves and a set of collection rods/surfaces
    - Go outside and orient the collector so it is perpendicular to the prevailing wind
        - This is to prevent sampling precipitation
        - Make sure there are no nearby obstructions that might affect sampling
    - Remove the covering bag and any material covering the ports for the collection rods and/or the collector inlet
    - Put on the gloves
    - Install the collection rods (from the top)

Reproduced with permission of the copyright owner. Further reproduction prohibited without permission.

- ➢ If it is snowing minimize exposure of the rods/surfaces to ambient conditions prior to inserting them into the collector
- ➢ Verify the surfaces are correctly aligned
  - ❖ The plastic tabs on the top of the collection rods should be parallel to the Jet plates

- Turn on the blower and check the flow rate (corresponding to 1.5 m^3 min^{-1} at ambient conditions)

2. Recovering Sample
   - Get the alternate set of collection rods/surfaces, clean plastic bags and gloves
     - ➢ We have special bags for the collection rods, although 2 gallon Ziplocs might work
   - Go outside and turn off the blower
   - Clear off any precipitation from around where the ports for the collection rods are
   - Put on the gloves
   - Remove each collection rod and place it in a clean plastic bag, taking care not to knock any sample off the surface
     - ➢ Having another person to hand these to can be useful, but this can be done by one person successfully
   - While the rod is removed, visually inspect the jet to see if it is riming up
     - ➢ Remove the rime if it is (with your gloves on)
     - ➢ This may not be possible to do for Jet 3/SMALL
   - Replace each collection rod with one from the alternate set before moving on to the next rod
   - Verify collection surface alignment
   - Turn the blower back on (again, check that the flow rate corresponds to 1.5 m^3 min^{-1} at ambient conditions)
   - This should take about 5 minutes (consecutive samples are possible)

Reproduced with permission of the copyright owner. Further reproduction prohibited without permission.

- Current protocol involves melting the collected samples in the field, and pipetting directly from the surface into vials/bottles for subsequent weighing and aliquoting
  - ➢ It is not clear that this procedure is necessarily appropriate for all conditions
  - ➢ We have also scraped the collected rime directly off using Teflon-coated scrapers and this has also worked well
    - ❖ Different scrapers must be used for each collection surface (and must be cleaned between samples)
    - ❖ The collected material is kept frozen until the return to the lab
- All collected material must be removed from each collection surface (even if not all of it is aliquoted) and the rods/surfaces placed into new clean bags for re-use
  - ➢ Do not rinse the collection surfaces with DI during an event unless there is a known problem

3. After an event
   - Depending upon the build-up of rime on the internal surfaces of the collector, it may or may not be necessary to clean the main body between events
   - If there was substantial build-up, remove the collector from the stand and take it inside
   - Do not disassemble the collector but scrub it as possible with DI and rinse it thoroughly
     - ➢ Some of the bolts can be loosened, but the collection rod ports can be used for reasonable access to the internal spaces of the collector
     - ➢ The exit stage can be removed for access to Stage 3/SMALL
     - ➢ Q-tips may be useful
   - If possible, place the main body into the large Nalgene tub for soaking
   - The collection rods/surfaces should be thoroughly scrubbed with DI and left to soak
   - The main body and rods need to be dried and either re-installed or bagged prior to the next event

Reproduced with permission of the copyright owner. Further reproduction prohibited without permission.

D. Appendix: The CSU 5-Stage Collector: Cleaning & Sampling Protocol

This appendix describes how to assemble and prepare the 5-Stage for successful field operation, and the steps required during sampling to achieve it. It ends with a short "quick" sampling checklist. The 5-Stage is used to obtain samples for trace metal quantification – do not use metal fasteners to assemble it.

D.1 Major Cleaning

This section describes how to clean the collector before/after a campaign.

1. Remove any material from inside the giant rectangular Nalgene tub, wash the insides (and under the cover) with dilute Triton-X and Kimwipes, rinse off with DI and start filling the tank
    - The tank will need to be half to two-thirds full and this takes several hours
    - Keep the tank largely covered while filling
    - There should not be any obvious grime on the tank's interior

2. Disassemble the 5-Stage collector
    - Remove all the lids and separate their neoprene gaskets (the handles can stay attached)
    - The main body can be separated between Stages 2 and 3 which assists handling
    - Remove the exit stage including the manifold plate and the Stage 5 lip

3. Wash all the parts individually

Reproduced with permission of the copyright owner. Further reproduction prohibited without permission.

- Do this three times – dilute Triton-X, methanol, dilute Triton-X
- Use gloves (and don't forget that the surface of the gloves and the Kimwipes and other tools are not "clean")
- Use Kimwipes, Q-tips, test-tube brush, toothbrush, etc.
  - Make sure that all internal surfaces get thoroughly cleaned (particularly the jets) which the toothbrush and Q-tips are good for
  - Limit the exposure of the internal surfaces to any metal objects
- After each wash, rinse thoroughly with DI
- After the last wash, place each item into the giant tub to soak
  - Only the 5-Stage lip floats (it is polypropylene)
  - As all surfaces soak together, external surfaces should also be cleaned well
  - The only item that does not go into the tub is the Jet 1 cover (its fasteners are metal). It can just be left to dry (internal surface facing down)
  - While washing, it is a good idea to check to make sure that all the epoxy seams remain sealed and that the physical and chemical integrity of the collector is not compromised in any way (e.g. no imbedded metal or visible grime on internal surfaces, and/or cracks in the Delrin).

4. Close the tank's lid when there is enough water to adequately cover the collector's parts and leave it to soak for a few days. DI can be added periodically for dilution.

5. While the collector is soaking, clean all of the spatulas
   - Clean all the spatulas using the same general procedure outlined
     - Dilute Triton-X, rinse with DI, methanol, rinse with DI, dilute Triton-X, rinse thoroughly with DI
     - Blades and handles
   - Do this even though the rubber spatulas should be kept clean at all times anyway

Reproduced with permission of the copyright owner. Further reproduction prohibited without permission.

- There are several large 4 liter Nalgene wide-mouth bottles which are used to soak the spatulas in DI
  - ➢ Handles should be "up" in the bottles
- After soaking for a few days (the DI can be refreshed during this step), the spatulas can be removed carefully
  - ➢ Wear gloves and minimize handling
  - ➢ Hold the spatula only by the very end of the handle between a finger and thumb
  - ➢ Remove excess DI by either flicking your wrist quickly while holding a spatula's handle, or rapping the handle on a convenient clean, plastic surface (e.g. bottle lip)
    - ❖ Water must be removed from both the handle and the blade
    - ❖ Do not dry or wipe off the handle with a Kimwipe
  - ➢ Place each spatula individually into its own Ziploc bag and seal it
  - ➢ Place complete sets of spatulas (2 x large, 2 x small, 1 x small notched for Stages 1 – 5) together
    - ❖ There are at least 6 complete sets and some extras

6. Carefully remove the 5-Stage parts from the tub after soaking and place them on a clean surface to dry
   - Use large garbage bags to prepare the surface
   - Place parts to minimize the possibility of contamination while drying
   - Cover loosely with garbage bags while drying
   - If necessary, a clean spatula can be used to push water off the internal surfaces to assist drying
   - This may take some time to complete (a day)

7. Assemble the collector (when it is dry)
   - The Stage 5 lip must be installed

Reproduced with permission of the copyright owner. Further reproduction prohibited without permission.

- There are notches carved in it – the lip should extend the same distance over the edge of the collection surface.
- There are markings on the exit stage and manifold plate to orient them correctly

- If blanks are not going to be taken immediately, cover over the cryovial holes (or insert cryovials), exit stage outlet, and the Jet 1 inlet with parafilm (and place the Jet 1 cover on for shipping)

8. Take blanks
   - Prior to a field campaign take a more extensive set of blanks than you would in the field
   - Use either spray or squirt bottles (spray is preferred)
   - Do not use excessive amounts of DI when taking the blank
     - Spray every collection surface down with lots of fresh DI and let it run out
       - For Stage 1, go through the Jet 1 inlet
       - Attach a 5 ml cryovial and spray down again for the blank itself
     - Take a blank off the underside of every lid
       - Collect the blank using the pipette tip
     - Take blanks of an assortment of spatula blades
       - Do enough to get good statistics
   - After taking the blanks, let the collector dry again and prepare it for travel/storage
     - Cover all the openings and bag the collector
       - Do not travel with cryovials installed in the collector
       - Do not travel with the collector disassembled
       - Tape the lids on (use electrical/vinyl – not duct – tape)
       - When packing, take care that each stage is supported to minimize strain on the seams
       - Take a full set of cleaning equipment and substitute parts into the field

Reproduced with permission of the copyright owner. Further reproduction prohibited without permission.

D.2 Field Installation

The 5-Stage should only be operated on its dedicated stand. Unless extreme weather conditions exist, the 5-Stage can be stored between events on its stand (it actually did blow over at Whiteface so be conservative). Cryovials should be installed (these can be exchanged for new ones at the start of sampling) and the Jet 1 cover kept on. The windshield must be installed (even in radiation fogs) for consistency. The stand should not be kept at a 45° angle between events. A few large garbage bags slit down the side are sufficient to cover the collector and can be kept on with bungee cords. Make sure that the collector (including the exit stage) is completely protected. Keep the pump (GAST Regenair #R4P115) attached. A Sierra Instruments, Inc. mass flow meter (#760-N5-VI-PS-EZ) is installed between the pump and the 5-Stage (it is housed in the pump box). The flow straightener must be installed for an accurate reading, and be aware that the length and position of the flexible hosing used can affect the flow rate. The mass flow meter is calibrated at 25°C and sea level conditions, so appropriate corrections must be calculated to ensure that the volumetric flow rate is set a 2.0 m^3 min^{-1} during operation. The pump and mass flow meter should be protected from the environment prior to sampling (keep the pump box closed).

D.3 Sampling

As a general rule, do not let any part of the spatula that you have handled (even with gloves on) touch any part of the interior of the collector. This is why the spatulas are stored individually and is (one of the reasons) different ones are used for each stage and each sample during an event. The 5-Stage does not collect sufficient volume to "clean" itself once it has become contaminated during an event. Therefore if there is any chance a spatula, glove or cryovial/bottle is dirty or contaminated, replace it before contact with the 5-Stage.

1. Preparing to sample

Reproduced with permission of the copyright owner. Further reproduction prohibited without permission.

- If the collector is not on its stand (e.g. drying inside), take it outside and re-install it on its stand
- label 5 x 5 ml cryovials #1 - #5 for each stage and place in a clean small Ziploc
  - ➢ if using the cryovial/30ml bottle adapter for the first/all stages substitute 30 ml (or other size) bottles as needed
  - ➢ weigh bottles individually if necessary
- once outside
  - ➢ orient the collector in the direction of the prevailing wind (or at least the other collectors)
    - ❖ make sure there are no upstream obstacles that might impact sampling
  - ➢ remove the covering garbage bags
    - ❖ attach the cryovials/vials (retain caps in the small Ziploc)
    - ❖ wear gloves
- move the stand to the 45° sampling angle and bolt the arms in place

2. Sampling
   - remove the Jet 1 cover and place it in a clean plastic bag (small garbage or 2 gallon Ziploc)
   - plug in the blower
   - check the flow rate (the volumetric flow rate should be set for 2.0 m^3 min^{-1} at ambient conditions)
     - ➢ this should be checked periodically to establish the uncertainty (while some fluctuations are expected, there will not be a large change unless there is a problem)
   - the sf-CASCC should be run concurrently over the same sampling interval
     - ➢ 1+ hours may be necessary depending upon the LWC and drop-size distribution
     - ➢ ideally some volume should be recovered from each stage
       - ❖ collected water can be observed in the attached vials/bottles during operation

Reproduced with permission of the copyright owner. Further reproduction prohibited without permission.

- do NOT
  - hit the collector to "encourage" sample flow
  - operate the collector without the lids and vials/bottles attached
  - walk directly in front of the collector's inlet during operation
- Usually the 5-Stage is kept off-line for one sf-CASCC/CASCC2 sampling period after its sampling period to permit adequate time for collection
- If the collector's internal surfaces are wet from cleaning at the start of an event, waste the first 20 – 30 minutes of sample (the limiting factors are the rear stages).
  - Scrape down the internal surfaces with spatulas prior to the "real" start and replace the collection vials/bottles

- label a new set of 5 x 5 ml cryovials/30 ml vials

3. Recovering sample
   - unplug the blower
     - if current surge from plugging/unplugging is problematic, leave the pump on and instead loosen the hose clamp at the back and remove the flexible hose
   - replace the Jet 1 cover on Jet 1
   - DO NOT hit the top of the collector to encourage sampled drop flow
     - Given the large internal losses in the collector and that the collection efficiency curves do not include drops that do not deposit on the collection surface itself, we do not want to collect any drops that are not where they are "supposed" to be
   - remove Lid 1 and use the spatula to push sample off the collection surface only into the attached cryovial/bottle
     - it will likely require a few swipes with the spatula to remove most of the water
     - Do not let the spatula handle (or your glove) touch any of the internal surfaces
     - The underside of Lid 1 should not be contaminated during collection
   - remove the attached cryovial/bottle and cap it

Reproduced with permission of the copyright owner. Further reproduction prohibited without permission.

- note if any collected material is lost
  - switch to a larger vial for the next sampling period
- at this point if visible drops are collected on the backside of the jet plates, on the underside of the lid, etc. the spatula can be used to wipe them off
- let any "extra" water drain out completely

- replace the lid
- put the used spatula into a "used spatula" Ziploc
- attach the correct new labeled cryovial/bottle to the collector
- repeat for Stages 2 – 5 (V2 – V5)
- the time required to recover the samples is 5 - 10 minutes and it is easier with two people
- to re-start the collector:
  - remove the Jet 1 cover
  - re-attach the hose (if the blower remains on) or turn on the blower
  - Check the flow rate!
- In the log book, record if any water was lost during collection and whether large amounts of water were observed on non-collection surfaces. Indicate if the non-collection surfaces were wiped off with spatulas. Record the flow rate.

4. After Sampling
   - replace the Jet 1 cover
   - clean the collector after each use (including scrapers and lids)
     - the "severity" of the field cleaning depends upon the event - at a minimum it needs to be liberally rinsed internally after scrubbing (both with DI). The 4 liter Nalgene jars are useful for this.
       - use toothbrush, Q-tips, brushes to get at all surfaces (particularly the internal jets)
       - Don't forget to remove the pump hose prior to rinsing

Reproduced with permission of the copyright owner. Further reproduction prohibited without permission.

- take blanks as in the lab
  - ➢ individual stage blanks only (but use the spatulas to scrape)
  - ➢ do not take separate spatula or lid blanks unless there is some concern
- scrape the internal surfaces down with spatulas to remove as much water as possible
  - ➢ do NOT re-use the spatula used for the blank unless it is immediately after taking the blank
- Replace the Jet 1 cover and lids (also cleaned/rinsed)
- Either take the collector inside to dry or bag it on the stand ready for the next event
  - ➢ If left on the stand, make sure to re-attach the pump

5. Spatulas
   - Individual spatulas should be used once only during an event
   - Used spatulas should be rinsed with DI reasonably soon after their use (do not wait for days as the rubber may be absorbent)
   - Clean spatulas individually by scrubbing with DI between events
     - ➢ If they clearly start to develop a black film, use 1:100 Triton-X and/or alcohol to clean them and then scrub with DI.
     - ➢ Soak in DI in the 4 liter Nalgene bottles taken into the field

Reproduced with permission of the copyright owner. Further reproduction prohibited without permission.

D.4 5-Stage Collector – QUICK Sampling List

1. Label the "next" set of cryovials/bottles prior to retrieving the sample (and weigh if necessary)
2. Take at least one clean spatula set out with you (already separated into clean Ziplocs) (extras are useful to have handy)
3. Turn the blower off
4. Put the Jet 1 cover ON Jet 1
5. Put on gloves
6. Stage-by-stage, remove the lids, use the appropriate spatula to scrape down the collection surface, remove the cryovial/bottle, and cap it. Scrape down any non-collection surfaces (including lids) if needed. Replace the collector lid and insert a new labeled cryovial/bottle. Do not place a used spatula in the clean Ziplocs with the remaining clean spatulas. Minimize the time your fingers/hand are inside the collector and be careful not to touch the walls (even with gloves on). If there are any concerns about whether a spatula or vial is clean, just replace with another one. Do not hit the collector to assist sample recovery.
7. To resume sampling, take the Jet 1 cover OFF Jet 1 (and bag it)
8. Turn the blower on
9. CHECK THE FLOW RATE (set for 2.0 m^3 min^{-1} for all elevations/conditions). Don't forget to record the mean value in the log.
10. Once the sample is retrieved, rinse the used spatulas with DI

Reproduced with permission of the copyright owner. Further reproduction prohibited without permission.

E. Appendix: Drop stopping distance and characteristic times for varying ambient conditions

Ground-based intercepted clouds may occur and be sampled in highly dynamic environments. In particular, orographic clouds can have relatively high wind velocities associated with them. At ACE-2 in extreme conditions ambient horizontal velocities in excess of 17 m s^{-1} (approximately 40 mph) were recorded in-cloud. At Whiteface, ambient wind speeds did not exceed 10 m s^{-1}, and in the Davis fogs the mean ambient wind speed was generally 0.5 – 1 m s^{-1}. This appendix presents a first order analysis of whether or not elevated ambient wind speeds may impact the performance of the CASCC collectors. Focusing on the sf-CASCC and the CASCC2, the potential for changes in collection efficiency – particularly the size cut between sf-CASCC stages – will be investigated for a range of reasonable conditions. Anisokinetic sampling is discussed elsewhere (Chapter 2). Here stopping distances and characteristic times are used to investigate whether or not drops (particularly "off-axis" ones) can stop in time to follow the (turbulent) streamlines through the collector and be collected as theory predicts. Therefore, the two aspects to be investigated are whether (a) the sf-CASCC's Large fraction D_{p50} changes, and (b) whether all aspirated drops can reach the collection surfaces in both the sf-CASCC and the CASCC2.

This analysis does not consider whether or not there is a wind-ramming effect through the collectors. The large pressure drops through the 5-Stage/pump and FROSTY/pump systems and observed oscillations in the measured flow rate through each while sampling suggest that they will be less susceptible to wind-ramming than the CASCCs. However, collection efficiency, particularly in the 5-Stage may be affected. In Stage 1 (V1) of the 5-Stage, all incident drops of sufficient inertia at high ambient velocities should be collected as insufficient time/distance exist for them to "relax" to the collector's inlet velocity. The wind shield may interfere with this simple

Reproduced with permission of the copyright owner. Further reproduction prohibited without permission.

analysis. FROSTY is not oriented into the wind so this should not be an issue. Data are not available to consider this point.

E.1 High wind conditions and collector performance

The ACE-2 wind velocities prompted the question of whether or not high winds change the sampling efficiency of the collectors, particularly the sf-CASCC. Drops may not relax to the sampling velocity quickly enough, and smaller drops than predicted may be collected on the sf-CASCC's Large stage, given sufficient drop inertia due to ambient winds that exceed the sampling velocity. In particular, larger drops (up to 47μm were reported) entering the collectors on "off-axis" or skewed trajectories may be lost if they also do not relax to the sampling velocity. In order to investigate whether or not these issues are important, a simple comparison of residence times, collector dimensions, drop stopping distances and characteristic times was performed. Drop losses within the collector, but upstream of the collection rods can be thought of as the transmission efficiency (discussed in Appendix B). Transmission efficiencies have been assumed to be perfect in the field performance calculations (Chapters 3 and 4), although field observations indicate inlet losses occur.

E.1.1 Collector residence times

The dimension L_i – the distance from the inlet to the mid-point of the first collection rods/strands – and sampling velocity, Vel_i, are used to calculate the mean residence time, T_i, for the sampled air inside the collector:

$$T_i = {}^{L_i}\!/_{Vel_i} \qquad \text{(E-1)}$$

Reproduced with permission of the copyright owner. Further reproduction prohibited without permission.

where i indicates the collector. For the velocities reported by Demoz et al. (1996), $T_{sfC} \approx 21$ ms and $T_{C2} \approx 10$ ms ($L_{sfC} \approx 14$ cm and $L_{C2} \approx 8.7$ cm).

E.1.2 Drop stopping distance and characteristic times

Drops from 5 – 50 μm often have particle Reynolds numbers (Re_p) that exceed 1 and may not be in the Stokes flow regime. Re_p is defined as:

$$\mathrm{Re}_p = \frac{VelD_p}{\nu} \qquad \text{(E-2).}$$

For these high Re_p number drops (up to $Re_p < 1500$), their stopping distance can be calculated using the empirical correlation attributed to Mercer (1973, p. 41):

$$St = \frac{\rho_p D_p}{\rho_a}\left[\mathrm{Re}_0^{1/3} - \sqrt{6}\arctan\left(\frac{\mathrm{Re}_0^{1/3}}{\sqrt{6}}\right)\right] \qquad \text{(E-3)}$$

where the arctangent is in radians (there is a typo in the same equation given in Brockmann (1993), as equation E-3 was verified against the citation provided). A drop's initial Reynolds number, Re_0, is defined as:

$$\mathrm{Re}_0 = \frac{V_0 D_p}{\nu} \qquad \text{(E-4).}$$

Drop characteristic time is defined as the time to 95% of the stopping distance as calculated by (E-3). Fuchs (1964, p. 77) provides a useful equation for the characteristic time:

Reproduced with permission of the copyright owner. Further reproduction prohibited without permission.

$$\int_{Re_1}^{Re_2} \frac{d\,\mathrm{Re}}{C_D\,\mathrm{Re}^2} = -\frac{3\mu(t_2 - t_1)}{4D_p^2\rho_p} \qquad \text{(E-5).}$$

Taking the derivative form of (E-5), the equation can be re-arranged to find dt:

$$dt = -\frac{4D_p^2\rho_p d\,\mathrm{Re}}{3\mu C_D\,\mathrm{Re}^2} \qquad \text{(E-6).}$$

Equation E-6 is used in lieu of (E-5) because C_D is a function of Re in this range (Re < 1000). The empirical correlation used to determine C_D is:

$$C_D = \left(\frac{24}{\mathrm{Re}}\right)\left(1 + 0.15\,\mathrm{Re}^{0.687}\right) \qquad \text{(E-7)}$$

(Hinds, 1999, p. 44). Fuchs (1964) appears to be the original source of the equation presented by Mercer (1973), hence the applicability of using equations E-3 and E-5 together. For drops where Stokes flow was applicable, the stopping distance and characteristic time were calculated via:

$$St = V_0\tau' \qquad \text{(E-8),}$$

$$\tau' = \frac{\rho_p D_p^2}{18\mu} \qquad \text{(E-9), and}$$

$$\tau = 3\tau' \qquad \text{(E-10)}$$

where the Cunningham slip correction factor is ignored (Hinds, 1999). Equation E-10 converts the characteristic time to the 95% characteristic time so both Stokes and non-Stokes calculations can be compared.

Reproduced with permission of the copyright owner. Further reproduction prohibited without permission.

For a given set of conditions and drop size, Re_p was calculated using equations E-2 – E-4, and E-5 – E-10. If $Re_p < 2$, St and τ for Stokes conditions (slightly relaxed) were calculated. The Re_p criterion was relaxed as equation E-3 did not appear to be optimized for near-Stokes conditions. Otherwise, St was calculated using (E-3), and then equation E-6 was numerically integrated to determine the time necessary for the drop to travel 0.95S. Four sets of ambient conditions approximately corresponding to the 5-Stage design, Davis, Whiteface and ACE-2 sampling conditions were investigated. Drop diameters investigated were 5, 10, 12, 14, 16, 18, 20, 25, 30, 40, and 50 μm. Ambient wind speeds up to 20 m s^{-1} were considered. The diameters were chosen to investigate response around the sf-CASCC's D_{p50}.

The stopping distance and characteristic time results for the ACE-2 conditions are shown in figures E-1 and E-2. The maximum difference, for a given drop size and ambient velocity, between the four sets of conditions was only on the order of 5% (not shown). Therefore only the ACE-2 results will be presented as concerns raised during that campaign motivated this work.

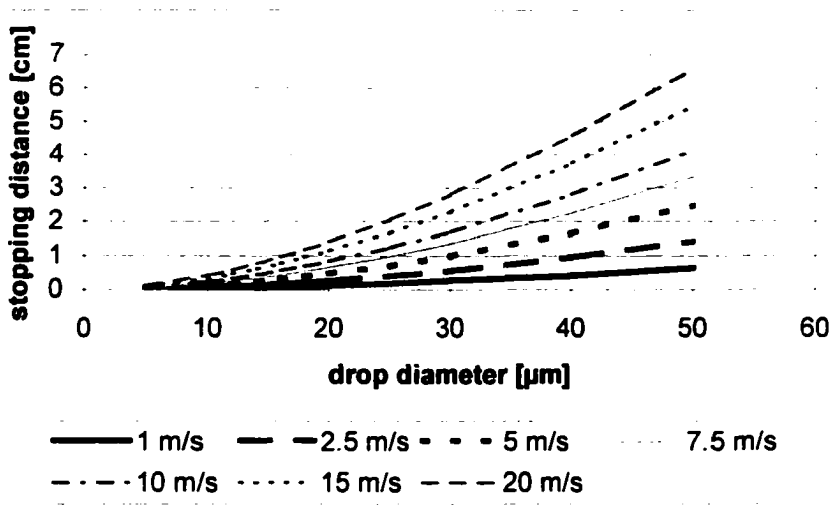

Figure E-1: ACE-2 conditions: drop stopping distance as a function of ambient wind speed

Reproduced with permission of the copyright owner. Further reproduction prohibited without permission.

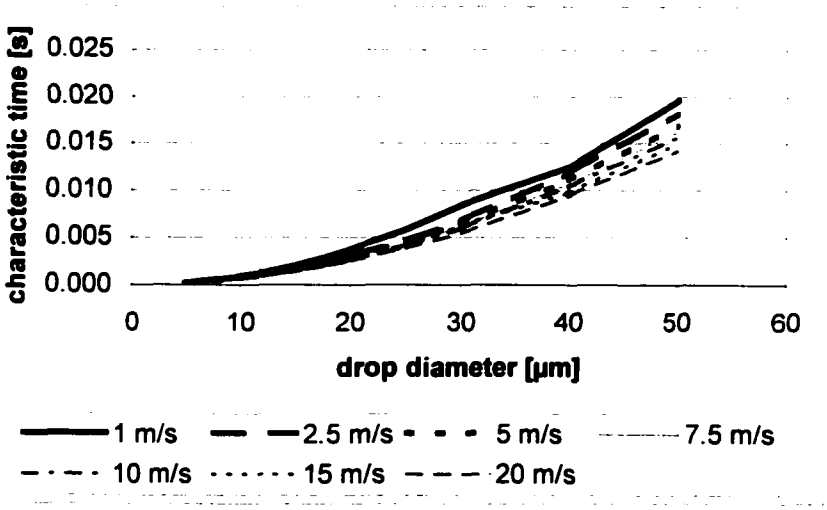

Figure E-2: ACE-2 conditions: time to 95% of the stopping distance as a function of ambient wind speed

Stopping distances increase with the drop inertia (from increasing size and/or velocity). The characteristic times decrease as the velocity increases consistent with results reported by both Fuchs (1964) and Hinds (1999). As drops have more drag in the transition regime than Stokes flow predicts, they stop more quickly (see Bird, Stewart and Lightfoot (1960, figure 6.3-1 (p. 192)) for a plot of C_D vs. Re). It is necessary to look at both drop stopping distance and characteristic time as the collectors represent a confined space, and the fluid inside the collector is moving. A drop may be not be collected if its stopping distance is greater than the length available for it to stop in even if its relaxation time is much shorter than the residence time upstream of the collection rods for the nominal sampling velocity.

Considering the residence vs. characteristic time comparison first, sf-CASCC's residence time upstream of the rods is at least an order of magnitude greater than the characteristic times for all drops up to 20 μm in diameter for all velocities. For larger drops, the sf-CASCC's residence time remains greater than their characteristic times, but decreases to a factor of 1.1 – 1.5 times the 50 μm drop's characteristic time. As the CASCC2 is both smaller and has a higher sampling

Reproduced with permission of the copyright owner. Further reproduction prohibited without permission.

velocity, its upstream residence time is only an order of magnitude greater than the characteristic times for 5 μm drops for all velocities. As the velocities and drop sizes increase, the CASCC2's upstream residence time remains larger than the characteristis times of drops only up to approximately 40 μm in diameter. The characteristic times for 50 μm drops exceed the CASCC2's upstream residence time by up to a factor of 2.

Comparing the stopping distances to the collector lengths upstream of the rods yields similar results. For both collectors, St for all drops at 1 m s^{-1} is at least an order of magnitude less than the respective L_is. As velocities increase, this remains true for smaller drop sizes only – through 30 μm at 10 m s^{-1} and 20 μm at 20 m s^{-1} for the sf-CASCC and 20μm and 15 μm for the CASCC2 for the same speeds. This is consistent with $L_{sfC} > L_{C2}$.

E.1.3 Implications

This is a first order approximation. A real simulation of ambient conditions would require extensive modeling using a computational fluid dynamics code. I assume equation E-3 is for the total stopping distance. These calculations assume that relaxation to a fluid at rest is required. Of course, the drops would only need to relax to the sampling velocity in the collectors.

The residence time calculations assume the drops come under the influence of the collector's sampling velocity only as they pass its entrance. Pressure measurements indicate there is a "bow-wave" that extends upstream of the collection surfaces which will affect impaction. The conditions inside the collector are expected to be highly turbulent which should impact drop deposition, but are not quantified.

Given these caveats, however, the results do suggest that the size cut of the sf-CASCC is not affected by high ambient winds. Drops < 25 μm in diameter should relax to the sampling velocity well upstream of the Teflon rods. Detailed modeling of the sf-CASCC to investigate cut-size

Reproduced with permission of the copyright owner. Further reproduction prohibited without permission.

changes in high wind conditions does not appear to be warranted unless future measurements indicate wind-ramming is occurring.

Due to the CASCC2's smaller size and higher sampling velocity, its performance is not quite the same as the sf-CASCC's. Most drops under most conditions should be collected the same by both. However, if turbulence scales with velocity, it is possible that the CASCC2 has higher losses to the walls upstream of the collection strands than might be observed in the sf-CASCC with a larger opening and longer upstream residence time. This is difficult to assess observationally.

Reproduced with permission of the copyright owner. Further reproduction prohibited without permission.

F. Appendix: the wind shield (baffle)

Axel Berner and his co-workers have spearheaded the development of wind shields or baffles for cloud water collectors (Berner *et al.*, 1998; Kruisz *et al.*, 1992). The presence of the wind shield downstream from the collector inlet – particularly one not oriented into the wind – in moderate or high winds can improve the collector's aspiration efficiency to approaching 100% (Berner *et al.*, 1998). Under varying ambient conditions, the non-ideal aspiration efficiency of the vertically–oriented inlets used in Berner and co-workers' collectors (Berner *et al.*, 1998; Kruisz *et al.*, 1992; Berner, 1988) without wind shields has resulted in inconsistent drop sampling, and has been suggested to explain some observed performance differences between co-located collectors (Schell *et al.*, 1992). While the benefit of a wind shield is a function of environmental conditions, idealized performance can be calculated based upon simple approximations. The goal is to create a stagnation region that does not distort the ambient drop distribution upstream of the wind shield from which drops can be aspirated into the collector. Wind shield design is governed theoretically by the assumed ambient conditions including the drop size distribution. Critical parameters include the maximum wind speed likely and smallest drop size lost. If the actual wind speed is lower, larger drops, if present, may be collected.

Berner and Kruisz (1997) published an equation for wind shield design:

$$W = \frac{8\left(D_{crit}^2 U_0\right)}{18\mu} \qquad \text{(F-1)}$$

where the density of water is implied in the numerator (and, in fact, must be included depending upon the units used). The factor of "8" in the numerator appears to represent the theoretical St_{crit}

Reproduced with permission of the copyright owner. Further reproduction prohibited without permission.

for flow past a cylinder (=1/8) (Friedlander, 2000, p. 107). St_{crit} is the maximum Stokes number for a drop corresponding to 0% collection efficiency. This interpretation is consistent with St_{crit} if W is defined as a half-width (or radius) (Friedlander, 2000). The assumptions behind equation F-1 are not given and the accompanying numerical example appears to have an error in it. Berner and Kruisz (1997) briefly describe some wind tunnel testing used to validate their approach. To my knowledge, these results were never quantifiably reported and for the parameters given, only the Stokes flow regime ($Re_p < 0.5$) appears to have been investigated. However, for the drop sizes and ambient conditions of most concern in this application, Stokes flow is not likely except for the smallest drops (< 5 μm approximately).

In response to an e-mail, Dr. Berner indicated that the following equation should be used to design the wind shield:

$$W = \frac{D_{crit}^2 U_0}{18\mu(0.4)} \qquad \text{(F-2)}$$

where, again, drop density is implied in the numerator (Berner, 1996). In this instance, St_{crit} was explicitly stated to be 0.4, although in retrospect it is not clear if W corresponds to a half-width or full width. The key point is that drops do not reach the baffle: in other words, their stopping distance upon reaching the stagnation region is short enough to avoid collection by the baffle (Berner, 1996). It is not known how the value of 0.4 is arrived at. It may be an empirical value derived from the unreported wind tunnel tests. It does not correspond to any reasonably appropriate St_{crit} value reported even allowing for variations in the definition of the Stokes number itself (Fuchs, 1964, p. 164). Further, it does not correspond to the 0% collection efficiencies reported for flow past a variety of objects in cross-flow (May and Clifford, 1967). A Stokes number (defined strictly as the ratio between the drop stopping distance/collector width) of this magnitude corresponds to a collection efficiency of approximately 10 – 30% for flow past simple objects (May and Clifford, 1967). As before, equation F-2 appears to imply that Stokes flow is an

Reproduced with permission of the copyright owner. Further reproduction prohibited without permission.

appropriate approximation. However, if this value is an empirical one it may incorporate non-Stokes flow effects.

In practice, both the FROSTY and 5-Stage wind shields need to extend beyond the length of the jet to avoid end effects and promote uniform sampling conditions along the entire jet length. This constraint results in a minimum size requirement for each collector's wind shield. Further, there is some limitation on wind shield placement relative to the inlets due to collector geometry. For the 5-Stage a square 55.9 cm x 55.9 cm wind shield could be located 10.2 cm behind the inlet centerline. For FROSTY, a 50 cm x 70 cm wind shield could not easily be located closer than 16 cm. For both collectors, these wind shield dimensions correspond approximately to the minimum size possible. Comparatively, the CWS impactor's single vertical inlet has a centerline 5 cm upstream of the 50 cm x 70 cm wind shield (Kruisz *et al.*, 1992). The depth of the stagnation region is not known. Therefore, the stopping distance calculations from the inlet centerline to the wind shields can be used to verify results (this implies that distance is the minimum depth of the stagnation region). These calculations cannot be used as a primary design tool. Given the difference between and the uncertainty regarding the two reported equations above, they were also not used as the primary basis to evaluate the wind shields' designs. The wind shields were modeled as simple discs in cross-flow (May and Clifford, 1967), although cylinders in cross-flow were also investigated as their use appeared to be implied in equation F-1. The Stokes numbers (as defined) were extracted for 0, 20, and 50% efficiency (see table F-1). Stopping distance calculations were performed using the empirically-derived formula for non-Stokes regime particles (equation E-3) (Mercer, 1973).

A range of conditions were investigated spanning the design conditions for both FROSTY (3000 m elevation standard atmosphere) and the 5-Stage (sea level, 25°C) as well as observed field conditions. For FROSTY, this included winds up to 15 m s^{-1} as experienced at SPL. Winds up to 11.7 m s^{-1} (25 mph) and temperatures down to freezing were used for the 5-Stage. Selected

Reproduced with permission of the copyright owner. Further reproduction prohibited without permission.

Table F-1: Stokes numbers as a function of collection efficiency for discs and cylinders in cross-flow (extracted from (May and Clifford, 1967)).

collection efficiency	Corresponding Stokes number	
	disc	cylinder
0%	0.1	0.06
20%	0.2	0.3
50%	0.4	0.8

results are shown in table F-2. Cylinders tend to yield smaller "no collection" diameters compared to the discs, but discs tend to have smaller diameters at 20% collection efficiency, consistent with the Stokes numbers reported in table F-1. As the wind speed increases, the drop diameters collected with a specific efficiency get smaller.

Given likely operating conditions, these results suggest virtually all drops in the sizes expected (and observed at Whiteface, SPL and Horsetooth by other devices) should not be interfered with, and the wind shields should not change the drop distribution aspirated into the collectors. The presumption is that if a drop is not collected in significant quantities by the wind shield then it will be aspirated into the collector with high efficiency. These results are consistent with limiting the use of the 5-Stage, however, in wind speeds in excess of 10 m s^{-1}. For higher wind speeds, a larger shield may be required depending upon the drop sizes of interest. As an additional check, equations F-1 and F-2 were used and yielded similar results, although the appropriate dimensions to use had to be assumed. Further, the stopping distances calculated for drops collected with 0% efficiency were generally smaller than or equal to the distance from the centerline of the inlet jet to the wind shield (within the uncertainty of the drop size determination). The error associated with assuming Stokes law holds for these

Reproduced with permission of the copyright owner. Further reproduction prohibited without permission.

Table F-2: Drop diameters for 10, 20 and 50% collection efficiency on the wind shields

scenario	disc			cylinder		
	D_0	D_{20}	D_{50}	D_0	D_{20}	D_{50}
	[μm]	[μm]	[μm]	[μm]	[μm]	[μm]
5-Stage: design (11.7 m s^{-1})	60	90	135	45	115	210
5-Stage: sea level, 0°C, 2 m s^{-1}	120	175	265	90	225	400
5-Stage: sea level, 0°C, 10 m s^{-1}	60	90	140	45	120	220
5-Stage: Whiteface & 5 m s^{-1}	80	120	180	60	150	270
5-Stage: Whiteface & 10 m s^{-1}	60	90	135	45	115	210
FROSTY: design & 15 m s^{-1}	45	80	125	40	105	195

particles is shown in figure F-1 which compares the "actual" drop diameter with the equivalent "Stokes law" diameter for the 5-Stage design conditions. Divergence between the two increases sharply as the drop size increases. While the difference is not large for 50 μm drops, Berner and co-workers report that 100 μm drops are not interfered with using their formula (Berner and Kruisz, 1997).

Finally, no drips have been observed to fall from the 5-Stage wind shield into the collector (the rear edge of the wind shield is behind the inlet which protrudes from the front of the collector.

How much the wind shield may help or hinder drop aspiration is actually difficult to ascertain without either modeling the entire flow field around the collector and its stand or performing wind tunnel experiments. Some theoretical development is possible – see (Berner *et al.*, 1998; Vincent, 1989) for example – but it is not clear how actual practice compromises the theory. The collectors themselves will distort the flow in front of the wind shields and the critical factor – the

Reproduced with permission of the copyright owner. Further reproduction prohibited without permission.

depth of the stagnation region – will also depend upon the collector. The stagnation region will be itself a function of atmospheric turbulence and velocity. In so far as these calculations and

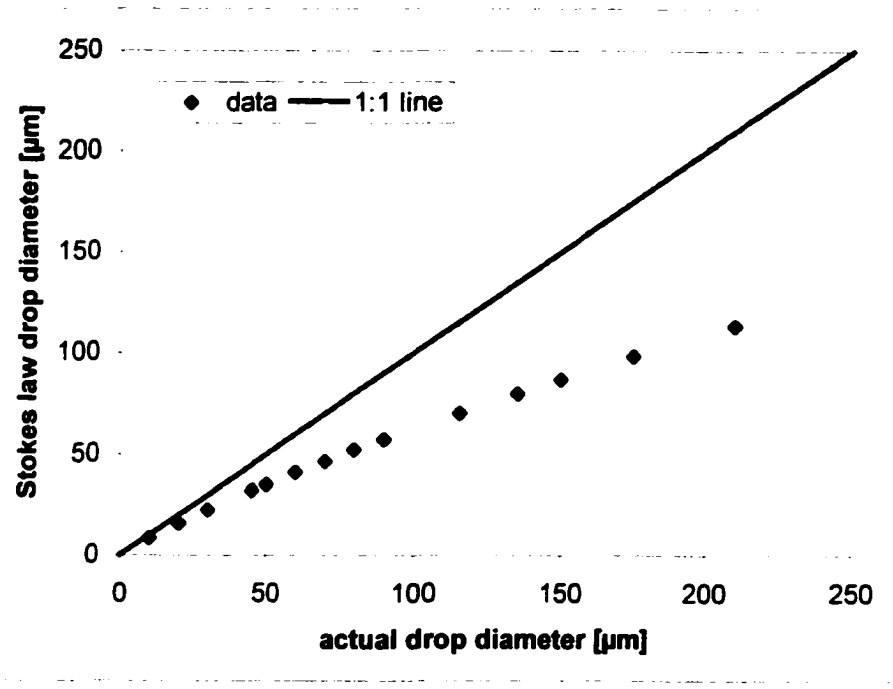

Figure F-1: Stokes law drop diameter vs. actual drop diameter for the 5-Stage wind shield design conditions (25°C, sea level, 11.7 m s^{-1} wind)

assumptions are applicable, however, the wind shields should not change the drop distribution. It is worth noting, moreover, that the 5-Stage collector is oriented in the direction of the wind (albeit at a 40° angle to it) which should help its aspiration efficiency. The wind shield is relatively more important for FROSTY whose inlet is at right angles to the ambient wind to avoid aspirating precipitation. CWS field performance reported at Jungfraujoch indicates that some drop losses are observed despite the wind shield in the extreme conditions experienced there (Baltensperger *et al.*, 1998). Field performance validation of the collectors with the wind shields attached may or may not be able to demonstrate their utility given the uncertainties involved in the calculations.

Finally, May and Clifford's experiments were performed where the Reynolds number of the discs varied from 165 – 8500 (May and Clifford, 1967). While their experiments extend into the

Reproduced with permission of the copyright owner. Further reproduction prohibited without permission.

turbulent regime, it is worth noting that the Re of the 5-Stage windshield is approximately 440,000 at design conditions.

Reproduced with permission of the copyright owner. Further reproduction prohibited without permission.

G. Appendix: Drop size distributions – instruments, problems and processing

This appendix describes the instruments used to measure ambient drop size distributions, identified problems with the data generated, estimates of the associated error, and the procedures used to process the raw data for use. Correction, processing and data validation steps are described in relation to the field campaigns with Whiteface as the model.

The goal is to determine the actual ambient drop volume size distribution. With this information, the distributions can then be aspirated (with varying efficiencies due to anisokinetic sampling conditions) into the collectors. The collection efficiency curves of the collectors are used to apportion mass between stages and the validity of the curves and/or field performance of the collectors evaluated. These calculations involve combining measurements made using several instruments with varying degrees of accuracy and precision and may result in relatively large error bars.

The symbols used in this appendix are defined in the List of Symbols, and the data processed by the methods described herein are in Appendix H.

G.1 Light scattering measurement probes

Drop size distribution measurements were obtained using two devices available from Particle Measurement Systems, Inc. (Boulder, CO). Their operation depends largely upon the same principles, despite that fact that the two instruments have somewhat different physical arrangements. The devices are the Classical Scattering Active Spectrometer Probe (CSASP) and the Forward Scattering Spectrometer Probe (FSSP) and are described in detail by Pinnick

Reproduced with permission of the copyright owner. Further reproduction prohibited without permission.

and co-workers (Pinnick *et al.*, 1981; Pinnick and Auvermann, 1979). Very few field studies report using a CSASP-HV-100 for drop size distribution measurements. Hering *et al.* (1987) and Novakov *et al.* (1994) do not report processing corrections, although the latter paper indicates that overflow counting problems were experienced. Drops in the measuring volume scatter light in a known way as they cross a laser beam based upon size-dependent classical scattering theory. This scattering is measured and a signal generated. The signal is distributed into one of 15 channels which correspond to varying drop diameters (determined via calibration). Both the FSSP and the CSASP are capable of scanning across varying size ranges in a sequential manner to more finely resolve the drop size distribution (table G-1).

Table G-1: CSASP and FSSP drop size ranges

Drop size ranges			
Device	Range number	size spectrum	bin size
CSASP			
	0	2 - 47 µm	3 µm
	1	2 - 32 µm	2 µm
	2	1 - 16 µm	1 µm
	3	0.5 - 8 µm	0.5 µm
FSSP			
	0*	2 - 47 µm	3 µm
	1	2 - 32 µm	2 µm
*for ACE2 and Storm Peak, this range only reported			

We used our CSASP-100-HV at Whiteface and Horsetooth. The CSASP scanned each range for 10 seconds, so a complete scan takes 40 seconds. The CSASP manual suggests that the signal/noise ratio is better in the "upper" channels of each range, although quantification is not provided. Our CSASP's software and some hardware were substantially upgraded in the Fall of 2000, and its operating method modified to provide more data processing information than previously available.

During ACE2, drop size distributions were provided by an FSSP-100 operated by UMIST and the Risø National Laboratory and were obtained after initial dN processing from the ACE2 main

Reproduced with permission of the copyright owner. Further reproduction prohibited without permission.

database. DRI operated a FSSP at Storm Peak Laboratory. DRI initially processed and provided the drop size number distribution data used in Chapter 3.

Only one paper (Pinnick and Auvermann, 1979) was found that described the performance of the CSASP itself. Therefore, while the results of that paper will be described in the following sections, most of the discussion about problems with drop size distribution measurements is based upon the extensive literature regarding interpretation/validation of the FSSP. It appears that many (but not all) of the issues raised are common to both, therefore my treatment of the CSASP data reflects known FSSP limitations. Many FSSP investigations were performed at aircraft speeds (velocities > 50-60 m s^{-1} approximately) and the higher velocities can impact the results (Wendisch *et al.*, 1996; Cerni, 1983) relative to ground-based systems/sampling velocities. Wendisch and co-workers (1996) and Baumgardner and Spowart (1990) present results for the probe's operation at non-aircraft speeds. The FSSP configuration is not always clearly indicated. The experimental conditions, where relevant and known, will be indicated.

Significant uncertainties may exist for many reasons described below. While some of the reported results conflict, they cumulatively suggest the magnitude of the uncertainty in the reported dN and dV distributions.

G.2 Known limitations to the CSASP/FSSP measurements

Pinnick and Auvermann (1979) report that the CSASP does not provide the size resolution indicated by the manufacturer (± 5% concentration in each bin). This study which compared four PMS spectrometer probes raised many issues that were later studied in extensive detail for the FSSP including:

(a) some drops were not counted,

Reproduced with permission of the copyright owner. Further reproduction prohibited without permission.

(b) the measured size distribution was broader than the actual size distribution (the distribution "spread"),

(c) some drops may be mis-sized,

(d) irregularly-shaped drops may not be counted properly,

(e) the scattering response function is not monotonically increasing over the range of interest,

(f) anisokinetic sampling conditions may modify the observed distribution, and

(g) variations in the laser illumination impact the measurements

(Pinnick and Auvermann, 1979). They used a longer CSASP inlet (45 cm) and slower sampling velocity (6.6 m s^{-1}) than the CSU version (about 15 cm and 25 m s^{-1}) which resulted in gravitational settling losses during sampling (Pinnick and Auvermann, 1979). For the discussion that follows, gravitational losses are ignored (estimated to be < 3% for 30 μm diameter drops in the CSU CSASP), and all particles are assumed to be spherical (see Chapter 2). All counted particles are assumed to be water drops. The CSASP-100-HV and the Gerber PVM-100 are assumed to sample at a high enough frequency that the drop distributions and measured liquid water content (LWC) are at equilibrium with the ambient humidity (Fairall, 1984).

G.2.1 Activity corrections

G.2.1.1 Particle undercounting due to dead-time

Particle undercounting was first reported for the CSASP by Pinnick and Auvermann (1979), and has since been reported by others for the FSSP (Brenguier *et al.*, 1994). High activity measurements lead to higher coincidence errors (Kowalski *et al.*, 1997). Activity correction is necessary to account for processing delays in the probe's electronics and several methods are available to do this (Dye and Baumgardner, 1984). It is a correction for "dead-time" when particles can pass unsensed through the sampling volume. The recommended activity corrections in many instances require the use of "non-standard" measurements of the probe's

Reproduced with permission of the copyright owner. Further reproduction prohibited without permission.

response during operation (Brenguier *et al.*, 1994; Baumgardner *et al.*, 1985; Dye and Baumgardner, 1984). The corrections are often of similar form to that initially proposed by Baumgardner (1983):

$$N_a = \frac{N_m}{1 - mA} \qquad \text{(G-1)}.$$

At aircraft speeds, uncorrected activity errors can exceed 15% for $N_{drops} > 500$ cc^{-1} (Baumgardner *et al.*, 1985). This simple correction procedure in equation G-1 is not exactly true, but at low drop concentrations, empirically-derived adjustments are likely to be adequate (Brenguier, 1989). In this discussion, all electronic processing issues in the spectrometers are grouped under "dead-time", but they also may reflect other issues (e.g. laser inhomogeneity) (Brenguier, 1989). Activity corrections are tabulated by the CSU CSASP for each range, but are otherwise not a function of drop size.

G.2.1.2 Coincidence errors

Drops passing closely together through the sensing volume of the spectrometer probes can be erroneously counted as one large particle. Coincidence errors are often lumped in with activity correction (see equation G-1), but can directly impact the reported size distribution (which equation G-1 does not address). Baumgardner (1983) reports that drops are systematically over-sized if they are coincident in the beam. A frequently cited study of FSSP coincidence problems by Cooper (1988) reports that coincident drops may be both counted and sized incorrectly resulting in distorted drop spectra even after activity corrections (significantly for $N_{drops} > 500$ cc^{-1}, but not so if $N_{drops} < 100$ cc^{-1}). Brenguier (1989) suggests that coincidence errors can also lead to changes in the velocity rejection criteria (discussed below) which may also distort the drop size distribution. As the particle number concentration increases, the likelihood of errors from dead-time and coincidence increase (Mossop, 1983)

Reproduced with permission of the copyright owner. Further reproduction prohibited without permission.

G.2.2 Laser inhomogeneities

PMS indicated the error in the FSSP's sizing resolution was 10% due to laser variations (Baumgardner, 1983), and similar inhomogeneities were reported for the CSASP (Pinnick and Auvermann, 1979). Variations in laser intensity may result in particle mis-sizing and drop distribution spreading (Wendisch *et al.*, 1996; Baumgardner and Spowart, 1990; Brenguier, 1989; Baumgardner, 1983). Wendisch and co-workers' (1996) results indicated particle under-sizing (up to 9 μm for drops 40 – 45 μm in diameter) due to this effect. Slits are used in the FSSP-300 and the newer "Fast-FSSP" to minimize this error (Brenguier *et al.*, 1998).

G.2.3 Multi-valued scattering

The PMS manuals indicate that the scattering response increases monotonically for the particle size range of the FSSP and CSASP (0.5 – 47 μm). Mie theory predicts for smaller water drops (< ≈ 5 – 6 μm diameter and index of refraction = 1.33) that the response can be multi-valued for the CSASP (Pinnick and Auvermann, 1979), as well as the FSSP (significant up to drops 8 μm in diameter) (Pinnick *et al.*, 1981). This has been studied at larger diameters (Wendisch *et al.*, 1996). One suggested approach to mitigate this problem is to re-group the bins (particularly the smaller ones) to keep all similar responses together (Pinnick *et al.*, 1981), and has been applied in many studies (Dye and Baumgardner, 1984; Cerni, 1983). For larger particles, the PMS calibration is sufficient (Pinnick *et al.*, 1981), although this depends upon the size and composition of the particles being measured (Dye and Baumgardner, 1984). Other authors shift the size ranges of the larger bins as well (Cerni, 1983). Baumgardner (1983) estimated that a sizing error of ≈ 10% resulted from neglecting Mie fluctuations, although this error is size-dependent. Corrections for Mie scattering resonances are a function of drop size, unlike many of the other correction procedures.

Reproduced with permission of the copyright owner. Further reproduction prohibited without permission.

G.2.4 The Velocity Acceptance Ratio (VAR)

The signal processing software in the CSASP/FSSP does not count all drops that pass through the laser beam. Rather it accepts or rejects signals based upon how much time the drop takes to pass though the system – they must take at least "average" time to be accepted. This is to avoid counting "partial" drop transits (e.g. drops that do not pass through the entire sensing annulus). This essentially changes the probe's depth of field. A Velocity Acceptance Ratio (VAR) is sometimes calculated and can be used to correct the measured concentration (Dye and Baumgardner, 1984) through modifying the physical depth of field to the effective one. This is not a drop size-dependent correction. The velocities measured are a function of sampling/air speed and may also impact how well the FSSP works (one study found significant differences for spectra measured at 100 m s^{-1} and 25 m s^{-1} (Wendisch *et al.*, 1996)).

G.2.5 Wind ramming

Choularton and co-workers (1986) report a correction procedure for ground-based FSSPs due to changes in the volumetric sampling rate during operation. The volumetric sampling rate (the product of the volume and the ventilation rate) can change if sampling is not in still air. They measured the transit time of the particles directly through their sensing volume and used the data to derive a frequency measure. Linear regressions of the field data characterized how performance changed as a function of ambient wind speed for their two FSSPs. Their correction equation is:

$$V_t' = V_t \times \frac{emp}{f_t} \qquad \text{(G-2)}$$

where emp is 1200 or 2100 depending upon which FSSP is being used (Choularton *et al.*, 1986). This correction may also be expressed more generally as:

Reproduced with permission of the copyright owner. Further reproduction prohibited without permission.

$$Windramming \propto \left(1 + {}^{u_a}/_{u_b}\right) \qquad \text{(G-3)}$$

(Vong and Kowalski, 1995). This is an adjustment mechanism for anisokinetic sampling in ground-based FSSPs which rely on fans. The correction is the same for all drop sizes. Both this adjustment and the VAR correction are for the sampling/sensing volume changing during operation.

G.2.6 Saturation errors

During ACE2 very high drop concentrations (> 2500 cc^{-1}) were observed during polluted events. Drop number concentrations were counted by both a FSSP-100 and a Droplet Aerosol Analyzer (DAA) and the results suggest that the FSSP's response, even via improved DMT electronics and corrected for activity and coincidence errors, still saturated (Bower *et al.*, 2000; Martinsson *et al.*, 2000). The number concentration where this effect becomes important is variously listed at > 1000 cc^{-1} (Martinsson *et al.*, 2000), or at > 1200 cc^{-1} (Bower *et al.*, 2000).

G.2.7 Measured size distribution "spread"

Unlike most sampling problems described here, this observed effect results at least in part from the other ones reported. The electronic response time and other factors (including coincidence, among others) has been found to spread out the measured spectrum at ambient speeds > 50 m s^{-1} (Baumgardner and Spowart, 1990; Baumgardner, 1983; Cerni, 1983), although Wendisch and co-workers (1996) suggested that at lower speeds, laser inhomogeneity is more important. Pinnick and Auvermann (1979) observed spreading in their CSASP distributions.

Reproduced with permission of the copyright owner. Further reproduction prohibited without permission.

One study determined the additional spread in known glass bead distributions with nominal mean diameters of 9.1 and 16.6 μm to be approximately 2.3 and 3 μm using Range 0 of a FSSP at 45 m s^{-1} (Cerni, 1983). The distributions remained artificially broadened despite corrections for Mie scattering and dead-time (Cerni, 1983). At aircraft speeds, Baumgarder (1983) estimated that the average amount of broadening was on the order of 3 – 4 μm, based upon glass bead studies. Politovich (1993) reported that the FSSP's dispersion (the ratio of the standard deviation to the mean radius) increased with size up to a diameter of 24 μm for her analysis of airborne data. The standard deviation was always greater than 0.2 times the mean radius measured.

Coincident errors can result in broadening on the order of 2 – 3 μm for cloud drops. The resulting spectrum may have too many large and not enough small drops, although airspeed effects were not considered (Cooper, 1988).

Baumgardner and Spowart (1990) measured 22 μm glass beads of known distribution at 15 m s^{-1} and found that the measured relative standard deviation increased to ≈ 21% from 14% in the actual one (or to 4.4 μm from 2.9 μm) using 3 μm bins. The mean increased from 21.2 μm to 23.8 μm (2.6 μm) (figure G-1). The FSSP's imprecision added approximately 3.3 μm (15%) to the spread in the existing distribution which is consistent with the increase in the reported mean for this example. It is also consistent with PMS' reported sizing confidence of ± 1 bin (Sherman, 1998). Mossop (1983) reported approximately a 10% error in sizing for glass beads 10 –15 μm and 25 – 35 μm in nominal diameter. Dye and co-workers (1984) reported at least a ± 1 μm uncertainty for repeated FSSP measurements of known particles. Their results suggest that the FSSP tends to over-size the smaller particles (D_p < 14 μm) and under-size the larger ones (Dye and Baumgardner, 1984). Wendisch and co-workers (1996) report similar sizing results, and their calibration error was comparable to the manufacturer's reported value (within < 15% or ± 1 bin range uncertainty). They also found that the amount of under-sized drops increased as the drop size increased: drops of 40 – 45 μm in diameter were spread out over 4 bins, whereas little broadening was found for drops in the 2 – 14 μm range (the first 4 bins of their range) (Wendisch

Reproduced with permission of the copyright owner. Further reproduction prohibited without permission.

et al., 1996). The PMS calibration is optimized for particles in the 10 – 15 μm range (Dye and Baumgardner, 1984). Dye and Baumgardner also observed broadening in the reported spectrum (D_p = 26 μm) on the order of ± 1 bin (Dye and Baumgardner, 1984). They studied six FSSPs and found that broadening varied between instruments (Dye and Baumgardner, 1984).

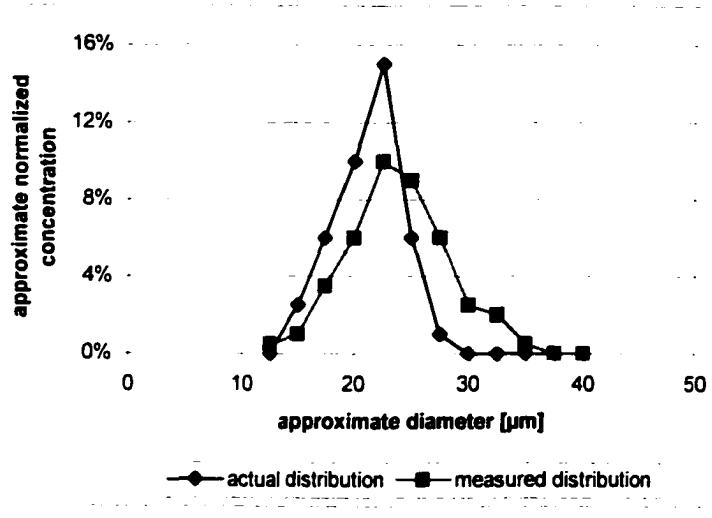

Figure G-1: Real vs. measured FSSP distribution (after figure 6 from Baumgardner and Spowart (1990))

G.3 Liquid water content via the drop size distribution

The dV distribution can be calculated from the dN distribution (see equation G-9) and the overall LWC determined by summation. This section motivates the processing method (section G-5).

Appendix I provides additional information regarding PVM and FSSP comparative performance, particularly as a function of varying drop spectra.

G.3.1 Laboratory results

By regrouping the bin distribution in a FSSP to reflect multi-valued Mie scattering or slowly changing response, the change in calculated LWC compared to the "standard" calibration was on

Reproduced with permission of the copyright owner. Further reproduction prohibited without permission.

the order of 16% (Pinnick *et al.*, 1981). This calculation was for a relatively small (most D_p < 10 μm) and narrow distribution and that more "typical" results will likely have up to a 52% error in the LWC (Cerni, 1983). Dye and co-workers (1984) for a calibration example given report data that suggests a 5% decrease in measured volume relative to actual volume. Wendisch and co-workers (1996) reported the "as-measured" effective diameter to be 7% less than the actual one, and the resulting LWC to be 23% lower.

G.3.2 Field results

Arends and co-workers (1992) compared field LWC measurements between four different methods including the PVM and the FSSP. The PVM-100 performed the best under both field and laboratory conditions. The PVM and FSSP LWCs generally agreed well, although some large differences between them were observed. FSSP dead-time, coincidence, Mie scattering, peak broadening, depth of field variability and inlet losses were investigated and could not account for the observed discrepancies. The PVM-100 should be used for LWC due to its consistency, and the FSSP for the drop size distribution only (Arends *et al.*, 1992). This treatment is followed by others (Schell *et al.*, 1992), and is the recommended procedure.

The Arends et al. (1992) study raised the question of the ability of the Gerber PVM-100 to measure LWC accurately for distributions with significant numbers of large drops (as indicated by D_{eff} or volume median or mean diameter). This is an important issue for the Davis fogs (see Chapter 4 and Appendix I).

G.4 General magnitude of the errors

The preceding discussion suggests that regardless of which drop sizes have the largest errors, the PMS instruments have considerable uncertainty in resolving the drop size distribution. Brenguier and co-workers (1994) report that uncorrected FSSP bin errors can be as large as 30%

Reproduced with permission of the copyright owner. Further reproduction prohibited without permission.

for sizes and 60% for concentrations. Most recently, Baumgardner (1995) reported sizing and concentration uncertainties in the FSSP to be on the order of 25% with corrections although the experimental data, hardware configurations and assumptions supporting this claim are not provided. These uncertainties result in a derived LWC error of 30 – 50% (Baumgardner, 1995).

G.5 Processing raw PMS probe data

The general method used to process the data is described in table G-2. The following detailed discussion focuses on Whiteface where data were obtained from the CSASP and the most processing was required. Data processing for Horsetooth (CSASP), ACE2 (UMIST FSSP) and Storm Peak Laboratory (DRI FSSP) are briefly described within the context of the Whiteface approach.

Several different processing methods have been reported in the literature to address the measurement deficiencies of the FSSP. Many of them require matrix inversions and substantial computer processing time (Wendisch *et al.*, 1996; Baumgardner and Spowart, 1990; Cooper, 1988). Additional non-standard measurements of the system's response including detailed electronic response, depth of field, VAR, true air speed/drop velocity, counting time interval, total beam diameter, and laser intensity profile may be required in order to obtain improved results (Wendisch *et al.*, 1996; Brenguier *et al.*, 1994; Baumgardner and Spowart, 1990; Brenguier and Amodei, 1989; Cooper, 1988; Choularton *et al.*, 1986; Baumgardner *et al.*, 1985; Dye and Baumgardner, 1984; Mossop, 1983). Generally, different groups make the corrections possible followed by scaling to an independent measurement of LWC (if available).

Reproduced with permission of the copyright owner. Further reproduction prohibited without permission.

Table G-2: General method for handling drop size distribution data

1. plot all raw size distribution data by diameter and grouped by collector sampling period • *check for any saturation/other errors* • *verify time against co-located PVM-100 or concurrent notes*
2. model data excluded due to saturation errors (Whiteface only) • *see detailed description in the text*
3. average data to match collector sampling periods • *use of mean values sufficient for the ensuing analysis if variation within the time period is minimal* • *if wide variations are observed in instrument operating parameters, it may be better to perform step #4 prior to this step*
4. adjust distribution data (as needed) for anisokinetic sampling conditions and other known instrument errors • *anisokinetic: due to use of CSASP inlet horn and inlet not pointed into the wind* • *instrument errors: see detailed description in the text (e.g. activity)*
5. adjust distribution data (as needed) for measuring water drops • *calibration spheres have varying refractive indices* • *due to modeling uncertainty, not performed for Whiteface data*
6. convert number distribution data to volume distribution • *compare total volume to mean LWC reported via the PVM-100* • *absolute quantities may vary, but trends should be similar*
7. scale calculated dV data against PVM-100 LWC • *D_{eff} < 20 μm only*
8. calculate effective diameter (D_{eff}) using the drop size distribution information • *compare to calculated effective diameter from the PVM-100 (if available)* • *absolute quantities may vary, but trends should be similar (D_{eff} < 20 μm)* • *flag time periods where D_{eff} > 20 μm for subsequent validation*
9. calculate number of drops in each bin and total for the scaled data • *results reasonable?*
10. calculate uncertainty for each dV bin • *include PVM LWC, drop distribution uncertainty at a minimum*

G.5.1 Available Whiteface data

The raw number counts in each bin were initially converted to the units of [# cc^{-1}] by multiplying them by (1/12.5) and (1/10). These factors are a function of the reported physical geometry for our CSASP-100-HV probe and are used to generate the [# cc^{-1}] units. All "dN" manipulation that follows is already converted into [# cc^{-1}] units.

Reproduced with permission of the copyright owner. Further reproduction prohibited without permission.

The CSASP was operated at Whiteface during the W185, W188, W197,and W198 events. During the W185 event, the collectors were oriented out of the wind on the order of 135° (Chapter 4), and these data are disregarded. During both the W188 and W197 events, the CSASP concentrations recorded were zero during part or all of the event. It is possible that there may have been a problem in whether or not drops were accepted or rejected, but this behavior remains unexplained. For the W188 event, non-zero distributions were available from approximately 19:00 through 24:00. For the W198 event, non-zero distributions were available throughout the entire event. These preliminary assessments were based upon unprocessed/uncorrected CSASP data, and additional data was removed as processing suggested.

G.5.1.1 Range combinations

Further inspection of the W188 and W198 CSASP raw data, revealed that the bins in Range 1 were often saturated in the 8 to 22 μm range (see figure G-2 for an example). We had an unresolvable error in the CSASP software, so drop concentrations > 80 cc^{-1} in any one bin were not counted. Range 2, due to its smaller bin size increment of 1 μm, was able to provide data for the bins up to 16 μm in diameter. Therefore, Range 1 and Range 2 were combined to provide a "better" distribution, although in many cases this was still not a complete one.

The data in Range 0 (up to 47 μm) during the two events was examined for the presence of any appreciable drop volume not available in Range 1 (i.e. 32 – 47 μm). While occasional drops were reported, a few sample calculations suggested that excluding Range 0 from the distribution would make negligible difference in the overall results. The sampling conditions of the CSASP may lead to the exclusion of larger drops (see the discussion of super-isokinetic sampling below). Range 3 was also neglected as it provided no additional data to that available in Range 2 and drops smaller than 3 – 4 μm in diameter were not of interest.

Reproduced with permission of the copyright owner. Further reproduction prohibited without permission.

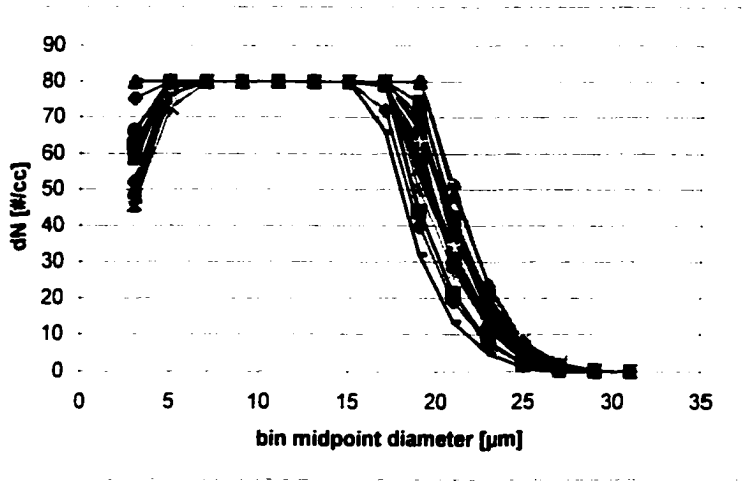

Figure G-2: Raw dN distributions plotted for Range 1 of the CSASP during the last W198 event sampling period. Only a portion (10 – 10:14) of the data for the time period is shown.

The combined CSASP distributions from 2 – 32 µm in diameter with bin increments of 1 and 2 µm were separated into cloud sampling periods. Typically a half-hour sampling period would contain ≈ 44 – 45 distributions (89 – 90 per hour). Each sampling period's distributions were sorted to reflect any missing data due to saturation. Any distributions that matched were averaged together, and the number of distributions averaged was tracked. The number of different distributions that resulted for a given sampling period ranged from 7 to > 20. After averaging, the distributions were converted to 1 µm bin increments which was necessary for the subsequent modeling.

G.5.1.2 Filling in the missing data

Log-normal, gamma and normal (gaussian) distributions were investigated to see which fit the existing CSASP data better. Log-normal and gamma distributions are often used to describe cloud drop size distributions (Pruppacher and Klett, 1997). In this instance, however, the long tails associated with these particular distributions were not justified, and better fits were observed using a simple gaussian fit to the dN data. Implicitly the data was assumed to be

Reproduced with permission of the copyright owner. Further reproduction prohibited without permission.

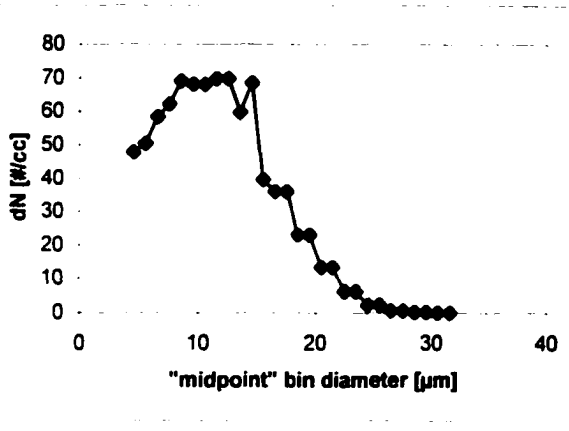

Figure G-3: Average of 4 individual distributions with a complete set of data points for the W198 event 9:00 – 10:00 sampling period. Range 1 data have two data points plotted per 1 µm bin hence "midpoint" is in quotation marks.

uni-modal where it needed to be "filled-in" which was reasonably supported where little or no data were missing (figure G-3). Each distribution with uniquely missing data from each sampling period was exported into the Origin v5.0 software (Microcal Software, Inc.) and a best-fit gaussian curve to the data was modeled using the following equation:

$$y = y_0 + \frac{Area}{w\sqrt{\pi/2}} \exp \frac{-2(x - x_c)^2}{w^2} \qquad \text{(G-4)}$$

and minimized subject to the calculated $\chi 2$ value. In some instances, the initial curve fit failed or was inadequate if the modeled data points were not at least 80 cc^{-1} (the saturation value). In practice, a 10% uncertainty was assumed in the curve fits, so a modeled value > 72 cc^{-1} was accepted. Where the initial fit still failed, additional data were "presumed" generally based upon extrapolating the calculated slope between existing data points into the saturated region, and the modeling repeated. In some instances, a slope greater than the existing data supported was used to "nudge" the fit in a particular bin to satisfy the minimum 72 cc^{-1} criteria. The use of "presumed" points was minimized. When an acceptable modeled fit was found, the y_0, Area, w, x_c and χ^2 values were recorded. After all the unique distributions for a particular time period were

Reproduced with permission of the copyright owner. Further reproduction prohibited without permission.

modeled, the existing physical distributions were filled in with the calculated modeled points and then a weighted average calculated based upon the number of distributions of each type to obtain the overall sampling period average. In no instance where physical data were available was a modeled point used (any extrapolated points required for the fitting of the gaussian were discarded).

Part of the investigation of the curve fitting procedure involved whether or not "better" results were achieved by fitting to dN or calculated dV data. Using the dN data constrained the peak of the distribution somewhat better than using the dV data as the dN values on either side of the saturated peak were similar in value resulting in more even weighting of the small and large diameter data in the curve fit. This was not the case for the dV fits, and significantly higher peak volume distributions were obtained, particularly where many data points were modeled. It is not known, however, how well the unknown peak values were modeled in either scheme. Therefore, dN data were uniformly used for the fits, and dN is the value measured by the CSASP.

Using this methodology, average dN distributions were obtained for all of the available sampling periods on W188 and W198.

G.5.1.3 Error introduced by the modeling

Model use implies additional uncertainty. Of the 883 total distributions available during W188 and W198, 68 had either no data omissions or one point only (approximately 8% of the total). Further, in general no data points > 20 μm needed to be modeled which are important to the dV distribution. In some instances, data points down to 3.5 μm (the smallest value used) had to be modeled, but usually some data were available between 3.5 – 10+ μm. Generally the agreement is quite good (on the order of 10%) in the size ranges in the peak of the distribution where it is most critical. As discussed previously, this level of error is less than that usually suggested for the physical measurement.

Reproduced with permission of the copyright owner. Further reproduction prohibited without permission.

G.5.1.4 Activity Corrections

PMS indicates that m = 0.0065 where A is provided in percent for the CSU CSASP. As two ranges were combined, the mean activity during a sampling period was averaged for each of the two ranges. Although the mean difference between the two was usually no more than 5% (table G-3), which is well within the measurement uncertainty, the average dN distributions were adjusted using equation G-1 as recommended by PMS. If only one size range had been used, the activity correction would not have been necessary. The activities reported are high enough (> 50%) that coincident errors may be important, although this cannot be determined with the data available.

Table G-3: Average activity correction by time period and sample range

Time	Activity > 16 µm [%]	Activity < 16 µm [%]	mean RSDs
W188 event			
1900-1930	78	84	4%
1930-2000	84	90	4%
2000-2030	79	86	4%
2030-2100	81	90	2%
2100-2130	81	88	3%
2130-2200	75	82	4%
2200-2230	76	82	3%
2230-2300	76	82	3%
2300-2330	74	80	3%
2330-2400	77	82	6%
W198 event			
130-200	89	94	1%
200-300	89	94	1%
300-400	74	82	32%
400-500	80	86	4%
500-600	77	83	3%
600-700	76	82	2%
700-800	76	82	3%
800-900	75	81	2%
900-1000	74	80	4%
1000-1100	73	78	4%

Reproduced with permission of the copyright owner. Further reproduction prohibited without permission.

G.5.1.5 Super-isokinetic sampling conditions in the CSASP

The inferred velocity (via pressure drop measurements) into the sampling volume of the CSU CSASP was approximately 26.5 m s^{-1} (not 35.8 m s^{-1} as indicated by PMS). This implies a velocity at the horn inlet of approximately 8.3 m s^{-1}. This generally exceeded the ambient horizontal component of the wind measured at the summit of Whiteface, although not by more than a factor of 2. Several studies mention or at least consider anisokinetic sampling into the spectrometer probes being used/investigated (Kowalski *et al.*, 1997; Arends *et al.*, 1992; Norment, 1987; Pinnick and Auvermann, 1979). Apparently the FSSP can be specially configured to avoid this issue during ground-based sampling (see (Kowalski *et al.*, 1997) and (Arends *et al.*, 1992) for example). Recently, Gerber and co-workers have disputed how effective the FSSP standard hardware configuration is for isokinetic sampling at ground-based speeds (Gerber *et al.*, 1999). Norment (1987) suggests size distribution distorting convergent flows are unavoidable as long as the sampling velocity exceeds the outside ambient velocity, although the exact effect is a function of the drop trajectories which are themselves a function of drop size and probe geometry. Super-isokinetic sampling should distort the size distribution of drops measured by the CSASP (neglecting how the converging flow in the inlet may affect drop loss). The "ambient" drop size distribution was determined from the measured CSASP distribution using the aspiration efficiency equations for thin-walled tubes (equations 2-9 and 2-10 (Chapter 2)) based upon average conditions during the sampling period. An 100% transmission efficiency was assumed as the alternate approach yielded what appeared to be unrealistic losses (Brockmann, 1993, p. 88). The results were converted to the appropriate bin range (2 μm) for the size distribution and collector efficiency curves and multiplied by the measured drop number concentration. As the inlet and ambient velocities at Whiteface were generally similar, only minor changes (within 10%) in the distribution resulted (figure G-4).

Reproduced with permission of the copyright owner. Further reproduction prohibited without permission.

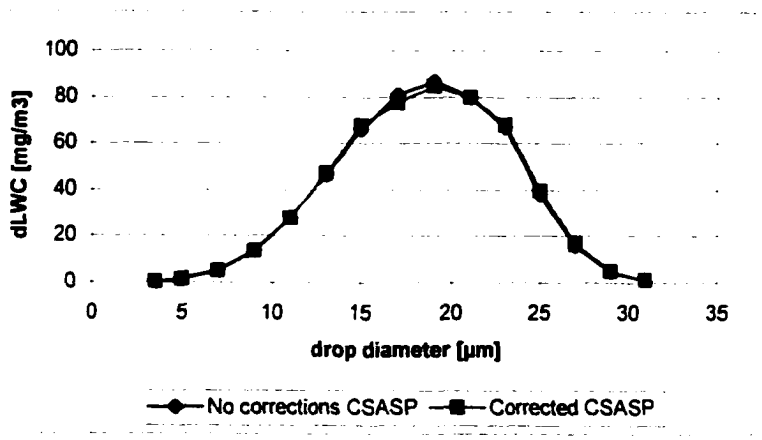

Figure G-4: Uncorrected and corrected for anisokinetic sampling CSASP derived LWC distributions (scaled to the PVM-100, W188 event, 19:00 – 19:30).

This calculation presumes isoaxial flow, and within ± 15° no significant error is added which appears reasonably within the horizontal wind direction variation observed at Whiteface. The vertical angle of the ambient wind at ACE2 was determined to be 17.5° on average (Flynn *et al.*, 2000) and resulted from more severe topography than at Whiteface (Chapter 7). No corrections were made for vertical variations in wind direction. The effect of anisoaxial sampling on the aspiration efficiency was investigated using the expressions in Brockmann (1993, p. 90). Losses, particularly of the relatively large drops, can be severe, although the range of applicable conditions to apply the expressions to is limited (see Chapter 2).

G.5.1.6 Additional losses

Professor J. C. Wilson suggested two other potential sampling artifact issues for the CSASP: drop evaporation and turbulent deposition in the inlet horn. The internal temperature of the CSASP can be relatively elevated compared to ambient conditions. Using the drop growth equations described elsewhere (see section 2.3.2.2), and conservative assumptions regarding drop residence time prior to measurement (0.001 s) and temperature inside the CSASP (35 –

Reproduced with permission of the copyright owner. Further reproduction prohibited without permission.

50°C) (Dawson, 2001), drop evaporation is negligible. Drop residence time is too short. Turbulent deposition inside the inlet horn was modeled using the equations from Brockmann (1993, p. 99):

$$\eta_{tube,turb_inert} = \exp\left(-\pi D_{nozzle} Le V_t / Q\right) \quad \text{(G-5)}$$

$$V_+ = (0.0006)(\tau_+)^2 \quad \text{(G-6)}$$

$$V_+ = 5.03\left(V_t / U\right)\mathrm{Re}_f^{1/8} \quad \text{(G-7)}$$

$$\tau_+ = 0.0395 Stk\, \mathrm{Re}_f^{3/4} \quad \text{(G-8)}$$

where Stk is the Stokes number using the tube diameter (D_{nozzle}) and average inlet fluid velocity. If the dimensionless particle relaxation time exceeds 12.9 then V_+ is approximately 0.1 (Brockmann, 1993, and references therein). The inlet was modeled in 2 consecutive sections: the mean values for the converging nozzle, and then the straight section into the measurement volume. The resulting efficiency curves are shown in figure G-5.

Note the effect of assuming a constant value for the dimensionless deposition velocity as the diameter increases. The larger drops have too much inertia to be much affected by turbulence. Additional losses are expected at the junction of the converging nozzle and the straight section (Brockmann, 1993), however these cannot be evaluated here. Examination of the inlet horn following the Winter 2000/2001 sampling campaign revealed a uniform layer of deposited material at the junction, as might be expected from turbulent deposition. As this effect may not be modeled well (there is some question of applicability at high Re_p), the error is within

Reproduced with permission of the copyright owner. Further reproduction prohibited without permission.

approximately 15% for the drop sizes of interest and it is not known if deposition occurred at Whiteface, no adjustment was made to the data.

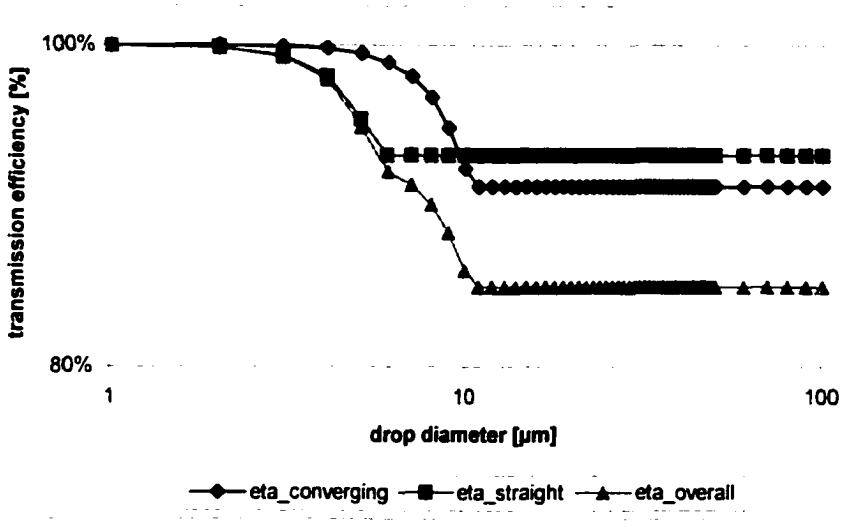

Figure G-5: Modeled turbulent inertial deposition efficiency in the CSASP inlet horn

Assuming a thin-walled nozzle may not necessarily be applicable to the CSASP inlet, but is a reasonable first approximation. Given the open questions regarding the CSASP and our on-going use of it, a more thorough investigation of the losses should be investigated either numerically or in the laboratory (Chapter 11).

G.5.1.7 Scaling of the drop distribution to the Gerber PVM LWC

The averaged dN distributions adjusted for both activity corrections and super-isokinetic sampling conditions were converted to a dV distribution using the equation:

$$dV = \left(\pi/6\right) D_p^3 dN \qquad \text{(G-9)}$$

Reproduced with permission of the copyright owner. Further reproduction prohibited without permission.

for each size bin where D_p is the midpoint diameter. dV was summed across all the size bins for a particular time period and the resulting distribution was then normalized and multiplied by the Gerber PVM liquid water content during the time period. The end result is a dV distribution expressed in [mg m^{-3}] that sums to the Gerber PVM LWC average for the time period. No corrections were possible for drop size distribution distortion aside from the activity correction in the two ranges. As alluded to earlier, a comparison of the LWC calculated from the corrected CSASP data and measured by the Gerber PVM yield significant differences – far greater than those reported during other investigations (figure G-6), with one exception (Fuzzi *et al.*, 1988). This suggests the CSASP data alone should not be used for LWC calculations. A better estimate in warm clouds may be determined using the collected sample volumes if no PVM data are available (Chapter 4).

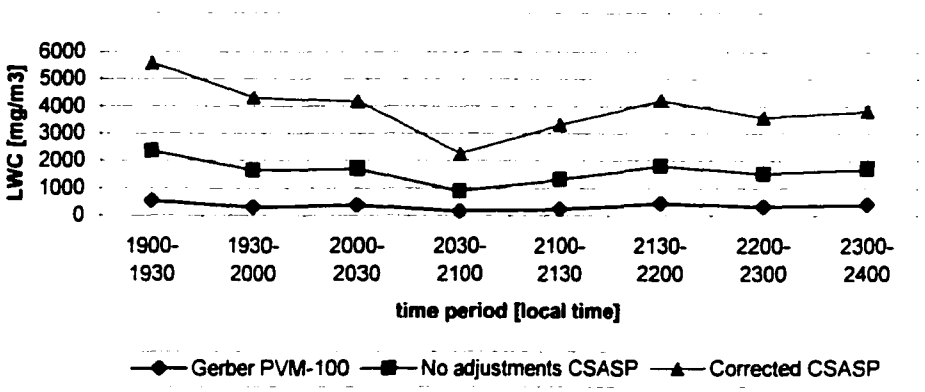

Figure G-6: W188 event – Measured vs. calculated LWC

G.5.1.8 Effective diameter

As a final check on the processed CSASP distributions, the effective diameter was calculated for all of the sampling periods and compared to the one calculated from the volume and surface area measurements made by the PVM. For the PVM data:

Reproduced with permission of the copyright owner. Further reproduction prohibited without permission.

$$D_{eff} = 60\frac{V}{SA} \qquad \text{(G-10)}$$

where D_{eff} is in [μm], V and SA are in the units provided by the PVM and the factor of 60 is used to both convert units and obtain diameter. D_{eff} via the CSASP is calculated as follows:

$$D_{eff} = \frac{\sum_{i=1}^{15} \pi D_i^3 n_i}{\sum_{i=1}^{15} \pi D_i^2 n_i} \qquad \text{(G-11)}$$

where the summation is over all the bins (after (Wendisch, 1998)).

For the W188 event the trend in D_{eff} via the CSASP and the PVM match well, although there is a consistent 1 – 2 μm offset between the two (figure G-7). However, this is well within the uncertainties associated with both measurement devices, and Baumgardner (1995) indicates that FSSPs cannot determine D_{eff} within 2 μm.

For the W198 event, the trends in D_{eff} by the two different methods sharply differ prior to 6 a.m. when they converge and trend closely together (figure G-8). The CSASP may not have been sampling representatively during the earlier time periods. Therefore, the CSASP data prior to 6 a.m. are discarded. Shifting the CSASP distributions based upon the PVM's D_{eff} improves the D_{eff} comparison, but the collector predicted/measured volume calculations that result are sharply in contrast to those where the size distribution measurements were known to be valid. While matching LWC and D_{eff} trends between the PVM and the CSASP is useful, it does not guarantee that the distributed mass is correct. However, there may be no other validation available.

Reproduced with permission of the copyright owner. Further reproduction prohibited without permission.

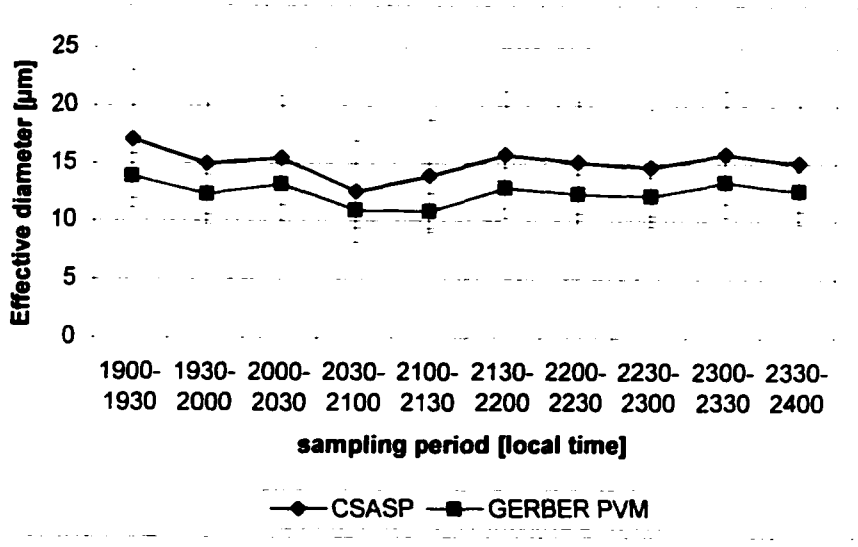

Figure G-7: W188 event: Effective diameter comparison by sampling period between the Gerber PVM and the CSASP (propagated error bars are ± 35% (CSASP) and ± 14% (PVM)).

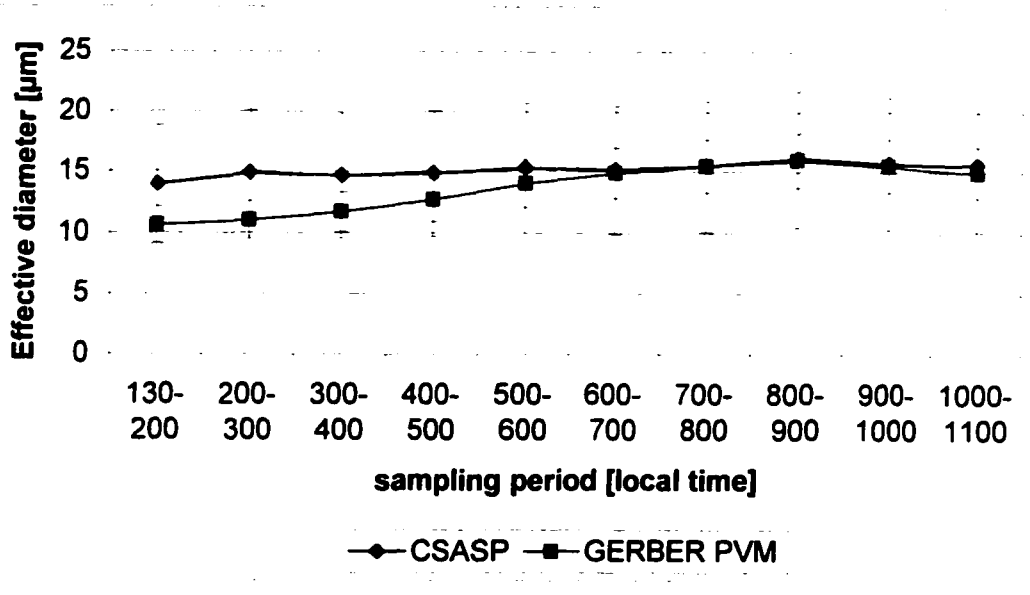

Figure G-8: Same as figure G-7 except for W198 event

The reported D_{eff}s were generally less than 20 µm for both the W188 and W198 events. This suggests that scaling to the Gerber PVM-100 is appropriate for the Whiteface conditions (see Appendix I).

Reproduced with permission of the copyright owner. Further reproduction prohibited without permission.

After correction, the ambient drop number distribution at Whiteface varies from approximately 200 cc^{-1} to 500 cc^{-1} for the time periods with validated distributions (table G-4). The W198 event has somewhat higher concentrations consistent with the generally higher LWC during this event and with continental distributions. Drop concentrations of approximately 450 cc^{-1} were measured at Kleiner Feldberg and from 400 – 600 cc^{-1} at Great Dun Fell which are both orographic cloudnsites (Arends *et al.*, 1997). Although this is after considerable manipulation, these results suggest activity corrections alone may be sufficient (Brenguier, 1989).

Table G-4: Derived number concentrations for the Whiteface events by sampling period

W188 event	N [# cc^{-1}]
1900-1930	300.9
1930-2000	237.8
2000-2030	282.8
2030-2100	223.0
2100-2130	224.3
2130-2200	308.2
2200-2300	270.4
2300-2400	307.2
W198 event	
600-700	434.0
700-800	479.3
800-900	494.7
900-1000	459.0
1000-1100	427.0

G.6 Comment on error calculations

The purpose of this section is to describe the basis for the uncertainty used for the Whiteface distributions drawing upon the preceding sections and the data presented.

Reproduced with permission of the copyright owner. Further reproduction prohibited without permission.

G.6.1 CSASP Field calibration

Prior to field operation at Whiteface, the CSASP calibration was checked and the velocity through the device measured (as previously mentioned).

Our CSASP calibration at a single point (15.7 μm glass beads) yielded a multi-modal curve with peaks in the 5 – 7 and 15 – 17 μm bins. This behavior has been observed by others and the first peak was removed from the analysis (Kowalski *et al.*, 1997). The measured mean diameter (13.9 μm) is within 2 μm (the range) of the reported actual mean. The calculated standard deviation is about 23% or 3.2 μm. Allowing for the uncertainty in the bead sizing (± 1.1 μm) yields an instrument uncertainty at this data point of approximately 3 μm (about 21.5%). This result is consistent with the previous discussion of sizing errors. The mean diameter uncertainty improves somewhat when the adjustment for varying refractive indexes between water (as calibrated for) and glass (as measured) is made, although the change is within the existing measurement uncertainty. No correction for different indices of refraction is thus made for any of the Whiteface data.

G.6.2 Error estimate for the Whiteface distributions

We have only the activity correction data available for the CSU CSASP, although normalization to the Gerber PVM does serve to correct the measured data for wind-ramming and similar sampling volume-dependent errors as well. Assuming the FSSP has similar limitations as the CSASP suggests that assuming 25% uncertainty in the concentration in each bin is not unreasonable for ground-based sampling. This uncertainty must be combined with the PVM-100's if PVM-scaled dV distributions are produced.

Reproduced with permission of the copyright owner. Further reproduction prohibited without permission.

G.7 ACE2 data

The raw FSSP data was processed by UMIST to account for coincident errors and wind-ramming effects per the methodology described by Choularton and co-workers (1986). Only Range 0 (approximately 3 μm bins) with the mid-point bin diameter was provided, although the data processing scheme does shift the exact range of each bin. No size-correction processing occurred. The provided 5 minute dN averages were averaged to match the longer sampling period for the collector samples. The processed distributions were reviewed and collector sample-averaged distributions > 1200 cc^{-1} were not used to avoid the saturation effects reported (Bower *et al.*, 2000; Martinsson *et al.*, 2000). The remaining data were separated into two groups – < 1000 cc^{-1} and 1000-to-1200 cc^{-1} – to investigate whether the results for the higher number concentrations differed significantly from those for the lower number concentrations. No apparent difference was discerned, and the two were combined. Finally, the number distributions were converted to volume distributions and normalized to the PVM-100 measurements after the method of Arends and co-workers (Arends *et al.*, 1992). Unfortunately, the UMIST PVM does not have the capability to provide D_{eff} measurements, so that could not be checked against the FSSP data.

G.8 Storm Peak Laboratory data

FSSP dN data supplied by DRI was processed for the "regular" suite of corrections prior to transmittal to CSU. This included Mie scattering and other standard corrections. The dV distributions were calculated, normalized to the PVM-100 (where available) and the D_{eff}s checked. The D_{eff}s were < 20 μm and no additional corrections were made. The PVM-100 and FSSP-100 data had apparently already been screened for time periods where the equipment malfunctioned (based upon copies of the field campaign's notes) and no additional data were excluded.

Reproduced with permission of the copyright owner. Further reproduction prohibited without permission.

G.9 Horsetooth data

CSASP-HV-100 data were processed similarly as above. Ranges 0, 1 and 2 were separated for 22:21 to 23:59, and 0:55 – 3:55. It is not known why there is a gap in data from 23:59 to 0:55 in the raw data files. Three ranges were initially included as Range 0 contained some information (e.g. drops > 32 μm in diameter) and Range 1 was saturated in some of the smaller (e.g. < 10 μm drop diameter) bins. Range 0 was retained for drops > 32 μm in diameter and selected data points from Range 2 were added to Range 1 where saturated. Otherwise the main basis for the distributions was Range 1. In a few instances, Range 2 was also saturated in the 2 – 4 μm bin range. In these instances, a value of 20,000 (2 x 9,999) was used. I assumed this was sufficient given measurement uncertainty and because few of these drops are collected. In instances where Range 2 data were used, I corrected the activity value for Range 1 and used the mean value for Range 1 and 2 (the activity values were broadly similar between all 3 ranges). After separating into time periods, the mean distribution was corrected for the mean activity and converted to dN units [# cc^{-1}]. Given the uncertainty of the measurement, making the activity corrections on the mean (instead of by individual distribution) seemed reasonable. The resulting dN data were corrected for super-isokinetic sampling into the CSASP. I used the CSASP velocity as measured at Whiteface to perform these adjustments and they were generally at the lower limit (or just beyond) the applicable range for the corrections based upon the velocity ratio (U_0/U_s). It is not known how much additional uncertainty this added, but there were very few large drops (D_p > 20 μm) where the most effect would be observed in the sampling periods with the calmest ambient wind. No PVM-100 LWC data was available due to equipment difficulties. Therefore, while the dV pattern is likely correct, it is not known how uncertain the derived LWC is. Therefore, I have normalized the dV distribution to the total volume calculated for the 1:00 – 2:00 sampling period (sampling period with complete data and highest calculated volume).

In support of the approximations made in the processing, the 2 – 4, 4 – 6, 6 – 8, and 8 – 10 μm dN values for the 1:00 – 3:55 time period were compared between Ranges 1 and 2. The mean

Reproduced with permission of the copyright owner. Further reproduction prohibited without permission.

Range 1/Range 2 ratios were 0.85 – 0.96 (based upon 224 – 250 activity corrected distributions), but the standard deviations were ≥ 0.50 and the range was from 0.0 – 15.58. Thus using means appears reasonable. This also suggests that there is considerable measurement uncertainty as others have found.

Reproduced with permission of the copyright owner. Further reproduction prohibited without permission.

H. Appendix: Data tables

Table H-1: Davis, CA Ammonia and Nitric acid gas-phase concentrations

date/time denuder ON [local]	date/time denuder OFF [local]	AMBIENT CONCENTRATION		COATED BLANK CONCENTRATIONS		95% C.L. MINIMUM DETECTION LIMIT	
		HNO_3 [ppbv]	NH_3 [ppbv]	HNO_3 [ppbv]	NH_3 [ppbv]	HNO_3 [ppbv]	NH_3 [ppbv]
1/6/99 19:30	1/7/99 7:30	0.061	4.8	0.009	0.072	0.007	0.006
1/7/99 7:30	1/7/99 16:04	0.050	6.6	0.013	0.099	0.010	0.008
1/7/99 16:04	1/7/99 22:55	0.039	5.0	0.016	0.126	0.013	0.010
1/7/99 22:55	1/8/99 9:35	0.017	5.1	0.010	0.080	0.008	0.007
1/8/99 9:35	1/8/99 16:02	0.086	9.4	0.017	0.134	0.013	0.011
1/8/99 16:02	1/9/99 2:35	0.025	12.7	0.010	0.081	0.008	0.007
1/9/99 2:35	1/9/99 11:13	0.039	8.2	0.013	0.100	0.010	0.008
1/9/99 11:13	1/10/99 2:22	0.030	8.9	0.007	0.056	0.006	0.005
1/10/99 2:22	1/10/99 10:35	0.064	6.4	0.014	0.105	0.011	0.009
1/10/99 10:35	1/10/99 22:29	0.025	4.4	0.009	0.072	0.007	0.006
1/10/99 22:29	1/11/99 10:00	0.029	3.3	0.010	0.075	0.008	0.006
1/11/99 10:00	1/11/99 19:12	0.034	7.4	0.012	0.093	0.009	0.008

ppbv calculated based upon 1020 mb and 5°C

Table H-2: Davis, CA total gas-phase peroxides (assumed to be H_2O_2)

event/date	time [local]	WITH MDL/2 mean H_2O_2 [ppbv]	WITHOUTMDL/2 mean H_2O_2 [ppbv]	% MDL/2	AVG MDL [ppbv]	AVG LOQ [ppbv]
D352						
12/18/99	3:22-4:00	-0.019		87%	-0.011	0.029
12/18/99	4-5:00	-0.017		78%	-0.011	0.029
12/18/99	5-6:00	-0.017		84%	-0.011	0.029
12/18/99	6-7:00	-0.014		93%	-0.011	0.029
12/18/99	7-8:00	-0.016		96%	-0.011	0.029
12/18/99	8-9:00	0.014	0.027	29%	-0.011	0.029
12/18/99	9-10:00	0.024	0.035	20%	-0.011	0.029
12/18/99	10-11:00	0.026	0.038	20%	-0.011	0.029
12/18/99	11-11:20	-0.020		100%	-0.011	0.029
D004						
no data						
D009						
1/9/99	3-4:00	0.022	0.035	16%	-0.038	-0.004

Reproduced with permission of the copyright owner. Further reproduction prohibited without permission.

1/9/99	4-5:00	0.007	0.014	11%	-0.038	-0.004
1/9/99	5-6:00	0.001	0.022	31%	-0.038	-0.004
1/9/99	6-7:00	0.022	0.022	0%	-0.038	-0.004
1/9/99	7-8:00	0.009	0.025	22%	-0.038	-0.004
1/9/99	8-9:00	0.004	0.012	13%	-0.038	-0.004
1/9/99	9-10:00	-0.006	0.010	31%	-0.038	-0.004
1/9/99	10-10:36	-0.008	-0.008	0%	-0.038	-0.004
D010						
1/10/99	2:45-4:00	-0.009		62%	-0.038	-0.004
1/10/99	4-5:00	-0.006		47%	-0.038	-0.004
1/10/99	5-6:00	-0.004		36%	-0.038	-0.004
1/10/99	6-6:52	0.014	0.019	8%	-0.038	-0.004
1/10/99	6:52-9:00	-0.002	0.015	27%	-0.038	-0.004
1/10/99	9-10:00	0.033	0.036	4%	-0.038	-0.004
D010B						
1/10/99	22:50-24:00	0.109		62%	0.105	0.179
1/11/99	0-1:00	0.086		82%	0.105	0.179
1/11/99	1-3:00	0.087		79%	0.105	0.179
1/11/99	3-5:00	0.099		48%	0.105	0.179
1/11/99	5-7:00	0.087		76%	0.105	0.179
1/11/99	7-8:00	0.114	0.126	24%	0.105	0.179
1/11/99	8-9:00	0.116	0.130	29%	0.105	0.179
1/11/99	9-9:42	0.106		46%	0.105	0.179
D011						
1/11/99	23-24:00	0.009		89%	0.011	0.048
1/12/99	0-1:00	0.055	0.057	4%	0.011	0.048
1/12/99	1-3:00	0.053	0.076	33%	0.011	0.048
1/12/99	3-5:00	0.040	0.049	32%	0.011	0.048
1/12/99	5-7:00	0.065	0.078	18%	0.011	0.048
1/12/99	7-8:00	0.019		62%	0.011	0.048
1/12/99	8-9:00	0.035		47%	0.011	0.048
1/12/99	9-9:42	0.023		67%	0.011	0.048
D013						
1/13/99	5:50-9:17	0.051	0.054	8%	0.011	0.048

Column 3 includes "MDL/2" in average where 1 minute data < MDL

Column 4 omits any 1 minute data points < MDL and is edited for time periods with < 50% of data is < MDL

Column 6 is the mean calibration MDL for the sampling period (not quite the same as the MDLs used to edit 1 minute data points out)

Column 7 is the LOQ based upon the mean calibration MDL

Column 6 is 3 sigma and Column 7 is 10 sigma

multi-hour sampling period averages are weighted for where data exists (e.g. an "hourly" average is treated as 45 minutes of data)

Table H-3: Davis, CA MOUDI data

size-cut D_{p50}* [µm]	PRE D009 EVENT			POST D009/PRE D010 EVENT			POST D010 EVENT		
	Nitrate [µg m^{-3}]	Sulfate [µg m^{-3}]	Ammonium [µg m^{-3}]	Nitrate [µg m^{-3}]	Sulfate [µg m^{-3}]	Ammonium [µg m^{-3}]	Nitrate [µg m^{-3}]	Sulfate [µg m^{-3}]	Ammonium [µg m^{-3}]
> 20.5	0.154	0.029	0.034	0.112	0.018	0.032	0.091	0.021	0.034

Reproduced with permission of the copyright owner. Further reproduction prohibited without permission.

11.4 - 20.5	0.135	0.016	0.047	0.143	0.016	0.039	0.125	0.017	0.038
6.4 - 11.4	0.251	0.033	0.078	0.192	0.024	0.056	0.225	0.028	0.054
3.66 - 6.4	0.696	0.078	0.224	0.464	0.054	0.138	0.308	0.040	0.097
2.06 - 3.66	1.678	0.201	0.515	1.097	0.134	0.343	0.579	0.077	0.184
1.15 - 2.06	2.628	0.356	0.864	3.802	0.432	1.232	3.576	0.444	1.195
0.65 - 1.15	2.232	0.265	0.699	2.972	0.287	0.930	2.757	0.280	0.889
0.37 - 0.65	1.360	0.115	0.411	1.772	0.139	0.535	1.157	0.121	0.358
0.22 - 0.37	0.961	0.067	0.285	1.185	0.085	0.359	0.743	0.084	0.244
< 0.22	0.205	0.023	0.064	0.334	0.024	0.101	0.109	0.034	0.032
47 mm blank	0.055	0.000	0.008	0.029	0.000	0.008	0.033	0.000	0.007
37 mm blank	0.018	0.000	0.003	0.000	0.000	0.002	0.000	0.000	0.002
extraction blank	0.000	0.000	0.000	0.000	0.000	0.000	0.000	0.000	0.002
95% CL MDL	0.028	0.021	0.004	0.019	0.014	0.003	0.025	0.018	0.004

** at 23 liters min^{-1} flow rate*

for sampling periods, see Appendix J

Table H-4: Davis, CA revised LWC and effective diameter

event/date	time [local]	effective diameter [µm]	LWC [mg m^{-3}]
D352			
12/18/99	3:22-4:00	19.5	64.0
12/18/99	4-5:00	>20	210.4
12/18/99	5-6:00	>20	329.5
12/18/99	6-7:00	>20	279.7
12/18/99	7-8:00	>20	293.7
12/18/99	8-9:00	>20	326.6
12/18/99	9-10:00	>20	266.7
12/18/99	10-11:00	>20	181.2
12/18/99	11-11:20	>20	44.4
D004			
1/4/99	20:05-21:00	>20	217.0
1/4/99	21-22:00	>20	227.5
1/4/99	22-23:00	>20	181.4
1/4/99	23-24:00	>20	176.9
1/5/99	0-1:00	>20	209.7
1/5/99	1-2:00	>20	214.3
1/5/99	2-3:00	>20	192.2
1/5/99	3-4:00	>20	193.5
1/5/99	4-5:00	>20	183.4
1/5/99	5-6:00	>20	183.1
1/5/99	6-7:00	>20	171.2
1/5/99	7-8:00	>20	145.2
1/5/99	8-10:00	>20	125.3

Reproduced with permission of the copyright owner. Further reproduction prohibited without permission.

D009			
1/9/99	3-4:00	>20	165.9
1/9/99	4-5:00	>20	177.0
1/9/99	5-6:00	18.2	47.5
1/9/99	6-7:00	18.1	55.2
1/9/99	7-8:00	18.4	50.8
1/9/99	8-9:00	19.3	50.6
1/9/99	9-10:00	>20	71.7
1/9/99	10-10:36	19.8	28.8
D010			
1/10/99	2:45-4:00	18.0	56.8
1/10/99	4-5:00	17.8	55.5
1/10/99	5-6:00	>20	67.2
1/10/99	6-6:52	>20	59.5
1/10/99	6:52-9:00	19.9	44.7
1/10/99	9-10:00	18.7	33.8
D010B			
1/10/99	22:50-24:00	>20	140.9
1/11/99	0-1:00	>20	130.5
1/11/99	1-3:00	>20	85.2
1/11/99	3-5:00	>20	92.9
1/11/99	5-7:00	>20	106.8
1/11/99	7-8:00	>20	106.3
1/11/99	8-9:00	>20	98.5
1/11/99	9-9:42	>20	48.7
D011			
1/11/99	23:00-24:00	>20	179.1
1/12/99	000-1:00	>20	178.6
1/12/99	1-3:00	>20	154.9
1/12/99	3-5:00	>20	107.1
1/12/99	5-7:00	>20	136.7
1/12/99	7-8:00	>20	142.0
1/12/99	8-9:00	>20	97.5
1/12/99	9-9:42	>20	69.5
D013			
1/13/99	5:50-9:17	>20	119.5

effective diameter via Gerber PVM-100 data

LWC from PVM-100 if effective diameter < 20 μm only

Table H-5: Davis, CA ambient conditions during events

EVENT	WIND SPEED [m s^{-1}]	WIND DIRECTION [degrees]	WIND DIRECTION STD. DEVIATION [degrees]	TEMPERATURE [°C]	PRESSURE [mb]
	mean±std. dev. (range)	mean±std. dev.	mean	mean±std. dev. (range)	mean±std. dev.
D352	0.6±0.4 (calm - 1.4)	154±110	105	4.7±1.4 (3.6 - 8.9)	1013.9±0.4

Reproduced with permission of the copyright owner. Further reproduction prohibited without permission.

D004	1.1±0.4 (calm - 2.0)	185±31	135	2.8±0.6 (2.2 - 4.2)	1027.7±0.5
D009	1.4±0.7 (0.2 - 2.6)	172±32	155	2.9±0.5 (1.5 - 3.6)	1027.3±0.7
D010	1.5±0.7 (calm - 2.8)	82±112	132	2.8±0.1 (2.6 - 3.1)	1023.6±0.5
D010B	1.2±0.6 (calm - 2.5)	161±129	195	2.4±0.4 (1.6 - 3.1)	1019.2±0.7
D011	2.2±0.6 (0.3 - 3.6)	143±161	94	2.9±0.2 (2.5 - 3.8)	1019.9±0.7
D013	2.5±0.7 (1.4 - 4.1)	160±172	72	5.3±0.1 (5.1 - 5.6)	1022.5±0.8

calculations used 5-minute stored averages (except std. dev. of wind direction)
event averages only shown

Table H-6: Davis, CA calculated deposition velocities and sampling time periods

event/date	time [local]	water [cm s^{-1}]	nitrate [cm s^{-1}]	sulfate [cm s^{-1}]	nitrite [cm s^{-1}]	ammonium [cm s^{-1}]
D352						
12/18/98	3:27-5:00	3.1	1.2	1.8	2.8	1.6
12/18/98	5-7:00	3.3	1.4	2.3	3.3	1.7
12/18/98	7-9:00	2.8	1.4	3.2	2.8	1.7
12/18/98	9-11:00	3.2	1.6	3.8	4.0	2.5
D004						
1/4/99	20:20-22:10	6.6	2.9	3.7	7.5	5.4
1/4/99-1/5/99	22:10-0:10	9.2	3.2	4.1	11.4	6.2
1/5/99	1:05-2:05	9.2	3.6	4.7	10.4	8.5
1/5/99	2:05-4:05	13.1	6.2	7.6	8.9	13.4
1/5/99	4:05-6:05	9.9	4.5	6.0	10.8	8.5
1/5/99	6:05-8:05	12.2	6.5	8.5	14.3	10.3
1/5/99	8:05-10:05	10.9	4.8	6.0	11.3	8.7
D009						
1/9/99	2:55-5:05	5.7	2.7	3.6	7.2	3.8
1/9/99	5:05-7:05	0.8	0.8	1.2	1.8	1.0
1/9/99	7:05-9:05	0.8	0.6	0.8	1.5	0.7
1/9/99	9:05-10:45	0.8	1.9	2.4	3.7	2.1
D010						
1/10/99	2:30-5:05	3.1	1.4	1.7	4.3	1.6
1/10/99	5:05-7:05	6.5	1.7	2.0	8.4	1.7
1/10/99	7:05-9:05	5.9	1.3	1.5	8.6	1.4
1/10/99	9:05-10:15	4.5	1.4	1.7	8.9	1.5
D010B						
1/10/99-1/11/99	22:40-1:05	9.6	4.0	4.3	9.6	4.9
1/11/99	1:05-3:05	7.3	2.2	2.6	11.2	3.0
1/11/99	3:05-5:05	4.6	1.5	2.4	6.9	2.1
1/11/99	5:05-7:05	5.1	1.7	2.7	9.2	2.6
1/11/99	7:05-9:05	11.4	3.6	4.9	10.7	6.6

Reproduced with permission of the copyright owner. Further reproduction prohibited without permission.

1/11/99	9:05-9:50	2.9	1.6	2.3	6.9	2.5
D011						
1/11/99-1/12/99	22:50-1:10	6.0	2.4	3.0	8.5	4.7
1/12/99	1:10-3:10	7.1	3.1	3.7	9.3	5.0
1/12/99	3:10-5:10	6.3	1.9	2.2	10.0	3.0
1/12/99	5:10-7:10	6.8	2.5	3.4	10.6	4.4
1/12/99	7:10-9:10	5.5	1.9	3.7	7.8	4.0
1/12/99	9:10-10:10	0.9	0.2	0.6	1.5	0.6
	mean	6.0	2.4	3.3	7.5	4.1
	min	0.8	0.2	0.6	1.5	0.6
	max	13.1	6.5	8.5	14.3	13.4

based upon mean of 2 LARGE plates only

Table H-7: Davis, CA bimodal drop distribution parameters

event/date	sampling period [local time]	LARGE MODE			SMALL MODE		
		mass diameter [μm]	gsd	mass fraction [%]	mass diameter [μm]	gsd	mass fraction [%]
D004							
1/4/99	20:04-22:00	29.2	1.23	98%	8.4	1.51	2%
1/4/99-1/5/99	23-1:00	29.2	1.23	88%	6.6	1.3	12%
1/5/99	2-4:00	29.2	1.23	95%	6.6	1.4	5%
D009							
1/9/99	4-6:00	26	1.23	85%	10.2	1.62	15%
1/9/99	7-9:00	24.6	1.35	93%	10.2	1.4	7%
D010							
1/10/99	4-6:00	33.9	1.35	75%	7	1.51	25%
1/10/99	6:52-9:00	36	1.23	75%	6	1.51	25%

derived from those calculated by Wendisch et al. (1998)

Table H-8: Davis, CA Copper cloud water concentrations (Caltech collectors only)

Event/ collector	Sample name	Copper	
		concentration [μg l^{-1}]	RSD [%]
D009			
CASCC2			
	Bulk #1	3.88	8.9%
	Bulk #2	5.30	8.2%
	Bulk #3	12.1	7.2%
	Bulk #4	24.4	6.9%
	Bulk #5	28.8	6.9%
	Bulk #6	34.9	6.9%

Reproduced with permission of the copyright owner. Further reproduction prohibited without permission.

Bulk #7		27.1	6.9%
sf-CASCC			
	Large #1	5.1	1.2%
	Large #2	6.8	0.2%
	Large #3	17.0	0.4%
	Large #4	29.2	0.1%
	Large #5	30.1	1.5%
	Large #6	33.7	0.0%
	Large #7	27.0	0.5%
	Small #2	8.1	0.1%
	Small #3	10.8	0.2%
	Small #4	16.6	1.5%
	Small #5	30.1	0.1%
	Small #6	40.3	1.5%
	Small #7	48.0	0.8%
D010			
CASCC2			
	Bulk #1	29.1	0.6%
	Bulk #2	21.6	1.0%
	Bulk #3	27.5	3.0%
	Bulk #4	23.1	1.0%
	Bulk #5	13.5	2.3%
	Bulk #6	12.9	2.1%
sf-CASCC			
	Large #1	22.1	0.1%
	Large #2	16.0	0.1%
	Large #3	15.8	0.4%
	Large #4	12.5	1.4%
	Large #5	10.4	0.4%
	Large #6	9.6	0.4%
	Small #1	15.5	1.6%
	Small #3	45.1	2.8%
D011			
CASCC2			
	Bulk #1	1.7	10.9%
	Bulk #2	2.0	10.0%
	Bulk #3	1.1	31.5%
	Bulk #4	0.9	34.0%
	Bulk #5	1.1	31.4%
	Bulk #6	2.7	9.0%
	Bulk #7	3.0	8.7%
	Bulk #8	46.9	6.8%
sf-CASCC			
	Large #1	1.0	11.0%
	Large #2	1.3	6.9%
	Large #3	1.5	2.7%
	Large #4	0.9	12.2%

Reproduced with permission of the copyright owner. Further reproduction prohibited without permission.

	Large #5	1.1	7.0%
	Large #6	2.3	14.3%
	Large #7	2.2	0.7%
	Large #8	76.7	2.2%
	Small #1	-12.2	-9.6%
	Small #2	-0.3	-117.7%
	Small #3	-0.1	-392.7%
	Small #4	0.5	93.5%
	Small #5	0.0	861.3%
	Small #6	-9.0	-10.4%
	Small #7	-11.0	-5.0%
	Small #8	-7.0	-11.3%

blanks measured but are not reported (no impact on results)

Table H-9: Davis, CA nitrite cloud water concentrations (Caltech collectors only)

Event/ Sample Name	Nitrite [μN]
pre-campaign blanks	
CASCC2	n.a.
sf-CASCC Large	n.a.
sf-CASCC Small	n.a.
DI	n.a.
D352	
CASCC2	
Bulk #1	40.8
Bulk #2	41.7
Bulk #3	23.4
Bulk #4	42.3
Bulk #5	42.5
Bulk #6	46.1
Bulk #7	52.6
Bulk #8	86.4
Bulk #9	165.9
sf-CASCC	
Large #1	69.6
Large #2	49.1
Large #3	23.9
Large #4	44.9
Large #5	45.5
Large #6	47.0
Large #7	52.4
Large #8	95.5
Large #9	186.8
Small #2	18.4
Small #3	10.2

Reproduced with permission of the copyright owner. Further reproduction prohibited without permission.

Small #4	13.6
Small #5	16.4
Small #6	21.7
Small #7	32.9
Small #8	34.3
Small #9	38.6
pre-D004 blanks	
CASCC2	0.0
sf-CASCC Large	0.0
sf-CASCC Small	0.0
DI	0.0
D004	
CASCC2	
Bulk #1	14.3
Bulk #2	13.8
Bulk #3	8.3
Bulk #4	10.2
Bulk #5	11.2
Bulk #6	12.4
Bulk #7	12.3
Bulk #8	13.7
Bulk #9	14.4
Bulk #10	16.2
Bulk #11	18.4
Bulk #12	20.1
Bulk #13	37.8
sf-CASCC	0.0
Large #1	16.5
Large #2	15.8
Large #3	8.5
Large #4	10.8
Large #5	11.0
Large #6	12.3
Large #7	12.4
Large #8	14.3
Large #9	15.3
Large #10	17.2
Large #11	18.7
Large #12	20.7
Large #13	39.6
Small #2	9.2
Small #3	6.0
Small #4	7.4
Small #5	7.4
Small #6	8.4
Small #7	9.4

Reproduced with permission of the copyright owner. Further reproduction prohibited without permission.

Small #8	9.5
Small #9	9.9
Small #10	10.6
Small #11	11.8
Small #12	12.5
Small #13	16.4
pre-D009 blanks	
CASCC2	0.0
sf-CASCC Large	0.0
sf-CASCC Small	0.0
DI	0.0
D009	
CASCC2	
Bulk #1	37.9
Bulk #2	50.1
Bulk #3	96.0
Bulk #4	109.9
Bulk #5	113.9
Bulk #6	101.8
Bulk #7	98.6
Bulk #8	96.8
Large #1	43.0
Large #2	57.8
Large #3	102.8
Large #4	133.7
Large #5	134.9
Large #6	114.2
Large #7	118.7
Large #8	115.9
Small #1	21.1
Small #2	25.9
Small #3	46.9
Small #4	52.8
Small #5	50.2
Small #6	51.5
Small #7	46.3
Small #8	76.9
pre-D010 blanks	
CASCC2	0.0
sf-CASCC Large	0.0
sf-CASCC Small	0.0
DI	0.0
D010	

Reproduced with permission of the copyright owner. Further reproduction prohibited without permission.

CASCC2	
Bulk #1	96.5
Bulk #2	74.8
Bulk #3	57.0
Bulk #4	48.1
Bulk #5	32.9
Bulk #6	34.1
sf-CASCC	
Large #1	99.7
Large #2	90.1
Large #3	71.8
Large #4	58.4
Large #5	45.2
Large #6	42.3
Small #1	30.5
Small #2	23.7
Small #3	33.6
Small #4	26.5
Small #5	37.3
Small #6	36.8
pre-D010B blanks	
CASCC2	0.0
sf-CASCC Large	0.0
sf-CASCC Small	0.0
DI	0.0
D010B	
CASCC2	
Bulk #1	44.8
Bulk #2	25.7
Bulk #3	13.2
Bulk #4	16.9
Bulk #5	20.0
Bulk #6	27.4
Bulk #7	23.2
Bulk #8	25.2
sf-CASCC	
Large #1	46.1
Large #2	30.5
Large #3	15.4
Large #4	18.5
Large #5	19.6
Large #6	30.0
Large #7	24.4
Large #8	28.1
Small #1	15.7

Reproduced with permission of the copyright owner. Further reproduction prohibited without permission.

Small #2	19.4
Small #3	16.4
Small #4	15.9
Small #5	13.5
Small #6	14.5
Small #7	21.5
Small #8	19.7
pre-D011 blanks	
CASCC2	0.0
sf-CASCC Large	0.0
sf-CASCC Small	0.0
DI	0.0
D011	
CASCC2	
Bulk #1	43.4
Bulk #2	46.8
Bulk #3	32.2
Bulk #4	18.6
Bulk #5	25.9
Bulk #6	34.5
Bulk #7	32.9
Bulk #8	34.8
sf-CASCC	
Large #1	45.5
Large #2	50.6
Large #3	34.5
Large #4	21.3
Large #5	28.7
Large #6	38.6
Large #7	33.6
Large #8	40.0
Small #1	9.7
Small #2	23.8
Small #3	21.7
Small #4	17.9
Small #5	16.6
Small #6	18.9
Small #7	18.4
Small #8	20.5
pre-D013 blanks	
CASCC2	0.0
sf-CASCC Large	0.0
sf-CASCC Small	0.0
DI	0.0

Reproduced with permission of the copyright owner. Further reproduction prohibited without permission.

D013	
CASCC2	
Bulk #1	75.9
sf-CASCC	
Large #1	88.6
Small #1	27.4

sample numbering corresponds to Reilly (2000)

Table H-10: Davis, CA CSU 5-Stage cloud water data

Event/sample	Chloride [μN]	Nitrate [μN]	Sulfate [μN]	Nitrite [μN]	Sodium [μN]	Ammonium [μN]	Potassium [μN]	Magnesium [μN]	Calcium [μN]	Sample Weight [g]	pH	Mn [μg l⁻¹]	Fe [μg l⁻¹]	Cu [μg l⁻¹]
pre-D004 blanks														
Stage 1	0.00	0.00	0.00	n.a.	0.26	0.52	0.73	3.37	4.27			0.09	1.53	n.a.
Stage 2	0.00	0.00	0.00	n.a.	0.37	0.46	0.76	3.37	4.05			0.20	0.96	n.a.
Stage 3	0.00	0.96	0.00	n.a.	-0.03	-0.14	0.01	3.14	4.27			0.04	0.67	n.a.
Stage 4	0.00	0.00	0.00	n.a.	-0.41	-0.27	0.00	3.44	3.78			0.05	1.48	n.a.
Stage 5	0.00	0.00	0.00	n.a.	-0.26	-0.19	0.10	3.31	4.15			0.04	1.33	n.a.
D004														
Sample set #1 (1/4/99 20:04-22:00)														
Stage 1	3.7	85.2	14	18.2	2	237.5	2	3	5.4	11.3	6.5	2.5	83.5	n.a.
Stage 2	6.62	148.51	23.39	19.64	4.14	338.46	3.50	4.07	5.13	4.1	6.63	5.53	116.8	n.a.
Stage 3	8.57	268.74	39.52	18.39	4.76	469.76	4.30	3.84	5.00	1.9	6.45	10.08	281.0	n.a.
Stage 4	99.70	862.93	113.32	15.20	19.31	1184.69	86.51	1.68	11.64	0.4	6.18	7.83	213.9	n.a.
Stage 5	n.a.	n.a.	n.a.	n.a.	n.a.	n.a.	n.a.	n.a.	n.a.	0	n.a.	n.a.	n.a.	n.a.
Stage 1 sample is composite of 2 consecutive samples with allowance for missing mass														
Sample set #2 (1/4/99 23:00 - 1/5/99 1:00)														
Stage 1	2.85	77.17	12.74	11.64	0.59	226.92	1.43	0.55	6.82	16.7	6.51	3.04	53.4	n.a.
Stage 2	4.51	136.24	20.37	13.62	1.07	305.60	2.04	1.11	8.26	5.3	6.61	4.82	187.1	n.a.
Stage 3	6.18	253.10	34.18	12.87	1.39	422.73	2.53	0.82	4.06	2.6	6.51	1.85	43.2	n.a.
Stage 4	68.66	684.70	85.46	16.06	21.55	946.05	57.87	10.08	19.67	0.3	6.45	13.93	1025.0	n.a.
Stage 5	182.9	1196.9	171.62	22.40	121.81	1210.13	208.77	77.76	496.2	1.8	6.9	19.21	558.1	n.a.
Sample set #3 (1/5/99 2-4:00)														
Stage 1	4.37	51.80	13.50	14.36	2.62	253.96	3.51	0.95	8.62	20.4	6.72	2.86	46.6	n.a.
Stage 2	3.27	81.33	16.82	16.04	1.14	302.29	2.47	1.12	9.29	3.3	6.62	2.06	44.5	n.a.
Stage 3	7.32	178.33	30.87	17.43	3.65	410.70	4.08	1.74	8.14	1.8	6.52	8.65	410.5	n.a.
Stage 4	21.23	613.53	84.73	14.96	4.51	865.84	15.89	1.95	8.62	0.5	6.28	6.63	137.8	n.a.
Stage 5	240.9	1510.5	200.06	38.67	165.02	995.91	467.04	103.49	948.5	0.4	6.8	26.60	169.6	n.a.

Reproduced with permission of the copyright owner. Further reproduction prohibited without permission.

pre-D009 blanks													
Stage 1	0.00	0.00	0.00	0.00	0.66	3.99	0.84	0.76	0.71		0.54	17.0	0.4
Stage 2	0.00	1.54	0.00	0.00	0.63	3.92	0.84	0.56	1.39		0.48	13.5	0.2
Stage 3	0.00	2.21	0.00	0.00	0.70	9.66	0.80	0.42	2.45		0.94	40.5	0.2
Stage 4	0.00	3.32	0.00	2.37	1.06	13.05	0.89	0.68	2.19		1.31	23.4	0.2
Stage 5	0.00	2.15	0.00	3.11	0.71	16.34	0.79	0.00	1.47		1.83	65.1	0.2
D009													
Sample set #1 (1/9/99 4-6:00)													
Stage 1	8.44	401.48	73.88	65.88	3.54	718.90	5.02	2.12	8.88	8.3	6.66	9.57	114.0	9.7
Stage 2	8.21	545.85	93.96	74.94	3.47	988.59	4.75	2.05	8.41	2.6	6.72	2.84	41.4	4.0
Stage 3	10.98	894.53	139.43	70.36	4.78	1317.65	10.87	2.27	9.40	2.4	6.84	1.83	22.1	4.2
Stage 4	19.56	1790.2	252.04	56.13	22.84	2418.60	16.82	2.41	13.58	1	6.63	12.23	635.0	19.6
Stage 5	127.7	6325.4	818.3	54.6	1797.8	7481.84	100.55	30.50	46.79	0.6	7.35	31.32	409.2	23.6
Sample set #2 (1/9/99 7-9:00)														
Stage 1	19.53	771.81	141.30	110.71	8.70	1233.02	12.08	7.90	16.80	7.6	6.78	38.67	842.0	24.1
Stage 2	31.05	1703.1	290.16	168.73	13.36	2496.63	15.58	5.83	30.97	2	6.65	30.64	880.9	30.7
Stage 3	88.48	1938.6	314.45	99.18	11.07	2538.99	14.56	4.54	17.14	1.8	6.08	27.29	557.9	27.6
Stage 4	75.18	4387.5	689.48	68.99	229.86	5478.40	29.37	16.62	37.90	0.7	6.56	37.48	2641.4	36.3
Stage 5	303.5	22907.	2727.92	77.83	86.69	24914.50	92.12	74.18	111.2	0.1	5.88	n.a.	n.a.	n.a.
pre-D010 blanks													
Stage 1	0.00	1.97	0.00	0.00	0.66	5.45	0.78	0.34	0.03		0.17	17.1	0.70
Stage 2	0.00	0.00	0.00	0.00	0.64	1.72	0.89	1.92	3.77		0.42	17.4	0.46
Stage 3	0.00	1.33	0.00	0.00	0.63	3.14	0.78	1.13	2.80		0.05	7.0	-0.04
Stage 4	2.19	1.53	1.81	0.00	2.02	2.81	0.70	2.10	3.43		-0.09	4.1	0.33
Stage 5	0.00	0.00	0.00	0.00	0.88	1.70	0.77	0.98	-0.41		0.16	8.8	-0.02
D010													
Sample set #1 (1/10/99 4-6:00)													
Stage 1	17.32	985.92	125.94	89.89	3.94	1498.30	8.57	2.35	12.79	2.9	6.72	15.83	262.8	10.8
Stage 2	25.37	1483.5	184.91	81.62	6.06	2307.72	11.93	4.31	31.71	0.6	6.64	20.84	715.1	22.9
Stage 3	42.73	2395.7	289.99	62.29	8.10	3418.39	17.49	3.55	28.41	0.8	6.45	17.01	322.6	n.a.
Stage 4	n.a.	n.a.	n.a.	n.a.	n.a.	n.a.	n.a.	n.a.	n.a.	0	n.a.	n.a.	n.a.	n.a.
Stage 5	257.3	11680.	1256.71	41.76	71.12	14786.90	179.36	148.59	253.0	0.7	6.3	42.24	591.2	37.3
Sample set #2 (1/10/99 6:52-9:00)														
Stage 1	14.53	852.94	93.42	55.44	5.11	1136.90	8.95	3.32	14.00	3.3	6.56	10.35	193.8	6.4
Stage 2	24.52	1317.4	143.09	53.06	5.60	1600.43	10.44	2.89	22.66	0.4	6.5	n.a.	n.a.	n.a.
Stage 3	104.2	2523.8	300.68	63.56	1398.5	2919.09	64.18	8.71	31.37	0.3	6.42	n.a.	n.a.	n.a.
Stage 4	130.4	6620.3	681.09	33.88	163.24	8154.76	40.62	9.39	40.71	0.2	6.1	n.a.	n.a.	n.a.
Stage 5	479.6	12286.	1137.43	61.58	123.77	16132.29	392.39	228.29	745.6	0.8	6.37	53.43	529.2	30.7

n.a. indicates not available

Reproduced with permission of the copyright owner. Further reproduction prohibited without permission.

Table H-11: Whiteface Mtn., NY copper cloud water concentrations (Caltech collectors only)

Event/ collector	Sample name	Cu [μg l^{-1}]	RSD [%]
pre-W188 blanks			
	CASCC2	1.0	19.8%
	sf-CASCC Large	3.0	6.7%
	sf-CASCC Small	1.3	19.8%
	DI	1.6	19.8%
W188			
CASCC2			
	Bulk #1	1.8	22.6%
	Bulk #2	4.0	12.4%
	Bulk #3	2.0	20.7%
	Bulk #4	1.1	34.5%
	Bulk #5	8.6	8.8%
	Bulk #6	2.7	16.3%
	Bulk #7	1.7	22.7%
	Bulk #8	1.5	26.5%
	Bulk #9	1.0	37.8%
	Bulk #10	1.1	32.9%
	Bulk #11	1.6	24.4%
	Bulk #12	2.5	17.0%
	Bulk #13	2.6	16.4%
	Bulk #14	5.0	11.1%
	Bulk #15	5.0	11.0%
	Bulk #16	1.5	26.2%
	Bulk #17	1.5	25.5%
	Bulk #18	0.5	69.6%
	Bulk #19	3.5	13.5%
sf-CASCC			
	Large #1	1.4	26.3%
	Large #2	0.3	114.2%
	Large #3	-0.5	-57.2%
	Large #4	1.0	35.4%
	Large #5	-0.9	-28.6%
	Large #6	0.8	41.0%
	Large #7	2.0	19.8%
	Large #8	-1.0	-24.5%
	Large #9	-0.5	-52.9%
	Large #10	7.7	9.7%
	Large #11	-0.7	-36.3%
	Large #12	-0.2	-176.4%
	Large #13	0.4	84.4%
	Large #14	0.1	428.2%
	Large #15	3.2	14.6%
	Large #16	0.1	287.1%
	Large #17	1.2	29.7%

Reproduced with permission of the copyright owner. Further reproduction prohibited without permission.

	Large #18	1.2	29.0%
	Large #19	1.5	24.4%
	Small #1	0.5	66.9%
	Small #2	1.1	33.3%
	Small #3	0.0	1359.0%
	Small #4	0.2	174.7%
	Small #5	0.4	96.1%
	Small #6	1.9	21.7%
	Small #7	2.6	16.4%
	Small #8	3.1	14.7%
	Small #9	1.0	36.2%
	Small #10	3.4	13.8%
	Small #11	1.1	32.8%
	Small #12	1.3	29.9%
	Small #13	1.9	21.4%
	Small #14	3.1	14.6%
	Small #15	3.7	13.0%
	Small #16	0.9	41.5%
	Small #17	1.1	33.4%
	Small #18	3.2	14.5%
	Small #19	1.3	29.8%
pre-W197 blanks			
	CASCC2	1.2	19.8%
	sf-CASCC Large	1.5	19.8%
	sf-CASCC Small	1.0	19.8%
	DI	0.5	19.8%
W197			
CASCC2			
	Bulk #1	3.9	10.7%
	Bulk #2	2.7	13.0%
	Bulk #3	2.6	13.4%
	Bulk #4	5.1	9.6%
	Bulk #5	5.1	9.5%
	Bulk #6	6.2	8.9%
	Bulk #7	10.2	7.9%
sf-CASCC			
	Large #1	17.6	7.5%
	Large #2	6.3	9.5%
	Large #3	4.9	10.6%
	Large #4	9.9	8.3%
	Large #5	9.6	8.4%
	Large #6	10.3	8.2%
	Large #7	12.4	7.9%
	Large #8	23.3	7.2%
	Small #1	4.1	9.8%

Reproduced with permission of the copyright owner. Further reproduction prohibited without permission.

	Small #2	2.1	13.8%
	Small #3	1.6	16.8%
	Small #4	3.6	10.3%
	Small #5	2.9	11.6%
	Small #6	7.8	8.0%
	Small #7	4.0	9.9%
	Small #8	10.8	9.5%
pre-W198 blanks			
	CASCC2	1.1	19.8%
	sf-CASCC Large	1.7	6.7%
	sf-CASCC Small	2.1	6.7%
	DI	1.1	19.8%
W198			
CASCC2			
	Bulk #1	5.0	9.3%
	Bulk #2	4.7	9.5%
	Bulk #3	2.9	11.9%
	Bulk #5	1.9	15.7%
	Bulk #6	1.6	17.5%
	Bulk #7	2.7	12.4%
	Bulk #9	2.2	14.0%
	Bulk #10	0.9	27.4%
sf-CASCC			
	Large #1	16.8	7.4%
	Large #2	9.4	8.0%
	Large #3	5.9	8.8%
	Large #4	3.6	10.4%
	Large #5	2.5	12.1%
	Large #6	1.9	13.9%
	Large #7	7.6	8.3%
	Large #8	0.4	46.1%
	Large #9	0.9	22.6%
	Large #10	0.4	48.6%
	Small #1	3.1	12.2%
	Small #2	0.8	29.6%
	Small #3	0.7	35.0%
	Small #4	3.4	11.6%
	Small #5	2.0	15.7%
	Small #6	2.0	15.4%
	Small #7	0.8	30.5%
	Small #8	1.8	16.8%
	Small #9	-0.1	-140.8%
	Small #10	-0.4	-47.3%

Reproduced with permission of the copyright owner. Further reproduction prohibited without permission.

Table H-12: Whiteface Mtn., NY CSU 5-Stage data

Event/sample	Chloride [µN]	Nitrate [µN]	Sulfate [µN]	Sodium [µN]	Ammonium [µN]	Potassium [µN]	Magnesium [µN]	Calcium [µN]	Sample Weight [g]	pH	Mn [µg l^{-1}]	Fe [µg l^{-1}]	Cu [µg l^{-1}]	Cu RSD [%]	Total peroxides [µM]
pre-W188 blanks															
Stage 1	0.00	0.00	0.00	0.32	0.00	0.63	2.07	4.86			0.53	44.1	3.9	6.7%	n.a.
Stage 2	0.00	0.00	0.00	0.42	0.52	0.73	2.14	2.58			0.30	43.9	0.9	19.8%	n.a.
Stage 3	0.00	0.00	0.00	0.68	0.00	0.84	2.10	2.44			0.29	37.2	2.2	6.7%	n.a.
Stage 4	0.00	0.00	0.00	0.32	0.00	0.00	2.12	2.75			0.37	38.4	2.5	6.7%	n.a.
Stage 5	0.00	0.00	0.00	1.09	0.00	0.82	2.05	2.53			0.42	45.0	1.6	19.8%	n.a.
W188															
Sample set #1 (7/8/98 0-1:00)															
Stage 1	n.a.	n.a.	n.a.	n.a.	n.a.	n.a.	n.a.	n.a.	0	n.a.	n.a.	n.a.	n.a.	n.a.	n.a.
Stage 2	10.53	64.33	375.86	5.16	121.3	3.43	5.96	118.97	0.75	3.53	5.38	53.0	3.8	20.1%	n.a.
Stage 3	15.74	172.9	952.84	5.45	233.0	5.86	12.10	139.51	0.3	3.12	n.a.	n.a.	n.a.	n.a.	n.a.
Stage 4	25.40	247.4	1423.29	14.99	339.9	17.38	8.08	150.59	0.8	2.99	8.65	96.8	-2.0	-28.5%	n.a.
Stage 5	23.69	164.5	883.16	9.67	234.2	9.16	26.79	140.86	1.5	3.21	5.99	119.2	6.5	14.4%	n.a.
pre-W198 blanks															
DI	*not reported here*										0.44	40.6	2.4	6.7%	n.a.
Stage 1	2.78	1.00	0.85	2.28	0.00	1.20	2.04	7.05			0.38	33.1	1.3	19.8%	n.a.
Stage 2	0.00	1.45	10.51	0.42	0.00	0.00	1.92	2.15			0.36	30.9	1.0	19.8%	n.a.
Stage 3	3.28	1.24	0.00	2.91	0.00	1.18	1.89	1.66			0.30	36.3	0.8	19.8%	n.a.
Stage 4	0.00	0.00	0.00	0.52	0.53	0.43	1.89	1.89			0.25	32.5	0.8	19.8%	n.a.
Stage 5	2.75	2.40	0.62	2.81	0.00	1.13	1.93	2.25			0.27	29.5	0.6	19.8%	n.a.
W198															
Sample set #1 (7/17/99 2-3:00)															
Stage 1	65.12	1328.	1072.90	28.16	716.2	23.24	283.53	1286.76	1.75	3.06	170.1	1573.	16.4	18.6%	9.0
Stage 2	54.92	729.3	983.04	27.29	650.7	16.35	93.36	991.71	0.75	3.07	69.55	932.5	15.0	11.1%	8.2
Stage 3	27.46	418.4	1355.03	5.55	546.7	4.91	9.80	65.46	5.3	3.01	10.07	132.8	5.7	10.0%	24.5
Stage 4	24.20	349.5	1003.47	4.34	465.8	4.05	4.89	43.11	5.6*	3.08	4.55	46.5	5.2	10.3%	n.a.
Stage 5	31.19	319.0	868.95	9.39	402.5	10.70	15.92	57.15	5.5	2.88	4.02	52.4	3.4	12.5%	41.0
Sample set #2 (7/17/99 4-5:00)															
Stage 1	25.69	462.9	1036.67	10.98	383.1	9.02	93.52	370.57	5.6	3.16	47.11	443.2	17.1	10.5%	7.6
Stage 2	19.62	296.6	930.09	7.22	352.7	5.50	31.54	302.15	1.8	3.22	29.27	732.3	4.2	22.6%	7.8
Stage 3	12.21	179.3	639.47	2.87	258.8	2.66	4.74	43.79	5.35*	3.25	3.34	50.2	0.5	49.8%	10.9
Stage 4	14.41	210.0	683.73	2.76	296.0	3.98	12.93	45.66	5.25	3.25	4.82	38.7	-0.5	-41.0%	19.0
Stage 5	23.54	199.7	670.97	8.40	279.7	6.42	17.43	55.32	4.85	3.27	4.56	41.1	1.0	28.2%	15.5
Sample set #3 (7/17/99 6-7:00)															
Stage 1	25.16	487.3	732.67	9.29	339.6	6.13	90.80	295.62	13.9	3.2	31.61	242.3	1.4	21.1%	30.4
Stage 2	18.89	308.5	658.43	6.11	312.8	4.83	16.70	122.44	5.4	3.21	10.16	156.3	1.1	26.9%	33.9

Reproduced with permission of the copyright owner. Further reproduction prohibited without permission.

Stage 3	14.96	290.2	584.56	1.88	299.6	2.44	4.50	35.44	5.35*	3.23	4.14	50.7	1.2	24.9%	39.4
Stage 4	16.79	282.3	580.35	3.02	302.0	4.22	9.85	39.91	5.45	3.22	3.47	42.1	-0.8	-47.0%	36.7
Stage 5	32.44	262.4	539.66	9.39	287.2	12.41	25.61	84.32	4.05	3.29	5.49	37.5	-0.8	-44.3%	34.6
Sample set #4 (7/17/99 8-9:00)															
Stage 1	23.01	337.4	612.20	5.43	239.5	3.03	53.71	161.64	21.8	3.22	23.77	244.1	0.1	221.4%	4.7
Stage 2	15.64	221.2	552.63	2.75	219.9	2.32	7.30	68.83	8.4	3.24	5.41	84.9	1.8	18.1%	3.9
Stage 3	17.71	192.8	462.90	6.24	193.4	6.60	4.13	36.43	5.45	3.29	1.97	32.5	0.0	-1090%	4.4
Stage 4	16.00	195.1	433.51	3.59	193.1	4.28	5.75	57.14	5.55*	3.36	2.17	28.2	-0.1	-192%	7.5
Stage 5	41.78	212.5	445.61	12.94	216.4	15.14	42.60	160.83	4.55	3.46	6.63	45.2	-0.1	-252%	7 0
Sample set #5 (7/17/99 10-11:00)															
Stage 1	27.08	270.6	644.24	9.46	274.8	14.65	43.76	202.76	9	3.31	15.72	222.4	2.2	15.9%	22.9
Stage 2	11.83	177.5	555.69	2.82	245.5	2.10	9.13	84.80	6.5	3.33	5.84	83.7	2.2	16.0%	24.6
Stage 3	10.20	152.7	459.34	2.74	211.5	2.45	3.31	29.02	5.55	3.37	1.74	31.4	0.6	42.3%	23.6
Stage 4	10.65	156.3	440.91	1.04	207.1	1.44	3.97	29.69	4.45	3.38	1.57	31.1	1.2	23.9%	25.9
Stage 5	39.71	202.4	551.86	18.46	260.9	21.22	43.84	154.79	3.3	3.41	4.80	45.6	0.4	62.5%	15.8

**mass lost prior to weighing*

n.a. indicates not available

Table H-13: Whiteface Mtn., NY simulated drop distributions

event/date	sampling period [local time]	LARGE MODE			SMALL MODE		
		mass diameter [μm]	gsd	mass fraction [%]	mass diameter [μm]	gsd	mass fraction [%]
W198							
7/17/98	2-3:00	25	1.18	5%	11	1.3	95%
7/17/98	4-5:00	34	1.15	7%	13.5	1.47	93%

Table H-14: Whitefact Mtn., NY calculated effective diameters

event/ sampling period	CSASP D_{eff} [μm]	GERBER D_{eff} [μm]
W188 (7/7/98)		
19:00-19:30	17.1	13.88
19:30-20:00	15.0	12.32
20:00-20:30	15.5	13.23
20:30-21:00	12.6	10.98
21:00-21:30	13.9	10.86
21:30-22:00	15.8	12.87
22:00-22:30	15.1	12.33
22:30-23:00	14.6	12.15
23:00-23:30	15.8	13.38
23:30-24:00	15.0	12.61
W198 (7/17/98)		
1:30-2:00	13.97	10.60

Reproduced with permission of the copyright owner. Further reproduction prohibited without permission.

2:00-3:00	14.93	11.02
3:00-4:00	14.71	11.71
4:00-5:00	14.92	12.73
5:00-6:00	15.36	14.06
6:00-7:00	15.19	14.91
7:00-8:00	15.50	15.50
8:00-9:00	16.12	15.99
9:00-10:00	15.74	15.48
10:00-11:00	15.63	14.97

Table H-15: Whiteface Mtn., NY validated dV distributions

midpoint bin diameter	event/time period												
	W188	W188	W188	W188	W188	W188	W188	W188	W198	W198	W198	W198	W198
	19:00-19:30	19:30-20:00	20:00-20:30	20:30-21:00	21:00-21:30	21:30-22:00	22:00-23:00	23:00-24:00	6:00-7:00	7:00-8:00	8:00-9:00	9:00-10:00	10:00-11:00
[µm]	[mg m^{-3}]	[mg m^{-3}]	[mg m^{-3}]	[mg m^{-3}]	[mg m^{-3}]	[mg m^{-3}]	[mg m^{-3}]	[mg m^{-3}]	[mg m^{-3}]	[mg m^{-3}]	[mg m^{-3}]	[mg m^{-3}]	[mg m^{-3}]
3.5	0.2	0.1	0.2	0.2	0.2	0.2	0.2	0.2	0.3	0.4	0.3	0.3	0.3
5	1.5	1.1	1.7	1.7	1.3	1.6	1.6	1.8	2.6	2.9	2.7	2.7	2.5
7	5.0	4.2	5.9	6.9	5.2	5.6	5.7	6.1	9.4	10.4	9.8	9.5	8.8
9	13.4	12.4	15.3	17.2	14.2	15.6	15.3	16.5	24.6	26.2	24.5	24.0	22.3
11	27.7	27.9	30.0	29.5	27.9	32.1	30.2	32.9	48.0	50.7	48.8	47.0	44.2
13	47.0	46.9	47.0	36.5	41.6	52.6	47.1	52.2	73.3	79.2	81.7	76.2	72.4
15	67.8	61.7	62.0	32.9	48.3	71.3	59.6	68.1	86.3	95.1	104.8	96.0	91.4
17	77.7	59.5	61.7	20.8	41.5	75.2	58.7	70.0	91.2	104.5	120.7	105.6	99.1
19	85.0	43.0	58.0	11.2	26.1	72.8	48.8	64.5	86.4	98.5	118.4	99.8	91.0
21	80.0	27.3	49.2	5.2	13.7	62.5	33.8	53.4	64.4	81.0	105.3	83.2	74.6
23	68.2	13.9	27.8	2.0	5.1	34.3	16.0	28.1	37.1	50.4	72.1	54.3	47.8
25	39.6	5.3	10.9	0.6	1.3	13.2	5.4	10.2	15.5	22.9	35.6	26.3	21.8
27	16.5	1.5	3.0	0.1	0.2	3.3	1.2	2.5	4.4	7.4	12.4	8.9	7.0
29	5.0	0.4	0.6	0.0	0.0	0.7	0.2	0.5	1.0	2.0	3.5	2.5	1.9
31	1.2	0.0	0.1	0.0	0.0	0.1	0.0	0.1	0.1	0.3	0.5	0.4	0.3

Table H-16: Whiteface Mtn., NY ambient cloud sampling data (selected events)

event/ sampling period	mean wind speed [m s^{-1}]	std. dev. wind speed [m s^{-1}]	mean wind dir. [deg.]	std. dev. wind dir. [deg.]
W188 (7/7/98)				
19:00-19:30	5.0	0.6	262	9.6
19:30-20:00	3.9	0.3	266	8.9
20:00-20:30	4.1	0.3	261	9.7
20:30-21:00	4.6	0.3	263	4.6
21:00-21:30	4.6	0.3	256	5.8
21:30-22:00	4.3	0.2	251	10.8

Reproduced with permission of the copyright owner. Further reproduction prohibited without permission.

22:00-22:30	3.9	0.3	254	10.0
22:30-23:00	4.5	0.7	246	10.5
23:00-23:30	5.5	0.5	248	9.5
23:30-24:00	5.4	0.4	247	5.1
W198 (7/17/98)				
1:30-2:00	6.1	0.3	262.7	11.3
2:00-3:00	5.8	0.3	262.2	13.4
3:00-4:00	5.9	0.8	260.0	12.0
4:00-5:00	7.1	0.7	263.5	9.5
5:00-6:00	5.8	0.4	265.2	14.2
6:00-7:00	6.4	0.4	265.8	11.9
7:00-8:00	7.0	0.6	263.1	12.5
8:00-9:00	6.1	0.3	260.8	12.2
9:00-10:00	4.7	0.9	262.6	18.9
10:00-11:00	3.8	0.5	262.8	21.8

Table H-17: ACE-2 ambient conditions by event

event	WIND SPEED [m s^{-1}] mean±std. dev.	WIND DIRECTION [degrees] mean±std. dev.	TEMPERATURE [°C] mean±std. dev.
T188	11.7±0.3	334±16	16.0±0.1
T189	13.7±0.3	337±4	15.4±0.1
T195	8.8±0.7	331±9	15.9±0.2
T201	14.5±0.4	350±5	16.2±0.2
T203	14.3±0.5	338±4	16.3±0.1

based upon data obtained from ACE-2 main data base
event averages only shown

Table H-18: ACE-2 validated dV data for polluted/intermediate events

midpoint bin diameter	event/sampling time period														
	T188 2100-2130	T188 2130-2200	T188 2200-2240, 47-52	T188 2324-2400	T188 000-100	T188 100-200	T189 000-100	T189 0100-0200	T189 0200-0300	T189 0300-0400	T189 0400-0500	T189 0500-0600	T189 0600-0700	T189 0700-0800	T195 0604-0755
[μm]	[mg m^{-3}]	[mg m^{-3}]	[mg m^{-3}]	[mg m^{-3}]	[mg m^{-3}]	[mg m^{-3}]	[mg m^{-3}]	[mg m^{-3}]	[mg m^{-3}]	[mg m^{-3}]	[mg m^{-3}]	[mg m^{-3}]	[mg m^{-3}]	[mg m^{-3}]	[mg m^{-3}]
1.2	0.0	0.0	0.0	0.0	0.0	0.0	0.0	0.0	0.0	0.0	0.0	0.0	0.0	0.0	0.0
3.55	0.0	0.1	0.1	0.1	0.1	0.0	0.1	0.1	0.1	0.0	0.0	0.0	0.1	0.1	0.0
5.9	1.2	1.3	1.4	1.4	1.6	1.2	1.4	1.3	1.3	1.3	1.2	1.4	1.8	2.1	0.9
8.25	17.4	17.6	16.7	21.0	22.4	19.4	18.9	17.0	15.6	17.8	18.5	20.3	18.3	21.9	18.0
10.6	93.0	91.3	84.4	116.1	120.0	122.8	97.8	87.9	77.2	100.9	113.2	109.6	70.5	70.9	108.1
12.95	60.7	55.7	49.5	72.0	76.3	88.3	61.5	54.3	46.2	69.1	80.0	72.1	33.7	28.8	56.5
15.3	12.3	11.3	9.8	14.9	15.6	19.6	12.0	10.7	8.8	14.3	17.9	15.1	5.5	4.5	9.5
17.65	13.1	12.0	10.4	16.2	16.6	22.1	12.6	11.3	9.0	15.3	20.4	16.3	5.1	4.1	11.1
20	3.4	3.4	2.9	4.8	4.5	6.4	3.2	3.0	2.2	4.0	6.0	4.4	1.1	0.9	4.2
22.35	0.4	0.5	0.5	0.8	0.7	0.9	0.5	0.4	0.3	0.5	0.8	0.5	0.1	0.1	0.7
24.7	0.1	0.2	0.2	0.3	0.2	0.3	0.2	0.1	0.1	0.1	0.2	0.1	0.0	0.0	0.2

Reproduced with permission of the copyright owner. Further reproduction prohibited without permission.

27 05	0.1	0 2	0.2	0 2	0.2	0 3	0 2	0 1	0.1	0.1	0 2	0 1	0 0	0 0	0 1
29 4	0 1	0 2	0 2	0 3	0 2	0 3	0 2	0 1	0 1	0 1	0 2	0 1	0 0	0 1	0 1
31 75	0 0	0 0	0 0	0.0	0 0	0 1	0.0	0 0	0 0	0 0	0 0	0.0	0 0	0 0	0 0
34 1	0 0	0 1	0 1	0 0	0 1	0 1	0.0	0.0	0.0	0 0	0 0	0 0	0 0	0 0	0 0
36 45	0.0	0.0	0.0	0 0	0.0	0 1	0 0	0 0	0.0	0 0	0 0	0 0	0 0	0 0	0 0
38 8	0.0	0 0	0 0	0 0	0.0	0.0	0.0	0.0	0.0	0.0	0 0	0 0	0 0	0 0	0 0
41 15	0 0	0.0	0 0	0 0	0.0	0 0	0 0	0 0	0.0	0 0	0 0	0.0	0 0	0 0	0 0
43.5	0 0	0.0	0.0	0.0	0 0	0.0	0 0	0 0	0 0	0.0	0 0	0 0	0 0	0 0	0 0
45 85	0 0	0 0	0 0	0 0	0 0	0 0	0 0	0 0	0 0	0 0	0 0	0 0	0 0	0 0	0 0
total LWC	201 9	194 0	176.5	248.2	258 7	281 8	208.6	186.6	161.0	223 6	258 7	240 2	136 6	133.5	209 4

screened for dN < 1200 cm^{-3}

Table H-19: ACE-2 validated dV data for the clean event

midpoint bin diameter [µm]	event/sampling time period T203 1730-1900 [mg m^{-3}]	T203 1900-2000 [mg m^{-3}]	T203 2000-2100 [mg m^{-3}]	T203 2100-2200 [mg m^{-3}]	T203 2200-2300 [mg m^{-3}]
1 2	0.0	0 0	0.0	0.0	0.0
3 55	0 0	0 0	0 0	0 0	0 0
5 9	0 0	0 0	0 0	0 0	0 0
8 25	1 2	0 1	0 1	0 4	0 1
10 6	18.2	1 8	1.5	4 5	4 1
12.95	24 9	12.3	12 8	17 0	18.3
15 3	11 9	13 6	17 8	20 0	19.7
17 65	36 0	45.7	84 1	73 8	99 2
20	72.8	79 5	103 9	93.3	110 6
22 35	50 6	55 8	16 8	26 3	14 0
24 7	24 5	30 7	3 8	8 2	4 4
27 05	23 6	31 1	4 3	6 6	5 4
29 4	22 8	15 4	3 2	4 3	3 7
31 75	4 0	1 2	0 2	0 4	0 2
34 1	6 0	1 4	0 1	0 3	0 2
36 45	4 5	0 5	0 0	0 1	0 1
38 8	3 1	0 2	0 0	0 1	0 0
41 15	1 1	0 1	0 0	0 1	0 0
43 5	0 1	0 0	0 0	0 0	0 0
45 85	0 0	0 0	0 0	0 0	0 0
total LWC	305 4	289 4	248 6	255 3	280 1

screened for dN < 1200 cm^{-3}

Reproduced with permission of the copyright owner. Further reproduction prohibited without permission.

Table H-20: ACE-2 cloud water data (sf-CASCC only)

Event/sample	Date	Start time [local]	End time [local]	Chloride [μN]	Nitrate [μN]	Sulfate [μN]	Sodium [μN]	Ammonium [μN]	Potassium [μN]	Magnesium [μN]	Calcium [μN]	Mn [μg l^{-1}]	Fe [μg l^{-1}]	pH	Total Peroxide [μM]	S(IV) [μM]	Sample weight [g]
pre-ACE2 blanks																	
sf-CASCC Large				-0.12	0	0	3.55	1.99	0.78	2.27	2.97	0.33	2.0		n.a.	n.a.	
sf-CASCC Small				0	0	0	1	2.52	0.68	2.22	3	0.12	1.1		n.a.	n.a.	
Spray bottle				0	0.85	0	0.5	0.33	0	2.29	2.94	0.17	n.a.		n.a.	n.a.	
squirt bottle				0	0	0	0.15	0	0.69	2.21	2.77	0.07	-1.5		n.a.	n.a.	
T188																	
Large #1	7/7/97	19:28	20:00	2303.44	394.64	772.58	2340.6	340.3	66.55	532.	407	28.53	307.2	4.01	65.0	2.8	19.3
Large #2	7/7/97	20:00	20:30	2587.55	430.04	832.41	2596.4	406.55	70.31	593	458	30.82	424.9	4.1	63.7	1.0	21.3
Large #3	7/7/97	20:30	21:00	3500.36	582.59	1062.2	3528.3	451.29	96.93	807	645	41.95	538.6	4.14	74.8	3.5	20.4
Large #4	7/7/97	21:00	21:30	4413.47	774.34	1314.6	4378.1	530.74	118.23	1003.	819.7	56.96	720.7	4.34	84.9	0.7	15.8
Large #5	7/7/97	21:30	22:00	4043.03	719.49	1233.6	4016.1	528.58	108.31	920.44	764.79	48.97	518.1	4.25	85.5	-1.0	14.1
Large #6	7/7/97	22:00	22:40*	3830.25	607.66	1037.8	3741.2	429.9	98.19	855.35	693.32	51.03	907.4	4.76	78.3	1.4	28.1
Large #7	7/7/97	23:24	0:00	6188.16	979.46	1453.7	5834.5	533.63	151.29	1328.4	1066.1	69.27	655.1	5.7	86.8	n.a.	26.5
Large #8	7/8/97	0:00	1:00	4129	552	1031.1	3976.4	427.63	103.9	898.87	664.1	41.97	483.9	4.87	73.2	-0.8	46.8
Large #9	7/8/97	1:00	2:00	3582.3	452.63	931.2	3468.6	400.49	90.4	788.62	548.65	39.37	597.7	4.36	58.5	0.3	58.5
Large #10	7/8/97	2:00	3:00	3295.94	533.7	987.36	3318.9	445.13	90.48	769.17	551.06	n.a.	n.a.	3.97	n.a.	n.a.	58.4
Large #11	7/8/97	3:00	4:00	3721.14	723.55	1230.9	3778.8	588.22	106.15	879.29	671.3	41.66	410.6	3.88	54.4	0.7	35.8
Large #12	7/8/97	4:00	5:00	3297.72	502.08	875.58	3231.4	500.77	89.46	727.95	456.39	n.a.	n.a.	4.18	n.a.	n.a.	51.7
Large #13	7/8/97	5:00	6:00	3884.48	559.96	978.27	3844.4	397.85	76.41	858.13	450.16	28.83	432.6	4.01	57.0	2.9	41.2
Large #14	7/8/97	6:00	7:00	5637.15	818.17	1513.7	5547.8	700.03	105.63	1253.4	617.88	n.a.	n.a.	3.82	n.a.	n.a.	19.6
Large #15	7/8/97	7:00	8:00	5392.53	583.12	1229	5122.6	503.13	132.97	1163.9	512.12	32.12	406.9	3.84	42.5	3.7	63.3
Small #1	7/7/97	19:28	20:00	412.725	86.04	510.9	455.42	302.6	17.995	110.3	73.7	5.67	181.0	3.72	66.0	1.8	55.2
Small #2	7/7/07	20:00	20:30	298.02	68.21	507.73	315.88	313.32	14.4	77.14	53.15	4.39	66.4	3.65	66.0	1.9	61.9
Small #3	7/7/97	20:30	21:00	277.66	81.01	582.17	294.0	382.63	15.43	74.57	53.84	5.26	147.8	3.58	81.0	1.9	50.9
Small #4	7/7/97	21:00	21:30	452.53	126.54	707.6	475.5	460.48	21.22	115.21	73.72	6.85	187.8	3.54	86.0	1.1	39.8
Small #5	7/7/97	21:30	22:00	508.94	144.46	759.49	537.64	510.97	25.06	129.71	83.27	8.26	238.4	3.54	91.9	0.6	37.8
Small #6	7/7/97	22:00	22:40*	699.64	133.8	628.89	696.05	409.89	26.48	161.81	101.01	7.7	135.0	3.66	83.7	0.1	57.9
Small #7	7/7/97	23:24	0:00	948.52	242.56	844.63	989.35	541.23	36.05	236.83	162.24	15	317.5	3.58	92.2	0.5	64
Small #8	7/8/97	0:00	1:00	340.6	83.25	516.84	344.49	381.24	19	85.89	54.54	4.91	85.7	3.69	77.9	1.5	107.6
Small #9	7/8/97	1:00	2:00	270.5	61.69	458.29	250.36	314.92	16.12	66.58	41.06	3.71	82.0	3.66	62.8	0.0	128.8
Small #10	7/8/97	2:00	3:00	300.77	76.27	486.93	268.84	329.2	15.54	67.89	42.48	n.a.	n.a.	3.59	n.a.	n.a.	133.5
Small #11	7/8/97	3:00	4:00	341.82	125.25	625.19	297.27	439.75	22.82	77.33	49.21	4.28	92.4	3.5	57.7	0.6	111.8
Small #12	7/8/97	4:00	5:00	267.21	71.12	357.14	243.11	314.74	13.64	62.53	34.78	n.a.	n.a.	3.82	n.a.	n.a.	116.7
Small #13	7/8/97	5:00	6:00	308.41	89.5	418.45	272.15	347.08	16.53	69.86	35.22	3.01	59.7	3.7	60.5	1.9	117.6
Small #14	7/8/97	6:00	7:00	617.11	171.38	855.41	575.62	618.44	33.01	138.52	59.89	n.a.	n.a.	3.43	n.a.	n.a.	71.1
Small #15	7/8/97	7:00	8:00	269.28	62.93	410.9	231.35	285.71	15.04	60.58	31.93	3.06	132.3	3.67	41.5	0.3	137.8
pre-T189 blanks																	
sf-CASCC Large				2.78	1.51	0	1.09	3.27	0.21	2.08	3.41	0.242	6.6		0.0	1.3	
sf-CASCC Small				2.41	1.69	0	0.95	3.8	0.36	1.89	3.13	0.132	6.1		0.0	0.6	

Reproduced with permission of the copyright owner. Further reproduction prohibited without permission.

T189																		
Large #1	7/8/97	23:02	0:00	3974.68	587.83	1049.8	3970.0	400.37	103.75	896.38	491.12	25.34	128.6	3.76	66.7	2.7	31.7	
Large #2	7/9/97	0:00	1:00	5640.01	898.01	1479.4	5520.7	506.8	142.23	1259.6	639.69	35.46	377.9	3.55	68.6	1.0	35.3	
Large #3	7/9/97	1:00	2:00	5014.11	598.03	1218.7	4780.3	473.6	124.65	1086.0	555.62	30.81	377.7	3.78	74.8	2.7	35.7	
Large #4	7/9/97	2:00	3:00	5791.28	894.05	1547.8	5680.5	578.02	146.79	1291.2	621.92	n.a.	n.a.	3.54	n.a.	n.a.	27.9	
Large #5	7/9/97	3:00	4:00	4395.44	668.51	1192.5	4328.1	453.91	111.83	984.18	436.16	20.9	374.2	3.54	63.2	1.4	49.7	
Large #6	7/9/97	4:00	5:00	3288.27	489.78	901.65	3254.2	358.85	85.18	736.38	287.88	n.a.	n.a.	3.6	n.a.	n.a.	70.1	
Large #7	7/9/97	5:00	6:00	3489.72	428.72	903.92	3382.0	384.64	87.51	761.22	248.75	12.21	222.3	3.6	65.1	2.3	61.4	
Large #8	7/9/97	6:00	7:00	3983.83	392.09	983.94	3779.7	420.24	96.18	854.09	246.39	n.a.	n.a.	3.59	n.a.	n.a.	29.4	
Large #9	7/9/97	7:00	8:00	6526.88	451.21	1334.2	6038.7	519.29	146.89	1360.3	337.14	9.25	129.6	3.57	n.a.	1.7	29.5	
Small #1	7/8/97	23:02	0:00	391.4	125.7	621.9	347.73	346.9	20.07	87.37	60.95	5.91	95.8	3.42	75.7	-0.2	89.1	
Small #2	7/9/97	0:00	1:00	501.79	163.93	754.3	450.19	414.66	21.99	109.69	71.01	5.74	107.1	3.35	70.2	0.5	94.5	
Small #3	7/9/97	1:00	2:00	481.3	130.84	647.2	441.68	397.48	23.66	107.02	70.63	6.11	114.4	3.48	85.2	1.2	89.1	
Small #4	7/9/97	2:00	3:00	616.96	185.05	922.6	562.0	518.04	34.56	134.17	86.33	n.a.	n.a.	3.31	n.a.	n.a.	84.5	
Small #5	7/9/97	3:00	4:00	341.71	118.6	586.5	284.42	331.85	18.59	72.85	47.86	4.09	94.5	3.42	65.7	0.3	107.3	
Small #6	7/9/97	4:00	5:00	258.62	72.51	447.4	208.23	270.07	10.94	54.39	28.43	n.a.	n.a.	3.52	n.a.	n.a.	122	
Small #7	7/9/97	5:00	6:00	270.56	65.8	440.9	222.75	278.15	13.22	59.11	29.73	2.58	52.7	3.56	67.5	0.0	113.3	
Small #8	7/9/97	6:00	7:00	350.99	78.16	573.28	317.34	359.57	15.91	78.55	34.03	n.a.	n.a.	3.49	n.a.	n.a.	61.7	
Small #9	7/9/97	7:00	8:00	665.12	124.41	739.66	630.77	448.11	26.62	149.42	53.19	3.22	54.8	3.47	72.3	1.3	57.4	
pre-T195 blanks																		
sf-CASCC Large				1.49	1.29	0	0.66	2.72	0.16	1.83	3.59	0.052	2.2		0.0	1.1		
sf-CASCC Small				0	0	0	0.33	1.97	0.12	1.73	3.21	0.092	1.2		0.0	-0.9		
DI				1.7	0	0	0.66	-0.28	0.26	1.74	3	0.034	2.8		0.0	-0.3		
T195																		
Large #1	7/14/97	6:04	7:55	425.23	126.32	275.63	448.75	129.8	13.53	107.57	64.81	6.08	67.3	3.89	66.3	0.1	73.3	
Small #1	7/14/97	6:04	7:55	122.23	53.05	268.5	82.69	157.71	5.83	23.74	28.18	3.81	46.2	3.81	67.9	1.0	83.1	
T201																		
Large #1	7/20/97	20:00	20:30	6090.87	197.42	803.27	5460.2	187.3	128.1	1221.9	361.58	13.17	120.9	4.21	n.a.	1.3	96	
Small #1	7/20/97	20:00	20:30	1096.23	87.49	394.79	1055.2	184.58	30.13	242.33	85.23	6.19	83.8	3.84	n.a.	1.0	11.2	
T203																		
Large #1	7/22/97	17:30	19:00	221.35	8.87	36.065	196.63	16.765	5.645	45.06	16.535	0.85	13.6	5.1	59.4	-0.3	239	
Large #2	7/22/97	19:00	20:00	270.24	8.62	49.82	244.83	15.48	6.58	57.26	23.68	n.a.	n.a.	4.99	n.a.	n.a.	223.5	
Large #3	7/22/97	20:00	21:00	406.6	12.94	76.95	383.82	26.11	10.35	87.78	33.81	1.11	11.6	4.83	54.0	-0.3	176	
Large #4	7/22/97	21:00	22:00	368.32	19.96	86.5	349.13	24.55	9.24	83.02	32.52	n.a.	n.a.	4.5	n.a.	n.a.	190.3	
Large #5	7/22/97	22:00	23:00	396.04	21.59	98.93	385.44	28.07	57.32	92.38	36.59	0.78	12.4	4.43	64.1	-0.3	161.9	
Small #1	7/22/97	17:30	19:00	333.51	23.53	69.45	325.61	37.38	11.4	74.57	29.34	1.44	18.5	4.89	57.9	-1.0	43.2	
Small #2	7/22/97	19:00	20:00	180.27	10.9	42.89	156.56	22.81	4.4	37.54	14.13	n.a.	n.a.	4.85	n.a.	n.a.	31.4	
Small #3	7/22/97	20:00	21:00	206.88	12.7	54.04	190.22	27.08	5.33	45.16	19.11	1.11	12.8	4.72	51.7	0.0	34.7	
Small #4	7/22/97	21:00	22:00	168.47	10.68	49.96	140.74	21.65	3.82	35.9	16.84	n.a.	n.a.	4.55	n.a.	n.a.	36.9	
Small #5	7/22/97	22:00	23:00	129.95	9.99	46.58	100.25	19.24	2.65	26.39	12.21	0.66	9.0	4.44	62.7	-0.5	33.1	

** Sample 6 from 22:00 to 22:40 AND 22:47 to 22:52*

Reproduced with permission of the copyright owner. Further reproduction prohibited without permission.

Table H-21: Storm Peak Laboratory, CO ambient sampling conditions data

Event/ Sample	time period	temperature [°C]	relative humidity [%]	wind speed [m s^{-1}]	wind direction [degrees]	pressure [mb]
EVENT 2						
CHRCC						
#1	23:13 - 23:45	-3.0	102.2	5.0	269	682.7
#2	23:50 - 0:20	-3.1	102.1	4.5	285	682.3
#3	0:25 - 0:50	-2.9	102.3	5.4	246	682.0
#4	0:55 - 1:25	-2.4	103.1	6.3	233	681.1
#5	1:30 - 1:55	-2.4	103.3	4.3	249	680.7
FROSTY						
#1	22:40 - 23:45	-3.0	102.3	5.5	272	682.9
#2	23:50 - 0:50	-3.0	102.2	5.1	265	682.1
#3	0:55 - 1:56	-2.4	103.1	5.5	240	680.9
EVENT 3						
CHRCC						
#2	19:20 - 19:40	-7.7	97.7	9.6	mainly from N	676.5
#3	19:45 - 20:00	-7.8	97.7	9.6	mainly from N	676.5
#4	20:05 - 20:20	-7.9	97.3	10.0	mainly from N	676.3
#5	20:30 - 20:45	-8.0	97.0	11.3	mainly from N	676.2
#6	20:50 - 21:10	-8.4	95.5	12.5	mainly from N	676.3
FROSTY						
#1	19:00 - 20:00	-7.7	97.8	9.6	203	676.5
#2	20:05 - 21:00	-8.0	96.8	10.9	152	676.3
#3	21:05 - 22:00	-9.2	94.8	9.7	107	676.8
#4	22:00 - 23:00	-10.1	94.3	9.2	50	677.0
#5	23:00 - 0:00	-10.9	93.4	8.9	102	676.7
#6	0:00 - 1:00	-11.9	92.8	10.2	347	676.4
#7	1:00 - 1:55	-12.8	91.4	9.2	334	676.8
EVENT 8						
CHRCC						
#3	21:56 - 22:22	-14.8	92.0	7.4	345	680.9
#4	22:26 - 22:56	-14.7	91.9	8.4	353	680.7
#5	23:02 - 23:32	-14.6	91.5	8.8	357	680.5
#6	23:36 - 23:57	-14.7	90.9	9.1	357	680.2
#7	0:03 - 00:28	-14.8	91.0	9.9	355	680.0
#8	0:32 - 0:57	-14.8	91.3	10.8	349	679.9
#9	1:02 - 1:27	-14.7	91.4	11.0	353	679.8
#10	1:31 - 1:56	-14.6	91.6	11.6	350	679.8
FROSTY						
#1	21:00 - 21:57	-15.0	91.8	6.1	149	681.1
#2	22:02 - 23:00	-14.7	91.9	8.0	354	680.7
#3	23:02 - 0:00	-14.7	91.3	9.0	357	680.3
#4	0:03 - 1:01	-14.8	91.2	10.3	352	679.9
#5	1:02 - 2:00	-14.7	91.5	11.3	352	679.8
#6	2:03 - 3:00	-14.5	91.4	11.4	350	679.8
#7	3:02 - 4:00	-14.5	91.4	11.5	345	679.7

Reproduced with permission of the copyright owner. Further reproduction prohibited without permission.

#8	4:02 - 5:00	-14.4	91.5	11.1	337	679.6
EVENT 9						
CHRCC						
#3	18:03 - 18:18	-11.6	93.8	2.1	mainly from N	677.6
#4	18:23 - 18:38	-11.6	93.6	2.2	mainly from N	677.5
#5	18:43 - 18:58	-11.6	93.5	2.0	mainly from N	677.5
#6	19:03 - 19:18	-11.6	93.7	2.0	mainly from N	677.4
FROSTY				anemometer failure in here?		
#1	17:02 - 18:00	-11.7	93.8	2.5	mainly from N	677.8
#2	18:02 - 19:00	-11.6	93.7	2.1	mainly from N	677.5
#3	19:02 - 20:00	-11.6	94.1	2.4	mainly from N	677.4
#4	20:02 - 21:00	-11.3	94.4	10.1	mainly from N	677.4
#5	21:02 - 22:00	-11.1	94.3	13.4	mainly from N	677.3
EVENT 10						
CHRCC						
#2	16:23 - 16:38	-10.7	94.6	5.8	350	675.5
#3	16:42 - 16:57	-10.8	94.4	6.1	351	675.4
#4	17:02 - 17:17	-10.9	94.4	6.2	349	675.3
FROSTY						
#1	16:00 - 17:00	-10.7	94.5	6.0	346	675.5
#2	17:02 - 18:00	-11.0	94.5	5.8	352	675.3
#3	18:02 - 19:00	-11.1	94.5	5.0	353	675.4
#4	19:02 - 20:00	-11.2	94.4	5.8	353	675.5
#5	20:02 - 21:03	-11.3	94.4	8.2	348	675.3
#6	21:05 - 22:00	-11.3	94.5	8.7	353	675.2
#7	22:02 - 23:00	-11.2	94.4	8.7	355	674.9
#8	23:02 - 0:00	-11.3	94.2	9.1	351	674.7
#9	0:02 - 1:00	-11.4	94.2	9.5	349	674.3
#10	1:01 - 2:00	-11.5	94.2	10.1	340	674.0
EVENT 14						
FROSTY						
#1	13:30 - 14:30	-12.0	91.0	6.3	337	674.4
#2	14:30 - 15:30	-12.0	91.2	5.5	344	674.7
#3	15:30 - 16:30	-12.1	90.4	4.0	353	674.9
#4	16:30 - 17:30	-13.2	91.4	4.7	331	675.1
#5	17:30 - 18:30	-13.8	92.1	6.2	336	675.4
#6	18:30 - 19:30	-14.2	91.0	6.5	319	675.9

note: "mainly from N" indicates mostly from N quadrant (315 to 45 degrees)
mean of 5 minutes averages reported

Table H-22: Storm Peak Laboratory, CO validated dN data for EVENT 8

	CHRCC Sample number & time period							
midpoint bin diameter [μm]	#3 21:56 – 22:22 [# cm^{-3}?]	#4 22:26 – 22:56 [# cm^{-3}?]	#5 23:02 – 23:32 [# cm^{-3}?]	#6 23:36 – 23:57 [# cm^{-3}?]	#7 0:03 – 00:28 [# cm^{-3}?]	#8 0:32 – 0:57 [# cm^{-3}?]	#9 1:02 – 1:27 [# cm^{-3}?]	#10 1:31 – 1:56 [# cm^{-3}?]
3.23	12.79	7.04	6.46	5.69	4.84	4.01	3.33	3.14
5.37	28.20	15.26	14.04	12.21	9.77	7.80	6.16	5.49
7.51	54.99	31.58	30.90	25.25	19.18	14.91	10.71	9.19

Reproduced with permission of the copyright owner. Further reproduction prohibited without permission.

9.66	91.64	60.94	63.76	49.97	35.83	27.53	19.04	16.08
11.8	69.37	57.74	63.83	54.64	41.42	31.56	22.96	20.37
13.94	22.19	27.02	25.84	31.40	33.50	29.07	27.48	26.95
16.09	6.09	8.51	5.49	7.74	14.54	18.69	25.93	29.84
18.23	1.68	2.22	1.47	1.93	4.04	9.50	15.10	21.44
20.37	0.37	0.51	0.29	0.48	1.13	3.70	5.54	7.68
22.51	0.09	0.10	0.05	0.10	0.28	1.23	1.74	2.39
24.66	0.03	0.02	0.02	0.03	0.06	0.25	0.37	0.57
26.8	0.01	0.01	0.02	0.02	0.03	0.08	0.10	0.16
28.94	0.01	0.01	0.02	0.02	0.03	0.05	0.04	0.06
31.09	0.01	0.01	0.02	0.02	0.03	0.04	0.04	0.05
33.23	0.01	0.01	0.02	0.02	0.03	0.04	0.04	0.04
D_{eff} [µm]	11.3	12.0	11.8	12.3	13.2	14.6	15.6	16.2
	FROSTY Sample number & time period							
midpoint bin diameter [µm]	#1 21:00 – 21:57 [# cm^{-3}?]	#2 22:02 – 23:00 [# cm^{-3}?]	#3 23:02 – 0:00 [# cm^{-3}?]	#4 0:03 – 1:01 [# cm^{-3}?]	#5 1:02 – 2:00 [# cm^{-3}?]	#6 2:03 – 3:00 [# cm^{-3}?]	#7 3:02 – 4:00 [# cm^{-3}?]	#8 4:02 – 5:00 [# cm^{-3}?]
3.23	no data	9.23	6.10	4.43	3.22	3.09	2.46	1.26
5.37	no data	20.19	13.12	8.79	5.80	5.23	4.02	2.02
7.51	no data	40.61	28.01	17.07	9.95	9.25	6.94	2.82
9.66	no data	72.90	56.65	31.64	17.67	16.59	11.09	4.02
11.8	no data	62.03	58.99	36.49	22.00	23.46	14.31	4.62
13.94	no data	24.49	28.78	31.57	27.77	33.54	21.36	6.68
16.09	no data	7.22	7.05	16.93	28.26	35.72	25.98	8.90
18.23	no data	1.92	1.84	6.98	18.30	24.47	21.28	8.36
20.37	no data	0.43	0.42	2.51	6.59	9.23	9.47	4.13
22.51	no data	0.09	0.08	0.79	2.06	3.04	3.41	1.67
24.66	no data	0.02	0.02	0.16	0.47	0.70	0.80	0.41
26.8	no data	0.01	0.02	0.06	0.13	0.20	0.26	0.13
28.94	no data	0.01	0.02	0.04	0.05	0.07	0.08	0.04
31.09	no data	0.01	0.02	0.04	0.04	0.05	0.05	0.02
33.23	no data	0.01	0.02	0.04	0.04	0.05	0.05	0.02
D_{eff} [µm]		11.7	12.1	14.0	15.9	16.3	16.9	17.3

Table H-23: Storm Peak Laboratory, CO validated dN data for EVENT 9

midpoint bin diameter [µm]	**CHRCC Sample number & time period**				**FROSTY Sample number & time period**				
	#3 18:03 - 18:18 [# cm^{-3}?]	#4 18:23 - 18:38 [# cm^{-3}?]	#5 18:43 - 18:58 [# cm^{-3}?]	#6 19:03 - 19:18 [# cm^{-3}?]	#1 17:02 - 18:00 [# cm^{-3}?]	#2 18:02 - 19:00 [# cm^{-3}?]	#3 19:02 - 20:00 [# cm^{-3}?]	#4 20:02 - 21:00 [# cm^{-3}?]	#5 21:02 - 22:00 [# cm^{-3}?]
3.23	1.39	1.68	1.58	1.75	incomplete data	1.55	1.53	incomplete data	no data
5.37	1.89	2.07	1.65	1.50	incomplete data	1.87	1.50	incomplete data	no data
7.51	3.29	3.69	2.61	1.97	incomplete data	3.16	2.05	incomplete data	no data

Reproduced with permission of the copyright owner. Further reproduction prohibited without permission.

9.66	5.42	6.40	4.13	2.68	incomplete data	5.22	2.74	incomplete data	no data
11.8	6.53	8.26	4.83	2.64	incomplete data	6.38	3.19	incomplete data	no data
13.94	8.90	11.76	6.64	3.40	incomplete data	8.82	4.29	incomplete data	no data
16.09	11.02	13.39	7.90	4.49	incomplete data	10.43	5.30	incomplete data	no data
18.23	11.00	11.22	7.08	4.96	incomplete data	9.57	5.27	incomplete data	no data
20.37	7.50	5.86	3.81	3.33	incomplete data	5.68	3.32	incomplete data	no data
22.51	3.32	1.85	1.15	1.35	incomplete data	2.13	1.37	incomplete data	no data
24.66	0.76	0.49	0.33	0.37	incomplete data	0.54	0.40	incomplete data	no data
26.8	0.26	0.27	0.21	0.25	incomplete data	0.25	0.29	incomplete data	no data
28.94	0.14	0.19	0.17	0.21	incomplete data	0.17	0.25	incomplete data	no data
31.09	0.12	0.18	0.18	0.21	incomplete data	0.16	0.25	incomplete data	no data
33.23	0.12	0.19	0.18	0.21	incomplete data	0.16	0.24	incomplete data	no data
D_{eff} [µm]	18.0	17.4	17.7	18.9		17.8	18.8		

Table H-24: Storm Peak Laboratory, CO validated dN data for EVENT 10 (FROSTY only)

midpoint bin diameter [µm]	FROSTY Sample number & time period									
	#1 16:00 – 17:00 [# cm^{-3}?]	#2 17:02 – 18:00 [# cm^{-3}?]	#3 18:02 – 19:00 [# cm^{-3}?]	#4 19:02 – 20:00 [# cm^{-3}?]	#5 20:02 – 21:03 [# cm^{-3}?]	#6 21:05 – 22:00 [# cm^{-3}?]	#7 22:02 – 23:00 [# cm^{-3}?]	#8 23:02 – 0:00 [# cm^{-3}?]	#9 0:02 – 1:00 [# cm^{-3}?]	#10 1:01 – 2:00 [# cm^{-3}?]
3.23	no data	no data	incomplete data	0.97	2.00	1.62	1.22	0.74	0.19	0.64
5.37	no data	no data	incomplete data	1.55	3.44	2.65	1.89	1.32	0.29	0.88
7.51	no data	no data	incomplete data	2.82	6.66	5.67	3.80	2.55	0.46	1.53
9.66	no data	no data	incomplete data	5.08	11.63	11.08	7.44	4.77	0.70	2.94
11.8	no data	no data	incomplete data	6.03	13.36	13.99	10.22	6.21	0.77	4.68
13.94	no data	no data	incomplete data	7.03	14.95	16.48	14.77	9.51	1.24	8.24
16.09	no data	no data	incomplete data	9.00	16.89	18.46	19.92	14.15	2.56	12.62
18.23	no data	no data	incomplete data	11.10	15.29	17.36	20.15	15.88	4.20	13.64
20.37	no data	no data	incomplete data	10.69	8.87	11.51	13.15	11.22	4.12	8.93
22.51	no data	no data	incomplete data	7.66	3.28	5.15	5.59	4.27	1.68	3.91
24.66	no data	no data	incomplete data	2.35	0.51	1.01	1.15	0.78	0.24	0.76
26.8	no data	no data	incomplete data	0.39	0.13	0.23	0.30	0.30	0.10	0.25
28.94	no data	no data	incomplete data	0.09	0.05	0.07	0.08	0.08	0.03	0.08
31.09	no data	no data	incomplete data	0.04	0.03	0.03	0.02	0.02	0.01	0.04
33.23	no data	no data	incomplete data	0.02	0.02	0.02	0.01	0.01	0.01	0.03

Reproduced with permission of the copyright owner. Further reproduction prohibited without permission.

D_{eff} [µm]		19.1	16.9	17.4	17.8	18.1	19.2	18.3

Table H-25: Storm Peak Laboratory, CO validated dN data for EVENT 14 (FROSTY only)

midpoint bin diameter [µm]	FROSTY Sample number & time period					
	#1 13:30 - 14:30 [# cm^{-3}?]	#2 14:30 - 15:30 [# cm^{-3}?]	#3 15:30 - 16:30 [# cm^{-3}?]	#4 16:30 - 17:30 [# cm^{-3}?]	#5 17:30 - 18:30 [# cm^{-3}?]	#6 18:30 - 19:30 [# cm^{-3}?]
3.23	1.72	2.33	87.83	incomplete data	no data	no data
5.37	4.33	4.90	13.69	incomplete data	no data	no data
7.51	9.73	8.23	6.54	incomplete data	no data	no data
9.66	21.39	16.69	11.13	incomplete data	no data	no data
11.8	28.49	24.37	14.85	incomplete data	no data	no data
13.94	30.32	27.40	17.32	incomplete data	no data	no data
16.09	22.73	20.94	15.90	incomplete data	no data	no data
18.23	9.60	10.50	10.02	incomplete data	no data	no data
20.37	2.69	4.25	4.92	incomplete data	no data	no data
22.51	0.74	1.57	2.18	incomplete data	no data	no data
24.66	0.15	0.37	0.60	incomplete data	no data	no data
26.8	0.02	0.08	0.15	incomplete data	no data	no data
28.94	0.00	0.01	0.03	incomplete data	no data	no data
31.09	0.00	0.00	0.00	incomplete data	no data	no data
33.23	0.00	0.00	0.00	incomplete data	no data	no data
D_{eff} [µm]	14.6	15.3	15.3			

Table H-26: Storm Peak Laboratory, CO CHRCC LWC data (via PVM-100)

Event/ sample	time period	LWC [mg m^{-3}]
EVENT 8		
#3	21:56 - 22:22	72.2
#4	22:26 - 22:56	93.0
#5	23:02 - 23:32	93.0
#6	23:36 - 23:57	104.1
#7	0:03 - 00:28	129.5
#8	0:32 - 0:57	144.3
#9	1:02 - 1:27	171.1
#10	1:31 - 1:56	184.5
EVENT 9		

Reproduced with permission of the copyright owner. Further reproduction prohibited without permission.

all data are bad		
EVENT 10		
#2	16:23 - 16:38	134.2
#3	16:42 - 16:57	157.8
#4	17:02 - 17:17	145.6

note: no D_{eff} data available

Table H-27: Storm Peak Laboratory, CO FROSTY LWC (via PVM-100)

Event/ sample	time period	LWC [mg m^{-3}]
EVENT 8		
#1	21:00 - 21:57	44.7
#2	22:02 - 23:00	85.9
#3	23:02 - 0:00	98.3
#4	0:03 - 1:01	137.4
#5	1:02 - 2:00	178.2
#6	2:03 - 3:00	209.3
#7	3:02 - 4:00	255.1
#8	4:02 - 5:00	278.0
EVENT 9		
all data are bad		
EVENT 10		
#1	16:00 - 17:00	151.8
#2	17:02 - 18:00	150.7
#3	18:02 - 19:00	134.9
#4	19:02 - 20:00	164.1
#5	20:02 - 21:03	141.1
#6	21:05 - 22:00	171.3
#7	22:02 - 23:00	419.2
#8	23:02 - 0:00	348.8
#9	0:02 - 1:00	276.9
#10	1:01 - 2:00	283.2
EVENT 14		
#1	13:30 - 14:30	179.4
#2	14:30 - 15:30	212.7
#3	15:30 - 16:30	258.6
#4	16:30 - 17:30	297.1
#5	17:30 - 18:30	271.3
#6	18:30 - 19:30	389.1

note: no D_{eff} data available

Table H-28: Storm Peak Laboratory, CO selected CHRCC collected mass data

Event/ sample	Mass [g]
EVENT 2	
#1	18

Reproduced with permission of the copyright owner. Further reproduction prohibited without permission.

#2	24.4
#3	12.9
#4	10.3
#5	14.8
EVENT 3	
#1	1.7
#2	5
#3	4
#4	4.1
#5	0.3
#6	4.6
EVENT 8	
#2	0.1
#3	1.4
#4	7.4
#5	5.4
#6	2.8
#7	2.5
#8	5.1
#9	3.8
#10	5.3
#11	2
#12	2.2
EVENT 9	
#1	8.5
#2	12.2
#3	7.1
#4	2.4
#5	0.4
#6	0.2
#7	20.1
EVENT 10	
#1	5.1
#2	3.3
#3	4.6
#4	3.7
#5	0.6
#6	8.9

note: see field notes for where losses occur in collecting mass data with incomplete collection were not included in the analyses

Table H-29: Storm Peak Laboratory, CO selected FROSTY collected mass data

Event/ sample	LARGE Mass [g]	MEDIUM Mass [g]	SMALL Mass [g]
EVENT 2			
#1	12.2	4	0.2

Reproduced with permission of the copyright owner. Further reproduction prohibited without permission.

#2	17.2	2.4	0.2
#3	7	1.8	0.3
EVENT 3			
#1	7.6	0.2	0.2
#2	3.2	0.4	
#3	10.2	0.7	0.3
#4	8	0.3	0.2
#5	7.4	0.8	0.1
#6	5	0.6	0.1
#7	1.9	0.4	
EVENT 8			
#1	0.5	0.3	0.4
#2	0.7	0.6	0.8
#3	0.8	0.5	0.7
#4	1.5	0.9	0.4
#5	3.1	1.2	0.3
#6	4.4	1.2	0.2
#7	5.4	1	0.1
#8	7.1	1	0.1
EVENT 9			
#1	4.4	1.2	0.2
#2	3.4	1.1	0.2
#3	4	0.8	0.1
#4	2.6	0.6	0.1
#5	1.7	0.7	0.1
EVENT 10			
#1	1.7	0.8	0.3
#2	1.9	1	0.4
#3	1.7	0.6	0.3
#4	3.7	0.7	0.1
#5	2.8	1	0.2
#6	3.2	1.1	0.2
#7	5.3	1.4	0.2
#8	8.1	1.7	0.2
#9	9.2	1.5	0.1
#10	5.9	1.2	0.1
EVENT 14			
#1	5.1	2.8	1.1
#2	6.1	2.5	0.8
#3	8.7	3.9	0.8
#4	10.8	3.2	0.3
#5	9.1	2.3	0.2
#6	10.5	1.9	0.2

note: see field notes for where losses occur in collecting mass
data with incomplete collection were not included in the analyses

Reproduced with permission of the copyright owner. Further reproduction prohibited without permission.

Table H-30: Storm Peak Laboratoy, CO selected CHRCC composition data

Event/sample	Nitrate [μN]	Sulfate [μN]
EVENT 2		
CHRCC Sample #2	17.03	30.17
CHRCC Sample #3	22.63	47.26
CHRCC Sample #4	35.00	77.55
CHRCC Sample #5	33.83	73.83
EVENT 8		
CHRCC Sample #3	250.41	313.41
CHRCC Sample #4	194.66	213.87
CHRCC Sample #5	151.37	173.51
CHRCC Sample #6	141.88	166.55
CHRCC Sample #7	156.77	177.75
CHRCC Sample #8	122.85	138.14
CHRCC Sample #9	76.49	119.05
CHRCC Sample #10	64.83	91.44
EVENT 9		
CHRCC Sample #10	22.58	52.23
CHRCC Sample #11	22.80	53.21
CHRCC Sample #12	22.23	54.42
CHRCC Sample #13	26.16	60.29
CHRCC Sample #14	23.46	54.60

Table H-31: Storm Peak Laboratory, CO selected FROSTY composition data

Event/sample	Nitrate [μN]	Sulfate [μN]
EVENT 2		
FROSTY LARGE #2	19.86	40.05
FROSTY MEDIUM #2	28.66	65.16
FROSTY SMALL #2	62.51	164.24
FROSTY LARGE #3	44.31	86.12
FROSTY MEDIUM #3	60.69	131.46
FROSTY SMALL #3	98.42	194.48
EVENT 8		
FROSTY LARGE #2	140.89	173.60
FROSTY MEDIUM #2	164.72	213.90
FROSTY SMALL #2	191.80	252.36
FROSTY LARGE #3	94.01	127.36
FROSTY MEDIUM #3	125.23	154.92
FROSTY SMALL #3	141.46	183.08
FROSTY LARGE #4	56.49	70.31
FROSTY MEDIUM #4	78.20	99.54
FROSTY SMALL #4	93.82	143.60
FROSTY LARGE #5	33.08	43.59
FROSTY MEDIUM #5	39.55	59.88
FROSTY SMALL #5	53.82	80.70

Reproduced with permission of the copyright owner. Further reproduction prohibited without permission.

EVENT 9		
FROSTY LARGE #2	16.73	31.78
FROSTY MEDIUM #2	20.14	40.97
FROSTY SMALL #2	24.22	57.14

Table H-32: Horsetooth Mtn., CO ambient sampling conditions data

SAMPLING PERIOD	time	mean wind speed [m s^{-1}]	mean wind direction [deg.]	std. dev. wind direction [deg.]	mean temperature [°C]	ambient pressure [mb]
1	17:15-18:55	1.3	185.0	203.3	1.9	771.1
2	19:36-21:00	1.1	43.1	161.2	1.4	769.6
3	21:04-22:00	1.3	66.8	202.4	0.9	770.3
4	22:05-23:00	0.6	65.0	130.3	0.7	770.8
5	23:02-1:00	0.9	47.8	183.7	0.5	771.0
6	1:00-2:00	1.3	62.0	161.5	0.2	770.9
7	2:00-3:00	0.8	81.0	172.6	-0.1	770.9
8	3:00-4:00	0.5	84.6	151.3	-0.1	770.3

Table H-33: Horsetooth Mtn., CO FROSTY cloud data

Event/sample	Chloride [µN]	Nitrate [µN]	Sulfate [µN]	Sodium [µN]	Ammonium [µN]	Potassium [µN]	Magnesium [µN]	Calcium [µN]	pH	sample weight [g]
pre-event blanks										
DI (squirt bottle)	0.0	0.0	2.8	0.7	0.0	0.0	2.7	3.7		
DI (small volume vial)	0.0	0.0	0.0	0.6	1.2	0.0	2.6	3.3		
FROSTY set #0										
LARGE	0.0	0.2	2.6	0.8	1.2	1.0	2.7	23.1		
MEDIUM	0.0	0.5	2.2	1.0	0.0	0.9	3.2	6.7		
SMALL	0.0	0.0	3.6	1.6	1.2	1.1	2.6	3.9		
FROSTY set #1										
LARGE	0.0	0.0	0.0	0.8	1.5	0.0	2.6	3.6		
MEDIUM	0.0	3.0	0.0	0.7	0.0	0.0	2.6	13.0		
SMALL	0.0	0.7	2.3	0.8	1.1	0.0	2.6	4.1		
H114										
Sample set #1 (4/14/98 17:15-18:55)										
LARGE	31.3	542.0	420.1	46.9	314.1	23.9	36.9	685.6	6.9	0.12*
MEDIUM	39.8	1563.2	1297.	51.9	1828.5	29.6	48.6	1590.3	6.6	0.1*

Reproduced with permission of the copyright owner. Further reproduction prohibited without permission.

SMALL	n.a.	n.a.	n.a.	n.a.	n.a.	n.a.	n.a.	n.a.	5.7	0.045*
Sample set #2 (4/14/98 19:36-21:00)										
LARGE	7.9	95.5	66.7	6.4	203.9	3.1	3.0	6.6	6.0	4*
MEDIUM	0.0	121.0	113.9	1.7	128.5	2.1	3.7	191.0	6.8	3*
SMALL	2.5	158.7	198.8	3.1	411.1	3.9	3.1	8.3	5.5	0.7
Sample set #3 (4/14/98 21:04-22:00)										
LARGE	1.8	51.6	53.3	3.1	60.8	2.2	4.1	110.7	6.9	5.4
MEDIUM	1.9	134.4	117.2	3.2	196.6	2.2	4.3	115.4	6.4	1.1
SMALL	13.9	233.1	201.5	16.2	375.4	11.3	18.4	45.3	6.0	0.11*
Sample set #4 (4/14/98 22:05-23:00)										
not reported										
Sample set #5 (4/14/98 23:02 - 4/15/98 1:00)										
LARGE	2.1	50.6	98.7	3.8	117.1	2.2	3.4	52.4	6.1	8.3*
MEDIUM	1.7	136.0	263.4	4.6	331.7	2.4	3.9	78.9	4.9	2.6
SMALL	5.2	257.1	472.9	11.1	698.9	6.7	6.9	67.8	4.5	0.9
Sample set #6 (4/15/98 1:02-2:00)										
LARGE	3.4	142.0	241.0	4.3	396.8	2.9	4.2	32.8	5.6	1.2*
MEDIUM	2.2	182.7	302.3	2.4	402.5	2.3	4.1	158.0	6.7	1.4
SMALL	3.1	352.6	538.3	4.0	949.1	6.3	5.1	23.7	5.4	0.7
Sample set #7 (4/15/98 2:02-3:00)										
LARGE	19.5	305.0	372.0	16.2	343.1	10.1	11.5	431.2	6.6	0.3*
MEDIUM	6.6	384.9	463.1	3.8	633.0	4.5	7.4	157.9	4.0	0.5
SMALL	12.1	638.4	688.8	6.2	1001.7	8.4	11.1	66.7	3.6	0.3
Sample set #8 (4/15/98 3:02-4:00)										
LARGE	n.a.	n.a.	n.a.	n.a.	n.a.	n.a.	n.a.	n.a.	n.a.	0
MEDIUM	n.a.	n.a.	n.a.	n.a.	n.a.	n.a.	n.a.	n.a.	n.a.	0.1
SMALL	31.8	1602.5	1675.	22.8	2712.3	20.7	26.4	201.0	4.2	0.3

**mass removed/lost prior to weighing or weight estimated*

Table H-34: Horsetooth Mtn., CO normalized dV data for selected sampling periods

midpoint bin diameter [µm]	Sampling period and time		
	#6 1-2:00 relative dV [%]	#7 2-3:00 relative dV [%]	#8 3 - 3:55 relative dV [%]
3	1%	5%	7%
5	5%	14%	20%
7	11%	23%	28%
9	18%	23%	24%
11	20%	15%	12%

Reproduced with permission of the copyright owner. Further reproduction prohibited without permission.

13	19%	10%	5.6%
15	14%	5.7%	2.1%
17	7.9%	2.6%	0.7%
19	3.0%	0.9%	0.2%
21	1.0%	0.24%	0.05%
23	0.27%	0.08%	0.04%
25	0.06%	0.03%	0.02%
27	0.03%	0.03%	0.05%
29	0.03%	0.06%	0.01%
31	0.02%	0.06%	0.03%
33.5	0.01%	0.09%	0.06%
36.5	0.01%	0.10%	0.10%
39.5	0.01%	0.08%	0.11%
42.5	0.01%	0.09%	0.07%
45.5	0.01%	0.17%	0.00%
sum	100%	100%	100%

note: no PVM LWC data available

Reproduced with permission of the copyright owner. Further reproduction prohibited without permission.

I. Appendix: Performance of the Gerber PVM-100

The purpose here is to motivate the development of the revised liquid water content (LWC) values for the Davis fogs. It consists largely of a literature review of previous investigations into the performance of the Gerber PVM-100 where the usual comparison was to the LWC derived from the drop size distribution measured by a Forward Scattering Spectrometer Probe (FSSP) (Particle Measurement Systems, Inc., Boulder, CO) (see Appendix G which includes a discussion of the FSSP data processing steps indicated below).

I.1 The Gerber PVM

The Gerber Particle Volume Monitor (Gerber Scientific, Inc., Reston, VA) or PVM was developed to measure cloud LWC and is described in detail by Gerber (1991). The PVM operates based upon drop forward scattering of an incident laser beam. This information is processed through a filter to provide the LWC. There are two versions of the PVM which have been used by numerous investigators: the PVM-100 (ground-based) and the PVM-100A (aircraft platform (Gerber *et al.*, 1994)). The PVM-100's LWC response is reported to be 100% for drops up to 40 μm in diameter falling off to approximately 80% for 55 μm, 50% for 70 μm and 25% for 100 μm drops (see figure 4, (Gerber, 1991)). Calibration is limited, however, to drops up to 30 μm in diameter (Gerber, 1991). The performance of the PVM-100A and PVM-100 was later reported to be good for drops from 4 – 45 μm in diameter (Gerber *et al.*, 1994). The filters for LWC and particle surface area (PSA) (available in later versions of the PVMs) are good to ± 10% and therefore so is their calibration (the PSA filter was only systematically tested for the PVM-100A, but results may be similar for the PVM-100 (Gerber, 2001))(Gerber *et al.*, 1994).

Reproduced with permission of the copyright owner. Further reproduction prohibited without permission.

I.2 Laboratory observations of the Gerber PVM's performance

During the initial development of the PVM-100 and the PVM-100A, several tests were performed with drop size distributions of varying volume median diameters (VMDs) – 10, 20, 30, and 40 μm. Results from these tests compared to a reference filter measurement of the LWC were in excellent agreement (nearly 1:1) up to 30 μm. For 40 μm there was a 50% discrepancy between the filter and the PVM (with the PVM < filter LWC) and an additional 50% discrepancy between the FSSP and the filter (FSSP > filter LWC). The FSSP gave consistently higher LWC measurements than the filter which became worse as the LWC increased. Calibration was developed based upon the results for VMD = 10 and 20 μm only (for VMD = 30 μm they suggest the LWC is about 18% too low on average). The discrepancy between the FSSP and the PVM is suggested to be FSSP sampling errors. According to these investigators, corrections must be made to the PVM LWC if large drops are present. The study does not address why there is still not a 1:1 correspondence between the different LWC measuring methods despite corrections (Gerber *et al.*, 1994).

To resolve issues raised in field studies (described below), two different PVM-100A instruments were operated in two different wind tunnels and used to measure the LWC of broadly varying drop distributions (Wendisch *et al.*, 2000). Tunnel LWC was also independently measured. The tests were at aircraft speeds and the LWC ranged from 0.08 to 2.1 g m^{-3} with a range of VMDs – 16, 22, and 29 μm. Only the PVM's LWC channel was recorded. For VMD = 16 μm there was a 1:1 correspondence between the filter LWC and the PVM LWC from 0 to 0.8 g m^{-3}. For larger VMDs, the PVM LWC is generally lower than the filter LWC (about 20% for VMD = 29 μm), although it is difficult to tell from the figure provided if the difference is outside the uncertainty for VMD = 22 μm and LWC < 0.4 g m^{-3}. No temperature or airspeed dependence was found in the two tunnels. Due to drop generation limitations, as the VMD increased the LWC tended to

Reproduced with permission of the copyright owner. Further reproduction prohibited without permission.

increase as well. They found that the two PVM instruments studied had different responses to increasing drop size (decreasing LWC response started at varying points in the 20 – 30 μm diameter range), although they converged at larger VMDs. This suggests that each PVM may have its own individual response function, and is in contrast to the 45 μm limit cited by the manufacturer. They suggest for a VMD of 50 μm, only about 50% of the "true" LWC would be indicated by the PVM, decreasing to 40% at a VMD of 60 μm.

I.3 Field Observations of the Gerber PVM's performance

A prototype PVM was inter-compared with several different measurement devices in May 1987 (Valente *et al.*, 1989). The prototype worked reasonably well in the orographic clouds measured and gave values within 0.045 g m^{-3} of the other instruments. The suggested PVM upper drop bound was 30 μm in diameter.

The Arends *et al.* (1992) study is discussed in detail in the development of how the drop distribution processing is performed (see Appendix G). Relevant findings were that at VMDs > 20 μm, the PVM-100 and the FSSP measured different LWCs, and the deviations most often occurred at low LWC (< 0.05 g m^{-3}). Calibration errors were not ruled out as a source of this discrepancy. The PVM and the FSSP were in good agreement (within 10%) for LWCs < 0.3 g m^{-3} and VMDs < 20 μm. They concluded that the PVM may underestimate LWC if the VMD is larger and suggested that the PVM-100 is good for drops < 30 μm in diameter.

Vong and Kowalski (1995) report generally very good agreement between LWC measured by a PVM and derived from an FSSP during a Spring 1993 orographic cloud study at the Cheeka Peak Observatory, WA. Their analysis indicated that coincidence errors could be a problem if the reported FSSP activity exceeded 50% but that for a volume mean diameter range of 11 – 19 μm (13 μm "typically"), a drop concentration range from 200 – 450 cm^{-3}, and taking wind ramming

Reproduced with permission of the copyright owner. Further reproduction prohibited without permission.

into consideration, the LWCs between 0.2 – 0.5 g m^{-3} agreed well (Vong and Kowalski, 1995). During later side-by-side operation of two PVMs and a FSSP in an orographic cloud, Kowalski and co-workers (1997) reported that there was no sensitivity in the LWC between the two for volume mean diameters from 6 – 22 μm and 0 – 1 g m^{-3} LWC – both PVMs yielded the same results when co-located They report that activity corrections alone are insufficient on days of high number concentration (> 600 cm^{-3} per Brenguier (1989)), and discount wind-ramming as an issue for their data set (Kowalski *et al.*, 1997). They do not address how the FSSP may change size distributions (Kowalski *et al.*, 1997). Additionally, consistently larger LWCs were reported in the higher (75 cm vertical separation) of two horizontally co-located PVMs regardless of which one it was. The difference in measurements was four times the reported uncertainty range for the PVM and highlights the importance of "accurate" co-location (although this is expected to be sampling site dependent) (Kowalski *et al.*, 1997).

Wendisch (1998) reports results from two ground-based field campaigns where multiple PVMs and FSSPs were compared. For D_p < 25 μm and reasonably narrow distributions, he reports that the FSSP and PVM LWC can agree quite well where the FSSP data is corrected for activity, changing VAR, Mie scattering and wind ramming (Wendisch, 1998). However, while the LWCs agree, the drop size distribution is not necessarily correct (Wendisch, 1998). He found that a low concentration of large drops, such as might occur in fogs (e.g. D_p > 25 μm, D_{eff} > 18 μm), may result in considerable discrepancies between the two measurement devices (Wendisch, 1998; Wendisch *et al.*, 1998). He suggests that the PVM is not sensitive to low drop concentrations (Wendisch, 1998), and cites additional measurements that support this conclusion (Wendisch *et al.*, 1998). The effective diameter channel from the PVM is not available for the two campaigns discussed. Gerber and co-workers (1999) dispute this assessment and indicate the drop trajectory convergence in the ground-based FSSP's sampling tube leads to spurious drop counts, similar to the problem noted by Norment (1987) for other probe configurations. Further, Gerber *et al.* (1999) indicate that it is difficult to compare results across different studies where the exact configuration of the FSSP is not known.

Reproduced with permission of the copyright owner. Further reproduction prohibited without permission.

Finally, our experience suggests that the preferred method is to calculate D_{eff} using the LWC and PSA channels as there have been instrument difficulties with the R_{eff} channel provided, particularly when R_{eff} values are low. When "out-of-cloud" the R_{eff} and PSA data should be disregarded (Sherman, 1998).

Reproduced with permission of the copyright owner. Further reproduction prohibited without permission.

J. Appendix: Microorifice Uniform Deposit Impactor (MOUDI) protocol

A MOUDI impactor (Marple *et al.*, 1991) was used to sample pre- and post-fog size-resolved aerosol for selected January 1999 events in Davis. The MOUDI is an 8 stage impactor and was operated with an afterfilter. With the inlet, this provides 10 aerosol fractions. This appendix briefly summarizes its use.

J.1 MOUDI preparation

The MOUDI housing and all substrate holders were thoroughly cleaned with a weak surfactant and 2-propanol interspersed with heavy DI rinses. The parts were shielded with clean plastic and allowed to dry. Gloves were worn while handling the MOUDI which was kept to a minimum.

A clean aluminum foil work surface was prepared to load the substrate holders with 47 mm Teflon (Zylon brand) substrates. Clean stainless steel tweezers were used to handle all substrates. A 37 mm Teflon (Zefluor brand) filter was placed in the afterfilter holder. Two complete sets of substrate and afterfilter holders were loaded. Each set included one 47 mm blank which was identically loaded into a holder. One set (with the exception of the blank) was installed in the MOUDI and the other was kept in a clean large plastic tub in preparation for substrate change-out at the end of sampling. No steps were taken to prevent particle bounce within the impactor as the high humidities should preclude this being a factor. There was no observational evidence of clogging (from condensing water) during sampling.

J.2 MOUDI sampling

Reproduced with permission of the copyright owner. Further reproduction prohibited without permission.

The MOUDI was operated at the site adjacent to the 5-Stage and the denuders. Its sampling periods correspond to pre-/post-fog denuder measurements. At the start of sampling, the attached pump was manually turned on and the pressure drop through the MOUDI set according to the manufacturer's instructions for a 30 lpm flow rate. The pressure drop was given a few minutes to stabilize in case there were initial fluctuations. Then, the twin magnehelic readings were recorded, and the MOUDI body was protected by plastic during sampling. An aluminum precipitation cover was placed to prevent large drops (but not aerosol) from entering the inlet.

At the conclusion of sampling, the magnehelic readings were again recorded, the pump shut down and the MOUDI returned to the field lab. On a clean work surface, the used substrates were loaded into individually labeled 50 ml PP centrifuge tubes and frozen prior to extraction. While the used substrates and holders were removed, the previously loaded set was installed in the MOUDI. The MOUDI was kept protected until the end of the fog event when it was re-installed and re-started. The MOUDI was generally turned either on or off within thirty minutes of the end or start of a fog event. This "contamination" is mitigated by the long overall sampling periods (8 to 14+ hours).

Observations of the substrates showed the characteristic pattern of the impinging jets (rotation was not used). Some of the impacted aerosol was almost black in colour.

Upon returning to CSU, all of the MOUDI filters and blanks were extracted in the centrifuge tubes using 4.8 ml of DI and 0.2 ml ethanol. The tubes were rotated at least an hour to ensure complete soluble extraction. For some substrates, evidence of the impaction pattern remained after extraction suggesting an insoluble component in the aerosol. All extracts were analyzed for cations and anions on the IC. Despite attempting to minimize the analytical detection limits, only ammonium, nitrate, and sulfate were present in reportable quantities in the samples.

Reproduced with permission of the copyright owner. Further reproduction prohibited without permission.

J.3 MOUDI sampling periods and cut-sizes

The MOUDI was operated before and after three of the January events – D009, D010, D010B. As the events were back-to-back, the "post-D009" sampling period is the same as the "pre-D010" sampling period. These time periods were:

a) Pre-D009: 1/8/99 16:00 to 1/9/99 02:30 (all times are local)

b) Post-D009/pre-D010: 1/9/99 11:10 to 1/10/99 02:21

c) Post-D010/pre-D010B: 1/10/99 10:33 to 1/10/99 22:28

d) Post-D010B: 1/11/99 10:00 to 1/11/99 19:12

The flow rate was not independently measured in the field well. Subsequent laboratory investigation indicated that the flow rate was not 30 lpm, but 23 lpm. The pressure drop through the impactor is changed by using the slightly thicker Zylon substrates instead of aluminum. This error was consistent throughout all sampling so while the cut-sizes between stages shift, the relative shift should be the same for all time periods. The revised cut-sizes were calculated using cascade impactor design theory (Marple and Rubow, 1986) and are shown in Table J - 1.

Table J-1: MOUDI design and revised (23 lpm) stage cut-sizes

	30 lpm D_{p50} [µm]	23 lpm D_{p50} [µm]
inlet	> 18	> 20.5
stage 1A	10	11.4
stage 2A	5.6	6.4
stage 3A	3.2	3.66
stage 4A	1.8	2.06
stage 5A	1	1.15
stage 6A	0.56	0.65
stage 7A	0.32	0.37
stage 8A	0.18	0.22
afterfilter	< 0.18	< 0.22

Reproduced with permission of the copyright owner. Further reproduction prohibited without permission.

K. Appendix: Compiled IC statistics

This appendix contains the compiled IC statistics for all four campaigns. Data presented include the 95% confidence level minimum detection limit, precision, accuracy and duplicate analysis (if available). Tables K - 1, K - 2, and K - 3 contain the Horsetooth, ACE2, and Whiteface information, respectively. The Davis data (tables K - 4, K - 5, and K - 6) have been separated into three separate tables in order to easily present all of it. The Davis data is more extensive due to (a) high concentrations of ammonium, (b) quantification of nitrite, and (c) the use of non-standard injection volumes.

Reproduced with permission of the copyright owner. Further reproduction prohibited without permission.

Table K-1: Compiled Horsetooth IC statistics

Horsetooth IC Statistics (taken from Davis, CA January 1998 compilation)									
	Chloride	Nitrate	Nitrite	Sulfate	Sodium	Ammonium	Potassium	Magnesium	Calcium
Minimum Detection Limit (95%CL) [µN]									
	2.9	2.22	1.65	1.42	0.78	1.01	0.38	3.46	4.72
(anions: 12 DI blanks, 20 std 1s (except nitrite (5 std 1s))									
(cations: 18 DI blanks, 19 std 1s)									
(use Standard 1s to determine standard deviation)									
Precision (%RSD)									
*> 10 µN**	2.07%	0.50%	3.29%	1.39%	0.47%	1.34%	1.92%	8.08%	7.52%
#	7	11	8	13	7	11	7	2	5
range [µN]	13.74-95.14	14.6-5341.19	9.58-25.13	24.59-768.5	13-176.28	86.26-7007.06	12.54-67.43	21.15-24.68	23.93-52.87
mean [µN]	38.61	1021.43	19.51	230.49	38.25	1569.73	27.35	22.97	40.48
< 10 µN	4.05%	14.24%		0.00%	1.31%	3.41%	27.99%	6.09%	1.82%
#	10	4		4	10	4	10	15	12
range [µN]	0-9.5	0-1.49		0-0	.72-8.62	0-1.16	0-11.28	2.85-7.12	3.6-7.33
mean [µN]	4.98	0.6		0	4.47	0.78	4.14	4.39	5.03
(*nitrite used single analysis for all (excluding any 0.00 values))									
Accuracy									
Dionex Standard 1 (anions: 12 msmnts.; cations: 10 msmnts.) [µN]									
nominal value	8.46	16.11		31.23	4.35	11.09	2.56	8.23	24.96
measured/nominal	102.4%	96.7%		97.1%	110.7%	94.4%	130.9%	137.7%	124.7%
blank corrected					*96.2%*	86.8%	125.8%	103.2%	109.1%
Dionex Standard 2 (anions: 12 msmnts.; cations: 10.) [µN]									
nominal value	76.16	145.01		281.08	173.99	443.5	102.31	329.15	998
measured/nominal	99.3%	108.1%		97.5%	103.2%	99.7%	103.3%	95.3%	99.6%
Dionex Standard 3 (anions: 13 msmnts.;cations: 10.) [µN]									
nominal value	211.55	402.8		780.78	347.98	886.99	204.61	658.3	1996.01
measured/nominal	97.4%	89.1%		89.9%	102.4%	98.2%	101.9%	93.5%	97.3%
Standard Comparison [µN]									
nominal value	3000	10			3000				
meas./nom.	95.6%	111.3%			102.1%				
#	2	5			2				
nominal value	5000	20			5000				
meas./nom.	100.8%	93.4%			96.9%				
#	1	4			1				
nominal value	7500	50			7500				
meas./nom.	96.6%	98.0%			100.7%				
#	2	5			2				
(standard comparison if > Dionex standards or no standard available)									

Reproduced with permission of the copyright owner. Further reproduction prohibited without permission.

Table K-2: Compiled ACE2 IC statistics

ACE2 IC Statistics	Na^+	NH_4^+	K^+	Mg^{2+}	Ca^{2+}	Cl^-	NO_3^-	SO_4^{2-}
Minimum Detection Limit (95% CL)								
MDL [µN]	0.09	0.59	0.37	2.3	3.11	0.64	0.54	0.2
(cations: 24 measurements & anions: 10 measurements)								
Precision (%RSD)								
range [µN]	81.99-8964.11	23.01-619.69	5.26-237.47	23.12-1918.78	18.82-1079.99	168.06-6532.06	8.62-899.95	35.47-1481.88
mean [µN]	1768.92	280.07	51.75	400.82	231.27	2167.96	263.88	653.03
number of sets	25	24	25	25	24	24	25	25
RSD% [%]	1.68%	1.44%	2.45%	1.67%	2.13%	0.92%	0.90%	0.59%
Accuracy (compared to diluted Dionex Standards)								
nominal [µN]	131.74	338.33	76.73	253.09	763.84	59.83	116.13	224.77
measured mean [µN]	132.72	334.29	81.28	235.56	738.47	59.29	128.87	224.27
measured/ nominal [%]	1%	-1%	6%	-7%	-3%	-1%	11%	<1%
std. dev./ mean [%]	1.3%	3.5%	1.4%	1.6%	1.5%	<1%	1%	1%
(cations: 11 samples, 19 measurements & anions: 8 samples, 13 measurements)								
nominal [µN]	4.39	11.28	2.56	8.44	25.46	10.39	20.16	39.02
Measured mean [µN]	4.38	10.91	2.97	8.90*	29.59*	9.68	20.9	40.9
measured/ nominal [%]	<1%	-3%	16%	6%	16%	-7%	4%	5%
std. dev./ mean [%]	2%	4.6%	8.5%	12.5%	8.6%	2%	1%	1%
(cations: 11 samples, 20 measurements & anions: 8 samples, 13 measurements) *(*blank corrected (consistent non-zero blank))*								
Duplicate Measurements (duplicate aliquot prepared concurrently)								
range [µN]	195.52-5461.71	6.57-349.30	5.62-128.28	44.52-1224.88	16.26-522.91	219.09-6158.76	8.69-395.04	35.66-813.73
mean [µN]	1709.13	174.04	49.11	384.05	200.44	1792.9	133.83	459.21
number of sets	8	8	8	8	8	8	8	8
RSD% [%]	0.95%	2.69%	4.02%	0.89%	1.36%	1.97%	1.15%	1.24%
not statistically different results at 95% CL								
Diluted Sample Measurements (check for Na^+/Cl^- swamping)								
RSD% [%]	5.99%	8.69%	5.36%	6.42%	9.26%	1.98%	0.19%	0.31%
(used only where specifically indicated (single NH4+ measurement)) *No blank corrections except as marked*								

Reproduced with permission of the copyright owner. Further reproduction prohibited without permission.

Table K-3: Compiled Whiteface IC statistics

Whiteface IC Statistics								
	Sodium	Ammonium	Potassium	Magnesium	Calcium	Chloride	Nitrate	Sulfate
Minimum Detection Limit (95% CL) [µN]								
method: DI/low std	1.64	0.67	0.41	3.35	4.11	0.24	0.63	0.98
(cations: 29 DI injections, 61 (Na+), 66 (NH4+), 68 (K+) std 0.5 (1 µN) injections for "s", t = 1.96)								
(anions: 52 DI injections, all "s" from 59 std 1 (2 µN) injections, t = 1.96)								
method: threshold	1.11	1.25	1.2	2.91	3.25	2.24	1.17	1.89
(cations: 12 calibrations, threshold detection area = 500, t = 2.26)								
(anions: 11 calibrations, threshold detection area = 900, t = 2.31)								
Precision (%RSD: concentration units in µN)								
<10 µN								< 22 µN
RSD	*8.5%*	*24.9%*	*13.5%*	*31.4%*	*10.3%*	*7.0%*	*11.6%*	*11.0%*
count	80	9	82	62	17	19	5	6
min	-0.34	0.00	0.00	1.66	1.15	0.00	0.00	0.00
max	9.82	4.60	9.95	16.73	11.83	10.70	1.48	21.72
mean	3.01	0.73	4.00	4.65	6.67	5.14	1.02	5.35
>10 µN								> 22 µN
RSD	*5.2%*	*2.9%*	*3.7%*	*2.2%*	*4.6%*	*4.2%*	*2.2%*	*0.9%*
count	6	79	6	24	67	41	54	48
min	12.94	13.30	10.48	10.33	10.06	10.35	11.35	26.40
max	298.91	1124.39	15.16	99.10	442.46	88.63	1341.66	1509.76
mean	134.79	239.29	12.89	39.75	66.70	31.49	326.27	612.29
(calculated from (mostly) pairs of replicate injections (including between runs) of the same sample)								
(if the pair of replicates straddled the 10 µN cut, it was included in the lower calculation range)								
(Sulfate cut point raised to (about) 20 µN due to lack of data)								
Accuracy (diluted from a purchased standard, concentration units in µN)								
Dionex Check #3								
count	22	22	22	22	22	26	26	26
nominal value	6.52	16.63	3.84	12.34	37.43	8.46	16.11	31.23
mean/ nominal*	*104.9%*	*93.0%*	*99.9%*	*150.2%*	*128.7%*	*95.1%*	*97.7%*	*99.2%*
min	5.97	14.44	3.34	13.42	41.41	7.46	15.16	29.23
max	8.40	18.61	5.41	25.65	60.63	8.50	18.23	33.53
**cation results for check #1 are blank-corrected*								
Dionex Check #2								
count	26	26	26	26	26	26	26	26
nominal value	173.99	443.50	102.31	329.15	998.00	76.16	145.01	281.08
mean/ nominal	*102.7%*	*97.5%*	*102.9%*	*94.7%*	*100.3%*	*98.9%*	*105.2%*	*94.4%*
min	163.48	406.48	99.72	290.72	951.43	73.89	151.06	261.82
max	187.85	469.42	112.26	323.81	1058.81	78.96	157.75	276.51
Dionex Check #3								
count	20	20	20	20	20	26	26	26
nominal value	260.99	665.25	153.46	493.73	1497.01	211.55	402.80	780.78
mean/ nominal	*102.3%*	*96.2%*	*102.7%*	*93.5%*	*99.2%*	*96.5%*	*90.6%*	*92.9%*
min	245.66	603.11	148.90	433.32	1414.59	199.61	359.33	715.23
max	279.80	688.34	166.77	485.15	1552.95	208.01	378.40	753.31
Duplicate analysis (concentration units in µN)								
+/- 1 s	14	17	16	20	15	15	15	11
+/- 2 s	3	3	5	1	3	5	2	2
+/- 3 s	1	2	2	1	3	0	1	2
>+/- 3 s	5	1	0	1	2	0	2	5
min	-0.34	13.71	1.02	2.53	5.75	0.00	8.68	20.11
max	6.79	478.69	12.74	58.60	251.64	41.12	608.94	926.66
mean	1.65	177.63	3.82	10.82	43.41	12.34	155.78	391.17
(Duplicate samples prepared concurrently in the field although not always analyzed in the same IC run								
(Where replicates of any sample occurred, each analysis compared individually)								
(all totals are not the same due to peak identification errors)								
("+/- 1 s" means the +/- 1 s bands around the two points compared overlap)								

Reproduced with permission of the copyright owner. Further reproduction prohibited without permission.

Table K-4: Compiled Davis IC MDL and precision statistics only

Davis IC statistics – MDL and precision only									
(standard injection volumes only, except where otherwise noted)									
(all concentration units in µN, unless otherwise indicated)									
	Chloride	Nitrate	Sulfate	Nitrite	Sodium	Ammonium	Potassium	Magnesium	Calcium
	[µN]	[µN]	[µN]	[µN]	[µN]	[µN]	[µN]	[µN]	[µN]
Minimum Detection Limit (95% CL) [µN]									
via threshold area detection limit method based upon calibration equations									
	2.23	1.3	1.24	2.07	0.83	1.03	1.14		
via DI water injection response									
					0.74	1.09	0.64	4.61	6.88
						0.72 (@ 100 µl)			
	(anion threshold area response: 26 calibration curves, 900 area units, t = 1.96)								
	(cation threshold area response: 21 calibration curves, 500 area units, t = 1.96)								
	(cation DI response: 123 injections (121 for K^+) over 21 runs, t = 1.96)								
Precision: all species (except NH_4^+ < 3000 µN only)									
RANGE	< 10 µN	< 20 µN	< 20 µN	< 20 µN	< 10 µN	< 10 µN	< 10 µN	< 10 µN	< 20 µN
RSD	8.01%	12.49%	5.28%	10.10%	4.52%	42.81%	8.94%	31.67%	17.19%
# of sets	55	21	34	36	69	15	65	90	83
min. conc'n	0.00	0.00	0.00	0.00	-0.49	-0.34	-0.01	-0.09	-1.26
max. conc'n	9.87	16.49	19.22	20.51	9.93	3.68	10.81	12.94	27.86
mean conc'n	3.60	2.22	6.60	9.60	3.51	0.79	4.06	3.37	9.21
RANGE	> 10 µN	> 20 µN	> 20 µN	> 20 µN	> 10 µN	3000 >x> 10 µN	> 10 µN	> 10 µN	> 20 µN
RSD	4.10%	1.06%	3.94%	4.00%	2.53%	4.43%	19.74%	7.69%	6.07%
# of sets	68	83	90	69	29	76	31	8	14
min. conc'n	10.00	52.64	20.43	21.42	10.32	102.23	10.00	10.01	21.06
max. conc'n	497.70	9587.70	1791.72	170.26	702.25	2977.89	50.34	34.08	67.82
mean conc'n	65.01	1088.19	257.50	63.83	50.88	841.60	19.97	18.80	37.19
						< 20 µN, 11.5% (@ 100 µl)			
						> 20 µN, 1.1% (@ 100 µl)			
	(where a pair straddled the division between precision ranges, it was assigned to the lower one)								
Precision: NH_4^+ > 3000 µN									
	concentrations via dilution compared to those from undiluted measurement @ 10 µl injection volume								
RSD						6.47%			
# of sets						13			
min. conc'n						5248.49			
max. conc'n						15871.35			
mean conc'n						11778.93			
	comparison of replicates of measurements @ 10 µl injection volume								
RSD						1.10%			
# of sets						12			
min. conc'n						1852.23			
max. conc'n						15496.20			
mean conc'n						7206.33			

Reproduced with permission of the copyright owner. Further reproduction prohibited without permission.

Table K-5: Compiled Davis IC standard accuracy statistics

Davis IC statistics – Accuracy: standard Dionex check standards and injection volumes only	Cl^- [µN]	NO_3^- [µN]	$SO_4^{=}$ [µN]	NO_2^- [µN]	Na^+ [µN]	NH_4^+ [µN]	K^+ [µN]	Mg^{2+} [µN]	Ca^{2+} [µN]
Accuracy									
	Dionex Check #1								
# of injections	51	51	51		40	40	40	40	40
min conc'n	7.29	14.51	28.71		5.66	8.83	8.44	11.52	12.04
max conc'n	8.56	16.60	32.37		6.91	11.46	10.71	19.58	21.48
mean conc'n	8.00	15.58	30.27		6.34	10.10	9.50	16.20	17.08
nominal conc'n	8.05	15.72	29.97		6.52	10.39	9.59	15.43	18.71
mean/nominal	99.4%	99.1%	101.0%		97.2%	97.2%	99.0%	105.0%	91.3%
	Dionex Check #2								
# of injections	51	51	51		37	37	37	37	37
min conc'n	70.97	137.53	266.21		11.35	17.96	17.08	27.90	32.10
max conc'n	76.58	142.15	272.83		14.58	22.88	20.96	36.48	41.20
mean conc'n	74.69	138.80	269.06		13.09	20.45	19.17	31.84	36.89
nominal conc'n	74.61	138.87	268.84		13.05	20.79	19.18	30.86	37.43
mean/nominal	100.1%	100.0%	100.1%		100.3%	98.3%	99.9%	103.2%	98.6%
	Dionex Check #3								
# of injections	51	51	51		40	40	40	40	40
min conc'n	194.06	373.56	750.16		156.51	249.35	230.70	359.31	433.41
max conc'n	200.93	395.71	783.83		182.60	292.77	270.20	442.38	529.97
mean conc'n	197.77	384.36	770.05		174.53	276.94	256.82	403.57	486.92
nominal conc'n	198.20	384.18	769.84		173.99	277.19	255.77	477.44	499.00
mean/nominal	99.8%	100.0%	100.0%		100.3%	99.9%	100.4%	98.1%	97.6%
	Dionex Check #4								
# of injections	43	45	45		37	37	37	36	36
min conc'n	825.30	1572.92	3055.88		233.51	365.75	349.94	548.59	663.39
max conc'n	854.23	1661.10	3220.68		279.04	431.63	409.04	662.57	802.29
mean conc'n	838.39	1597.96	3122.11		259.89	406.70	382.39	611.39	739.94
nominal conc'n	840.20	1598.64	3116.36		260.99	415.78	383.65	617.16	748.50
mean/nominal	99.8%	100.0%	100.2%		99.6%	97.8%	99.7%	99.1%	98.9%
	(note anions check #4 is undiluted)								
	Dionex Check #5								
# of injections					37	37			
min conc'n					1081.32	1728.33			
max conc'n					1282.90	2245.22			
mean conc'n					1214.83	1991.73			
nominal conc'n					1217.93	1940.30			
mean/nominal					99.7%	102.7%			

Reproduced with permission of the copyright owner. Further reproduction prohibited without permission.

Table K-6: Compiled Davis IC high ammonium and nitrite accuracy statistics

Davis IC statistics – Accuracy: high ammonium and nitrite only									
	Chloride	Nitrate	Sulfate	Nitrite	Sodium	Ammonium	Potassium	Magnesium	Calcium
	[µN]	[µN]	[µN]	[µN]	[µN]	[µN]	[µN]	[µN]	[µN]
	for ammonium @ 10 µl (via calibration standard) over 2 runs only								
# of injections						12			
min conc'n						4342.78			
max conc'n						4619.98			
mean conc'n						4476.25			
nominal conc'n						4400.00			
mean/nominal						101.7%			
	for ammonium @ 10 µl (via calibration standard) over 1 run only								
# of injections						3			
min conc'n						10037.20			
max conc'n						10388.70			
mean conc'n						10222.03			
nominal conc'n						10000.00			
mean/nominal						102.2%			
	for ammonium @ 10 µl (via Dionex Check #5) over 2 runs only								
# of injections						4			
min conc'n						2114.25			
max conc'n						2151.52			
mean conc'n						2130.94			
nominal conc'n						1940.30			
mean/nominal						109.8%			
	for ammonium @ 100 µl								
mean/nominal						< ± 1.5%			
	(for all species concentrations quantifiable @ 10 µl injection volume, accuracy good to ± 10%)								
	for nitrite only via dilution of a separate liquid standard								
# of injections				33					
min conc'n				37.05					
max conc'n				39.61					
mean conc'n				38.24					
nominal conc'n				40.00					
mean/nominal				95.6%					
	for nitrite only via dilution of a separate liquid standard								
# of injections				19					
min conc'n				186.38					
max conc'n				199.10					
mean conc'n				191.79					
nominal conc'n				200.00					
mean/nominal				95.9%					
	note that cation analysis of nitrite standards consistent with these reported results								

Reproduced with permission of the copyright owner. Further reproduction prohibited without permission.